Alaska Department of Transportation & Public Facilities
Alaska University Transportation Center

Seismic Performance of Steel Pipe Pile to Cap Beam Moment Resisting Connections

Final Report

Prepared By:

Steven J. Fulmer
Mervyn J. Kowalsky
James M. Nau

North Carolina State University
Raleigh, North Carolina

January 2013

Prepared For:

Alaska University Transportation Center
Duckering Building Room 245
P.O. Box 755900
Fairbanks, AK 99775-5900

Alaska Department of Transportation
Research, Development, and Technology Transfer
2301 Peger Road
Fairbanks, AK 99709-5399

IN/AUTC 13.02

DOT FHWA-AK-RD-13-02

REPORT DOCUMENTATION PAGE

Form approved OMB No.

1. AGENCY USE ONLY (LEAVE BLANK)	2. REPORT DATE	3. REPORT TYPE AND DATES COVERED
FHWA-AK-RD-	January 2013	Final Report (7/2010-6/2013)

4. TITLE AND SUBTITLE

Seismic Performance of Steel Pipe Pile to Cap Beam Moment Resisting Connections

5. FUNDING NUMBERS

AUTC#410001
DTRT06-G-0011
T2-10-05

6. AUTHOR(S)
Steven J. Fulmer, Mervyn J. Kowalsky, James M. Nau
North Carolina State University, Raleigh, North Carolina

7. PERFORMING ORGANIZATION NAME(S) AND ADDRESS(ES)
Alaska University Transportation Center
P.O. Box 755900
Fairbanks, AK 99775-5900

8. PERFORMING ORGANIZATION REPORT NUMBER

INE/AUTC 13.02

9. SPONSORING/MONITORING AGENCY NAME(S) AND ADDRESS(ES)
Alaska Department of Transportation
Research, Development, and Technology Transfer
2301 Peger Road
Fairbanks, AK 99709-5399

10. SPONSORING/MONITORING AGENCY REPORT NUMBER

FHWA-AK-RD-13-02

11. SUPPLENMENTARY NOTES

12a. DISTRIBUTION / AVAILABILITY STATEMENT

No restrictions

12b. DISTRIBUTION CODE

13. ABSTRACT (Maximum 200 words)

This research, a joint effort between AUTC and North Carolina State University, is a continuation of an ngoing project that investigated bridge and marine structure design practices, aiming to identify improved connection design approaches to produce the necessary ductility and energy absorbing capacities required for satisfactory designs in Alaska. Through earlier testing, researchers not only proved what methods were inadequate (such as the current practice of fillet-welding the cap beam to the pile as well as an alternative welding methods) but also confirmed that a new method of using a plastic hinge-relocating concept was more successful. This method utilized a round steel column capital in which the top portion welded to the cap beam is thicker than the bottom thinner portion welded to the pile. The approach successfully reduced the inelastic demands of the cap beam weld, and forced the inelastic action to occur in the pile itself. Current research includes optimizing the new design to improve displacement capacity and ductility in bridge and marine structure design, as well as investigating additional connection designs proposed by ADOT&PF engineers. The research will result in a series of design recommendations consistent with the various levels of seismicity found within Alaska. The primary benefit will be the improved design and performance of steel bridges and marine structures containing similar connections.

14- KEYWORDS: Bridge design (Esusb), Earthquake engineering (Ttkfre), Earthquake resistant design (Esdc), Steel pipe (Rbmdxnpks), Steel bridges (Pdybmmms), Steel structures (Pbcs), Piles (Supports) (Pbpbvvm), Structural tests (Gbbs), Structural analysis (Ge), Structural engineering (Ttkfr), Structural connection (Fcacjv), Dynamic structural analysis (Geb), Static structural analysis (Get), Finite element method (Gej), Ductility (Rkmlm)

15. NUMBER OF PAGES
680

16. PRICE CODE

N/A

17. SECURITY CLASSIFICATION OF REPORT	18. SECURITY CLASSIFICATION OF THIS PAGE	19. SECURITY CLASSIFICATION OF ABSTRACT	20. LIMITATION OF ABSTRACT
Unclassified	Unclassified	Unclassified	N/A

SI* (MODERN METRIC) CONVERSION FACTORS

APPROXIMATE CONVERSIONS TO SI UNITS

Symbol	When You Know	Multiply By	To Find	Symbol
		LENGTH		
in	inches	25.4	millimeters	mm
ft	feet	0.305	meters	m
yd	yards	0.914	meters	m
mi	miles	1.61	kilometers	km
		AREA		
in^2	square inches	645.2	square millimeters	mm^2
ft^2	square feet	0.093	square meters	m^2
yd^2	square yard	0.836	square meters	m^2
ac	acres	0.405	hectares	ha
mi^2	square miles	2.59	square kilometers	km^2
		VOLUME		
fl oz	fluid ounces	29.57	milliliters	mL
gal	gallons	3.785	liters	L
ft^3	cubic feet	0.028	cubic meters	m^3
yd^3	cubic yards	0.765	cubic meters	m^3
	NOTE: volumes greater than 1000 L shall be shown in m^3			
		MASS		
oz	ounces	28.35	grams	g
lb	pounds	0.454	kilograms	kg
T	short tons (2000 lb)	0.907	megagrams (or "metric ton")	Mg (or "t")
		TEMPERATURE (exact degrees)		
^oF	Fahrenheit	5 (F-32)/9 or (F-32)/1.8	Celsius	^oC
		ILLUMINATION		
fc	foot-candles	10.76	lux	lx
fl	foot-Lamberts	3.426	candela/m^2	cd/m^2
		FORCE and PRESSURE or STRESS		
lbf	poundforce	4.45	newtons	N
lbf/in^2	poundforce per square inch	6.89	kilopascals	kPa

APPROXIMATE CONVERSIONS FROM SI UNITS

Symbol	When You Know	Multiply By	To Find	Symbol
		LENGTH		
mm	millimeters	0.039	inches	in
m	meters	3.28	feet	ft
m	meters	1.09	yards	yd
km	kilometers	0.621	miles	mi
		AREA		
mm^2	square millimeters	0.0016	square inches	in^2
m^2	square meters	10.764	square feet	ft^2
m^2	square meters	1.195	square yards	yd^2
ha	hectares	2.47	acres	ac
km^2	square kilometers	0.386	square miles	mi^2
		VOLUME		
mL	milliliters	0.034	fluid ounces	fl oz
L	liters	0.264	gallons	gal
m^3	cubic meters	35.314	cubic feet	ft^3
m^3	cubic meters	1.307	cubic yards	yd^3
		MASS		
g	grams	0.035	ounces	oz
kg	kilograms	2.202	pounds	lb
Mg (or "t")	megagrams (or "metric ton")	1.103	short tons (2000 lb)	T
		TEMPERATURE (exact degrees)		
^oC	Celsius	1.8C+32	Fahrenheit	^oF
		ILLUMINATION		
lx	lux	0.0929	foot-candles	fc
cd/m^2	candela/m^2	0.2919	foot-Lamberts	fl
		FORCE and PRESSURE or STRESS		
N	newtons	0.225	poundforce	lbf
kPa	kilopascals	0.145	poundforce per square inch	lbf/in^2

*SI is the symbol for the International System of Units. Appropriate rounding should be made to comply with Section 4 of ASTM E380.
(Revised March 2003)

TABLE OF CONTENTS

LIST OF FIGURES

LIST OF TABLES

LIST OF SELECTED NOTATIONS

$ALR =$ Axial Load Ratio

$D / t_{des} =$ Design D/t Ratio

$F_{loss} =$ Allowable System Strength Loss

$f_{cc} =$ Elastic Stress Distribution Factor

$H =$ Height Above Grade

$H =$ Distance from P.O.C. to Cap Beam Soffit

$H_{CP} =$ Height to Point of Contraflexure

$H_{IG} =$ Height to In-ground Hinge

$M_{IG} =$ In Ground Hinge Moment Capacity

$M_T =$ Top Hinge Moment Capacity

$O =$ Applicable Strain Hardening Overstrength Factor

$S_{pz} =$ Elastic Modulus of Protected Zone

$X_d =$ Design Depth of Hinging

$Z_{hinge} =$ Plastic Modulus of Intended Hinge Region

$\varepsilon_{\max} =$ Maximum Strains in Region of Discontinuity

$\varepsilon_n =$ Normal Strains in Region of Discontinuity

$\Delta =$ Displacement

$\Delta_y =$ Effective Yield Displacement

$\Delta'_y =$ First Yield Displacement

$\Delta_{y,\exp} =$ Effective Yield Displacement From Experimental Results

$\Delta'_{y,\exp}$ = First Yield Displacement From Experimental Results

$\sigma_{\max}$ = Maximum Stress in Region of Discontinuity

σ_n = Normal Stress in Region of Discontinuity

μ = Displacement Ductility Unless Noted Otherwise

$\mu_{\Delta all}$ = Allowable System Displacement Ductility

$\mu\varepsilon$ = Microstrain

ACKNOWLEDGEMENTS

The authors of this report wish to acknowledge the Alaska DOT&PF (AKDOT&PF) and the Alaska University Transportation Center (AUTC) for supporting the research work considered in this project through a series of grants. Special acknowledgement goes to Elmer Marx of the Alaska DOT&PF and Billy Connor of the AUCT who were closely involved in this research as the primary technical contacts between NCSU and AKDOT&PF/AUTC. In addition, acknowledgement should be given to the entire AKDOT/AUTC technical staff who was involved with this project.

The assistance of the entire staff and all graduate students of the Constructed Facilities Laboratory at NCSU is greatly appreciated. A special thanks is extended to Yuhao Feng, Chad Goodnight, Greg Lucier, Nichole King, and Kelly Herrick all of whom helped extensively throughout the course of the project.

ABSTRACT

This report discusses research work conducted to evaluate and improve upon the seismic performance of hollow steel pipe pile to cap beam moment resisting connections. Past research has shown that directly welding circular hollow steel piles to a steel cap beam, regardless of weld configuration, does not mitigate the undesirable failure mode of brittle cracking in critical welded regions of the connection as the pier is subjected to inelastic displacement levels. This finding was further validated in this research project, suggesting specific attention should be given to capacity protecting critical welded regions of the connection.

To do so, the concept of modified weld protected connections was developed based on capacity design principles. The concept was aimed at developing connection configurations that would improve the seismic capacity of steel pier systems by relocating damage in the pile elements away from critical welded regions in addition to strengthening critical welded regions to remain in the elastic range of response. Three such connection configurations were developed with two being shown to fulfill both key criteria. Ultimately, design recommendations were generated in regards to standard welded connections, modified weld protected connections, and the ductility capacity of systems utilizing a composite connection configuration.

SUMMARY OF FINDINGS

This report discusses original research work conducted to evaluate and improve upon the seismic performance of hollow steel pipe pile to cap beam moment resisting connections. These connections are intended to serve in steel pier bridge substructure systems which are subjected to lateral loading, due seismically induced forces and are expected to perform in the non – linear response range. Past research has shown that directly welding circular hollow steel piles to a steel cap beam, regardless of weld configuration, does not mitigate the undesirable failure mode of brittle cracking in the critical welded regions of the connection as the pier is subject to inelastic displacement levels. This finding was further validated in the scope of the research work discussed in this document, suggesting specific attention should be given to capacity protecting critical welded regions of the connection.

To achieve this goal, the concept of modified weld protected connections was developed based on capacity design principles. The concept was aimed at developing connection configurations that would improve the seismic capacity of steel pier systems by fulfilling two key criteria. First, the location of damage in the pile elements of the system needed to be relocated below the welded region of the connection, and secondly the welded region needed to be strengthened to remain in the elastic range of response considering increased moment demands due to hinge relocation. It was postulated that following these two key criteria would allow the limit state of flexural hinging, in the form of pile wall local buckling, to develop prior to any cracking.

Three potential modified weld protected connections were developed and evaluated in this research. The first consisted of a cruciform gusset plate style connection, which was shown to relocate damage away from critical welds. However, this connection was not capable of producing the desirable failure mode of pile wall local buckling, as pile wall cracking developed. Next, a fabricated flared column capital section was developed and was shown to both effectively relocate damage and to produce the desirable pile wall local

buckling mode of failure. Lastly, a composite connection configuration was developed which utilized an annular grouted region with shear stud connectors that facilitated force transfer from the pile to a larger stub pipe pile component that was welded to the cap beam.

Large scale quasi – static experimental testing, scaled dynamic shake table experimental testing, and analytical investigations all showed this composite system to be capable of relocating damage away from the welded regions of the connection and to produce the desirable failure mode of pile wall local buckling. Further, the performance of this connection configuration was shown to be minimally impacted by construction tolerance offsets, lending confidence to a designer that adequate behavior can be expected under non – ideal construction conditions. Given the successful performance of this style of connection, an analytical parametric study was conducted to relate ductility capacity for a given allowable strength loss, pile D/t ratio, and vertical dead load magnitudes for systems containing these composite connections. Ultimately, from the research results design recommendations were generated with regards to basic welded connections, modified weld protected connections, and the ductility capacity of systems utilizing the composite connection configuration.

In addition to the connection research that was conducted, an alternate truss style steel pier system was evaluated within this project and was shown to have behavior dominated by compression brace buckling and gusset plate weld cracking when subjected to lateral loading. Due to multiple sources of inelasticity and an undefinable/unreliable brittle cracking failure mode, the use of this type of system is not recommended when a ductile response is required. However, with improved seismic detailing it may be possible to produce a desirable with the truss style steel pier detail.

Chapter 1: Introduction

1.1 Background – Steel Pier Bridges

Although the bridge construction industry is historically dominated by the use of reinforced concrete for the construction of typical bridge piers, the use of steel as a bridge pier construction material has its place in history as well as the future. The benefits of the use of steel for the construction of bridge piers or bents includes but is not limited to speed and ease of construction, as well as the utilization of what is inherently a very ductile material. The state of Alaska has an inventory of existing driven pile steel piers and, in some cases, prefers to design new bridges with this type of system. These bridge piers typically consist of hollow driven steel pipe piles, not filled with concrete, and multi-wide HP steel cap beams as shown in shown in Figure 1.1 through Figure 1.3. In some cases, the system uses battered piles which are not considered in the research covered in this project that was jointly funded by the Alaska Department of Transportation and Public Facilities (AKDOT&PF) and the Alaska University Transportation Center (AUTC).

The research work presented in this document was aimed at evaluating the seismic performance capabilities of hollow steel pipe pile to cap beam moment resisting connections utilized in the construction of driven pile steel piers. Transverse, and in some cases longitudinal, super-structure displacements produced by seismic loading generate a double curvature bending moment gradient along the length of the driven steel pile as shown in Figure 1.4. The connection between the pipe pile and cap beam elements of the system must be capable of transferring this bending moment demand. Typical of a capacity design procedure, the required moment resisting capacity of the connection can be taken as the over-strength moment capacity of the pipe pile element, assuming a plastic hinging failure mechanism at the top of the pile members is expected to be the controlling mode of failure. However, the majority of the research discussed in this document focuses not only on the

ability of the connection design to develop the moment capacity of the pipe pile, but more importantly to accommodate large inelastic rotations necessary to facilitate a ductile system response as is required of systems expected to resist seismically induced forces.

Figure 1.1 Steel Bridge Pier (Compliments AKDOT)

Figure 1.2 Steel Bridge Pier (Compliments AKDOT)

Figure 1.3. Mooring Dock Steel Pier – Juneau, AK

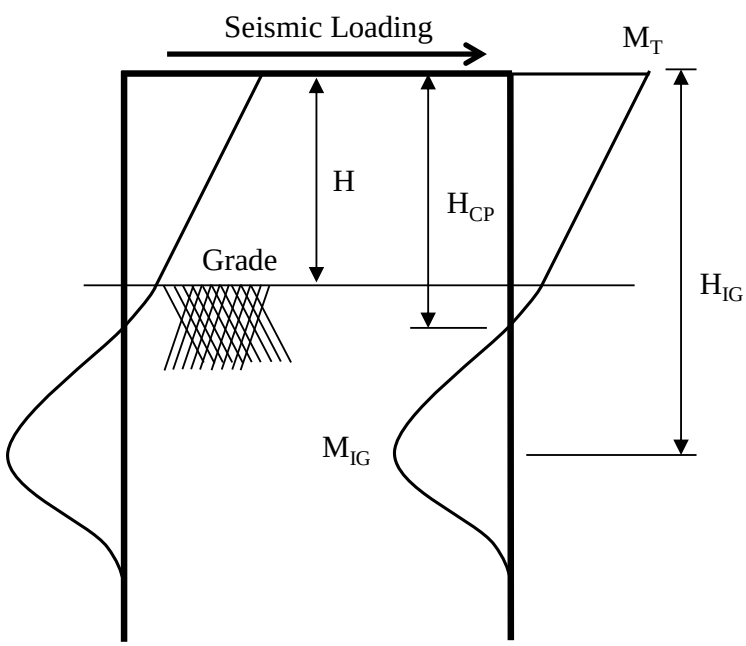

Figure 1.4 Pile Bending Moment Pattern for Driven Pile System

1.2 The Need for Research: Potential Limit States

When subjected to design level seismic events, structures are expected to perform in the non-linear response range and to sustain damage as is discussed in many texts including (Priestley, et. al., 2007). This damage must however be controllable, prevent collapse, and in the case of demands less than the design seismic event preferably be repairable. As a base material, steel is a desirable construction material due to its ductile characteristics. However, steel connections, if not detailed properly, can be problematic when subjected to large inelastic deformations as is discussed in many documents including (Bruneau, et. al., 1998). In accordance with the principals of capacity design, undesirable modes of failure of a system, such as brittle connection failures, should be avoided in order to develop plastic hinges at intended location. Should undesirable modes of failure develop prior to the formation of pile plastic hinges, issues such as structural collapse, irreparable damage, or lack of system ductility could occur.

Based on the geometry of steel pier systems and the anticipated pile hinging mechanism, obvious potential limit states include yielding of connection elements, cracking of connection elements, cracking of base pile material, or most preferably local buckling of the pile wall to form flexural hinges. Past research at North Carolina State University has indicated that basic welded connections, regardless of weld geometry, may be incapable of producing desirable ultimate limit states and may possess limited ductility capacity. The past work showed the behavior of basic welded connections to be dominated by cracking at or near critical welded regions. This past research consisted of a portion of the phase 1 steel pier testing program that is described in detail in (Fulmer, et. al., 2010, 2009) and (Cookson, K.A., 2009). Further conclusions regarding the behavior of welded connections from the past work will be discussed in detail in subsequent chapters of this document.

1.3 Research Goals and Scope

The scope of the research covered in this document, which includes work from phases 1 and 2 of the steel pier testing program, was aimed at better understanding and improving upon the non – linear behavior of steel pipe pile to cap beam moment resisting connections. The research hypothesis assumed that the behavior of basic welded connections is controlled by undesirable failure modes, and that the performance of the system could be improved by alternative connection designs. Better understanding of how steel pipe pile to cap beam connections behave, and improving upon their configuration, would allow for the application of Performance Based Seismic Design (PBSD) to systems containing these types of connections. PBSD aims to design a structure to reliably achieve a specific level of damage for a prescribed seismic hazard as is done in a Direct Displacement-Based Design (DDBD) procedure for example.

As will be discussed throughout this document, in order to achieve a reliable pile hinging failure mode, steel pipe pile to cap beam connection configurations should provide a specific method of protecting critical welded regions by relocating damage away from these interfaces. These connections fall into what has been defined in this work as modified weld protected connections as opposed to standard welded connections which do not provide a means of damage relocation. Further discussion regarding these two categories of connection designs, is provided throughout this document.

The methods that have been utilized to achieve these research goals include laboratory experimental testing of full scale pier systems as well as dynamic testing of scaled systems, and three dimensional detailed Finite Element Modeling (FEM). These two components, experimental work and Finite Element Modeling, have been used interdependently where in some cases FEM assisted in planning of experimental work and in others where experimental work allowed for calibration of the FEM procedure. Further, the FEM model was used to

conduct a parametric study to determine reliable deformation capacity as a function of D/t ratio and dead load magnitude for a particular connection configuration.

Chapter 2: Literature Review

2.1 General Discussion

An extensive review of the literature revealed a limited amount of published research work that was applicable to the specific steel pier system considered in the scope of the work discussed here. However, two journal articles were found that provided relevant information to the scope of this research project. The work of Steunberg et al. (1998) examined the behavior of a circular steel pipe pile welded to a steel plate embedded in a concrete cap beam, while the second study by Nishikawa et al. (1998) was focused on strengthening of systems with connections of the steel pipe pile to a restrained testing base consisting of a pocketed and welded configuration. While relevant from the perspective of pipe wall local buckling behavior, the second study did not directly reflect any connection investigated in the research discussed throughout this document.

2.2 Relevant Articles

2.2.1 Steel Pile/Precast Concrete Cap Beam Study (Steunenberg et. al., 1998)

The research discussed in the paper by Steunenberg et. al. (1998) focused on a single laboratory test that evaluated the performance of a steel pile with, a D/t ratio of 25, welded to a steel plate that was embedded in a concrete block using anchor rods as shown in Figure 2.1. The connection of the pile to the plate consisted of a full joint penetrating weld which was placed in an overhead position to simulate actual construction practices. The specimen was subjected to reverse cyclic lateral load and was ultimately able to achieve a displacement ductility of 8, according to the authors of the paper, after local buckling formed at the base of the pile as shown in Figure 2.2. Although this seemed to be a positive result indicating that standard welded connections may provide adequate system behavior, a review of the testing

results indicates otherwise. The yield displacement reported in the article was 30 mm. However, as can be seen in Figure 2.3, this structure appears to not have reached first yield at 30 mm. nor effective yield which extrapolates the first yield displacement by the ratio of nominal system strength to first yield strength. From Figure 2.3, it is appears that a ductility one displacement value would be approximately 50 mm. indicating a maximum ductility of approximately four and a reliable ductility capacity of slightly over two based on the lack of repeating cycles at +/- 200 mm. and the loss of strength at +/- 300 mm.

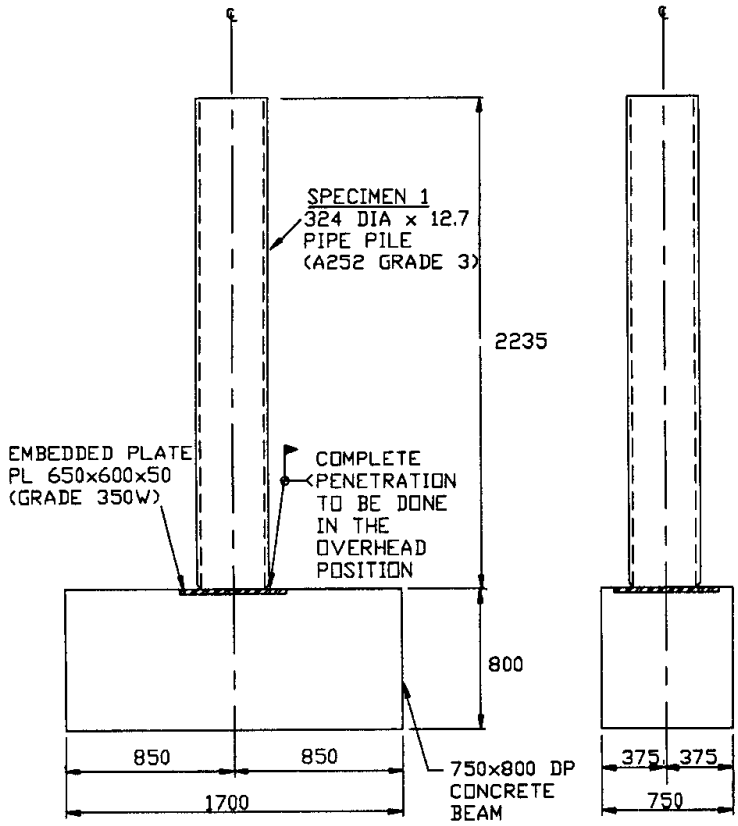

Figure 2.1 Test Specimen Details (Steunenberg, et. al., 2007)

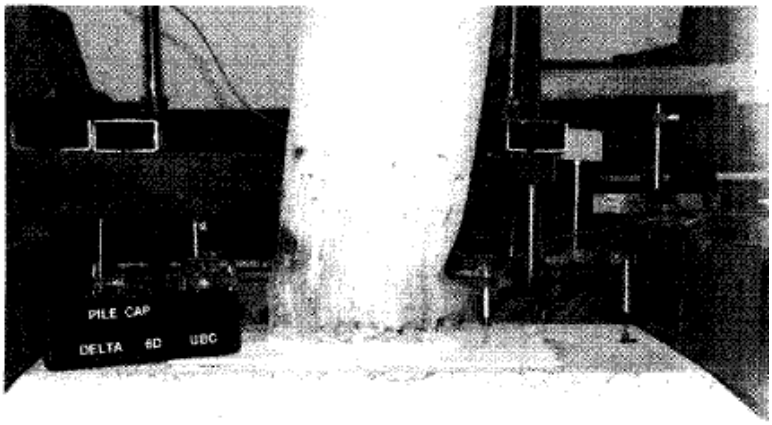

Figure 2.2 Locally Buckled Pile at Base Connection (Steunenberg, et. al., 2007)

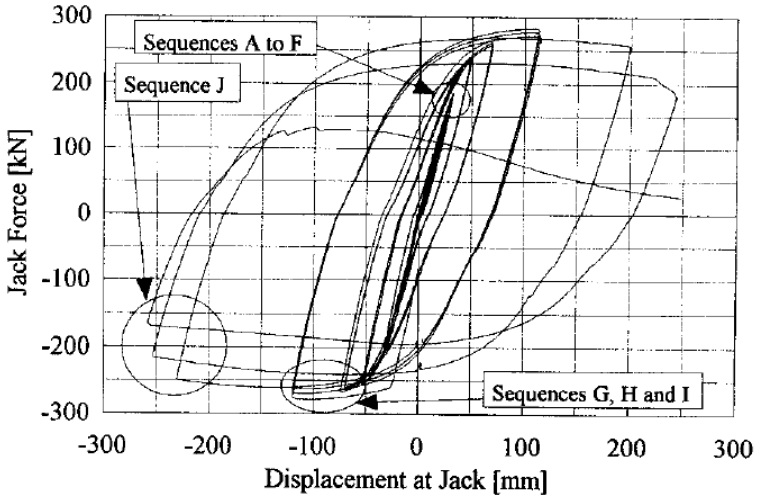

Figure 2.3 Experimental Force Displacement Hysteresis (Steunenberg, et. al., 2007)

Although the dimensions and diameter-to-thickness (D/t) ratio of the pile tested were similar to the dimensions used in this research project several differences in the test specimens existed. First, the steel plate embedded in concrete likely produced a more stiff connection interface than would have been the case if the connection was to a flexible steel cap beam. As will be discussed later in this document, this effect is likely significant. Secondly, no axial load was applied during testing as would exist in an actual pier and as would develop in a multi-column pier test regardless of whether or not gravity load was

applied to the specimen due to global equilibrium requirements. Although this specimen was able to develop pile hinging in the form of local buckling which mitigated connection cracking, the force displacement response indicates that these structures may be of limited ductility capacity.

2.2.2 Retrofitting of Steel Bridge Columns (Nishikawa, K., et. al., 1998)

The research considered in the study by Nishikawa et. al., 1998 focused on retrofitting of existing columns as the title indicates. The study considered both square and circular sections. However, only the results of the circular specimens are presented here as the basis of this research project is to determine the performance capabilities of hollow circular section piles.

The study assumed that local buckling of the pile would occur before connection cracking, as was reportedly experienced following the Kobe earthquake of 1995. The goal of the research study was to prolong the life of the structure by controlling the growth of outward local buckling. This would be achieved by placing an outside reinforcing pipe around the column with a specified tolerance. The lack of contact between the two elements was intended to ensure that the outer ring provided no strength or stiffness to the structure until buckling occurred. Following the occurrence of local buckling the outward bulges which were expected to develop should come in contact with the outer ring which in turn will control the growth of these bulges and prolong the life of the structure as shown in Figure 2.4.

The experimental results, detailed in Figure 2.5, indicated that the method was moderately successful as shown in Figure 2.6 which provides positive side force displacement envelopes for the two D/t values tested. As shown, the retrofitted column responses, depicted by the dashed lines, experienced a slight increase in post buckling

ductility capacity as compared to the non-retrofitted specimen responses shown by solid lines. However, this conclusion is not of great importance to the basic scope of this research project since the basic system configuration differed from that considered in the research covered in this document, which does not specifically focus on retrofit.

Regardless, the fact that connection cracking did not occur prior to pile local buckling is of importance to this project. However, the connection utilized during this testing was a pocketed type connection where the pile was passed through an upper plate and then welded to both a lower plate and the upper plate as shown in Figure 2.5. The significant difference between this type of system and connection of piles to a cap beam soffit indicates that a direct comparison of these results to the results of this research project is not possible. Nevertheless, the study does provide what could be a viable connection alternative, namely a pocketed connection. In addition the study provides a potential retrofitting concept which was applied to develop a modified connection configuration in this research project intended to enhance the performance of the pier system as will be discussed in later chapters.

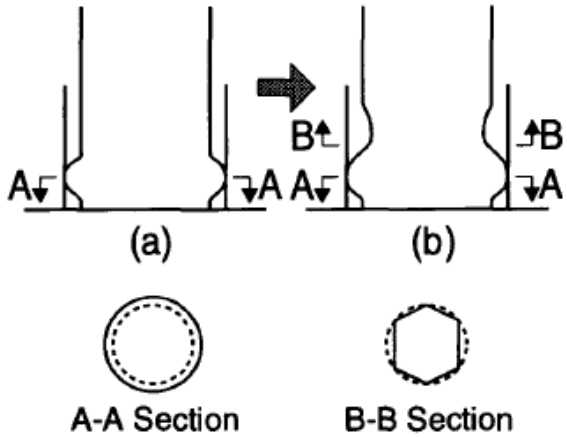

Figure 2.4 Buckling Control with Outer Ring (Nishikawa, K., et. al., 1998)

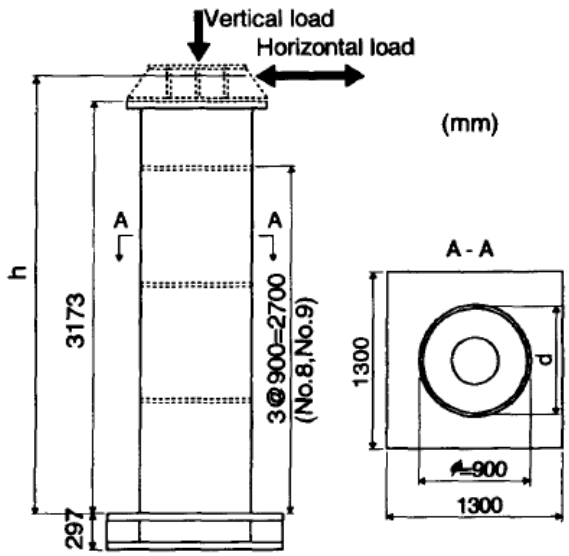

Figure 2.5 Test Specimen Detail (Nishikawa, K., et. al., 1998)

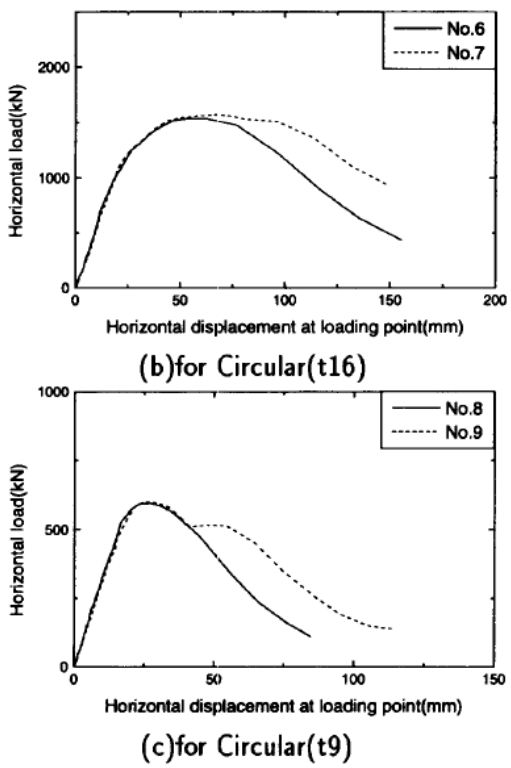

Figure 2.6 Positive Side Force-Displacement Envelopes (Nishikawa, K., et. al., 1998)

2.3 Literature Review Conclusions

Although the two studies reviewed in this chapter are of limited applicability to the scope of the research discussed in this document, both did indicate that basic welded connections may be capable of precluding connection cracking and developing pile wall local buckling. However, the considerable physical differences between a plate embedded in concrete, a pocketed base connection, and an actual steel cap beam connection place restrictions on the relevance of this conclusions to the steel pier systems considered in this research. As will be discussed in subsequent chapters, the study by Nishikawa et. al., 1998, did provide a concept that was used to modify a successful connection configuration in an attempt to improve post pile wall buckling behavior.

Chapter 3: Past Experimental Research

3.1 General Discussion

Past experimental research at North Carolina State University (NCSU) was conducted on full scale two column piers containing standard welded connections, which are defined as connections which do not specifically attempt to protect critical regions by relocating damage. This research work comprised a portion of the phase 1 steel pier testing conducted at NCSU that was funded by AKDOT&PF and is described in detail in both (Fulmer, et. al., 2009, 2010) and (Cookson, K.A., 2009). However, a summary of this work is provided in this chapter to enhance the discussion in subsequent chapters regarding the later experimental and analytical work that is basis of this document. Further, it is important to understand research findings which led to the development of modified weld protected connections. This later research work that is the basis of this document is comprised of a portion of phase 1 and all of phase 2 of the steel pier testing at NCSU.

3.2 Past Experimental Research Details

3.2.1 Introduction

The main goal of the past research program was to model as accurately as possible a typical steel bridge pier used in Alaska for evaluation of the connection behavior. The use of full scale two pile pier specimens helped to ensure that the influence of axial forces due to global overturning resistance and proper boundary conditions were captured. Although laboratory limitations were considered throughout the design, an attempt was made to minimize the influence of these limitations in order to achieve the main goal of capturing the response of the system when subjected to lateral load as accurately as possible.

A very important aspect of the specimen design in the past work was coordination with AKDOT&PF engineers to ensure that the design was in fact representative of their existing bridge inventory. Table 3.1 provides a representative sampling of the steel bent bridge inventory provided by AKDOT&PF to NCSU. As shown in Table 3.1, the pile heights range from 10-20 ft. above grade and the pile diameters from 12-30 in. Taking into account the fact that pinned based supports shown in Figure 3.1 were used to model the point of inflection that would exist in an actual system subjected to double bending, the decision was made to set a target pile height at 10-14 ft. which would correlate to an approximate 20-28 ft. pile length from the cap beam to the in ground point of fixity for an actual system depending on soil conditions. The decision was also made to use 16 in. diameter piles to produce a reasonable aspect ratio. The pile thickness was chosen as 1/2 in. to generate a D/t ratio of 32 which is within the typical range of AKDOT practice. ASTM A500 Grade B&C material designations were chosen for the pile elements.

The design of the cap beam was controlled by capacity design principles. In order to ensure that flexural hinging occurred at the tops of the piles, other failure mechanisms (beam hinging, joint failure, etc.) had to be capacity protected. From the design calculations which are included in (Fulmer, et. al., 2009), a double wide HP14x89 cap beam section comprised of ASTM A572 Grade 50 material was chosen since it was determined to remain elastic when subjected to the anticipated over-strength demands of a pile hinging mode of failure. In addition, cap beam transverse stiffeners were placed over the extreme fibers of the HSS piles to mitigate cap beam flange damage. The design resulted in the specimen configurations shown in Figure 3.2 and Figure 3.3.

Table 3.1 Sampling of AKDOT Steel Pier Inventory (Compliments AKDOT)

Name	Weld Type	Weld Size [in]	Pile Diam.	Pile thickness [in]	Pile Height above ground [ft]	Number of Piles per bent	Cap Beam	# of Spans	Span Length [ft]	Location		Figure reference
										Latitude	Longitude	
208	Field Fillet	0.25	12"	N/A	10	4	HP14x73	3	75	57.618	-152.315	N/A
1196	Field Fillet	0.25	12"	0.833	14	4	HP14x73	3	33	59.478	-139.608	N/A
1754	Field Fillet	0.75	30".	N/A	16.5	4	2W36x280	3	50	61.150	-149.700	Figure 1.2 and Figure 1.6
1820	Field Fillet	0.375	16"	N/A	20	4	2HP10x57	3	35	60.178	-149.365	Figure 1.4
1136	Field Fillet	0.375	16"	0.5	10	2	2HP14x89	1	80	60.105	-149.448	Figure 1.7
1945	Field Fillet	0.3125	20".	0.625	20	3	2W18x36	23	30	54.852	-163.408	Figure 1.1
1714	Field Fillet	0.375	12"	0.375	N/A	2	W24x84	1	74	61.560	-149.038	Figure 1.3 and Figure 1.5

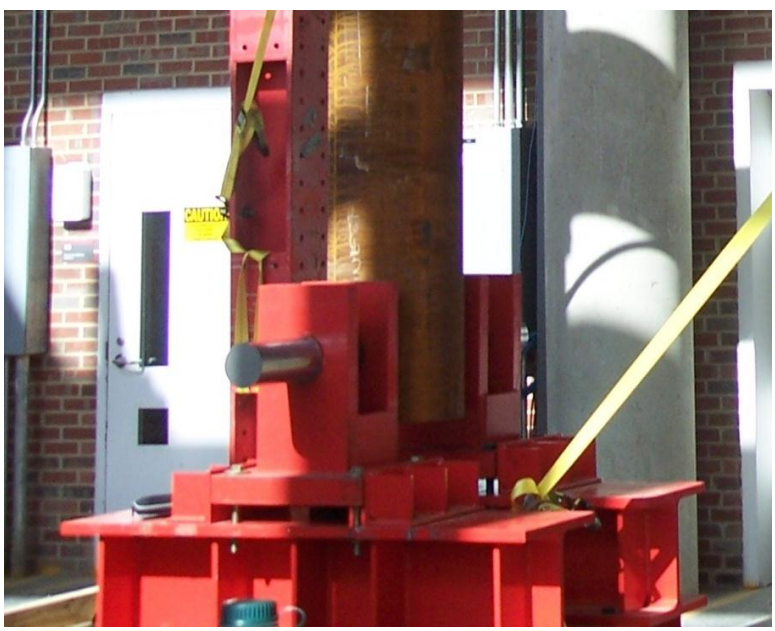

Figure 3.1 Pinned Base Supports Used in Phase 1 Testing

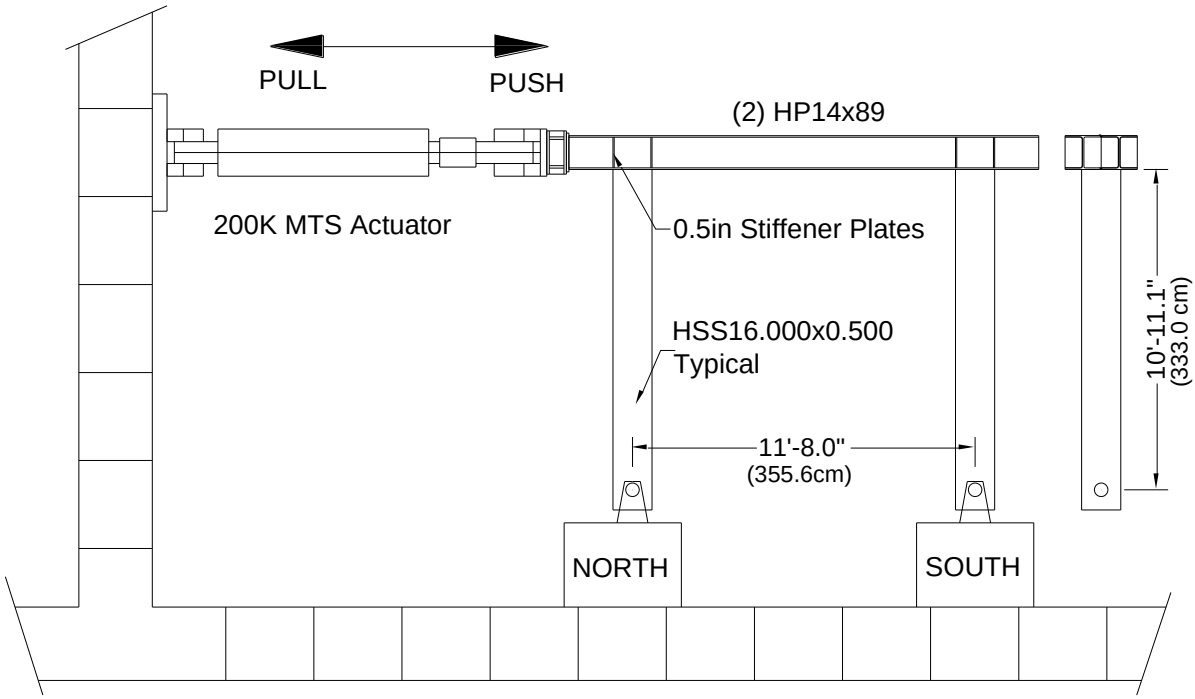

Figure 3.2 Phase 1 Laboratory Experimental Set Up

Figure 3.3 Phase 1 Laboratory Experimental Set Up

3.2.2 Lateral Loading of the Test Specimens

Structural analysis was conducted prior to testing with anticipated material properties of the piles to determine that a 220 kip MTS servo-controlled actuator would be adequate to test the specimen. The other major consideration when designing the lateral loading system was actuator stroke. The 220 kip MTS actuator had a total stroke capacity of 40 in. For the purpose of reverse cyclic testing, the lateral loading system was designed to allow for a balanced set up that would provide plus or minus 20 in. of stroke. It was anticipated that this magnitude of actuator stroke would be capable of testing the pier to failure. The lateral load history applied to past experimental specimens consisted of a balanced reverse cyclic loading procedure as shown in Figure 3.4.

This load history, termed a three cycle set, is the same procedure utilized in both the experimental and analytical portions of the later work that is presented in this document and is defined in detail in subsequent chapters. In general, this loading history is defined by single reverse cyclic force-controlled steps that increase by increments of ¼ of the system's first yield force until the full first yield force cycle is reached, followed by three cycle sets of displacement ductility increments. In this protocol a displacement ductility of 1 is defined as the experimental first yield displacement extrapolated by the ratio of anticipated nominal system strength to the first yield system strength. Increasing levels of displacement ductility were imposed in the order of 1, 1.5, 2, 3, 4, 6, etc. until failure. This style of balanced load history effectively evaluates the full reverse cyclic capabilities system. Again, a more detailed explanation of this load history procedure is provided in subsequent chapters.

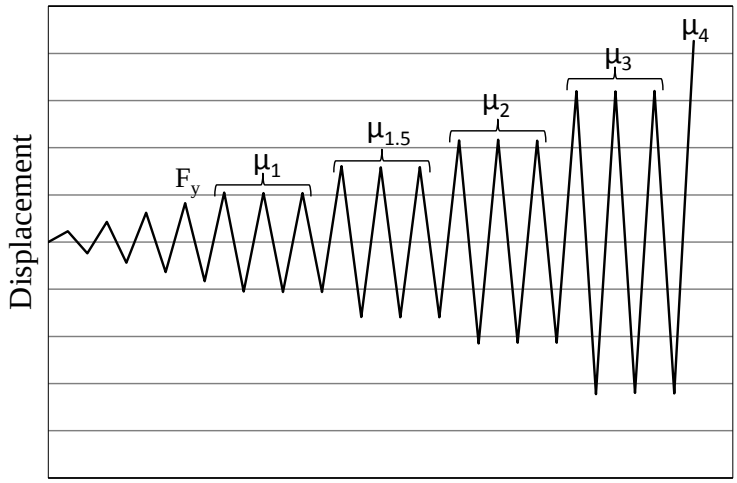

Figure 3.4 Typical Three Cycle Set Load History

3.2.3 Standard Welded Connection Configurations

As has been noted, the prior work considered only standard welded connection configurations. Four experimental evaluations were conducted with nominally identical global specimen parameters (cap beam size, pile size, and pier dimensions) with the only differentiation being three separate welding details used to form the moment resisting connection between the pile and cap beam elements of the system. These welding details included a fillet weld, a complete joint penetration weld (CJP), and a complete joint penetration weld with a full depth reinforcing fillet weld as shown in Figure 3.5 through Figure 3.7 respectively. In all cases, the welding was conducted in an overhead field like condition by certified welders to replicate actual construction practice. In addition, the piers containing CJP welds and CJP welds with full depth reinforcing fillet welds were subjected to full visual and ultrasonic testing (UT). Further welding details and documentation of quality are provided in (Fulmer, et. al., 2009).

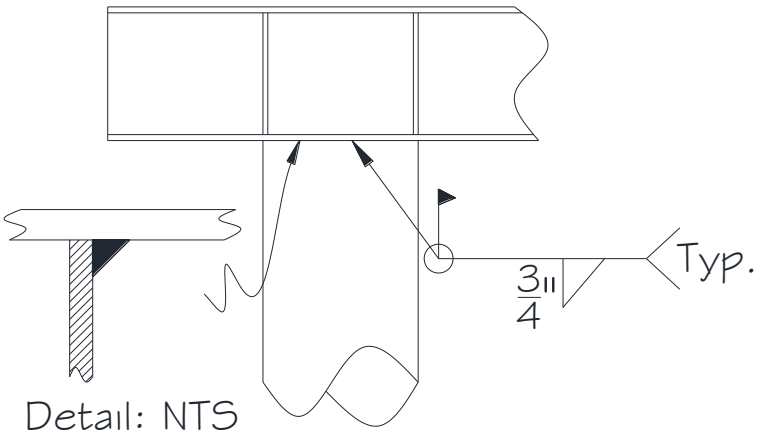

Figure 3.5 Standard Welded Connection – Fillet Weld

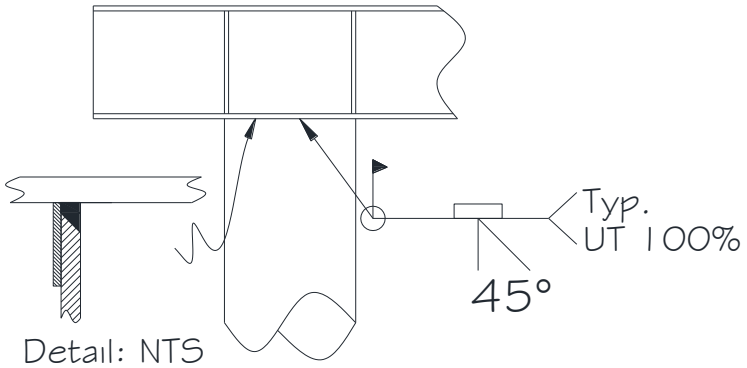

Figure 3.6 Standard welded Connection – CJP

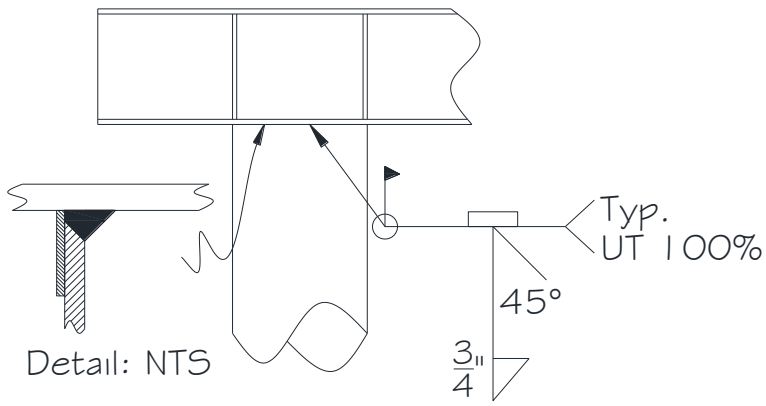

Figure 3.7 Standard welded Connection – CJP with Full Depth Reinforcing Fillet

3.3 Summary of Experimental Results

3.3.1 Fillet Weld Evaluation

As is indicated in Table 3.1, the typical detail utilized during construction of the existing bridge inventory consisted of a field conducted fillet weld. The connection requires no backing bar and provides no root opening as can be seen in Figure 3.5 which depicts a section cut of the 1/2 in. pile wall and the bottom flange of the HP section cap beam. It is important to note that due to a construction error the actual welds used in the experimental test was undersized by approximately 1/16 in. Although this was an error, the situation is actually more indicative of the existing bridge inventory which has many fillet weld connections with throat thicknesses less than the pile wall thickness.

Structural analysis conducted prior to testing provided a system first yield force of 73 kips on which the initial portion of the loading history was based. This yield force was calculated on the basis of material properties provided by mill certifications (see Figure A 2 through Figure A 4) which indicated a yield stress of approximately 54 ksi for the ASTM

A500 Gr. B&C dual certified piles. During testing, the average first yield displacement of the system was observed to be 2.99 in which was considerably higher than the calculated estimate of 2.04 in. from basic structural analysis considering cap beam flexibility. One reason for the higher than expected yield displacement, was the effect of base displacement which was attributed to rocker bearings located in the base supports. From the recorded first yield displacement of 2.99 in., the equivalent yield displacement or ductility 1 displacement was calculated as 3.89 in.

Regardless of the base displacement issue, the specimen was found to respond adequately within the elastic range. No signs of failure were observed during the load controlled portion of the load history prior to first yield nor were any observed during the ductility 1 and 1.5 levels. However, rapid degradation of the connection was observed during the first positive cycle of the second ductility level. During this cycle cracking developed at the toe of the fillet weld on the south column as can be seen in Figure 3.8. The effect of this cracking in regards to the strength of the specimen can be seen in Figure 3.9 and Figure 3.10 which provide the force displacement hysteresis and the load history respectively. It should be noted that the force displacement hysteresis appears to be shifted towards the positive direction due to the effects of base displacement which is plotted in Figure 3.11. The first negative cycle of the second ductility level led to additional cracking in the fillet weld of the south column. As a result, the specimen was assumed to be failed and the test was concluded.

Figure 3.8 Fillet Weld Test – Cracking of South Column

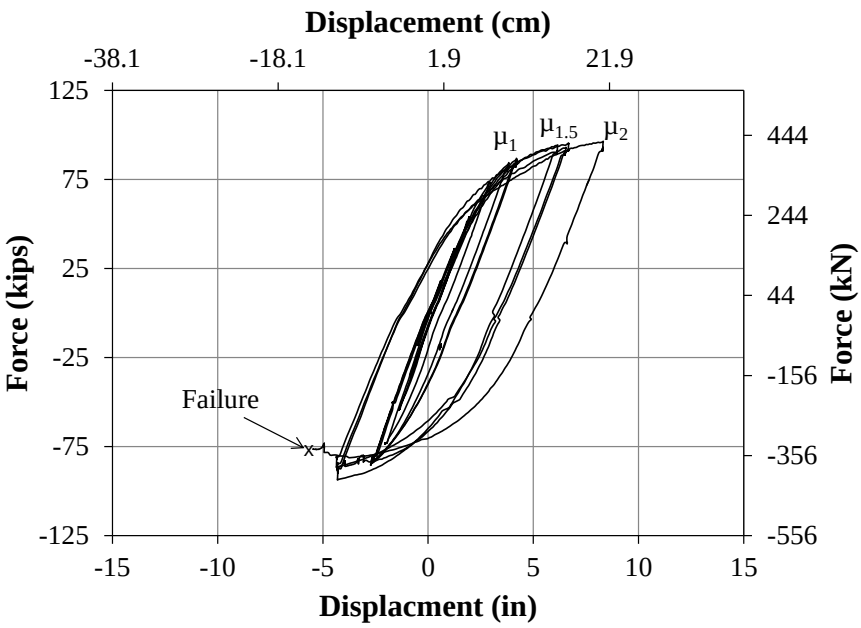

Figure 3.9 Fillet Weld Test – Force Displacement Hysteresis

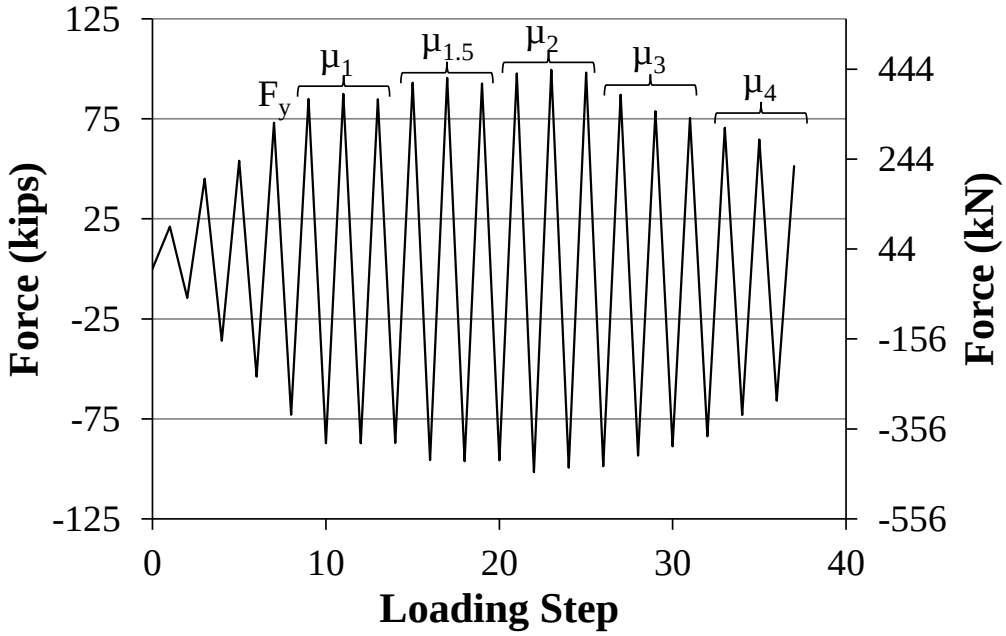

Figure 3.10 Fillet Weld Test – Load History

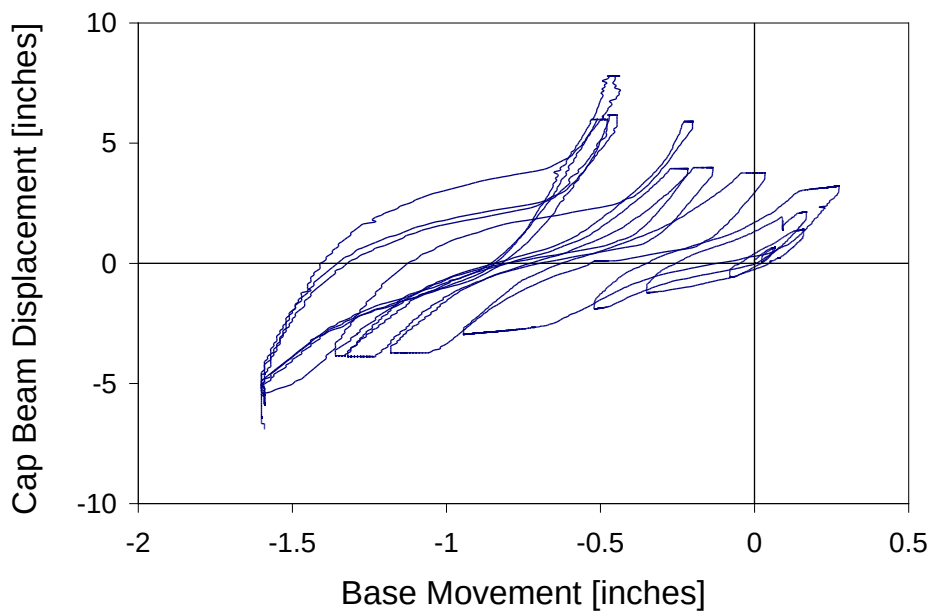

Figure 3.11 Fillet Weld Test – Base Displacement vs. Cap Beam Displacement

3.3.2 Complete Joint Penetration Weld Evaluation

Unlike the fillet weld detail, the CJP detail shown in Figure 3.6 required a 1/4 in. root opening and a circular 3/8 in. thick steel backing bar per American Welding Society (AWS) D1.1 (AWS, 2008) specifications as noted in (Fulmer, et. al., 2009). However, the global system was nominally identical to that of the pier with fillet welds as has already been mentioned. Consequently the calculated first yield force of 73 kips and the force controlled cycles of the displacement history were also identical as the pile material was from the same heat and consisted of the same material properties.

During testing of this specimen, a loading error occurred early in the test. Following the 1/2 F_y positive or push cycle, the specimen was significantly overloaded and data was lost during this time as is seen in Figure 3.12. As shown in Figure 3.13 estimates from extrapolation of the force displacement hysteresis indicate that the overload cycle reached approximately -100 kips and -15.74 in. of displacement in the pull direction. Unfortunately, due to the time during testing at which the overload cycle occurred, no first yield displacement could be established for this specimen. For this reason the load history of a previous test pier containing CJP welds with reinforcing fillets was utilized, resulting in an equivalent yield or ductility one value of 3.24 in.

During the overload cycle, a fracture developed at the weld toe on the beam flange side of the weld on the north column as is seen in Figure 3.14. After the three cycle set load history was reinstated, the next crack that formed was during second pull cycle of ductility 1.5 on the south column at the cap beam weld toe as seen in Figure 3.15. Multiple small cracks also developed on the south side of the south column. The crack seen at the weld toe of the north column also grew in length during this cycle. The cracks already formed on both columns continued to propagate both in length and width during the first cycle of the ductility 2 level and propagated through the weld in the case of the cracking on the south column during the second cycle of ductility 2 as shown in Figure 3.16. The cracking

observed on the north pile was also seen to propagate through the weld during the third cycle of ductility 2 as shown in Figure 3.17. The test was continued into ductility three regardless of the reduction in strength which was more than 20%. After the first cycle of ductility 3 the cap beam showed distortion near both columns, as seen in Figure 3.18, and an additional crack had formed in the north column at the cap beam weld toe. At this point the test was stopped due the extent of damage and loss of strength of the test specimen.

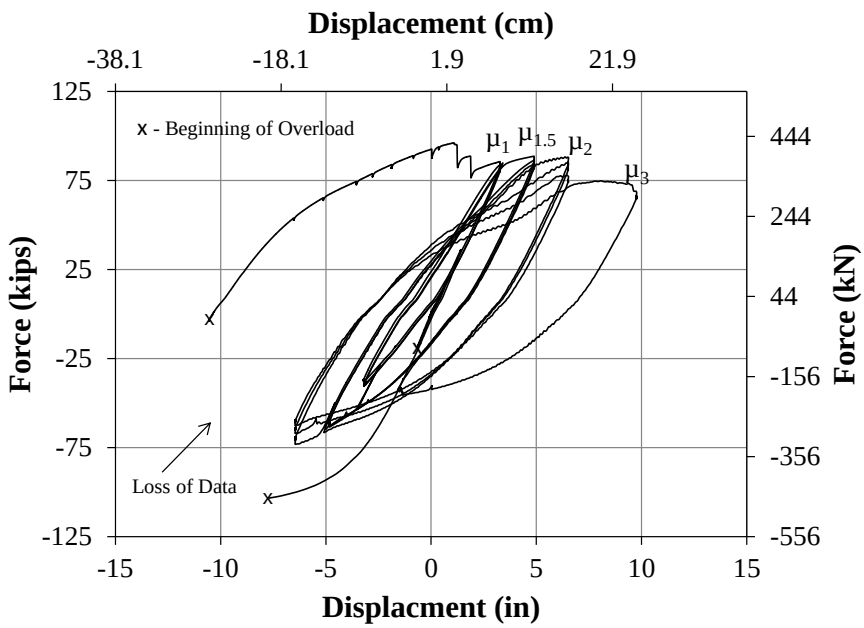

Figure 3.12 CJP Weld Test – Force Displacement Hysteresis

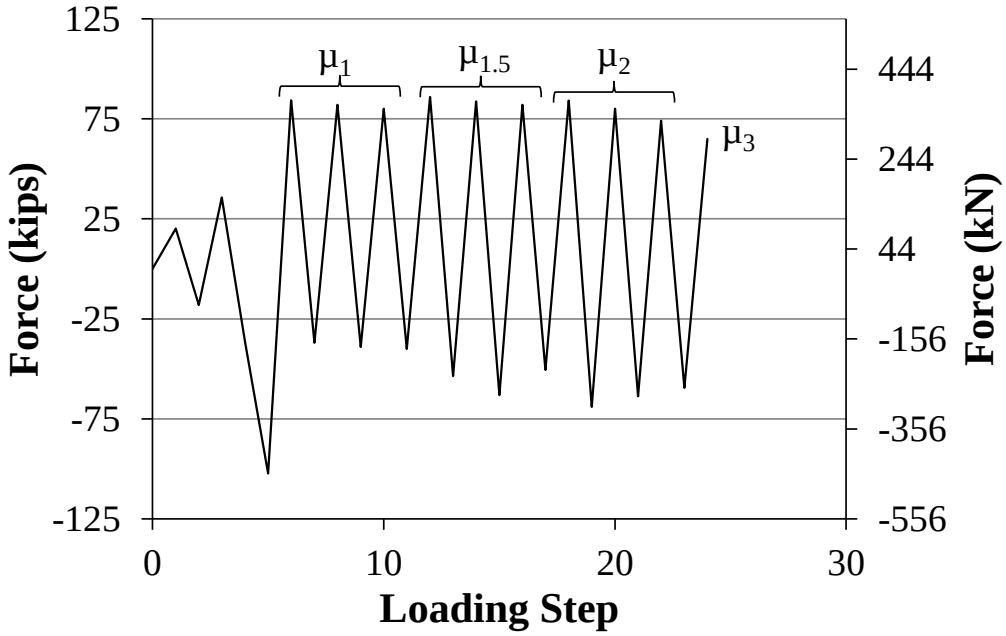

Figure 3.13 CJP Weld Test – Load History

Figure 3.14 CJP Weld Test – North Column Crack During Overload Cycle

Figure 3.15 CJP Weld Test – South Column Cracking – Ductility 1.5 Second Pull cycle

Figure 3.16 CJP Weld Test – South Column Propagation of Cracking through the Weld

Figure 3.17 CJP Weld Test – North Column Propagation of Cracking through the Weld and Cap Beam Distortion

Figure 3.18 CJP Weld Test – Cap Beam Distortion

3.3.3 Complete Joint Penetration Weld with Full Depth Reinforcing Fillet

As in the case of the basic CJP weld, the detail of a CJP weld with a full depth reinforcing fillet weld, shown in Figure 3.7, also required a 1/4 in. root opening and a circular 3/8 in. thick steel backing bar per AWS D1.1 (AWS, 2008) specifications as noted in (Fulmer, et. al., 2009). Again, the global system was nominally identical to that of the piers with fillet welds and basic CJP welds. Consequently the calculated first yield force of 73 kips and the force controlled cycles of the loading history were also identical as the pile material was from the same heat and consisted of the same material properties.

This welding detail was utilized in 2 of the 4 specimens evaluated in the past research due to improvement in performance that was experienced during the first of the two tests as compared to the fillet weld and basic CJP weld details. During testing of the first specimen, the observed average first yield displacement was found to be 2.49 in. and was used to establish a new displacement history for the remainder of the test. From the first yield displacement, the equivalent yield displacement or ductility 1 displacement was calculated as 3.24 in. resulting in the force displacement response and load history shown in Figure 3.19 and Figure 3.20 respectively. As in the case of the fillet weld evaluation, base displacement due to the rocker bearings used in the test set up was experienced, but at reduced level as can be seen in Figure 3.21.

As has been mentioned, the first CJP with reinforcing fillet weld specimen generally performed in a more acceptable manner than specimens with fillet welds or basic CJP welds. No signs of failure were observed through the displacement ductility 1, 1.5, and 2 levels. The specimen was accidentally subjected to an overload cycle corresponding to a displacement ductility of 5 during the transition from ductility 2 to 3 as can be seen in Figure 3.19. Although no damage was observed during this overloading, reversal to the negative or pull correct ductility 3 displacement led to a crack forming at the weld toe in the north column.

This crack extended from the extreme fiber of the south face to approximately the neutral axis as shown in Figure 3.22. It is possible that this crack was due to damage sustained during the overload cycle. For this reason and the fact that only minor strength loss had been experienced, as is shown in Figure 3.20, the test was continued. Ultimately the specimen was able to develop local buckling as is seen in Figure 3.23 when subjected to ductility 4 displacements. This buckling led to significant strength degradation and base material fracture at a location of local buckling on the south column shown in Figure 3.24. The failure mechanism of this specimen can be summarized as a combination of local buckling and associated strength loss, base material fracture, and weld fracture possibly due to the overload cycle.

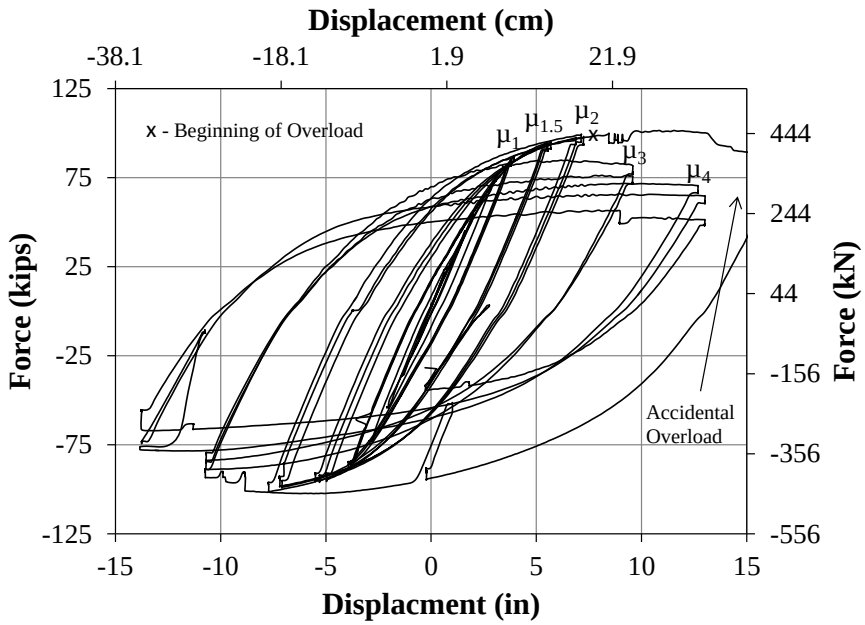

Figure 3.19 (1) CJP w/ Reinforcing Fillet Weld – Force Displacement Hysteresis

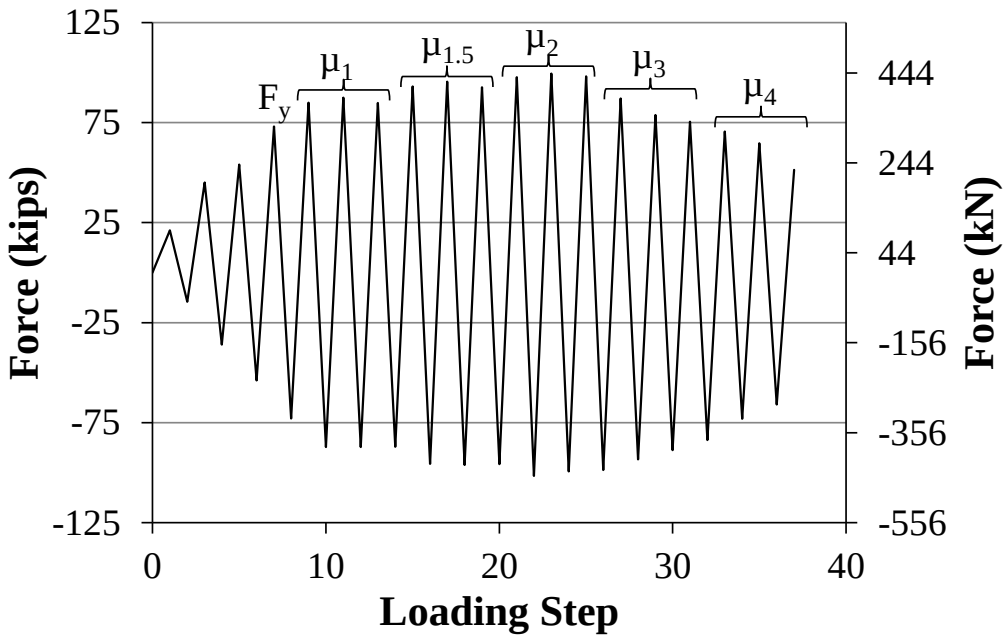

Figure 3.20 (1) CJP w/ Reinforcing Fillet Weld – Load History

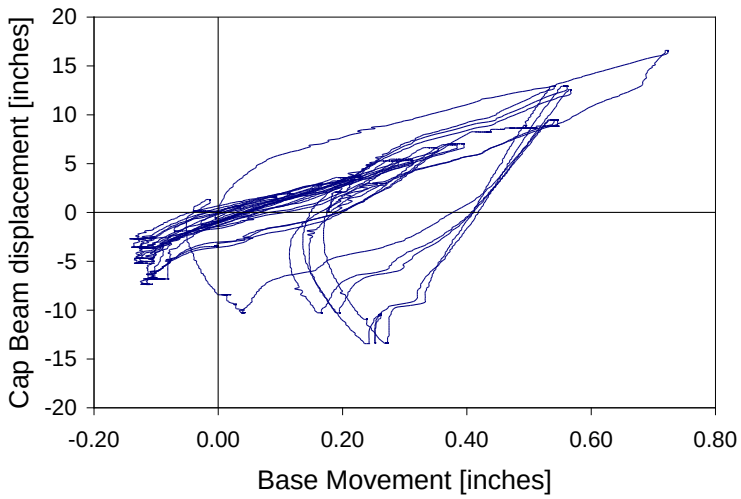

Figure 3.21 (1) CJP w/ Reinforcing Fillet Weld – Base Displacement vs. Cap Beam Displacement

Figure 3.22 (1) CJP w/ Reinforcing Fillet Weld – Cracking at Weld Toe North Column South Face

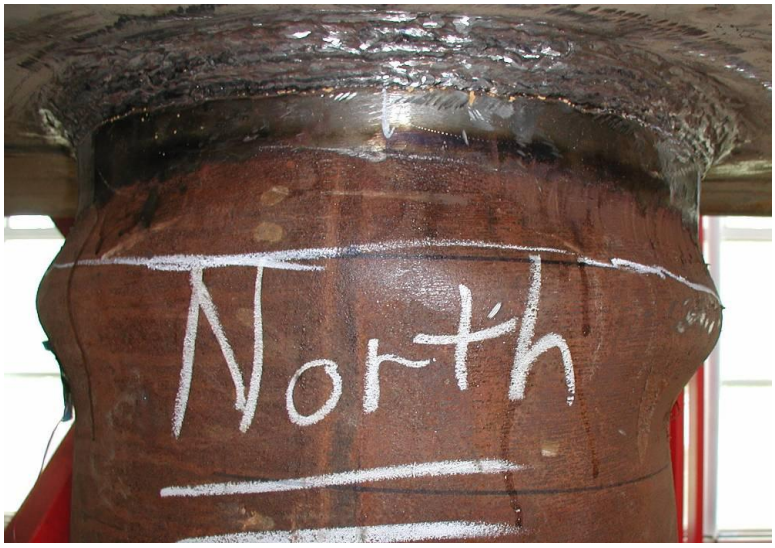

Figure 3.23 (1) CJP w/ Reinforcing Fillet Weld – Local Buckling of North Column

Figure 3.24 (1) CJP w/ Reinforcing Fillet Weld – Base Material Fracture South Column

The improved system response that was observed with this weld detail included both increased levels of reliable and ultimate displacement response as well the ability of the connection to form the preferable failure mechanism of pile wall local buckling. Although it is important to note that cracking at the weld toe was not mitigated, it was determined that the results warranted a second trial of this weld detail to evaluate repeatability of the results.

In the second experimental evaluation, the observed average first yield displacement was 2.54 in. nearly identical to that of the first evaluation which was 2.49 in. This resulted in an equivalent yield displacement of 3.30 in. During the test, no visual signs of failure and no strength loss were observed prior to the third cycle of ductility 3 as is shown in Figure 3.25 and Figure 3.26. However, ultimate failure occurred rapidly during the third push cycle of ductility 3. A large crack rapidly formed at the weld toe and propagated around a significant portion of the south face of the south column as seen in Figure 3.27 and Figure 3.28. This crack significantly affected the strength of the system as can be seen in Figure 3.25. The last pull cycle of ductility three was completed and the test was assumed to be completed given the significant cracking on the south column and approximately 30% strength loss. Although minor levels of local buckling began to develop below the weld region, as shown in Figure 3.29, the buckled region was not as pronounced as in the first evaluation and did not appear to be associated with strength loss prior to the brittle cracking mechanism which formed on the south column leading to rapid strength loss in a single cycle of loading.

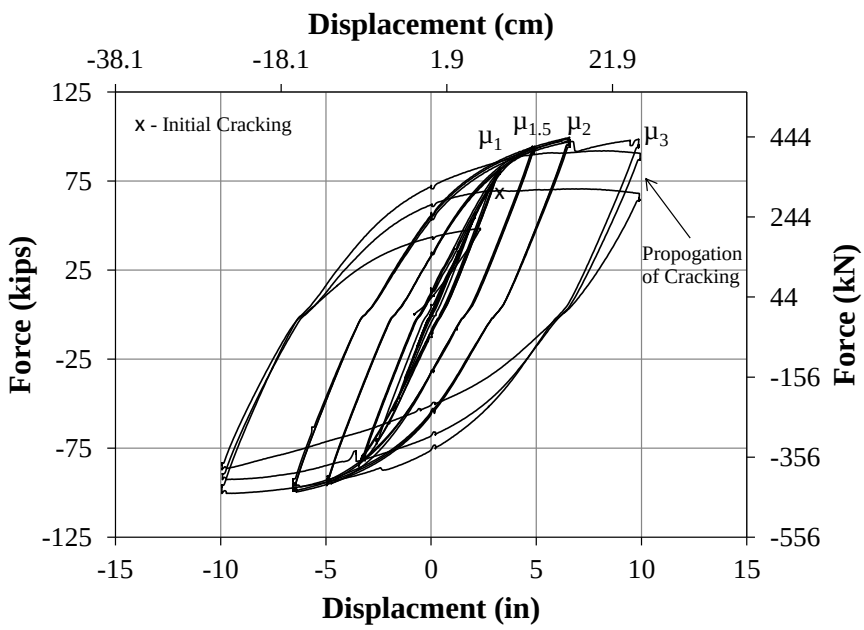

Figure 3.25 (2) CJP w/ Reinforcing Fillet Weld – Force Displacement Hysteresis

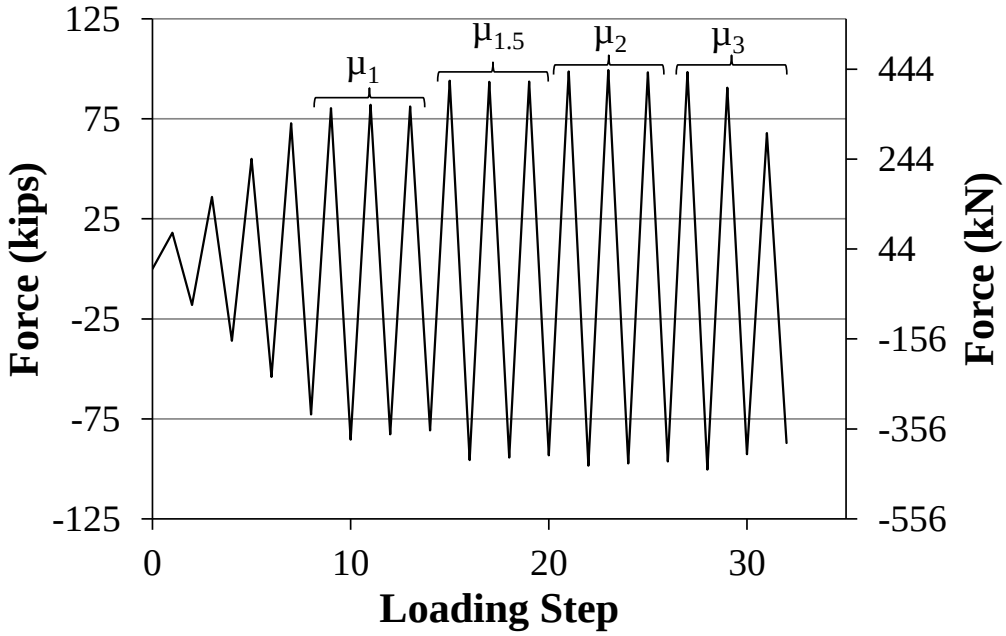

Figure 3.26 (2) CJP w/ Reinforcing Fillet Weld – Load History

Figure 3.27 Cracking on South Column

Figure 3.28 Cracking on South Column – Post Test

Figure 3.29 Minor Local Buckling on the South Column

3.4 Summary and Conclusions from Past Work

The results of the past experimental testing, summarized in Table 3.2, showed that in all cases the ultimate limit state of the system was controlled by brittle cracking in or near the

welded regions as has been discussed in this chapter. With the exception of one case, this cracking occurred prior to the development of the more desirable limit state of pile wall local buckling. Although the use of CJP welds drastically improved the behavior of the connection in comparison to the use of fillet welds, in no cases did the more desirable ductile failure mode of pile wall local buckling control. In addition, the reliable displacement ductility capacity from each test was considerably limited noting that the fillet weld specimen was barely capable of entering the non-linear range.

However, it should be noted that although the reliable ductility values were relatively low, the associated drift magnitudes were reasonably large particularly for the specimens with CJP welds and full depth reinforcing fillets. This is partially due to the definition of displacement ductility ($\Delta/\Delta_{y,exp}$) and the considerably high elastic flexibility of this type of system. Regardless, the undesirable failure mode of brittle cracking at or near welded regions, which developed in each of the 4 tests, warranted concern regarding the standard welded connection configurations considered in the past work.

Table 3.2 Past Work Summary

Configuration	Failure Ductility	Failure Description	Reliable Ductility	Equivalent Reliable Drift
3/4" Fillet	2	South Column North-Mid Face Crack at Weld Toe in Base Metal	1	0.028
45° CJP	3	Multiple Cracks in Both Columns at Weld Toe in Base Metal and Through Weld	1.5-2	0.035 - 0.047
45° CJP w/ 3/4" Backer Fillet (#1)	4	South Column North Face Crack at Weld Toe In Base Metal	3	0.070
45° CJP w/ 3/4" Backer Fillet (#2)	3	South Column South Face Crack at Weld Toe in Base Metal	2-3	0.049 - 0.072

Chapter 4: Research Methods

4.1 General Discussion

As has been mentioned, the research methods used in this project include full scale quasi – static experimental tests as was done in the past work, as well as detailed Finite Element Modeling of steel piers containing both standard and modified weld protected connections. In addition, scaled dynamic shake table evaluations of steel piers with a modified weld protected connection configuration was conducted. This body of work consisted of portions of the first phase and of the entire second phase of the steel pier project at NCSU. Sections provided in this chapter are aimed to explain the details of each research method prior to discussing results and findings in later chapters. These details include the design of the full scale specimen, the design of the laboratory set up components, the definition of the lateral load history used in the project, and the various components related the development of the Finite Element Models.

4.2 Lateral Load History

The applied load history used in both the full scale quasi-static experimental evaluations as well as the Finite Element Analysis evaluations in this research is termed a three cycle set history. The definition of this load history consists of an initial elastic portion based on the anticipated yield force of the system and a second section based on the experimentally determined yield displacement of the system. More specifically, single reverse cyclic load controlled cycles of 1/4 first yield force increments are applied to the pier until a full first yield force cycle was reached where the first yield force is determined in accordance with Eq.(4.1). In Eq.(4.1), S represents the section modulus of the pipe pile members, f_y represents the anticipated yield stress of the pile material, and X represents the shear span from the pinned supports to the critical pile hinging section.

The second section of the load history was defined by displacement controlled incremental ductility levels where displacement ductility 1 (μ_1), or effective yield, is defined by Eq.(4.2) and subsequent displacement ductility levels are defined by Eq.(4.3). In Eq.(4.2), $\Delta'_{y,exp}$ represents the experimentally determined first yield displacement while M_p and M_y represent the full plastic moment capacity and the first yield moment capacity of the pipe pile members respectively. This load history definition results in a balanced force and displacement patterns as shown in Figure 4.1 and Figure 4.2 respectively.

A critical assumption in this definition of a three cycle set load history is that plastic hinge sections form in the pile elements and that the rest of the system remains in the elastic range of response. Further, the simplified equations provided in Eq.(4.1) through Eq.(4.3) assume an equal distribution of shear forces between the pile members which in the elastic range of loading is only accurate for a two column pier with no applied vertical load. These equations also neglect P-Delta effects which would arise from axially induced loads generated from overturning resistance of the pier or from applied vertical loads should they be considered in the test or analysis.

$$F_y = \frac{2 f_y S}{X} \tag{4.1}$$

$$\mu_1 = \Delta_y = \Delta_{y,\exp} \frac{M_p}{M_y} \tag{4.2}$$

$$\mu_i = i\mu_1 \tag{4.3}$$

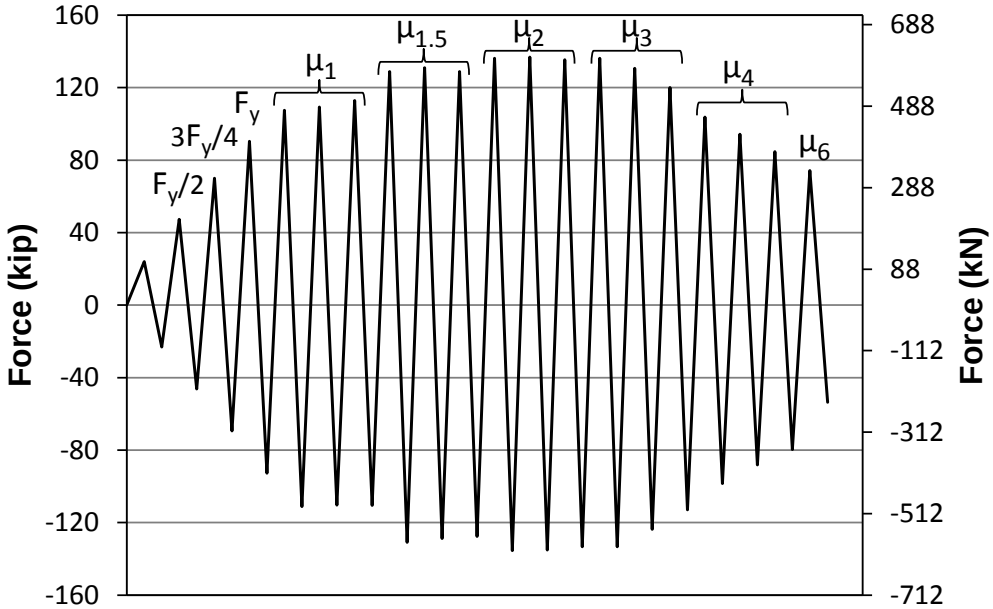

Figure 4.1 Exmaple 3 Cycle Set Load History

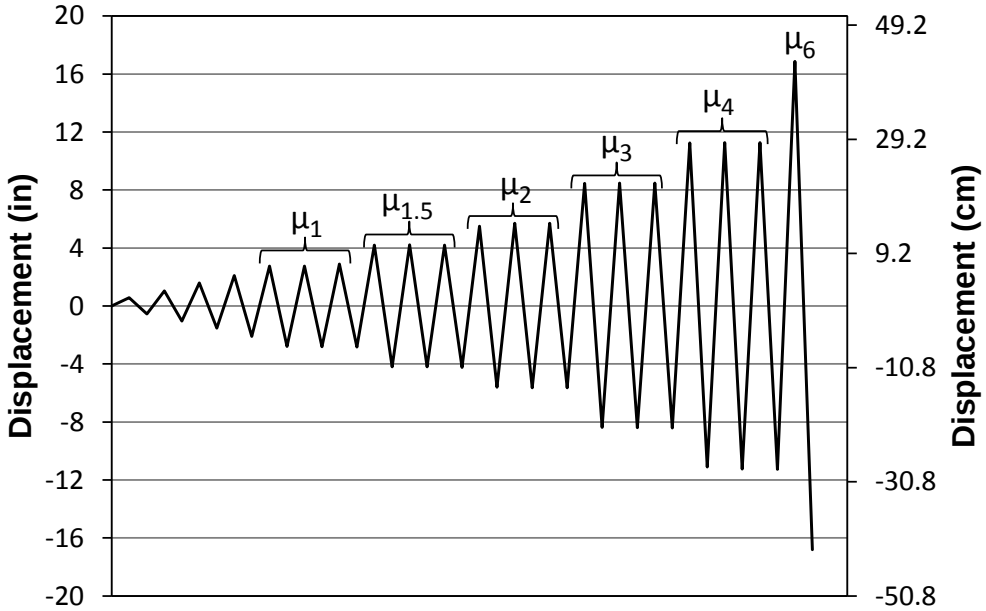

Figure 4.2 Example 3 Cycle Set Displacement History

4.3 Full Scale Quasi-Static Experimental Evaluations

4.3.1 Design of the Global Test Specimen

As was the case with the prior research, this phase of work also considered full scale two column bridge piers representative of actual structures in Alaska. It was intended that throughout entire range of testing, the global specimen parameters, such as member sizes, would remain the same with only variable being connection configuration. In line with the past research work, ASTM A500 Gr.B (likely dual certified C) were used as the pile column elements and a double wide ASTM A572 Gr. 50 double wide HP14x117 cap beam was used to complete the system. Although the details of each specimen are discussed throughout this document, detailed design drawings are provided in the appendix such that the precise details of each specimen can be reviewed by a reader as necessary.

Based on laboratory restrictions and a desire to maintain reasonable pile aspect ratio and pile spacing geometry, the shear span from the pinned connections that were used to the center of loading was set at 11 ft. – 2 in. and the center to center spacing of the piles was set at 12 ft. The design of the cap beam as well as test frame components was again based on capacity design principles and an assumed pile hinging mode of failure. However, it was recognized that pile hinge relocation away from the interface would likely occur in the project and as hinges were relocated away from the cap beam interface, moment demand (and shear) demands on the cap beam element would increase due to extrapolation of the moment gradient. As a result, the design calculations were conducted based on an assumed minimum shear span from the pinned base support to the hinge location of 8 ft. – 6 in. Additionally, material over-strength factors were considered to predict expected material properties in the design calculations per the recommendations of *ANSI/AISC 341-10* (AISC, 2010) and "AASHTO Guide Specifications for LRFD Seismic Bridge Design" (AASHTO, 2009) material over strength R_y and R_t values. This resulted in the use of the material properties shown in Table 4.1.

The basic global specimen configuration, shown in Figure 4.3, was developed based on the design calculations provided in Figure 4.4 and Figure 4.5. However, it should be noted that some of the connection configurations which were tested required different member sizes and configurations to be utilized. The design of these alternate members will discussed where necessary in this document to highlight differences in system response.

Table 4.1 Expected Material Properties for Design

Material	F_y (ksi)	R_y[1,2]	$\mathbf{F_{y,exp}}$ **(ksi)**	F_u (ksi)	R_t[1]	$\mathbf{F_{u,exp}}$ **(ksi)**
ASTM A500 Gr. B& C Dual Cert. (Piles)	46.0	1.4	**64.4**	62.0	1.3	**80.6**
ASTM A572 Gr. 50 (Cap Beam & Stiffeners)[3]	50.0	1.1	**55.0**	65.0	1.1	**71.5**
ASTM A36 (Various Test Frame Components)	36.0	1.5	**54.0**	58.0	1.2	**69.6**

[1] based on (AISC, 2010)

[2] based on (AASHTO, 2009)

[3] R_y values only covered in (AISC, 2010)

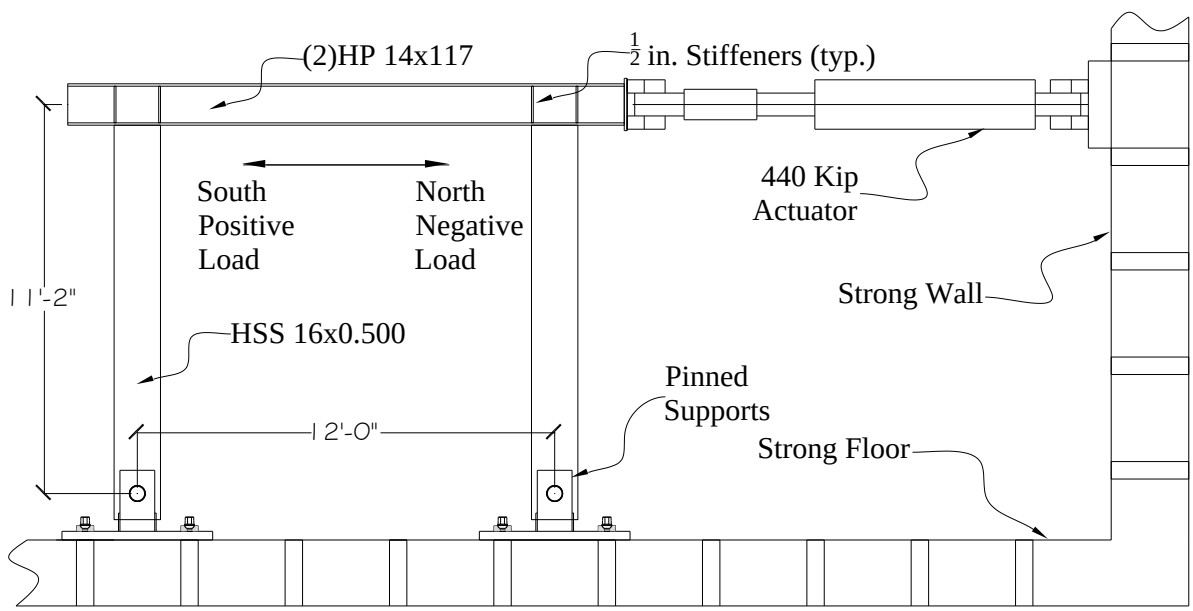

Figure 4.3 Phase 2 Basic Specimen Laboratory Configuration

Basic Specimen Design:

(1) Pile: HSS16x0.500 ASTM A500 Gr. B

$f_{y\_min} := 42ksi$ ASTM minimum yield stress

$f_{u\_min} := 58ksi$ ASTM minimum tensile stress

$f_{y\_exp} := f_{y\_min} \cdot 1.4$ $f_{y\_exp} = 58.8\,ksi$

$f_{u\_exp} := f_{u\_min} \cdot 1.3$ $f_{u\_exp} = 75.4\,ksi$

$O_{sh} := \frac{f_{u\_exp}}{f_{y\_exp}}$ $O_{sh} = 1.28$ overstrength factor to account for potential strain hardening

Assuming a pile hinging mode of failure:

$f_{y\_pile} := f_{y\_exp} \cdot O_{sh}$

$Z_{pile} := 112in^3$ plastic modulus of for HSS 16x0.500

$V_{span\_min} := 8.5ft$ minimum expected shear span

$M_{pile} := f_{y\_pile} \cdot Z_{pile}$ $\boxed{M_{pile} = 703.73 \cdot kip \cdot ft}$ expected overstrength pile moment capacity

$V_o := \frac{M_{pile}}{V_{span\_min}}$ $\boxed{V_o = 82.79 \cdot kip}$ associated shear, at max considered depth of hinging (actuator force/2)

To check shear failure of the pile per AISC specifications G6:

$$F_{cr} := \min\left[\max\left[\frac{1.6 \cdot 29000ksi}{\sqrt{\frac{132}{16}} \cdot \left(\frac{16}{0.465}\right)^{\frac{5}{4}}}, \frac{0.78 \cdot 29000ksi}{\left(\frac{16}{0.465}\right)^{\frac{3}{2}}}\right], 0.6 \cdot f_{y\_min}\right] \qquad F_{cr} = 25.2 \cdot ksi$$

$\phi V_{n\_pile} := 0.9 F_{cr} \cdot 0.5 \cdot 22.7in^2$ $\boxed{\phi V_{n\_pile} = 257.42 \cdot kip}$ as expected, pile is adequate for shear demand

Figure 4.4 Phase 2 Specimen Design Calculations

(2) Basic Cap Beam: Double HP14x117 ASTM A572 Gr. 50.

Flexural Capacity Per AISC Specification Chapter F:

$f_{y\_min} := 50ksi$ ASTM minimum yield stress for A572 material

$S := (2) \cdot 172in^3$ for double HP14x117

Check Element Compactness:

Flange Slenderness -- $\frac{0.5 \cdot 14.9in}{0.805in} = 9.25$ $0.38 \cdot \left(\frac{29000ksi}{f_{y\_min}}\right)^{0.5} = 9.15$ close, neglect non-compact flange

Web Slenderness -- $\frac{11.25in}{0.805in} = 13.98$ $3.76 \cdot \left(\frac{29000ksi}{f_{y\_min}}\right)^{0.5} = 90.55$ web compact

Lateral Torsional Buckling will be neglected as HPs will be doubled and welded at flanges. Full pin weld in accordance with AWS D1.1 should be used to ensure composite action about Y axis.

Note the demand on the cap at cap centerline and pile centerline:

$M_{o\_cap} := M_{pile} \cdot \frac{11.17ft}{V_{span\_min}}$ $M_{o\_cap} = 924.79 \cdot kip \cdot ft$

$\phi M_{y\_cap} := 0.9 f_{y\_min} \cdot S$ $\phi M_{y\_cap} = 1290 \cdot kip \cdot ft$ cap beam adequate for flexure

By inspection, interaction of axial forces and moment capacity can be neglected as maximum considered axial force to gross axial yield strength is approximately 2%.

Shear capacity evaluation per AISC Specification G2:

$V_{o\_cap} := \frac{2M_{o\_cap}}{12ft}$ $V_{o\_cap} = 154.13 \cdot kip$

$\phi V_{n\_cap} := 2.0(1.0) \cdot 0.6 \cdot f_{y\_min} \cdot (11.25in) \cdot (0.805in) \cdot 1.0$ $\phi V_{n\_cap} = 543.38 \cdot kip$ cap beam adequate for shear

By inspection, include 1/2" transverse cap beam stiffeners at extreme fiber of pile connection.

Figure 4.5 Phase 2 Specimen Design Calculations (Continued)

4.3.2 Design of Testing Fixtures

In addition to the specimen design, alternate laboratory testing fixtures were designed for the second phase of testing. In an effort to simplify testing set up and to mitigate base movement that was experienced in the past experimental work, pinned base assemblies that could be directly post tensioned to the laboratory reaction floor with 1-3/8 in. post tensioning bars were designed. The pinned base assemblies, shown in Figure 4.6, were designed to use 5 in. diameter steel pins passing through sleeves in the pile as shown in Figure 4.7 through Figure 4.9. Design calculations for the assemblies which considered ASTM A36 material, are provided in Figure 4.12.

Sizing of the cap beam loading plate and the connecting fillet welds shown in Figure 4.11 was also necessary prior to testing. Based on engineering judgement, the plate was sized as 1 in. thick and a calculated minimum length of 22 in. of 5/8 in. fillet weld was provided between the plate and cap beam. The plate was detailed to connect to a 440 kip MTS actuator that was used in this phase of the project. As was the case with the first phase of testing, the 440 kip actuator used had a total stroke capacity of 40 in. allowing for plus or minus 20 in. of specimen displacement which was judged to likely be adequate for testing.

Figure 4.6 Laboratory Pinned Base Assemblies

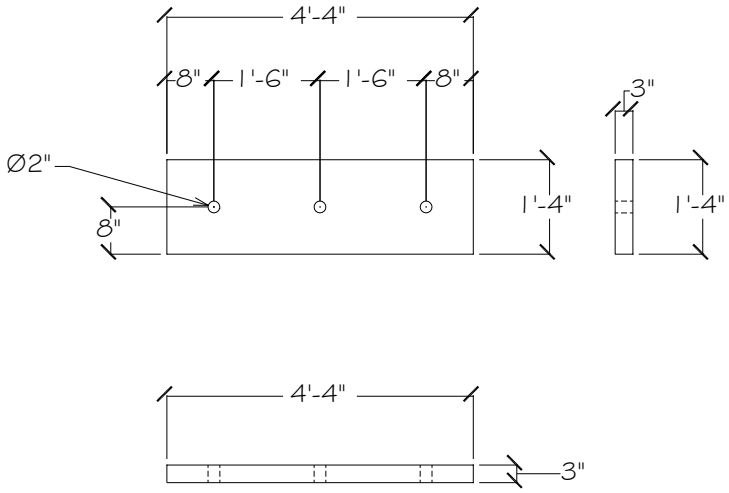

Figure 4.7 Base Assembly – Part P1

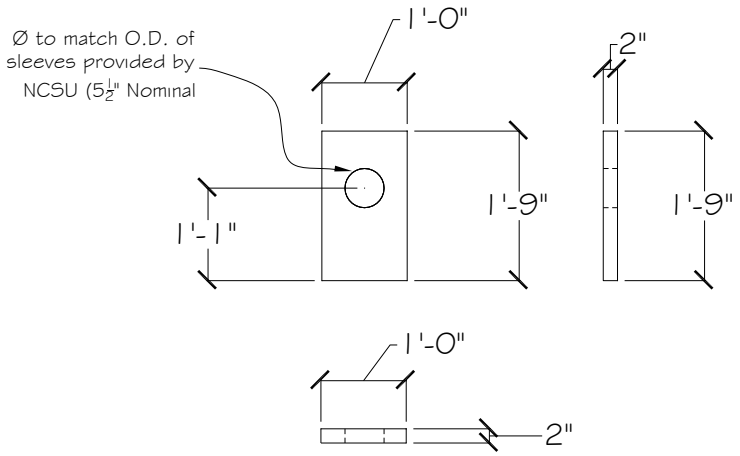

Figure 4.8 Base Assembly – Part P2

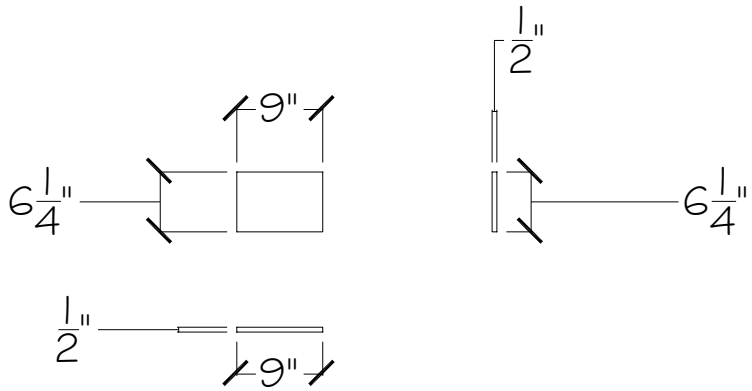

Figure 4.9 Base Assembly – Part P3

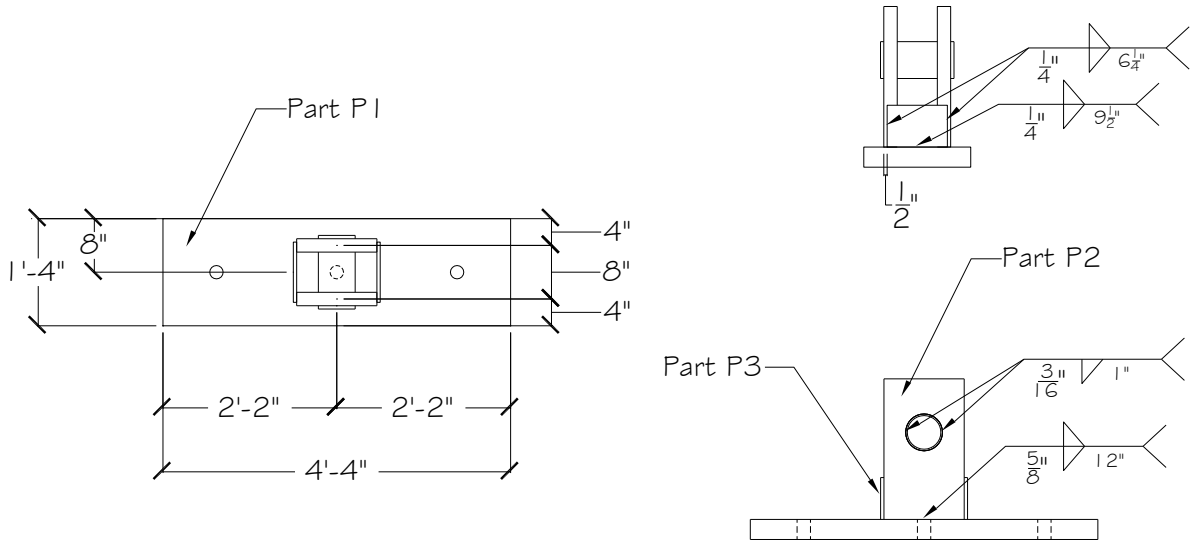

Figure 4.10 Assembled Pinned Base Fixtures

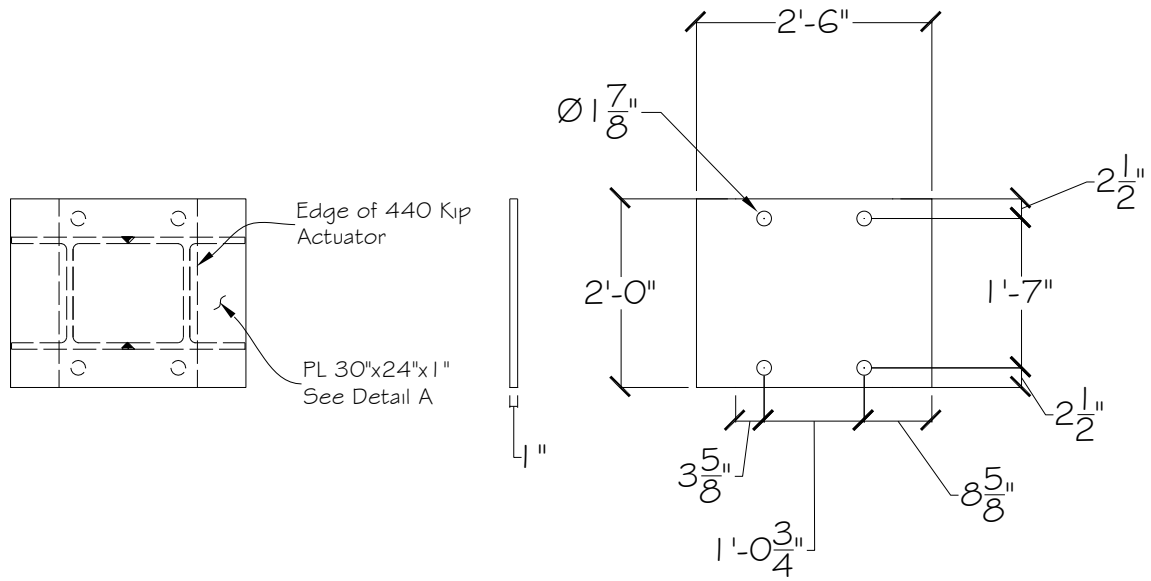

Figure 4.11 Actuator Loading Plate Details

Testing Set Up Design:

(1) Base Shoes, ASTM A572 Gr. 50

Description: Base assemblies are constructed of 3in thick base plate 16in wide spaning 3ft (plus 8in either side) and two verical plates (2" x 12") forming the pin region that are connected to the base plate with 5/8" fillet welds on both sides.

$f_{y\_min} := 36ksi$ ASTM minimum yield stress

$e_p := 1.333ft$ eccentricity between strong floor and pin centerline

Flexure of vertical plates:

$M_{o\_shoe} := 0.5 \cdot V_o \cdot e_p$ $\boxed{M_{o\_shoe} = 55.18 \cdot kip \cdot ft}$

$$I := \frac{2 \cdot (2in) \cdot (12in)^3}{12}$$

$\phi M_{y\_shoe} := f_{y\_min} \cdot I \cdot (6in)^{-1}$ $\boxed{\phi M_{y\_shoe} = 288 \cdot kip \cdot ft}$ vertical plates adequate for flexure

Shear yielding of shoes at net area of pin hole:

$V_{o\_shoe} := 0.5 \cdot V_o$ $\boxed{V_{o\_shoe} = 41.4 \cdot kip}$

$\phi V_{n\_shoe} := 1.0 \cdot (0.6) f_{y\_min} \cdot 2 \cdot (2in) \cdot (12in - 5in) \cdot 1.0$ $\boxed{\phi V_{n\_shoe} = 604.8 \cdot kip}$ vertical plates adequate for shear

Flexure of base plate (conservative assumption):

$$I := \frac{16in \cdot (3in)^3}{12}$$

$\phi M_{y\_shoe\_base} := f_{y\_min} \cdot I \cdot (1.5in)^{-1}$ $\boxed{\phi M_{y\_shoe\_base} = 72 \cdot kip \cdot ft}$ base plate adequate for flexure

Check adequacy of eccentrically loaded weld group:

Utilizing AISC 13ed. Table 8-4 Angle = 0 degress special case load out of plane:

$D := 10$ 10/16 inch fillet weld $L := 12$ 12 inches of weld

$C_1 := 1.0$ for EE70XX Electrodes $C := 1.25$ coefficient for a= 1.07

$\phi R_n := 2 \cdot (0.75) \cdot C \cdot C_1 \cdot D \cdot L \cdot kip$ $\boxed{\phi R_n = 225 \cdot kip}$ Good, 5/8" Fillet weld Adequate

Figure 4.12 Pinned Base Assembly Design Calculation

4.3.3 Laboratory Instrumentation Summary

Multiple systems of instrumentation were used during the testing series. These systems included traditional measurement devices such electrical resistance foil strain gauges, linear sting potentiometers, inclinometers, and accelerometers (in some cases). In addition to the traditional equipment, a motion sensing system that tracks the location of LED markers adhered to the experimental specimen during testing was employed. More specifically, the Optotrak system is a motion capturing device that utilizes a combination of LED markers, strobers, multiple tracking cameras, and a data acquisition station, as shown in Figure 4.13, to record the three dimensional motion of the markers throughout the duration of a test. The system captures X, Y, and Z location data at a prescribed frequency with a reported accuracy of 0.1 mm. By applying a grid of markers to a specimen as is shown in Figure 4.14 and Figure 4.15, post processing of the recorded data allows for calculations of strains and cross section curvatures.

For these calculations, the initial gauge length between markers is taken as the distance between any two given markers recorded at time zero prior to the beginning of the test. The magnitude of average strain between the two markers of interest can then be calculated for the remainder of the test by dividing the change in three dimensional distance between the markers by the initial reading as described in Eq.(4.4). This system allows for an average value of strain to be calculated between any two markers. Since the markers are attached in a grid system, the total of the absolute value of strain at either extreme fiber of a cross section divided by the diameter of the pipe pile provides the curvature of that cross section at that given time as shown in Eq.(4.5).

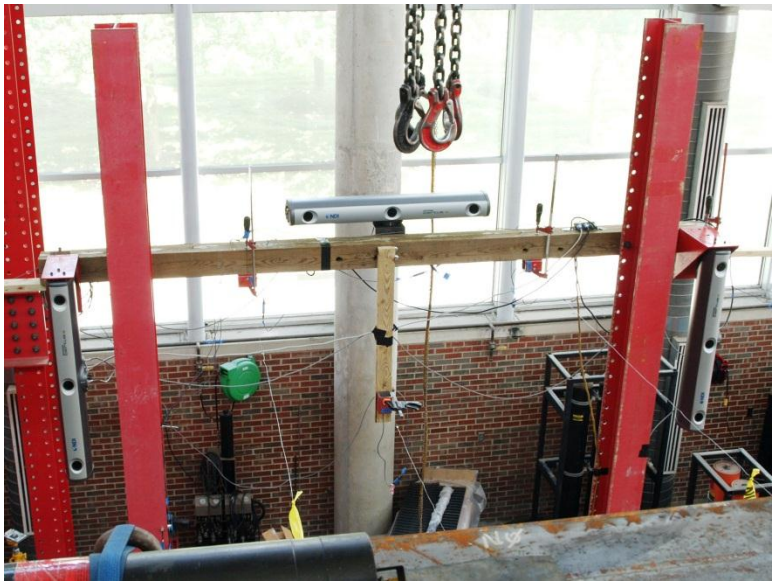

Figure 4.13 Optotrak Motion Capturing Camera

Figure 4.14 Sample Grid Application of Optotrak Markers

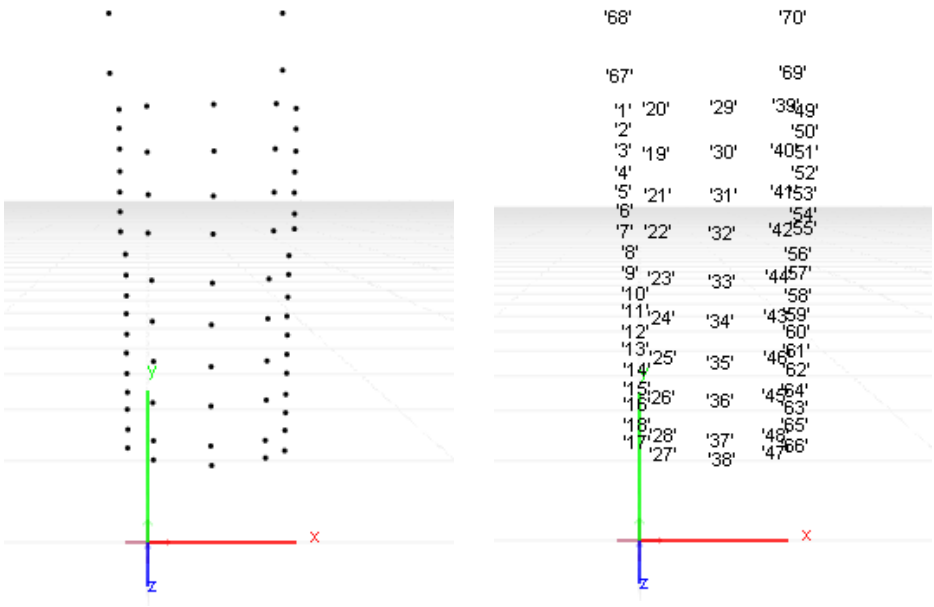

Figure 4.15 Sample of Optotrak 3D Grid Snapshots

The largest benefits of the system over traditional electric resistance strain gauges is the ability to capture strain values at magnitudes much higher than that of the traditional gauges and the ability to capture strain values over a larger area. The markers are applied to the specimen using a Dow Corning 3140 adhesive and data can collected as long as the markers stay attached. It was typically seen that the Optotrak markers were able to remain adhered to the specimen for the duration of the test and provide reliable data beyond buckling or fracture. By employing the grid system it is also possible to capture the strain variance along the height of the pile or through a cross section of the pile. It is important to note that although the primary use of the Optotrak system in this testing series was for the calculation of strains, any measurement related to the relative motion of points on the specimen can be derived from the raw data. Further, it should be noted that although the markers typically remained adhere to the specimen throughout the entire test, data collected around regions of local buckling and fracture are not indicative of engineering strains after these actions occur. This issue will be discussed where applicable to results presented in this document.

Although the instrumentation used during testing was similar between each specimen, some variations did exist due to the exact connection configuration that was being considered in each test. As a result the instrumentation layout for each test will be discussed as the testing observations are presented in subsequent chapters. However, in general the layout for each test was focused around studying the behavior of the connection region with little concern for the remainder of the system.

$$\varepsilon_{ijt} = \frac{\sqrt{\left(X_{it} - X_{jt}\right)^2 - \left(Y_{it} - Y_{jt}\right)^2 - \left(Z_{it} - Z_{jt}\right)^2} - \sqrt{\left(X_{i0} - X_{j0}\right)^2 - \left(Y_{i0} - Y_{j0}\right)^2 - \left(Z_{i0} - Z_{j0}\right)^2}}{\sqrt{\left(X_{i0} - X_{j0}\right)^2 - \left(Y_{i0} - Y_{j0}\right)^2 - \left(Z_{i0} - Z_{j0}\right)^2}} \quad (4.4)$$

$$\phi_t = \frac{\left|\varepsilon_{+t}\right| - \left|\varepsilon_{-t}\right|}{D} \quad (4.5)$$

4.4 In-House Material Testing

Throughout the scope of the research discussed in this document, several instances of in-house material testing are noted. In all cases, these tests were conducted to, and the steel coupons tested were manufactured to, the standard of ASTM A370 – 10. The tests were conducted in a MTS Universal Testing Machine utilizing hydraulic wedge grips. Load was monitored with the internal load cell of the machine and strains were monitored using combination of strain gauges, extensometers, and the Optotrak system which will be subsequently discussed.

4.5 Detailed Finite Element Modeling

4.5.1 General Discussion

Detailed Finite Element Modeling (FEM), also referred to as Finite Element Analysis (FEA) in this document, was conducted as a complimentary research method to that of the experimental investigations. The FEM simulation component of the research utilized the program Abaqus to conduct quasi-static stress based analysis which considered both geometric and material non-linearity. When possible, the non-linear steel material model was calibrated from actual coupon testing data and conformed to hardening rules appropriate for cyclic response. Both shell and 3D solid elements were utilized to model the connections as accurately as possible while attempting to maintain computational efficiency.

In most cases the entire test pier was modeled, as shown in Figure 4.16, neglecting the opportunity to utilize extensive sub-modeling and symmetric condition reduction in an effort to increase accuracy. However, the steel pier models did contain sub-modeled beam elements in the elastic region of the piles to reduce the size of the model and ease the application of pinned boundary conditions. A multiple point constraint feature was used to require the nodes at the base of the three dimensional hollow pile sections to conform to the same rotations and displacements as the top node of the one dimensional beam sections.

Geometric non-linearity was considered in order to capture P-Delta effects as well as local buckling behavior of the pile members. Typically, the same three cycle set loading protocol utilized in the experimental component of the research was also used in the FEM simulations to allow for a direct comparison between the two methods. It should be noted, throughout the research program FEA was used in some cases to verify the results of experimental evaluations and in other cases to develop connection configurations and predict behavior prior to experimental tests.

Connectivity within the model, typically representative of welds in the experimental specimens, was modeled using a mesh independent tie definition. This method of defining connectivity restricts nodes on independent parts within a specified spatial tolerance to conform to the same displacements and rotations during the analysis. Although this method of modeling makes the analysis easier to conduct since welds are not required to be modeled, the associated limitations and assumptions should be noted. The most prominent of these limitations is the inability of this modeling procedure to capture the potential limit state of weld cracking, or base material cracking, since no welds were included and no cracking models were defined. Additionally, since no extreme convergence study was conducted in any particular area of the models, any stress and strain concentrations in very small areas should be understood to be of questionable accuracy.

However, this basic modeling procedure was shown to capture local buckling, connection behavior, global behavior, and stress and strain concentrations over reasonably sized regions in a manner comparable to that of the experimental investigations. In addition, some models required the definition of hard contact between elements within the analysis. This was achieved with an Abaqus feature that allows for the definition of hard contact between surfaces independent parts and allows separation after the contact occurs. Additional specific details related to the various models developed in this research will be discussed where applicable.

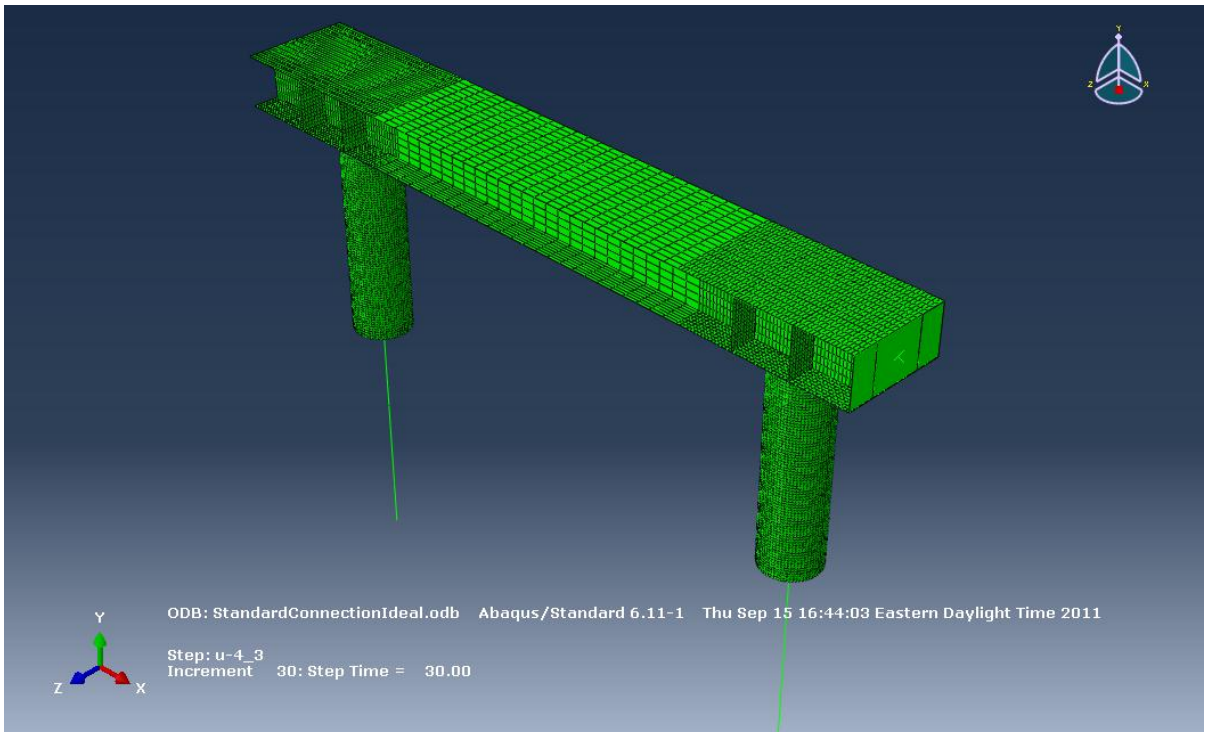

Figure 4.16 Steel Pier Finite Element Model

4.5.2 Material Models

As has been mentioned, when possible actual material stress strain data from coupon testing was used to calibrate the steel material model used in the FEA. The material model definition used in Abaqus defines an elastic portion of the stress strain curve based on an input of elastic modulus which in every case was assumed 29000 ksi. The plastic portion of the stress strain curve was defined by an input of tabular plastic stress – plastic strain data from material testing. For this input, plastic strain is determined by subtracting a strain value equal to the first plastic stress value divided by the elastic modulus, from the actual strain value found from testing. This half cycle input data was used by the program to calibrate the various parameters associated with the non – linear kinematic hardening model that was used to represent the behavior of steel subjected to cyclic loading inelastic loading.

When actual stress – strain data was not available, bi-linear material models were used and were based on the anticipated material properties shown in Table 4.2. The ultimate stress was typically associated with a plastic strain 0.14 as a reasonable value to define the slope of the hardening curve. It should also be noted that the material model associated with the sub-modeled beam element pile sections did not consider the non – linear kinematic hardening model as this was not allowed by the program. Alternatively, a bi - linear hardening model was used although inelastic behavior in this section of the pile was not anticipated.

Table 4.2 Expected Material Properties for FEA

Material	F_y (ksi)	R_y[1,2]	$\mathbf{F_{y,exp}}$ **(ksi)**	F_u (ksi)	R_t[1]	$\mathbf{F_{u,exp}}$ **(ksi)**
ASTM A500 Gr. B& C Dual Cert. (Piles)	46.0	1.4	**64.4**	62.0	1.3	**80.6**
ASTM A572 Gr. 50 (Cap Beam & Stiffeners)[3]	50.0	1.1	**55.0**	65.0	1.1	**71.5**
ASTM A36 (Various Test Frame Components)	36.0	1.5	**54.0**	58.0	1.2	**69.6**

[1] based on (AISC, 2010)

[2] based on (AASHTO, 2009)

[3] R_y values only covered in (AISC, 2010)

4.5.3 Automatic Stabilization Controls

During the development of the Finite Element simulations, it was found that consideration of geometric non-linearity with a large displacement formulation allowed the model to capture the effects of local buckling. However, it was also found the solution diverged and the model failed as local buckling of the pile walls developed. To solve non-linear problems, Abaqus uses an iterative Newton method that increments loads applied to the model and solves the non-linear problem initially based on the tangent stiffness of the structure to solve for nodal displacement. Convergence is then checked by comparing applied loads to the sum of the internal nodal forces as well as nodal force equilibrium.

Incrementing this process with updated stiffness matrices allows the program to eventually converge. The process of incrementing loads divides an input load (or displacement) over a time period that comprises a step. Hence, all models are treated as a dynamic problem although no mass, damping, or accelerations are defined in the system. When automatic incrementation is specified, the program will attempt to solve a static problem step in one single increment. However, this is not possible with non-linear problems which require incrementation of the input displacement or load.

As instabilities such as local buckling develop, strain energy is transferred within the model and the global iterative solution process may diverge. One solution to this problem, provided by the program, is to include adaptive automatic stabilization control. This process inserts a small artificial amount of mass into the system along with an adaptive magnitude of a damping factor such that damping forces can develop as local instabilities occur generating an increase in nodal velocities. These damping forces are then included in the iterative equilibrium checks that compare applied forces into the summation of internal nodal forces. The inclusion of these damping forces locally dissipates the strain energy transfer that occurs and helps the solution reach convergence which checks not only for global force equilibrium but also nodal equilibrium. Although this does generate some modeling errors, the method was shown to accurately capture specimen behavior when compared to the experimental tests which helps to lend confidence to the accuracy of the solution. Further, allowing the program to adaptively determine the necessary magnitude of the damping factor may reduce the associated error.

4.6 Scaled Dynamic Shake Table Evaluations

In addition to the full scale quasi – static experimental evaluations that were conducted in this research project, dimensionally scaled experimental shake table testing was also conducted. The single direction shake table at NCSU's Constructed Facilities Laboratory is

driven by a two – stage servo controlled hydraulic actuator with a total force capacity of 50 kips. The shake table dimensions are 8 ft. x 8 ft. with an 8 in. square grid of 5/8-11 tapped holes for base restraint of test specimens. Given the dimensions of the table, scaling of the pier specimens was required, as would be the case with most experiments that would be tested on this piece of equipment.

The shake table is limited to a total displacement capacity of +/- 5 in., which had to be considered when selecting ground motions and associated displacement time histories for testing. Tuning of the table prior to testing was based on traditional PID signal tuning to the servo valve. The accuracy of the resulting table acceleration histories, as compared to the intended inputs, was evaluated by comparing the acceleration and displacement response spectrums generated from the original acceleration time history and those from recorded acceleration time histories captured with accelerometers attached to the shake table. Further details regarding the calibration and tuning of the shake table, as well as the design of test specimens for shake table testing, will be discussed in subsequent chapters of this document where applicable.

4.7 Nonlinear Time History Analysis

In an effort to predict dynamic behavior prior to experimental shake table testing of specimens, and to assist in the selection of acceleration time histories, nonlinear time history analysis (NLTHA) was conducted with the FEM program Abaqus. The analysis used line elements representing the pile and cap beam members of the actual system, as well as lumped masses over the pile elements to represent superstructure dead load. The elements selected for the analysis were formulated to capture section plasticity through cross section integration over a given number of section points and a given number of integration points along the element. This formulation did not require calibration of a hysteretic rule associated with a plastic hinge length to capture system non – linearity. However, it should be noted this

analytical technique was not capable of capturing the effects of pile wall local buckling on system strength, which had to be considering when using the analytical results to plan experimental testing. Further details regarding this NLTHA will be discussed in subsequent chapters of this document.

Chapter 5: Evaluation of Standard Welded Connections

5.1 General Discussion

From the conclusions drawn from the past research work, it appeared that it would be necessary to explicitly protect critical welded regions of pipe pile to cap beam connections in order to produce the more desirable limit state pile of hinging in the form of pile wall local buckling. However, the fifth test of the first phase of experimental testing program attempted to mitigate brittle cracking, at or near welds, with one additional standard welded detail. Finite Element Analysis was also conducted in order to further evaluate the behavior of piers with standard welded connections, to verify the laboratory results which had been observed, and to further study what appeared to be a propensity for cracking near the critical connection region.

5.2 Evaluation of a CJP Weld with a Double Sided Reinforcing Fillet Weld

As has been mentioned, in addition to the standard welded connections that were tested in the past work at NCSU, one additional configuration which falls in the standard category was considered in the current research scope. The weld configuration consisted of a CJP weld with full depth reinforcing fillet welds both inside and outside the pile as shown in Figure 5.1. This configuration required the use of a splice weld 12 in. below the connection to facilitate construction with the interior reinforcing fillet weld. For reporting purposes, it is important to note that this test was conducted in the first phase steel pier testing at NCSU, but is considered in the current scope of work in this document which again aims to verify the hypothesis that standard welded connections are incapable of mitigating connection cracking.

The connection design was an attempt to determine whether the brittle cracking experienced in prior tests was more of a stress based failure or strain based failure since the larger weld should reduce the stress in the weld itself but not necessarily the associated plastic strains at the interface weld toe interface. Consideration was given to the fact that the detail would induce more heat effects and introduce the possibility for more defects. The addition of the necessary splice weld also added to the negative effects of the configuration as more welding was required which not only increased the potential of defects but also decreased economy. However, it was felt that regardless of these issues the connection still had potential to improve the connection behavior and was the final obvious possible weld geometry detail that could be considered.

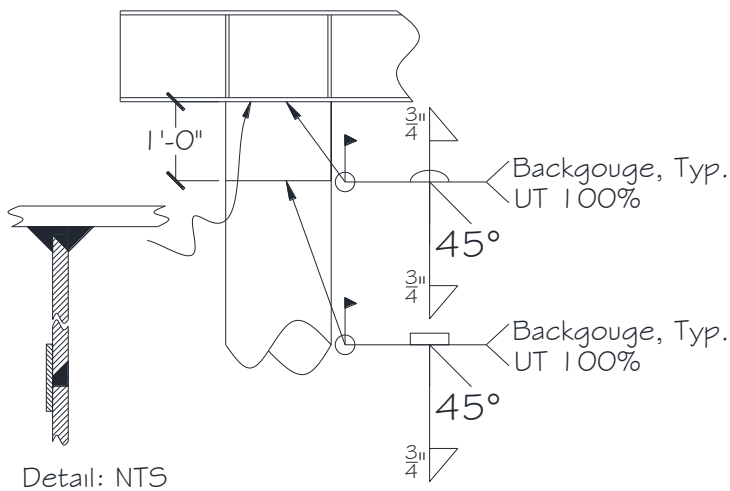

Figure 5.1 Standard Welded Connection – CJP Weld with Full Depth Reinforcing Fillet Both Sides

Considerable effort was made to ensure that during the construction process each step taken could be realistically reproduced in the field as had been done in the past research work. In order to incorporate the inside fillet weld shown in Figure 5.2, it was necessary to use a stub column (which was detailed as 12 in. long) which would first be welded to the cap beam in a sequence indicated by a WPS provided in the appendix of this document. Prior to the welding of the stub column to the cap beam, the proper location of the stub column on the

cap beam was marked by placing the cap beam on the piles which had already been erected and marking their location. This step was used to ensure alignment of the stub column to the pile. The welding of the stub column to the cap beam, shown in Figure 5.3, was then conducted in an underhand position on the ground prior to the placement of the cap beam onto the piles, as could be done in the field. Next, the cap beam was placed on the piles and the splice welds between the stub columns and piles were completed. During construction, full visual weld inspection was conducted and, following construction, UT inspection of the welds was conducted. Reports from both inspection processes are provided in the appendix of this document.

Figure 5.2 Phase 1 Test 5 – Inside Reinforcing Fillet Weld

Figure 5.3 Completed Stub Column Weld

For the experimental evaluation, a first yield force of 73 kips was used to define the elastic cycles of the three cycle set load history, based on mill certifications (provided the appendices of this document) that indicated a yield stress of approximately 54 ksi value. The average first yield displacement for this test was found to be 2.84 in. resulting in an equivalent yield magnitude of 3.69 in. The overall response of the test 5 (phase 1) specimen was very similar to that of second pier tested with CJP welds and full depth reinforcing fillets on the outside in the prior research work. No visual signs of failure or strength degradation were observed prior to a displacement ductility level of 3.

The ultimate failure mechanism in test 5 (phase 1) occurred in the third push cycle of ductility 3 and consisted of a large fracture at the weld toe on the south side of the south column as shown in Figure 5.4. The crack was associated with over 20% strength loss as shown in Figure 5.5 and Figure 5.6. Since the full cycle had not been completed, the decision was made to continue pushing the specimen but the crack began to propagate quickly and reduce the ability of the pier to carry load. For this reason the test was concluded and the detail was assumed to possess a reliable ductility capacity of likely 2.

During testing, the specimen was found to be capable of developing minor levels of local buckling on both columns suggesting the more desirable failure mode was beginning to develop. The first signs of local buckling were noted during the second push cycle of ductility 3 at a location just above the splice weld on the north face of the south column and near the cap beam weld on the north face of the north column. The second pull cycle of ductility 3 led to slight local buckling developing near the cap beam weld on the south face of the south column and near both the cap beam weld and splice weld on the south face of the north column as can be seen in Figure 5.7. However, the buckling did not propagate to significant levels which would be expected to lead to strength loss over multiple cycles of loading.

Ultimately, the failure of the pier was attributable to brittle connection region cracking leading to significant strength loss in a single cycle of loading as had been shown to occur with the other standard welded connection details. The configuration was not capable of producing considerable pile wall local buckling and was there for considered to be inadequate and unreliable. It appeared from the results of the experimental evaluation, that the weld toe failure observed was likely strain related as opposed to stress related. The inside reinforcing fillet weld did not prolong the life of the structure lending to the conclusion that the failure may be strain controlled.

Figure 5.4 Failure Crack – Ducitlity 3 Cycle 3

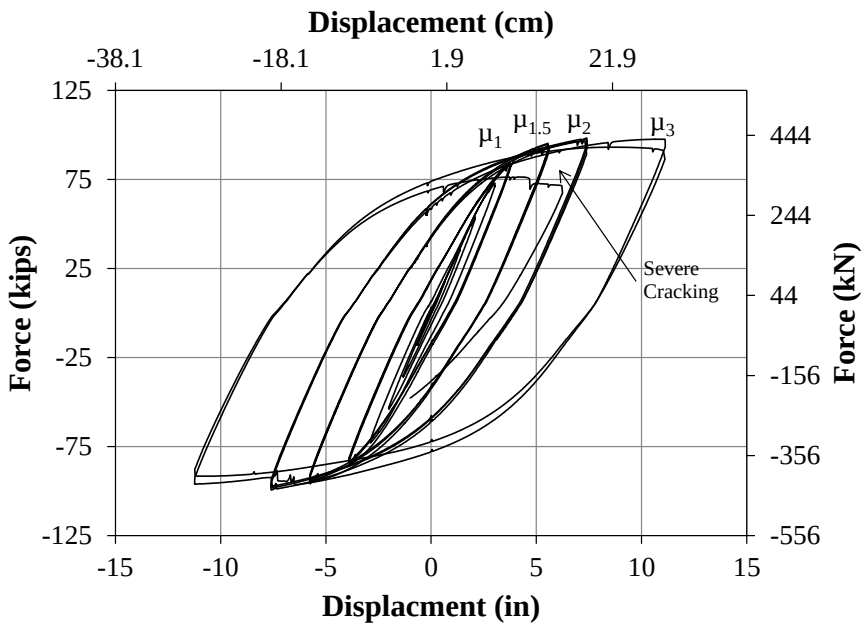

Figure 5.5 Phase 1 Test 5 – Force Displacement Hysteresis

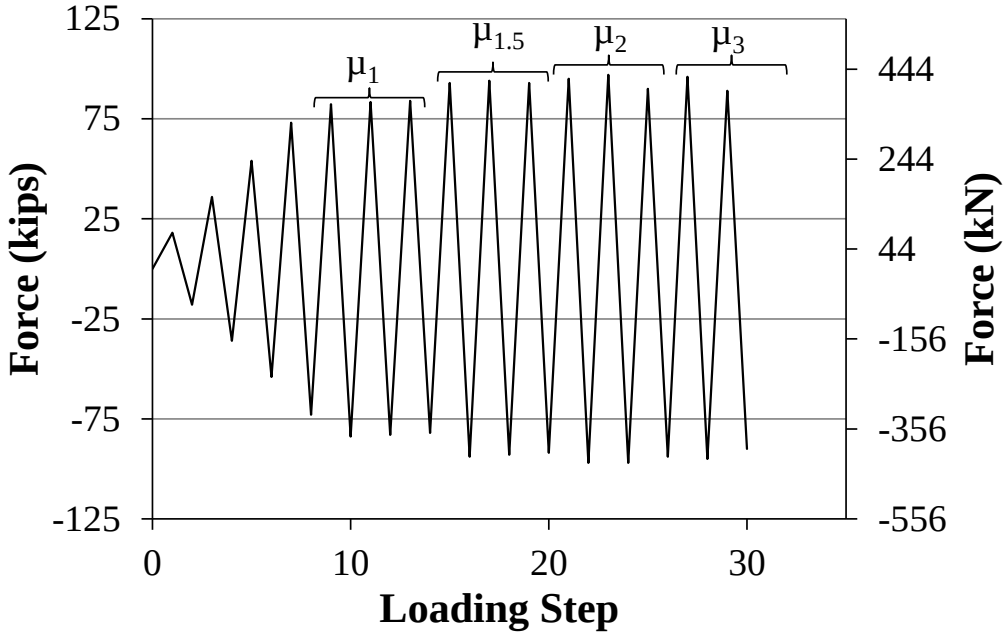

Figure 5.6 Phase 1 Test 5 – Load History

Figure 5.7 Double Buckling of North Column

5.3 FEA of Standard Welded Connections

In an effort to verify and better understand the experimental results that had been observed for the piers containing standard welded connections, FEA was conducted to further evaluate the behavior of this type of configuration. The Finite Element Model, shown in Figure 5.8, considered ideal geometry (pile spacing, pile length, and stiffener placement) and was subjected to a three cycle set load history which was calibrated with the first yield displacement found by the model. The average first yield deflection was predicted to be 2.19 in. as is also shown in Figure 5.8. The analysis utilized stress – strain data from coupon testing of actual material taken from the pile elements of the system to calibrate the non – linear kinematic hardening rule that described the plastic portion of the material model. It is important to note, the model used mesh independent tie definitions to define connectivity between the piles and the cap beam as has already been discussed. Hence, the actual weld geometry was not modeled rendering the results of the analysis applicable for comparison to the results of any standard welded specimen.

The results of the simulation showed the onset of local buckling to occur at the ductility 3 level as shown in Figure 5.9. Note this was the same ductility level at which minor levels of local buckling were noted to occur in each experimental evaluation with the exception of the pier containing fillet welds which was limited to a maximum displacement ductility of 2. The analysis, which did not have the capability to capture material fracture, was conducted through the ductility 4 cycles which showed the severity of the buckled region to propagate as shown in Figure 5.10. This was similar to that of the first experimental evaluation with CJP welds and full depth reinforcing fillet welds which was able to survive the ductility 4 cycles and showed the buckled region to propagate in severity. Hence, the analytical results indicated that the desirable form of pile wall local buckling leading to gradual strength loss over multiple cycles may control, should connection region cracking be mitigated as shown in Figure 5.11. However, mitigation of connection region cracking was not experienced in any of the experimental evaluations as has been highlighted.

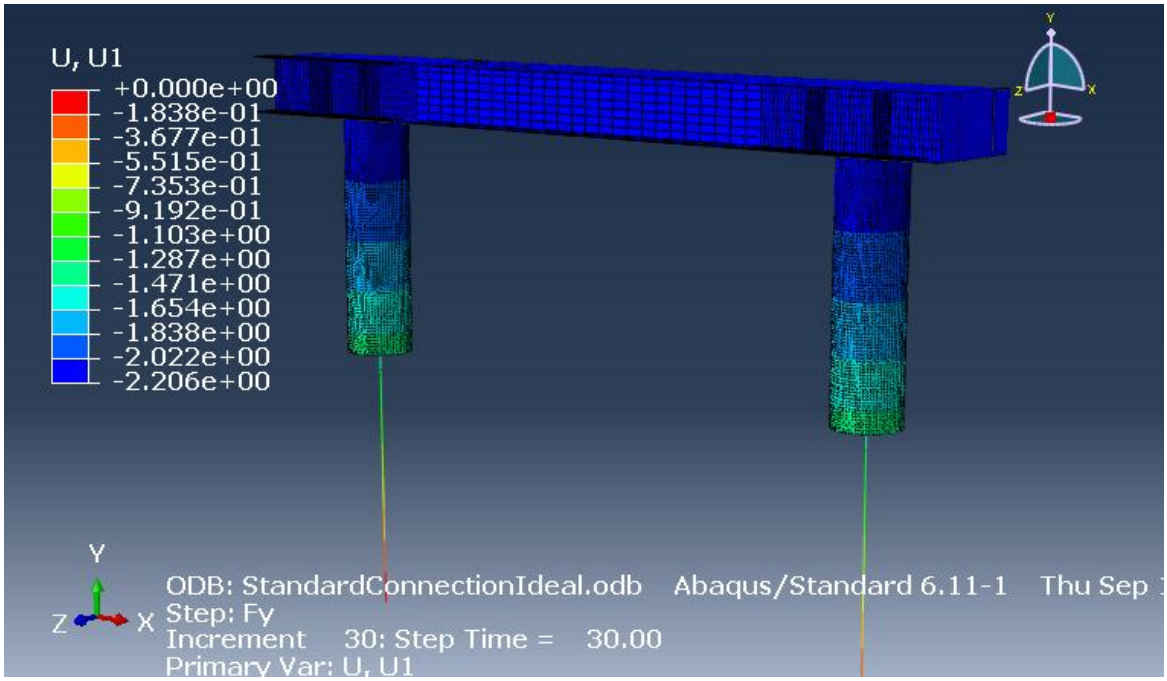

Figure 5.8 Standard Welded Connection Detail – FEM First Yield Conditions

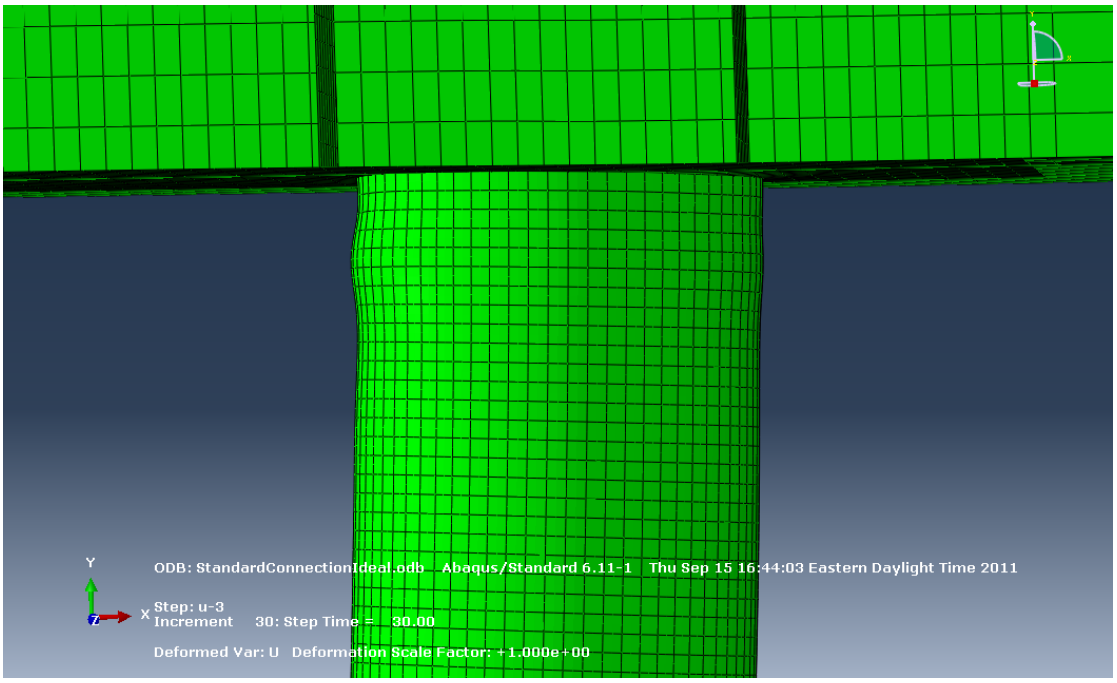

Figure 5.9 FEM – Onset of Local Buckling at the Ductility 3 Level

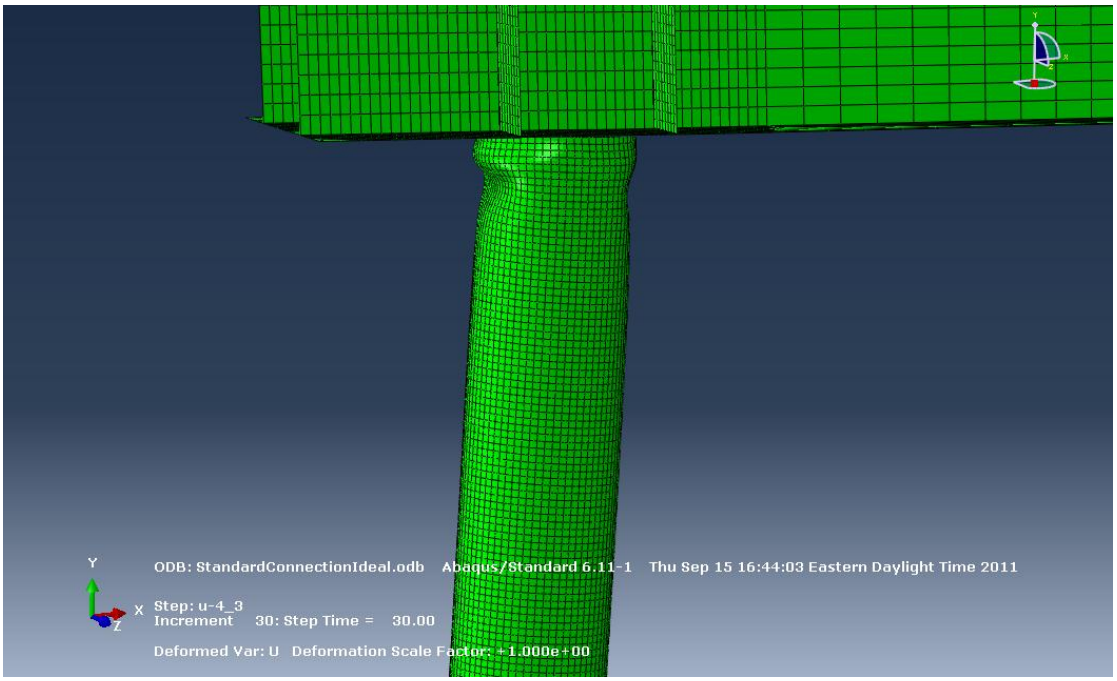

Figure 5.10 FEM – Propagation of Local Buckling at Ductility 4 Level

The general hysteretic shape of the analytical results as well as the strength capacity of the system match that of the experimental test well as shown in Figure 5.12 which compares the response to that of the test 5 (phase 1) evaluation as an example. It should be noted that the magnitudes of the displacement peaks do not match between the analysis and that of test 5 (phase 1) as the load histories were based on different first yield displacements. Regardless, the similarity in the global behavior in terms of hysteretic shape and strength capacity, lends to confidence in the analytical results that are not readily comparable to experimental laboratory measurements.

These results, in particular, include tensile strain concentrations that were shown to develop in what would be the weld toe region of the actual system as shown Figure 5.13 and Figure 5.14. These figures depict the concentrations at the ductility 3 displacement level which was the maximum ductility level experienced by any of the experimental specimens prior to the development of crackin. The analysis predicted these tensile strain

concentrations, immediately below the cap beam soffit, to be associated with strain magnitudes of approximately 0.09 on the tension face of the tension pile in either direction of loading.

Although there are no valid reasons to believe that this predicted magnitude of strain is largely incorrect, a detailed convergence study in this region was not conducted. For this reason, the results should be considered more informative as a potential explanation for the observed cracking behavior than as a conclusive strain demand at fracture. The tension strain concentration may explain the propensity for cracking tension face with any particular standard welded detail. It is also worth noting, this form of strain concentration was not shown to be as severe on the compression face as local buckling develop at the ductility 3 level as shown in Figure 5.15 and Figure 5.16.

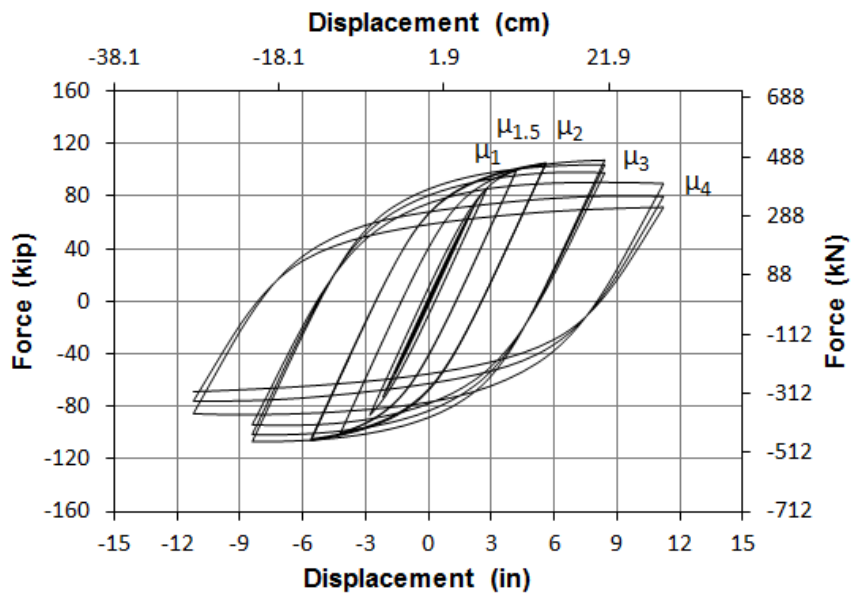

Figure 5.11 FEM – Force Displacement Hysteresis

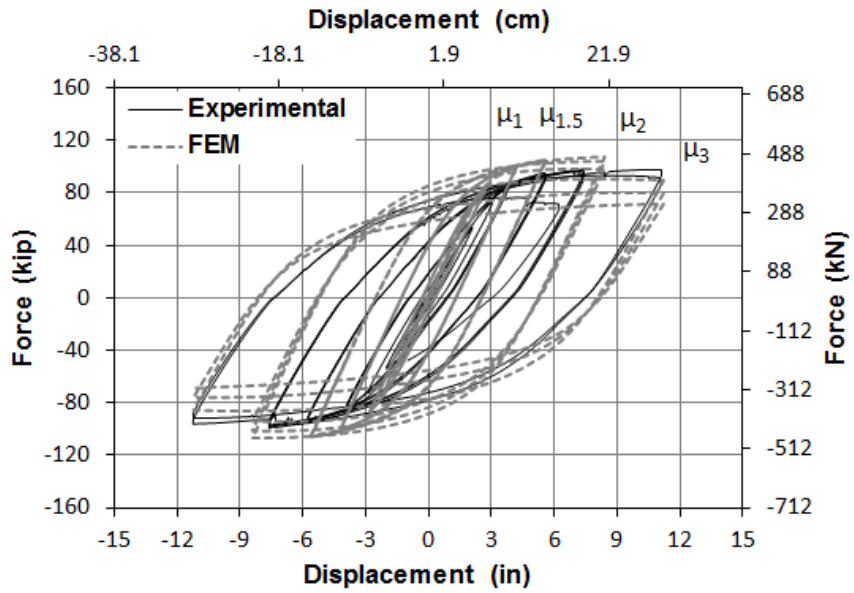

Figure 5.12 Comparison of FEM vs. Phase 1 Test 5 Force Displacement Response

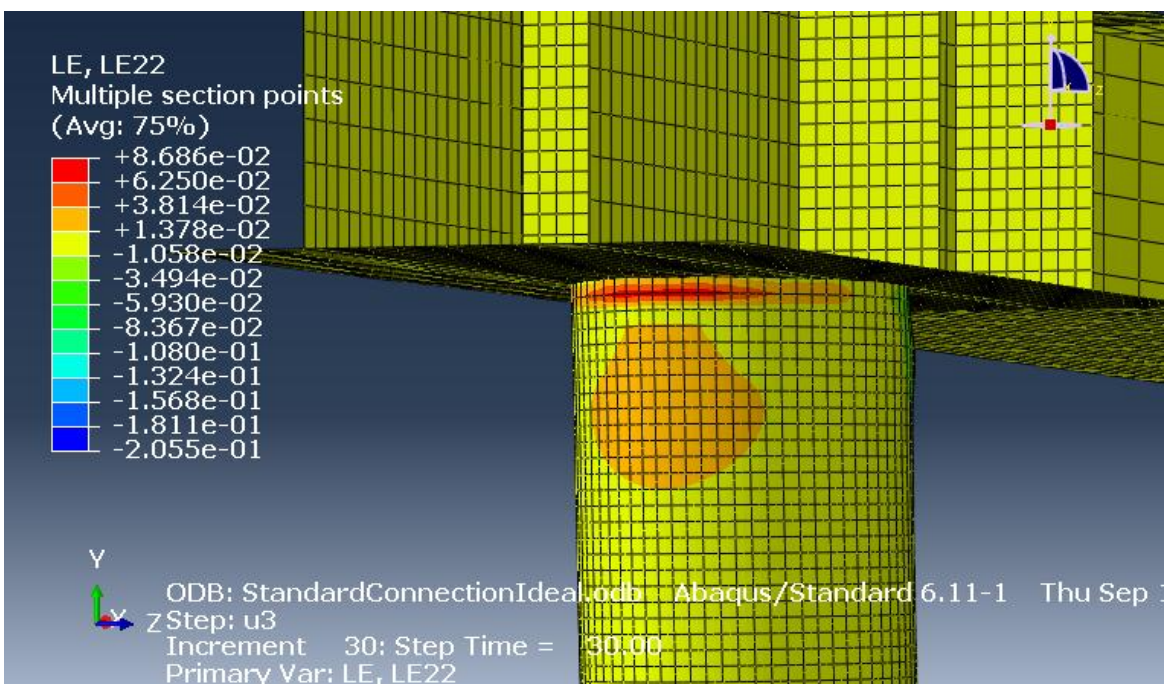

Figure 5.13 FEM – Local Tension Strain Concentration at Weld Toe Region

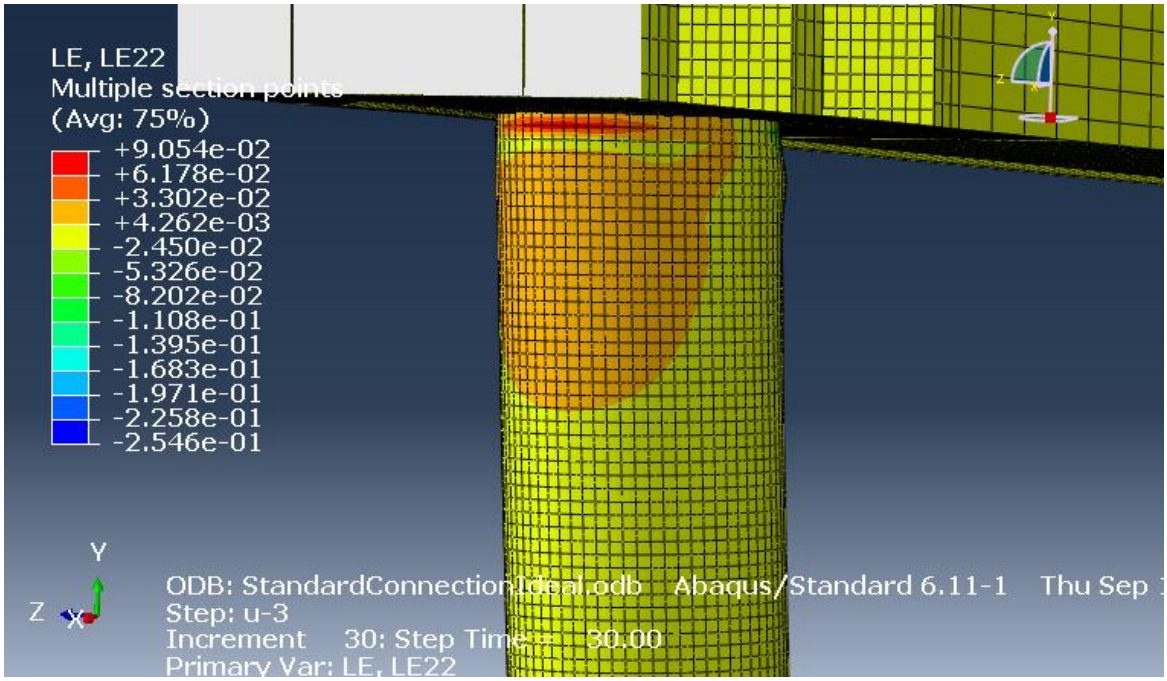

Figure 5.14 FEM – Local Tension Strain Concentration at Weld Toe Region

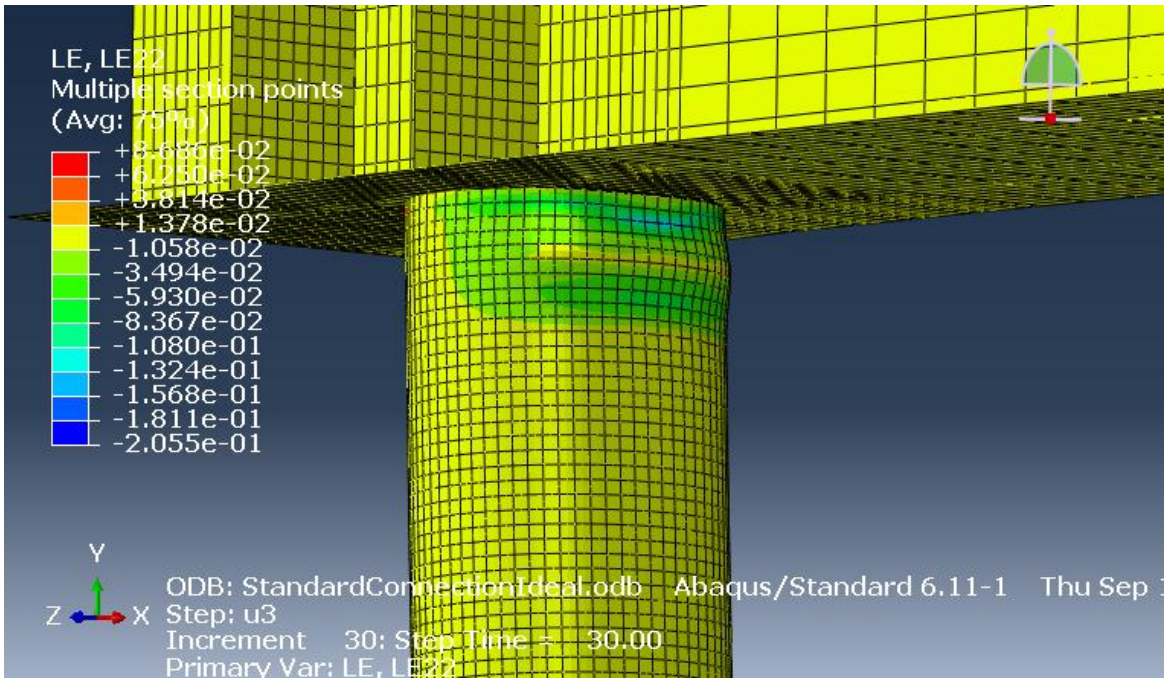

Figure 5.15 FEM – Compression Strains at Weld Toe Region

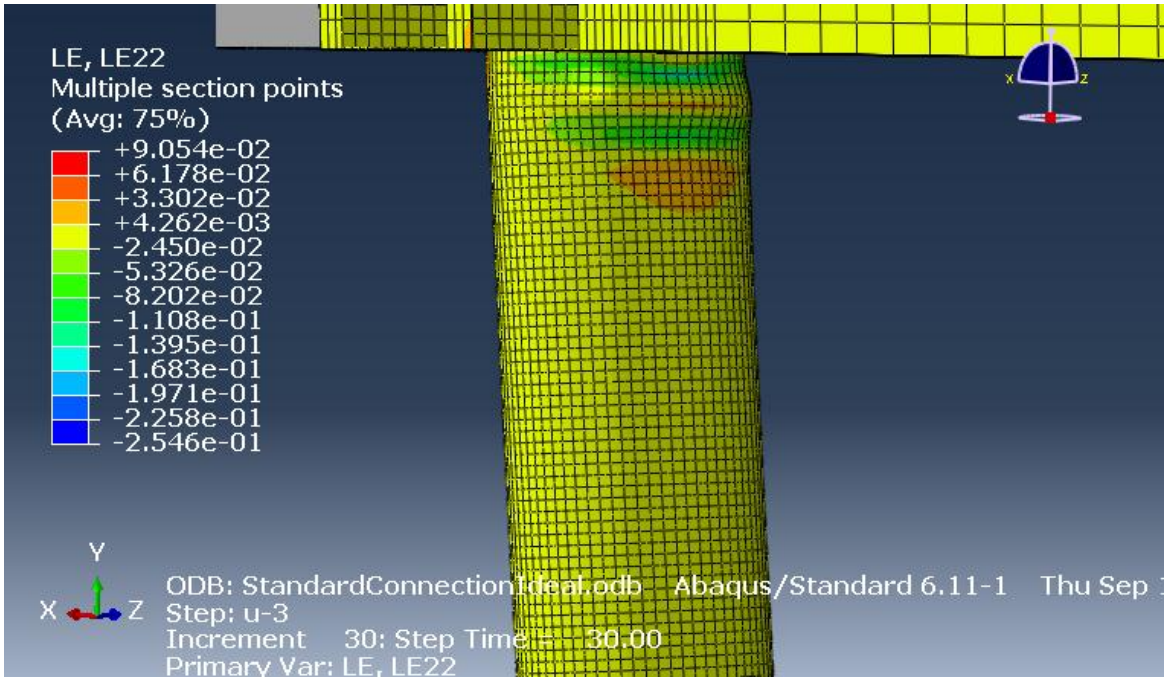

Figure 5.16 FEM – Compression Strains at Weld Toe Region

In addition to the strain considerations that have been discussed, the simulation provided insight into another issue noted during the experimental testing of the standard welded connection piers. As has been mentioned in prior chapters, the anticipated first yield displacement based on typical centerline modeling that considered cap beam flexibility was 2.04 in. However, in all cases of the standard welded connections, the experimentally determined average first yield displacement between the positive and negative cycles, was larger than this calculated value by between 21% and 47%. In some cases a portion of the elevated values that were experienced could be attributed to unanticipated base displacements as has been mentioned. However, it was also noticed during testing that, due to construction errors, the placement of the transverse cap beam stiffeners was in many cases considerably far out of alignment. These stiffeners were intended to be placed directly over the extreme fibers of the piles to transfer forces from the cap beam to the pile walls to develop the capacity of the pile section. Although no exact measurements were taken, a review of photographs taken during testing indicated that the stiffeners were typically out of

alignment by 0-3 in. as shown in Figure 5.17. Further, it should be noted that the as-built alignment of the internal stiffeners (between the double section HP cap beams) could not be visually inspected.

Although the cap beam was designed to remain elastic based on calculated flexural demands, in each test instances of cap beam bottom flange prying was noted typically near the tension face of each pile as full strength of the pile section was developed. This prying action, shown in Figure 5.18, was predicted to occur by the Finite Element Analysis simulation as shown in Figure 5.19, which also predicted a first yield displacement of 2.19 in. However, when a FEM simulation was conducted with cap beam stiffeners arbitrarily offset by 3 in., as shown in Figure 5.20, the cap beam bottom flange prying action that was noted in the experimental tests was also predicted by the simulation as shown in Figure 5.21. Further, the simulation with offset stiffeners indicated an elevated first yield displacement magnitude of approximately 4.6 in as shown in Figure 5.22. From these results, it appeared that the misplacement of the stiffeners led to the observed prying action at the cap beam soffit and consequently a less rigid joint behavior than standard analysis would anticipate. It is possible that this effect contributed to the elevated first yield displacement levels that were observed during testing.

Figure 5.17 Offset Stiffeners with Standard Welded Connection

Figure 5.18 Cap Beam Bottom Flange Prying Action

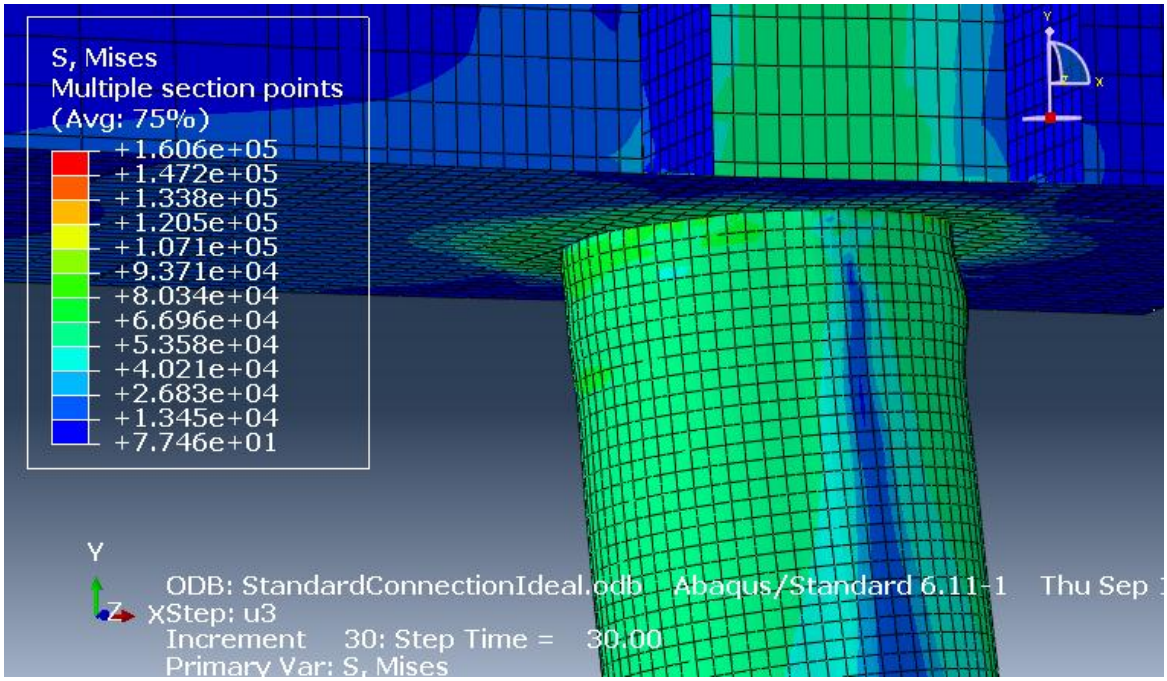

Figure 5.19 FEM – Ideally Placed Stiffeners Ductility 3 (2X scale factor)

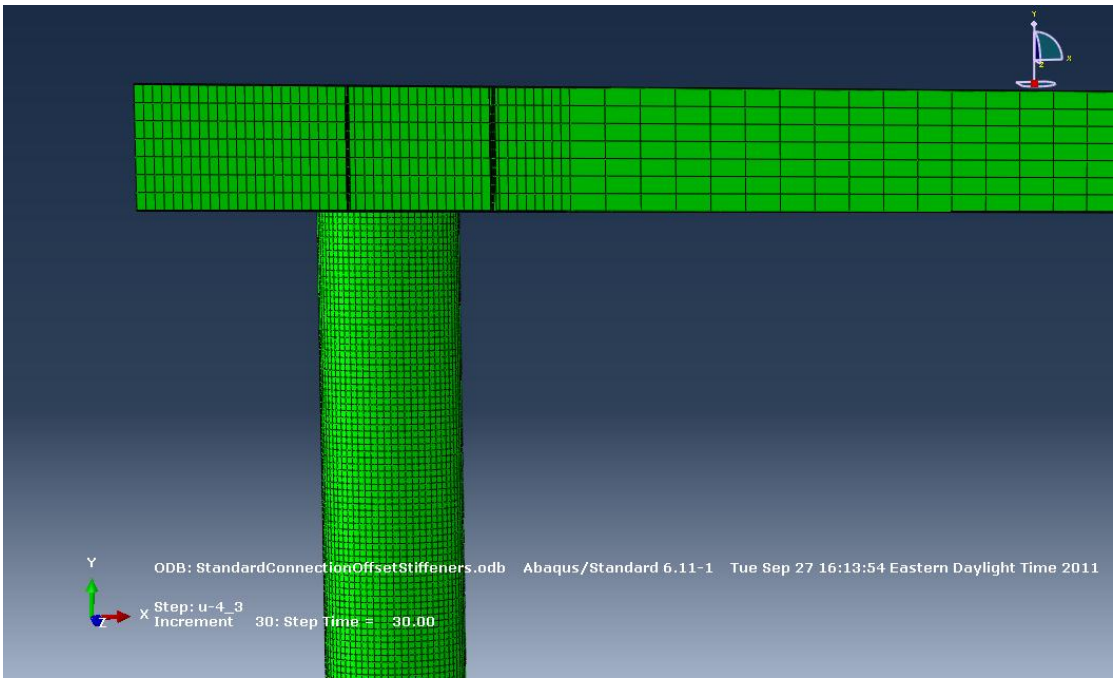

Figure 5.20 FEM – Pier with Offset Stiffeners

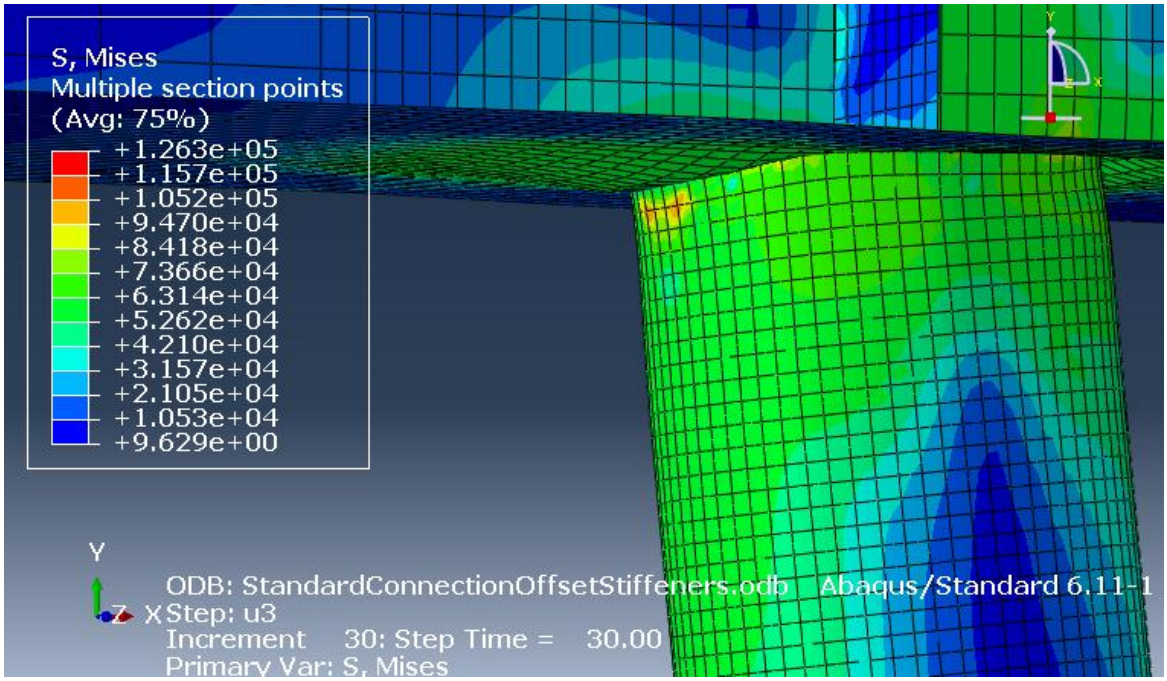

Figure 5.21 FEM – Offset Stiffeners Ductility 3 (2X scale factor)

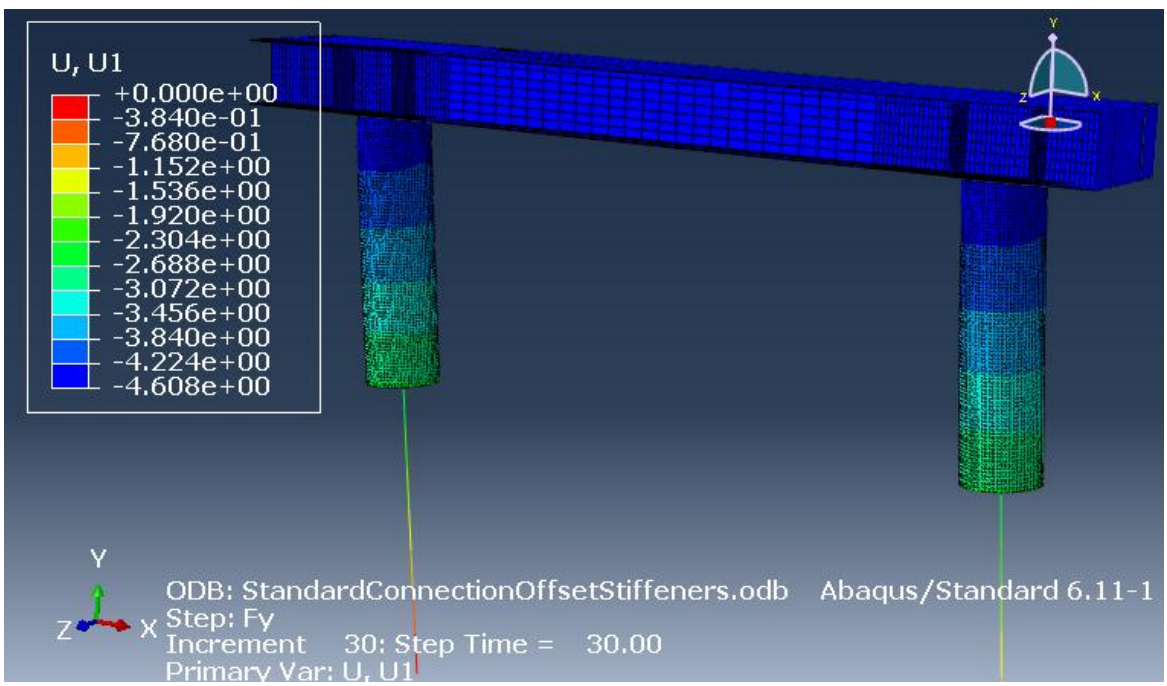

Figure 5.22 FEM – Offset Stiffeners First Yield Displacement (in)

5.4 Conclusions Regarding Standard Welded Connections

As has been discussed throughout this chapter and prior chapters, the failures observed during testing of the standard welded connection specimens would generally be considered unsatisfactory. Although each specimen did begin to develop minor levels of the more desirable limit state of local buckling, in each case brittle cracking leading to rapid strength degradation was experienced prior the propagation of the buckled region. Although the first evaluation of a system with complete joint penetrating welds and full depth outside reinforcing fillet welds was able to survive all cycles of loading at the displacement ductility 4 level, the results were not repeatable in a second evaluation. Further, it was shown that the intensive process of including interior reinforcing fillet welds did not improve the response of the system as brittle connection region cracking again controlled the ultimate limit state of the experimental specimen.

Finite Element Modeling conducted to better understand the connection behavior, showed that a local buckling failure mode would be likely to control the response of the system should cracking be mitigated. However, the model which was representative of systems containing any standard welded connection detail also showed a region of elevated strain concentration to develop immediately below the cap beam soffit near what would be the weld toe region of an actual system. This strain concentration was located at the region of the connection where cracking was experienced in the experimental evaluations. Although the model was incapable of capturing the cracking failure mechanism, the results did suggests the propensity of the system to develop this region of concentrated elevated strains may be the reason for the observed cracking failure modes.

In addition, the FEM simulation was capable of replicating the cap beam bottom flange prying action that was observed in the experimental tests. The action only developed in the simulation when the cap beam transverse stiffeners were offset as was the case in the

experimental evaluations. The prying action appeared to lead to larger than expected first yield displacements due to softening of the connection region. Therefore, it should be recommended that minimal construction tolerance be allowed in regards to stiffener placement when constructing this type of system to ensure the predicted behavior can be achieved by the actual structure.

Although by definition the systems evaluated with standard welded connections possessed limited reliable ductility capacity, it should be noted that the associated reliable drift capacity was of a reasonable magnitude in some cases. For example, as noted in Table 3.2, a reliable drift capacity of approximately 4.9% was associated with the detail with a CJP weld and single sided reinforcing fillet weld. This reasonable level of drift was associated with a displacement ductility capacity of 2, which may be judged as a low magnitude highlighting the need to also consider drift capacity and actual displacement capacity when reviewing the performance of a system. This is partially the result of the considerably high elastic flexibility of this type system which leads to reasonably large first yield displacements. Regardless, the work conducted on standard welded connections appeared to indicate that the undesirable and less reliable failure mode of connection region cracking would likely not be mitigated by any form of a standard welded connection. This suggested that relocation of damage and capacity protection of these critical regions may be necessary in order to ensure a reliable system response could be achieved.

Chapter 6: Evaluation of Modified Weld Protected Connections

6.1 Purpose of Modified Weld Protected Connections

As has been concluded in prior chapters, experimental and analytical research work conducted in regards to standard welded connections seemed to indicate that precluding the undesirable failure mode of connection region cracking would require explicitly protecting critical connection regions. In order to achieve this, goal a basic capacity design procedure concept was applied to the design of pipe pile moment resisting connections resulting in the idea of modified weld-protected connections. The capacity design procedure, common to many facets of earthquake engineering, protects less ductile failure modes such as weld cracking by ensuring a "weak link" exists and, importantly, is associated with a preferable ductile mode of failure as illustrated in Figure 6.1. In the case of the steel pipe pile piers under consideration, this more desirable mode of failure was flexural hinging in the form of pile wall local buckling. Should a connection configuration be capable precluding connection region cracking, allowing buckling to be the controlling failure mode, the ultimate displacement capacity of the system could be increased or decreased by selection of a smaller or larger D/t ratio for the pile elements of the system as will be discussed in subsequent chapters.

Application of the capacity design procedure to the multi-column piers under consideration led to the concept of flexural hinge relocation. As shown in Figure 6.2, the hinge relocation concept aims to move damage down the pile away from the cap beam soffit and critical welded regions. However, relocation of the hinge increases the bending moment demand in the protected zone as the full over-strength bending moment capacity associated with flexural hinging of the hinge zone is linearly extrapolated to the protected zone in

accordance with the relationship provided in Eq.(6.1), where (H) represents the distance from the point of contraflexure to the cap beam soffit, (X_d) the design depth of hinging, (Z_{hinge}) the plastic modulus of the hinge region, (S_{pz}) the elastic modulus of the protected zone, and (O) applicable strain hardening over-strength factors. Thus, in order to effectively protect the critical welded regions of the steel pipe pile to cap beam connection, two key criteria had to be met.

First, the location of damage in the pile element would be moved below the welded region as has been mentioned and secondly, the welded region would be strengthened to remain in the elastic range of response taking into account the increased bending moment demand. It was postulated by the researchers that following these two key criteria would allow the more desirable failure mode of flexural hinging, in the form of pile wall local buckling, to control the ultimate limit state of the system given that welded connections had been shown to avoid cracking in the elastic range of loading in past research. As is discussed throughout this chapter, these criteria led to multiple connection configurations that were evaluated with both experimental and analytical methods. For each design case considered in this chapter, the specific connection configuration used to meet the two noted key criteria varied and will be discussed where applicable.

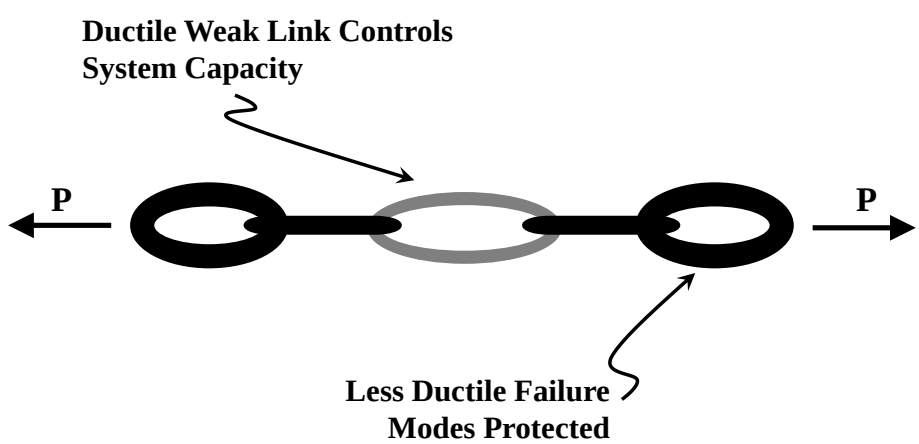

Figure 6.1 Capacity Design Concept Schematic Reproduced From: (Paulay and Priestley, 1992)

$$\frac{H - X_d}{f_{y,\exp} Z_{hinge} O} = \frac{H}{f_{y,\min} S_{pz}} \tag{6.1}$$

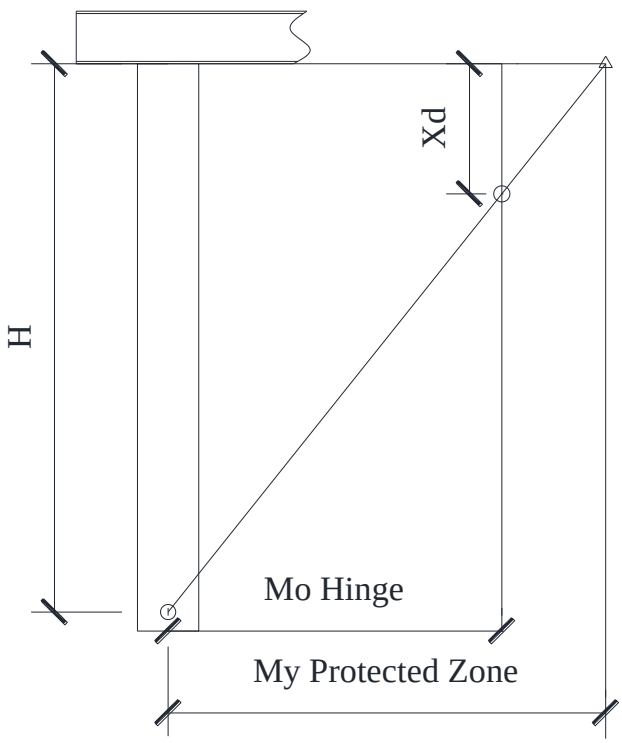

Figure 6.2 Flexural Hinge Relocation Concept

6.2 Kerf Connection

6.2.1 Introduction and General Discussion

The first test of the second phase of the steel pier project was aimed evaluating the performance of a cruciform gusset plate style connection shown in Figure 6.3. In particular,

the evaluation aimed to determine the configurations ability to effectively behave as a modified weld protected connection using both experimental and analytical methods. The connection consisted of gusset plates located in the joint zone oriented longitudinally and transversely to the cap beam as shown in the detail provided in Figure 6.4 and in Figure 6.5. This particular connection configuration required the use of an alternate cap beam configuration (opposed to the standard double HP cap beam) which had a centerline web directly over the longitudinal gusset plates. This resulted in the use of a built-up I shape cap beam for this particular evaluation. The design calculations for this alternate style of cap beam are provided in Figure 6.6. As is shown, a capacity design procedure was again employed to design the ASTM A572 Gr. 50 cap beam to remain within the elastic range of response as a pile hinging mode of failure developed as was done with the basic double HP configuration.

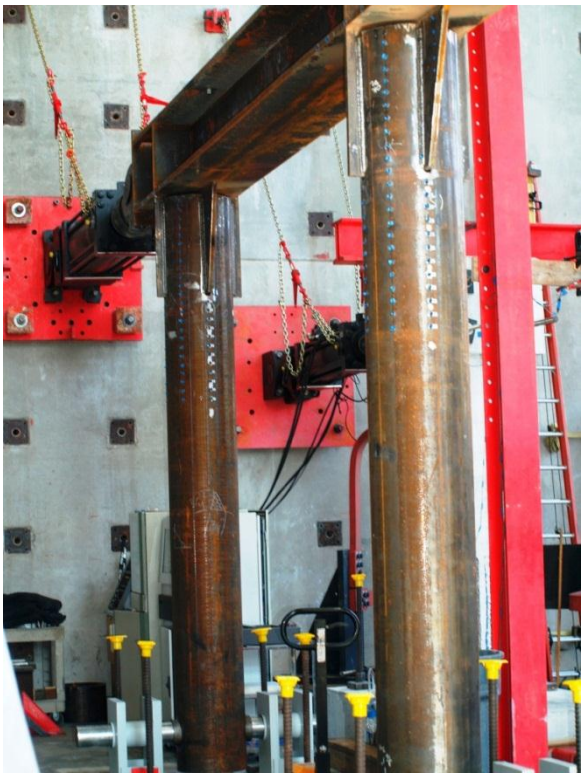

Figure 6.3 Kerf Connection Experimental Set Up

In an effort to achieve the goals of a modified weld-protected connection, the longitudinal gusset plates forming the connection were designed to remain in the elastic range of response when subjected to the flexural demands associated with hinging of the pile elements and were joined to the built up I section cap beam with complete joint penetration welds. It was assumed that the longitudinal plates would act as narrow rectangular sections in strong axis bending at the cap beam interface. From the over-strength pile hinging moment capacity, the extrapolated flexural demands at the cap beam interface was determined and the necessary length of gusset plate for the cross section to remain elastic was calculated as 36 in. for a 1 in. wide plate.

The gusset plates were joined to the HSS16x0.500 piles, which were field slotted by torching to allow for gusset plate insertion, with 5/8 in. fillet welds longitudinal to the pile axis. The welds were assumed to act in shear along the length of the weld in order to produce a moment couple that would resist the flexural demands associated with pile hinging. The necessary length of welding, which controlled the necessary depth of the gusset plate, was determined from the over-strength pile hinging demand. As has been discussed, the elements of the connection were designed to develop the full over-strength moment capacity of the pile to encourage the development of flexural hinges in the pile sections when the system was subjected to lateral loading. Detailed connection design calculations are provided in Figure 6.7. The connection detail, which is shown in Figure 6.5, was termed a "kerf" connection. Although the gusset plates oriented transverse to the cap beam were not assumed to carry any load as the pier was displaced longitudinally, they would be necessary should the pier be subjected double bending in the longitudinal direction of the bridge. Further, by inspection the transverse gussets are likely necessary to stabilize the longitudinal gusset in the out of plane direction.

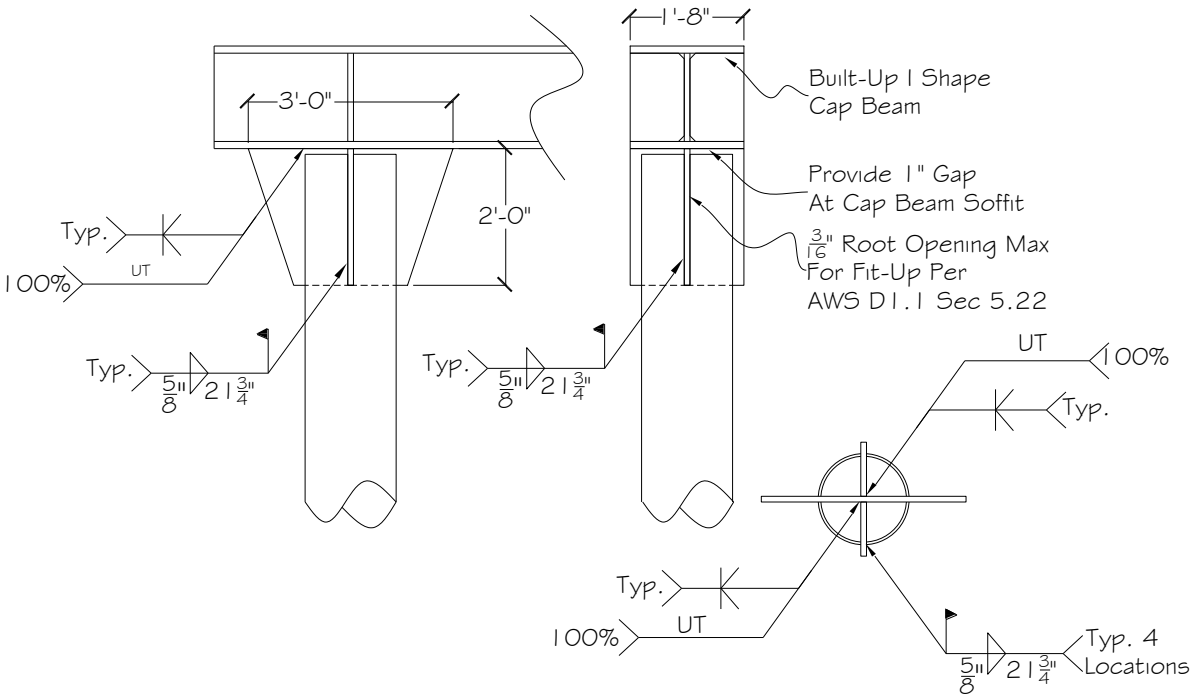

Figure 6.4 Kerf Connection Detail

Figure 6.5 Kerf Connection

(3) Plate Cap: Plate I Girder, ASTM A572 Gr. 50.

Flexural Capacity Per AISC Specification Chapter F:

$f_{y\_min} := 50ksi$ ASTM minimum yield stress

The minimum flange thickness to ensure flange compactness with a 20in wide flange can be determined.

$$t_{min} := \left[0.38\cdot\left(\frac{29000ksi}{f_{y\_min}}\right)^{0.5}\right]^{-1}\cdot 0.5\cdot(20in) \qquad t_{min} = 1.09\cdot in$$

Therefor, a 1.25in thick 20in wide flange plate will be used with a 1in thick web plate and total section depth of 18in to maintain box like cross section. Web compactness ok by inspection. Lateral Torsional buckling will be considered.

$$I_x := 2\left[\frac{20in\cdot(1.25in)^3}{12} + 20in\cdot 1.25in\cdot(8.25in)^2\right] + \frac{1in\cdot 15.5in^3}{12}$$

$$I_y := 2\cdot\left[\frac{1.25in\cdot(20in)^3}{12}\right] + \frac{15.5in\cdot(1in)^3}{12}$$

$$r_y := \left[I_y\cdot(20in\cdot 1.25in\cdot 2 + 15.5in\cdot 1in)^{-1}\right]^{0.5}$$

$L_b := 6ft$ Note: assumed that point of contraflexure will brace compression flange.

$$L_p := 1.76\cdot r_y\cdot\left[29000ksi\cdot\left(f_{y\_min}\right)^{-1}\right]^{0.5} \qquad L_p = 17.82\cdot ft$$

Note that full length of cap beam (12ft) is still within Lp. Yeilding will control the capacity design of this beam.

$$M_{o\_cap} := M_{pile}\cdot\frac{11.17ft}{V_{span\_min}} \qquad \boxed{M_{o\_cap} = 924.79\cdot kip\cdot ft}$$

$$\phi M_{y\_cap} := 0.9\,\frac{f_{y\_min}\cdot I_x}{10in} \qquad \boxed{\phi M_{y\_cap} = 1279.1\cdot kip\cdot ft}$$

built up cap adequate for flexure

By inspection, interaction of axial forces and moment capacity can be neglected as maximum considered axial force to gross axial yield strength is approximately 2%.

Shear capacity evaluation per AISC Specification G2:

$$V_{o\_cap} := 2\cdot V_o \qquad \boxed{V_{o\_cap} = 165.58\cdot kip}$$

$$\phi V_{n\_cap} := (1.0)\cdot 0.6\cdot f_{y\_min}\cdot(15.5in)\cdot(1in)\cdot 1.0 \qquad \boxed{\phi V_{n\_cap} = 465\cdot kip}$$

as expected, adequate

Figure 6.6 Built – Up I Section Cap Beam Design Calculations

(I) Kerf Connection

The kerf connection will be designed utilizing longitudinal fillet welds subjected to shear loading to develop the full moment strength of the pile. A total of four welds, two on each extreme fiber of the pile, will be considered. The strenth of the welds on the neutral axis will be neglected.

Note the demand from flexural hinging:

$M_{pile} = 703.73 \cdot kip \cdot ft$ expected overstrength pile moment capacity

$V_o = 82.79 \cdot kip$ associated shear, at max considered depth of hinging

The 1" thick gusset plate will be sized to remain elastic . Use ASTM A572 Gr. 50 material.

$f_{y\_min} := 50ksi$ ASTM minimum yield stress

The length of the gusset plate will be sized for the plate to remain flexurally elastic:

$$M_{o\_plate} := M_{pile} \cdot \left(\frac{11.17ft - 9in}{V_{span\_min}} \right) \qquad M_{o\_plate} = 862.69 \cdot kip \cdot ft$$

$$L_{min} := \left[\frac{M_{o\_plate} \cdot 6}{f_{y\_min} \cdot (1in)} \right]^{0.5} \qquad L_{min} = 35.25 \cdot in$$

Neglecting any strength reduction factors, **Use total length of plate equal to 36 inches.**

Check Shear Capacity:

$$\phi V_n := (1.0) \cdot (0.6) \cdot f_{y\_min} \cdot (1in) \cdot (36in) \cdot (1.0) \qquad \phi V_n = 1080 \cdot kip$$ Good

Use 1" x 36" gusset oriented along web of cap with full pin weld.

The necessary length of 5/8" fillet welding along the pile will be determined by considering the moment couple that must be developed between the two weld groups at either extreme fiber.

$$L_{w\_min} := \frac{M_{pile}}{16in} \cdot \left[(2) \cdot (0.75) \cdot 0.6 \cdot (70ksi) \cdot \frac{\sqrt{2}}{2} \cdot \frac{5}{8} in \right]^{-1} \qquad L_{w\_min} = 18.96 \cdot in$$

Use 23 inches of fillet welding along the longitudinal axis of the pile.
Use matching transverse gusset configuration.

Figure 6.7 Kerf Connection Design Calculations

6.2.2 Load History and Instrumentation Details

In the case of the kerf connection test, the material yield stress was estimated to be 55 ksi for the A500 Gr. B pile material based on mill certification test and in in-house material testing (see Figure A 6 through Figure A 10). This value, combined with the shear span of 8 ft. – 5 in. from the pinned supports to the base of the gusset assembly, resulted in a first yield force of 93.34 kips. Both the experimental and analytical evaluations, in the case of the kerf connection study, were based on the typical three cycle set load history which has been described in prior chapters. The application of this load history with the predicted material properties resulted in an experimentally determined first yield displacement of 1.91 inches generating a ductility 1 displacement of 2.50 inches. Application of the three cycle set load history produced the experimental force and displacement histories shown in Figure 6.8 and Figure 6.9 respectively.

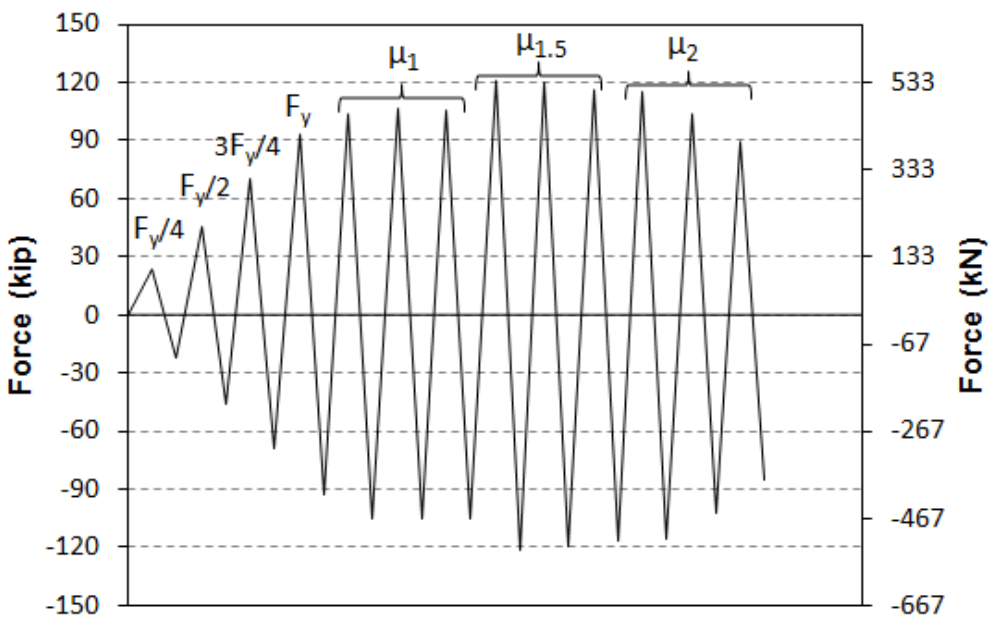

Figure 6.8 Kerf Connection Experimental Load History

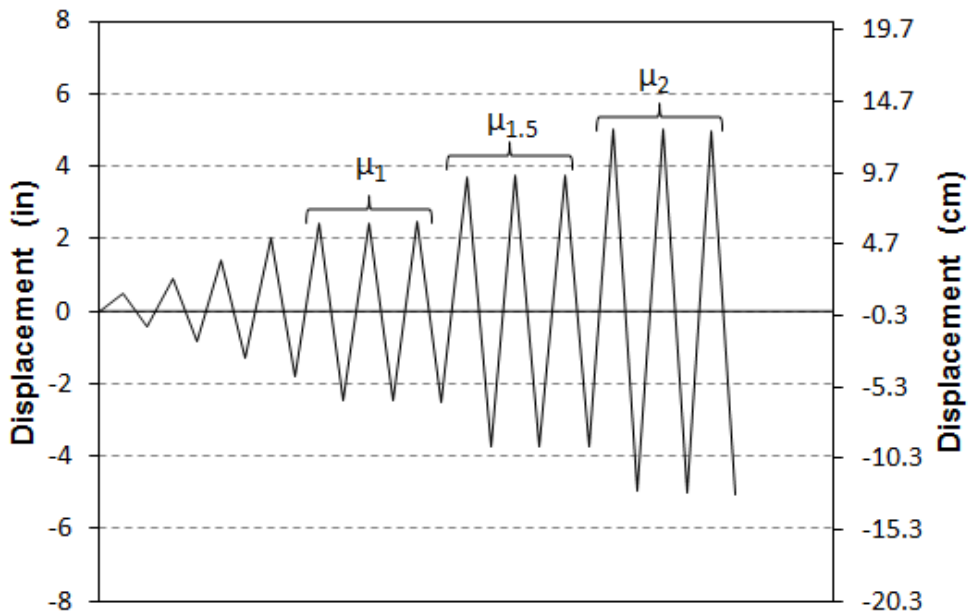

Figure 6.9 Kerf Connection Experimental Displacement History

The instrumentation used in the kerf connection evaluation consisted of traditional laboratory instrumentation as well as the Optotrak motion sensing system as was typical throughout the project. The traditional equipment consisted of inclinometers located 8 inches above the pinned bases to monitor drift magnitudes, linear string potentiometers attached to the bases to monitor any unanticipated base sliding, and strain gauges located on the extreme fibers of each pile cross section as shown in Figure 6.10. Also shown in Figure 6.10, a 2 inch spaced grid of Optotrak LED markers was placed on the east face each pile in both the connection and critical pile regions as also shown in Figure 6.10. The Optotrak markers were placed in a pattern to allow for calculation of strains in the intended pile hinging region as well as the intended capacity protected gusset plate region. Markers were also used to monitor cap beam displacements.

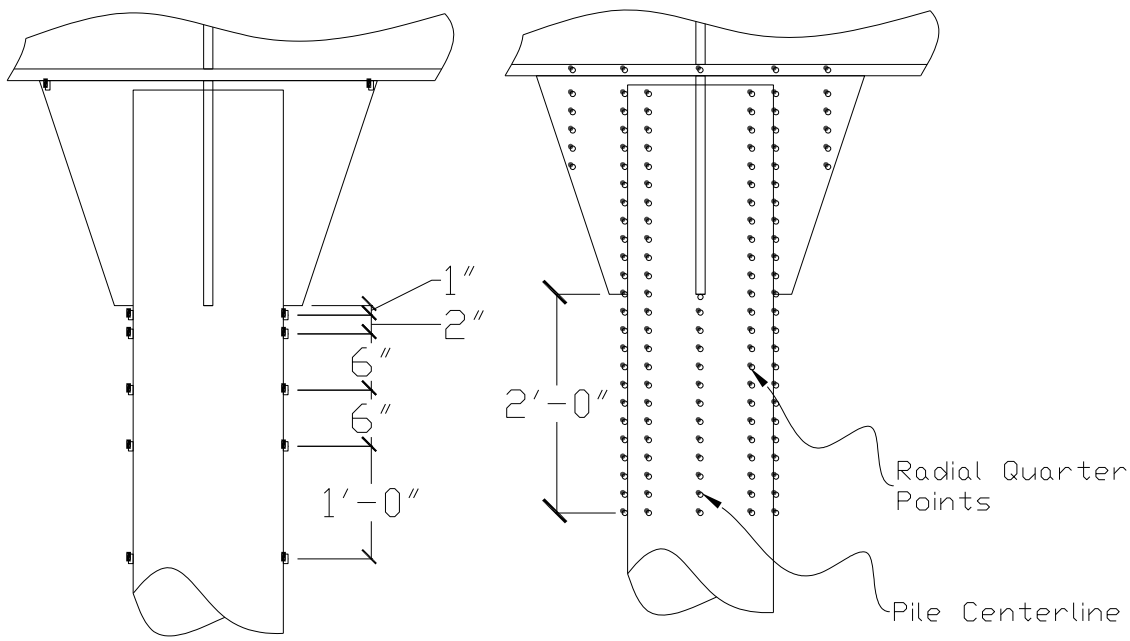

Figure 6.10 Kerf Connection (Left: SG Layout Right: Optotrak Layout)

6.2.3 Finite Element Analysis Simulation

Shell element based Finite Element Analysis was conducted prior to testing of the system in an effort to predict specimen behavior. The model consisted of 8 node linear shell elements that incorporated a multi-linear kinematic hardening material model which was based on actual in-house tensile material tests. The model also incorporated non-linear geometric formulations in order to capture the effects of local buckling on the overall specimen behavior. The three cycle set load history utilized in the simulation was based on the theoretical first yield force assuming a pile hinging mechanism below the gusset plate region and a FEA predicted first yield displacement of 1.56 in. In the case of the kerf connection, the analytical model, shown in Figure 6.11, took advantage of the relatively symmetric nature of the two column pier configuration to reduce the model size by employing a roller boundary condition at the centerline of the pier.

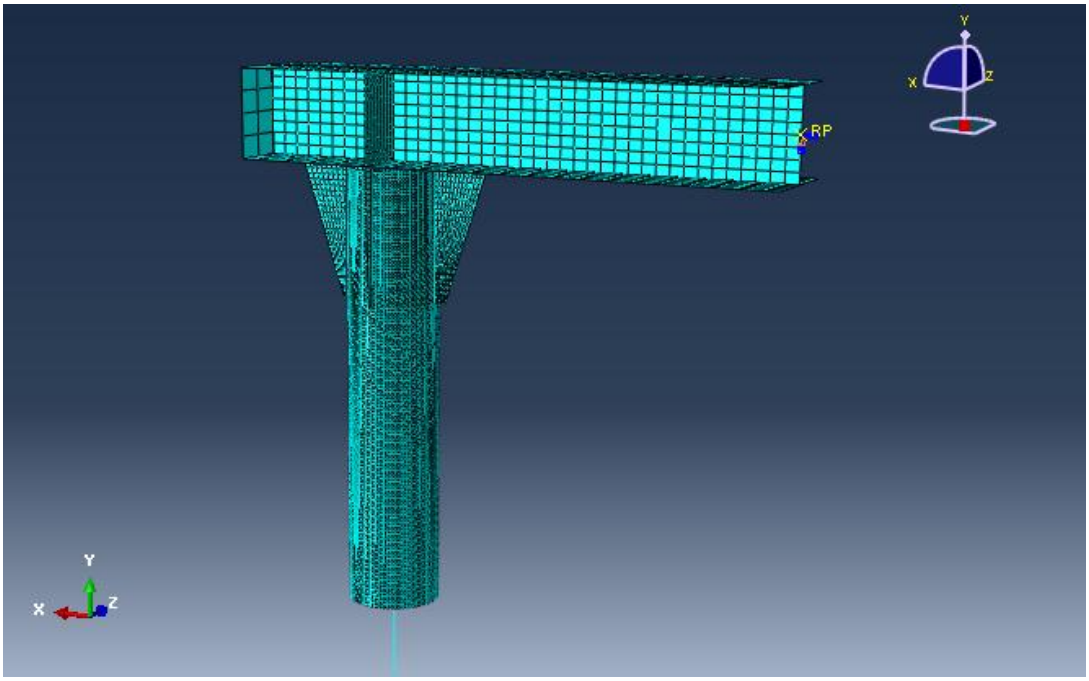

Figure 6.11 Kerf Connection Finite Element Model

The results of the numerical simulation indicated a stable response could be expected prior to the third ductility level where noticeable local buckling of the wall would develop resulting in strength degradation throughout the ductility three cycles with continued degradation in the ductility 4 cycles. These effects can be seen in Figure 6.12 and Figure 6.13 which visually illustrate the development of local buckling and indicate the associated strength degradation respectively. Further cycles of the load history showed an increase in local buckling and subsequent strength loss. However, base material and weld fracture were not considered in the FEA analysis as has been discussed. Related to this issue, it is important to note that considerable strain concentrations were expected to develop at the base of the gusset plate in the pile wall even at low levels of response as is shown in Figure 6.14. The observed strain concentration was potentially due to the abrupt stiffness change at the given interface between the pile wall and gusset plate. From this observed result, it was considered a possibility that weld or base material cracking may develop in this general region prior to the formation of the more desirable failure mode of pile wall local buckling.

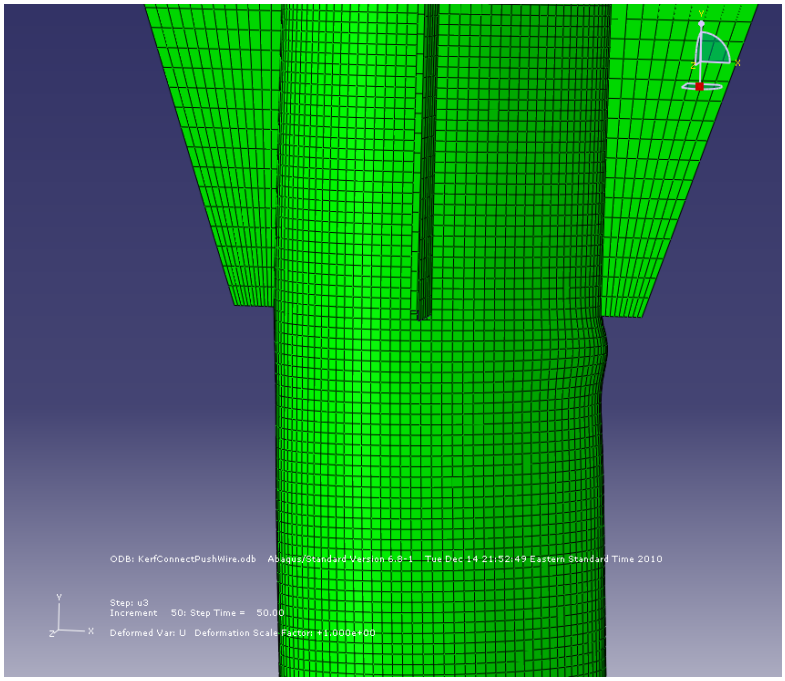

Figure 6.12 FEA - Local Buckling Ductility 3 Cycle 1

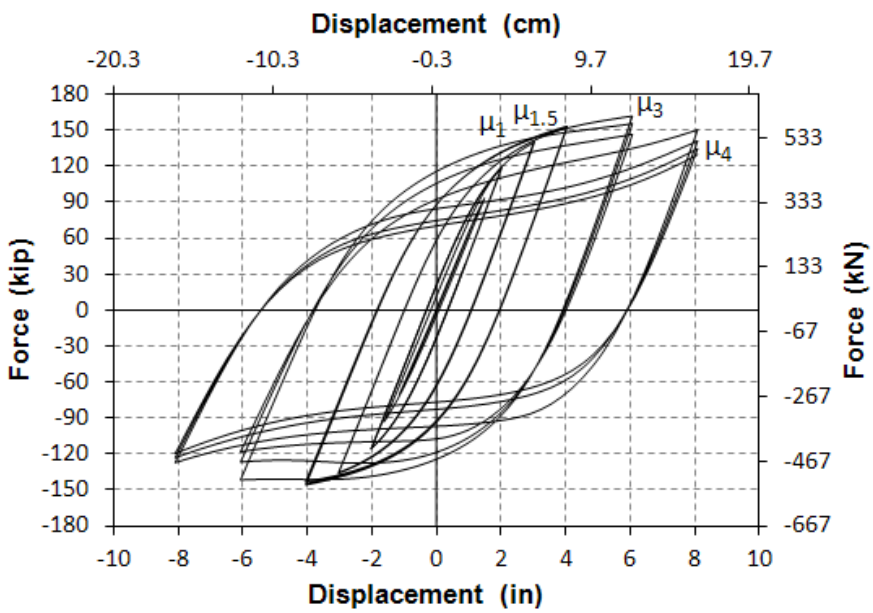

Figure 6.13 FEA-Force Displacement Hysteresis

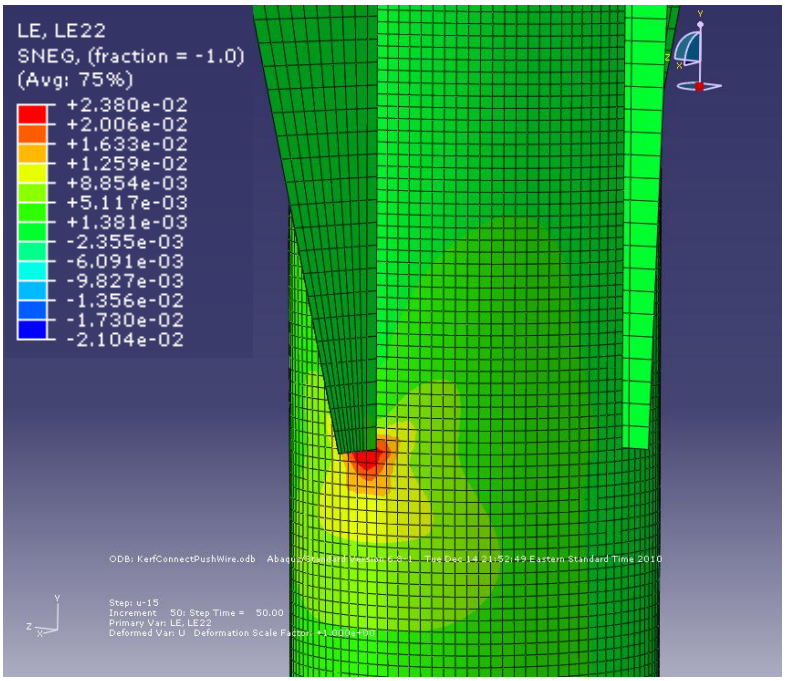

Figure 6.14 FEA- Example of Strain Concentration at Base of Gusset Plate

6.2.4 Experimental Summary

The results of experimental testing showed the specimen to perform well in the elastic portion of the load history as well as through the ductility 1.5 cycles as can be seen in Figure 6.15 and Figure 6.16. As is also shown by these figures, the specimen was able to achieve the full plastic moment capacity of the pile section correlating to a lateral load of 121 kips as shown by the plateau of the force – displacement response. As has already been noted, the experimental first yield displacement was found to be 1.92 inches leading to a ductility 1 displacement of 2.50 inches. Although this is larger than FEA predicted first yield displacement of 1.56 inches, the difference is likely attributable to calibration of the FEA kinematic hardening material model.

During the ductility 1.5 cycles, slight local buckling was noted in the extreme fibers of the piles, as is shown Figure 6.17, which corresponded to a minor loss in load as is evident in the force displacement hysteresis and cycle envelopes shown in Figure 6.15 and Figure 6.16 respectively. As the load history proceeded into the ductility 2 displacement level, cracking developed in the base pile material in the south (tensile) face of the north pile as is shown in Figure 6.18. The remaining cycles of the ductility 2 level lead to development and propagation of base material cracking at each of the four extreme fibers of the piles as is shown Figure 6.19 and Figure 6.20. At the conclusion of the ductility 2 cycles, cracking had propagated around the majority of each pile and the global strength capacity had been reduced by approximately 40%. At this point the test was assumed to be completed and the specimen was returned to a neutral position.

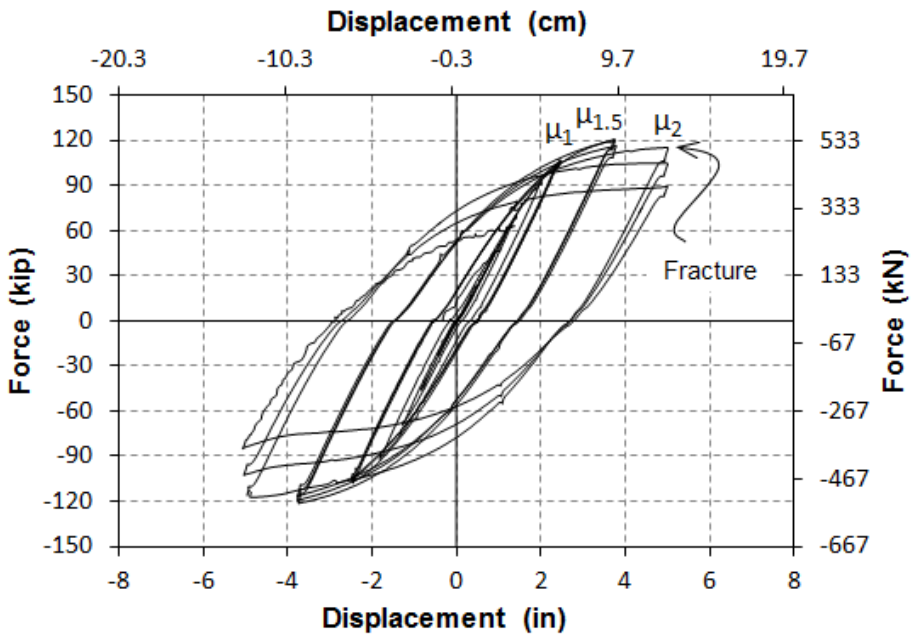

Figure 6.15 Phase 2 Test 1 Kerf Connection Force – Displacement Hysteresis

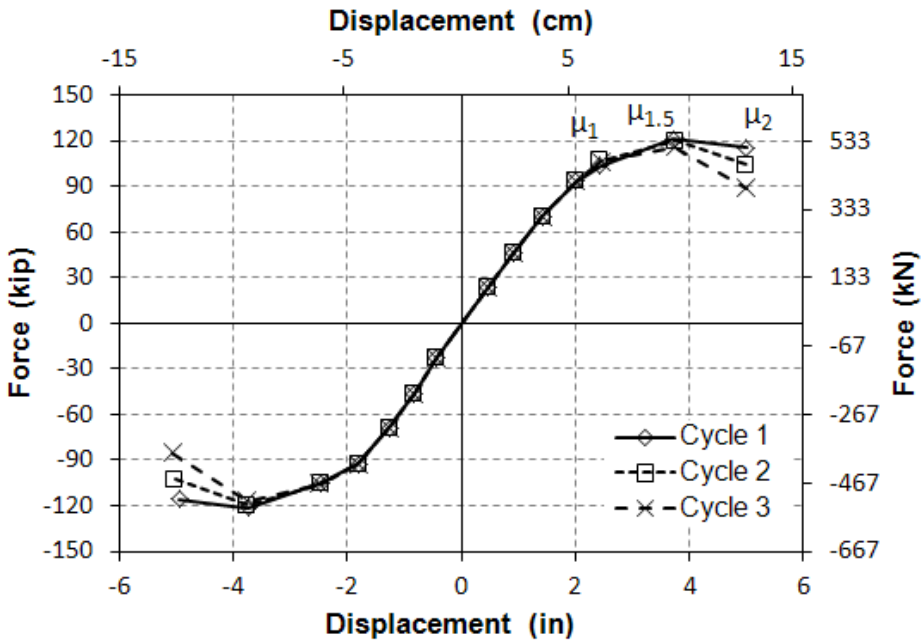

Figure 6.16 Phase 2 Test 1 Kerf Connection Force – Displacement Envelopes

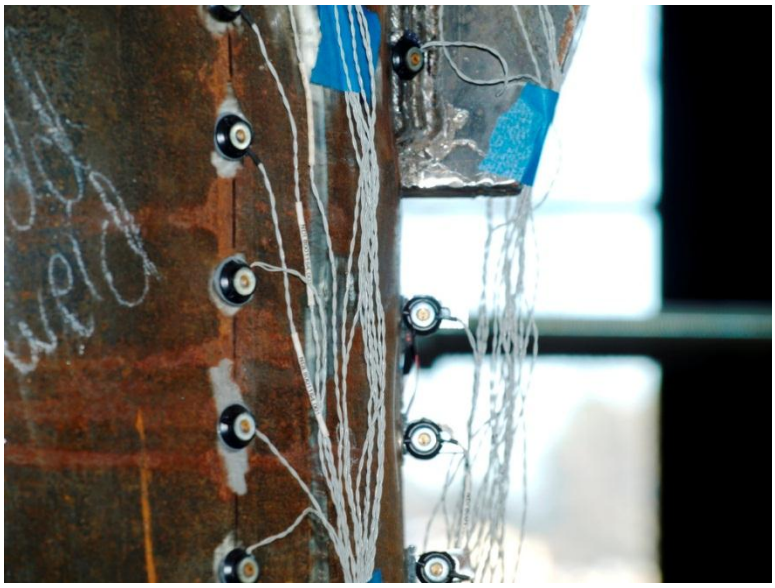

Figure 6.17 North Pile South Face, Ducitlity 1.5 Cycle -3, -112 kips, -3.75 in

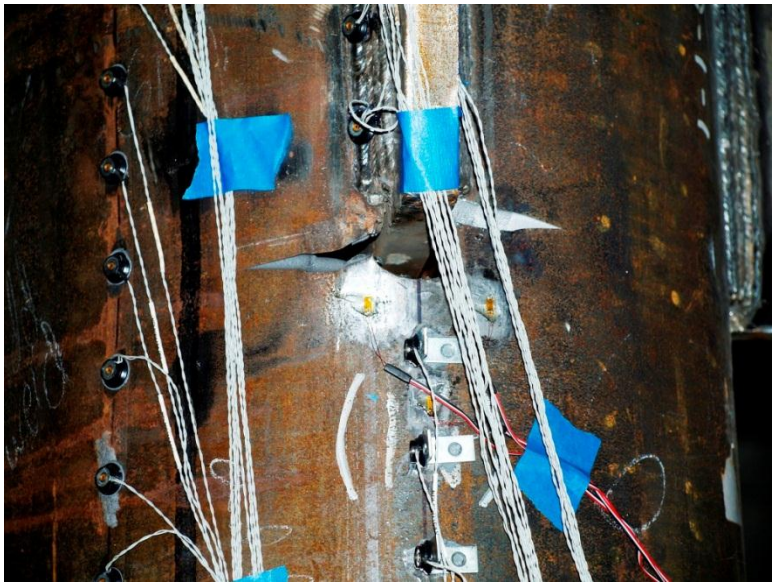

Figure 6.18 North Pile South Face, Ducitlity 2 Cycle 1, 112 kips, 5.00 in

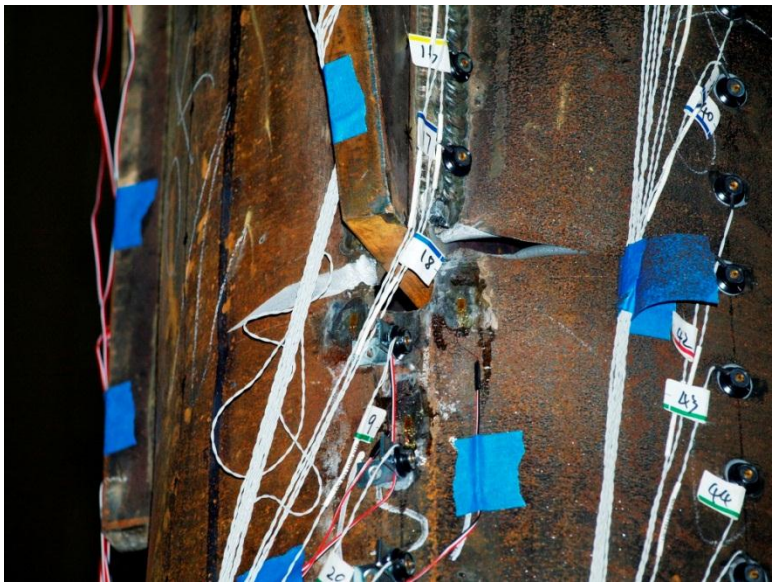

Figure 6.19 South Pile North Face, Ducitlity 2 Cycle -2, 100 kips, .00 in

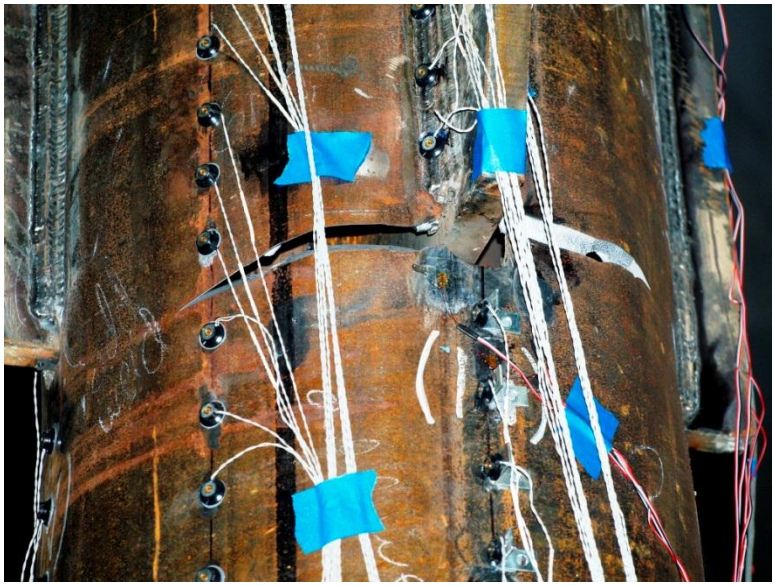

Figure 6.20 North Pile South Face, Ducitlity 2 Cycle 3, 85 kips, 5.00 in

Considering the results of the experimental test, it appeared that the FEA predicted strain concentration at the base of the gusset plate had generated the cracking failures that were observed. In order to evaluate the magnitude of the strain demand that was present in the cycles prior to cracking, both traditional strain gauge data and Optotrak data were evaluated. Figure 6.21 through Figure 6.24 plot the bending strain demands recorded by strain gauges located on the extreme fibers of each pile. Each graph plots the strain recording at a given vertical location below the critical section of the pile, in this case at the base of gusset plates, for the first cycle of each ductility level in a given direction of loading.

As was predicted by FEA, significant strain concentrations were shown to exist immediately below (1 in.) the gusset plate termination point. The intensity of the concentration appeared to be approximately equal on the tensile and compressive faces. At ductility 1.5, the displacement ductility level immediately prior to cracking, the data indicated strain levels in the range of 20000με - 35000με except on the north face of the north column which could be due to a malfunctioning strain gauge. This range of strain magnitudes recorded by the strain gauges immediately below the gusset plate termination

point, is confirmed by the strain hysteresis recorded from Optotrak data in the gauge length encompassing the termination of the gusset plate. This is shown in Figure 6.25 and Figure 6.26 which both indicate strains of approximately +/- 25000 με – 35000 με were present at a ductility level of 1.5. The concentrated nature of this strain demand is highlighted by Figure 6.19 and Figure 6.20 which show the Optotrak strain hysteresis on both faces of the south pile 3 in. below the termination of the gusset plate, to be limited to approximately 10000 με prior to the develop of the slight local buckling at ductility 1.5 which occurred near these gauge lengths.

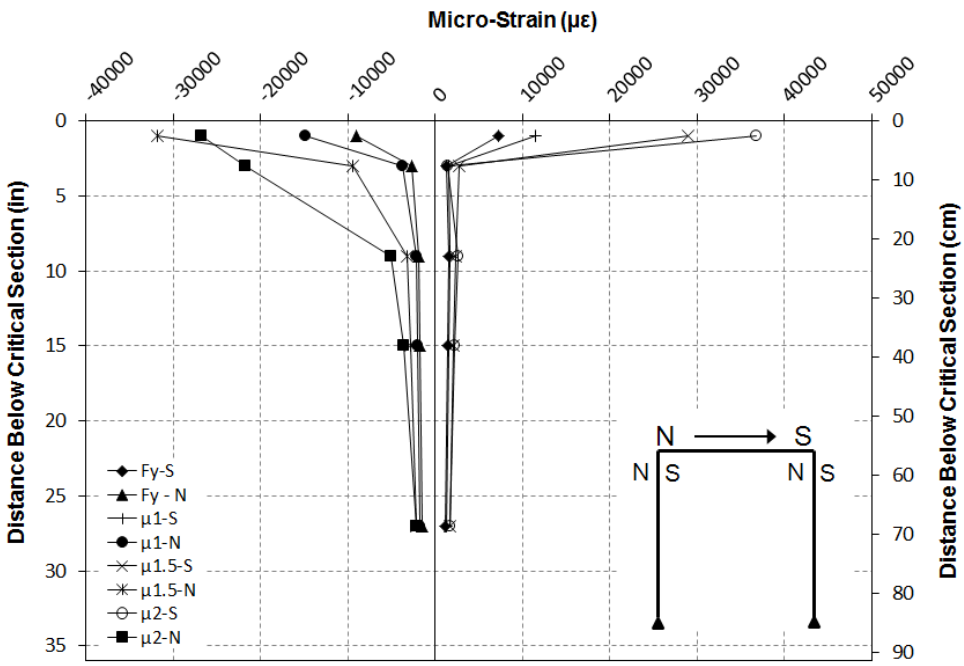

Figure 6.21 Test 1 - S. Col. - 1st Positive Cycles Strain Profiles

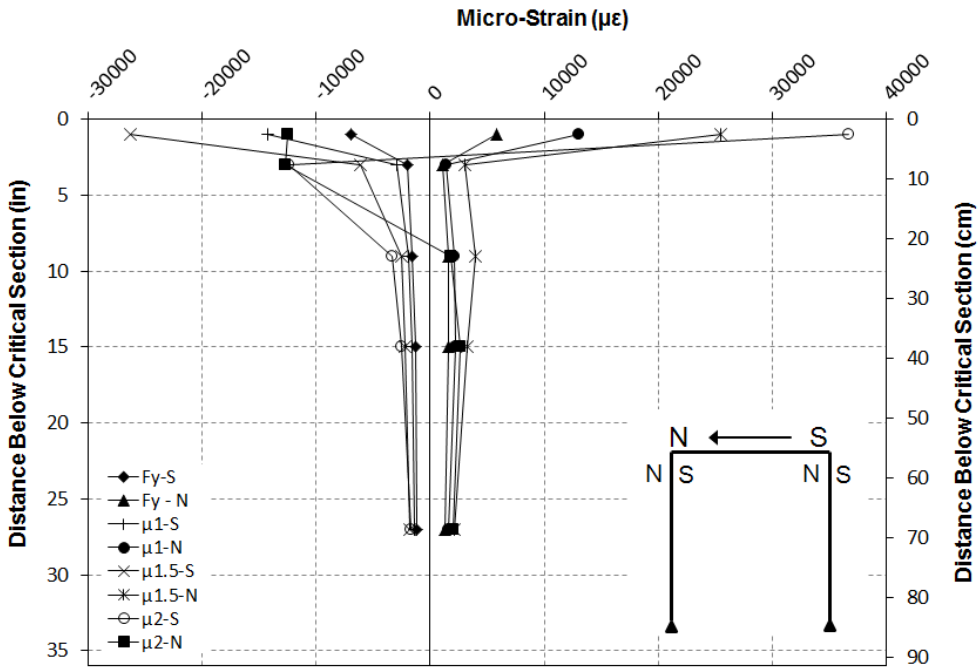

Figure 6.22 Test 1 - S. Col. - 1st Negative Cycles Strain Profiles

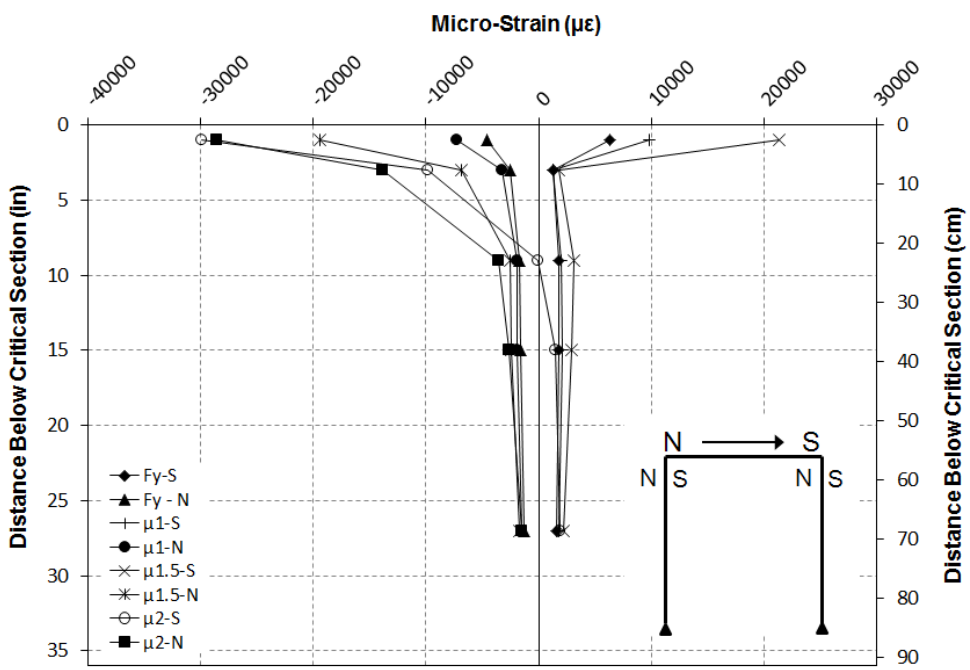

Figure 6.23 Test 1 - N. Col. - 1st Positive Cycles Strain Profiles

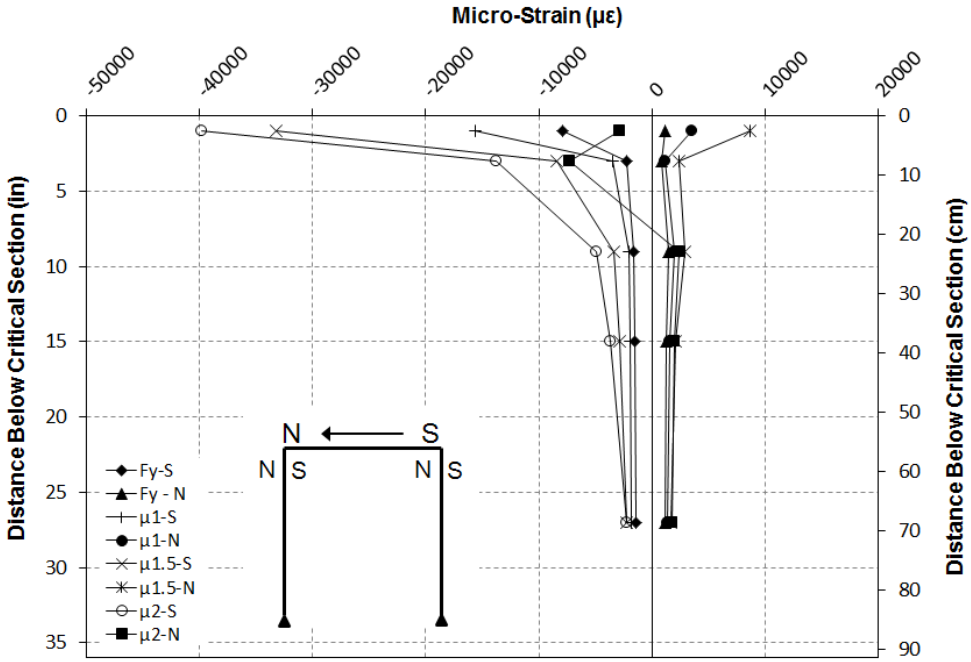

Figure 6.24 Test 1 - N. Col. - 1st Negative Cycles Strain Profiles

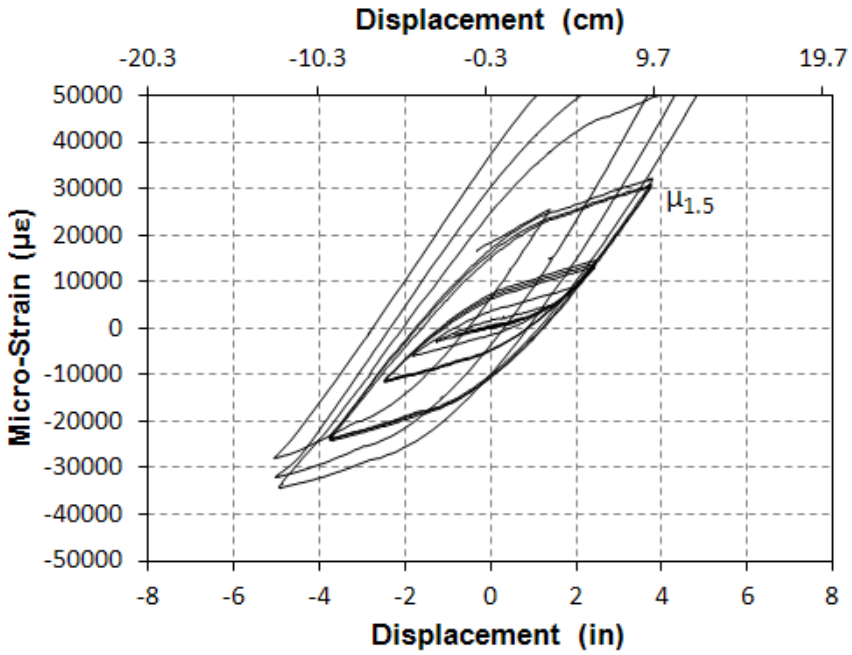

Figure 6.25 Optotrak Strain Hysteresis - S. Col. S. Face at Gusset Termination

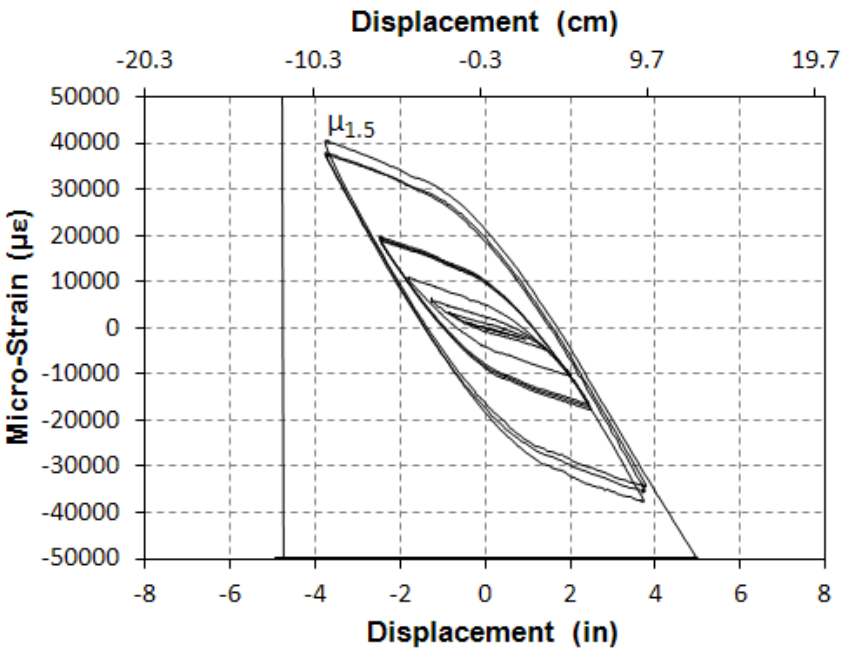

Figure 6.26 Optotrak Strain Hysteresis - S. Col. N. Face at Gusset Termination

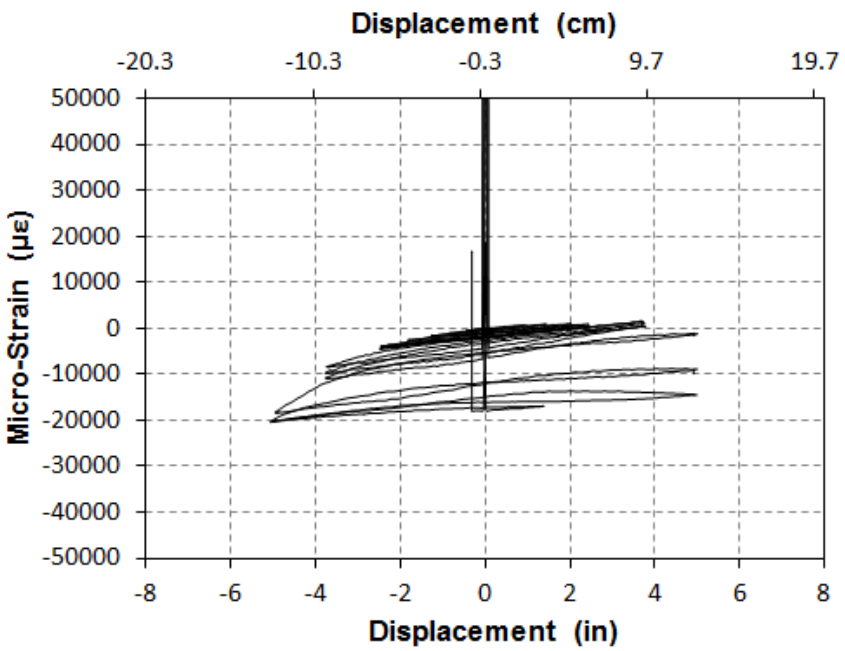

Figure 6.27 Strain Hysteresis - S. Col. S. Face 3 in. Below Gusset Termination

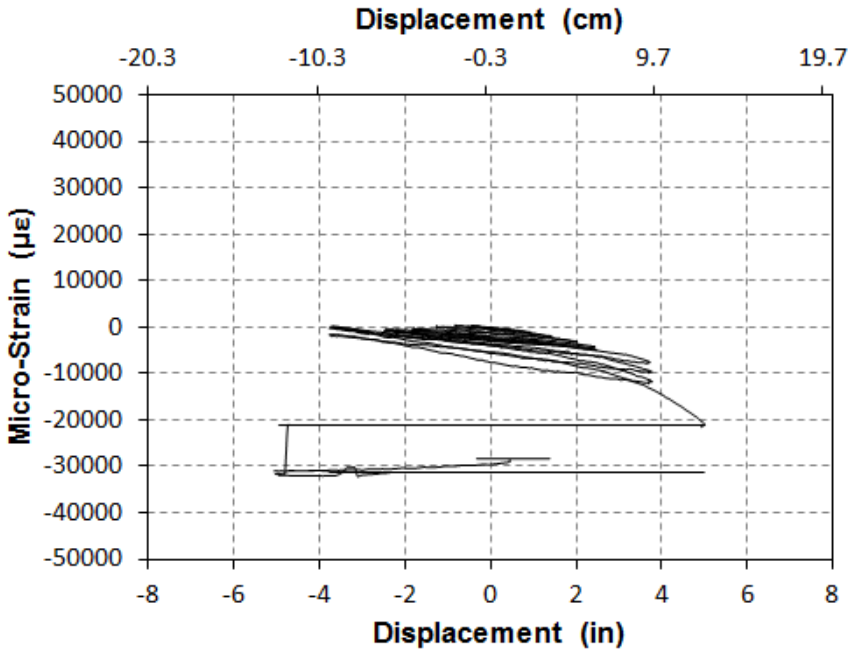

Figure 6.28 Strain Hysteresis - S. Col. N. Face 3 in. Below Gusset Termination

The strain demands predicated by the FEA modeling indicated a range of +/- 21000 με – 29000 με at the ductility 1.5 displacement level, suggesting good agreement between the modeling results and both styles of laboratory instrumentation. This result helps to support the conclusion that the model appropriately captured the localized response with the exception of incorporating cracking into the simulation. The strain distributions determined from modeling, at the ductility 1.5 level, are shown in Figure 6.29 and Figure 6.30.

It should be noted, that although a significant strain concentration has been shown to occur in the region encompassing the termination of the gusset plate, the associated magnitude of the strain (approximately 30000 με or 3%) seemed to be too low to induce cracking in the base material as most steel can exhibit 20%-30% ultimate elongation in direct tension tests. However, it is also well founded that stress and strain concentrations develop around discontinuities such as the base of the gusset slot. Noting that the strain gauges were approximately 1 inch from the end the slot and that the Optotrak strains calculated in this

region were determined from a gauge length of approximately 2.5 inches which encompassed but was not limited to the end of the slot (as shown in Figure 6.17), it is likely that the magnitude of the strains determined from these instruments was lower than the actual strain magnitude at peak concentration near the slot.

As shown in Eq.(6.2), theoretical mechanics, discussed in detail in (Boresi, 2003), can be used to estimate the maximum strain demand magnitude when the recorded strains are taken as the normal strain in the general region of the discontinuity (ε_n) and the maximum stress (σ_{max}) is considered to be equal to the normal stress in the region (σ_n) as the stress state is well into the plateau of the material response. In the case of a small hole in a large plate which is similar to the end of the slotted region, the elastic stress concentration factor (S_{cc}) approaches the value of 3. When these parameters are considered, the maximum strain at the discontinuity can be estimated by Eq.(6.3), which results in a value of 270000 με (27%) considering the recorded value of approximately 30000 με. Although this is only an estimate and considers several assumptions, it does display that the maximum strains experienced at the edge of the discontinuity were likely much larger than that captured by the FEA or laboratory instrumentation results.

$$\sigma_{\max}\varepsilon_{\max} = S_{cc}^{\ 2}\sigma_n\varepsilon_n \tag{6.2}$$

$$\varepsilon_{\max} = 9\varepsilon_n \tag{6.3}$$

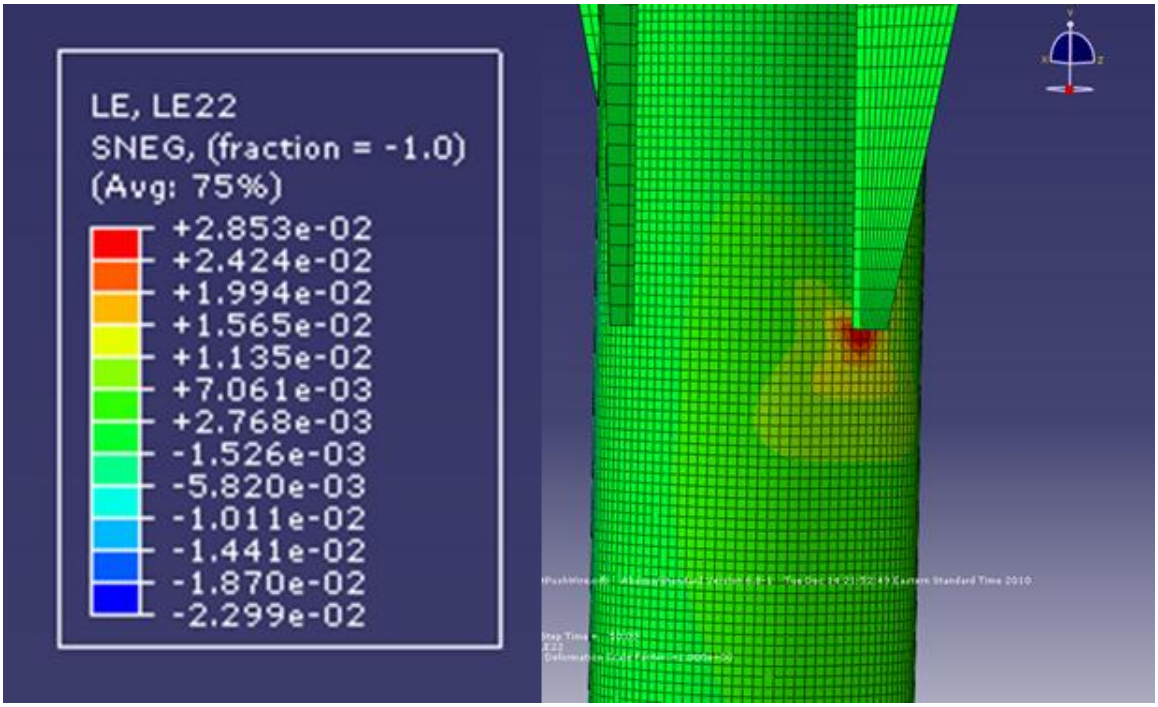

Figure 6.29 FEA- Strain Distribution at Ductility 1.5, 29000με Tensile

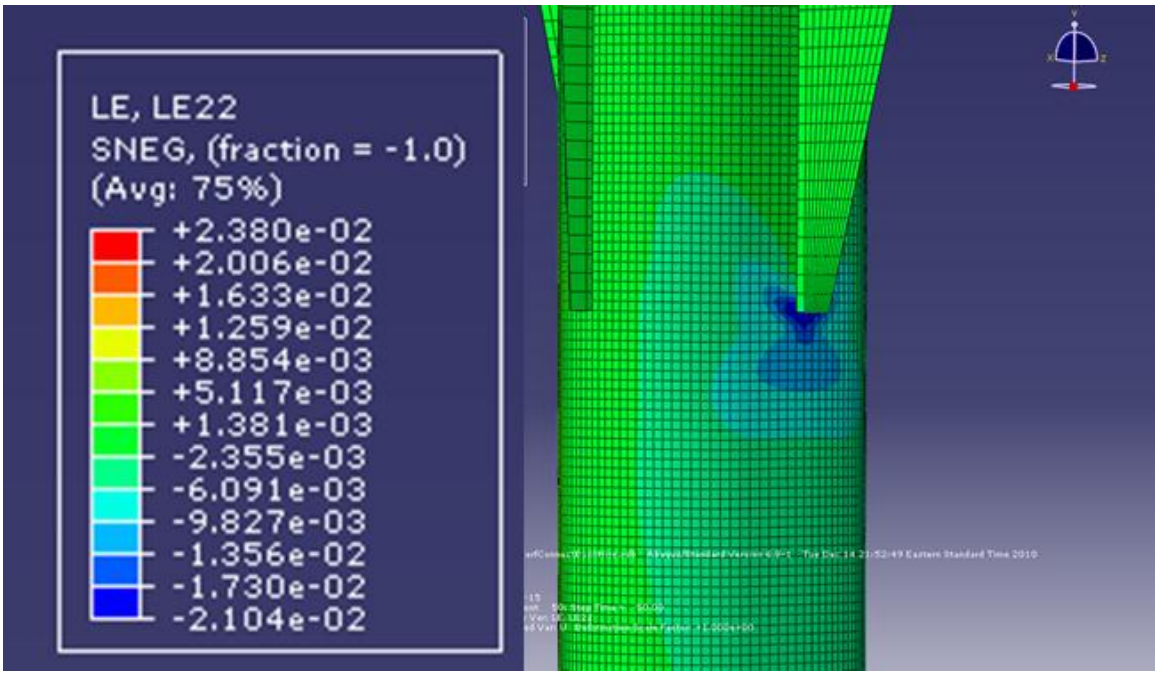

Figure 6.30 FEA- Strain Distribution at Ductility 1.5, 21000με Compressive

6.2.5 Kerf Connection General Conclusions

Although the test 1 kerf connection experimental specimen was able to develop the full moment capacity of the pile section, the ductility capacity of the assembly was limited. Based on the results of the evaluation, the connection design was able to achieve a reliable displacement ductility of 1-1.5 prior to brittle cracks forming in the base pile material similar to that depicted in the schematic provided in Figure 6.31. Although the required ductility of a system is a function of the design scenario involving seismic hazard, system configuration, and allowable damage levels, the reliable ductility capacity of this system would likely be insufficient in even low seismic regions for most applications.

Taking this into account, the researchers would not recommend the use of this style of connection in design without special considerations regarding the development of cracks in the low range of the non-linear response. Although the connection configuration was able to locate damage away from the cap beam interface and was able to capacity protect critical welds which were the two key criteria of modified weld protected connections, the geometry of the configuration did not allow for the desirable failure mechanism of pile wall local buckling to develop. It should also be noted, considerable differences existed between the FEA predicted Force – Displacement hysteretic behavior and that of the experimental evaluation. Although the general shapes were similar, the model overestimated the strength capacity of the system by approximately 25% which is likely the results of insufficient material model calibration. However, given the general poor performance of the experimental tests, the decision was made to not focus additional research effort on calibration of the Finite Element Model for this connection configuration.

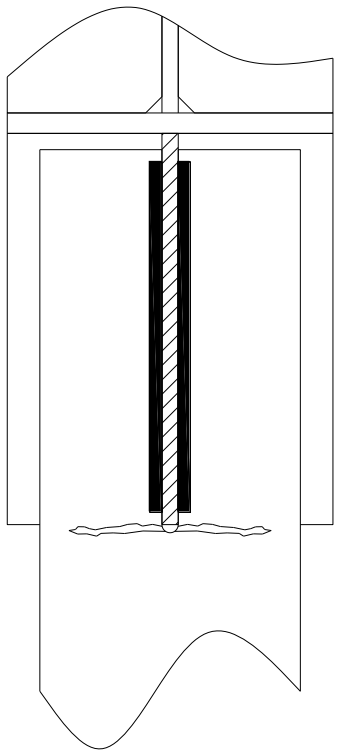

Figure 6.31 Kerf Connection – Brittle Cracking at Base of Gusset Plate

6.3 Column Capital Connection

6.3.1 Introduction and General Discussion

The sixth test of the first phase of steel pier testing at NCSU aimed at evaluating the performance and capabilities of a flared column capital connection to perform as a modified weld protected connection configuration. The capital assembly used in the configuration consisted of a rolled and welded circular pipe section formed from ASTM A572 Gr. 50 plate material which had a thicker upper region than that of the HSS16x0.500 piles intended to capacity protect the critical welded interface region between the capital and cap beam soffit. More specifically, the assembly shown in Figure 6.32, was fabricated by rolling plate into

two 180 degree sections which were then welded together with complete joint penetrating welds. After welding the plates, the lower 8 in. of the assembly was machined to reduce the thickness of the fabricated pipe section to match that of the HSS16x0.500 piles. This turned-down section was intended to behave as a buckling region to isolate damage away from any welded sections, noting that no welding between the upper thick section and lower thinner section existed. Details of the assembly are shown in Figure 6.33. Fabrication documentation for the capital assemblies including material certifications and UT inspection are provided in the appendix of this document.

Figure 6.32 Phase 1 Test 6 – Flared Column Capital Assembly

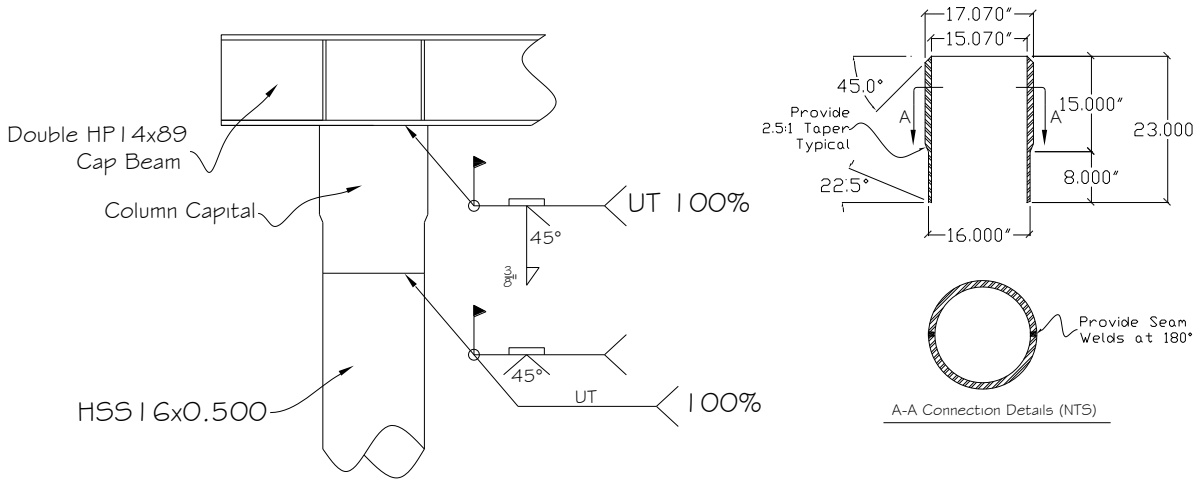

Figure 6.33 Column Capital Connection Detail

The design of this system was based on the principle that the critical section of the flared column capital (adjacent to the cap beam flange) should remain elastic as the full plastic flexural over-strength moment capacity at the intended hinge region just below the flared section was developed. Taking into account the moment demand extrapolated from the hinging region to critical welded region at the top of the assembly, a maximum depth of flared section (X_m) could be determined for a given flared section thickness as shown in Eq.(6.4) and Figure 6.34. The assembly was then detailed with a depth of flared section less than the maximum calculated value which, in the case of the test pier, resulted in a 15 in. deep flared section for a 1 in. flared section wall thickness.

Although no minimum depth of flared section was determined by calculations, it was assumed that 15 in. was a reasonable length by which to relocate damage to avoid areas of strain concentrations based on past experimental and analytical results. The capital assembly was designed to be connected to the cap beam with a CJP weld that included a 3/8 in. reinforcing fillet and to the HSS16x0.500 pile section with a CJP splice weld. By designing the section for the top weld to remain elastic, it was anticipated that the strains would remain low enough to preclude connection region cracking, similar to that seen in the prior tests, as

all standard welded details were shown to behave with no signs of failure in the elastic range of loading.

$$X_d \leq X_m = H - \frac{Hf_y Z_{hinge} O}{f_y S_{pz}} \tag{6.4}$$

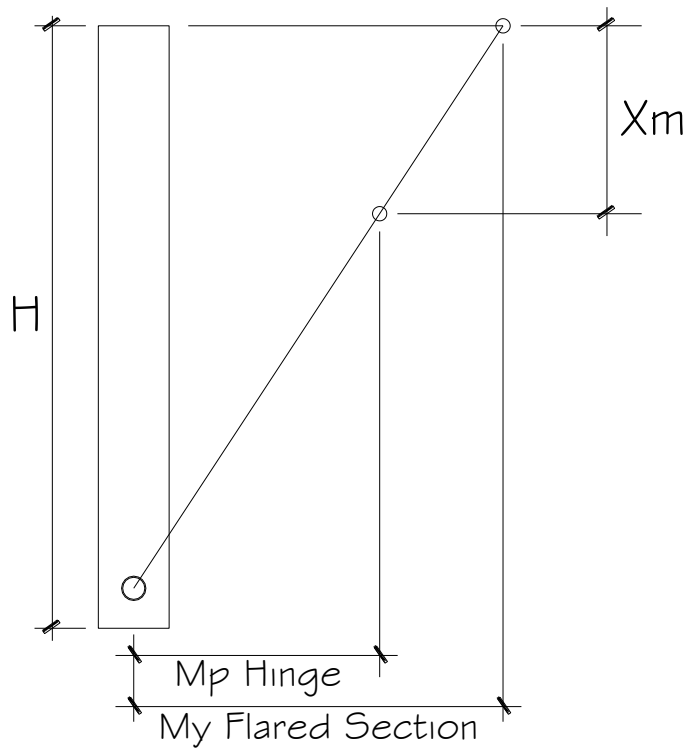

Figure 6.34 Capital Assembly Design Criteria

Typical of all experimental work in this project, consideration was given to the repeatability and practicality of the bent construction process. A process similar to that of test 5 (phase 1) was used and has been described in Figure 6.35. Both the top CJP weld and the lower splice weld were inspected by visual and UT technique and the resulting

documentation is provided in the appendix of this document. It is also important to note that a 3/8 in. reinforcing fillet was used in the top weld of the assembly to the cap beam flange. Although this may have been unnecessary given the elastic design intention of the joint, it was desired to help relieve the sharp geometry of a plane complete joint penetration weld as this had been shown to improve the performance of standard welded connections.

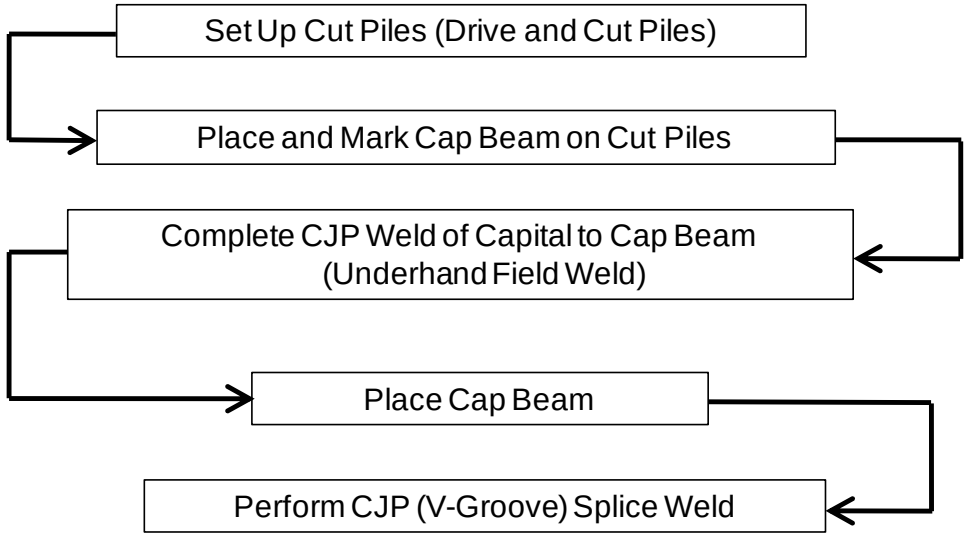

Figure 6.35 Construction Sequence of Test 6

6.3.2 Load History and Instrumentation

The experimental evaluation of the column capital configuration followed the typical three cycle set load history. Assuming a critical cross section formed immediately below the flared capital, as was the design intention, and taking into account the anticipated material yield stress of 54 ksi, a first yield force of 79.7 kips was used for the force controlled loading increments loading protocol. An experimentally determined average first yield displacement of 2.33 in. resulted in a ductility 1 displacement magnitude of 3.03 in.

Again, the instrumentation used in the experimental evaluation consisted of both traditional equipment and the Optotrak system. The traditional equipment consisted of

inclinometers at the base of pile section and electric resistance strain gauges oriented to evaluate bending strain demands along the pile and column capital elements of the system. The typical 2 in. spaced grid of Optotrak markers was placed on the west face of the south pile in the flared capital region, intended hinging region, and the pile region below the splice weld to monitor behavior through the full connection assembly region.

6.3.3 Experimental Summary

The column capital experimental specimen showed no signs of failure through the displacement ductility 1.5 level and began to develop slight local buckling in both piles during ductility 2 cycles although no evident associated strength loss was experienced at this displacement level as shown in Figure 6.36 and Figure 6.37. This local buckling progressed throughout the cycles of ductility 2, 3, and 4 as shown in Figure 6.38. The slow propagation of the local buckling on both columns allowed for degradation of the structure's strength to also take place over multiple cycles of loading and multiple displacement ductility levels as shown in the experimental Force – Displacement response. Ultimately, failure was dictated by base material rupture at a location of local buckling on the south column as shown in Figure 6.39. This rupture was not associated with a welded zone and occurred after approximately 30% strength loss was experienced by the pier.

As has been noted and is further indicated by Figure 6.40, the local buckling mechanism observed during testing occurred below the intended hinging region of the flared column capital which had a matching outer diameter and thickness to that of the HSS16x0.500 piles. Initial speculation of why this occurred included the possibility that the entire capital assembly was acting as a rigid end more than a flexural member for an unknown reason. As seen in Figure 6.41 through Figure 6.48, flexural strains were present in the capital indicating it was not acting as a rigid end block but as a flexural member as intended. These figures provide extreme fiber vertical strain profiles along the length of the columns from Optotrak data for the south pile and strain gauge data for the north pile. However, as shown the strains

were marginally higher immediately below the intended hinging region and splice weld, potentially explaining the observed local buckling behavior in this HSS16x0.500 pile. Further it is important to note, both forms of strain data collection indicate similar trends along the entire length of the instrumented regions and that the flared capital section did essentially remain in the elastic range of loading as was the design intention.

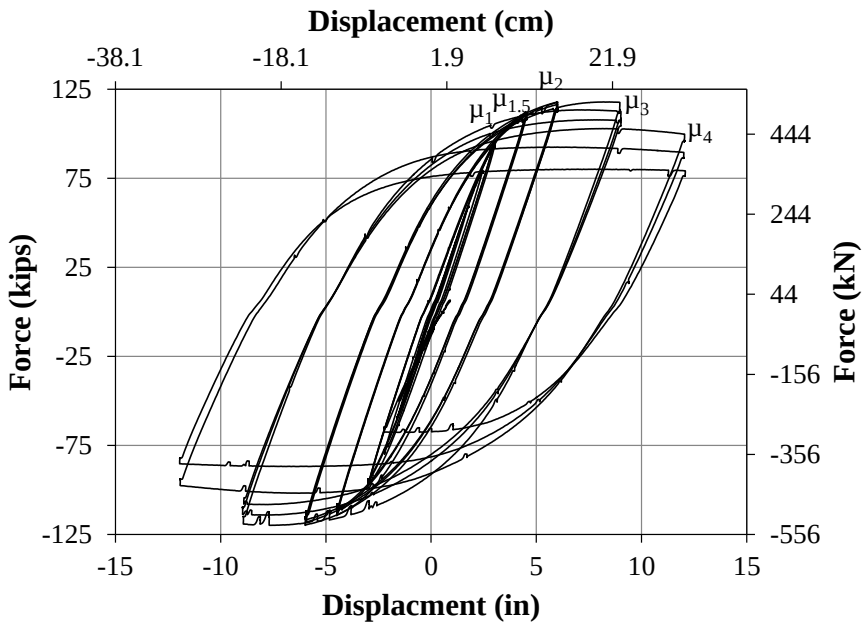

Figure 6.36 Phase 1 Test 6 Column Capital Force – Displacement Response

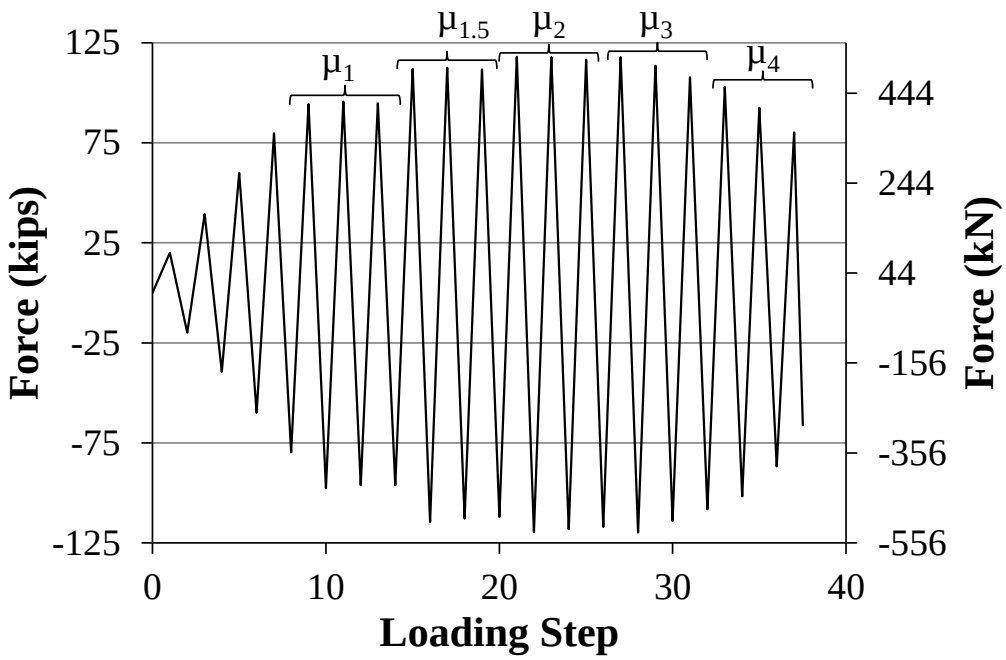

Figure 6.37 Phase 1 Test 6 Column Capital Force – Displacement Envelopes

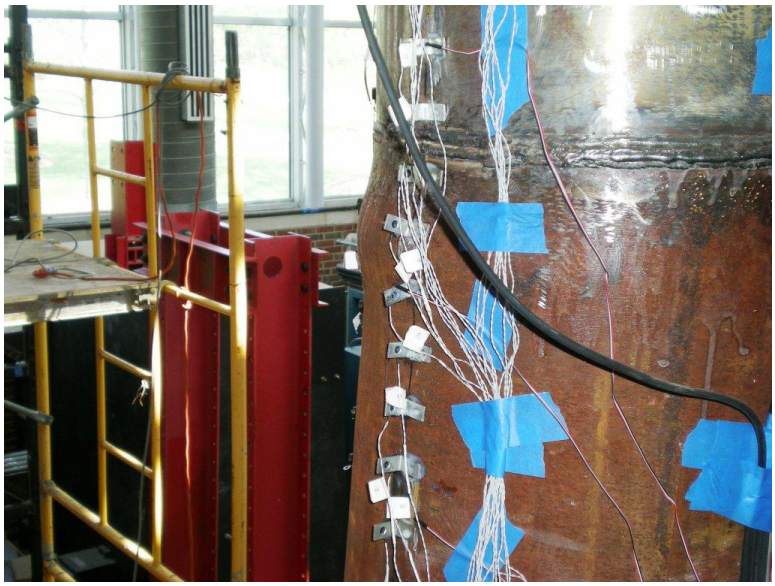

Figure 6.38 Propogation of Local Buckling – Ductility 3 Cycle 1

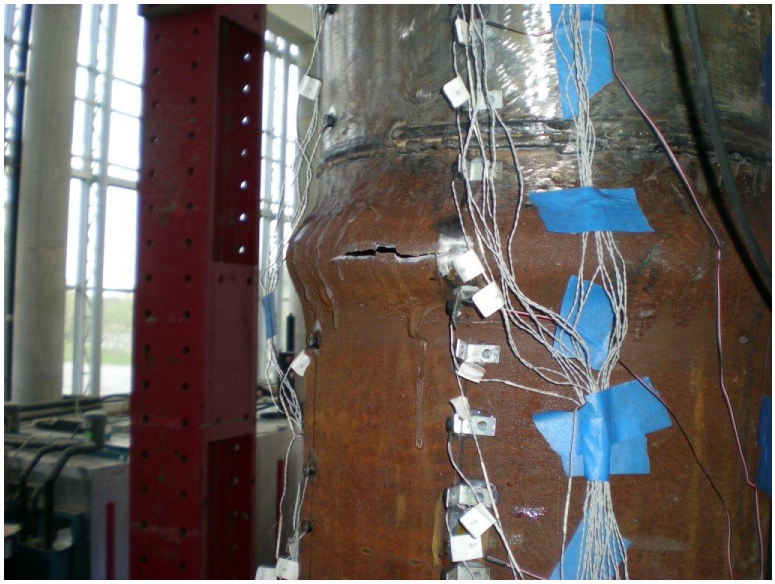

Figure 6.39 Phase 1 Test 6 Rupture – South Column North Face – Ductility 4 Cycle -3

Figure 6.40 Buckled Pile Wall Below Intended Hinging Region

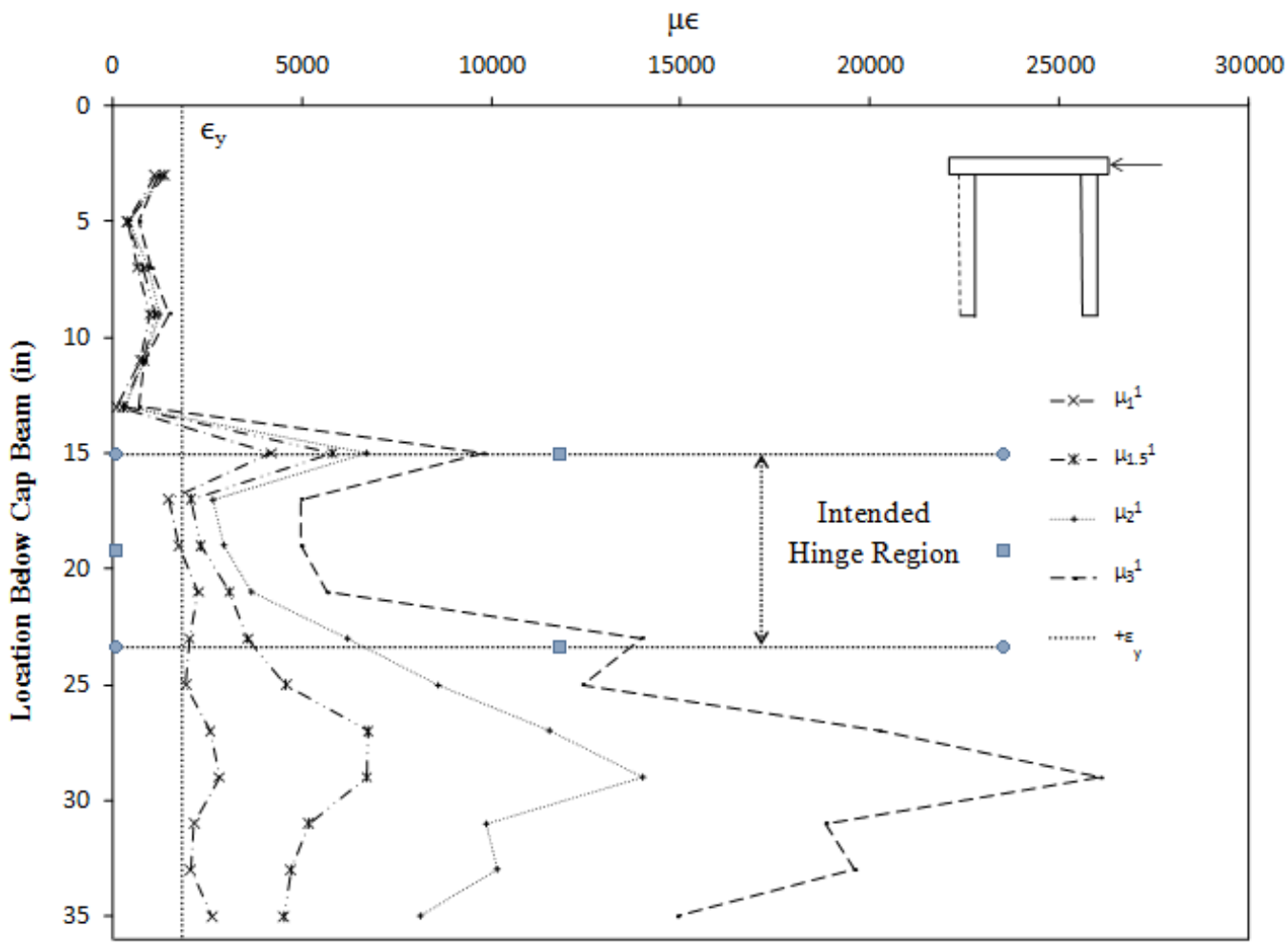

Figure 6.41 Optotrak Vertical Strain Profile – South Column South Face Push Direction

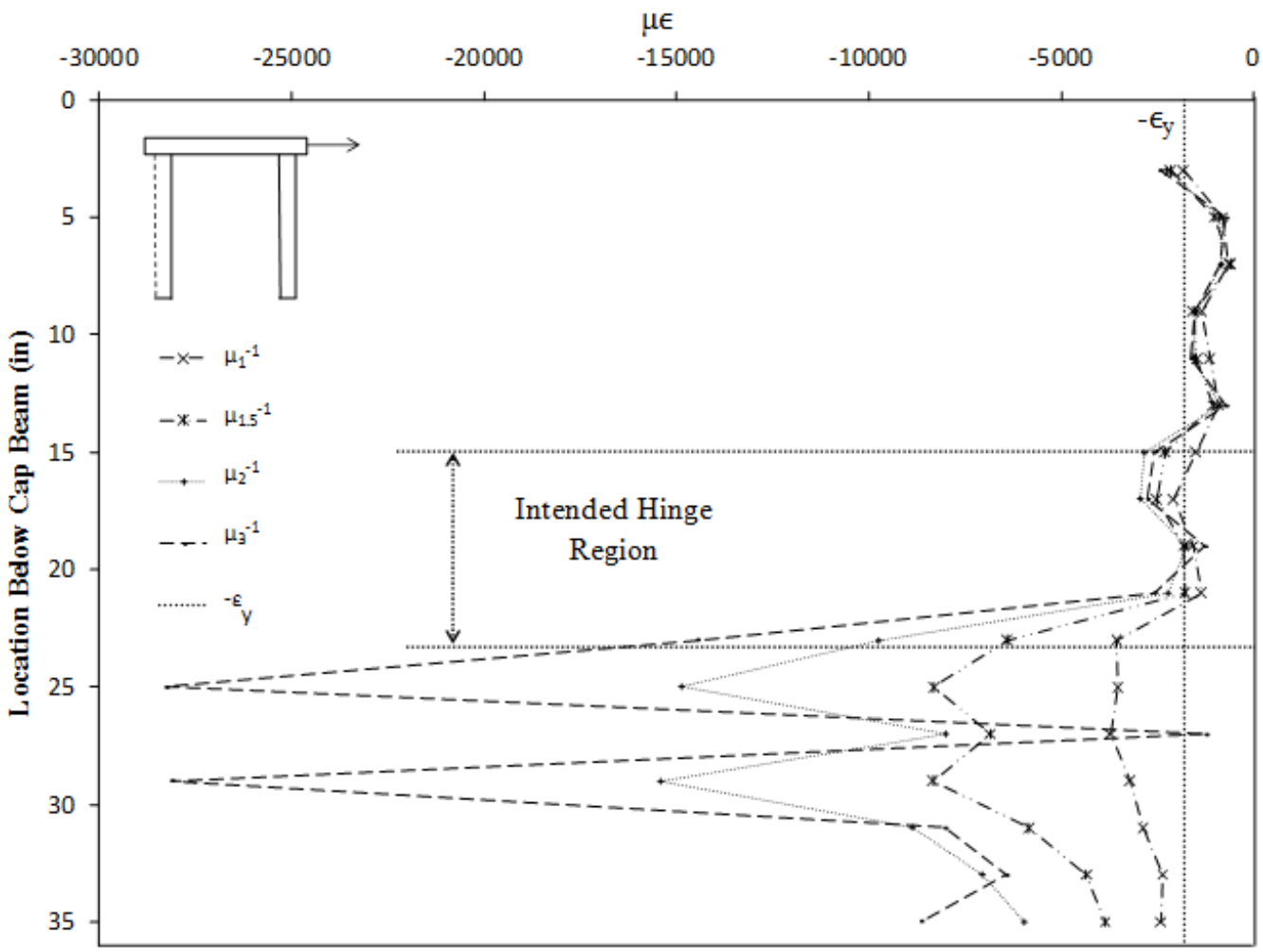

Figure 6.42 Optotrak Vertical Strain Profile – South Column South Face Pull Direction

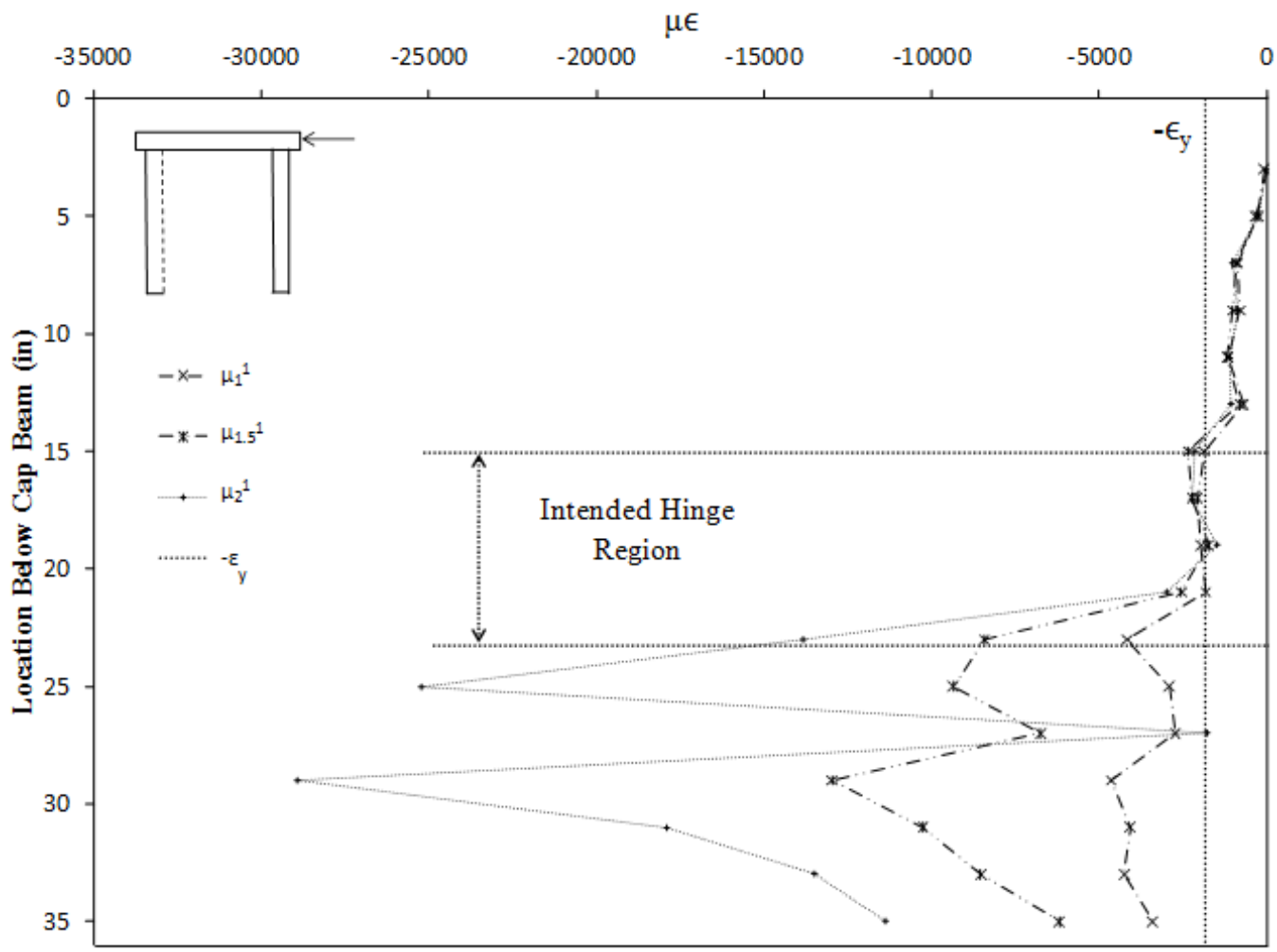

Figure 6.43 Optotrak Vertical Strain Profile – South Column North Face Push Direction

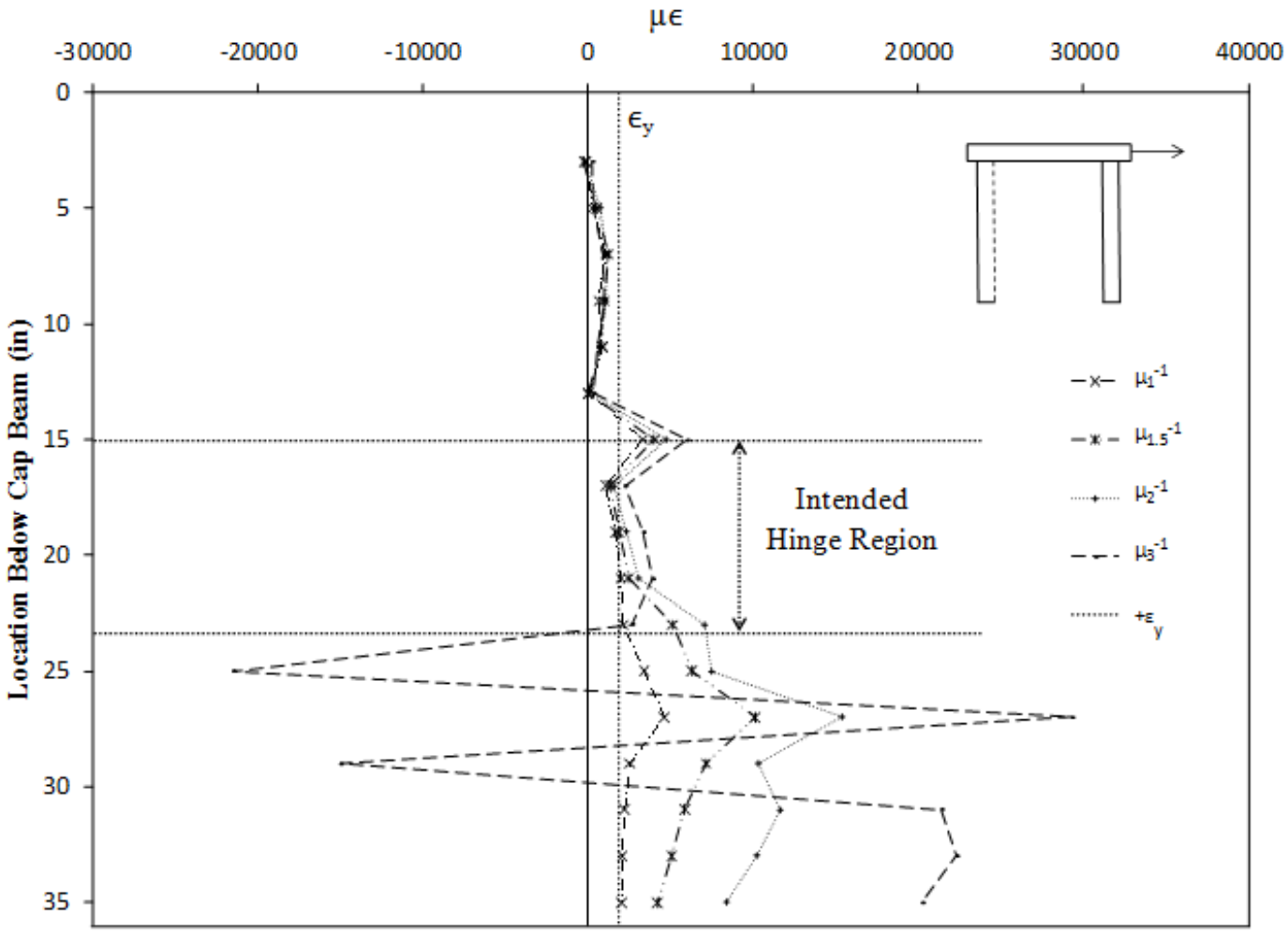

Figure 6.44 Optotrak Vertical Strain Profile – South Column North Face Pull Direction

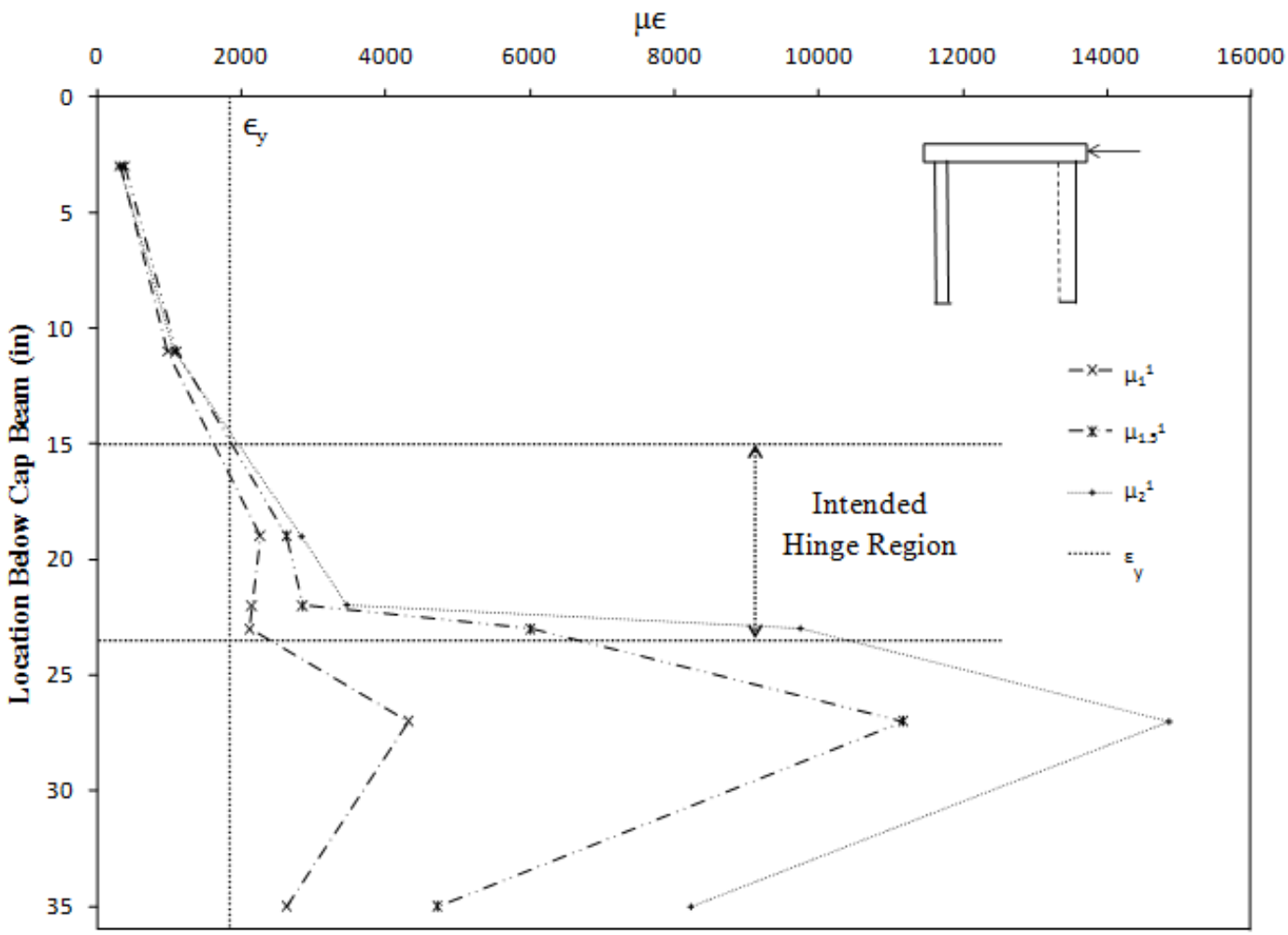

Figure 6.45 Strain Gauge Vertical Strain Profile – North Column South Face Push Direction

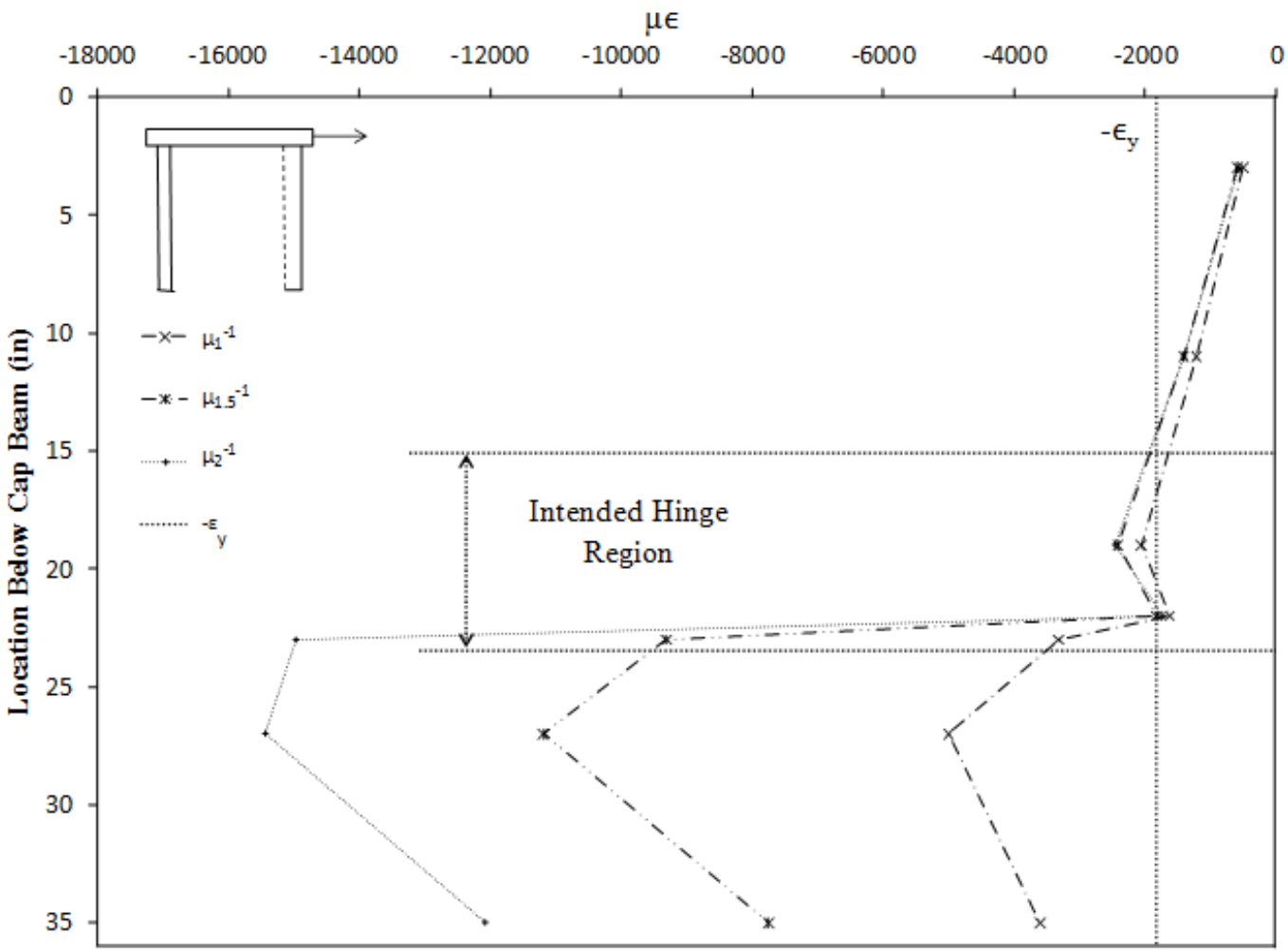

Figure 6.46 Strain Gauge Vertical Strain Profile – South Column South Face Pull Direction

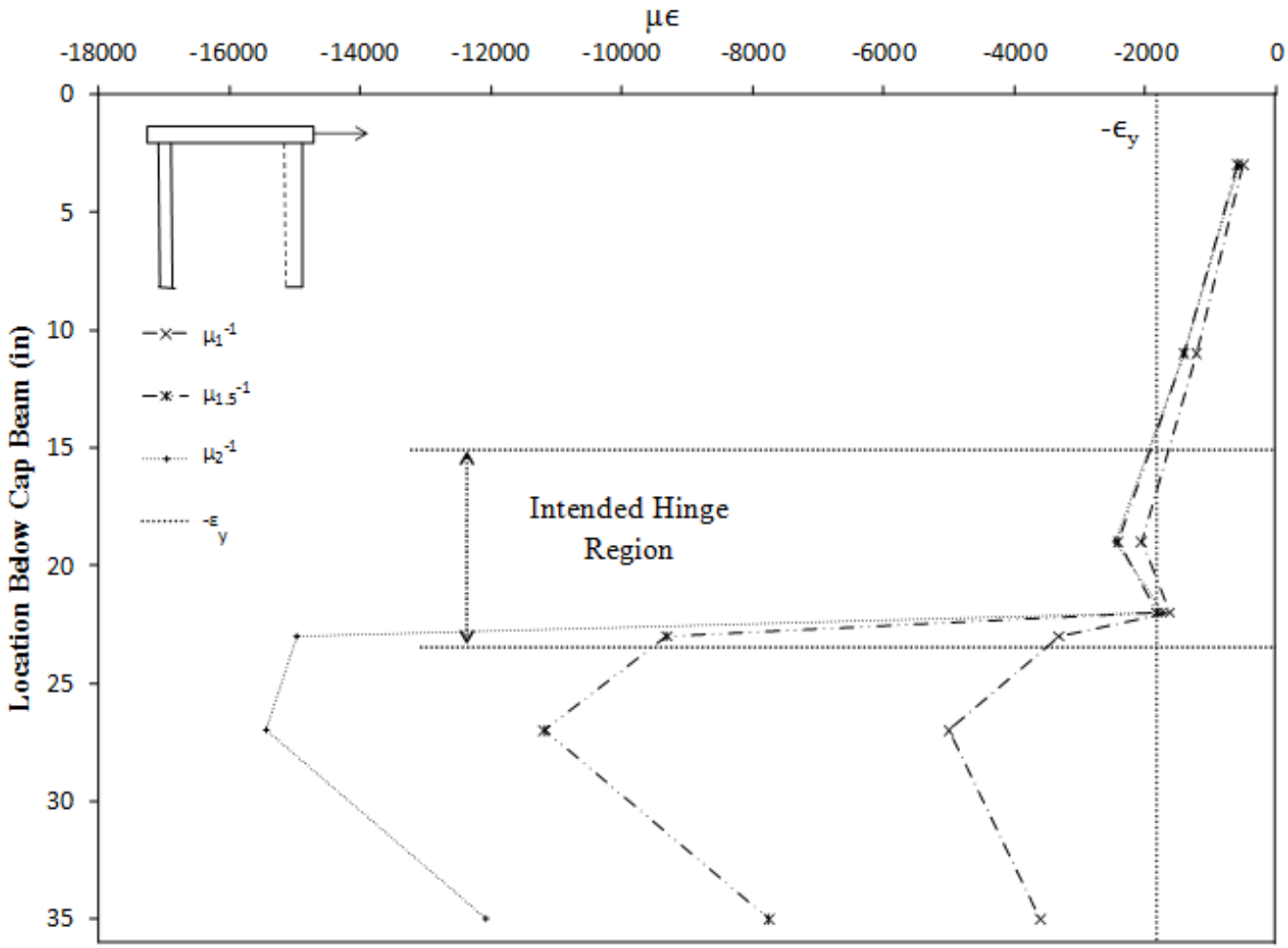

Figure 6.47 Strain Gauge Vertical Strain Profile – South Column South Face Pull Direction

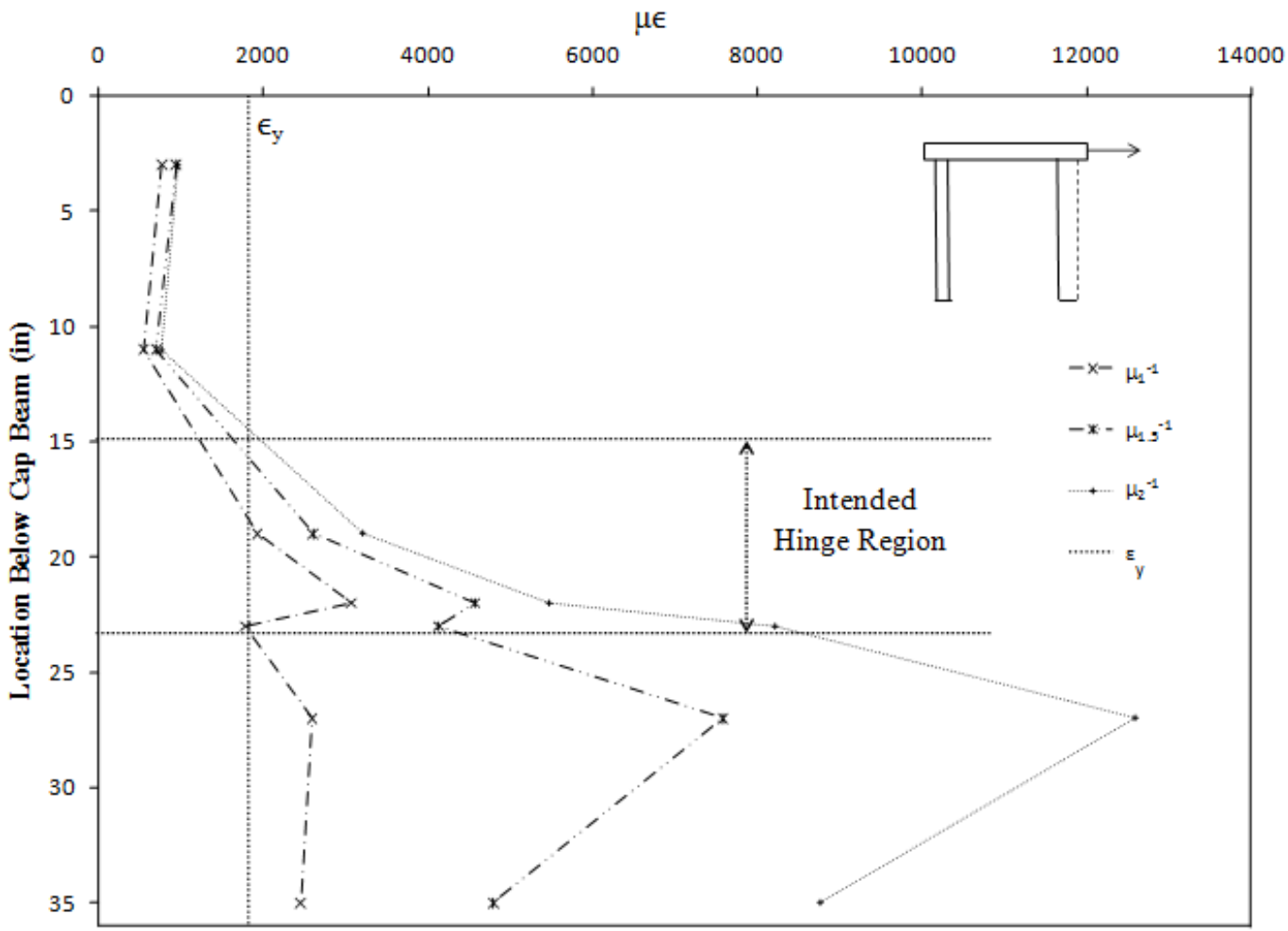

Figure 6.48 Strain Gauge Vertical Strain Profile – North Column North Face Push Direction

Noting that the anticipated yield stress of the ASTM A500 Gr. B piles was 58.8 ksi which was comparable to the approximate 54 ksi value reported by mill certificates, and that the expected material yield stress of the ASTM A572 Gr. 50 capital material was 55 ksi, differences in anticipated or reported material strength did not provide an apparent reason for the observed location of local buckling. However, it was possible that the cold forming and machining processes associated with the production of the capital assembly altered the ASTM A572 Gr. 50 material properties to a degree significant enough such that buckling was forced into the pile member below the splice weld.

Regardless of the observed location of local buckling, it is important to note that the capital connection configuration was capable of achieving the two main criteria considered in the development of modified weld-protected connections. First, damage was successfully located away from critical cap beam interface welds. Secondly, the critical welded region at the cap beam interface was strengthened to remain in the elastic range of response to protect interface welds. Although the configuration was unable to fulfill the secondary criteria of properly locating damage in the intended region away from the splice weld, it was capable producing the more desirable limit state of pile hinging in the form of pile wall local buckling while mitigating connection region cracking.

6.3.4 Column Capital General Conclusions

In general, the column capital connection specimen was considered more successful than any of the standard welded connection configuration as the detail was able to develop flexural hinging in the pile sections as shown Figure 6.49. The system would likely be assigned a reliable ductility of 3 or 4, at least one level greater than that of the standard welded details. Not only was the ultimate displacement ductility capacity increased by this configuration, but more importantly, the desirable and controllable failure mode of pile wall local buckling was observed. By inducing local bucking and base material fracture prior to brittle rupture at a weld region, the specimen experienced strength degradation over multiple

cycles and multiple displacement ductility levels. Should greater displacement capacity be desired, it may be possible with a similar detail to decrease the pile D/t ratio to produce higher reliable ductility capacity prior to strength loss as a result of local buckling and eventual base material fracture.

Figure 6.49 Phase 1 Test 6 – Ductility 4

6.4 Modified Column Capital Connection

6.4.1 Introduction and General Discussion

The third test of the second phase of the steel pier project was aimed at evaluating the performance of a steel pier containing modified column capital sections, as shown in Figure 6.50. The modified column capital elements of the pier, shown in detail in Figure 6.51, were a modified design from that of the basic column capital assembly discussed in prior sections of this document. More specifically, to ensure that a capacity protected region existed at the column to cap beam interface and that pile hinging in the form of local buckling was properly

located at the desired location, a specific reduced thickness section with a higher D/t ratio than the remainder of the capital assembly and HSS pile section was developed. The design intent was similar in nature to a reduced section I beam which also protects critical welded regions by isolating damage away from welds. This test served as both a validation of and improvement upon the performance of the basic column capital design evaluated in test 6 of phase 1 which did not contain a specific reduced section. As has been noted, the basic configuration was capable of capacity protecting the critical cap beam connection region, but did not properly locate damage in at the intended location potentially allowing damage to develop near the lower splice weld.

Figure 6.50. Steel Pier with Modified Column Capital Assemblies

Figure 6.51 Modified Column Capital Assemblies

6.4.2 Modified Capital Assembly Design and Pier Construction Process

In order to facilitate construction of the sytem, the modified column capitals were designed with an inner diameter matching that of the HSS pile section such that the CJP splice weld between the modified capital and pile section could be a prequalified weld. Considering the need for matching inner diameters along with the design intention of providing a reduced critical section within the capital element, a HSS pile section with a D/t ratio lower than is desired in the reduced section was required. Consequently, for the design of the test pier, ASTM A500 Gr. B HSS16x0.625 piles with a D/t ratio of 27.5 were chosen. This selection allowed a D/t ratio of approximately 36 to be used in the specific reduced section which is similar to that of the HSS16x0.500 piles that were used in other tests in this project, therefore facilitating comparison of any compression based failure modes.

Similar to the basic column capital design, the maximum depth of the upper flared section of the modified column capitals was determined for a given flared section thickness as was described in in Eq.(6.4) and Figure 6.34. For the test 3 experimental specimen, a design depth of hinging of 12 in. was chosen along for an outer diameter of 15.7 in. within the reduced section. This generated a reduced section thickness of 0.431 in. and a D/t ratio of 36.4 fulfilling the design intention of a D/t ratio similar to that of an HSS16x0.500 section. Combining the selection of depth of hinging along with the full over-strength plastic moment capacity of the reduced section (considering a material over-strength of 1.25) a required thickness in the upper section of the capital was found to be 0.9375 in. or 15/16 in.

The remaining details for fabrication included the length of the reduced section and the length of the lower section which would be splice welded to the HSS pile. The length of the reduced section was chosen as 16 in. (one nominal diameter) as a reasonable dimension to minimize any stiffening effects from the thick upper section that may diminish the ability for local buckling to develop in the intended reduced region. Lastly, the length of the lower section was chosen as 10 in. to provide a reasonable distance to avoid the potential of local buckling near the splice weld. Fabrication details as well as the completed capitals are shown in Figure 6.52 and Figure 6.53 respectively. As was done with the basic capital configuration, the modified column capitals were connected to the cap beam soffit with CJP welds that included a 3/8 in. reinforcing fillet weld and to the HSS16x0.625 piles with a CJP splice welds.

Typical of all experimental tests in this project, attention was given to ensure that a construction process as similar as possible to actual field conditions was employed when completing the connection detail shown in Figure 6.54. Consequently, the first step in the construction process was placement of the column capitals onto the piles which had been erected in the laboratory as shown in Figure 6.55, followed by placement of the splice weld in a horizontal welding position as shown in Figure 6.56. After completion of the splice weld, the cap beam was placed on top of the two column capitals. The CJP weld between the

capital and cap beam flange was then placed in the overhead position to complete the connection configuration. Following completion of this weld, UT inspection was performed on all welds prior to testing of the specimen. Additionally, visual inspection of the entire welding process was conducted. The applicable documentation of the welding process, welder certifications, and inspections are provided in the appendix of this document.

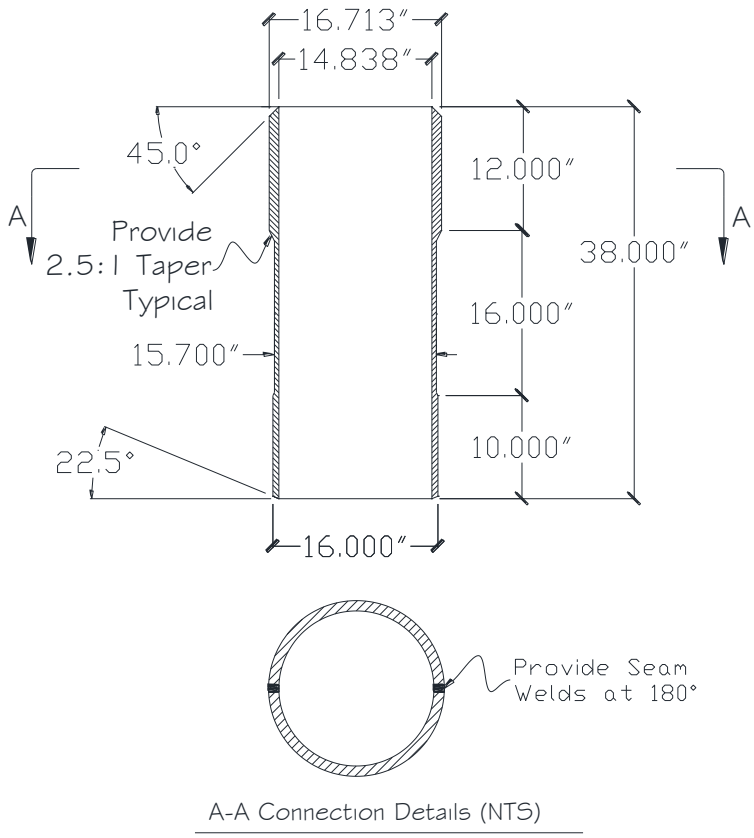

Figure 6.52. Modified Column Capital Details

Figure 6.53. Fabricated Modified Column Capitals

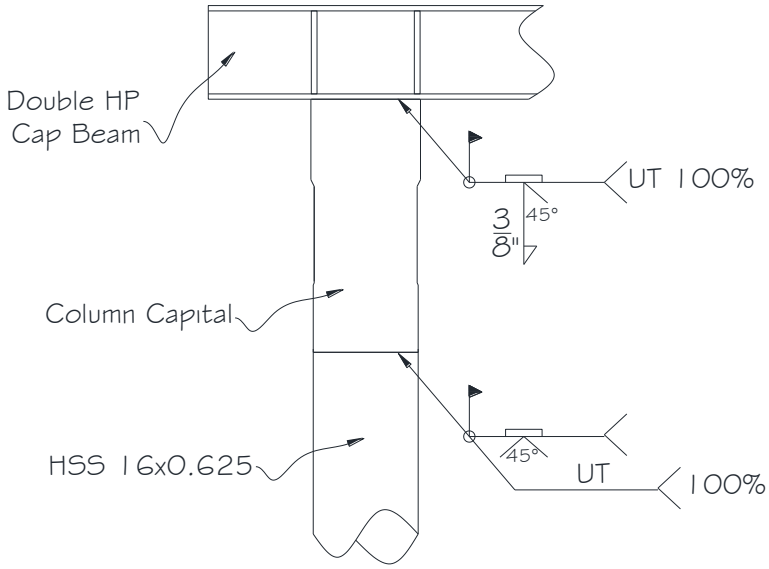

Figure 6.54 Test 3 Modified Column Capital Connection Detail

Figure 6.55 Placement of Modified Column Capitals

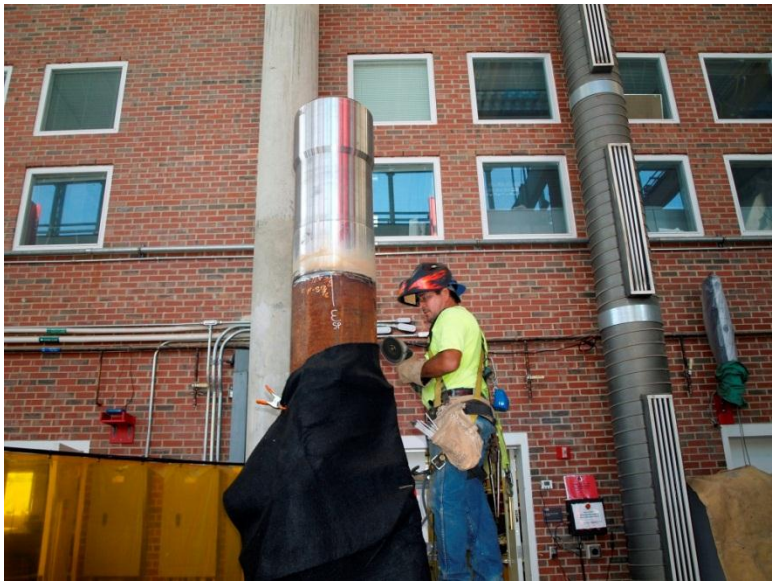

Figure 6.56 Splice Welding of Modified Capitals to the Erected Piles

6.4.3 Load History and Instrumentation Details

In the case of the modified column capital experimental test, the material yield stress was assumed be 54 ksi for the A572 Gr. 50 capital plate material based on mill certification test and in in-house material testing details of which are provided in Figure A 20 through Figure A 23. This value, combined with the shear span of 9.57 ft. from the pinned supports to the reduced section, resulted in a first yield force of 72.3 kips. Both the experimental and analytical evaluations of the modified column capital pier, were based on the typical three cycle set load history which has been described in prior chapters. The application of this load history with the predicted material properties resulted in experimentally determined first yield displacement of 1.64 in. and an associated ductility 1 displacement of 2.15 in. Application of the three cycle set load history produced the experimental force and displacement histories shown in Figure 6.57 and Figure 6.58 respectively.

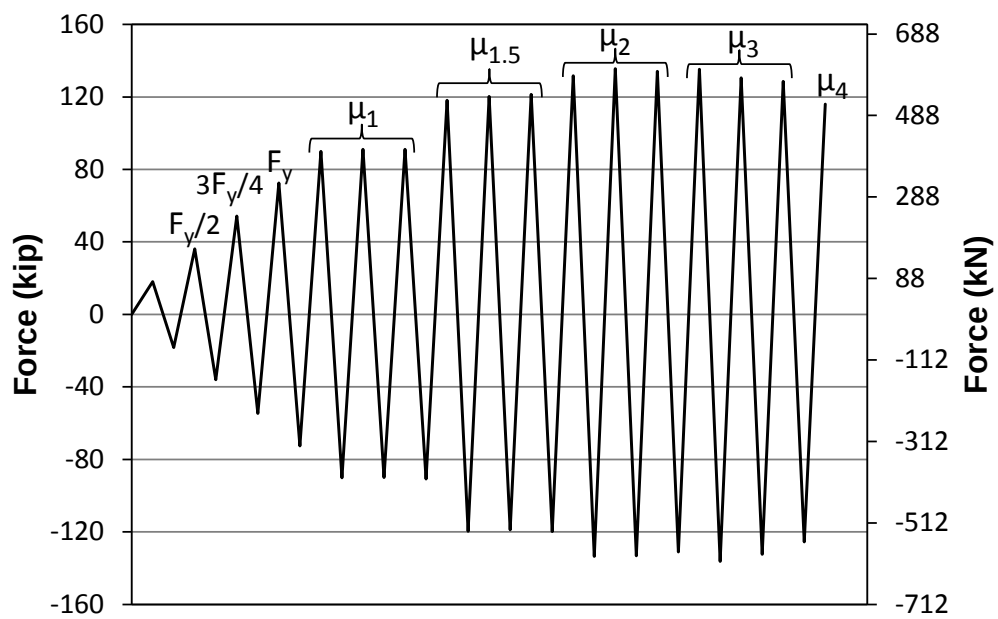

Figure 6.57 Modified Column Capital Connection Experimental Load History

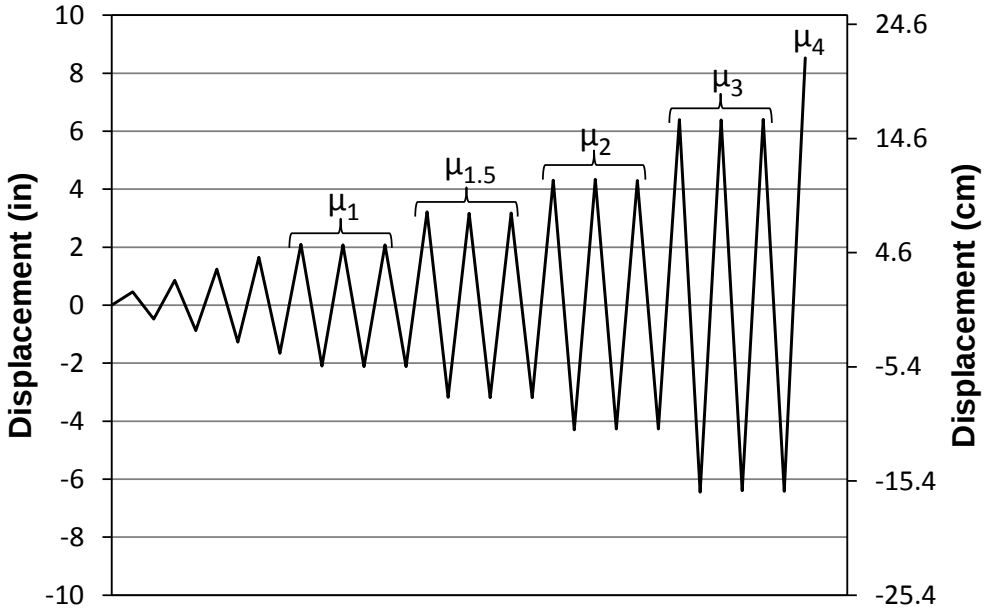

Figure 6.58 Modified Column Capital Connection Experimental Displacement History

The instrumentation used in the modified column capital evaluation consisted of traditional laboratory instrumentation as well as the Optotrak motion sensing system as was typical throughout the project. The traditional equipment consisted of inclinometers located 8 inches above the pinned bases to monitor drift magnitudes, linear string potentiometers attached to the bases to monitor any unanticipated base sliding, and strain gauges located on the extreme fibers of each pile cross section as shown in Figure 6.59. Also shown in Figure 6.59, a 2 in. spaced grid of Optotrak LED markers was placed on the east face each pile in the flared capital, reduced section, and HSS pile regions. The Optotrak markers were placed in a pattern to allow for calculation of strains in the intended reduced thickness hinging region as well as the intended capacity protected flared connection regions. Optotrak markers were also used to monitor cap beam displacements.

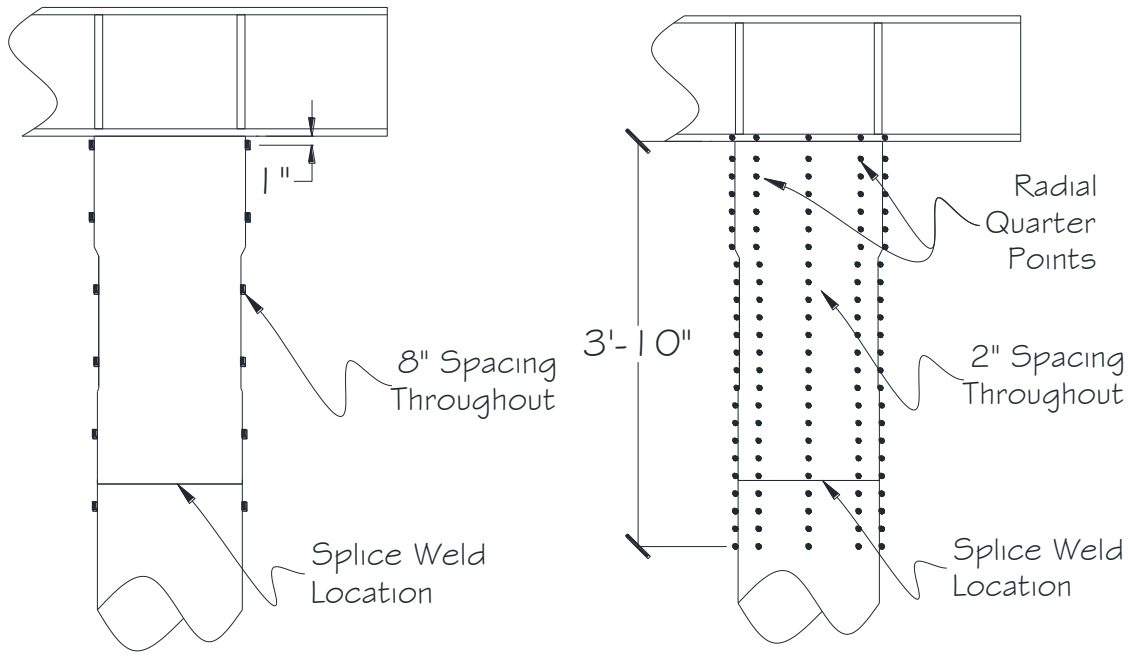

Figure 6.59 Modified Column Capital (Left: SG Layout Right: Optotrak Layout)

6.4.4 Experimental Summary

Experimental results showed the modified capital test pier to perform with no appreciable signs of damage that could be related to strength loss or any upper bound limit state throughout the first two cycles of ductility two as is shown in Figure 6.60 and Figure 6.61. Although no evidence of strength loss was apparent in the full Force-Displacement response or the Force-Displacement response envelopes, minor local buckling began to develop on the compression face of each pile during the third push cycle of ductility 2. As shown in Figure 6.62, the buckled region was located in the reduced section intended hinging region approximately 2 in. below the transition to the upper section of the column capital. Reversal to the third pull cycle of ductility 2 resulted in similar local buckling on the south face of the north column again not producing any apparent strength loss. However, no visual signs of local buckling occurred on the south face of the south column during this cycle.

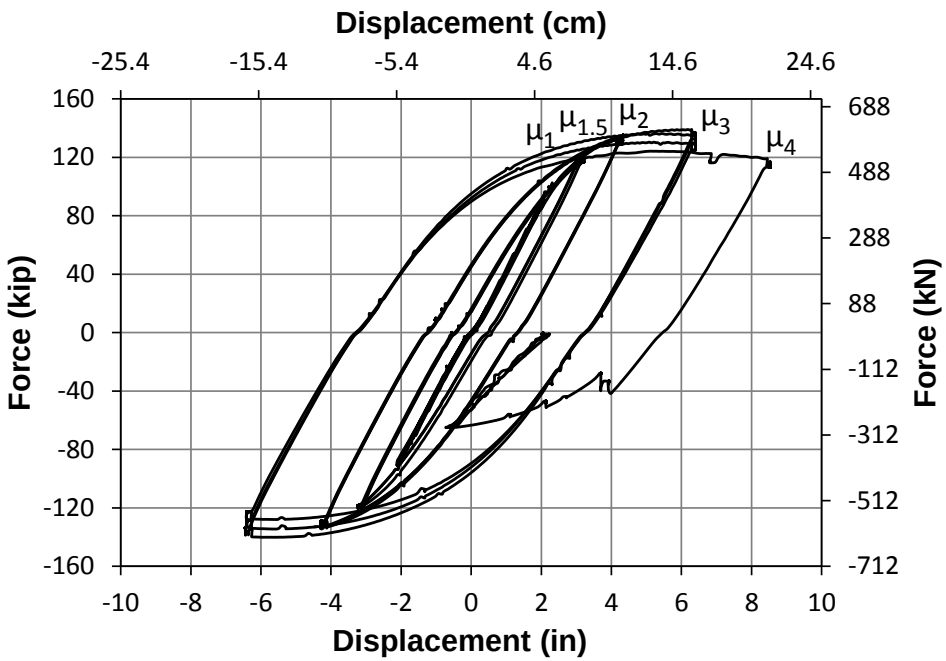

Figure 6.60 Phase 2 Test 3 Modified Capital Force-Displacement Hysteresis

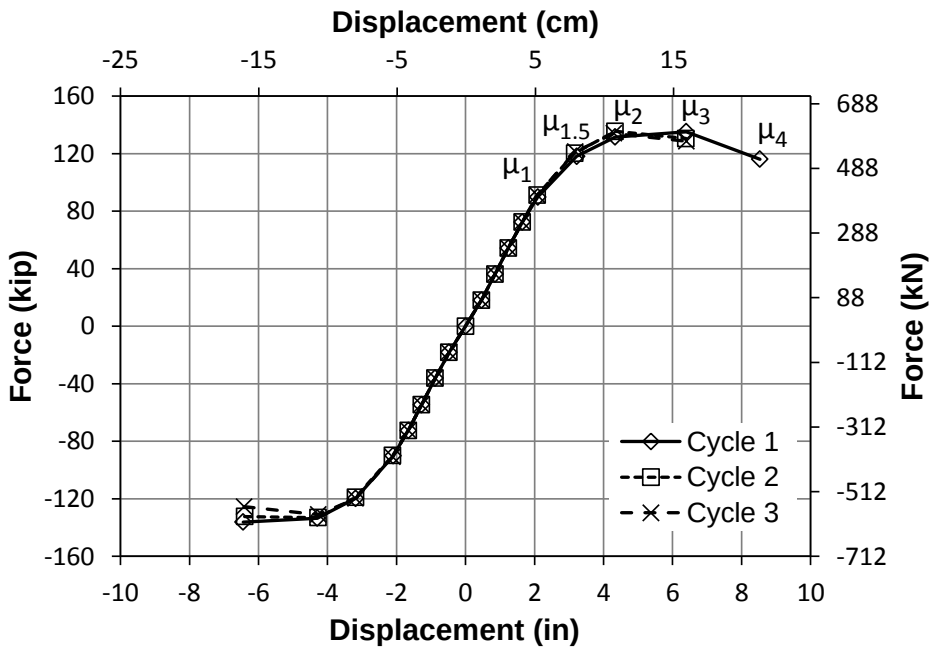

Figure 6.61 Phase 2 Test 3 Modified Capital Force-Displacement Envelopes

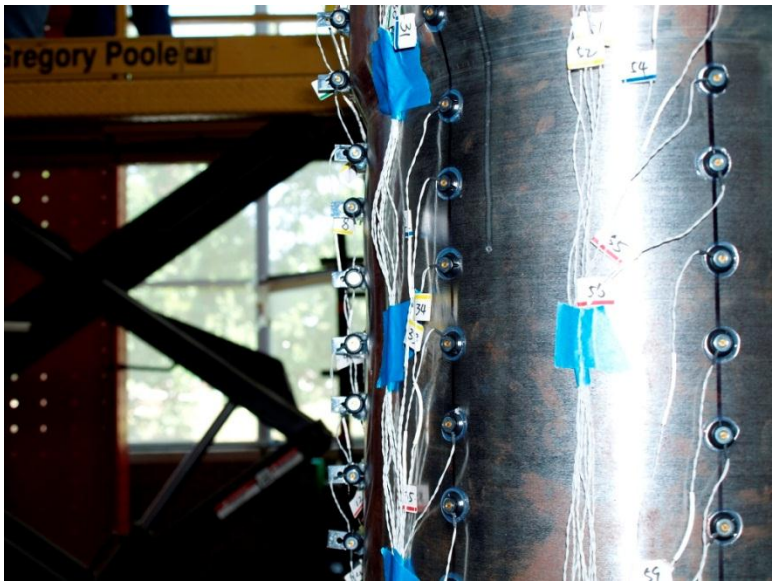

Figure 6.62 North Pile South Face, Ductility 2, Cycle 3, 130 kips, 4.29 in. Displacement

As the test progressed into the first push cycle of ductility 3, the local buckling which was experienced on the north face of the south pile during the third cycle of ductility 2, propagated to a larger magnitude in an outward circumferential manner as shown in Figure 6.63. Although a similar style of buckling propagation was also noted on the north face of the north pile, the magnitude at this location was less severe. Reversal to the first pull cycle of ductility 3 generated propagation of local buckling again in an outward circumferential manner on the compression faces of both piles. Regardless of further development of visual damage, the pier still exhibited no signs of strength degradation during the first cycle (positive and negative) of ductility 3 which corresponded to a displacement of 6.44 in.

The remaining cycles of ductility 3 produced further increases in the severity the locally buckled regions on both extreme fiber regions of each pile. As is shown in Figure 6.64, the regions continued to develop outward circumferential buckling which produced notable strength loss during these cycles. However, at the completion of the third ductility level, the maximum strength loss was limited to approximately 8%.

Figure 6.63 South Pile North Face, Ductility 3, Cycle 1, 136 kips, 6.34 in. Displacement

Progression of the test into the ductility 4 displacement level produced further propagation of buckling on both columns as shown in Figure 6.65 and Figure 6.66 with the buckled region on the south column becoming notably severe. Regardless of the magnitude of local buckling, the strength loss experienced was limited to approximately 15% at the ductility 4 displacement which corresponded to a displacement of 8.58 in., as shown in Figure 6.67. Upon reversal to the first pull cycle of ductility 4, a crack rapidly developed through the thickness of the wall around the circumferential buckling spanning approximately 1/3 of the cross section on the north face of the south pile as shown in Figure 6.68. The crack developed during the loading cycle as the pier was subjected to a negative (pull direction) load, while still at a residual positive displacement. Immediately upon restart of the test, following a pause for photographs, the crack rapidly propagated to approximately 1/2 of the cross section as shown in Figure 6.69. As loading of the pier continued, the width of the crack increased, as shown in Figure 6.69, while the strength and stiffness of the system continued to degrade as is evident on the Force-Displacement response. Due to the damage experienced by the south pile, the test was concluded.

Figure 6.64 North Pile South Face, Ductility 3, Cycle -2, -130 kips, -6.43 in. Disp.

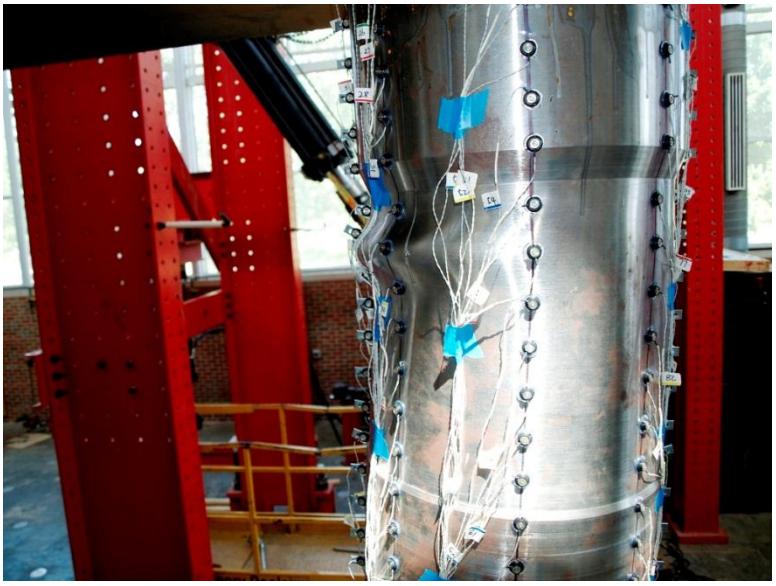

Figure 6.65 South Pile North Face, Ductility 4, Cycle 1, 115 kips, 8.58 in. Disp.

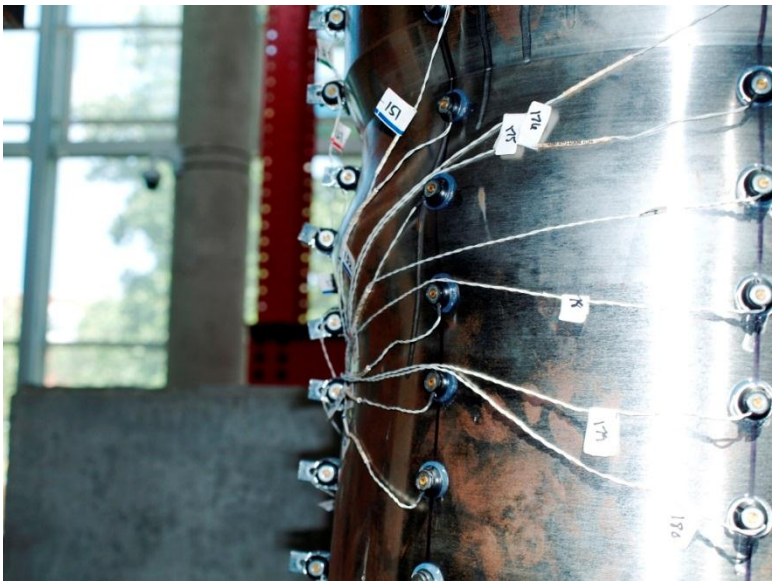

Figure 6.66 North Pile North Face, Ductility 4, Cycle 1, 115 kips, 8.58 in. Displacement

Figure 6.67 Displaced Pier Ductility 4, Cycle 1, 115 kips, 8.58 in. Displacement

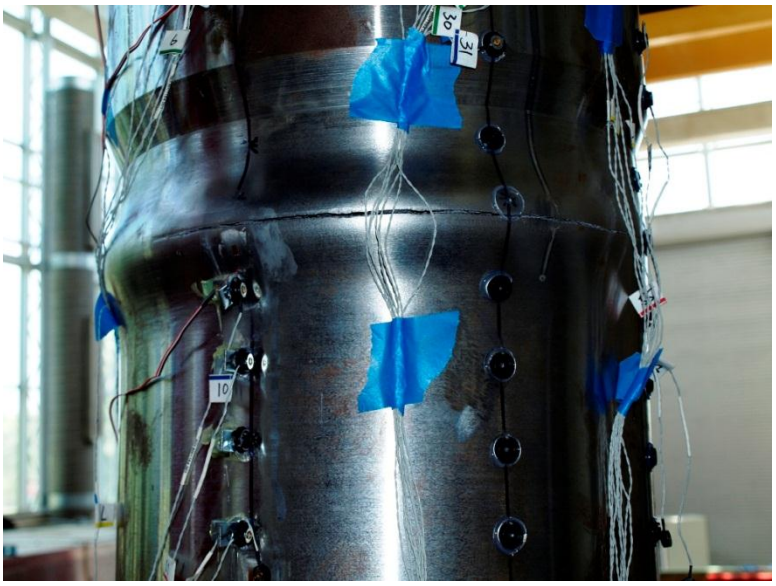

Figure 6.68 South Pile North Face, Ductility 4, Cycle -1, -33 kips, 3.13" Displacement

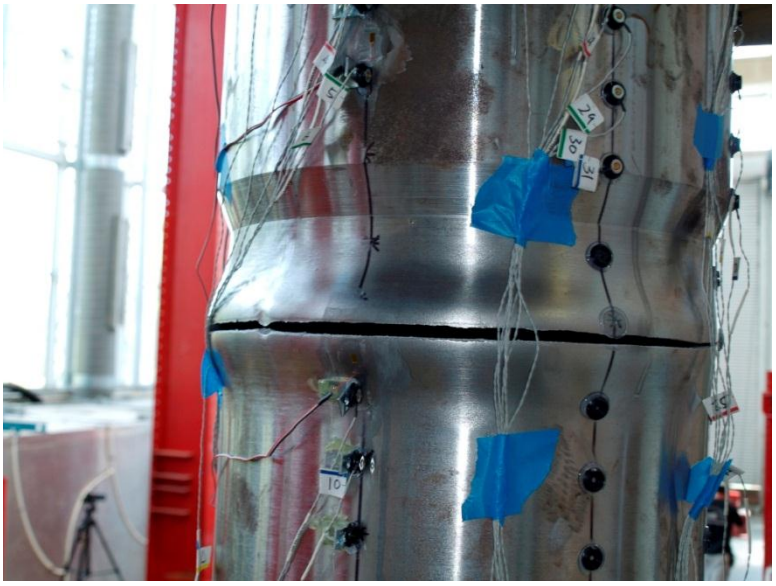

Figure 6.69 South Pile North Face, Ductility 4, Cycle -1, -47 kips, 2.14" Displacement

Following testing, Optotrak data analysis was conducted to evaluate the effectiveness of the column capital system to locate damage in the desired location while maintaining strains

in the elastic range at the capital to cap beam interface and protecting the splice weld region. Focusing on the extreme fibers of the south column, it is shown in Figure 6.70 through Figure 6.73 that the design intention was achieved. As is shown, plastic strains were essentially limited to the reduced thickness section with the exception of some inelasticity below the reduced section which falls within the intended design behavior. Although not provided in this document for brevity, similar results were generated from the response of the north pile as well as subsequent cycles of each ductility level. It should be noted that in some cases, the strain profiles appear to indicate tensile strain on a face which should be experiencing a compressive strain state. For example, in Figure 6.70, the strains for a displacement ductility of 4 indicate tension strains on a compression face. This behavior is due to the onset and development of local buckling which generates spatial changes between LED markers which are not indicative of engineering strains. Strain data beyond this point is of course not reliable, and should be disregarded with the exception of identifying locations of local buckling.

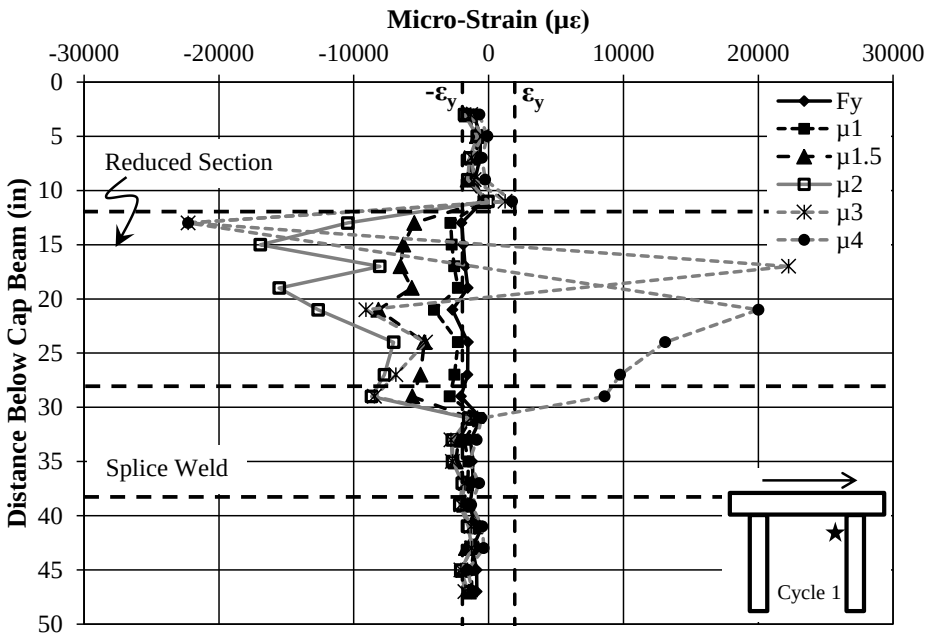

Figure 6.70 South Column North Face – Positive Cycle 1 Vertical Strain Profile

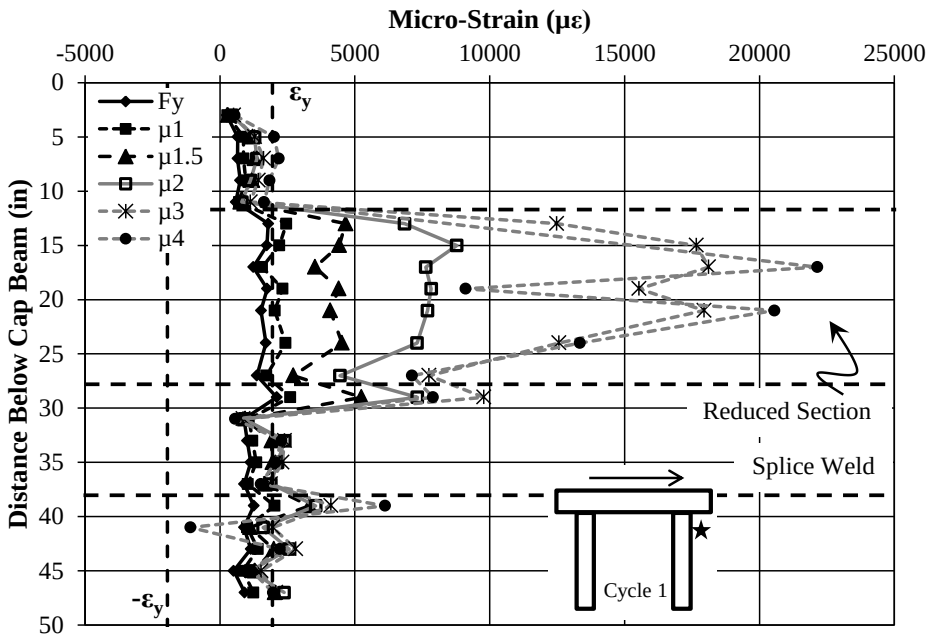

Figure 6.71 South Column South Face – Positive Cycle 1 Vertical Strain Profile

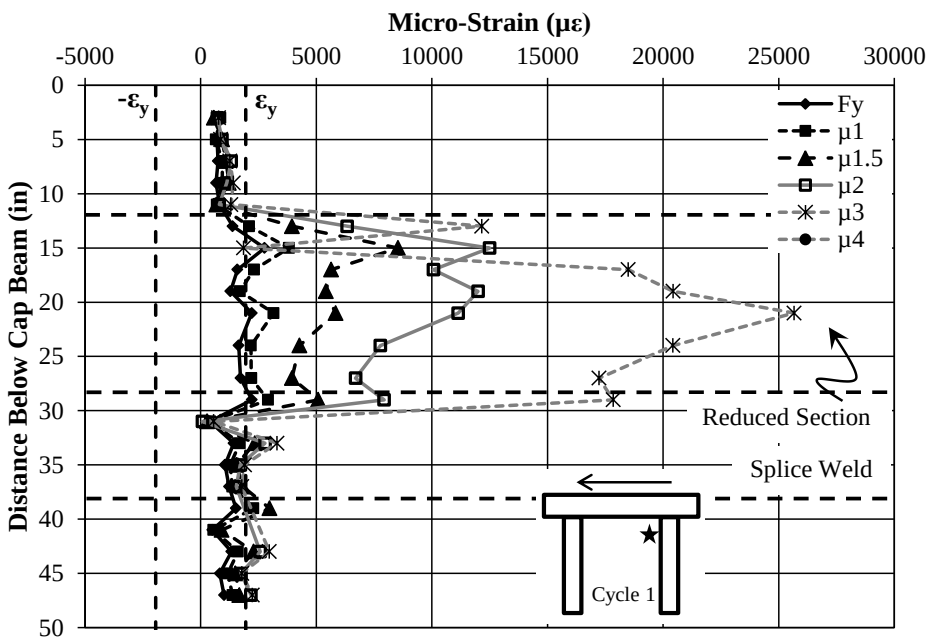

Figure 6.72 South Column North Face – Negative Cycle 1 Vertical Strain Profile

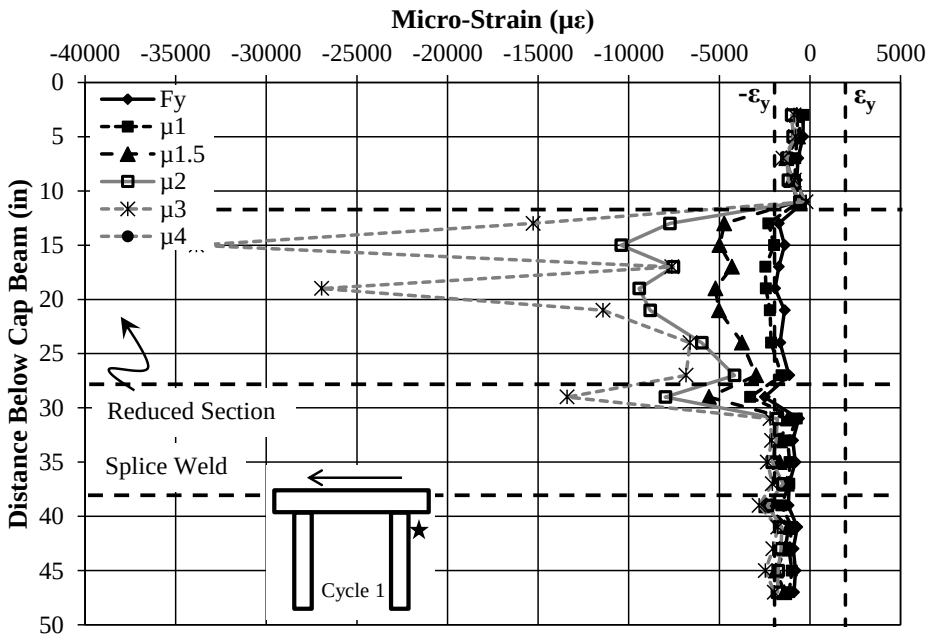

Figure 6.73 South Column South Face – Negative Cycle 1 Vertical Strain Profile

6.4.5 Finite Element Analysis: Standard and Modified Column Capital Connections

Finite Element Modeling simulations were conducted prior the experimental test not only to predict the behavior of the modified configuration, but also to better understand the behavior of the standard capital configuration which was evaluated in test 6 of the first phase of the project. The analytical methods were aimed at trying to understand why the buckling location in the past test did not occur where intended. It had been postulated that this may have been due to the rolling and machining processes having significant effects on the material properties of the fabricated capital assemblies. However, no in-depth evaluation had taken place prior to the FEM work being conducted.

The Finite Element Model developed to represent the standard column capital assembly, consisted of 20 node 3-dimensional brick elements in the pile and capital assembly and

considered the actual geometry of the standard capital assembly. However, a continuous mesh was used between the capital assembly and the HSS16x0.500 portion of the pile such that no modeling of the splice weld was necessary. Although any effects that the splice weld induced on the behavior of the past experimental test would not be captured by the model, it was found through the development process that this modeling technique was more efficient than making modeling assumption regarding the welded region.

Initially, the non-linear portion of the steel material model, that considered a kinematic hardening rule, was calibrated based on past in-house material tests of ASTM A500 Gr. B. material not the actual specimen or capital materials as no data was available at that time. Although this could have impacted the strength capacity exhibited by the FEM simulation, it is more important to note that the lack of material test data led to both the capital portion of the model and the pile portion of the model being defined with the same constitutive model. As has been discussed, it was suspected that the standard column capital experimental evaluation may have been influenced by altered material properties in the capital region which would not be captured by this simulation.

The initial FEM simulation produced a similar hysteretic Force-Displacement response compared to the phase 1 test 6 experimental evaluation as shown in Figure 6.74. In addition, the FEM simulation showed pile wall local buckling, leading to strength degradation, to be the controlling failure mode of the system. However, the analysis predicted the buckled region to develop approximately 3 in. below the flared section in what would have been the intended buckling region of the experimental specimen, not below the splice weld region as was shown during the experimental investigation. This predicted region of buckling is shown in Figure 6.75. Noting that actual geometry of the capital assembly was considered in the model, this prediction suggested that the observed behavior of the past test was due to either stiffening effects of the splice weld (which was not modeled) or actual material properties of the capital assembly which were not available at the time of the analysis.

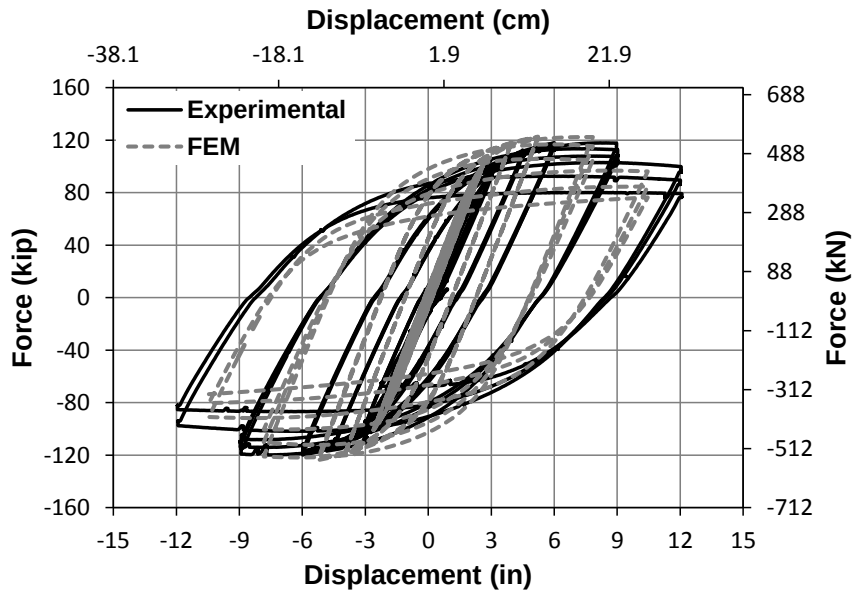

Figure 6.74 Standard Column Capital – Initial FEM vs. Experimental Response

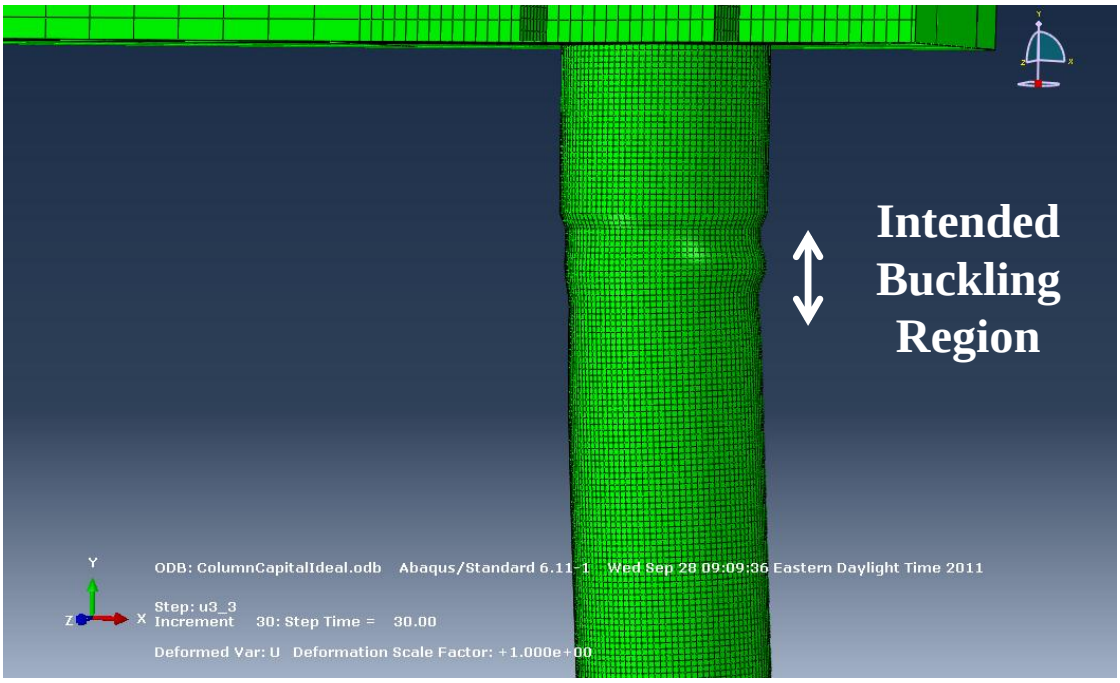

Figure 6.75 Standard Column Capital – Initial FEM Simulation Response

While aware of the potential errors that existed from the lack of a seemingly appropriate material model for the capital region of the FEM, analysis was conducted to generate an initial estimate of the behavior of the modified configuration prior the experimental test. As was the case with the standard configuration, the model was generated considering the actual geometry of the modified column capital including the specific reduced thickness section, using 20 node 3-dimensional brick elements. The model was subjected to the typical 3 cycle set load history based on an analytical first yield displacement, and showed local buckling to develop in the intended buckling reduced thickness section as shown in Figure 6.76. Further, strength degradation was shown to develop between the individual ductility levels as was shown to occur in past experimental evaluations as indicated in Figure 6.77.

However, less strength reduction was experienced in between cycles of a given displacement ductility level than was shown to occur in the standard configuration experimental test. Further, as was evident after the experimental test of the modified configuration, the ultimate strength capacity predicted by the simulation of approximately 100 kips was considerably lower than the experimental value that was found to be approximately 130 kips. Both results indicated that it may be necessary to more appropriately define a material model for the fabricated capital material, in order to accurately model the behavior of either the standard or modified configuration.

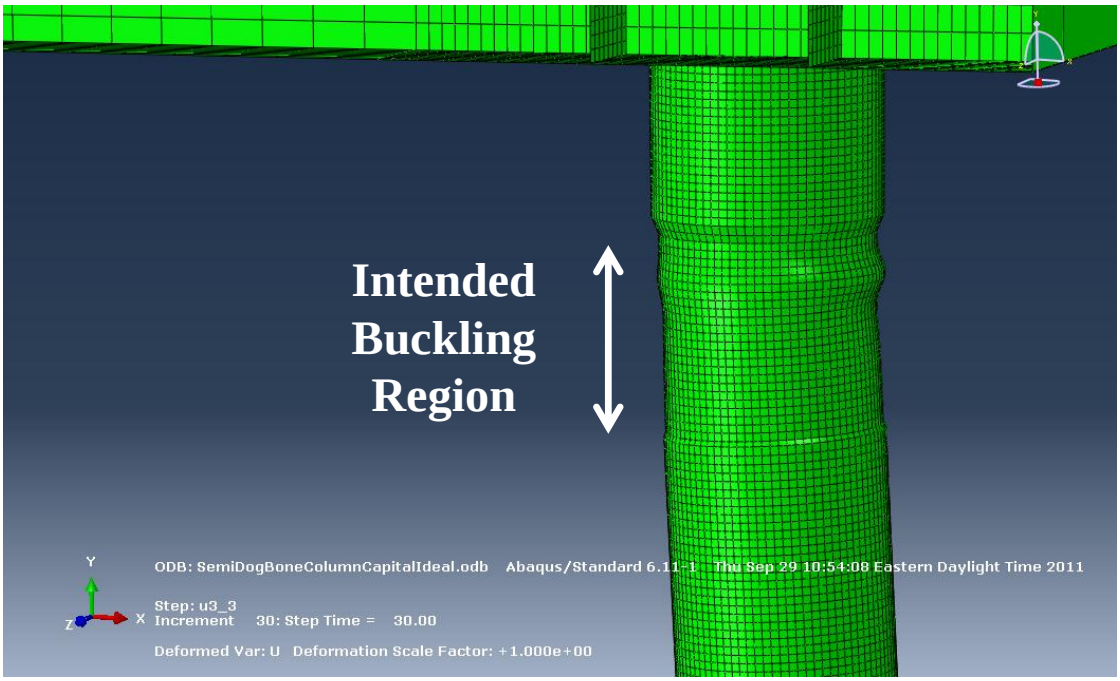

Figure 6.76 Modified Column Capital – Initial FEM Simulation Response

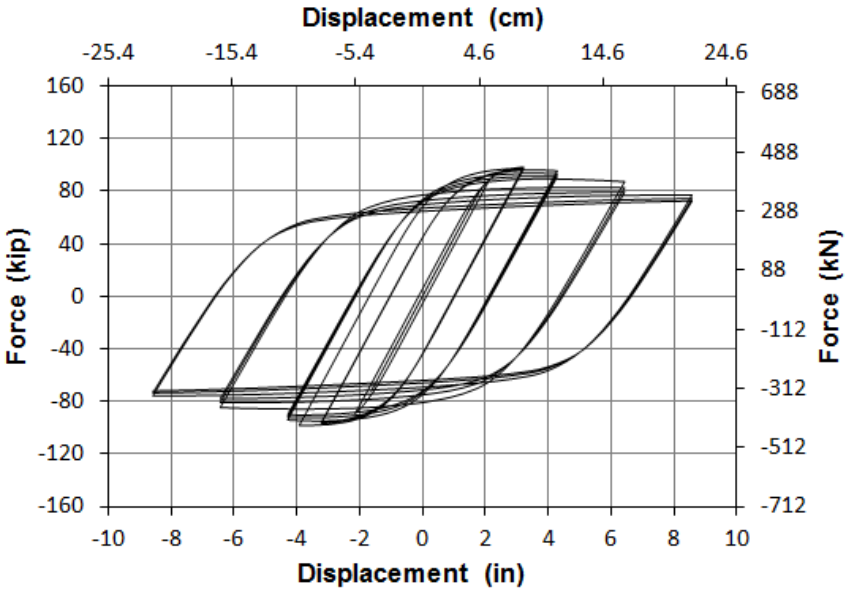

Figure 6.77 Modified Column Capital – Initial FEM vs. Experimental Response

Following the modified column capital experimental test, material was removed from the actual fabricated capitals from an area at the neutral axis that remained in the elastic range of loading for in-house material testing. The results of 4 coupon tension tests indicated that the mechanical material properties of the ASTM A572 Gr. 50 steel, that was used to fabricate the capitals, was altered during the fabrication process. Comparing the 4 tensile tests conducted following fabrication to 4 prior to fabrication, it is shown that both the yield stresses and ultimate stresses were increased by approximately 15% as summarized in Table 6.1. These results are also detailed in Figure A 20 through Figure A 27. Although these results were generated from the modified column capital material, assuming similar effects were generated in the fabrication of the standard capital assemblies, this finding likely explains why buckling did not occur in the intended region of the standard column capital experimental test.

Table 6.1 Modified Capital Material Properties Before/After Fabrication

Coupon	2% Offset Yield Stress (ksi)	Ultimate Stress (ksi)
Plate 1	48.5	79.6
Plate 2	53.7	79.7
Plate 3	53.5	78.6
Plate 4	52.9	79.9
Fabricated 1	65.0	87.3
Fabricated 2	62.9	86.6
Fabricated 3	65.7	88.0
Fabricated 4	67.9	89.3

The assumption was made that the material tests conducted were likely also representative of the standard column capital fabricated material and the results were used to re-calibrate the FEM steel material model. With the updated material model, the FEM simulation of the standard capital configuration was again conducted with no other changes. The results of the analysis again showed the global performance of pier to match well with that of the experimental specimen as shown in the Force-Displacement hysteresis provided in

Figure 6.78. More importantly, with the updated material model in the capital assembly region of mesh, the analysis predicted pile wall local buckling to occur in the HSS16x0.500 section below the intended hinging region of the capital assembly as shown in Figure 6.79. This prediction closely resembled that of the experimental buckling location, further indicating the likelihood that altered material properties following fabrication were the reason for buckling not occurring in the intended region of the capital.

The in-house material test results were also used to update the calibration of the steel material model in the capital assembly region of the modified column capital Finite Element Model. Again nothing else in the model was changed and the simulation was re-conducted. The results of the simulation showed the analysis to more appropriately capture the strength capacity of the pier. As shown in Figure 6.80, the analysis predicted an ultimate strength capacity of approximately 120 kips which is more comparable to the 130 kips exhibited by the experimental test. As may be expected, the analysis also showed the buckled region to form in the intended hinging reduced thickness section as occurred in the experimental test as well as the initial simulation without an explicit material model for the capital region. This is shown in Figure 6.81. The combination of these findings potentially suggests that the effects of fabrication on material properties be considered when designing or analyzing column capital connections. In addition, as shown in Figure 6.82, the analysis indicated that the strains in the flared capital section remained in the elastic range as large inelastic strains developed in the reduced thickness section. As has been discussed, this was also shown to be the case for the experimental evaluation and was the design intention.

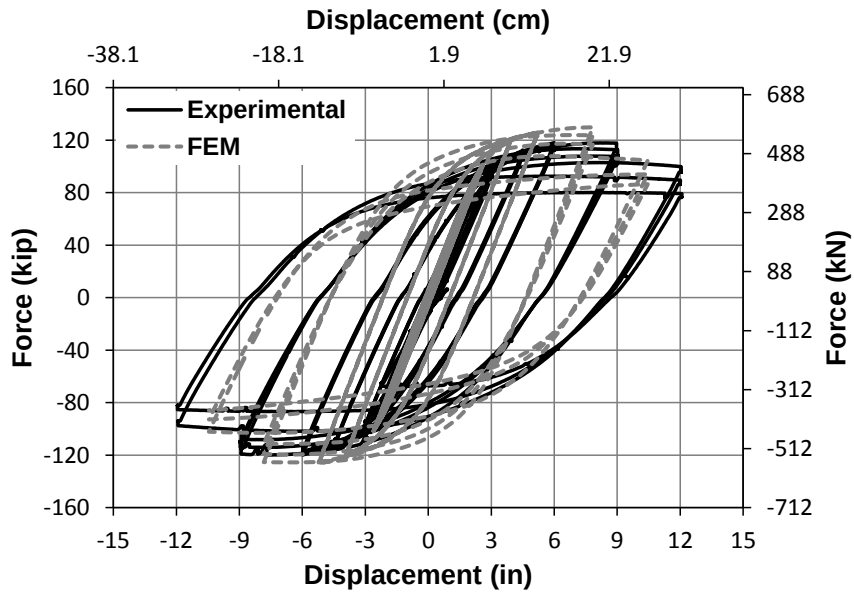

Figure 6.78 Standard Column Capital – Updated FEM vs. Experimental Response

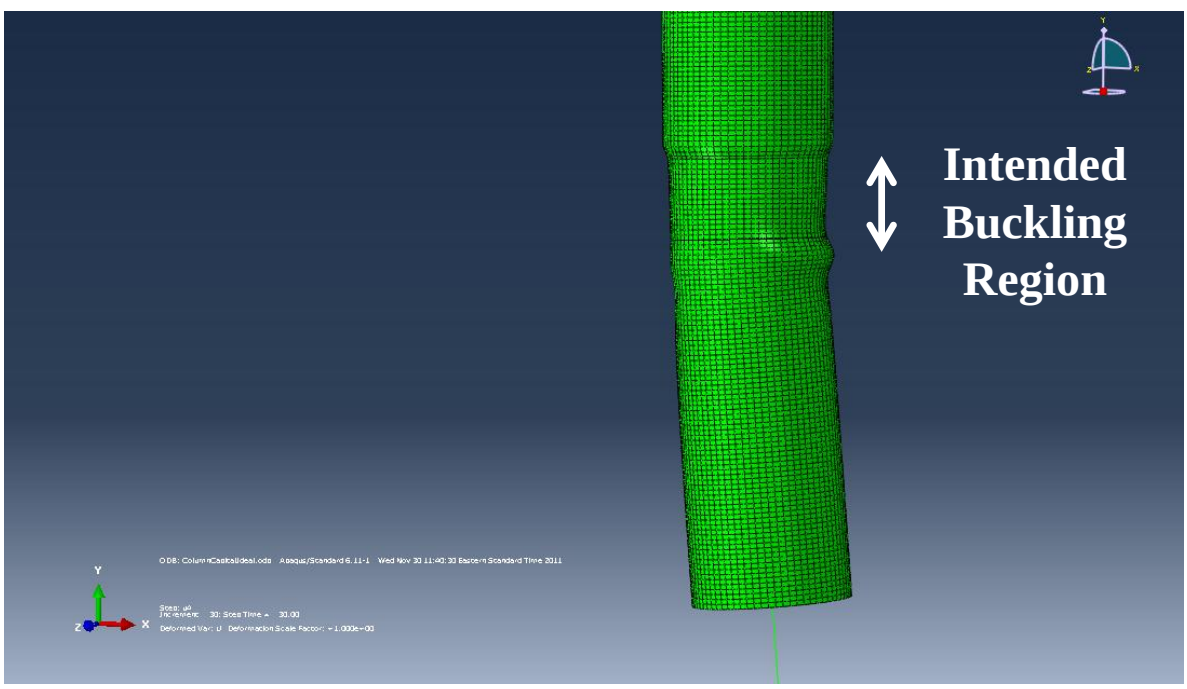

Figure 6.79 Standard Column Capital – Updated FEM Simulation Response

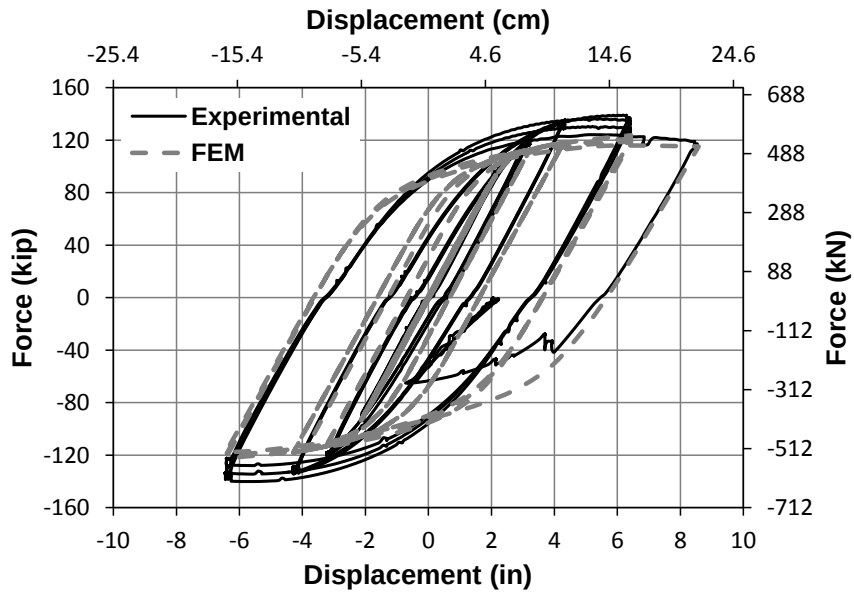

Figure 6.80 Modified Column Capital – Updated FEM vs. Experimental Response

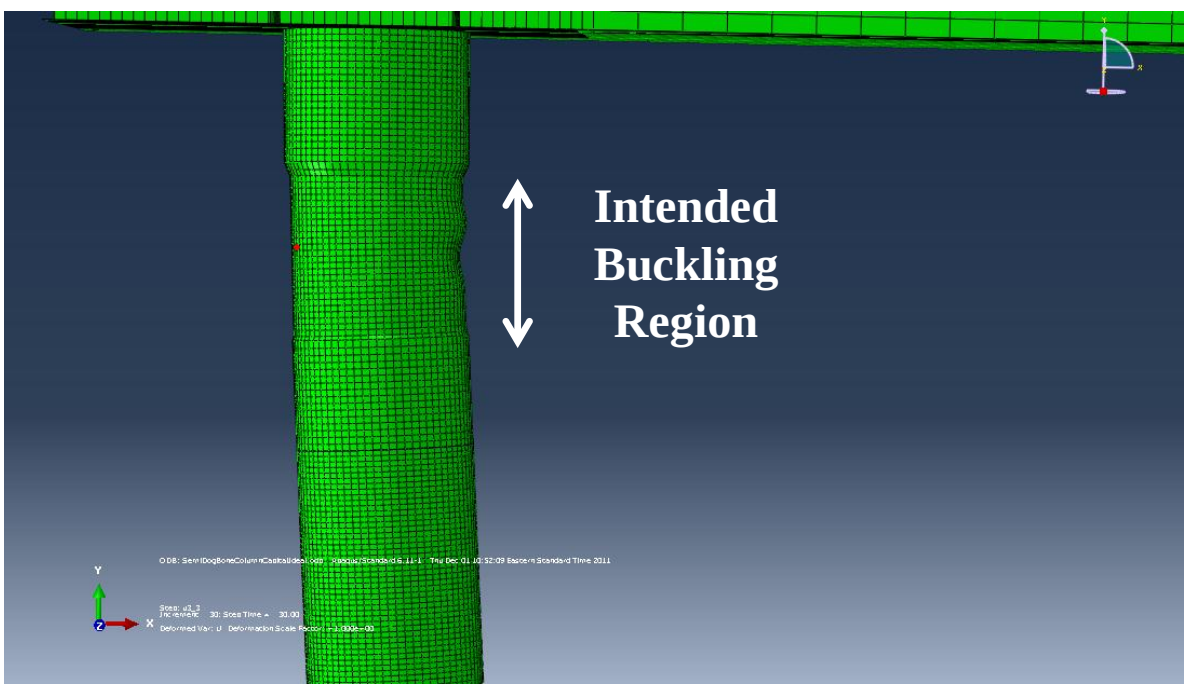

Figure 6.81 Modified Column Capital – Updated FEM Simulation Response

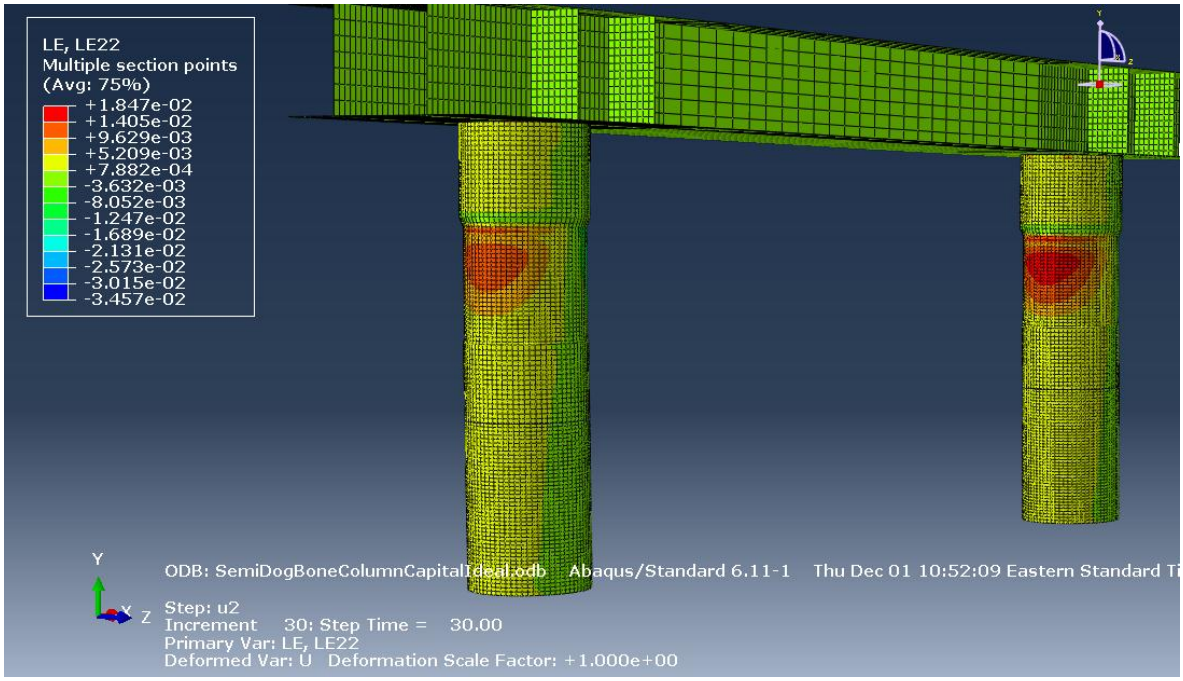

Figure 6.82 Modified Column Capital – Updated FEM Longitudinal Strains

6.4.6 Modified Column Capital General Conclusions

The experimental results, as well as those of data analysis and Finite Element Modeling, indicated that the modified reduced section column capital did effectively relocate damage, in the form of flexural hinging, away from the capital to cap beam interface. No signs of brittle weld failure were experienced as the preferable failure mode of pile wall local buckling was developed. However, the overall inelastic displacement capacity of the system was limited due to base material cracking of the locally buckled region on the south pile. Although the cracking that was experienced was expected to occur, it is preferable for a larger magnitude of local buckling and further strength degradation to occur prior to the formation of these cracks to develop a more stable failure mechanism. Ultimately, the system was limited to a reliable displacement ductility of 3 which corresponded to a reliable displacement of 6.43 in. or a drift of 4.3%. Nevertheless, the design intention to capacity protect the welded region at the capital to cap beam interface was achieved. Should a larger

reliable ductility capacity be required, reduction of the D/t ratio within the reduced section could likely meet the demand.

6.5 Grouted Shear Stud Connection (G.S.C.)

6.5.1 Development of the Grouted Shear Stud Connection Configuration

The second, fourth, fifth and sixth full scale quasi-static tests of the second phase of the steel pier project were aimed at developing and evaluating a modified weld-protected connection that consisted of a composite grouted pocket style configuration. More specifically, the connection consisted of a 24 in. x 0.500 in. stub pipe pile section that was connected to the cap beam with a complete joint penetration weld (CJP) and a 3/8 in. reinforcing fillet weld. The inner diameter of the stub pile contained 12 lines of welded 3/4 in. diameter 2-1/2 in. long shear stud connectors located at 30 degrees on center around the inside of the pipe with 4 shear studs in a given line. Similarly the top of the HSS16x0.500 pile section had 12 lines of 4 matching shear studs welded at 30 degrees on center around the cross section offset by 15 degrees radially and 2-1/2 in. vertically from the studs inside the larger stub pile. The shear stud pocket, shown in Figure 6.83, was grouted utilizing non-shrinking flowable grout after the piles had been inserted into the stub pipe section, to complete the moment resisting connections of the pier as shown in Figure 6.84. The grout used to complete the connection was a BASF Masterflow 928 product, which was expected to provide adequate working time and consistency to allow for vertical pumping of the grout material into the grout pocket. Additionally, the product was expected to provide adequate compressive strength per the connection design model which will be subsequently discussed.

Figure 6.83 Annular Shear Stud Pocket

Figure 6.84 Steel Bent with Completed Composite Connections

As was typical throughout the project, ASTM A500 Gr. B HSS16x0.500 piles were chosen as the column elements of the experimental pier specimens. The construction of the cap beams consisted of double ASTM A572 HP14x117 sections to provide both a capacity

protected cap beam as well as adequate bearing seat width for single span girders, should a designer choose not to utilize continuous spans. Further, in the case of the grouted shear stud connection, a multi-wide HP cap beam was necessary to accommodate the size of the 24 in. diameter stub pile sections. The 24 in. x 0.500 in. pipe sections were manufactured to the material standards of ASTM A500 Gr. B specification. The diameter of the stub pile was selected to provide an adequate gap for the placement of shear studs as well as to accommodate construction tolerances. The details of this configuration would allow for nominally +/- 1 in. of construction tolerance. However, this could be increased or decreased by a designer by altering the exact dimensions of the configuration while remaining within the basic design intentions that are recommended for this type of connection.

The design of the composite connection was based on the assumption that the total nominal strength of the shear stud connectors, on the pile side, should be capable of developing yielding of the HSS16x0.500 gross cross section. From known, or anticipated, material properties, a required number of 3/4 in. diameter shear studs could be determined and distributed around the cross section in an even pattern at 30 degrees on center. A matching number of studs were then placed on the stub pile side to facilitate load transfer in a truss like mechanism between the studs on either side of the connection. The nominal capacity of a single shear stud was determined utilizing the provisions of "AASHTO LRFD Bridge Design Specifications" (AASHTO, 2007) Section 6.10.10.4.3 as well as the *ANSI/AISC 360-05* (AISC, 2005) Section I3 both of which provide similar models shown in Eq.(6.5) through Eq.(6.7). As indicated in the equations, the model is a function of concrete compressive strength as well as the cross sectional area of the shear stud with an upper bound of stud shear rupture. Although the model is intended for use (in both codes) for composite construction between beams and a slab or bridge deck, it has been assumed conservative for use in this design given the highly confined nature of the annular grout pocket maintaining a logical upper bound of shear stud rupture.

$$Q_n = 0.5A_{sc}\left(f_c^{'}E_c\right)^{0.5} \leq A_{sc}F_u \qquad units: psi \tag{6.5}$$

$$E_c = 1746\sqrt{f_c^{'}} \qquad units: psi \text{ (AISC, 2005)} \tag{6.6}$$

$$E_c = 1820\sqrt{f_c^{'}} \qquad units: psi \text{ (AASHTO, 2005)} \tag{6.7}$$

Utilizing this model along with expected material properties of the grout and specified material properties of ASTM A108 shear stud connectors, it was found that a minimum of 47 shear stud connectors were necessary based on an anticipated yield stress of 58.8 ksi for the HSS16x0.500 ASTM A500 Gr. B piles. This anticipated yield stress was based on the recommendation (AASHTO, 2009) (AISC, 2010) of 1.4Fy where Fy is the ASTM minimum specified yield stress of 42 ksi . To generate a symmetrical condition, 12 lines of 4 shear studs at 30 degrees on center were used providing 48 shear studs on the pile side or 96 total per connection as shown in the detail provided in Figure 6.85. Further details of the connection are provided in Figure 6.86. It should also be noted that the 24 in. x 0.500 in. stub pile section, acting non-compositely at the cap beam connection, was designed to remain elastic as the full flexural over strength moment capacity of the piles was developed in order to fulfill the two key criteria of modified weld protected connection; damage relocation and protection of critical welded regions.

As was done with all other connection configurations, the physical construction associated with the experimental evaluations of the grouted shear stud connection, focused on replicating actual field construction conditions as much as reasonably possible. Consequently, the construction process of the specimens began with erecting the piles in the laboratory as if they had been driven in the field. The cap beam was then placed on top of the erected piles allowing the pile section to be inserted in to the larger stub pile which was shop welded to the double HP14x117 cap beam.

To complete the connection, the BASF Masterflow 928 grout material was then placed in the annular ring formed by to the pipe sections. To assist in minimizing the possibility of air voids within the annular grout pocket, the decision was made to pump grout vertically from the bottom of the connection to the top where 1 in. diameter holes had been left in the cap beam flange to allow air to escape the connection. A hand operated pumping system was utilized along with shut off valves that were cast into place and later removed to facilitated pumping of the grout as shown in Figure 6.87 and Figure 6.88. In addition to the pocketed connections, 4 in. x 8 in. cylinders were also cast for each specimen to ensure a minimum compressive strength of 5-6 ksi was obtained by the grout prior to testing of the specimen as this was assumed to be a minimum value considered in the design of the connection.

Figure 6.85 Pile Side Shear Studs (48 per pile)

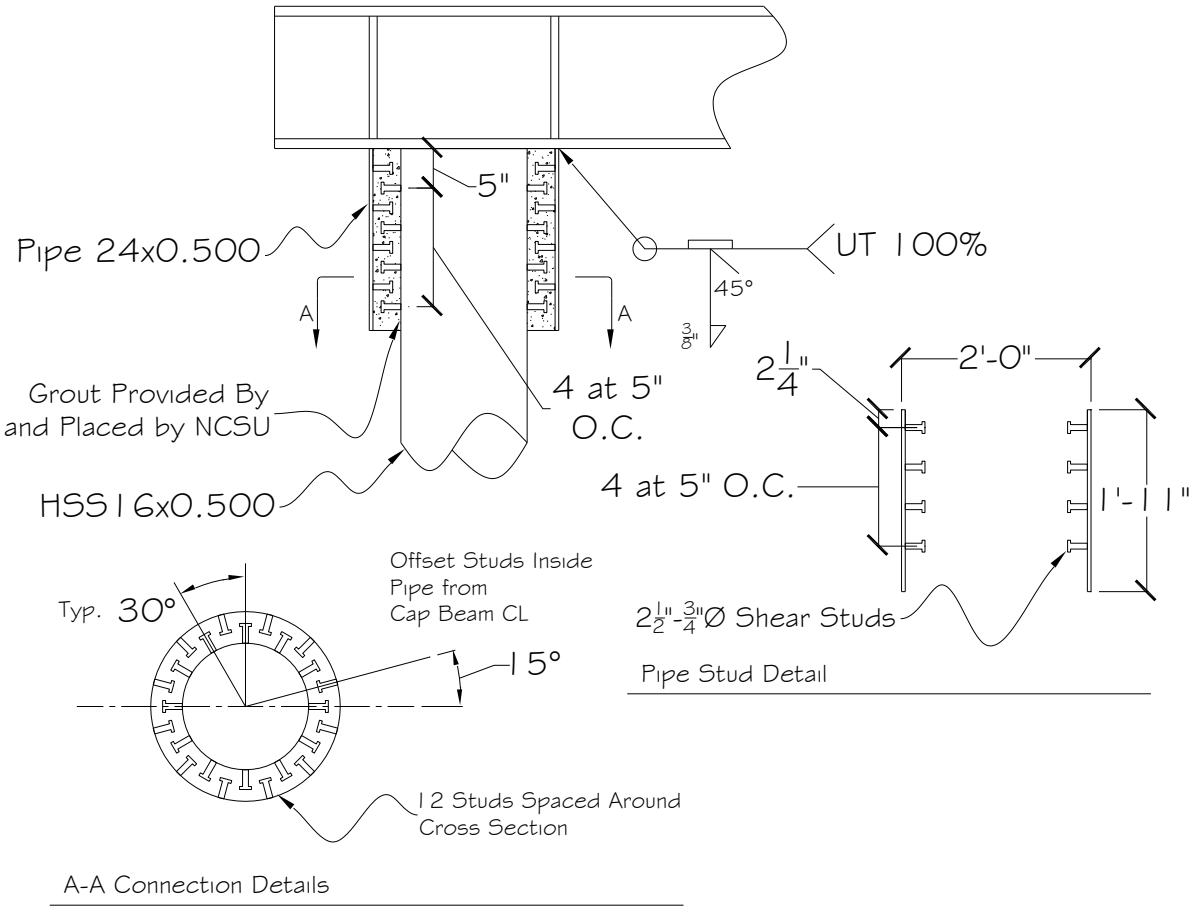

Figure 6.86 Grouted Shear Stud Composite Connection Details

Figure 6.87 Hand Operated Grout Pumping System

Figure 6.88 Formwork with Cast In Place Shut-Off Valve

6.5.2 Evaluation with No Construction Offset (Nominally Ideal)

The first experimental test of a grouted shear stud connection pier, test 2 of the second phase of the steel pier project, was aimed at evaluating the connection configuration when constructed with nominally ideal geometric conditions (i.e. no construction tolerance offsets of the piles). This was achieved in the laboratory by routinely checking construction dimensions during construction of the pier and ensuring the erected piles were correctly spaced as reasonably as possible prior to placement of the cap beam. In addition, visual inspection and measuring of the annular gap spacing prior to placement of the grout was conducted.

In the case of the first grouted shear stud connection test, the material yield stress was found to be 56.5 ksi for the A500 Gr. B pile material based on in-house material testing. This value, combined with the shear span of 8.65 ft. from the pinned supports to the base of the composite connection, resulted in a first yield force of 93.3 kips. The experimental evaluation was based on the typical three cycle set load history which has been described in prior chapters. The application of this load history with the predicted material properties resulted in an experimentally determined first yield displacement of 2.15 in. corresponding to a ductility 1 displacement of 2.82 in. Application of the three cycle set load history produced the experimental force and displacement histories shown in Figure 6.89 and Figure 6.90 respectively. It should also be noted that the average compressive strength of the grout material was found to be 6.85 ksi on the day of testing which was 19 days after casting.

The behavior of the specimen during testing was monitored using both traditional instrumentation and the Optotrak system. As shown in Figure 6.91, strain gauges were located on the extreme fibers of both the pile section and stub pile section to monitor bending strains. Also shown in Figure 6.91, a 2 in. spaced grid of Optotrak LED markers was placed on the east face of each pile in both the pile hinge region and the capacity protected stub pile region. In addition, inclinometers were located 8 in. above the pinned bases to monitor

drifts, linear string potentiometers were attached to the bases to monitor any unanticipated base sliding, and Optotrak markers were placed on the cap beam to monitor global displacements.

The first signs of the development a critical limit state occurred in third positive cycle of the ductility 2 loading stage where a small magnitude of pile wall local buckling began to develop on the north side (compression face) of the south HSS16x0.500 pile along with a small amount of slip between the grout block and the stub pile wall. Upon reversal to the third negative cycle of ductility 2, a similar magnitude of local buckling developed on the south side (compression face) of the north pile as well as grout block slipping as shown in Figure 6.96. In neither case was the buckling significant enough to produce any noticeable strength loss in either the full force-displacement response or the force-displacement response envelopes.

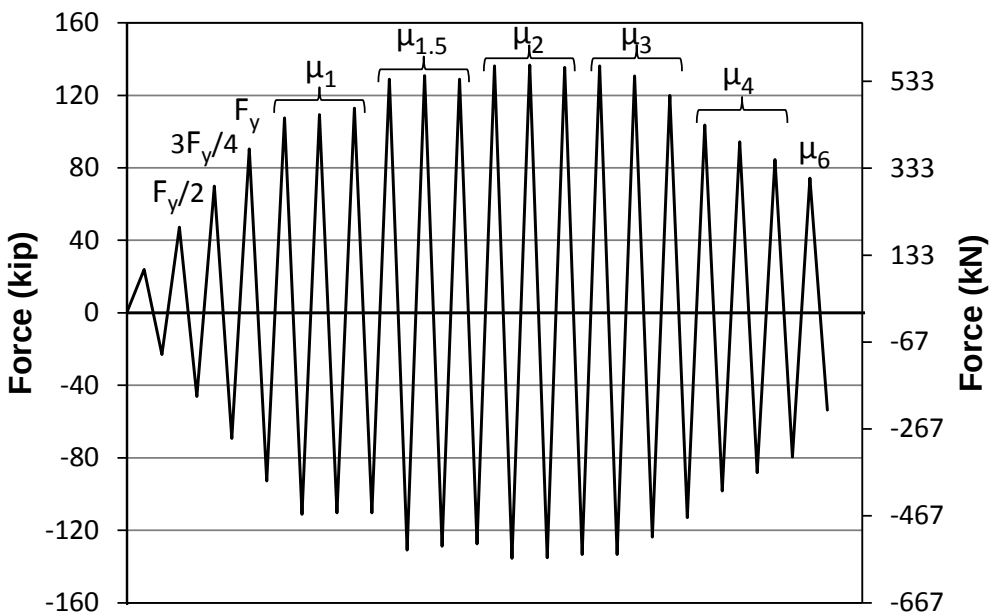

Figure 6.89 Nominally Ideal G.S.C. Experimental Load History

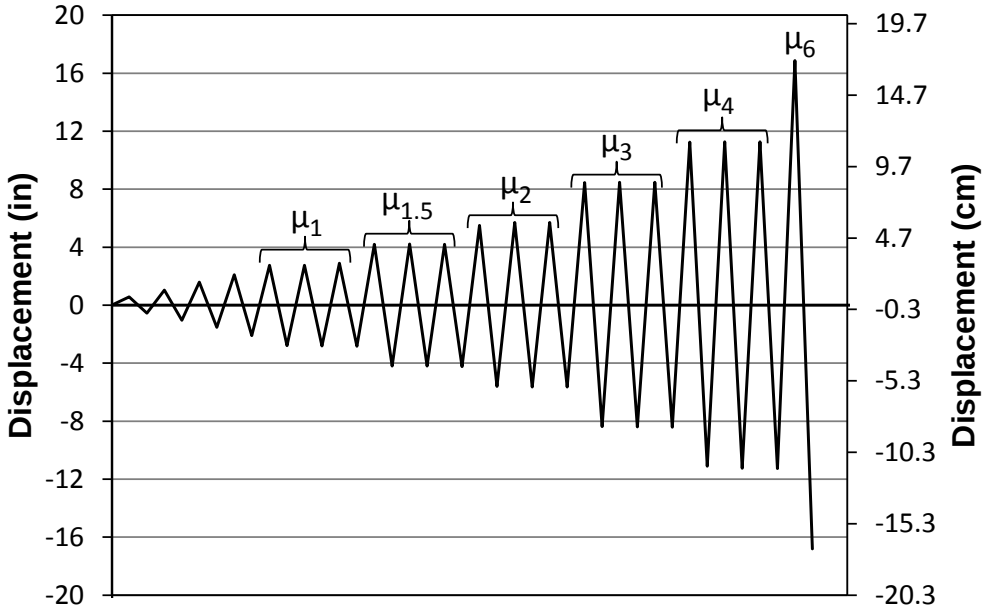

Figure 6.90 Nominally Ideal G.S.C. Experimental Displacement History

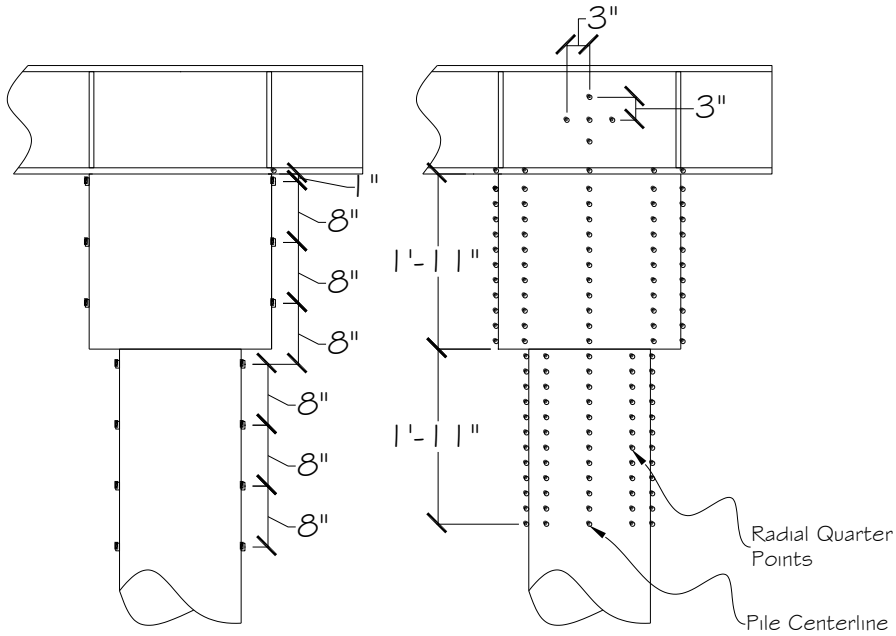

Figure 6.91 Nominally Ideal G.S.C. (Left: SG Layout Right: Optotrak Layout)

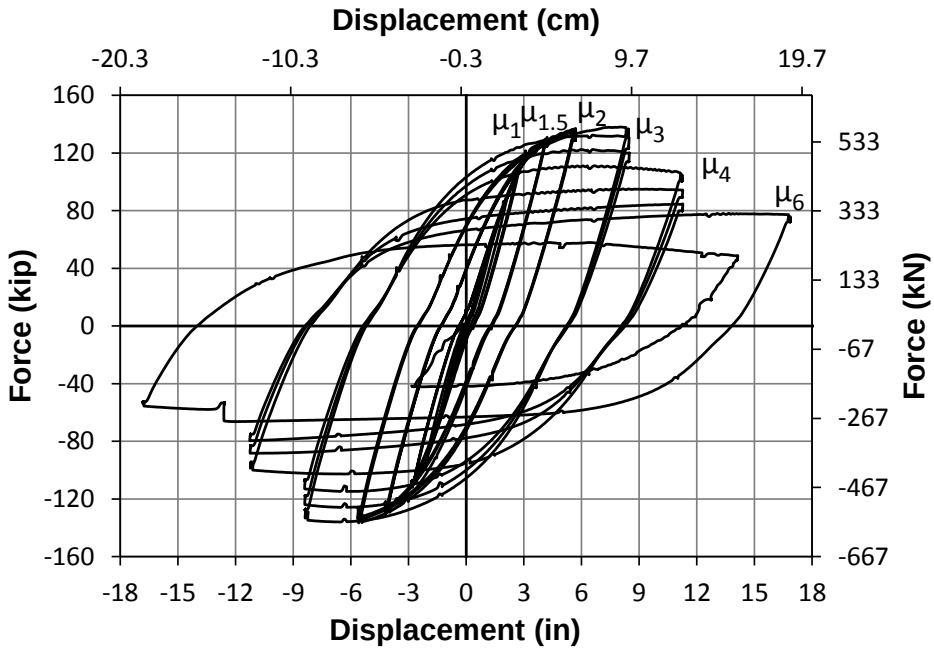

Figure 6.92 Nominally Ideal G.S.C. Force – Displacement Hysteresis

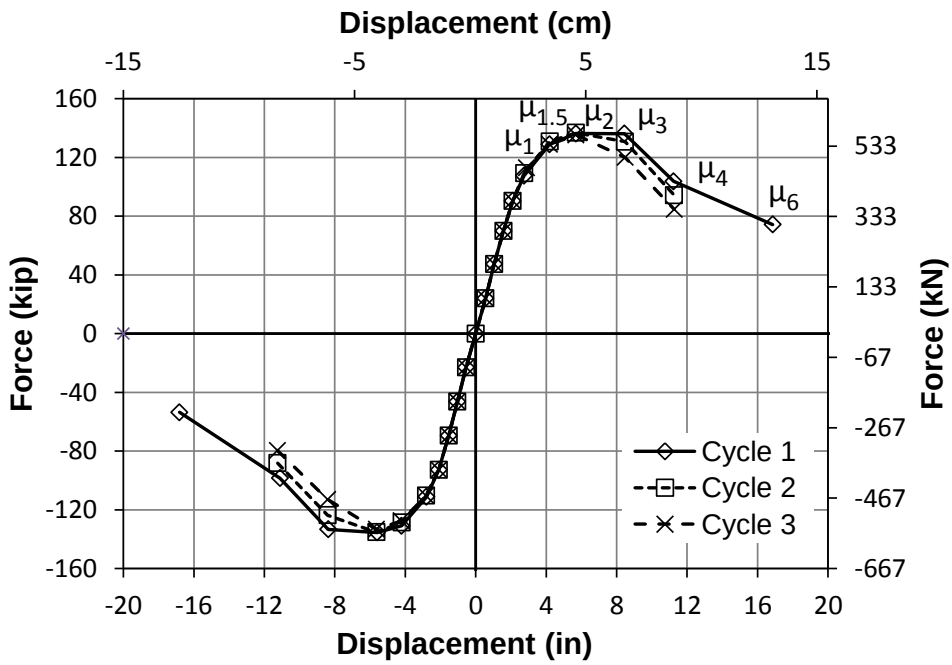

Figure 6.93 Nominally Ideal G.S.C. Force – Displacement Envelopes

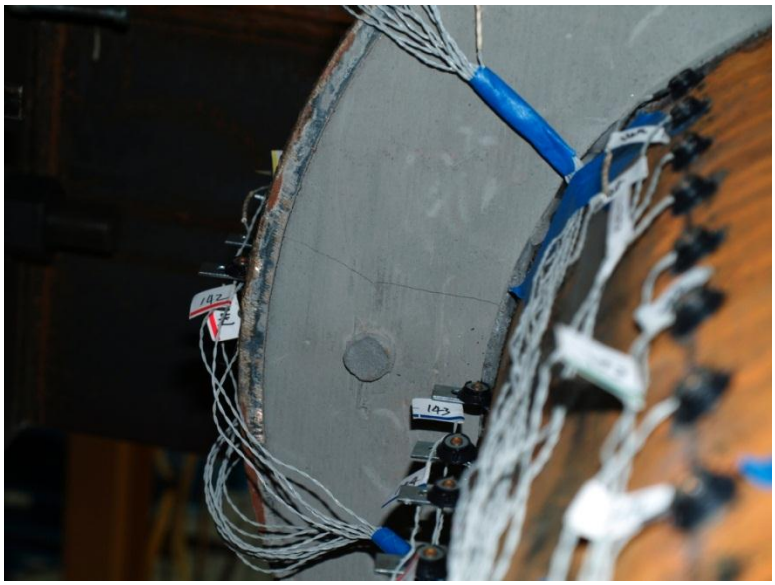

Figure 6.94 North Pile North Face, -Fy Cycle, -93.3 kips, Small Cracks

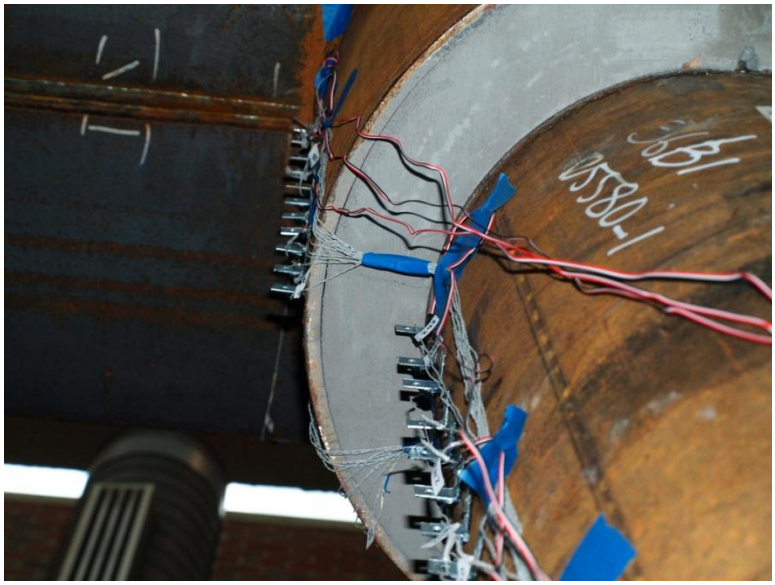

Figure 6.95 North Pile South Face, Ductility 2 Cycle 1, 134 kips, 5.62 in.

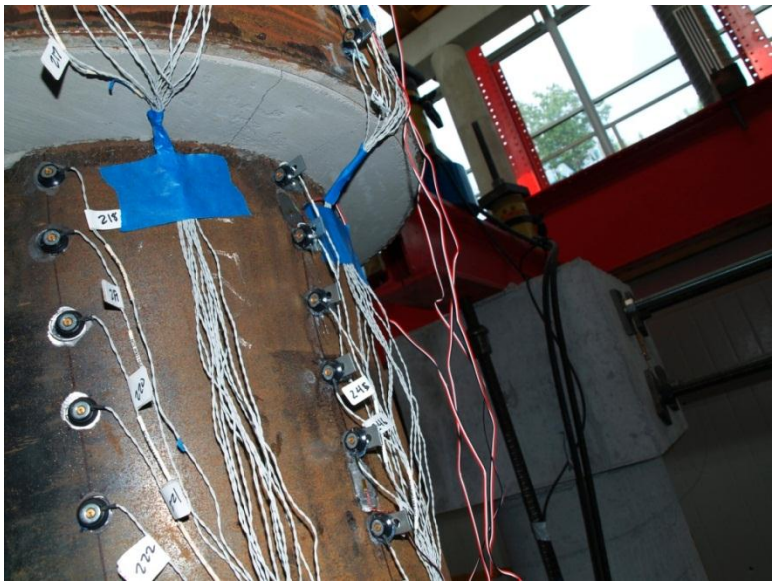

Figure 6.96 North Pile South Face, Ductility 2 Cycle -3, -132 kips, -5.62 in.

Progressing into the first positive and negative cycle of ductility 3, 8.44 in. of displacement as shown in Figure 6.97, led to an increase in the magnitude of local buckling on both piles but again no recognizable strength loss in the system. However, the second and third cycles of the ductility 3 level produced propagation of the pile wall local buckling which consequently led to strength reductions of approximately 10% and 15% respectively. Additionally during these cycles, grout located below the first row of shear studs began to spall as shown in Figure 6.98.

As the test progressed into the ductility 4 cycles, 11.25 in. of displacement as shown in Figure 6.99, the severity of local buckling increased inducing strength reduction magnitudes of approximately 25% to 40% throughout the ductility level. As the magnitude of the local buckling increased, small cracks began to develop in these regions of the pile wall as shown in Figure 6.100. As is also shown, grout began to spall to the depth of the first row of shear studs at this ductility level. Although at the completion of the ductility 4 cycles the damage, as well as the associated strength loss, was signification the pier remained in-tact and did not

exhibited any complete wall cracking. The test was therefore continued to a displacement ductility level of 6.

Figure 6.97 Ductility 3 Cycle 1, 134 kips, 8.44 in.

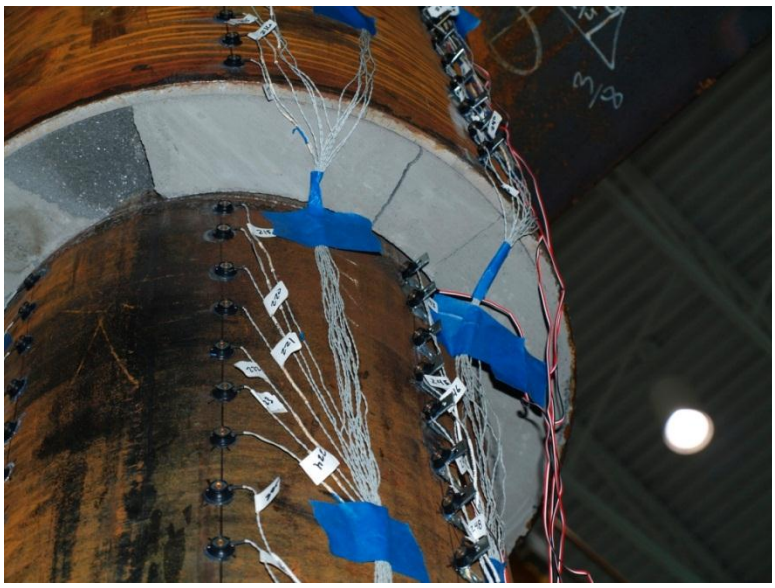

Figure 6.98 Ductility 3 Cycle 2, 126 kips, 8.44in.

Figure 6.99 Ductility 4 Cycle 1, 103 kips, 11.25 in.

Figure 6.100 Ductility 4 Cycle 3, North Pile South Face, 85 kips, 11.25 in.

As the test progressed to the first positive cycle of the ductility 6 level, associated with 16.88 in. of displacement as shown in Figure 6.101, pile wall cracking developed in the south face of the north column and propagated until the ductility 6 displacement was reached.

Similarly, as the specimen was displaced towards the first negative cycle, pile wall cracking developed on the north face of the south column at the location of prior buckling. This cracking propagated until the ductility 6 displacement was reached in the negative direction as shown in Figure 6.102. At this point, approximately 60% strength loss had been experienced so the specimen was returned to a neutral position and the test was assumed to be concluded.

Figure 6.101 Ductility 6 Cycle 1, 75 kips, 16.88 in.

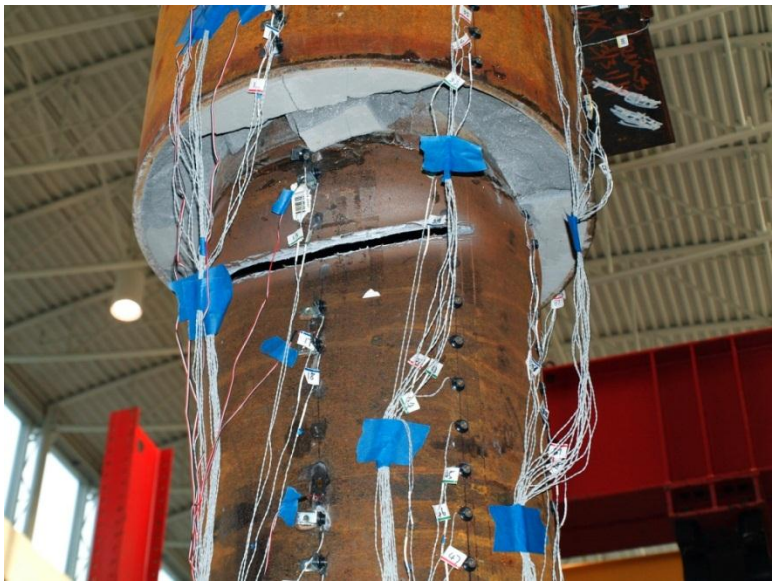

Figure 6.102 Ductility 6 Cycle -1, -54 kips, -16.88 in

Following testing, Optotrak data analysis was conducted to evaluate the effectiveness of the connection configuration to reduce strain demands within the connection itself and appropriately relocate damage. As is shown in Figure 6.103 through Figure 6.106, the connection did remain in the elastic range while large inelastic demands were forced below the bottom of the connection which terminated at 23 in. below the cap beam. As was intended in the design of the connection, a critical region developed immediately below the capacity protected connection on both extreme fibers of the south pile in both directions of loading. Strains in the approximate region of 30000-40000 ($\mu\varepsilon$) were developed in this critical region prior to the formation of local buckling at the ductility 3 stage of loading. Although not shown in this document, a nearly identical response was experienced on the north pile. It should be noted that in some cases, such as Figure 6.103, the vertical strain profile appears to enter the positive range on an extreme fiber that should be experiencing negative strains or vice versa. This condition is generated in a region where significant local buckling has occurred and the orientation of the Optotrak marker is no longer correctly indicative of engineering strains.

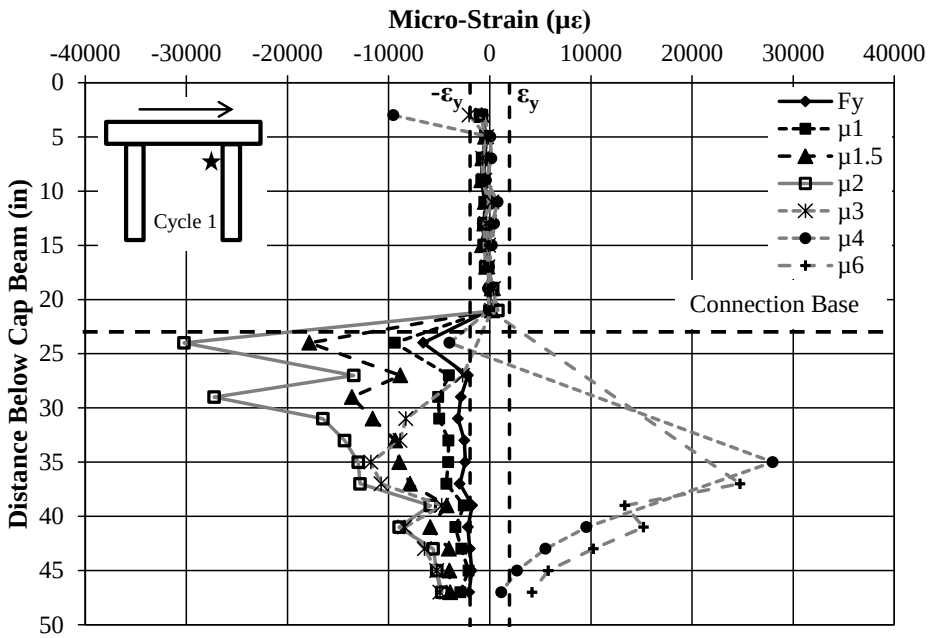

Figure 6.103 South Column North Face – Positive Cycle 1 Vertical Strain Profile

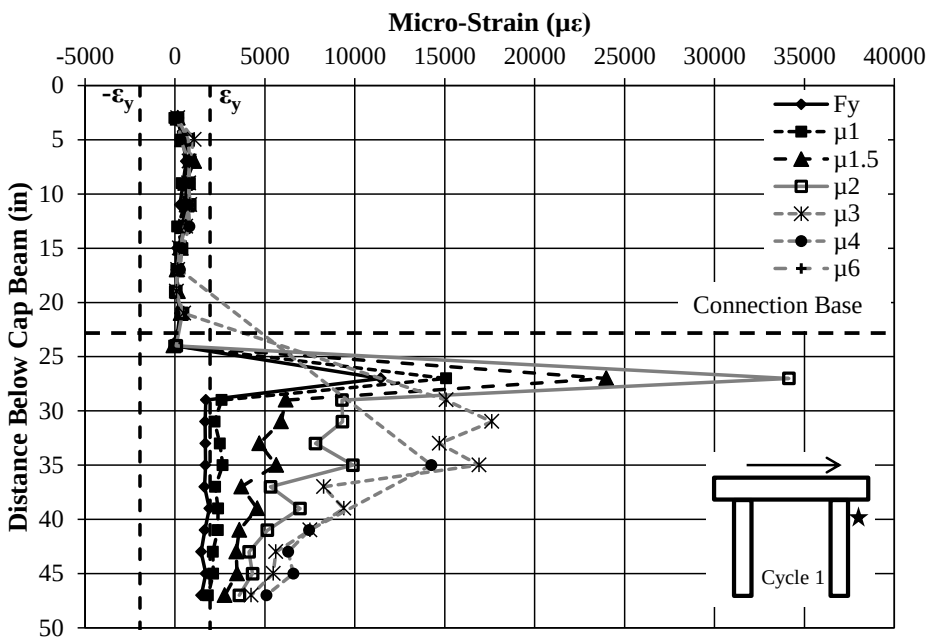

Figure 6.104 South Column South Face – Positive Cycle 1 Vertical Strain Profile

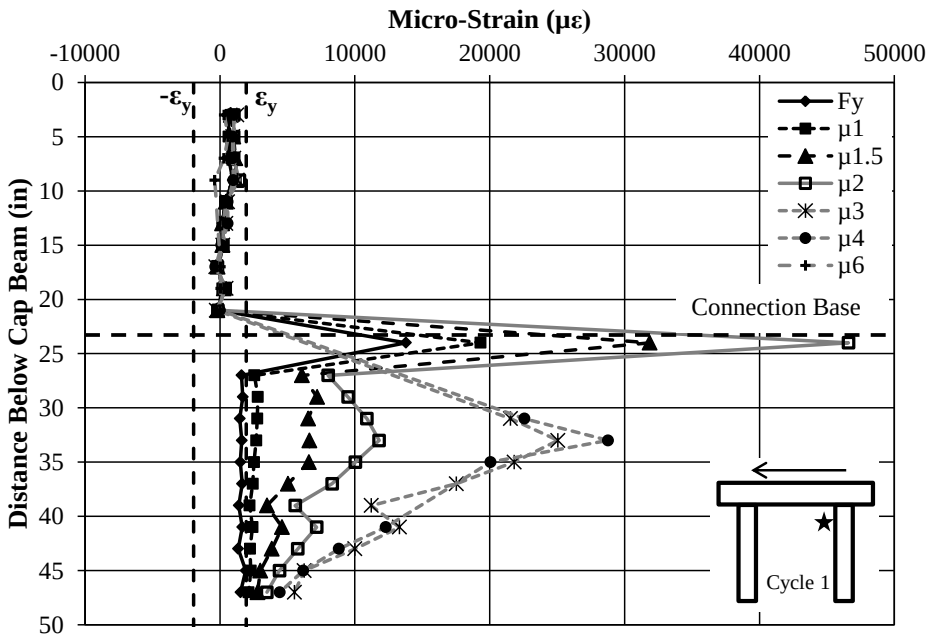

Figure 6.105 South Column North Face – Negative Cycle 1 Vertical Strain Profile

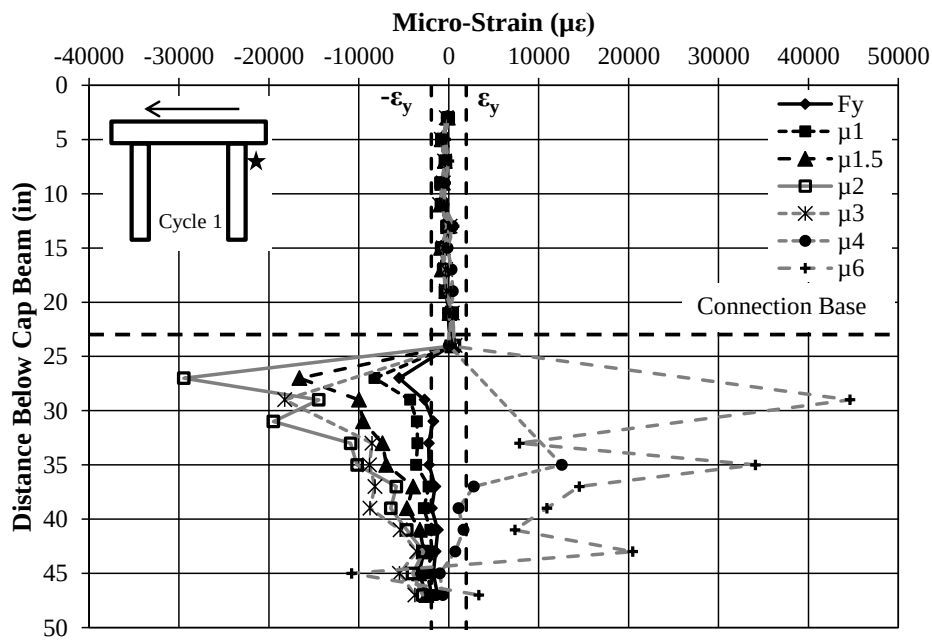

Figure 6.106 South Column South Face – Negative Cycle 1 Vertical Strain Profile

In an effort to verify the global behavior of the pier and the formation of local buckling within the pile section, as well as to better understand the behavior of the connection, detailed Finite Element Modeling of the pier and the connections was conducted. As was the case with the experimental evaluation, ideal geometry with no construction tolerance offsets was considered in the analysis. The model utilized 4-node shell elements as well as 20-node solid brick elements along with a non-linear kinematic hardening material model which considered expected stress strain behavior of the ASTM A500 Gr. B pile material. The non-linear portion of the material model was calibrated with stress – strain data acquired from in house material testing of the actual test 2 material (see Figure A 13).

For simplicity, the grout material was modeled with elastic material behavior and the resulting analytical errors will be discussed where applicable. Due to the harsh geometric conditions required to directly model the shear studs, connection between the grout and pipe elements was achieved by utilizing fastener definitions that considered the geometric pattern of the shear studs to join appropriate areas of each mesh. The model, shown in Figure 6.107, was subjected to a quasi-static displacement history matching that of the test 2 specimen to analytically replicate the experimental procedure.

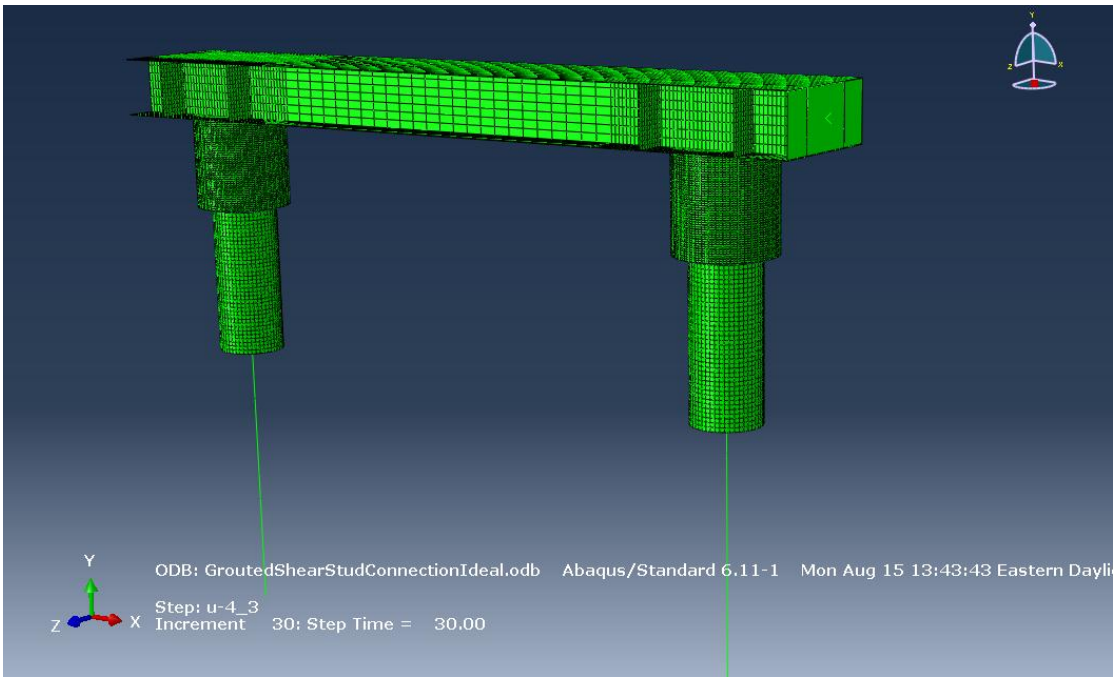

Figure 6.107 Abaqus FEM G.S.C. Pier

Similar to the experimental specimen, the FEM simulation began to develop local buckling of the pile wall below the base of the connection at the ductility 2 displacement level as can be seen in Figure 6.108. In addition, the simulation also indicates tensile strains in the pile wall prior to buckling in the range of approximately 25000-35000 (με), as shown in Figure 6.110, which is comparable to that of the experimental evaluation which indicated approximately 30000-40000 (με). Further, the analysis estimated the critical connection region to remain essentially elastic as the full moment capacity of the pile section was developed at the ductility 2 level as shown in Figure 6.109.

As was the case with the experimental evaluation, the buckling which developed in the simulation at the ductility 2 level increased in magnitude throughout the ductility 3 and 4 cycles as shown in Figure 6.111 and Figure 6.112 respectively. As expected, the propagation of buckling initiated a loss in the strength capacity of the system resulting in a hysteretic response similar in nature to that of the experimental specimen as shown in Figure 6.113.

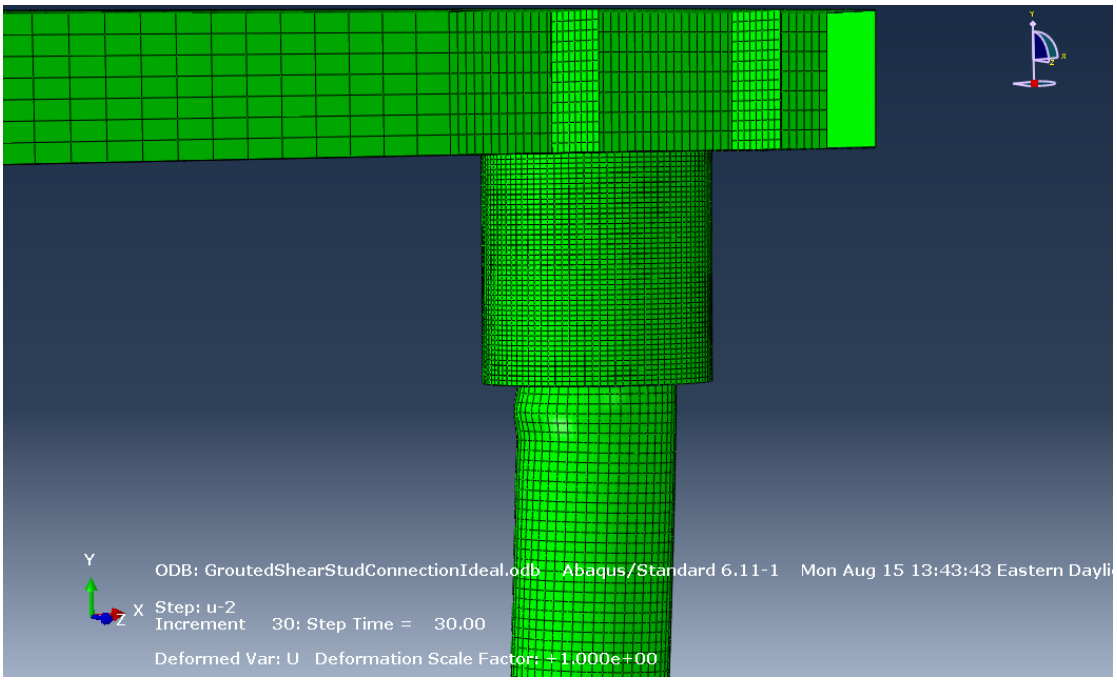

Figure 6.108 Minor Local Buckling of Pile at Ductility 2

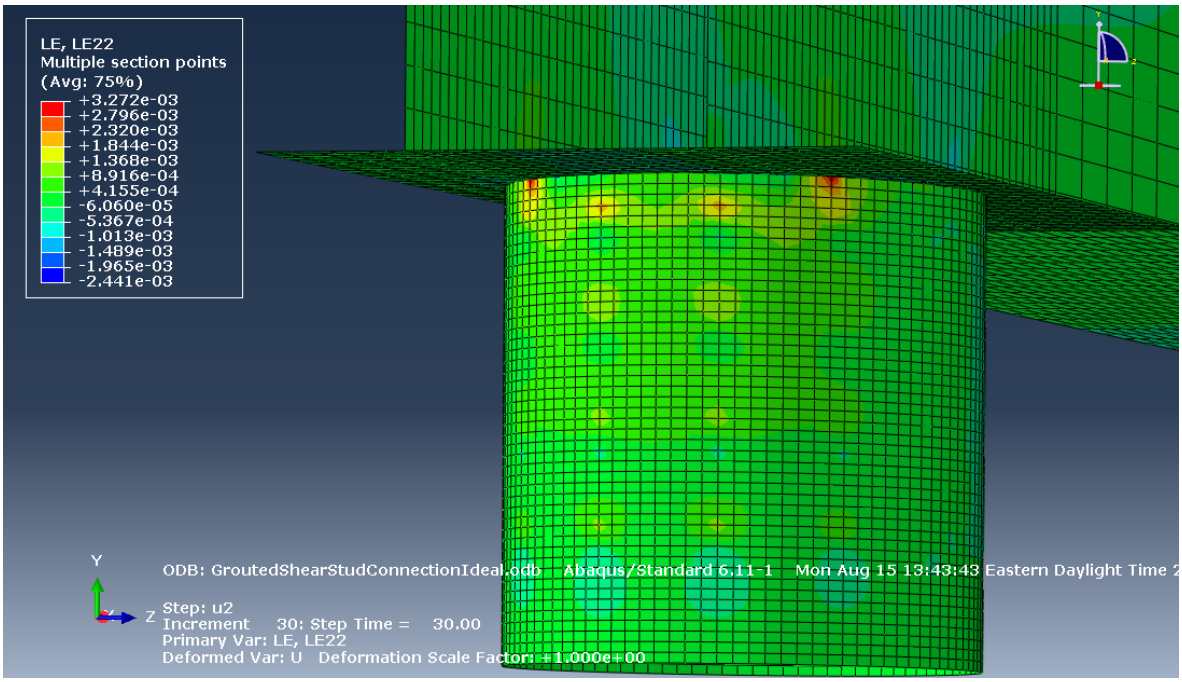

Figure 6.109 Stub Pile Strains at Ductility 2

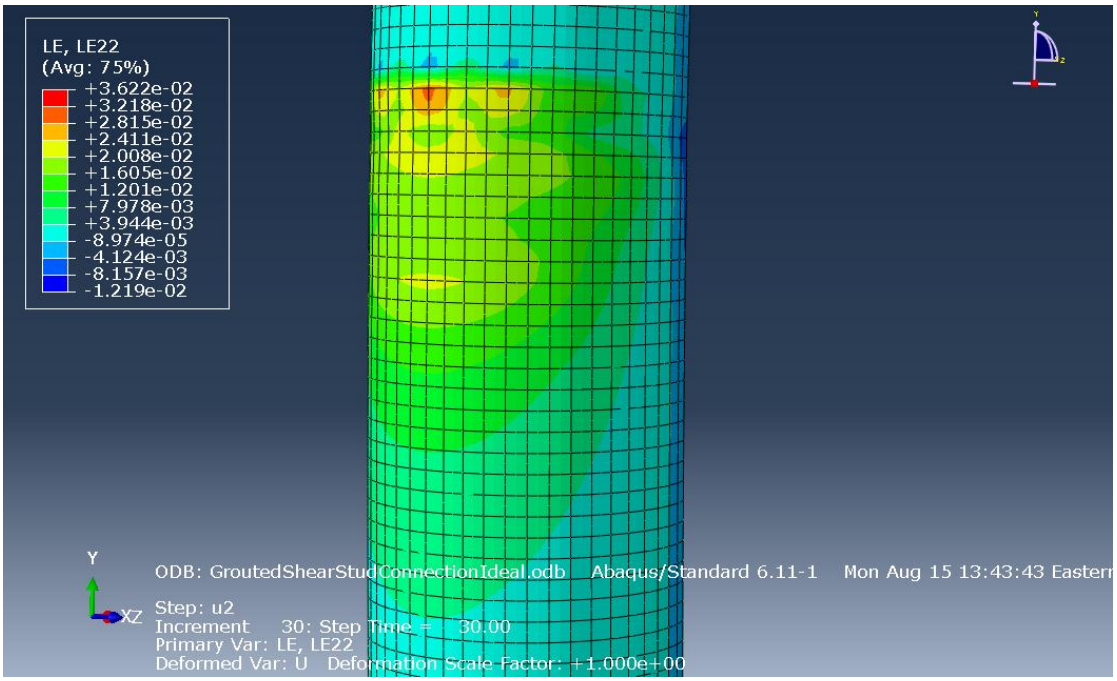

Figure 6.110 Longitudinal Strain Prior to the Development of Buckling

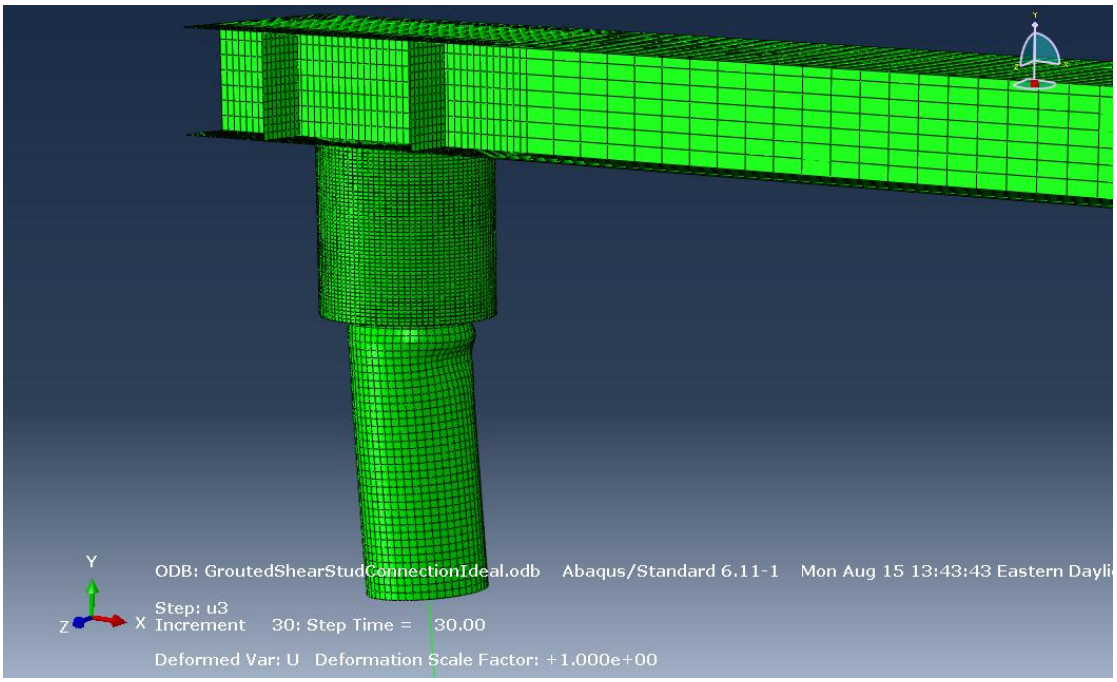

Figure 6.111 Propagation of Local Buckling

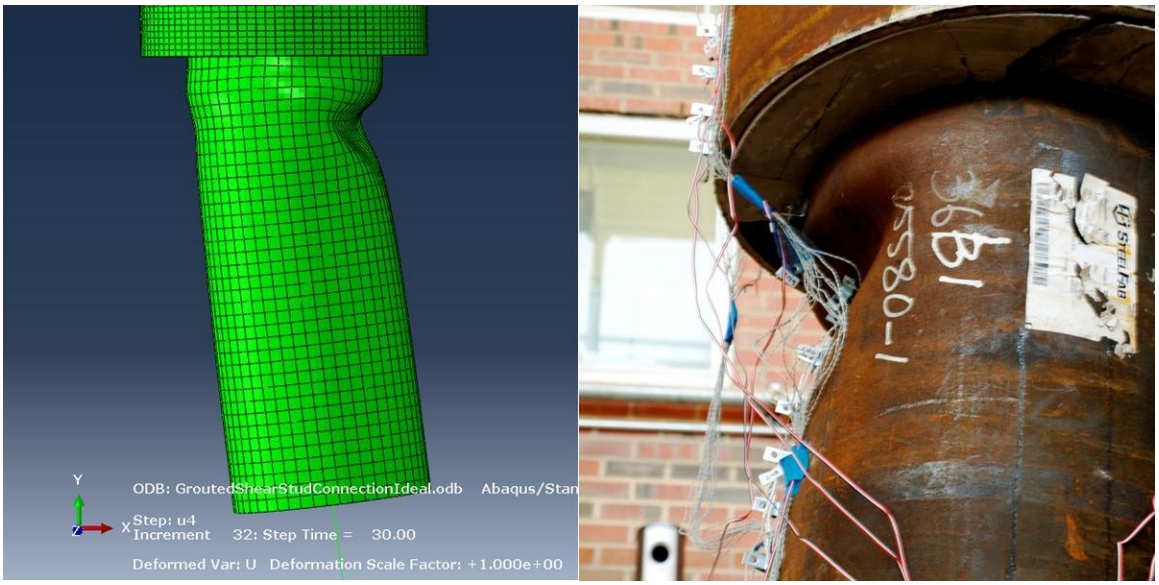

Figure 6.112 Comparison of Propagation of Local Buckling

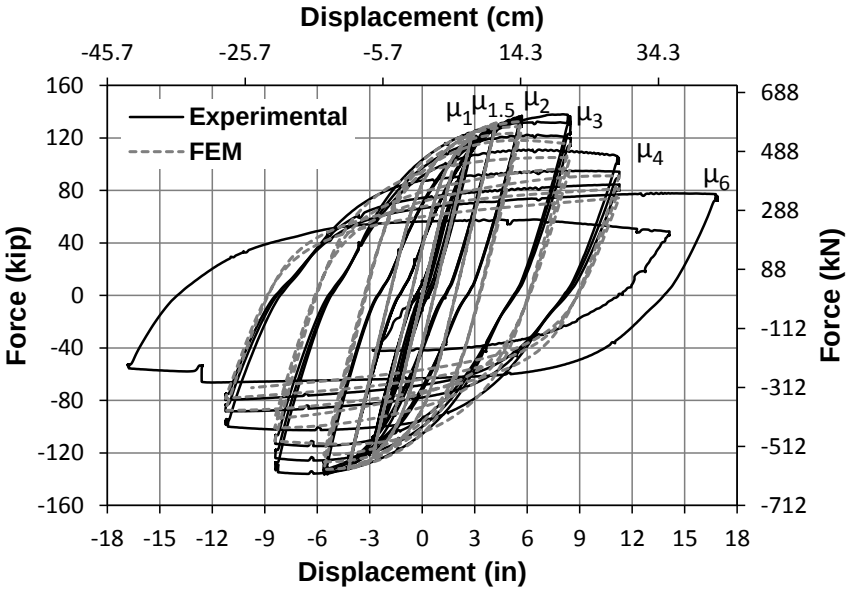

Figure 6.113 FEM vs. Experimental (Test 2) Force – Displacement Response

In an effort to quantify the behavior the grouted connection, Von Mises stresses within the grout section are shown in Figure 6.114 and Figure 6.115 at a ductility level of 2 as this corresponded to the maximum moment demand placed on the connection. It should however be noted that it would be inappropriate to draw conclusions regarding the exact values of the Von Mises stresses since the grout block is modeled with elastic material properties which is likely to develop stresses much higher than that of the capacity of the actual grout material. Hence, it is more appropriate view the results as a reasonable estimate of the actual stress condition by considering only the stress variations (i.e. stress gradient) within grout block while disregarding the actual values.

As shown in Figure 6.114, the grout block is most highly stressed at the top row of shear connectors on the stub pile side of the connection which is a logical conclusion based on the design action. Similarly, Figure 6.115 indicates that the grout at the bottom row of shear studs is most highly stressed on the HSS16x0.500 pile side of the connection which again is logical in accordance with the design action.

Regardless of the fact that stress intensities are highest at the extreme ends of the connection (top outside and bottom inside), the simulation also indicates that considerable levels of stress are also being developed at the other rows of shear studs beyond the extreme layers. In addition, reasonable levels of strain are shown to develop by the simulation in the pile section within the connection on both the compressive and tensile faces of the pile as shown in Figure 6.116 through Figure 6.118. The magnitudes of strain estimated by the simulation are generally however, typically below the yield strain of the pile material. Although these results are not fully conclusive and are based in part on some simplifying modeling assumptions, they seemed to indicate that a reduction in the number of shear connectors could produce undesirable results as each layer of shear studs was estimated be utilized to some degree based on the stress pattern.

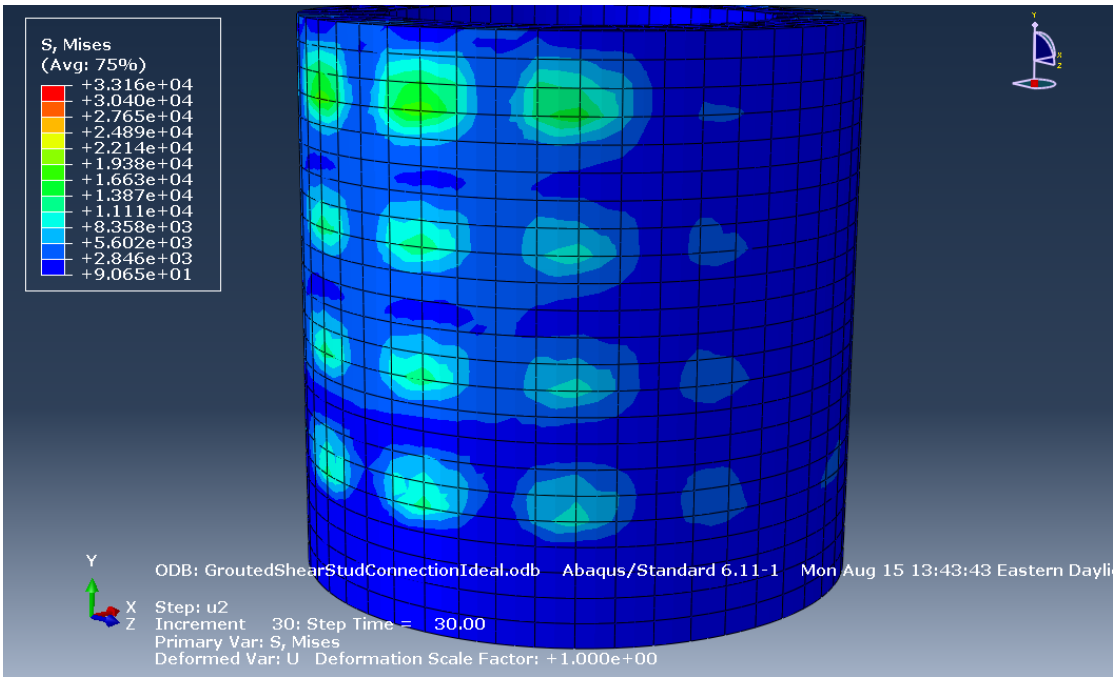

Figure 6.114 Von Mises Stresses in Grout Block at Ductility 2

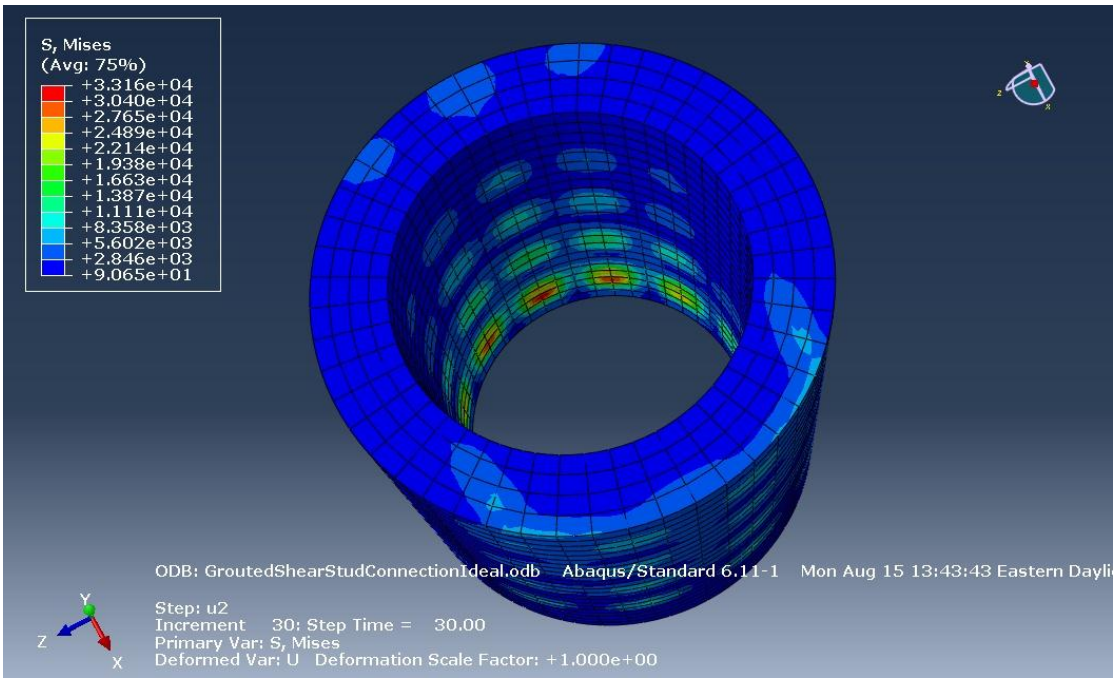

Figure 6.115 Von Mises Stresses in Grout Block at Ductility 2

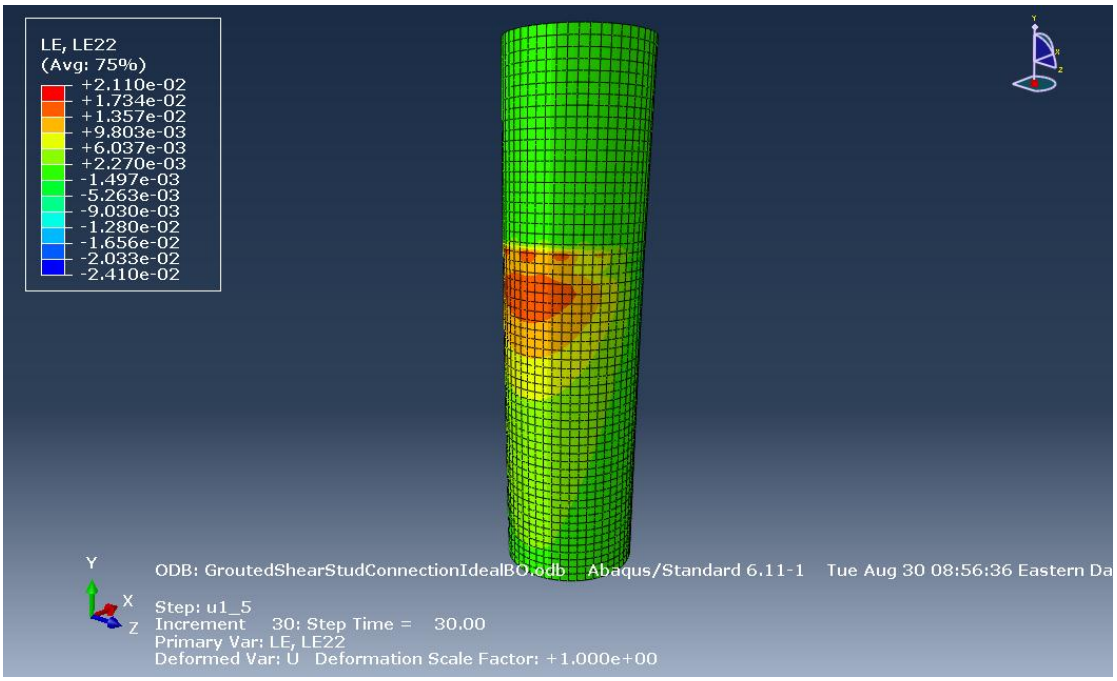

Figure 6.116 Longitudinal Pile Strains at Ductility 2

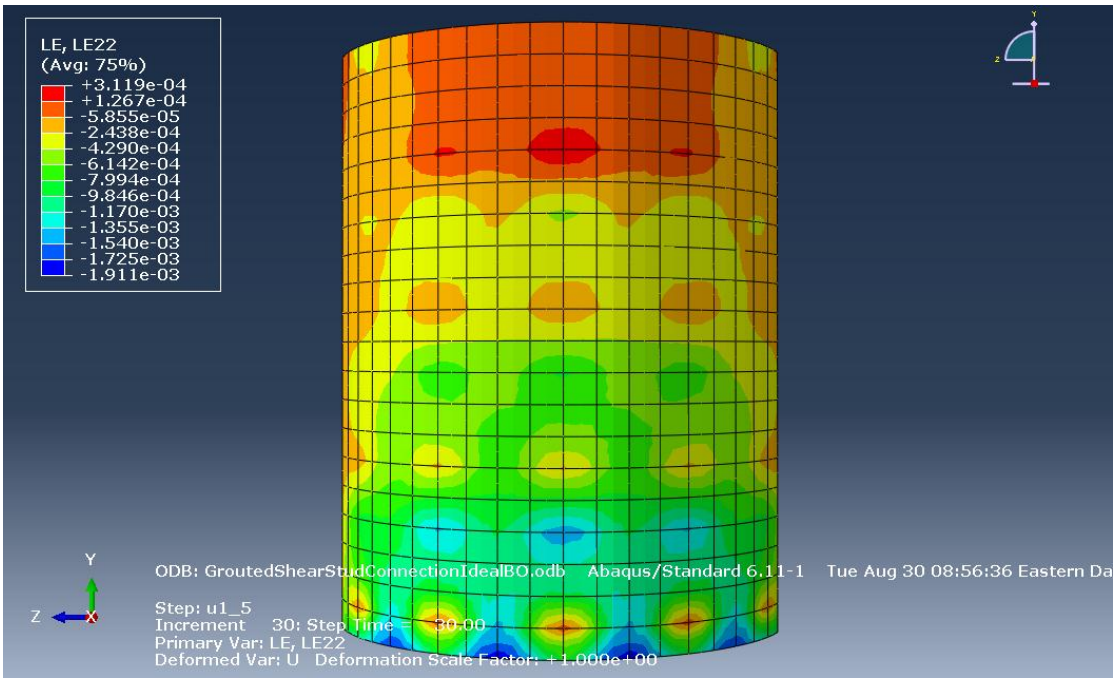

Figure 6.117 Pile Strains in the Connection Region Above the First Row of Studs

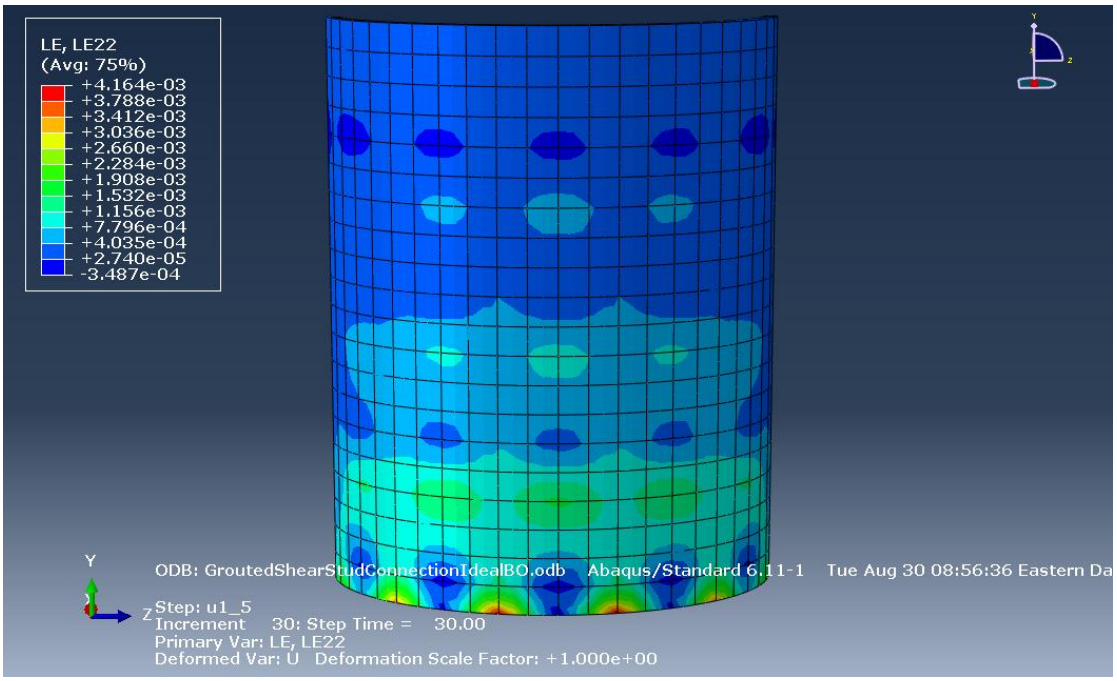

Figure 6.118 Pile Strains in the Connection Region Above the First Row of Studs

The physical results of experimental testing, as well as the results of Optotrak data analysis and Finite Element Analysis, indicated that the composite connection design considered in this test was effective in producing a desirable failure mode in the form of flexural hinging of the HSS16x0.500 pile wall. In addition, the configuration was shown to adequately protect the critical welded region between the stub pile and the cap beam soffit Consequently, undesirable failure modes such weld cracking or tearing the pile wall prior to local buckling were avoided. Although some damage did develop within the grout block at the base of the connection in the form of cracking and spalling, no adverse consequences were induced on the structural response due to these actions.

Although these actions may be considered as low level response limit states such as a serviceability limit state (hence some repair after seismic loading would be necessary) they would not constitute an ultimate limit state. As has been noted, the ultimate limit state in this case would be considered pile wall local buckling likely corresponding to a reliable

displacement ductility level of 3 or 4 depending on the exact considered allowable level of strength loss. These limit states correspond to 8.44 in. and 11.28 in. of lateral displacement, respectively, or 6.3% and 8.4% drift at the cap beam level. It should also be noted that, although associated with large levels of damage and loss of strength, the specimen was able to remain in-tact at a displacement ductility level of 6 associated with 16.88 in. of displacement. This is largely due to the development of a stable failure mode while avoiding more brittle failure mode such as welded connection cracking. From the results presented in this section, the design methodology of developing the axial yield capacity of the pile to determine the required number shear stud connectors appeared to be adequate and perhaps conservative, but no optimization options were immediately evident.

6.5.3 Evaluation with Fully Offset Construction

The fourth test of the second phase of the steel pier project aimed to evaluate the capabilities of the grouted shear stud connection configuration to act successfully as a modified weld protected connection when subjected to maximum possible construction tolerance offsets. As was the case with the nominally ideal specimen (test 2), the test 4 specimen was constructed by first erecting the piles within the laboratory, placing the cap beam over the piles, and vertically pumping the grout material into the annular cavity. However, to evaluate the effects of construction tolerance offsets, the cap beam was intentionally displaced longitudinally by approximately 1 in. such that minimum shear stud overlap of 1/2 in. would exist on the south extreme fiber of each connection as shown in Figure 6.119 and Figure 6.120. This nominal 1 in. offset corresponded to the maximum possible offset for the exact detail provided in the specimen design. It was hoped that the experimental evaluation would show adequate performance which, in turn, would provide a designer confidence in system performance regardless of construction tolerance issues. Hence, as long as the driven pile element fell within the stub pile element, a designer should be able to expect a ductile pile hinging mode of failure.

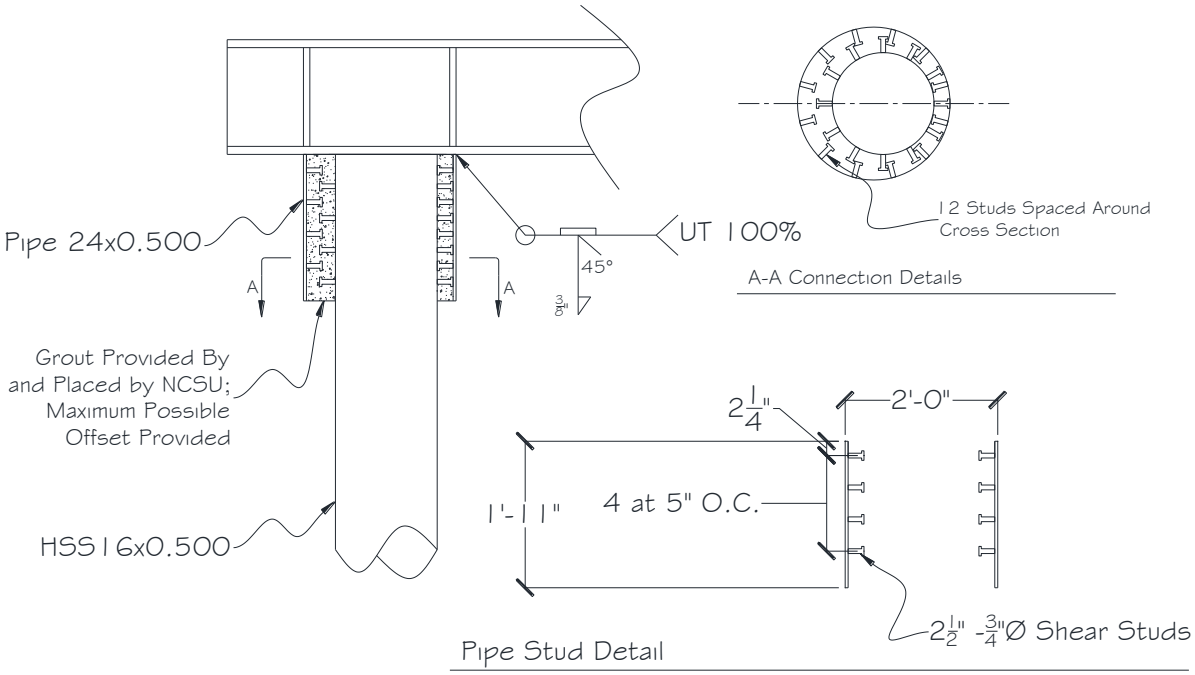

Figure 6.119 G.S.C. Detail with Full Construction Tolerance Offset (+/- 1in.)

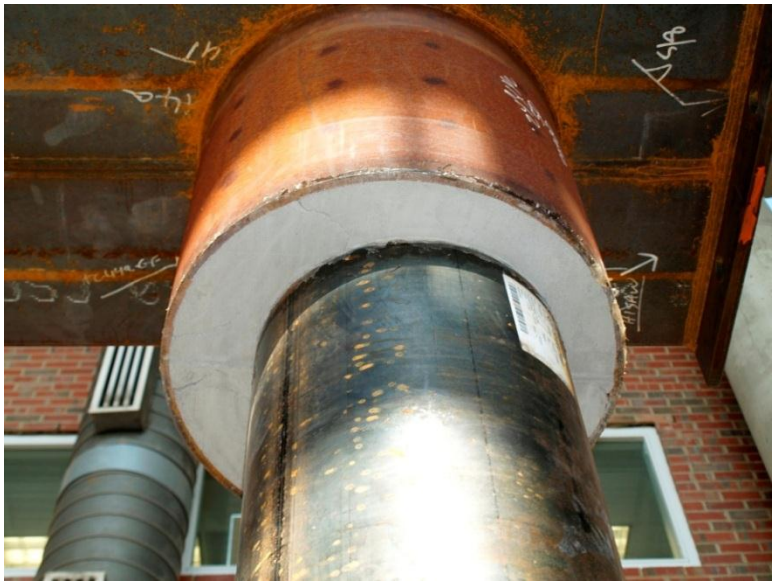

Figure 6.120 G.S.C. Construction Tolerance Offset

In the case of the grouted shear stud connection test with construction tolerance offsets, no in-house material testing was conducted prior to the experimental evaluation. Although the material certification report indicated a yield stress of approximately 69 ksi, which seemed unlikely high for the ASTM A500 Gr. B. material, a first yield force of 93.3 kips was considered which corresponds to a material yield stress of 56.5 ksi. This was done such that the response of the experimental test with nominally ideal geometry could be directly compared to that of the offset construction. The application of this assumed first yield force resulted in a first yield displacement of 2.11 in. which was nominally identical to that of the first G.S.C. test which indicated a first yield displacement of 2.15 in. The corresponding ductility 1 displacement for the offset test was 2.82 in. Application of the three cycle set load history produced the experimental force and displacement histories shown in Figure 6.121 and Figure 6.122 respectively. It should also be noted that an average compressive strength of the grout material was found to be 9.76 ksi on the day of testing, 14 days after grouting took place.

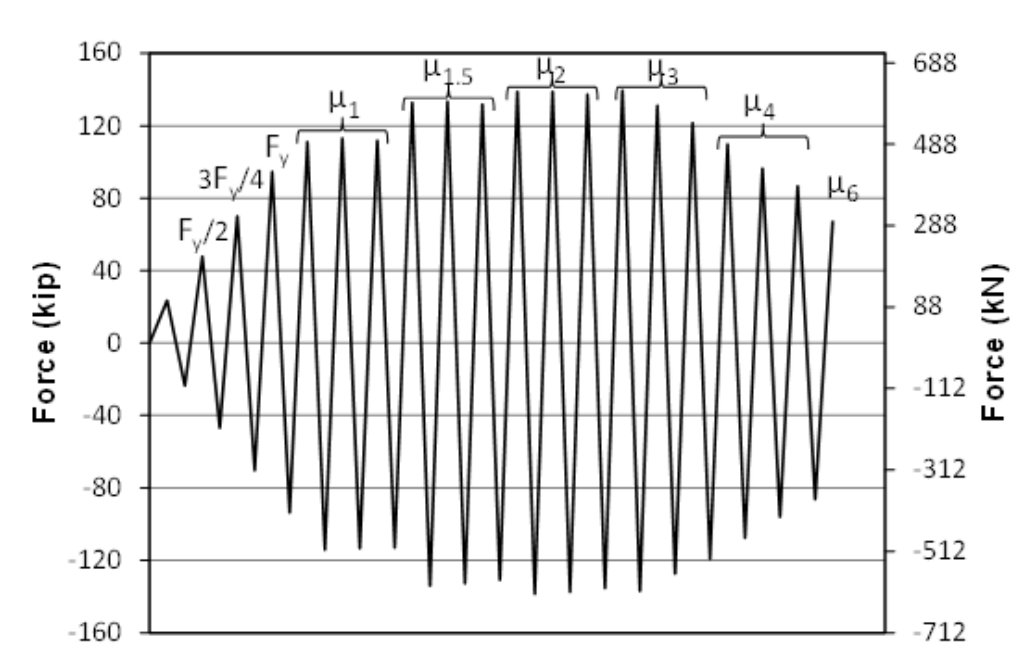

Figure 6.121 Full Offset G.S.C. Experimental Load History

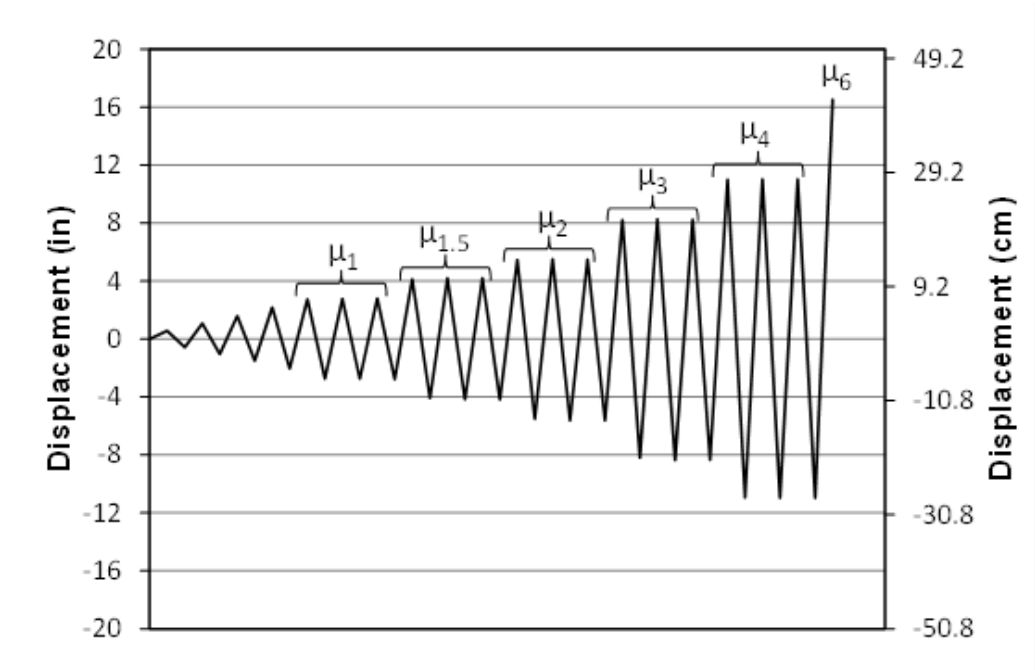

Figure 6.122 Full Offset G.S.C. Experimental Displacement History

As was the case with the ideal geometry specimen, behavior was monitored during testing using both traditional instrumentation and the Optotrak system. Although the Optotrak marker grid layout remained the same, the location of the electric resistance strain gauges was altered. As shown in Figure 6.123, a total of 24 gauges were placed inside the HSS 16x0.500 pipe pile in the connection region prior to construction of the pier. This configuration resulted in 6 gauges being located on each extreme fiber of each pile. The layout was chose in an effort to monitor the strain gradient along the pile wall in the connection region to better understand the connection behavior as was done analytically as has been discussed. The resulting data and associated conclusions from the strain gauge layout will be discussed subsequently in this section.

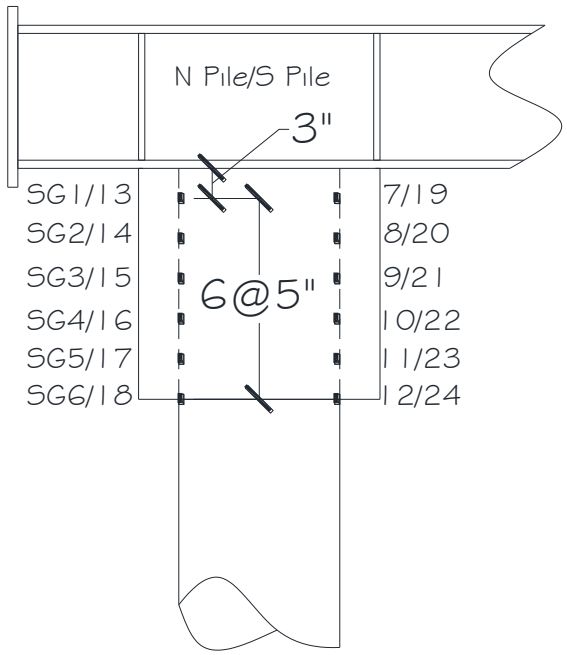

Figure 6.123 Full Offset G.S.C. Internal Strain Gauge Layout

The results of the experimental test showed the specimen to perform in an adequate manner with no appreciable signs of damage that could be related to strength loss or any upper bound limit state throughout the second ductility level as is shown in Figure 6.124 and Figure 6.125. However, minor signs of inconsequential damage were experienced as early as the negative 1/4 yield cycle where small cracks were observed at the base of the grout pocket of the south column as shown in Figure 6.126. Throughout the remaining elastic cycles as well as the ductility 1 and 2 cycles, more small cracks developed in addition to the formation of small gaps between the grout block and the pile and/or stub pile walls on the tensile faces of each column.

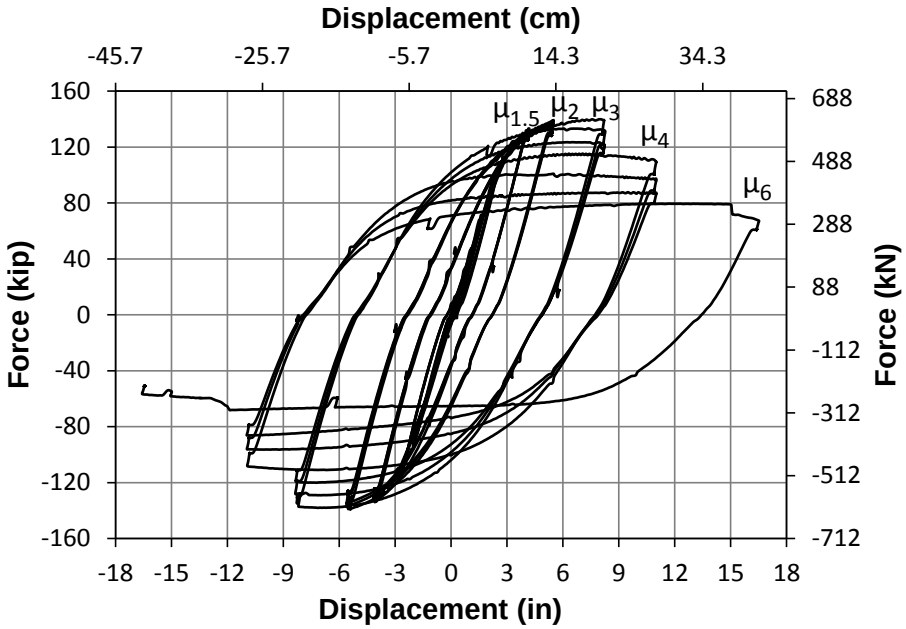

Figure 6.124 Full Offset G.S.C. Force-Displacement Hysteresis

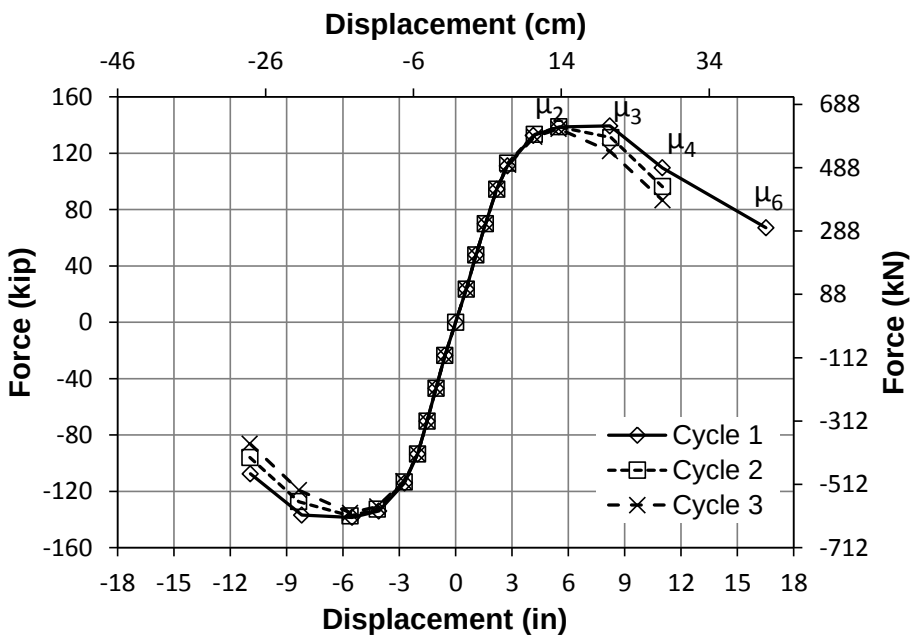

Figure 6.125 Full Offset G.S.C. Force-Displacement Envelopes

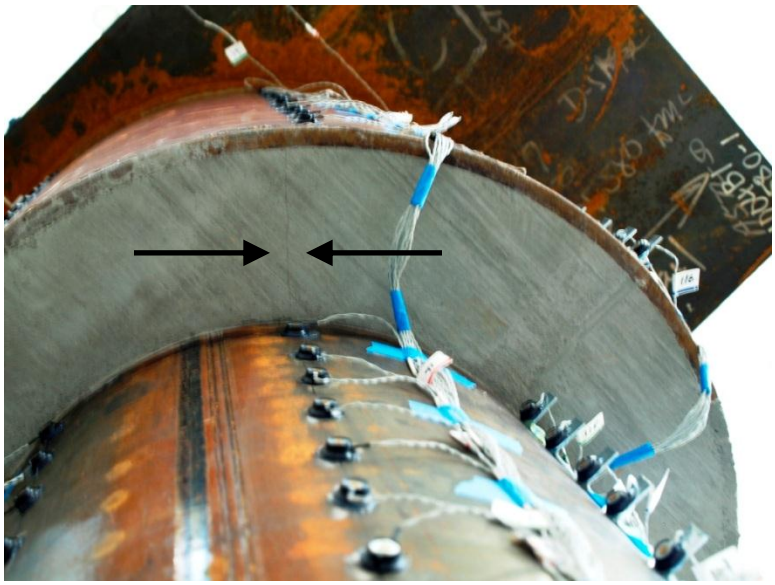

Figure 6.126 South Pile, -Fy Cycle, -23.3 kips,-0.57 in., Small Cracks

The first signs of the development of a critical limit state occurred in the second negative cycle of the ductility 2 loading stage where a small magnitude of pile wall local buckling began to develop on the south side (compression face) of the north pile along with a small amount of slip between the grout block and the stub pile wall as shown in Figure 6.126. Progressing into the third positive cycle of the ductility 2 loading stage led to the development of a similar magnitude of local buckling on the north face of the south pile. This observed response is similar in nature to that of test 2 where minor amounts of local buckling developed in the third positive and negative cycles of ductility 2. As in test 2, the observed local buckling at this stage of the load/displacement history was not significant enough to produce any noticeable strength loss in either the full Force-Displacement response or the Force-Displacement response envelopes. In addition to the local buckling, grout spalling below the first level of shear studs was experienced in the ductility 2 level but appeared to be inconsequential to the response of the system as was the case in the nominal ideal investigation.

Figure 6.127 North Pile South Face, Ductility 2 Cycle -2, -128 kips, -5.52 in.

Progressing into the first positive and negative cycle of ductility 3, 8.27 in. of displacement, led to an increase in the magnitude of local buckling on both piles but again no recognizable strength loss in the system. However, the second and third cycles of the ductility 3 level produced propagation of the pile wall local buckling which consequently led to strength reductions of approximately 6% and 13% respectively. Additionally during these cycles, grout located below the first row of shear studs began to spall as shown in Figure 6.128.

As the test progressed into the ductility 4 cycles, 11.03 in. of displacement as shown in Figure 6.129, significant local buckling had developed inducing strength reduction magnitudes of approximately 25% to 40% throughout the ductility level. Although the magnitude of the local buckling increased in this ductility level as shown in Figure 6.130, the formation of small cracks which were noted to develop in the pile wall in test 2 at this stage of loading were not noted in this test. In addition to the propagation of buckling, continued spalling of grout below the first level of shear studs was experienced as can also be seen in Figure 6.130. At the completion of the ductility 4 cycles, the damage as well as the

associated strength loss, was significant but the bent remained in-tact and did not exhibited any pile wall cracking. The test was therefore continued to a ductility level of 6.

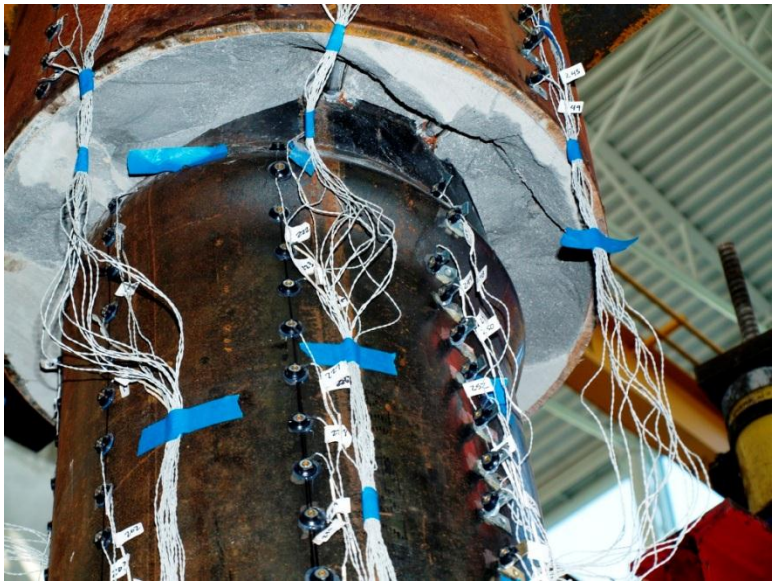

Figure 6.128 Ductility 3 Cycle -3, -119 kips, -8.27in.

Figure 6.129 Ductility 4 Cycle 1, 105 kips, 11.03 in.

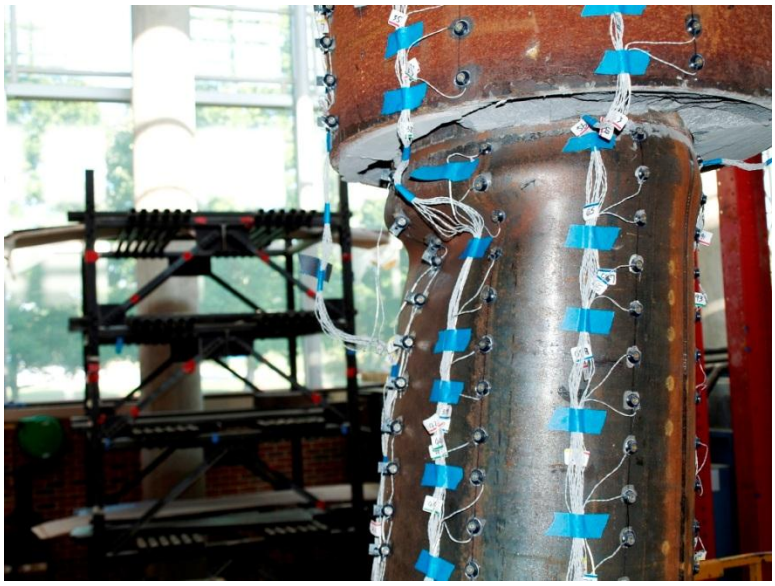

Figure 6.130 Ductility 4 Cycle 3, South Pile North Face, 87 kips, 11.03 in.

As the test specimen was loaded to the first positive cycle of the ductility 6 level, associated with 16.55 in of displacement as shown in Figure 6.131, small cracks began to develop on the north face of the south column at the location of local buckling. Loading reversal towards the first negative ductility 6 displacement led to cracking through the pile wall on the north face of the south column as well as the south face of the north column. Interestingly, as shown in Figure 6.132, the severity and orientation of the buckled pile wall induced fracture along the seam weld of the pile. Although this was inconsequential to the performance of pier due to the severe strength degradation which had already occurred, this cracking mechanism had not been seen in any past test. At this point, approximately 60% strength loss had been experienced along with considerable cracking so the specimen was returned to a neutral position and the test was assumed to be concluded.

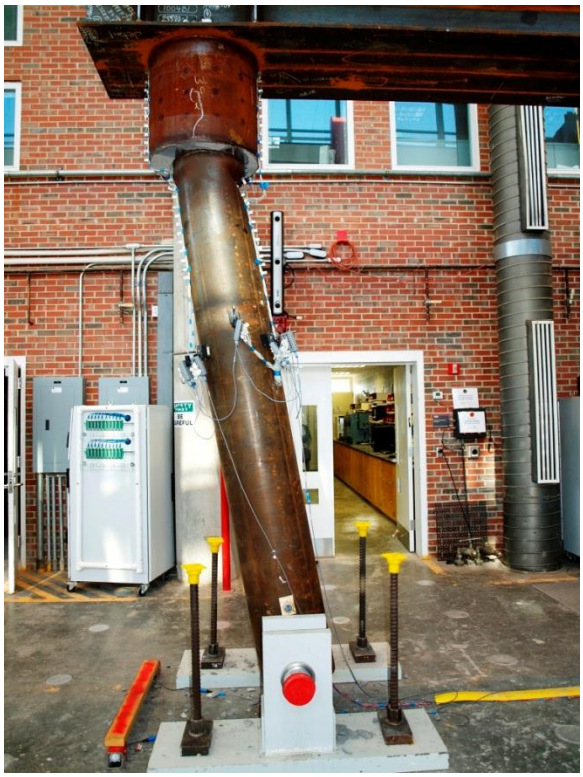

Figure 6.131 Ductility 6 Cycle 1, 67 kips, 16.55 in.

Figure 6.132 Ductility 6 Cycle -1, -52 kips, -16.55 in.

As has been noted throughout this section, the test specimen with offset pile placements performed in a manner nominally identical to that of test 2 which had no construction tolerance offset. For additional comparison of the global behavior of both tests, Figure 6.133 provides the Force – Displacement hysteretic response from each test to allow for a direct assessment regarding the effects of the tolerance offset. As is shown, it appears from this test that the global response of the pier was unaffected by the minimum overlapping of shear connectors on the side of the connection with the largest annular space. In addition to this conclusion, the similarity of two tests can also be viewed as a validation of the behavior of the connection since no adverse effects due to the offset were noticeable.

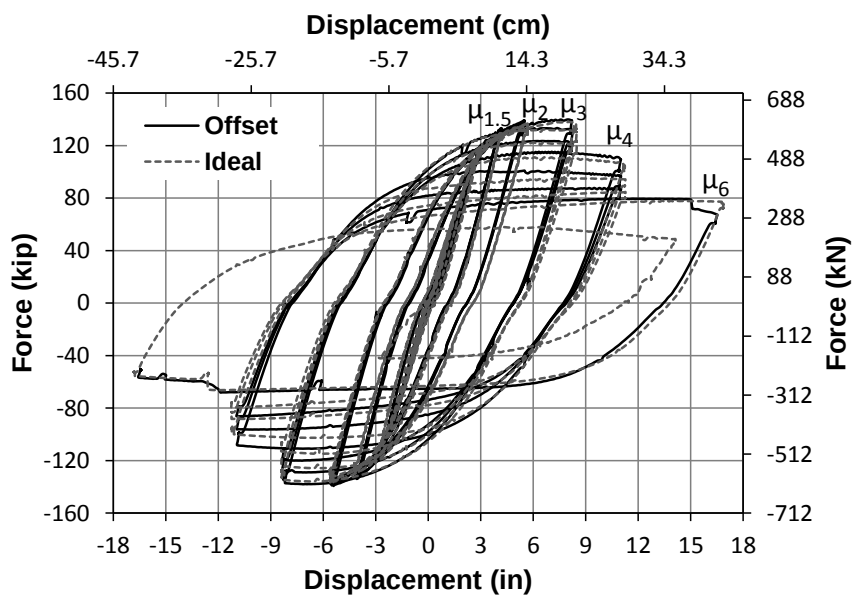

Figure 6.133 Offset (Test 4) vs. Ideal (Test 2)

Following testing, Optotrak data analysis was again conducted to evaluate the effectiveness of the connection configuration to reduce strain demands within the connection itself and appropriately relocate damage. As shown in Figure 6.134 through Figure 6.137, the connection did remain in the elastic strain range while large inelastic demands were

forced below the bottom of the connection as was the case without construction offsets. As was intended in the design of the connection, a critical region developed immediately below the capacity protected connection on both extreme fibers of the south pile in both directions of loading. Strains in the approximate region of 30000-40000 (με) were developed in this critical region prior to the formation of local buckling at the ductility 3 stage of loading. Also, the strain elevations presented here are nearly identical to those of the presented in the test 2 summary again indicating little or no effects were experienced due to the tolerance offset.

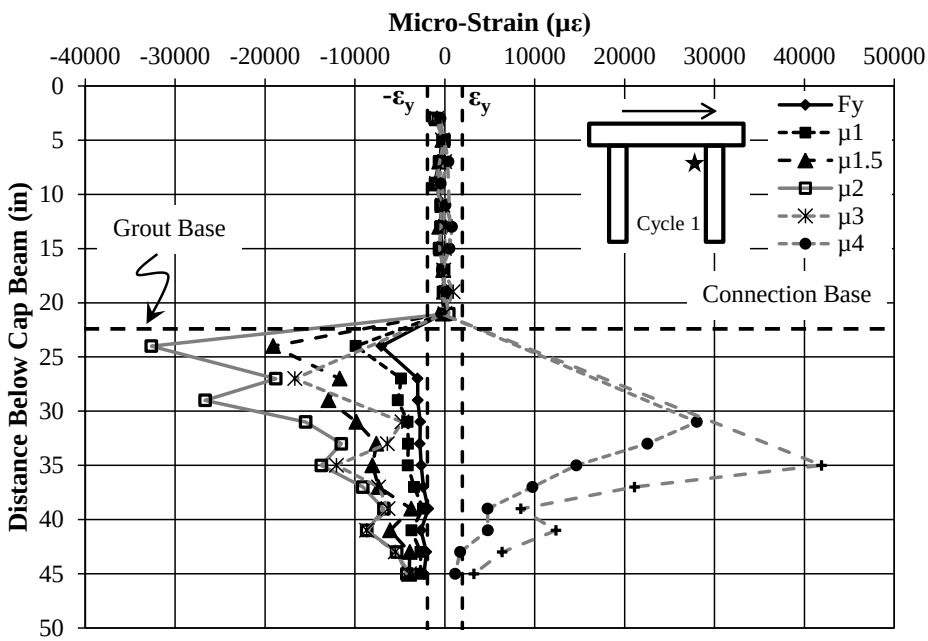

Figure 6.134 South Column North Face – Positive Cycle 1 Vertical Strain Profile

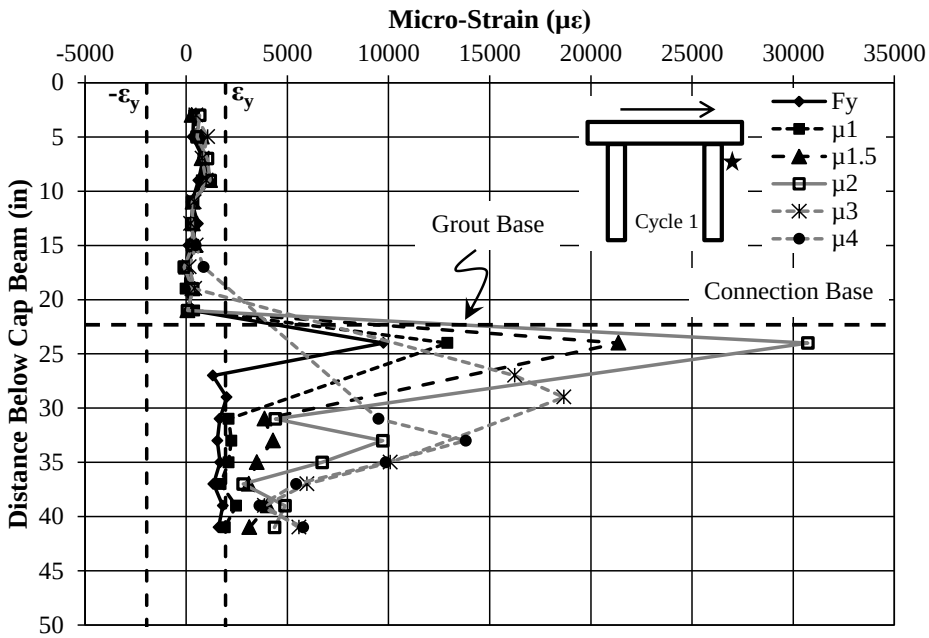

Figure 6.135 South Column South Face – Positive Cycle 1 Vertical Strain Profile

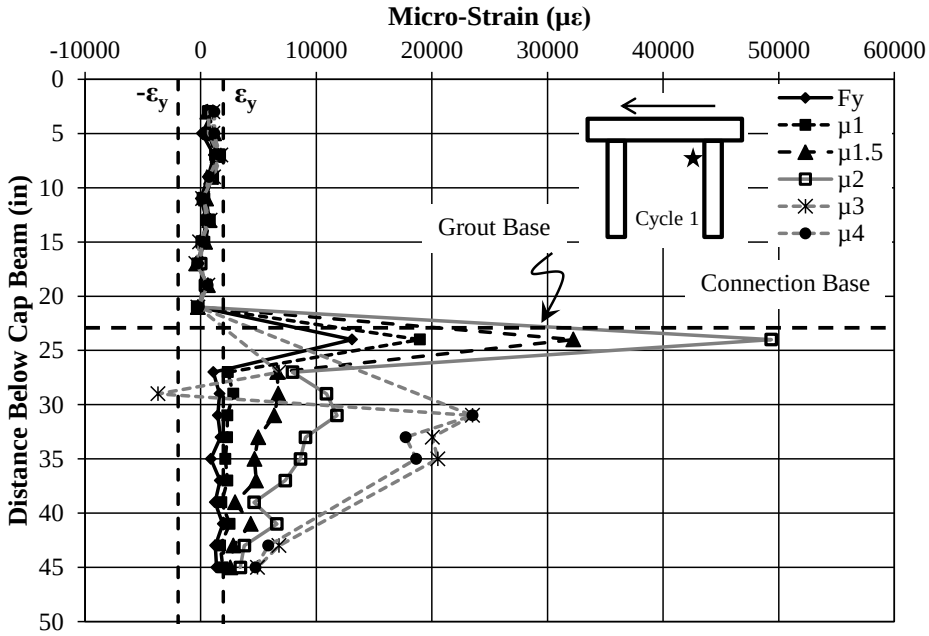

Figure 6.136 South Column North Face – Negative Cycle 1 Vertical Strain Profile

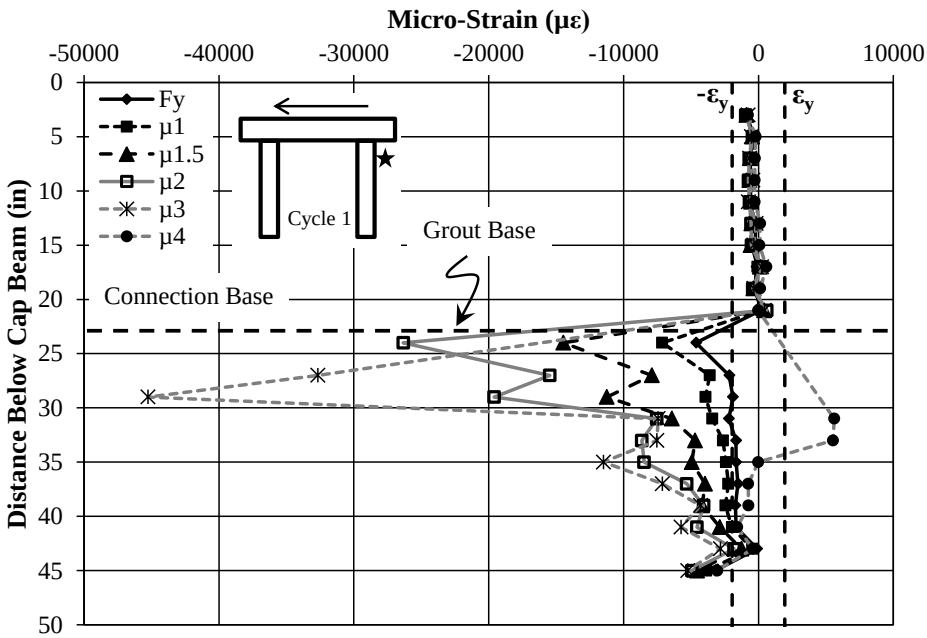

Figure 6.137 South Column South Face – Negative Cycle 1 Vertical Strain Profile

In an effort quantify the behavior of the connection throughout its length data was reviewed from the internal strain gauges shown in Figure 6.138, following testing. The strain elevations provided in Figure 6.139 through Figure 6.142 indicate a relatively linear strain gradient prior to the large strain accumulation which occurs at the base of the connection as local buckling develops. Also it is shown, as expected, that the top strain gauge in all cases provides a reading close to zero since by design full force transfer should have taken place at this point in the connection. Given the relatively linear nature of the strain gradient, it is not immediately apparent that a reduction in the number of shear studs (or overall size of the connection) is warranted as may be the case if the majority of the length was experiencing virtually zero strain. However, it is possible that should the number of shear stud connectors be reduced, higher demands on the studs further into the connection would generate larger strains higher into the connection while the overall behavior of the system remains un-altered. An analytical or experimental study with a reduced number of shear studs would be required to verify this possibility but has not been considered in this research.

Figure 6.138. Internal Strain Gauges

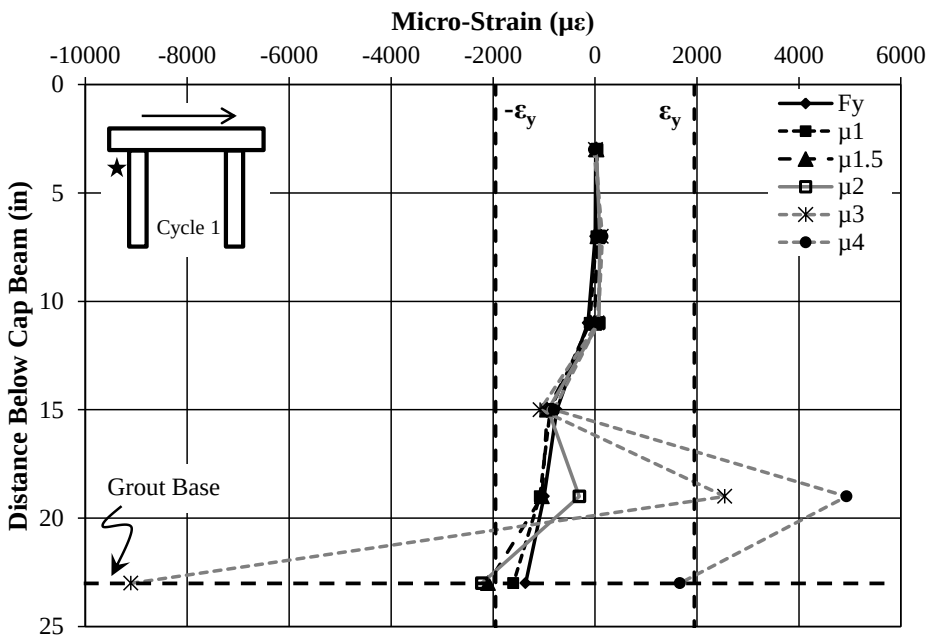

Figure 6.139. Test 4 – North Column North Face Connection Strain Elevation

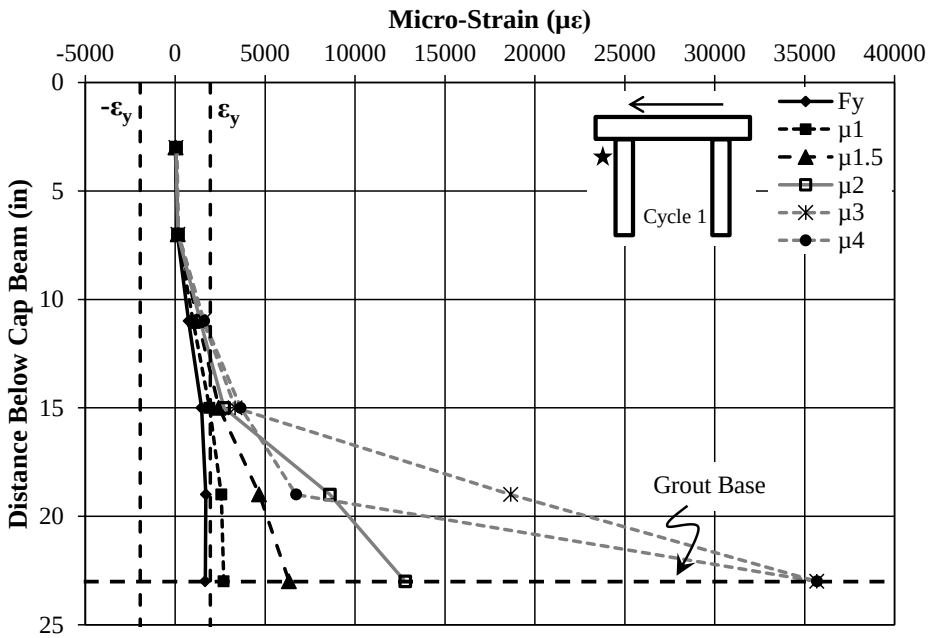

Figure 6.140. Test 4 – North Column North Face Connection Strain Elevation

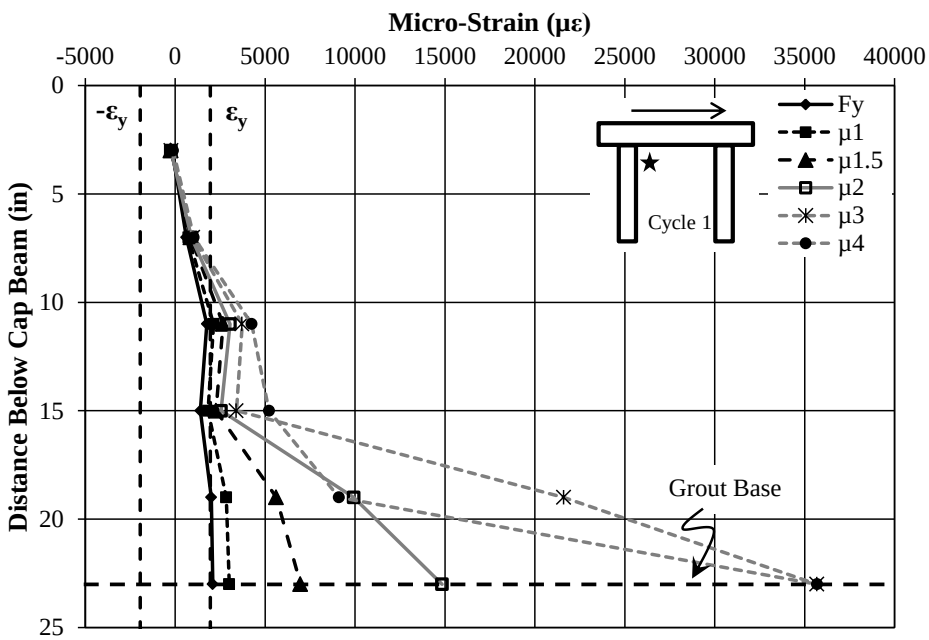

Figure 6.141. Test 4 – North Column South Face Connection Strain Elevation

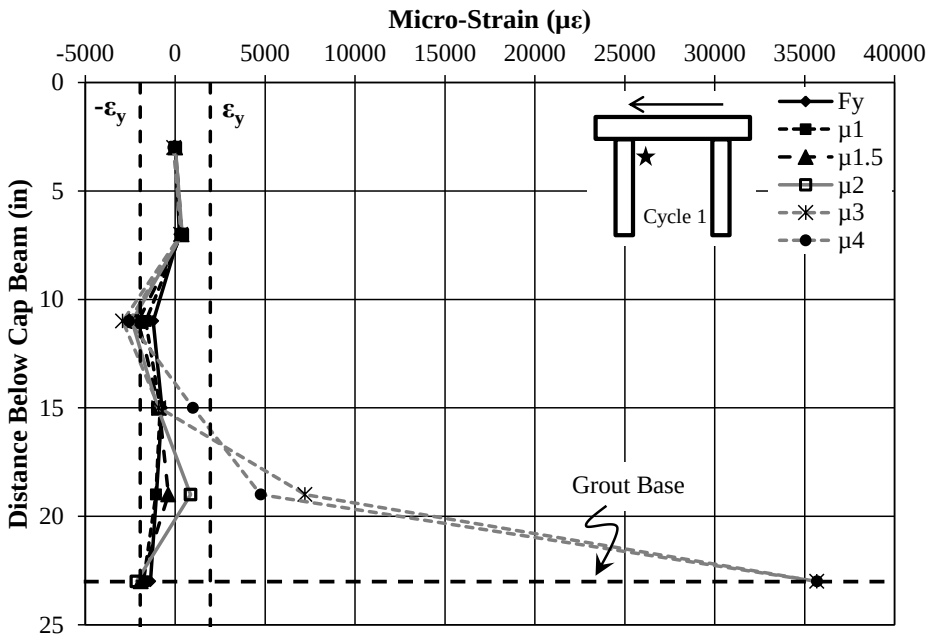

Figure 6.142. Test 4 – North Column South Face Connection Strain Elevation

The physical results of experimental testing, as well as the results of data analysis, indicate that the composite connection design considered in this test was effective in producing a desirable failure mode in the form of flexural hinging of the HSS16x0.500 pile wall regardless of the construction tolerance offset. Consequently, undesirable failure modes such as weld cracking or tearing of the pile wall prior to local buckling were again shown to be avoidable for this connection configuration. As was the case in test 2, some damage did develop within the grout block at the base of the connection in the form of cracking and spalling of the grout material, though no adverse consequences were induced on the structural response due to these actions.

Although these actions may be considered as low level response limit states, such as a serviceability limit state (hence some repair after seismic loading would be necessary), they would not constitute an ultimate response parameter. As has been noted, the ultimate limit state in this case would be considered pile wall local buckling likely corresponding to a

reliable displacement ductility level of 3 or 4 depending on the exact considered allowable level of strength loss. These limit states correspond to 8.44 in. and 11.28 in. of lateral displacement, respectively, or 6.3% and 8.4% drift at the cap beam level. In regards to all aspects of the response which have been discussed, the construction tolerance offset produced no adverse effects as the specimen performed in a nominally identical manner to that of the test 2 specimen which considered nominally ideal construction geometry.

Taking into account the results produced by the strain gauges placed within the connection region as well as the results of the FEM simulation, it is not immediately apparent that a reduction in the number of shear connectors or the overall size of the connection should be reduced. Hence, the design methodology of developing the axial yield capacity of the pile to determine the required number shear stud connectors appears to be adequate and no optimization options are immediately evident. However, should a more direct investigation relating to optimization of the design methodology may produce results that suggest otherwise, but this not considered in this research.

6.5.4 Evaluation with Modified Buckling Restrained Configuration

The fifth test of the second phase of the project was aimed at evaluating the hysteretic performance of a steel pier specimen which contained modified grouted shear stud connections that included an additional buckling restraint feature. As in test 2 and 4, the grouted shear stud composite connection was used to form flexural hinging in the pile section away from the cap beam interface. In the case of test 5, an additional 10 in. of length was provided in the connection design which was used to generate a 1/2 in. annular block-out around the HSS16x0.500 pile as the connection was grouted as shown in Figure 6.143 and Figure 6.144. The intention of the design was for the grout block to provide restraint against propagation of pile wall local buckling, associated with pile flexural hinging, in an effort to mitigate post buckling strength degradation.

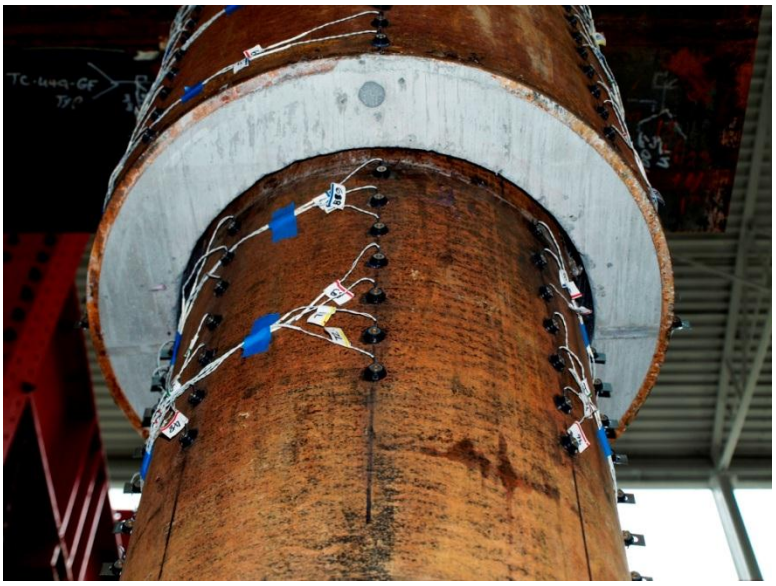

Figure 6.143 Buckling Restrained Grouted Shear Stud Connection

The concept was partially influenced by the work of (Nishikawa, K., et. al., 1998) which focused on strengthening existing structures with steel restraining rings as was discussed in the literature review section of this document. As in that past study, specific consideration was given in the design process to avoid altering system behavior prior to local buckling by avoiding premature contact of the pile wall as will be subsequently discussed. In addition, it should be noted that nominally ideal geometry was considered in this experimental evaluation, and that 2-11/16 in. shear studs were used in lieu of 2-1/2 in. studs due to availability issues.

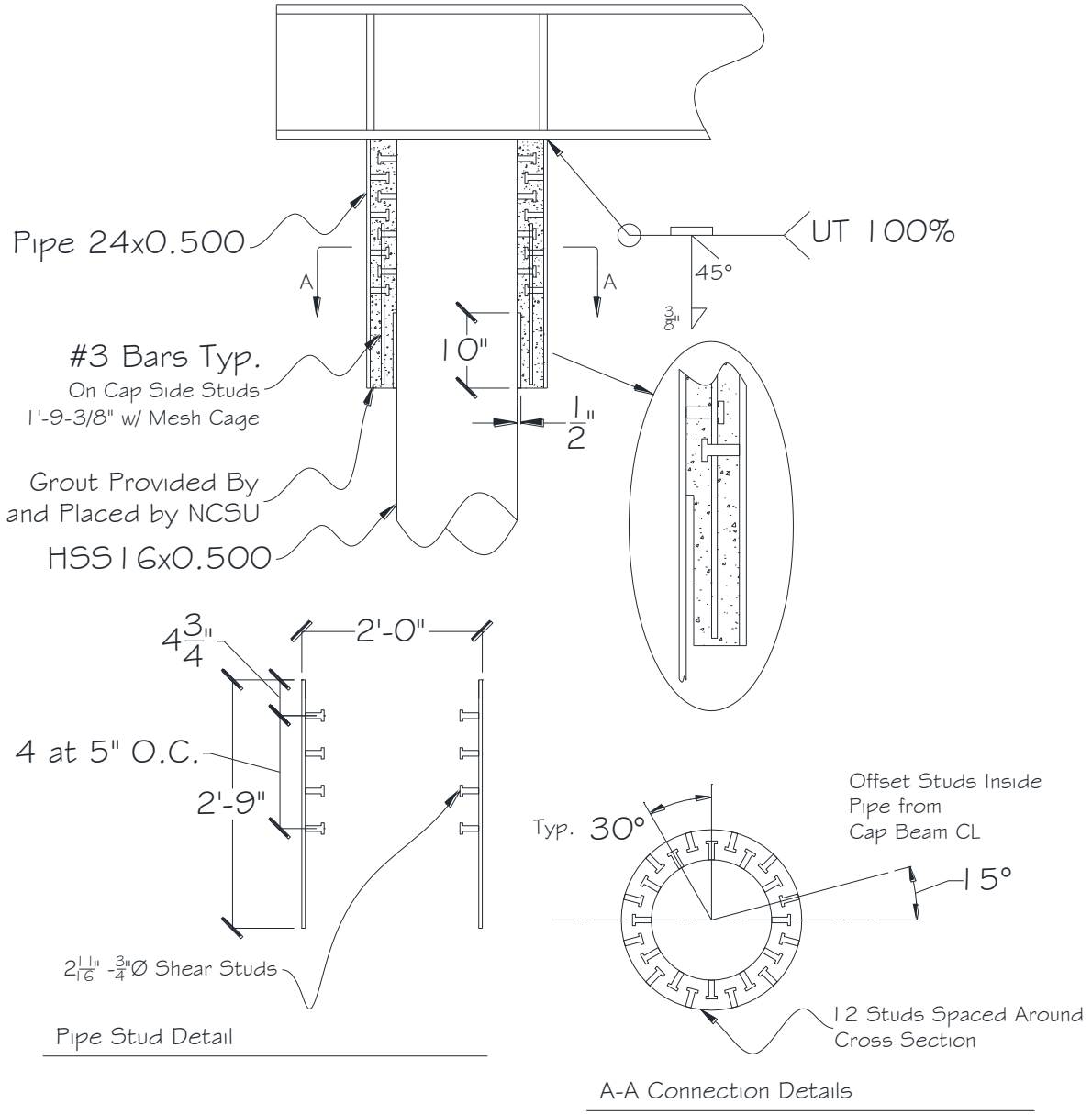

Figure 6.144 B.R. Grouted Shear Stud Connection Details

Design details regarding the annular block-out and grout ring that was intended to provide buckling restraint, included block-out sizing and reinforcement pattern. The block-out dimensions selected (10 in. x 1/2in.) were based on a combination of engineering

judgment and Finite Element Analysis results. The length of 10 in. (5D/8) was chosen based on the results of prior experimental tests which showed the buckled pile wall to be contained within a 10 in. region below the base of the standard grouted shear stud connection. The gap sizing of 1/2 in. was based on FEA results which indicated this dimension to be more effective at mitigating post buckling strength degradation than a gap of 3/4 in. as shown by comparing Figure 6.145 and Figure 6.146. Additionally, based on a combination of engineering judgment and FEM results (shown in Figure 6.147), the gap size of 1/2 in. was assumed to be a lower bound minimum that could be used while still avoiding contact of the pile wall and the grout block due to typical flexural displacements prior to local buckling. Lastly, the grout block reinforcement pattern, shown in Figure 6.148, consisted of #3 bars at each line of pile side shear studs as well as a welded wire mesh wrap. This pattern was selected as a reasonable means to restrain any cracking that may occur in the region as it was necessary to avoid grout spalling in this case.

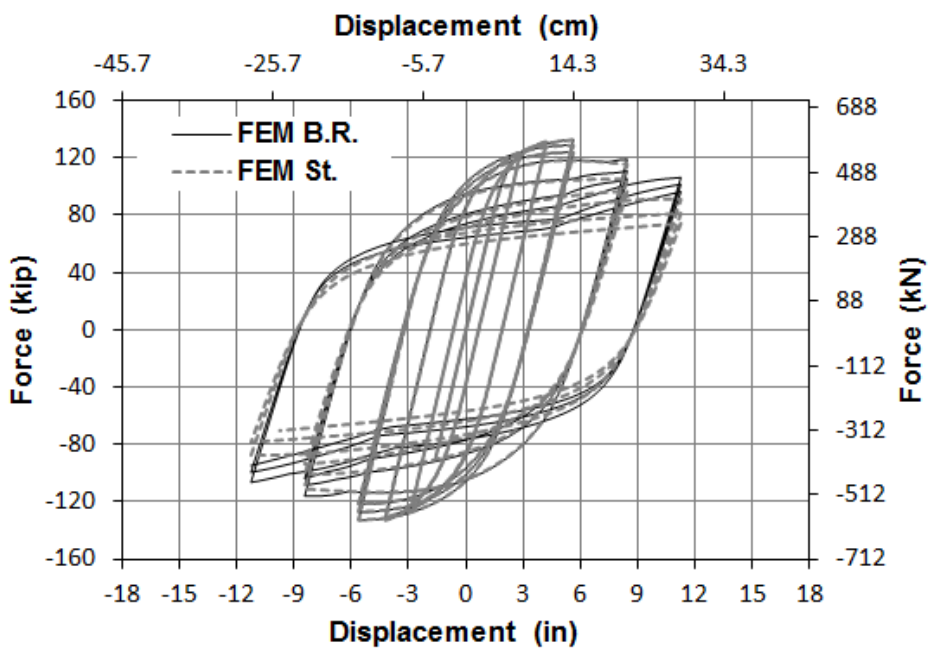

Figure 6.145 FEM 3/4 in. Block-Out vs. FEM Standard G.S.C.

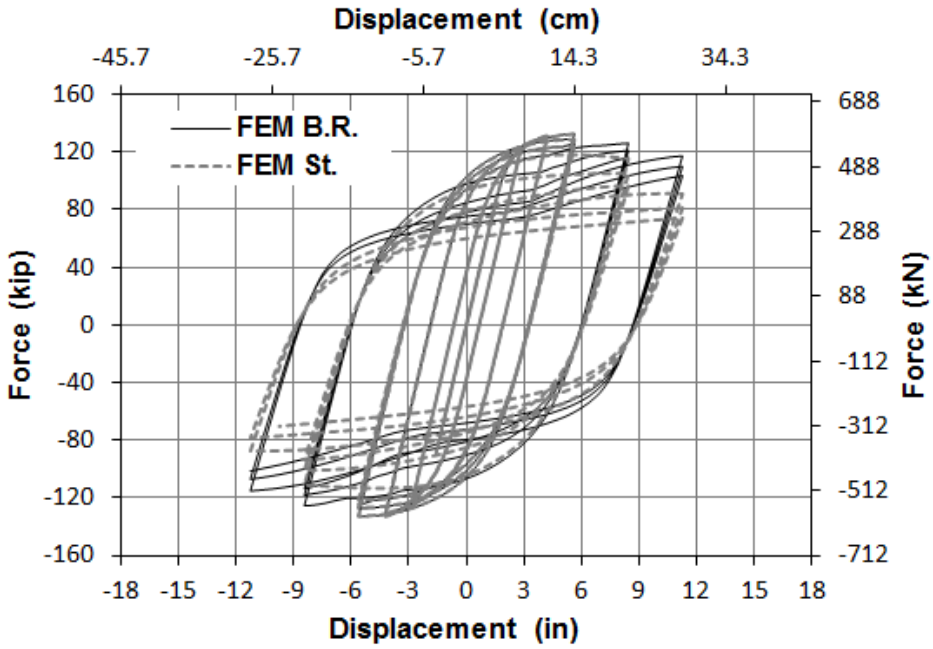

Figure 6.146 FEM 1/2 in. Block-Out vs. FEM Standard G.S.C.

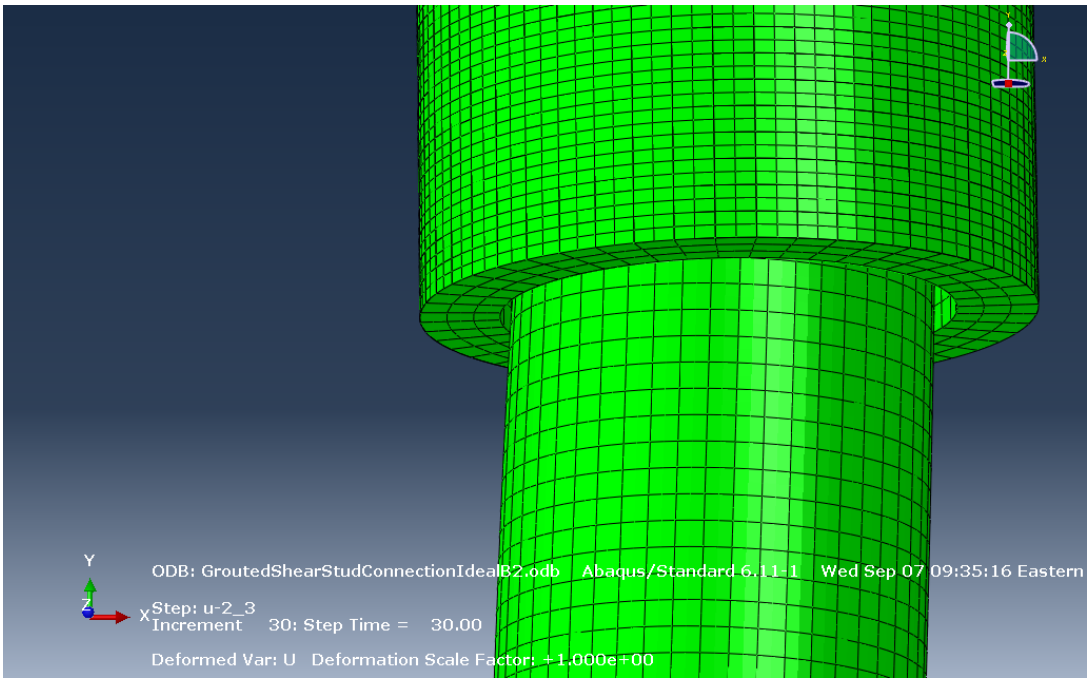

Figure 6.147 FEM 1/2 in. Block-Out – Ductility 2 Cycle -3 – Prior to Buckling

Figure 6.148 Grout Block Reinforcement and Block Out Material

Welding of the cap beam elements, stub piles to the cap beam, and shear stud connectors was conducted by the fabricator to eliminate the necessity of any field welding as was the case with the prior G.S.C. piers. Hence, it was intended that only grout placement was necessary to complete the connection at the laboratory. However, due to a fabrication error, the original shear stud connectors were placed in an incorrect pattern on the HSS16x0.500 piles. As a result, the studs were removed, the surface ground smooth and second set of studs were placed in the proper location. This work was conducted at NCSU's laboratory by professional welders.

To form the annular block-out, 1/2 in. thick insulating foam material was wrapped around the pile and banded with duct tape to create the necessary void in the proper location. Following casting, the insulating foam material was removed from the region using drills, hand saws, and acetone to break apart and disintegrate the material. Although the foam material could have likely been left in place and not have produced any noticeable effects, for research purposes the material was removed to ensure no impact on the response of the system was possible.

No in-house material testing was conducted prior to the experimental evaluation of the pier with modified grouted shear stud connections as it was intended that this evaluation would follow the load/displacement history of the prior to G.S.C. piers (tests 2 and 4) such that direct comparisons could be made with no need to normalize displacement magnitudes. However, material certification reports for the ASTM A500 Gr. B piles were reviewed prior to testing and indicated a 68 ksi yield stress which was again considerably higher than the 56.5 ksi value found for the first G.S.C. pier. However it should be noted, that in the case of the tolerance offset evaluation (test 2) which also had material certifications indicating elevated yield stress, the piers' ultimate strength capacity closely matched that of first G.S.C. pier leaving suspicion surrounding the mill certification tensile test results.

Regardless of the potentially high material properties, the decision was made to follow a matching load/displacement history to that of the first two G.S.C. peirs as has been noted. This resulted a first yield force of 93.3 kips which led to an experimentally determined first yield displacement of 1.96 in. which was reasonably close to the two prior evaluations. Although this first yield displacement corresponded to a ductility 1 displacement of 2.55 in., a value of 2.76 in. was used to match the prior displacement histories. Application of the three cycle set load history produced the experimental force and displacement histories shown in Figure 6.149 and Figure 6.150 respectively. It should also be noted that an average compressive strength of the grout material was found to be 10.08 ksi 2 days after testing, 24 days after grouting took place.

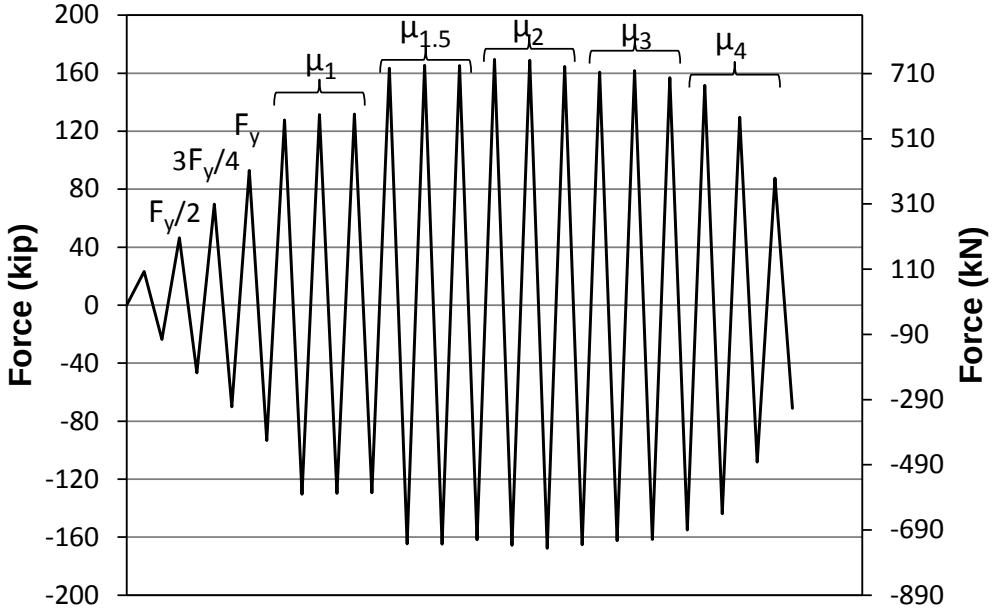

Figure 6.149 Modified B.R. – G.S.C. Experimental Load History

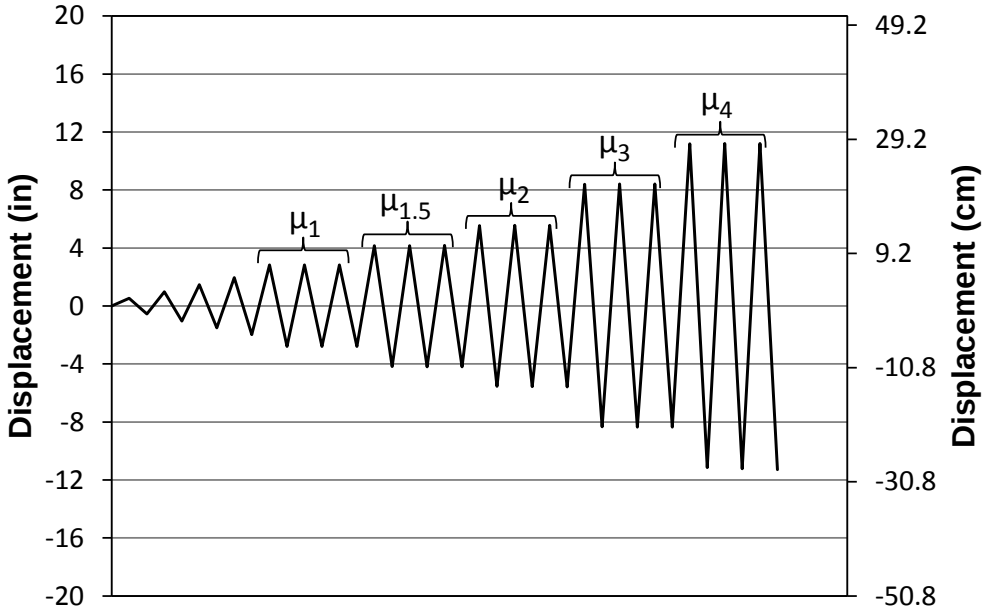

Figure 6.150 Modified B.R. – G.S.C. Experimental Displacement History

Similar to the prior grouted shear stud connection tests, the behavior of the modified buckling restrained configuration was monitored during testing using both the Optotrak system as well strain gauge instrumentation. As shown in Figure 6.151, the basic Optotrak marker grid remained the same with the exception of the instrumented stub pile region being longer as a consequence of the design configuration. Again, internal strain gauges were used to monitor the strain gradient along the pile wall in the connection region. However, in the case of the modified configuration, strain gauges were also placed inside the block out region on the outside of the HSS16x0.500 pile prior to placing the block-out and grout material, such that strains could be monitored in this region since no Optotrak data could have been collected within the internal region.

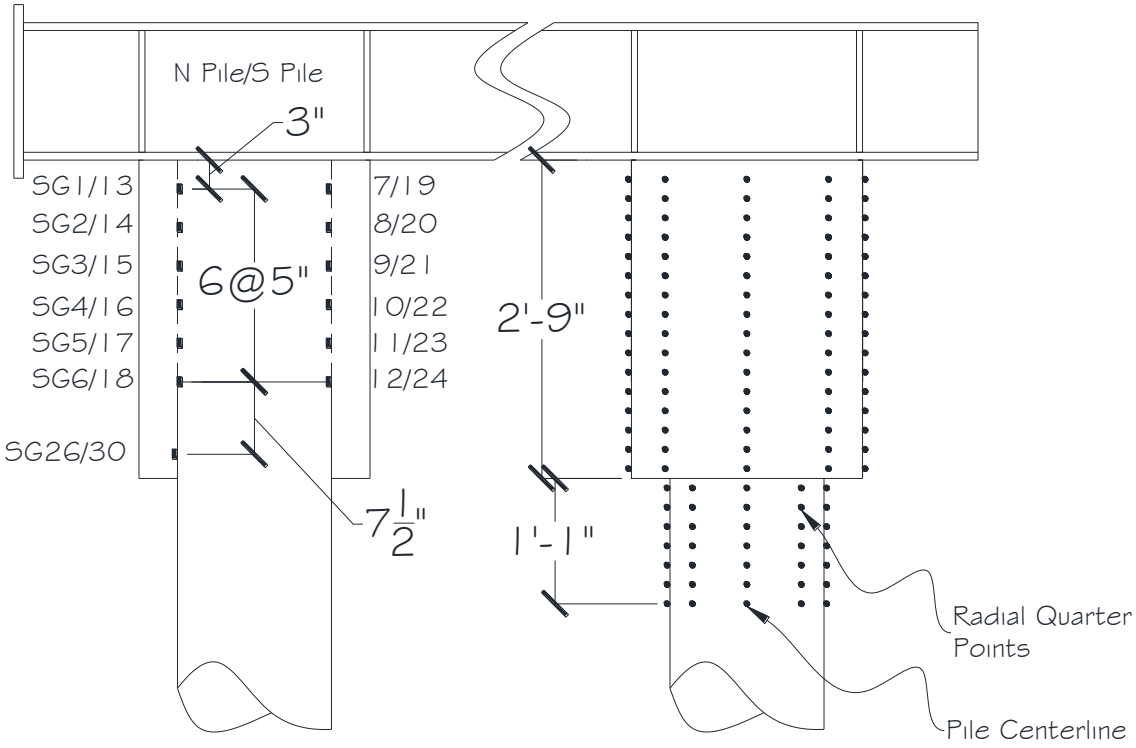

Figure 6.151 Modified B.R. – G.S.C. Instrumentation Layout

The initial force controlled cycles of the experimental test, as well as the ductility 1 displacement controlled cycles, showed no signs inadequate performance. As was the case throughout the entire test, no visual cracks or crushing of the grout material was experienced as had occurred as early as the elastic range of loading in prior G.S.C. tests. This is likely due to the presence of steel reinforcement in the lower grout block region which was shown to provide adequate restraint against crushing as was necessary to ensure the ability of the grout block to provide restraint against propagation of local buckling. Although cracking and crushing of grout at the base of the standard configuration was inconsequential in past tests, it was necessary to ensure this did not occur in the buckling restrained configuration as this area of the connection was responsible for restraining the propagation of pile wall local buckling.

As the test continued into the ductility 1.5 level, the lateral force necessary to develop the full system strength (which typically occurred between ductility 1.5 and 2) was approaching 160 kips. Although this force was approximately 23% higher than had been experienced in past tests, it was also reasonable based on the mill certifications which indicated a yield stress of 68 ksi as has already been noted. Further, this value of approximately 68 ksi yield stress was later verified with in-house material tests (see Figure A 31 and Figure A 32). As a consequence of the elevated level of lateral force, the north column (tensile column) pinned base supports slipped by approximately 1.5 in. prior to reaching the first positive ductility 1.5 displacement peak of 4.22 in as shown in Figure 6.152 through Figure 6.155.

Recognizing that the base shears were likely no longer evenly distributed with this level of slipping, and having no way to quantify the values, it was decided to stop the test in order to correct the base displacement. By removing the applied prestressing force to the north pinned base assemblies and striking the assemblies with a sledge hammer, the base connection was returned to its original position. After this was done, the prestressing force placed on the base shoe assemblies was increased by 50% which was estimated to be

adequate based on anticipated system strength as indicated by the mill certifications. The test was then continued starting with the first cycle of ductility 1.5 from a residual cap beam displacement of +0.59 in.

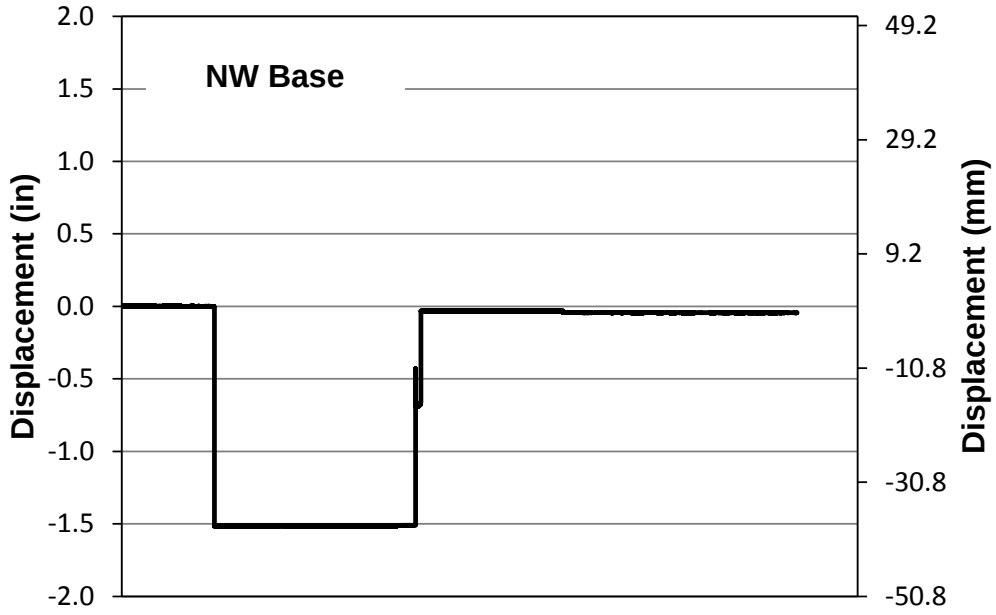

Figure 6.152 Test 5 – NW Base Displacement Reading Through Test

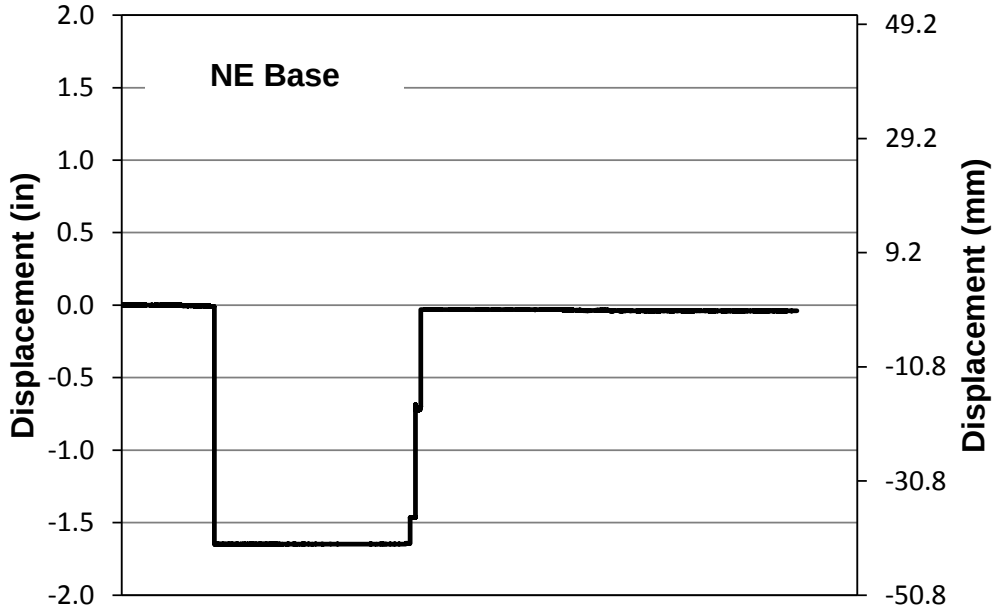

Figure 6.153 Test 5 – NE Base Displacement Reading Through Test

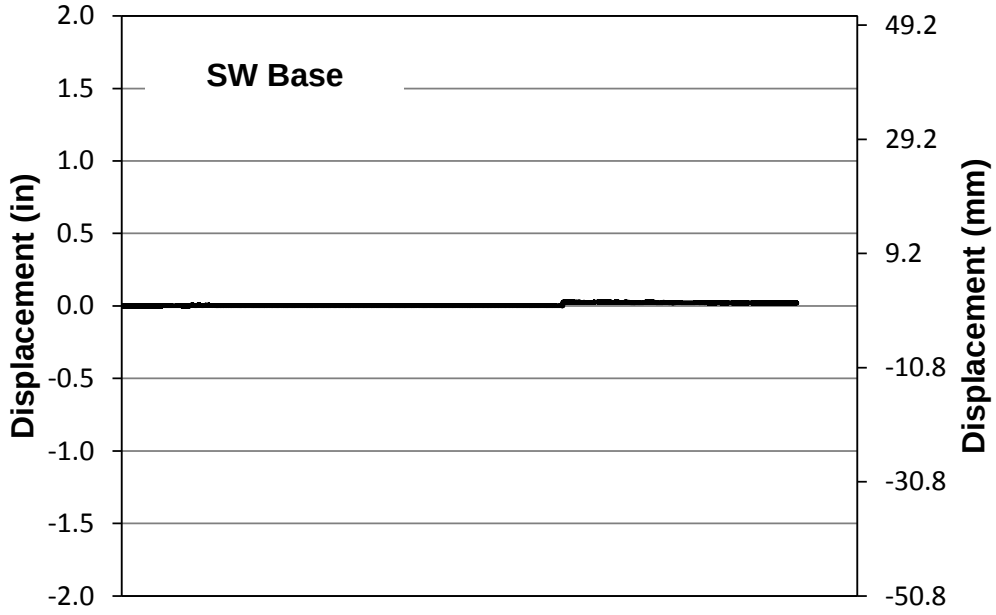

Figure 6.154 Test 5 – SW Base Displacement Reading Through Test

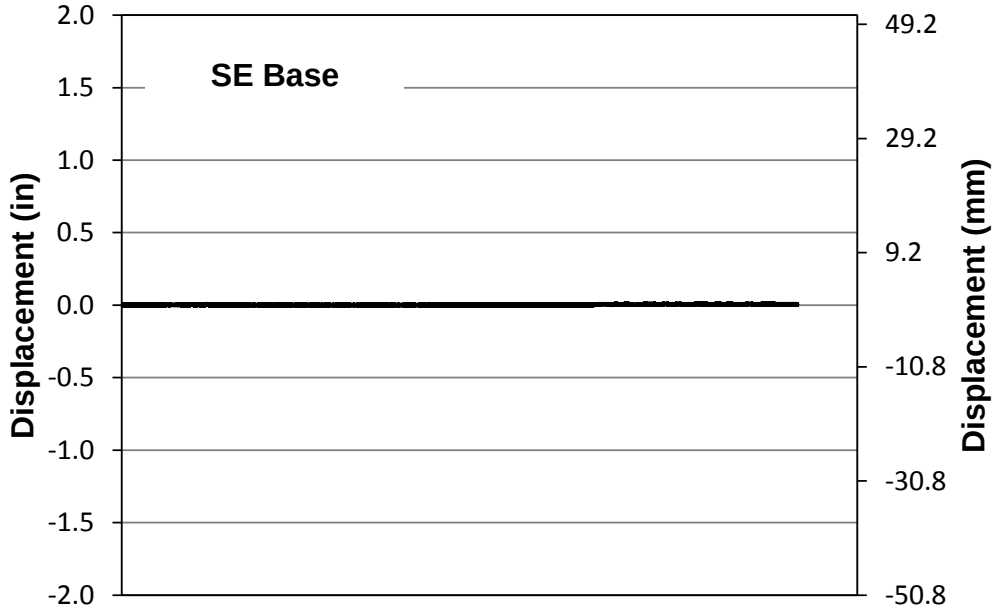

Figure 6.155 Test 5 – SE Base Displacement Reading Through Test

As the specimen was loaded to the full 4.22 in. of displacement associated with ductility 1.5, the system force reached 165 kips and there were no notable signs of damage, strength loss, or any other undesirable results. This remained the case throughout the subsequent ductility 1.5 cycles as well as the first positive and negative cycles of ductility 2 where the maximum system forces of +/- 172 kips was experienced. During the second pull cycle and third push cycles of ductility 2, associated with 5.63 in. of displacement, small reductions in the system strength to +/- 165 kips were experienced indicated the onset of local buckling may have occurred although no visual inspection was possible. These reductions in force, although minor, can be seen in the full Force – Displacement hysteresis as well as the cycle envelopes shown in Figure 6.156 and Figure 6.157 respectively. However, as has been noted, visual inspection of the pile wall was not possible since the region which was assumed to be experiencing the onset of buckling was located within the 1/2 in. annular block-out as was intended.

As the test progressed to the ductility 3 level, which was associated with 8.44 in. of displacement, further reduction in strength began to occur. However, prior to reaching the full ductility 3 displacement peak, a slight positive change in the tangent stiffness of the system occurred restoring some system strength. This can be seen in Figure 6.156 and more clearly in Figure 6.158 which reduces the hysteretic response to only the first cycle of ductility 3. The positive change in stiffness was assumed to be the result of the buckled region contacting the restraining grout block and was seen to be more pronounced in second and third cycles of ductility 3 as is shown in Figure 6.159 and Figure 6.160. As shown in the Force – Displacement envelopes, this stiffening effect was successful in mitigating the strength degradation to a negligible magnitude at the ductility 3 displacement level. It is also worth noting, that at this stage of loading the 1/2 in. annular block-out gap was nearly closed at the base of the connection but no contact had occurred as was the design intention. This can be seen in Figure 6.161, which also shows the absence of grout crushing during this test as has already been noted.

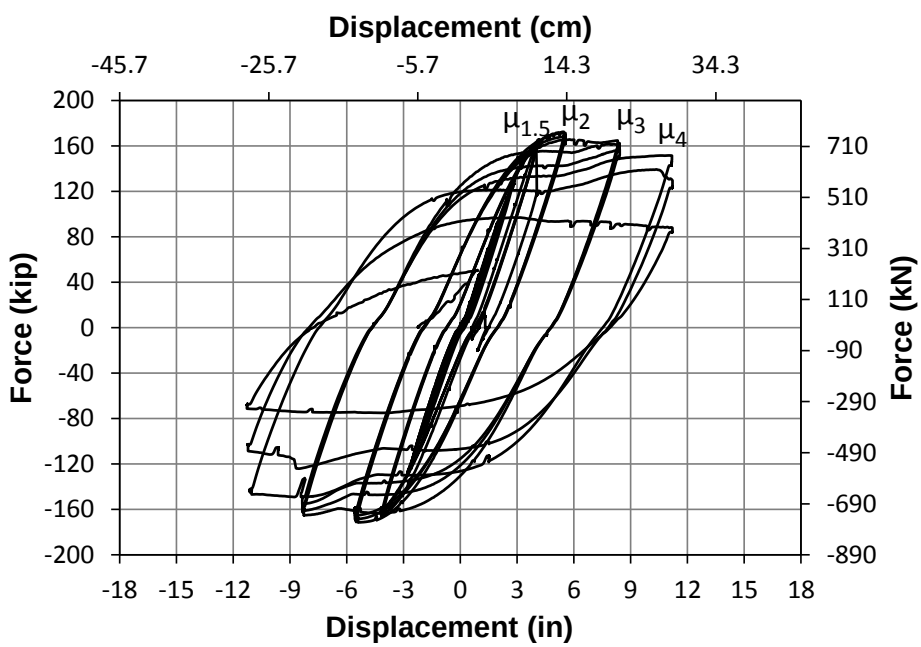

Figure 6.156 Buckling Restrained G.S.C. – Force-Displacement Hysteresis

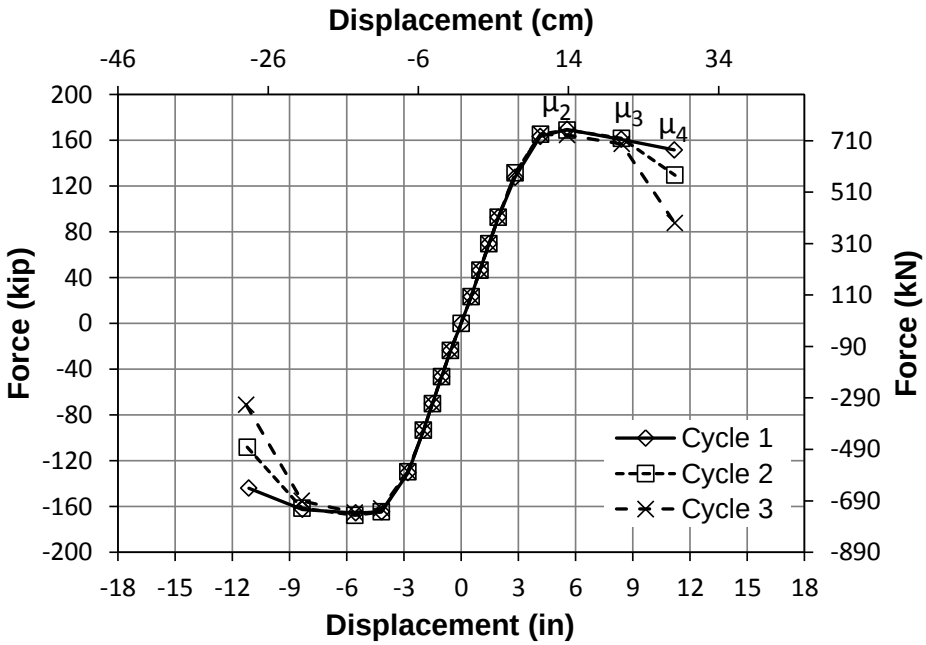

Figure 6.157 Buckling Restrained G.S.C. – Force-Displacement Envelopes

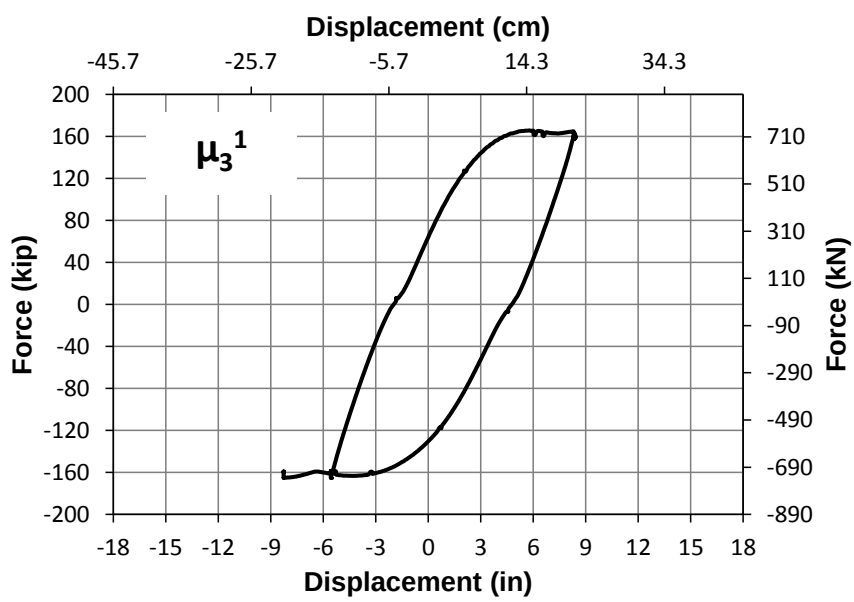

Figure 6.158 Single Cycle Loop – Ductility 3 Cycle 1

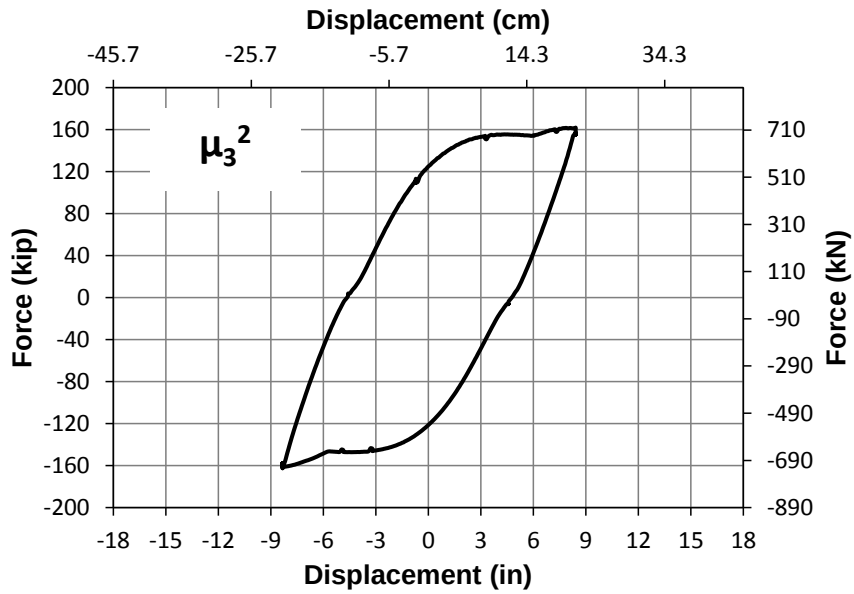

Figure 6.159 Single Cycle Loop – Ductility 3 Cycle 2

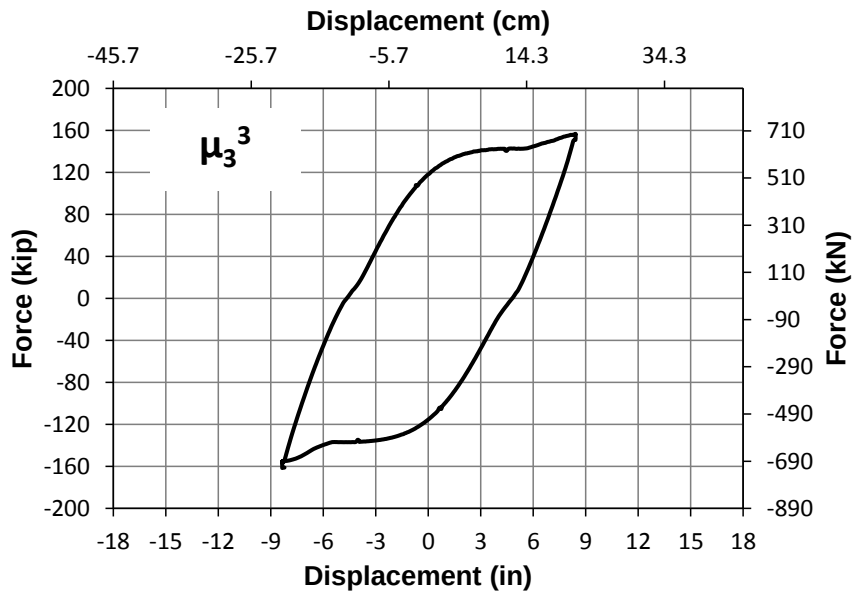

Figure 6.160 Single Cycle Loop – Ductility 3 Cycle 3

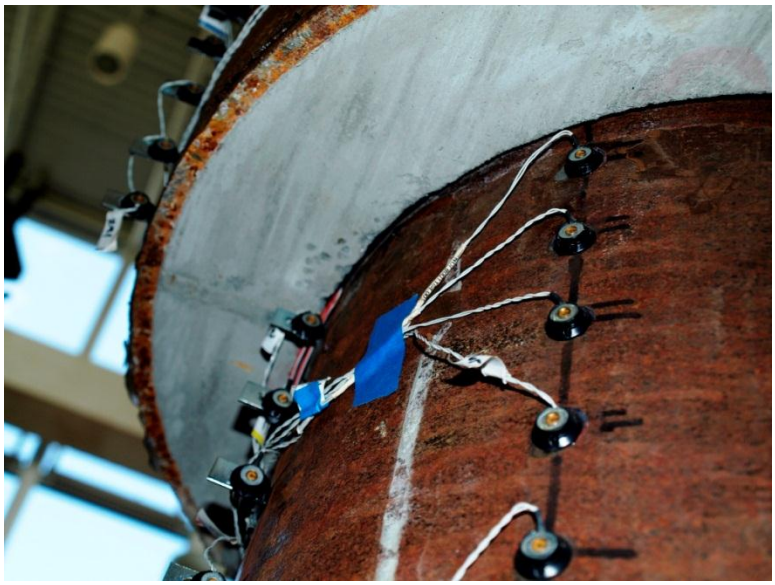

Figure 6.161 Ductility 3 Cycle 1, 8.44 in. Displacement, 165 kips

As the test progressed to the first positive and negative cycles of ductility 4, associated with 11.26 in. of displacement, continued strength degradation due to local buckling of the pile wall was experienced. Although the stiffening effect of the buckling restraint mechanism continued throughout the ductility 4 level, as is shown in Figure 6.162 and Figure 6.163, the ability of the mechanism to restore system strength to nearly negligible levels of loss, was less effective than in ductility 3. The inability of the mechanism to further restore strength is likely due in part to pile wall cracking which occurred on the tensile face of the south column during the second negative cycle of ductility 4 as shown in Figure 6.164. Similarly, the third positive cycle lead to cracking on tensile faces of both the north and south columns which produced further strength degradation. Although the third negative cycle of the ductility 4 level was conducted, approximately 40% strength loss had been experienced and multiple cracking locations existed. As a result the test was concluded.

Following testing, the piles were removed from the specimen by flame cutting the material below the length of the outer stub pile. By exposing the inside of the connection region, it was visually verified that buckling had in fact occurred as intended, leading to

contact with the restraining grout block as shown in Figure 6.165. Although somewhat visible during testing, the extent of cracking was also more clearly verified from the un-obstructed view.

As was done in test 4 in an effort quantify the behavior of the connection throughout its length, internal strain gauges were placed inside the pile at the extremities of the section prior to construction as shown has been noted. Post test data analysis produced the strain elevation presented in Figure 6.166 through Figure 6.169. Similar to test 4, the strain elevations presented indicate a relatively linear strain gradient prior to the large strain accumulation which occurs at the base of the connection as large levels of plasticity and eventual local buckling developed.

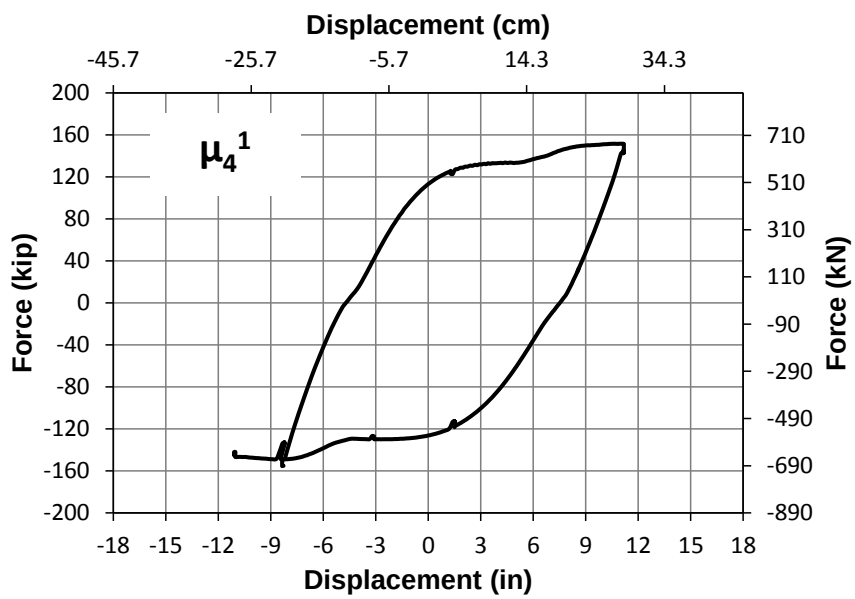

Figure 6.162 Test 5 – Single Cycle Loop – Ductility 4 Cycle 1

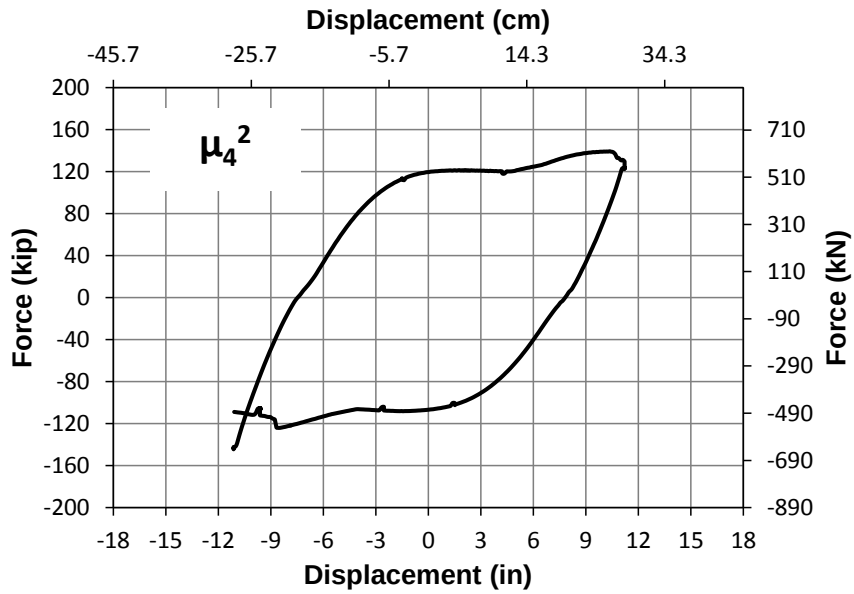

Figure 6.163 Test 5 – Single Cycle Loop – Ductility 4 Cycle 2

Figure 6.164 Ductility 4, Proceeding to Cycle -2, -2.85 in. Displacment, -107 kips

Figure 6.165 Test 5 – Buckled Region inside HSS16x0.500

As expected, it was also shown that the top strain gauge in all cases provides a reading close to zero since by design full force transfer mechanism should have taken place at this point in the connection. The conclusion made from the past experimental test as well as FEM results, that it is not immediately apparent that a reduction in the number of shear studs (or overall size of the connection) is warranted, remained applicable after reviewing the results of this experimental evaluation which continued to show a relatively linear strain gradient throughout the connection However, as noted earlier it is possible that should the number of shear stud connectors be reduced, higher demands on the studs further into the connection would generate larger strains higher into the connection while the overall behavior of the system remains un-altered.

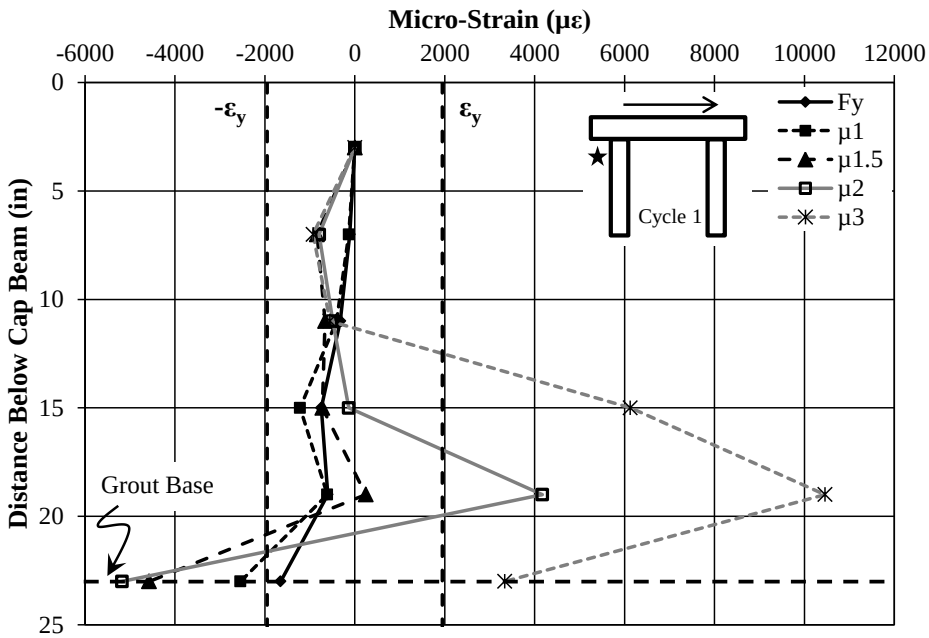

Figure 6.166 North Column North Face Connection Strain Elevation

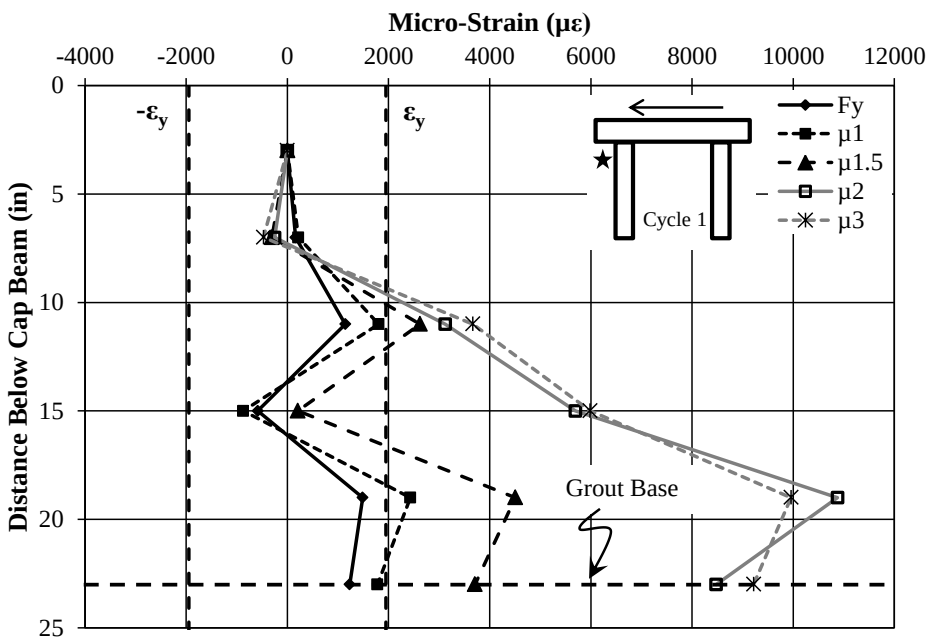

Figure 6.167 North Column North Face Connection Strain Elevation

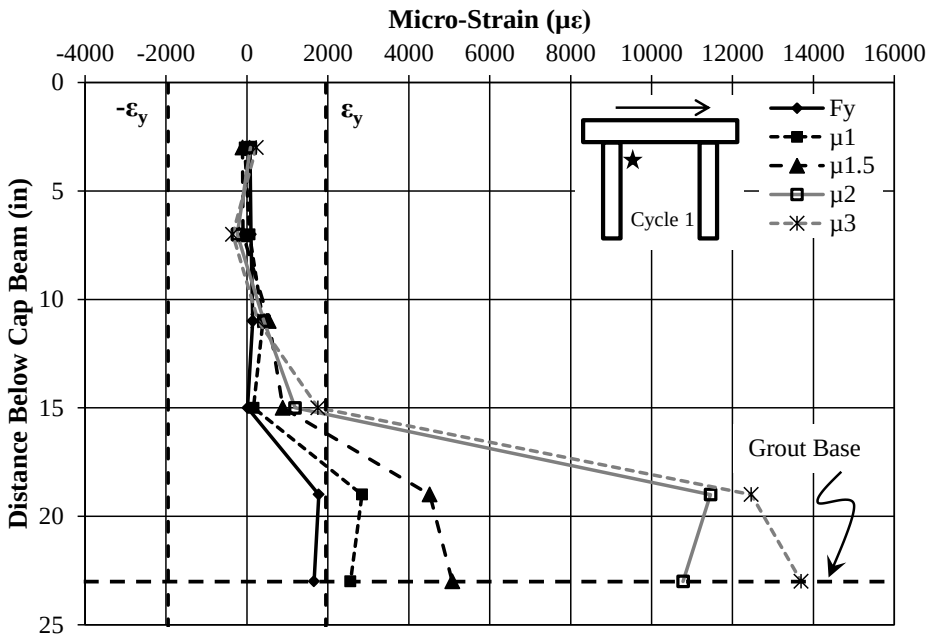

Figure 6.168 North Column South Face Connection Strain Elevation

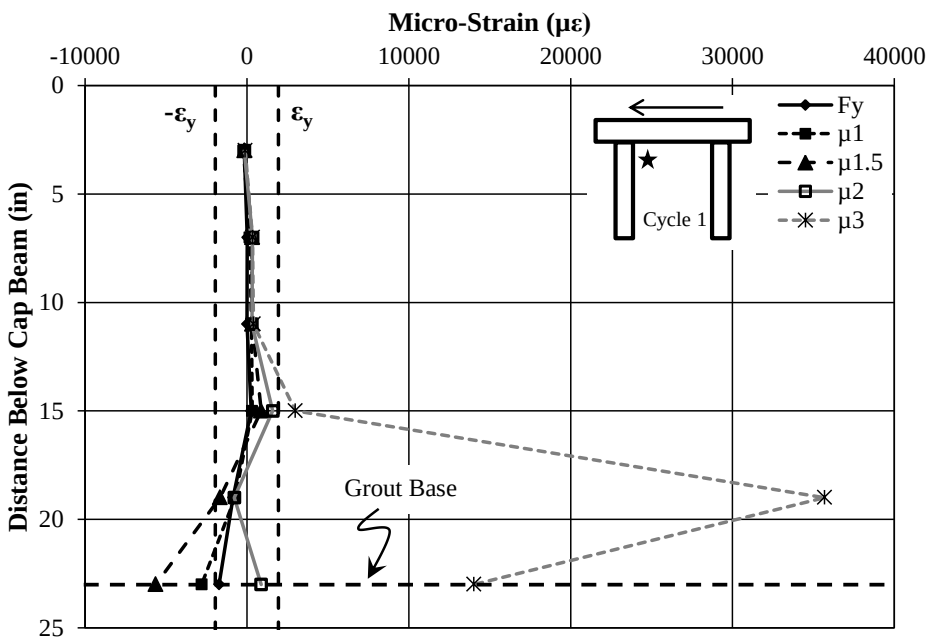

Figure 6.169 North Column South Face Connection Strain Elevation

In an effort to better quantify the ability of the buckling restraint feature to enhance the post buckling hysteretic performance of the pier, direct comparisons were made between the standard configuration with no buckling restraint feature (test 2) and the buckling restrained configuration of test 5. In order to facility the comparison, it was necessary normalize the system forces from each test due to the higher strength material and resulting higher system forces in test 5. This was achieved by dividing the force recordings from each test by the respective maximum values normalizing the results to unity. As has already been noted, test 5 was subjected to a nominally identical load/displacement history such that the comparisons can be made at given displacement levels with no need to normalize displacements by ductility level or any other means.

As shown in Figure 6.170, the general hysteretic shape prior to buckling is similar between the two specimens as was expected given that the buckling restraint features were not intended to alter the pre-buckling behavior of the pier. However, the stiffening effect of the buckling restraint began to alter the hysteric shape at approximately +/- 6 in. of displacement in the ductility 3 and 4 loops by producing the positive stiffness change that has been discussed. To more clearly evaluate results of the stiffening effects, normalized envelope Force – Displacement curves have been plotted in Figure 6.171 through Figure 6.173.

Regardless of the seemingly positive effects of the buckling restraint behavior, the magnitudes of associated strength increase are negligible when compared to the response of test 2. Further, in the case of the third cycle of ductility 4, the envelope response falls below that of the test 2 response. This is likely a result of the cracking which occurred at this level of response and did not occur until the ductility 6 level in test 2 (note ductility 6 is not shown on envelope comparisons). There is no supporting data to indicate that the effects of the buckling restraint mechanism encouraged the cracking to occur at an earlier stage of loading in test 5, but it is clear from the response of the test 5 specimen, that the configuration had no apparent positive effect on cracking mitigation. In conclusion to these comparisons,

regardless of the stiffening effects generated by the buckling restraint feature, the normalized response envelopes do not show an impactful improvement to the behavior of the pier as the associated magnitudes of strength increase are too low.

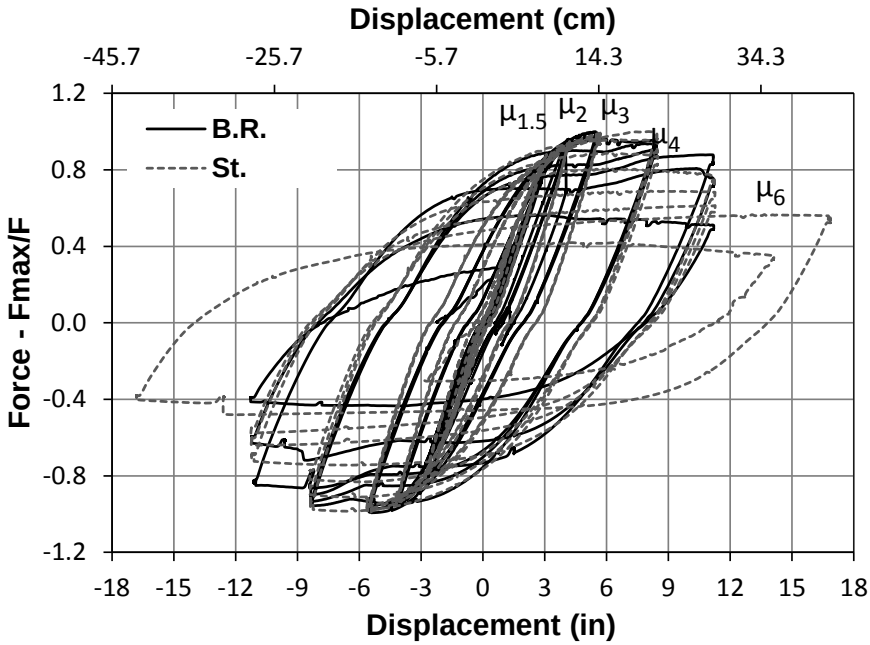

Figure 6.170 B.R. (Test 5) vs. St. (Test 2) – Normalized F-D Hystersis

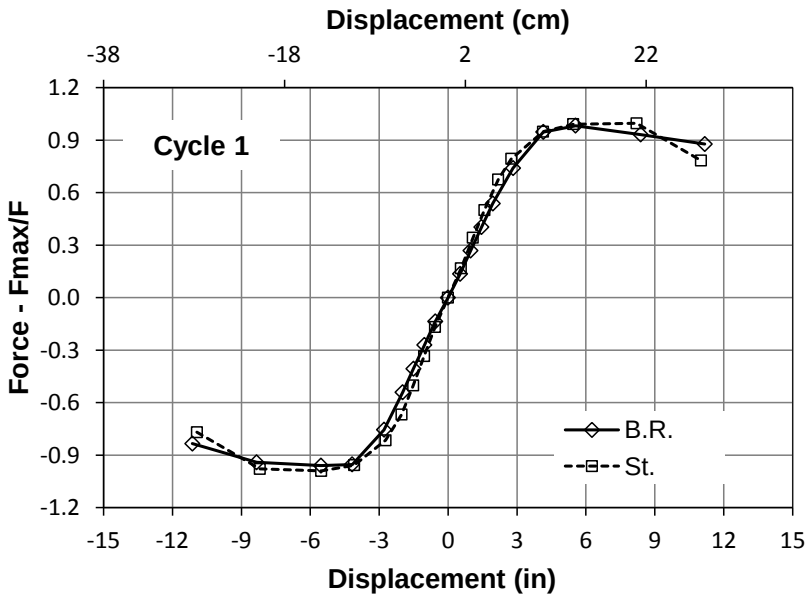

Figure 6.171 B.R. vs St. Configuration – Normalized Cycle 1 Envelopes

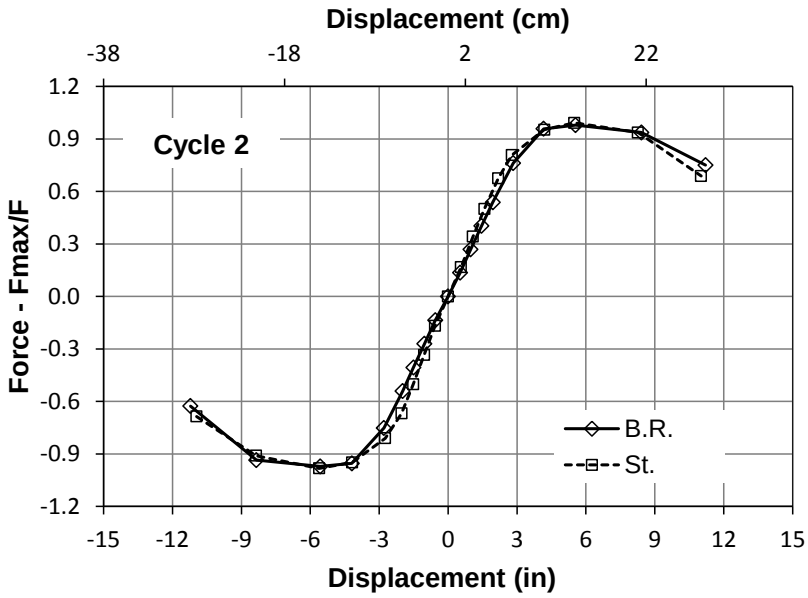

Figure 6.172 B.R. vs St. Configuration – Normalized Cycle 2 Envelopes

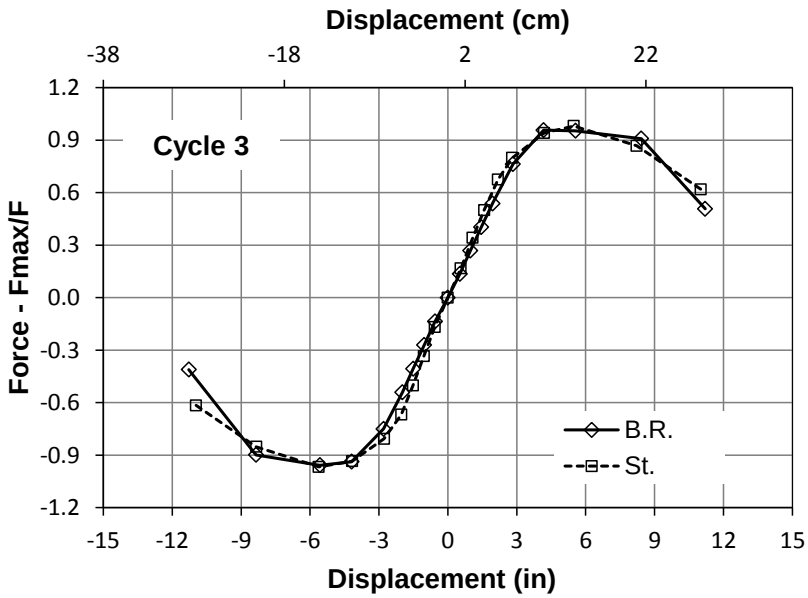

Figure 6.173 B.R. vs St. Configuration – Normalized Cycle 3 Envelopes

The physical results of experimental testing, as well as the results of data analysis, indicate that the buckling restrained grouted shear stud connection was effective at properly locating damage in the form of pile wall local buckling within the intended block-out location. Consequently, undesirable failure modes such as well cracking were again avoided. Further, restraint provided by the grout block did produce a post-buckling stiffening effect in the hysteretic response resulting in the restoration of some system strength as was the design intention.

However, the magnitude of strength that was restored in the system was insufficient to produce an impactful change in the system behavior particularly at the ductility 4 displacement level. This lack of impact is particularly evident in the comparison of normalized Force – Displacement envelopes between the standard configuration and buckling restrained configuration. Therefore, the ultimate limit state of this configuration remains pile wall local buckling which produces significant strength degradation in the

ductility 4 level resulting in an upper bound reliable displacement ductility of 3 (6.3% drift) as was the case with the standard configuration.

Considering the results which have been presented in this section along with the additional labor required to form the block-out region, the standard connection is recommended over the buckling restrained configuration. However, the test did serve as further validation of the capabilities of the standard connection design to properly relocate damage in the form of pile wall local buckling as the response of the system was un-altered prior to this limit state. Further, as reasonably linear strain gradient was again shown to develop along the length of the connection as was the case in test 4, it remains unapparent that a reduction in the number of shear connector or the overall size of the connection is warranted. Hence, the design methodology of developing the axial yield capacity of the pile to determine the required number shear stud connectors appears to be adequate and no optimization options are immediately evident.

6.5.5 Evaluation with Applied Dead Load

The sixth test of the second phase of the project was aimed at evaluating the performance and behavior of a steel pier specimen that was subjected to vertical dead loads in addition to lateral loading. The specimen contained standard grouted shear stud connections and considered ideal geometry (no construction tolerance offsets) such that the configuration was nominally identical to that of test 2. As shown in Figure 6.174 and Figure 6.175, the experimental specimen was subjected to vertical loads representative of superstructure dead weight using post tensioning bars and hydraulic jacks. The presence of the applied vertical load induced axial load on the piles in addition to that generated by lateral loading of the pier. This was done in an effort to evaluate the effect of additional compressive axial load on the pile wall local buckling failure mode which had been shown to be the controlling failure mode of piers containing the grouted shear stud connection

configuration. In addition, the influence of P-Delta effects on the system's behavior could also be evaluated.

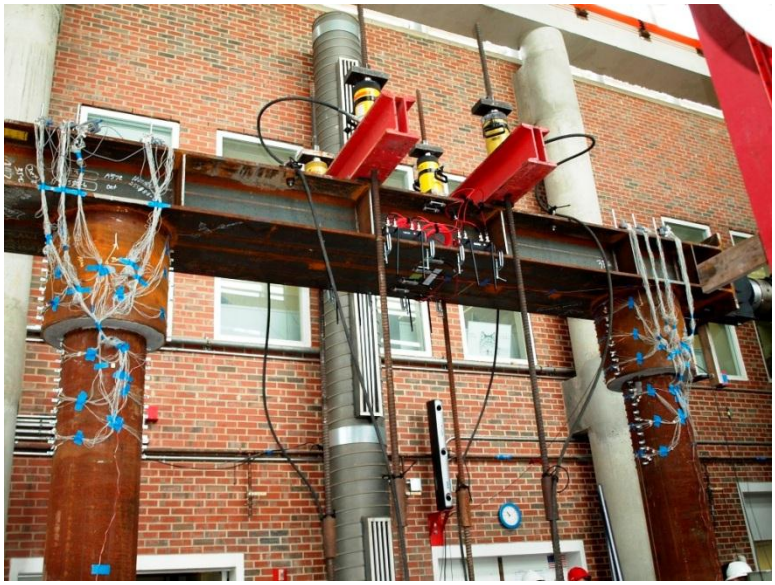

Figure 6.174 Steel Pier with Applied Vertical Dead Load

The magnitude and application method of the vertical load were both functions of reasonable upper bound estimates of bridge superstructure weight and laboratory restrictions. The reasonable upper bound superstructure dead load was based on a presumed steel I girder/CIP reinforced concrete bridge deck with the assumptions listed below. These assumptions resulted in a gravity load of 80 kips per pile. However, due to a fatigue rated pressure restriction of 3200 psi in the accumulation system that was used to maintain a reasonably constant load, the magnitude was reduced to 73 per pile kips for the experimental test.

- 8 in. thick CIP deck (8 ft. width attributable to each pile)
- 84 plf steel girders (2.5 attributable to each pile)
- 1000 plf guard rail (equally attributable to each pile)
- 20% of steel girder load for miscellaneous steel

- 10% deck load for concrete haunches
- 4 in. wear surface (8 ft. width attributable to each pile)
- 40 ft. spans

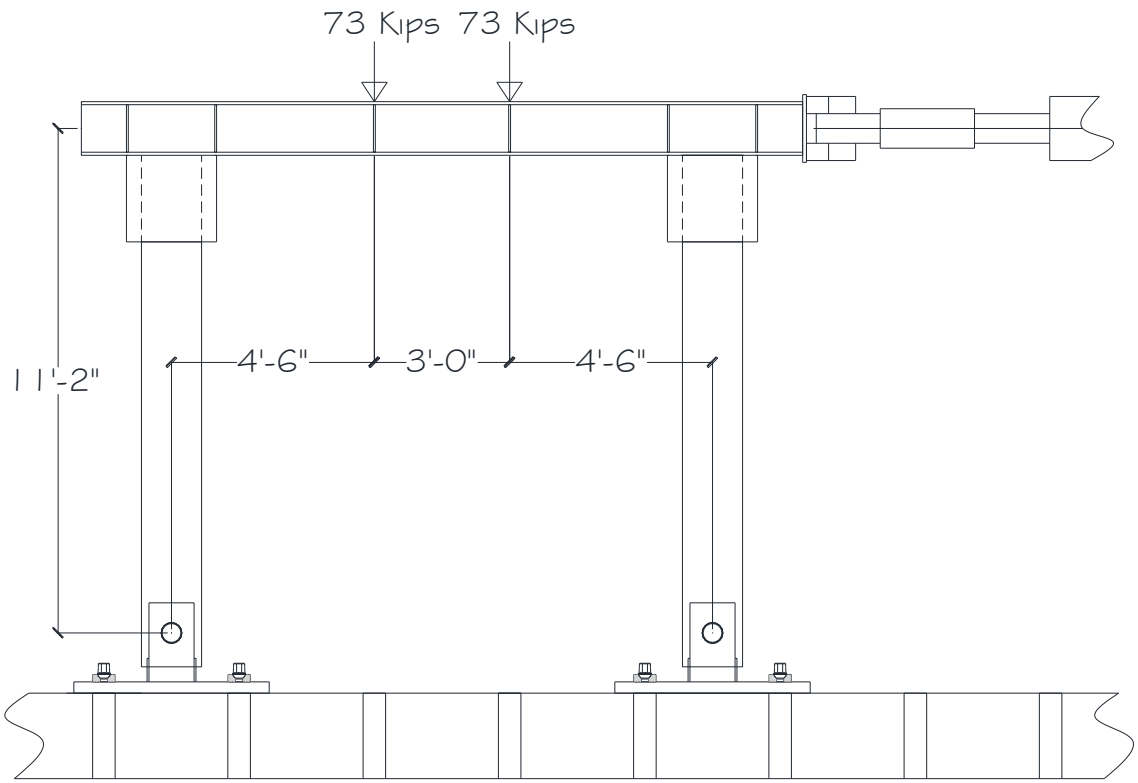

Figure 6.175 Experimental Set Up with Vertical Dead Load

Although the gravity load calculations assumed five I girder locations evenly spaced along a 16 ft. cap beam for a two column pier, the laboratory reaction floor layout provided only two feasible locations for application of the axial load. As shown in Figure 6.174 and Figure 6.175, these locations were 1.5 ft. left and right of the centerline of the cap beam. Although this differs from the assumed five girder locations, the cap beam was capacity protected and experienced strains below 400 $\mu\varepsilon$ at the soffit centerline (see Figure 6.176) as a result of the vertical and lateral loading. Further, it has been shown that the stub pile to cap

beam interface is capacity protected with the grouted shear stud connection configuration. Any variation in the moment to shear ratio at the joint was expected to have little effect on the response of the system. Hence, application of the vertical load at two locations (near the center of the cap beam) instead of the five girder locations was assumed to adequately model the effect of superstructure dead load.

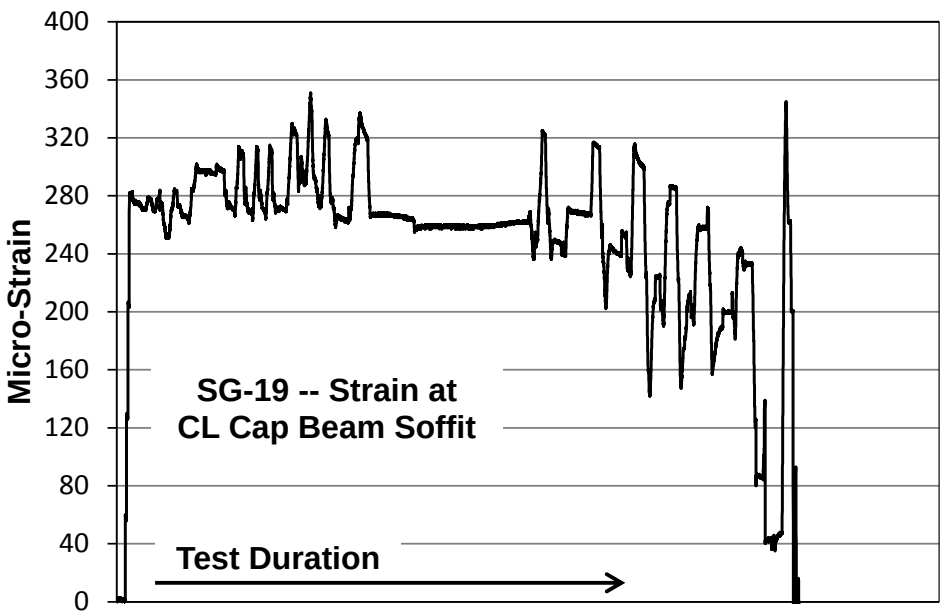

Figure 6.176 SG19 – Strain at Cap Beam Centerline Soffit

The application of the vertical load utilized 1-3/8 in. post-tensioning bars on either side of the specimen with a steel spreader beam placed across to the top of the cap beam bearing on neoprene pads. Four 120 kip hydraulic jacks were used to generate a nominal 36.5 kip force on each bar. The closed loop hydraulic system used only one pump providing even pressure across all four jacks such that load could be monitored by a single load cell on one jack. In addition, two 1 gallon pressure accumulators were included in the system to help maintain a constant load as the pier was displaced and changes in the required stroke of the jack were necessary. Further, it had been found from previous tests that up to 3 in. of axial

shortening of the pier could be expected after the development of local buckling creating further need for an accumulation system. As was previously mentioned, the fatigue pressure rating of 3200 psi of the accumulation system required the actual applied load of each jack to be reduced to 36.5 kips in lieu of the calculated 40 kips. Figure 6.177 shows the magnitude of total vertical load applied to the specimen throughout the duration of the test.

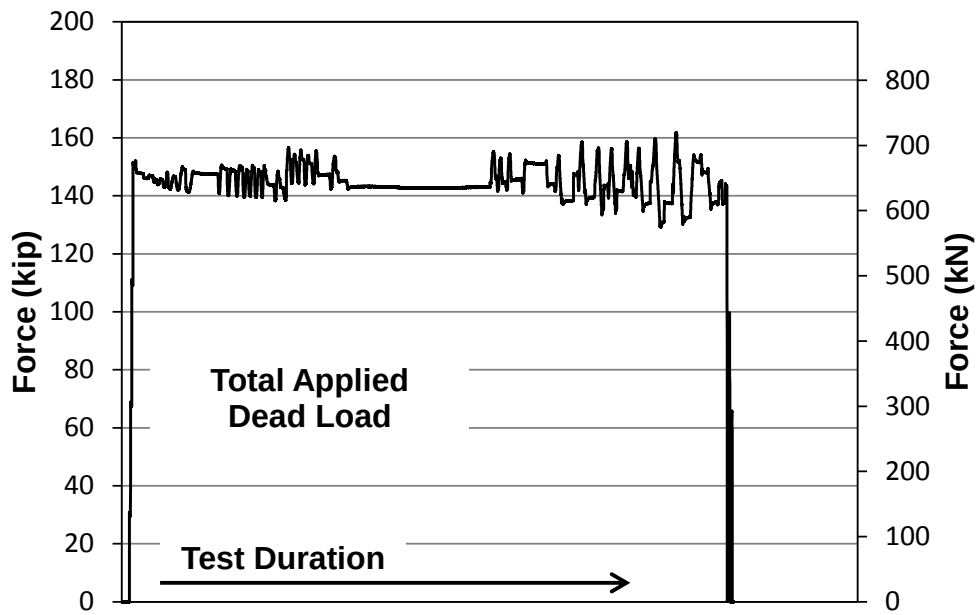

Figure 6.177 Total Applied Vertical Load

In an effort to predict the effects of superstructure dead load on the behavior of the pier prior to testing, Finite Element Modeling of the pier and connection was conducted. The model utilized 4-node shell elements as well as 20-node solid brick elements along with a non-linear kinematic hardening material model which considered expected stress strain behavior of typical ASTM A500 Gr. B pile material. In this case, the analytical material model was calibrated with tensile test data from the test 2 specimen material (see Figure A 13) which indicated a material yield stress of approximately 56.5 ksi. This was done such that direct comparisons could be made between the analytical results which considered

vertical dead load and the results from the analysis of test 2 which did not consider vertical dead load. In addition, no in-house testing of the test 6 materials was conducted prior to experimental evaluation. As has been noted for prior analyses, the grout material was modeled with elastic material behavior and the resulting analytical errors will be discussed where applicable.

The model was subjected to a quasi-static lateral displacement history matching that of the test 2 experimental specimen as was the plan for the experimental test 6 evaulation which would be subjected to axial dead load, as has been discussed. The vertical load was applied in the model at the same two locations on the cap beam as would be done for the experimental test. As shown in Figure 6.178, the vertical load was applied at each location as a distributed load over an area of similar size as the spreader beams which would be used in the laboratory set up.

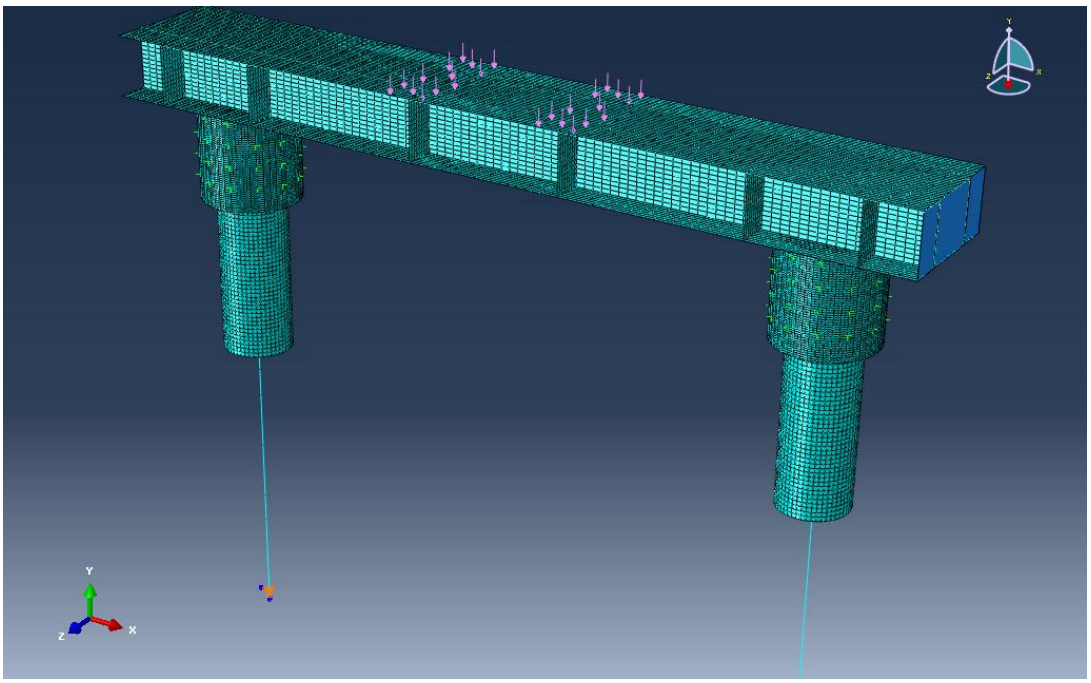

Figure 6.178 Finite Element Model with Vertical Dead Load

The results of the simulation showed the ultimate limit state of the system to be flexural hinging of the piles in the form of pile wall local buckling immediately below the base of the connection, as shown in Figure 6.179. As expected, this is the same failure mechanism as previously tested experimental specimens and previous Finite Element Models which were not subjected to vertical dead load. However, both the development of pile wall local buckling and strength degradation associated with propagation of buckling were shown by the analysis to occur at lower displacement ductility levels than with specimens not subjected to the vertical dead loads.

As shown in Figure 6.180, noticeable strength degradation in the predicted hysteretic Force – Displacement response occurred at the second ductility level for the pier subjected to dead load. The strength degradation was accompanied by small magnitudes of negative stiffness as the pier approached the ductility 2 displacement peaks. This was a result of P-Delta effects which were more severe with the presence of the vertical loads. As the model was subjected to the ductility 3 cycles, strength degradation and negative stiffness effects both increased in magnitude. Although flexural hinging in the form of pile wall local buckling also occurred in analyses without vertical loads, as has been mentioned, the onset of buckling and development of strength degradation both occurred later in the response. As shown in Figure 6.181, no considerable strength loss was experienced until the ductility 3 cycles without the presence of vertical loads and the effects of negative stiffness were not evident. From the results of the analysis, it was anticipated that the presence of the dead load in the experimental test would reduce the displacement capacity of pier system by inducing pile wall local buckling at lower displacement levels and produce negative stiffness in the hysteretic response of the pier as a result of P-Delta effects.

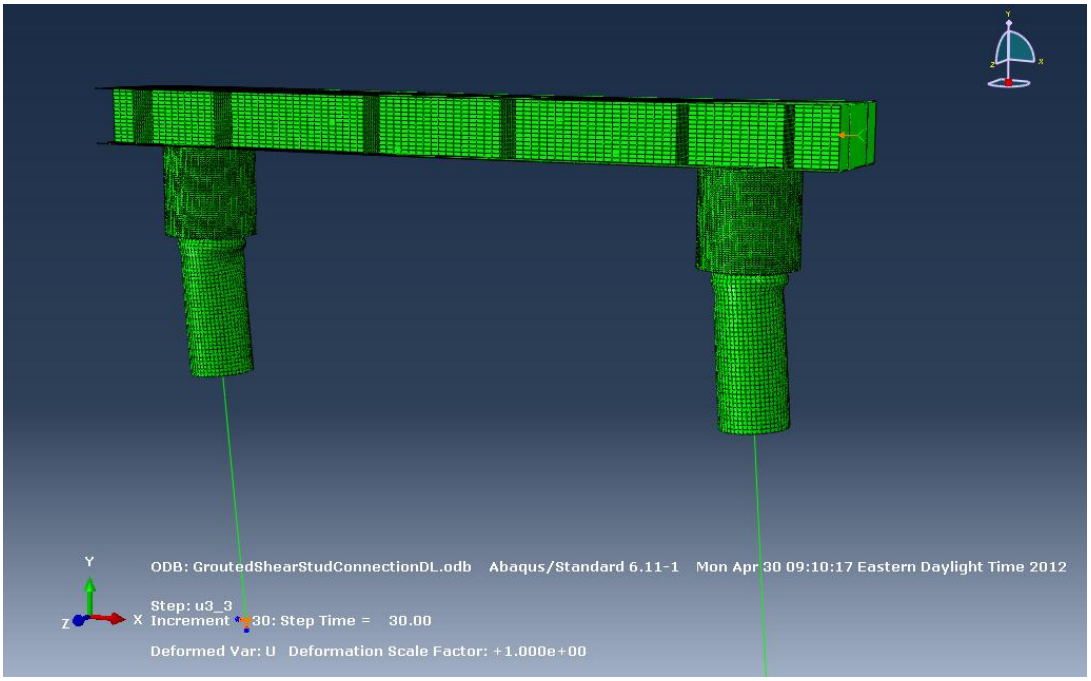

Figure 6.179 Pile Hinging of Displaced Pier – Ductility 3 Cycle 3

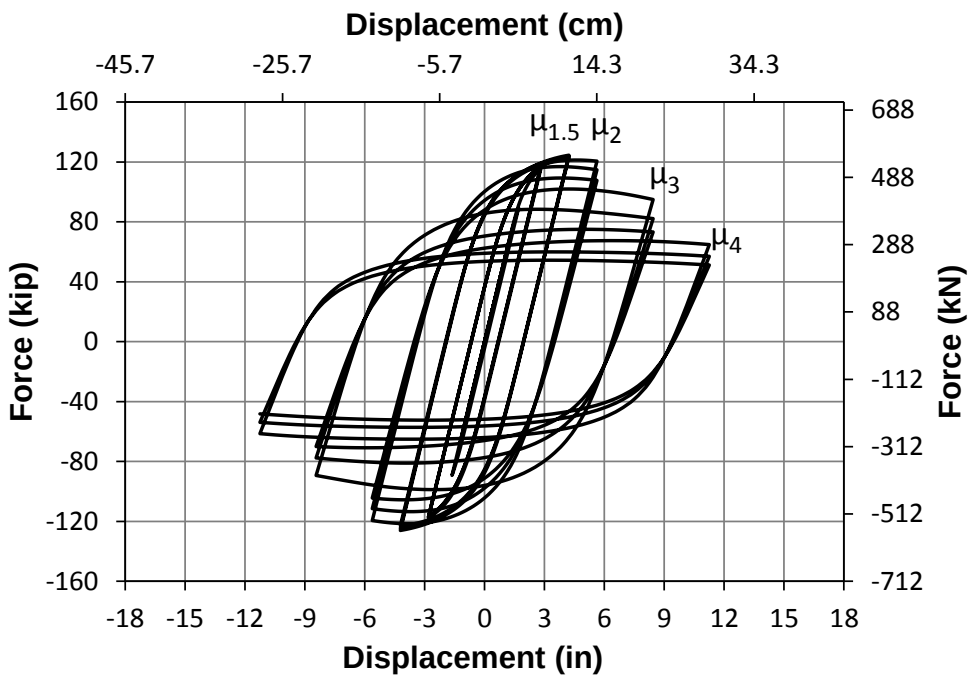

Figure 6.180 FEM with Vertical Dead Load-Displacement Hysteresis

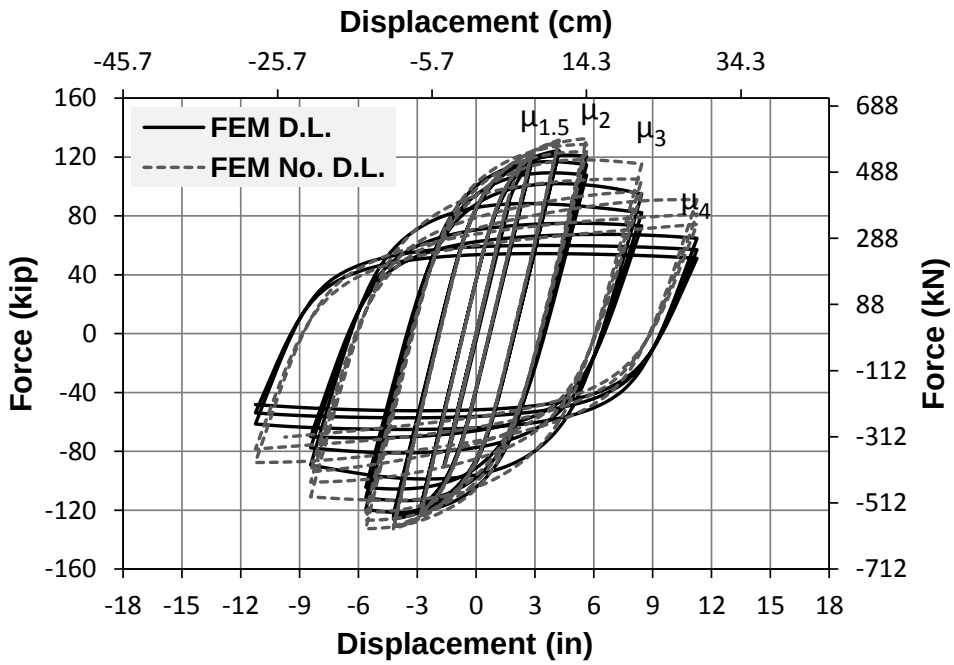

Figure 6.181 FEM Hysteresis Comparison – D.L. vs. No D.L.

As has been noted and as was the case with tests 4 and 5, no in-house material testing was conducted prior to the experimental evaluation of the pier with applied vertical dead loads. It was intended that this evaluation would follow the load/displacement history of the prior to G.S.C. piers to facilitate comparisons regarding the response of the system. However, material certification reports for the ASTM A500 Gr. B piles were reviewed prior to testing and indicated a yield stress of approximately 74 ksi (see Figure A 38), which was again considerably higher than the 56.5 ksi value found for the first G.S.C. pier. It should be noted, that this value is similar to that reported for test 5 (68 ksi) which did display larger system strength values than prior tests and required elevated levels of base restraint post tensioning force to resist sliding.

Following the load/displacement history applied to all prior G.S.C. piers resulted a first yield force of 93.3 kips which led to an experimentally determined first yield displacement of 1.95 in. which was reasonably close to the prior evaluations. Although this first yield

displacement corresponded to a ductility 1 displacement of 2.54 in., a value of 2.76 in. was used to match the prior displacement histories. Application of the three cycle set load history produced the experimental force and displacement histories shown in Figure 6.183 and Figure 6.183 respectively. It should also be noted that the average compressive strength of the grout material was found to be 7.74 ksi on the day of testing which was 28 days after casting.

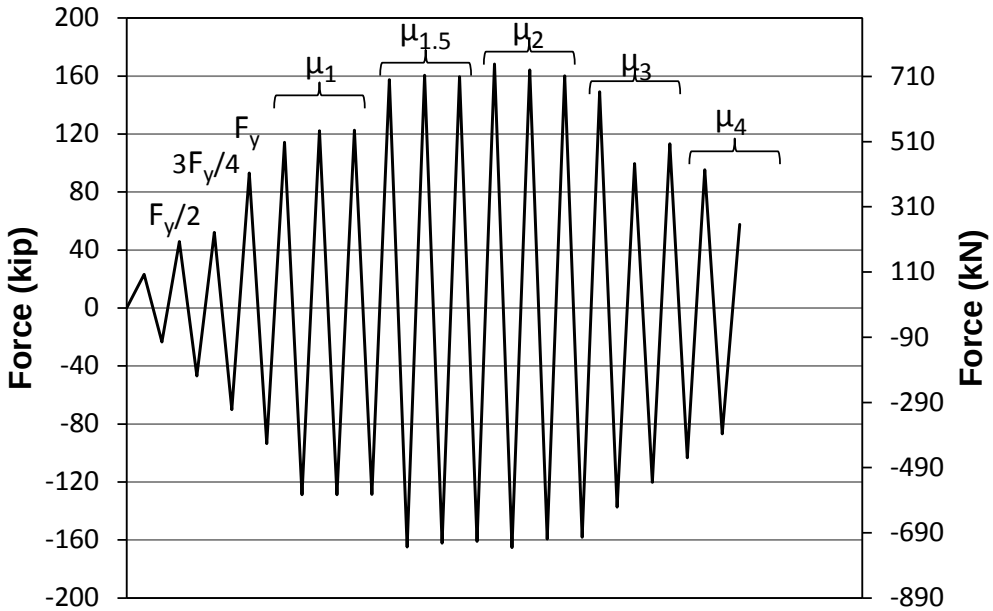

Figure 6.182 Vertical Dead Load – G.S.C. Experimental Load History

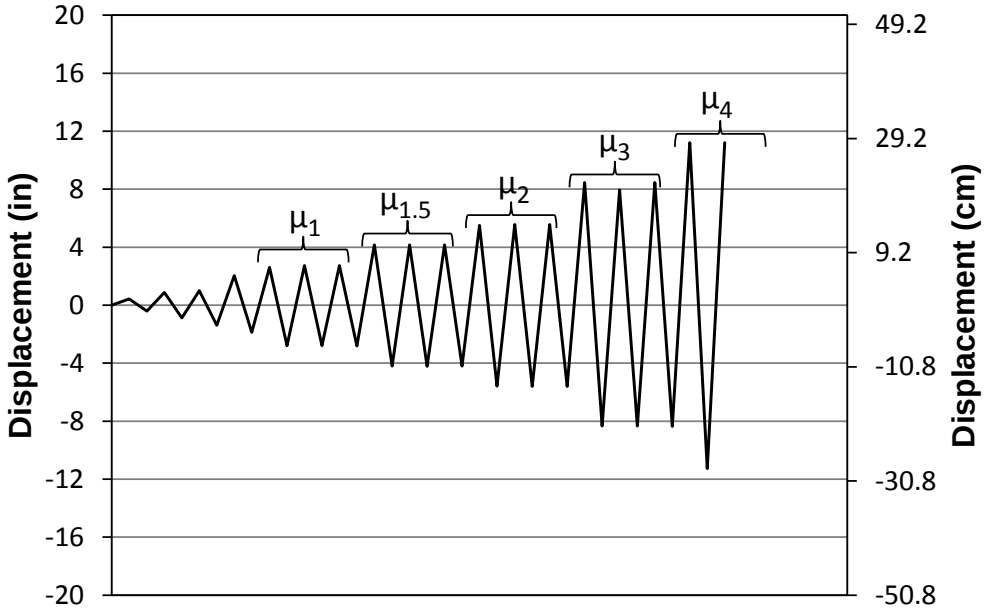

Figure 6.183 Vertical Dead Load – G.S.C. Experimental Displacement History

As was the case with other experimental evaluations, the response of the specimen during the laboratory tests was monitored using a combination of traditional strain gauges as well as the Optotrak system. Although the Optotrak marker grid remained the same as the past G.S.C. tests, the internal strain gauge layout was slightly modified. As shown in Figure 6.184, the number of internal strain gauges was reduced from 6 on each extreme fiber to 4. This was done to allow for strain gauges to be placed in other positions such as the cap beam soffit and pile buckling regions to monitor the effects of the additional axial compressive stress on the buckling behavior.

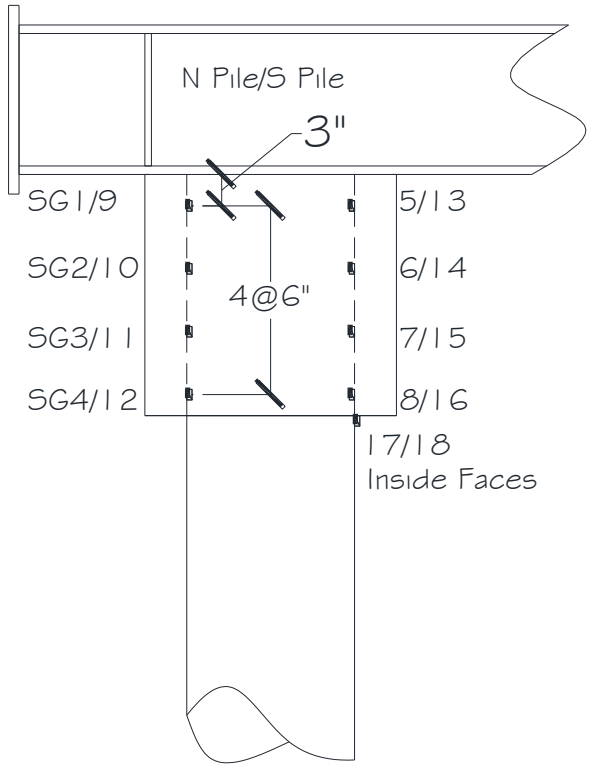

Figure 6.184 Vertical Dead Load – G.S.C. Instrumentation Layout

The initial force controlled cycles of testing as well as the ductility 1 and 1.5 displacement controlled cycles showed good performance of the pier. Unlike test 2, no cracking of the grout material was experienced until the first cycle of the ductility 1.5 level. Test 2 had experienced cracking as early as the +/- F_y cycles of loading. The difference is potentially due to the presence of the additional axial compressive load reducing the axial tension demands required to maintain global equilibrium. However, it should be noted that cracking and crushing of grout at the base of the connection in earlier tests was inconsequential and constituted only a serviceability limit state.

As the test continued into the ductility 2 level, the lateral force necessary to develop the full system strength (which typically occured between the ductility 1.5 and 2 levels) was approaching 170 kips. Although this force was approximately 23% higher than had been experienced in test 2, it was also reasonable based on the mill certifications which indicated a

yield stress of 74 ksi, as has already been noted. As the test continued through the first push and pull cycles of ductility 2, minor levels of local buckling were visually noted on the inside faces of each column which corresponds to the compression face of the of the column resisting compression for global equilibrium. It has been noted that these locations typically experience buckling prior to the outside faces of the piles.

The second and third cycles of ductility 2 led to increased local buckling on the inside faces of each column, as is shown in Figure 6.185, as well as minor buckling of the outside face of the south column. Although the strength loss associated with the local buckling at the ductility 2 level was less pronounced than that predicted by the FEM, losses of approximately 5% were experienced, as is shown in the full Force – Displacement hysteresis and the Force – Displacement envelopes provided in Figure 6.186 and Figure 6.187 respectively.

As the test continued to the ductility 3 displacement level, corresponding to 8.44 in. of displacement, the locally buckled regions that developed during ductility 2 propagated in an outward style, as is shown in Figure 6.188. This propagation of buckling led to further strength degradation along with negative stiffness in the hysteretic response as a result of P-Delta effects as was predicted by the FEM. Throughout the second and third cycles of ductility 3, further buckling and associated strength loss within the system was experienced. Additionally, minor levels of grout crushing at the base of the connection were experienced in these cycles as shown in Figure 6.189. However, this loss of cover grout was not associated with any negative effects and remained less severe than was experienced in past test without applied vertical dead load. At the conclusion of the ductility 3 cycles, the pier had experienced approximately 35% strength loss but had experienced no material cracking.

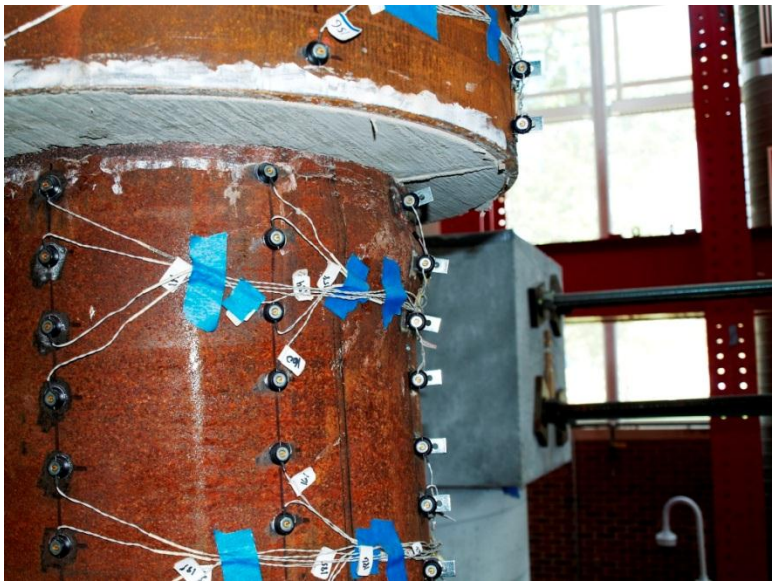

Figure 6.185 Test 6 – Ductility 2, Cycle -3, -5.63 in. Displacement, -158 kips

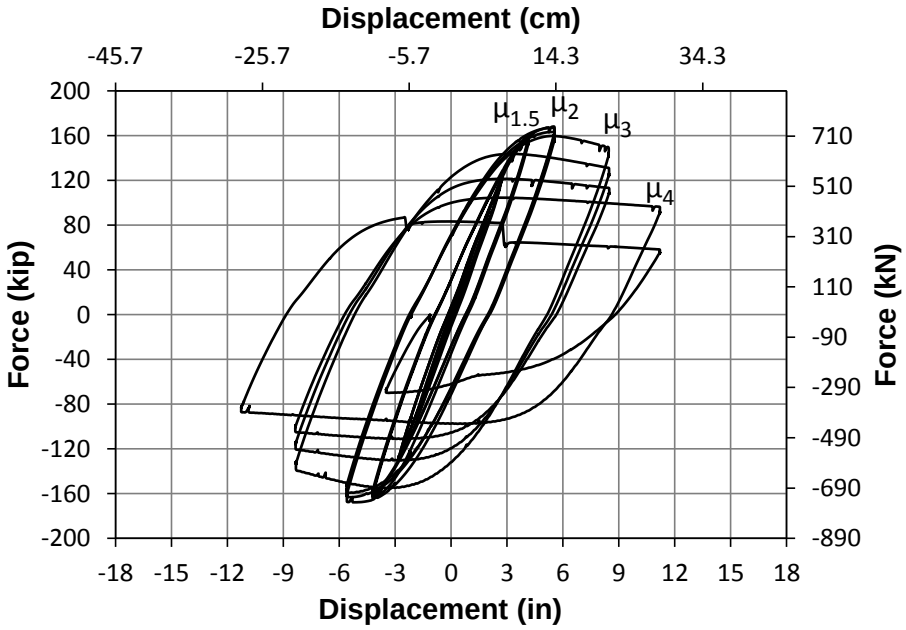

Figure 6.186 Vertical Dead Load – G.S.C. Force – Displacement Hysteresis

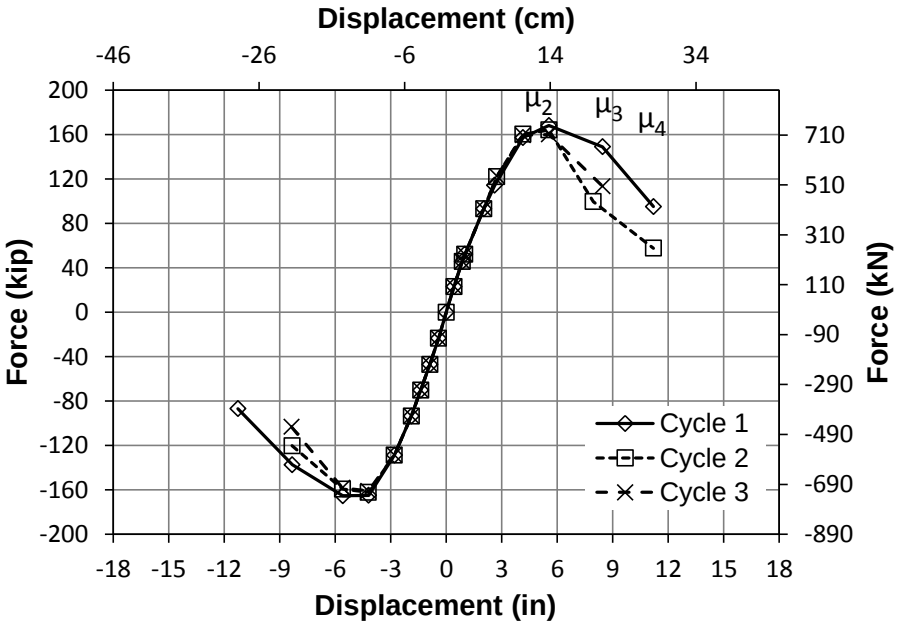

Figure 6.187 Vertical Dead Load – G.S.C.Force – Displacement Envelopes

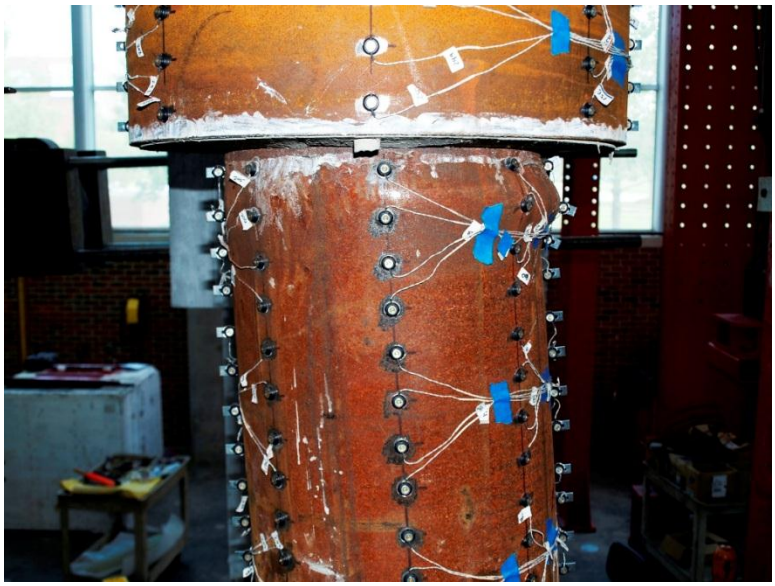

Figure 6.188 Test 6 – Ductility 3 Cycle -1, -8.44 in. Displacement, -137 kips

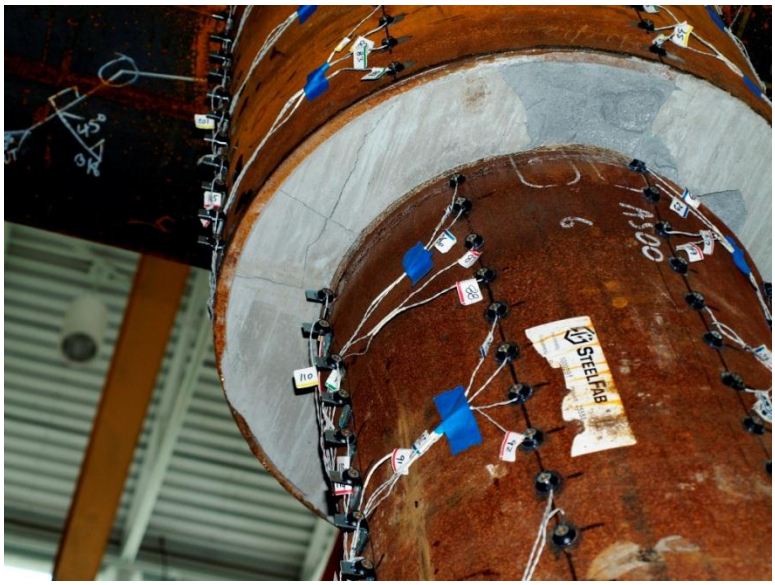

Figure 6.189 Test 6 – Ductility 3 Cycle -2, -8.44 in. Displacement, -120 kips

As the test progressed to the first positive and negative cycles of ductility 4, associated with 11.26 in. of displacement as shown in Figure 6.190, further strength degradation due to local buckling of the pile wall was experienced. Unlike past tests, the locally bucked region continued to maintain an outward shape while becoming more pinched as shown in Figure 6.191. Although the first push and pull cycles of ductility 4 were associated with 45% and 48% strength loss respectively, no cracking had been experienced and the test was continued.

As the specimen was being loaded to the second positive cycle of ductility 4, a loud popping sound was experienced. However, only small cracks not extending through the wall were visually noted on the south face of the north column. Loading was continued until another loud popping sound was experienced which was associated with the development of a large crack on the south face of the north column as shown in Figure 6.192. While monitoring the propagation of the crack, the specimen was loaded to the full ductility 4 cycle 2 displacement peak. At this point in the test, the crack had propagated around approximately 1/2 of the cross section and 66% strength loss had been experienced. The test was assumed to be concluded and the specimen was returned to a zero force position.

Figure 6.190 Test 6 – Ductility 4 Cycle 1, 11.26 in. Displacement, 95 kips

Figure 6.191 Test 6 – Ductility 4 Cycle 1, 11.26 in. Displacement, 95 kips

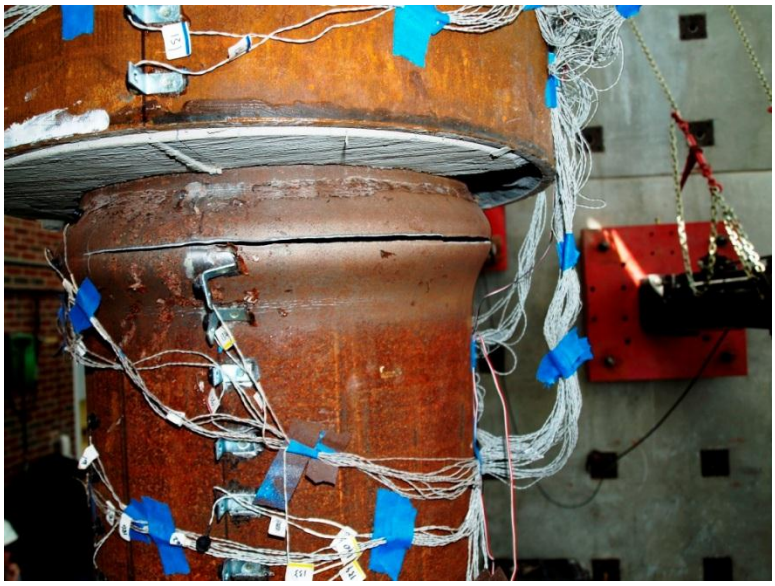

Figure 6.192 Progressing to Ductility 4 Cycle 2, 2.85 in. Displacement

As has been discussed for the other G.S.C. tests, internal strain gauges in the connection region of the pier were used in an effort to quantify force transfer characteristics within the connection length. A similar pattern of internal strain gauges was placed inside the piles at the extremities of the section prior to construction of the test 6 specimen. Post test data analysis was used to produce the strain elevation presented in Figure 6.139 through Figure 6.142, all of which indicate a relatively linear strain gradient prior to the large strain accumulation which occurs at the base of the connection as large levels of plasticity and eventual local buckling develop. Also it is shown, as expected, that the top strain gauge in all cases provides a reading close to zero since by design full force transfer should have taken place at this point in the connection.

When compared to similar strain elevations from tests 4 and 5, it appears that larger strain demands extend higher into the connection potentially as a results of the applied vertical load generating larger P-Delta moment demands. Additional analysis would be required to verify a reason for the observed results. Further, as strain values near or above yield were shown to develop over halfway into the connection region, it is not immediately

apparent that there were any underutilized shear studs. As was concluded from earlier tests as well as FEM results, a reduction in shear studs and alteration of the design model is not immediately warranted without additional study.

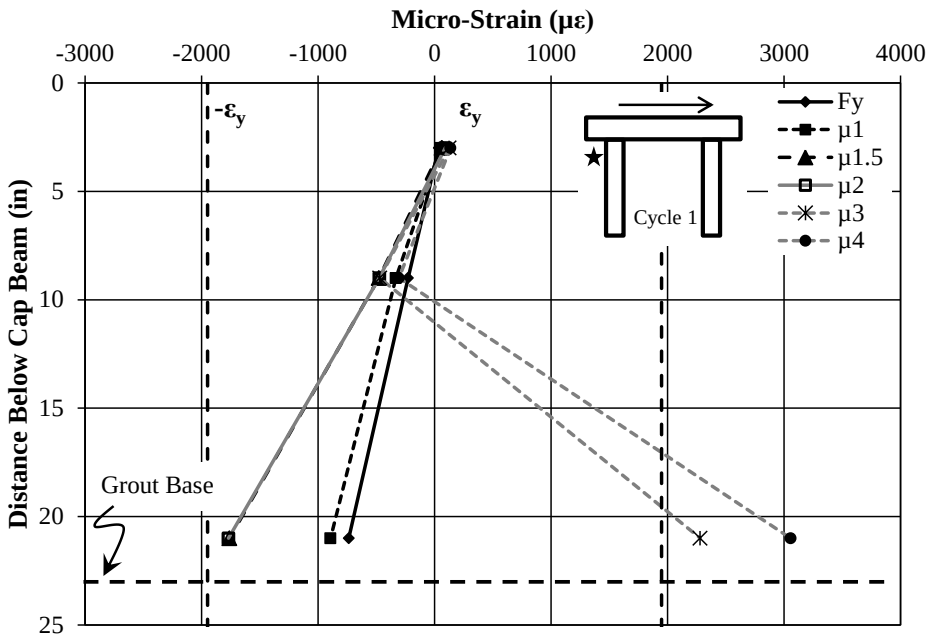

Figure 6.193 Test 6 – North Column North Face Connection Strain Elevation

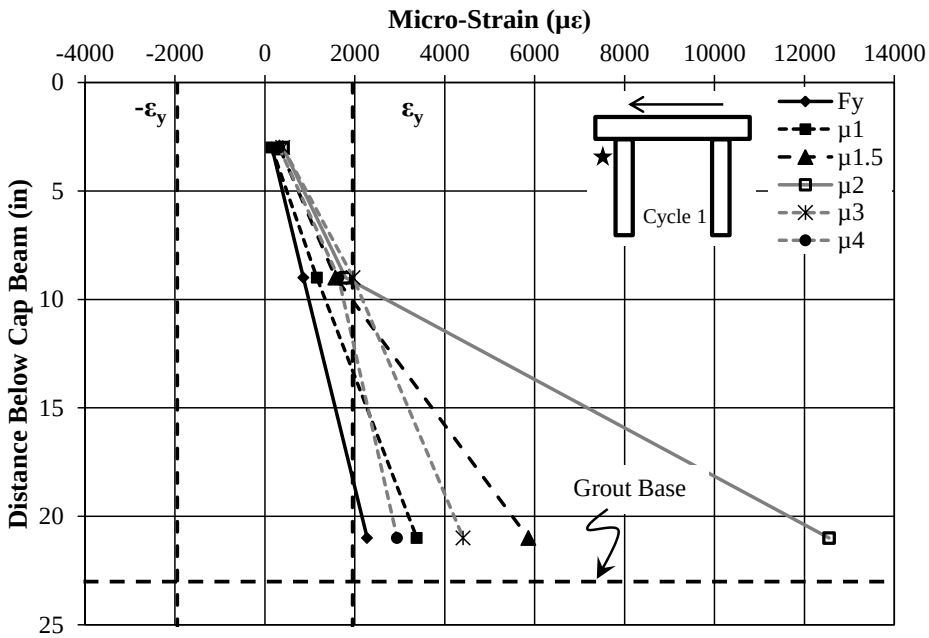

Figure 6.194 Test 6 – North Column North Face Connection Strain Elevation

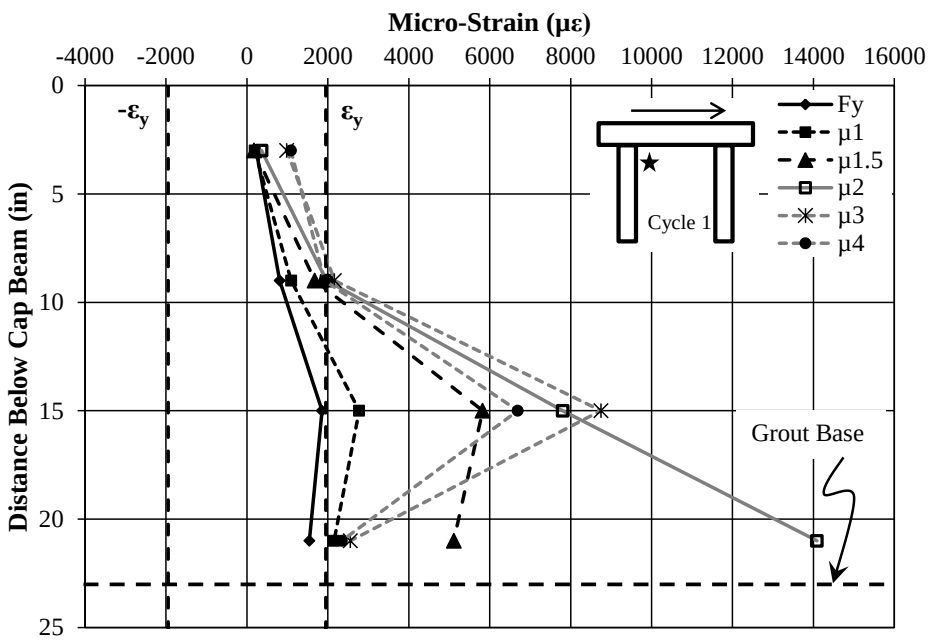

Figure 6.195 Test 6 – North Column South Face Connection Strain Elevation

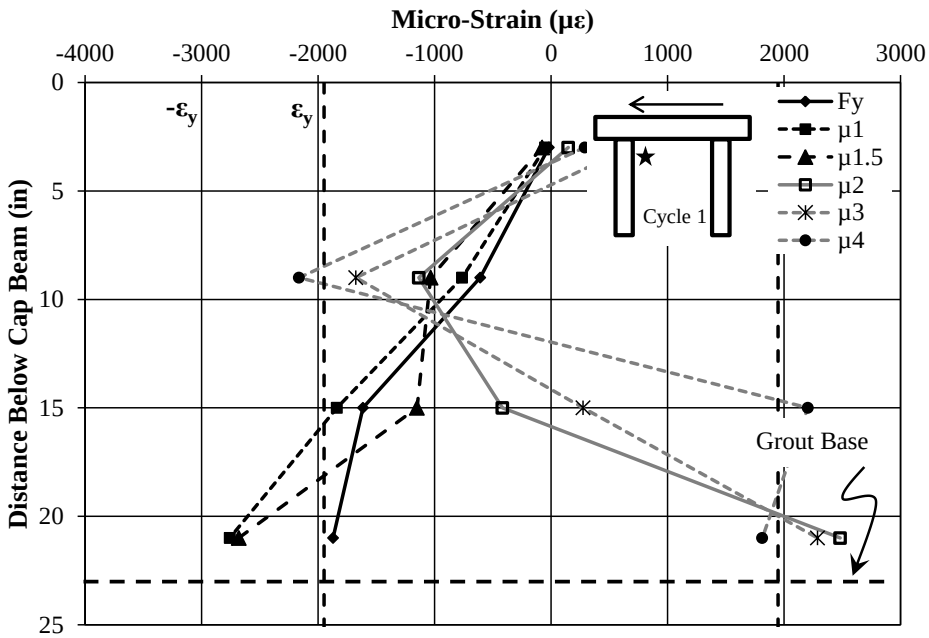

Figure 6.196 Test 6 – North Column South Face Connection Strain Elevation

In an effort to better quantify the effects that the applied vertical dead load had on the performance of the pier, direct comparisons are made in this section between the nominally identical piers of tests 2 and 6. In order to facilitate comparison of experimental data, it was necessary to normalize the system force recordings from each test due to the higher strength material and resulting higher system forces in test 6. This was achieved by dividing the force recordings from each test by the respective maximum values. As has already been noted, test 6 was subjected to the nominally identical load history of test 2 such that the comparisons can be made at given displacement levels with no need to normalize displacement by ductility level or any other means.

As shown in Figure 6.197, the general force displacement hysteretic shape prior to ductility two is similar between the two tests. Following ductility 2, the comparison shows the effects of local buckling to produce more drastic strength degradation in the case of test 6 with vertical dead load than in the case with no vertical dead load. This is particularly

evident in the ductility 3 cycles and in the individual backbone force displacement curves provided in Figure 6.198 through Figure 6.200. Further, as shown in Figure 6.201, when the pier is not subjected to vertical dead load, the P-Delta effects (from compressive overturning resistance) appear to be small enough to not generate negative stiffness in the force displacement response which was experienced with the presence of the applied vertical dead load.

Although the FEM predicted a larger magnitude of strength degradation in the ductility 2 cycles with the presence of vertical load than was actually shown to occur in the experimental test, the two general predictions from the FEM appear to be correct. The overall displacement capacity of the pier was reduced due to increased levels of strength degradation particularly at the ductility 3 level and negative stiffness in the force displacement response was generated from P-Delta effects.

It was also shown from experimental observations, that the presence of the vertical dead load reduced the propensity for the cover grout at the base of the connection to spall and also altered the shape of the buckled pile wall region. As was mentioned, test 6 experienced a predominately outward style of buckling of the pile wall as was shown in Figure 6.191, while the buckling in all cases that did not contain vertical dead load tended to be an inward collapse type mechanism as shown in Figure 6.201. Based on these conclusions, the presence of the vertical dead load appeared to effect the behavior of the pier but does not alter the connection behavior in any obvious and/or negative manner.

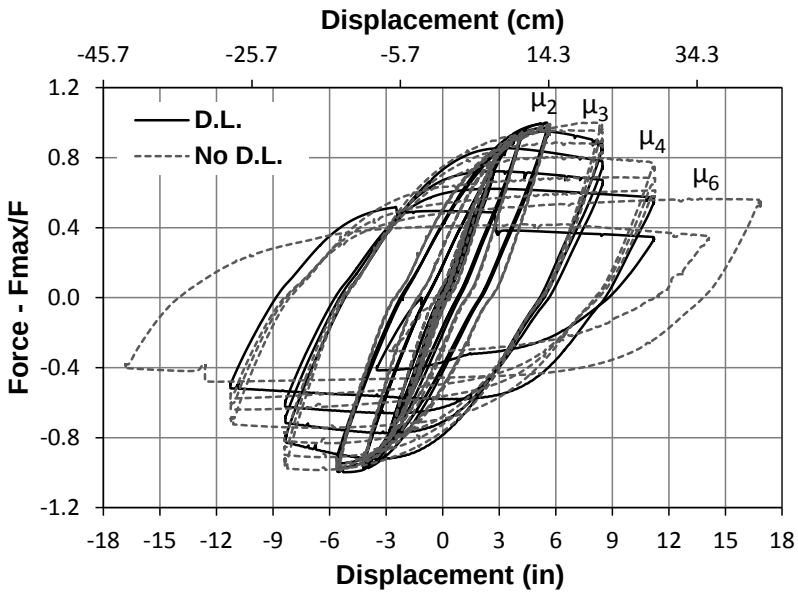

Figure 6.197 D.L. vs. No D.L. – Normalized F-D Hystersis

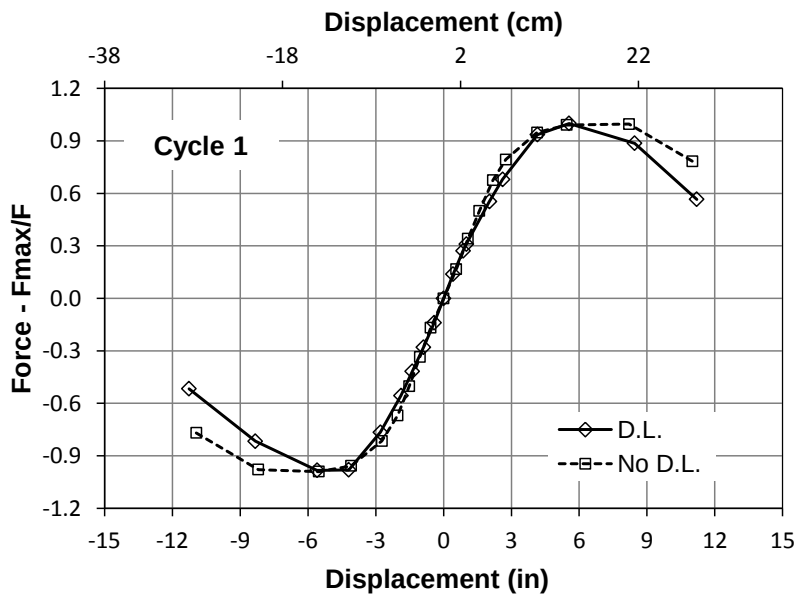

Figure 6.198 D.L. vs. No D.L. – Normalized Cycle 1 Envelopes

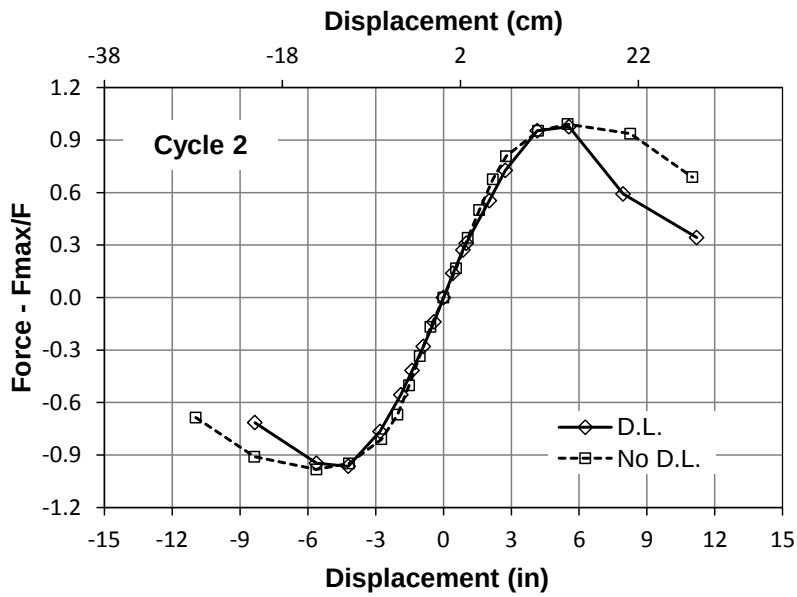

Figure 6.199 D.L. vs. No D.L. – Normalized Cycle 2 Envelopes

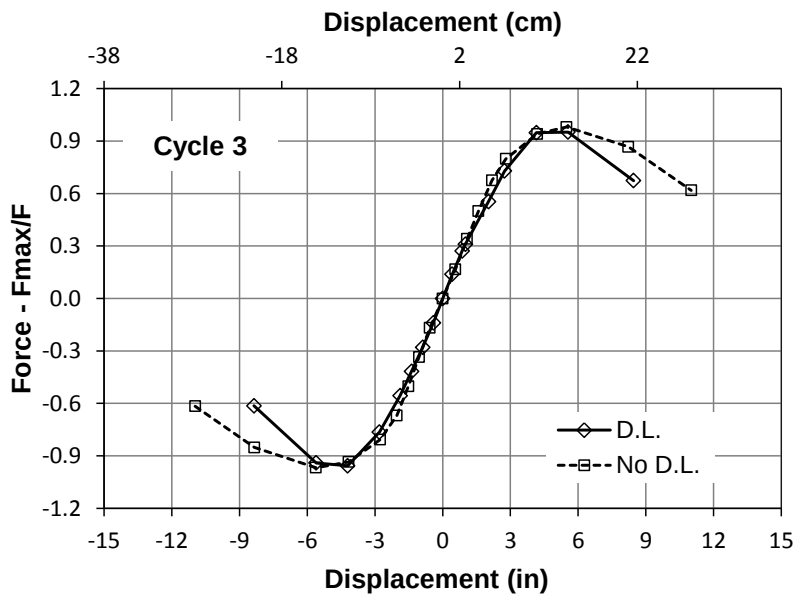

Figure 6.200 D.L. vs. No D.L. – Normalized Cycle 3 Envelopes

Figure 6.201. Test 2 – Ductility 4 Cycle -1, -11.25" Displacement, -98 kips

As has been noted, the experimental pier subjected to vertical dead loads appeared to exhibit a lower ultimate displacement ductility capacity as well as a slightly altered hysteretic shape resulting from P-Delta effects. Consequently, the equivalent viscous damping values for each ductility level of testing have been calculated in order to compare the structures' inelastic damping capabilities to that of the pier with no vertical dead loads (test 2) and with suggested values for a Ramberg – Osgood response (Priestley et al. 2007).

The method used to calculate the total equivalent viscous damping is based on a modified Jacobsen's approach (Jacobsen, 1930). Jacobsen's approach was based on an energy balance method which equated the area encompassed within a full force displacement cycle of a rigid – perfectly plastic oscillator to the input energy from a sinusoidal forcing function. The outcome of this approach showed the total hysteretic damping ratio to be equal to $2/\pi$ for a rigid – perfectly plastic oscillator. It was also shown that the total hysteretic damping of a non – rigid – perfectly plastic response can be determined by scaling the value of $2/\pi$ by the ratio of the area contained in the realistic hysteric loop (A_H) divided by the area contained in the rigid-perfectly plastic response (A_P) as shown in Eq.(6.8) and Figure 6.202

(Priestley et al. 2007). Since the loading history used to generate the actual response is not based on a sinusoidal forcing function, as considered in Jacobsen's derivation, it is necessary to apply the modification factor shown in Eq.(6.9) to avoid inappropriately large values of hysteretic damping (Montejo, 2008; Priestley et al. 2007). It is also necessary to apply a modification factor to the elastic viscous damping, assumed to be 5% in these calculations, which is added to the hysteretic viscous damping to obtain total equivalent viscous damping (EVD) as shown in Eq.(6.10).

This process is necessary to convert the specified elastic damping value to a secant stiffness related value as Jacobsen's approach was based on the secant stiffness method. Further, the secant stiffness approach is recommended for use with the DDBD approach (Priestley et al. 2007). The modification factor is a function of the displacement ductility level and a variable λ which is equal to -0.617 assuming a Ramberg-Osgood model for the ductile steel structure is applicable (Priestley et al. 2007). This λ also assumes that tangent stiffness damping is appropriate for the analysis as is suggested to be correct by (Priestley et al. 2007). Both the loading history and tangent stiffness modification factors have been calibrated using non-linear time history analysis to match maximum response displacements with the DDBD approach. The values of total equivalent viscous damping obtained from the combination of corrected elastic viscous damping and corrected hysteretic damping will be compared to the recommended values (Priestley et al. 2007) of total equivalent viscous damping based upon a Ramberg – Osgood response, provided by Eq.(6.11).

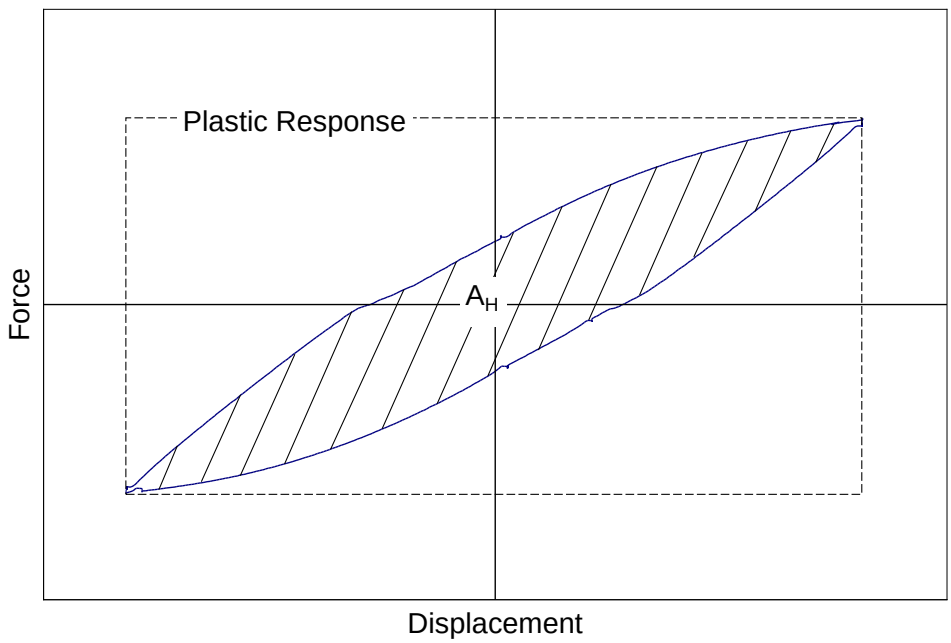

Figure 6.202 Jacobsen's Equivalent Viscous Damping Approach

$$\xi_{Jacobsen} = \frac{2}{\pi}\left(\frac{A_H}{A_P}\right) \tag{6.8}$$

$$\xi_{Hysteretic} = \xi_{Jacobsen}\left[\left(0.53\mu + 0.8\right)^{-\left(\frac{\mu}{40}+0.4\right)}\right] \tag{6.9}$$

$$\xi_{eq} = \mu^{\lambda}\xi_{Elastic} + \xi_{Hysteretic} \tag{6.10}$$

$$\xi_{eq,RO} = 0.05 + 0.577\left(\frac{\mu - 1}{\mu\pi}\right) \tag{6.11}$$

As shown in Figure 6.203, the results of the data analysis showed the piers both with and without applied vertical dead load to exhibit similar total EVD ratios at the ductility 1, 1.5, 2, and 3 levels. Further, in both cases the calculated values of EVD were shown to be of greater

magnitudes than the expected curve considering a Ramberg – Osgood type of response, throughout the entire range of ductility as shown in Figure 6.204 and Figure 6.205. These results suggest that the use of recommended expression would be conservative for Displacement – Based Design purposes, at least up to level of applied vertical dead load considered in the test 6 experimental evaluation.

However, it should be noted that while the test 2 response falls above the recommended R.O. curve, the general shape of three cyclic curves and that of the R.O. response are similar. Contrarily, while still falling above the R.O. response, the three cycle curves from test 6 exhibit a drop at the ductility 1.5 level that is not shown in the R.O. response or the test 2 responses. Although this does not indicate that the R.O. response should not be used for design with applied dead loads, it may suggest that that the presence of axial load effects the total EVD exhibited by a pier at some ductility levels. However, it is also possible that this is a result of the test 6 load history, which was defined to match the same load history as test 2, and did not consider the actual yield stress of the test 6 specimen materials. It is possible that this underestimated the yield displacement of the pier which would consequently generate less inelastic action at the ductility 2 level.

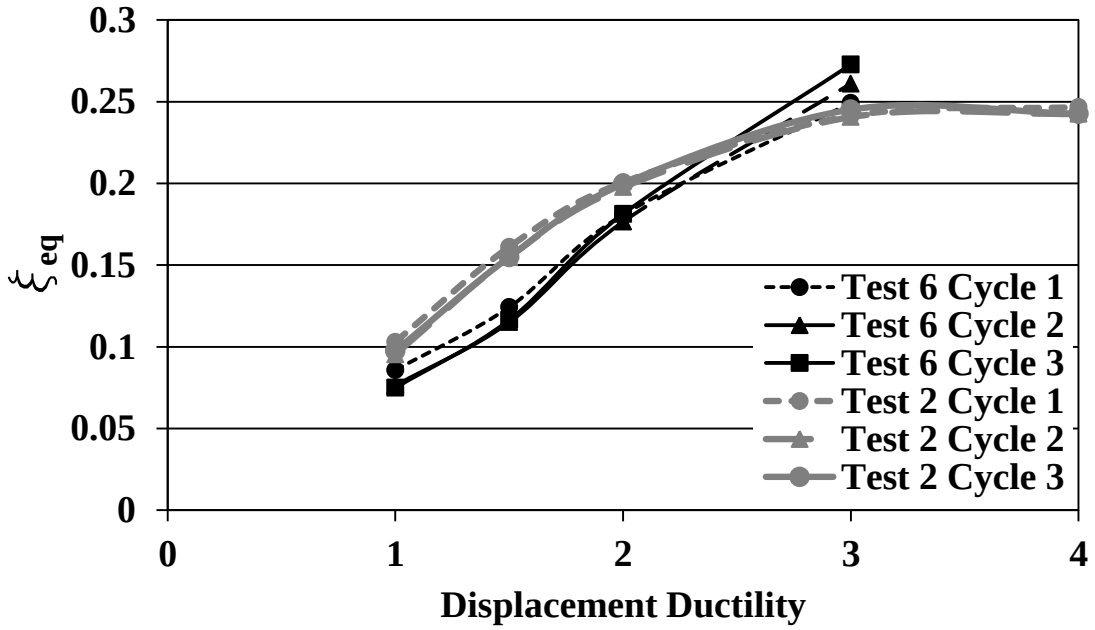

Figure 6.203 Total EVD Test 6 vs. Test 2

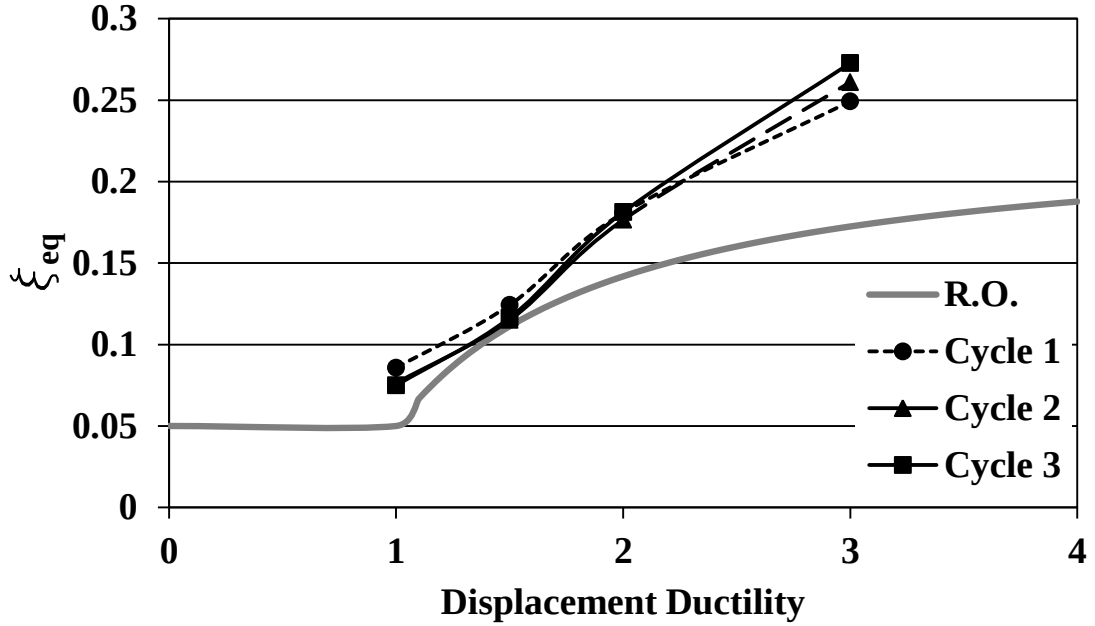

Figure 6.204 Total EVD Test 6 vs. Ramberg Osgood

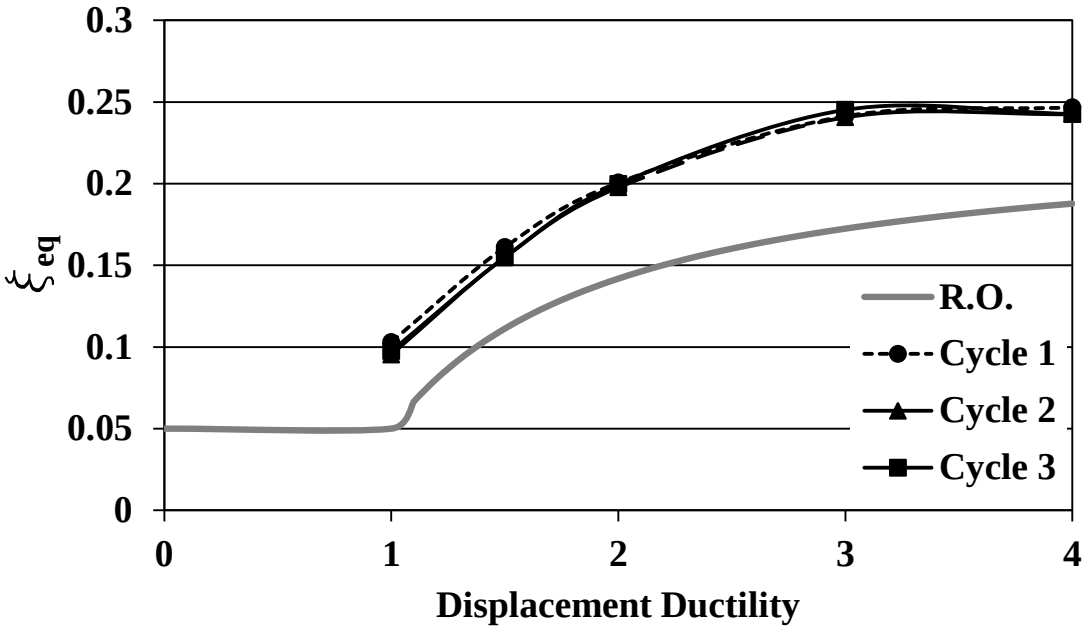

Figure 6.205 Total EVD Test 2 vs. Ramberg Osgood

Following the test 6 experimental evaluation, in-house material testing of the actual test 6 pile material was conducted in order to verify the material properties that were reported by the mill certifications in an effort to explain the differences in strength capacity between the experimental and analytical results. As has been shown, the experimental specimen exhibited an ultimate strength capacity of approximately 170 kips, while the analytical prediction conducted prior to testing indicated a maximum capacity of approximately 120 kips, a difference of 42%. The results of the two coupon tensile tests conducted, provided 2% offset material yield stresses of 71.2 ksi and 68.6 ksi, and ultimate tensile stresses of 79.5 ksi and 77.9 ksi as shown in Figure A 36 and Figure A 37 respectively. These values were found to be reasonably similar to those reported in the material certifications which were 67.5 ksi yield and 80.5 ksi ultimate, as shown in Figure A 38.

The in-house material test data was used to re-calibrate the analytical Finite Element steel constitutive model which again considered a non – linear kinematic hardening rule. The

results of the analysis which included the applied vertical dead loads and followed the same load history as the experimental evaluation, showed good agreement in both global and local behavior when compared to the experimental results. As shown in Figure 6.206, with the re-calibrated material model the analytical prediction exhibited an ultimate strength capacity of 160 kips compared to the experimental capacity of 170 kips. Although this was still a slight difference, the magnitude was reduced to approximately 6% difference and the general hysteretic shape remained similar to that of the experimental response including the intra-cycle strength degradation due to local buckling that was experienced.

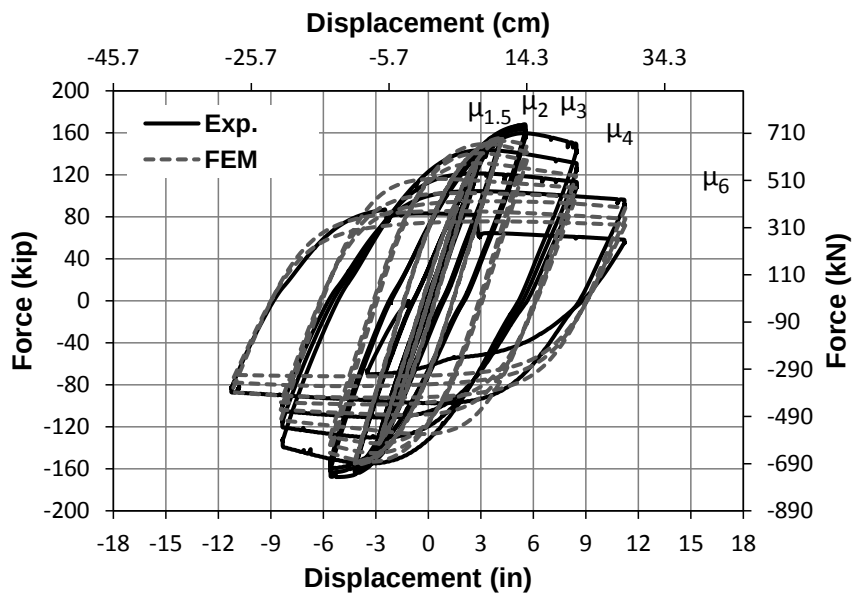

Figure 6.206 D.L. – FEM vs. Experimental Force – Displacement Response

The physical results of experimental testing, as well as the results of data analysis and Finite Element Modeling, indicate that the standard grouted shear stud connection was again effective at properly locating damage in the form of pile wall local buckling within the intended region at the base of the connection. Although this had already been shown in previous tests, test 6 served as a validation of the capability of the connection while the pier

was subjected to vertical dead load, which had not been considered in earlier experimental evaluations. However, as was anticipated by FEM results, the presence of vertical dead load reduced the ultimate displacement capacity of the pier by both inducing local buckling at lower levels of displacement and increasing the rate of post buckling strength degradation.

The test 6 specimen was shown to be limited to an ultimate displacement ductility capacity of 2 or 3 depending on the exact allowable level of strength degradation. These limit states correspond to 5.63 in. and 8.44 in. of lateral displacement, respectively, or 4.2% and 6.3% drift. As has been discussed, test 6 experienced more significant strength degradation throughout the ductility 3 cycles than had past tests with no applied dead load. This resulted in an approximate strength loss of 35% in the third cycles of ductility 3 compared to that of test 2 which exhibited 15% strength loss in these cycles. Hence, with a strict definition of reliable ductility corresponding to less than 20% strength loss through all cycles of a ductility level, the pier's ultimate displacement capacity would be reduced from a ductility of 3 to 2 with the presence of a reasonable upper bound vertical dead load. However, with a less strict definition of reliable ductility the capacities both with and without dead load may be increased by one level. Further, it should be noted that while seemingly low, both the ductility 2 and 3 displacement levels correspond to reasonable drift limits.

As has been shown, it may be necessary to consider lower D/t values should an increased deformation capacity be required beyond that which is provided by the grouted shear stud connection with HSS16x0.500 pile sections. Although the applied dead was shown to reduce the ultimate displacement capacity of pier, the test did serve as further validation of the capabilities of the connection design to properly relocate damage in the form of pile wall local buckling in the intended region and to capacity protect critical regions. Further, as strains near or above yield were shown to develop in the HSS16x0.500 pile over halfway into the connection region, it is not immediately apparent that any shear studs were underutilized as might be the case had the strain gradient more quickly approached zero.

6.5.6 Grouted Shear Stud Connection General Conclusions

In general, the grouted shear stud connection configuration was shown to effectively behave as a modified weld protected connection by fulfilling the two key criteria of such connections. First, damage associated with the more desirable failure mechanism of pile wall local buckling was relocated away from the pile to cap beam connection interface. Secondly, critical welded regions were protected by ensuring they remained in the elastic range of loading as full strength capacity associated with pile hinging was developed. In addition, it was shown that the presence of construction tolerance offsets within the connection region had no adverse effects on the performance of the pier, which could likely be considered advantageous from a design standpoint.

Although an attempt was made to modify the configuration to generate a buckling restraining mechanism intended to mitigate post – buckling strength degradation, the effectiveness of the additional feature was found to be marginal. Considering the additional labor and materials required to modify the connection, the use of the modified version would likely not be recommended in design. However, it should be noted that the inclusion of the buckling restraining mechanism did not have any adverse effects on the system.

As has been noted, the results produced by internal strain gauges as well as the results of the FEM simulation, it is not immediately apparent that a reduction in the number of shear connectors or the overall size of the connection should be reduced. Hence, the design methodology of developing the axial yield capacity of the pile to determine the required number shear stud connectors appears to be adequate and no optimization options are immediately evident. Although the inclusion of bond stress capacity between the HSS16x0.500 pile and the grout block, to develop the axial yield capacity of the pile could be considered, the resulting effect on the required number of shear connectors would likely be minimal. For example, considering a reasonable bond stress capacity of 0.8 MPa (116 psi) over the length of the connection would induce a reduction in required shear connectors of

approximately 10% for the configuration considered in the experimental tests. This would correspond to approximately 5 shear studs which likely not affect most designs as the required number must be rounded up to generate a symmetrical pattern. Further, the complicated action occurring within the connection would make it difficult to verify the assumed 0.8 MPa bond stress or to estimate an alternate value.

Having developed a connection capable of producing the desired pile hinging mode of failure, experimental and FEM evaluation were conducted to assess the impact of vertical dead loads on the performance of the system when subjected to lateral loading. As discussed in detail in prior sections, it was found that when the pier was subjected to a reasonable upper bound estimate of superstructure weight, pile wall local buckling was induced a lower displacement ductility level and the ultimate displacement capacity was reduced. Depending on the exact allowable level of strength loss considered in a design, these effects would likely reduce the piers' ductility capacity by approximately 1 level. As a result of this response, the decision was made to conduct a parametric study to better understand the interaction of dead load magnitude, D/t ratio, allowable strength loss, and ultimate displacement ductility capacity. The details, results, and recommendations of this study will be discussed subsequently in this document.

6.6 G.S.C. Dynamic Shake Table Testing

6.6.1 Test Specimen Design, Construction, and Scaling Parameters

In addition to the quasi – static large scale steel pier testing that was used in this research project, scaled dynamic shake table testing was also conducted. In this case, two nominally identical specimens containing grouted shear stud connections were constructed at a 3/8 length scale. This scale was chosen through a trial and error process considering the shake table's force capacity, dimensional capacity, and material availability. The purpose of these

two tests was to verify the capability of the grouted shear stud connection configuration to effectively act as a modified weld protected connection when subjected to actual dynamic loading. In addition, the results of the dynamic tests would allow for comparisons to be made in regards to the displacement capacity of this system when subjected to a three cycle set load history and when subjected to an actual ground motion. Although this second objective required that the connection properly relocate damage in form of pile wall local buckling, it was postulated by the researchers that this would be achieved.

As has been noted, a 3/8 length scale factor was used in the design of the model test specimens which considered the large scale tests with applied vertical dead load (phase 2 test 6) to be the prototype specimen. Although an attempt was made to maintain this factor in the design of the entire system, particular attention was paid towards maintaining the 3/8 factor in regards to the outer dimension of the pipe piles, the center to center spacing of the piles, and the shear span from the pinned base supports to the bottom of the grouted shear stud connection as these parameters were considered to be critical to the behavior of the pier. In addition, particular attention was paid towards maintaining the same D/t ratio between the prototype and the scaled model specimens as this would be critical to the anticipated pile wall local buckling failure mode.

The design process resulted in the use of ASTM A500 Gr. B. HSS6x0.188 piles, ASTM A500 Gr. B. HSS10x0.250 stub pile elements, and a double ASTM A992 W8x40 cap beam as shown in Figure 6.207 through Figure 6.208. Further, the design of the grouted shear stud connection resulted in the use of ASTM A108 1 – 1/8 in. x 1/4 in. diameter shear studs with 5 stud connectors in a given line spaced at 1 – 3/4 in. on center as shown in Figure 6.209. As was the case with the large scale pier, the studs were evenly distributed around the HSS6x0.188 pile in 12 vertical lines at 30 degrees on center with a matching pattern on the inside of the HSS10x0.250 stub pile offset by 7/8 in. vertically and 15 degrees radially. Design calculations for the system and connection region are provided in Figure 6.210 through Figure 6.213.

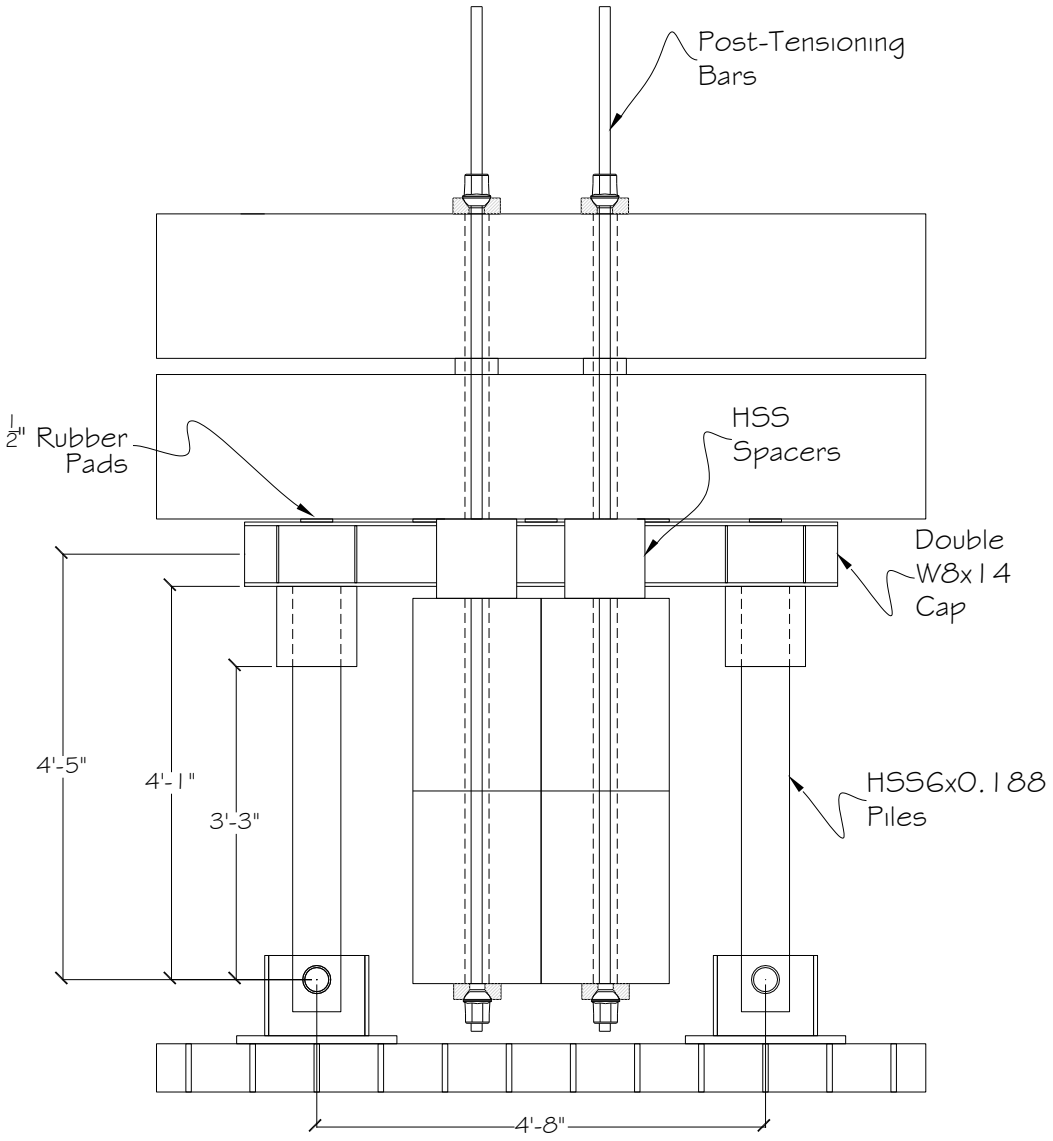

Figure 6.207 Scaled G.S.C. Steel Pier NS Elevation (Phase 2 Tests 8 & 9)

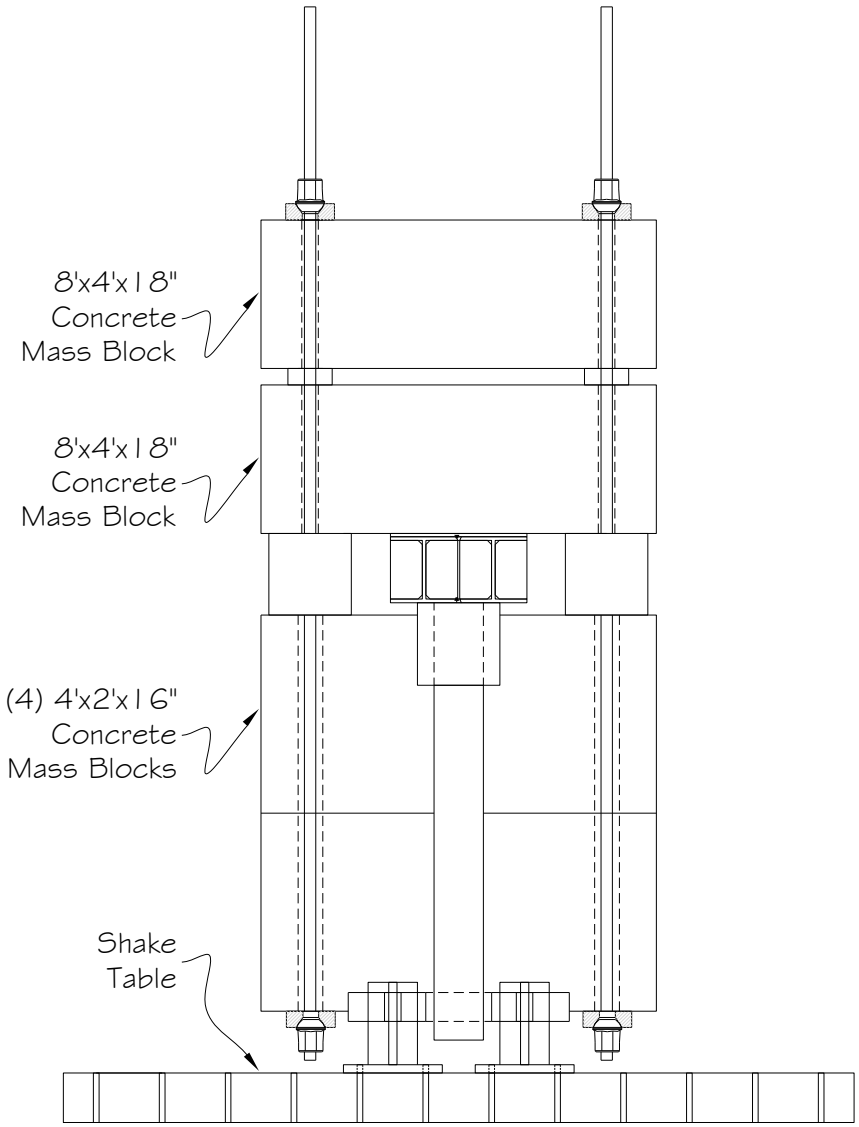

Figure 6.208 Scaled G.S.C. Steel Pier EW Elevation (Phase 2 Tests 8 & 9)

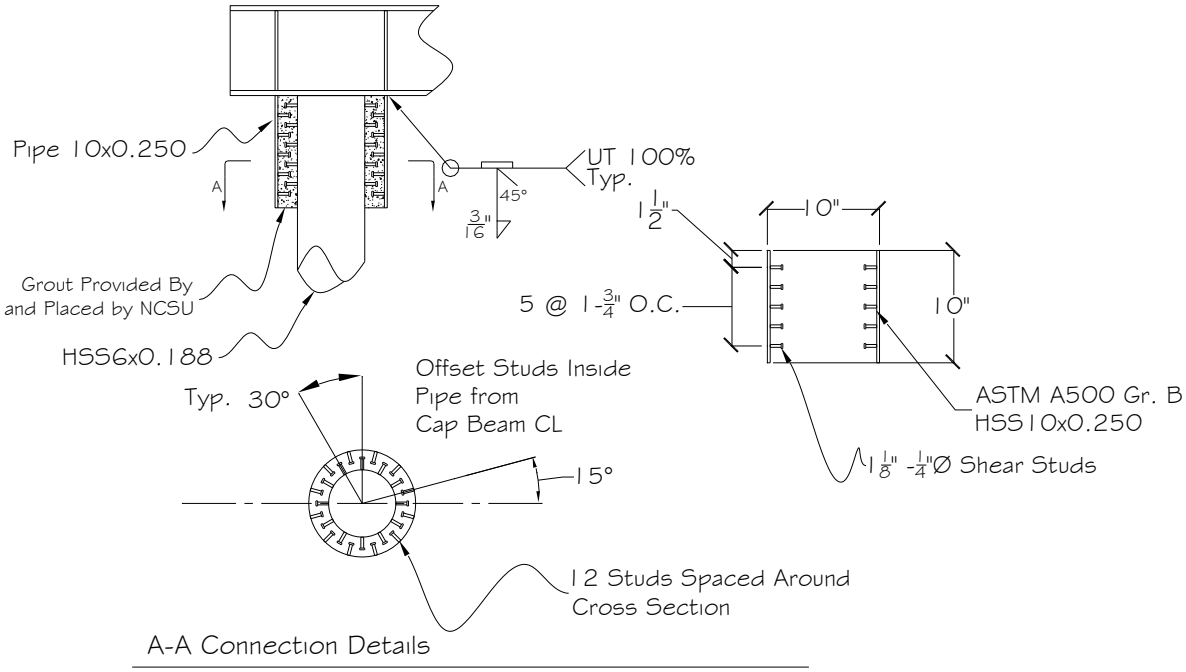

Figure 6.209 Scaled G.S.C. Details (Phase 2 Tests 8 & 9)

Scaled Specimen Design:

(1) Scaled Pile: HSS6.00x0.188 ASTM A500 Gr. B

From recommended **AISC 341-10 overstrength values**:

$R_y := 1.4$ $\quad f_y := 42ksi$ $\quad f_{y\_exp} := R_y \cdot f_y$ $\quad f_{y\_exp} = 58.80 \cdot ksi$

$R_t := 1.3$ $\quad f_u := 58ksi$ $\quad f_{u\_exp} := R_t \cdot f_u$ $\quad f_{u\_exp} = 75.40 \cdot ksi$

$O_{exp} := \frac{f_{u\_exp}}{f_{y\_exp}}$ $\quad O_{exp} = 1.28$ reasonbale exptected overstrength factor

Shape is compact for flexure Per AISC 360-05 for specified material properties. For the expected values of material properties:

$\frac{6.00in}{0.188in} = 31.91$ less than: $\frac{0.07 \cdot (29000ksi)}{f_{y\_exp}} = 34.52$ Shape is compact beyond requirment, Good.

Figure 6.210 Scaled Steel Pier Design Calculations

The flexural overstrength of the pile is given by:

$f_{y\_pile} := f_{y\_exp}$ $\quad Z_{pile} := 5.91in^3$ for HSS 6.00x0.188

$O := O_{exp}$ $\quad V_{span} := 39in$ design shear span

$M_{pile} := f_{y\_pile} \cdot Z_{pile} \cdot O$ $\quad \boxed{M_{pile} = 37.13 \cdot kip \cdot ft}$ expected overstrength pile moment capacity

$V_o := \frac{M_{pile}}{V_{span}}$ $\quad \boxed{V_o = 11.43 \cdot kip}$ associated shear at design depth of hinging per pile

$V_b := (2) \cdot V_o$ $\quad \boxed{V_b = 22.85 \cdot kip}$ base shear demand to form flexural hinging (2) pile pier

To check shear failure of the pile per AISC 360-05 specifications G6:

$$F_{cr} := \min\left[\max\left[\frac{1.6 \cdot 29000ksi}{\sqrt{\frac{50}{6.00}} \cdot \left(\frac{6.00}{0.188}\right)^{\frac{5}{4}}}, \frac{0.78 \cdot 29000ksi}{\left(\frac{6.00}{0.188}\right)^{\frac{3}{2}}}\right], 0.6 \cdot f_y\right] \qquad F_{cr} = 25.20 \cdot ksi$$

$\phi V_{n\_pile} := 0.9 F_{cr} \cdot 0.5 \cdot 3.18in^2$ $\quad \boxed{\phi V_{n\_pile} = 36.06 \cdot kip}$ >Vo, Good

(2) Scaled Cap Beam: Double W8X40 ASTM A992.

Flexural Capacity Per AISC 360-05 Specification Chapter F:

$f_{y\_A992} := 50ksi$ ASTM minimum yield stress

$S := (2) \cdot 35.5in^3$ for double HP8x36

$\phi M_y := (0.9) S \cdot f_{y\_A992}$ $\quad \boxed{\phi M_y = 266.25 \cdot kip \cdot ft}$

Figure 6.211 Scaled Steel Pier Design Calculations Continued

Check Element Compactness:

Flange Slenderness -- $\frac{0.5 \cdot 8.16in}{0.560in} = 7.29$ $\quad 0.38 \cdot \left(\frac{29000ksi}{f_{y\_A992}}\right)^{0.5} = 9.15$ flange compact

Web Slenderness -- $\frac{5.25in}{0.360in} = 14.58$ $\quad 3.76 \cdot \left(\frac{29000ksi}{f_{y\_A992}}\right)^{0.5} = 90.55$ web compact

Lateral Torsional Buckling will be neglected as HPs will be doubled and welded at flanges. Full penetration weld in accordance with AWS D1.1 should be used to ensure composite action about Y axis. Yielding about X axis will be checked.

The bending moment demand at the end of the cap beam is limited to the extrapolated pile hinging moment capacity:

$M_{o\_cap\_end} := M_{pile} \cdot \frac{52in}{V_{span}}$ $\quad M_{o\_cap\_end} = 49.51 \cdot kip \cdot ft$ <<My, Good

The maximum bending moment at the center of the span can conservatively be determined by assuming a centerline point load equal to the anticipated applied inertial load:

$M_{o\_cap\_CL} := \frac{22kip \cdot 54in}{4}$ $\quad M_{o\_cap\_CL} = 24.75 \cdot kip \cdot ft$ <<My, Good

Shear capacity evaluation per AISC 360-05 Specification G2:

$\frac{5.75in}{0.455in} = 12.64$ less than $2.24 \cdot \sqrt{\frac{29000ksi}{f_{y\_A992}}} = 53.95$

Therefore: $C_v := 1.0$ and $\phi_v := 1.0$

$\phi V_{n\_cap} := (2.0)\phi_v \cdot 0.6 \cdot f_{y\_A992} \cdot (8.25in) \cdot (0.360in) \cdot C_v$ $\quad \boxed{\phi V_{n\_cap} = 178.20 \cdot kip}$ by inspection, Good

Figure 6.212 Scaled Steel Pier Design Calculations Continued

Grouted Shear Stud Connection Design:

(1) Connection Design

Description: The grouted shear stud connection will be designed utilizing the theory developed for the full sized specimens. ASTM A108 stud connectors will be used and a minimum grout strength of 6 ksi will be assumed.

$A_{g\_HSS6x188} := 3.18in^2$

For: 1/4" Shear Studs with minimum 6 ksi grout; from AISC Specification I3:

$A_{sc} := \frac{\pi}{4} \cdot \left(\frac{1}{4}in\right)^2$ $\qquad A_{sc} = 0.05 \cdot in^2$

$f_u := 65ksi$ for ASTM A108 Stud Connectors

$f'_c := 6ksi$

$E_c := 1746 \cdot \sqrt{\frac{f'_c}{ksi}}$

$Q_n := \min\left(0.5 \cdot \frac{A_{sc}}{in^2} \cdot \sqrt{\frac{f'_c}{ksi}} \cdot E_c, \frac{A_{sc}}{in^2} \cdot \frac{f_u}{ksi}\right) \cdot kip$ $\qquad \boxed{Q_n = 3.19 \cdot kip}$ nominal capacity of each stud

$N := \frac{f_{y\_exp} \cdot A_{g\_HSS6x188}}{Q_n}$ $\qquad \boxed{N = 58.60}$ total required number of shear studs

Use: 12 vertical rows, evenly distributed around cross section with (5) 1-1/8" x 1/4" Dia. studs in each vertical line. Pipe side studs to match pattern.

Figure 6.213 Scaled Grouted Shear Stud Connection Calculations

Unlike the prior large scale grouted shear stud connection piers, the scaled shake table specimens were constructed in an inverted position as shown in Figure 6.214. Constructing the piers in this inverted position allowed for the placement of grout material in the annular ring of the connection to be done by hand with small shovels as opposed to the vertical pumping system that was used with the large scale specimens. Although this construction sequence deviates from realistic field conditions, it was felt necessary to minimize any possible air voids which may be more impactful to the behavior of the system at the reduced

length scale. Further, the process was necessary to minimize construction tolerance offsets which were critical given the 8 in. grided bolted restraint system associated with the shake table. As was done with the large scale specimens, a BASF Masterflow 928 flowable high strength grout product was used to form the composite connection. 4 in. x 8 in. cylinders were cast at the same time as the two scaled piers to ensure that an adequate compressive strength was achieved prior to testing. Four cylinder tests provided an average strength of 10.5 ksi after 137 days of curing, which was larger than the assumed value of 6 ksi in the design calculations.

Figure 6.214 Inverted Construction of Scaled G.S.C. Piers

Prior to conducting any experimental and analytical investigations, similitude scaling calculations were conducted in order to determine other applicable scaling factors associated with the 3/8 length scale model. As shown in Figure 6.215, by mandating that the stress and gravitational acceleration scale factors were 1/1 which was desired, other necessary scale factors including mass and time could be calculated with dimensional analysis. As shown, for the 3/8 length scale the applicable mass and time scales were found to be 9/64 and 79/129 (0.612) respectively. Considering, the 9/64 mass scale factor and the 160 kip dead load

determined to be an upper bound estimate of superstructure weight applicable to the prototype specimen (phase 2 test 6), it was determined that 22.5 kips of dead load should be applied to the scaled pier.

This was achieved by utilizing (2) 8 ft. x 4 ft. x 18 in. and (4) 4 ft. x 2 ft. x 16 in. concrete mass blocks. The two larger mass blocks were placed on top of the pier on (5) 4 in. wide by 1/2 in. thick neoprene bearing pads evenly spaced between the piles at 14 in. on center to represent girder locations. The four smaller mass blocks were placed underneath the pier and stressed to the upper mass blocks with four post tensioning bars as shown in Figure 6.207, Figure 6.208, and Figure 6.216. It is important to note, HSS spacers were placed on top of the lower blocks to act as shims between the two sets of mass blocks. This was done such that the cap beam would not be stressed between the mass block system in an effort to mitigate cap beam stiffening effects which would alter the flexibility of the pier system. In addition, large steel angles were stressed to both ends of the cap beam and to the mass block system. This was done to restrain the mass block system in the direction of shaking while still attempting to avoid any stiffening effects on the system. Although not involved in the design of the pier or test set up, it should be noted that the calculated time scale factor of 0.612 was used to time scale each record considered in the investigations such that the similitude scaling factors would remain consistent.

(I) Scaling Parameters

Control Scaling Parameters

$\boxed{S_L := \frac{3}{8}}$ Length Scale

$\boxed{S_\sigma := 1}$ Stress Scale

$\boxed{S_a := 1}$ Gravitational Acceleration Scale

Dimensionaly Dependant Scaling Parmeters:

$S_A := S_L \cdot S_L$ $\quad S_A = \frac{9}{64}$ Area Scale Factor

$S_F := S_A \cdot S_\sigma$ $\quad S_F = \frac{9}{64}$ Force Scale Factor

$S_M := S_F \cdot S_L$ $\quad S_M = \frac{27}{512}$ Moment Scale Factor

$S_m := S_F \cdot S_a^{-1}$ $\quad \boxed{S_m = \frac{9}{64}}$ Mass Scale Factor

$S_t := \sqrt{\frac{S_L}{S_a}}$ $\quad \boxed{S_t = 0.612}$ Time Scale Factor

Figure 6.215 Similitude Scaling Calculations

Figure 6.216 Scaled Steel Pier with Mass Block System on Shake Table

6.6.2 NLTHA Details

Non – linear time history analysis (NLTHA) was conducted prior to the experimental shake table testing in order to predict the response of the steel pier system to various acceleration time histories in effort to select a suite of ground motions for testing. In addition, the FEA program was also used to apply baseline correction to the input acceleration time histories on order to obtain displacement histories for testing. This was necessary as the input to the shake table at NCSU needed to be in the form of a displacement vs. time.

The FEA model used for the NLTHA was a line element model which considered both material and geometric non – linearity. The cap beam elements consisted of a box shape cross section representative of the double W8x40 webs and flanges, while the piles consisted

of pipe elements with the appropriate design dimensions of the HSS6x0.188 piles. The connection region of the model consisted of analytically rigid elements, which was considered a reasonable simplifying assumption for the dynamic analysis. Mass was represented by lumping 1/2 of the total 22.5 kip mass over the pile/cap beam joints. The various regions of this model are shown schematically in Figure 6.217.

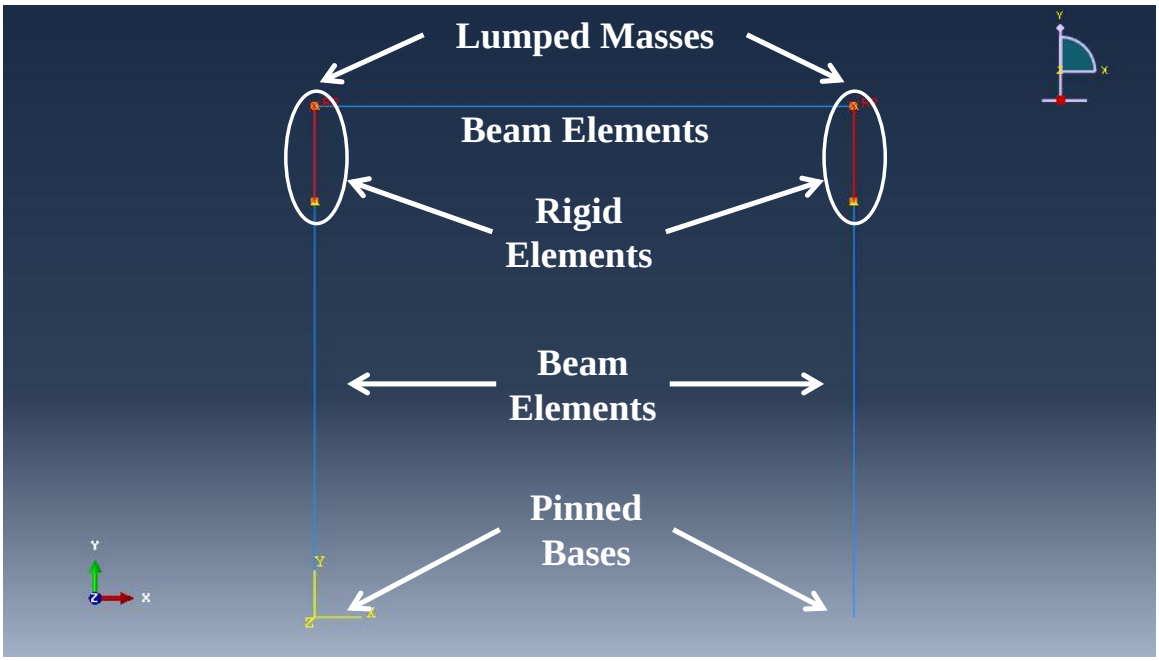

Figure 6.217 Dynamic Line Element Model Schematic

As has been noted in prior chapters, the formulation of the line elements used in the model evaluated cross section plasticity with an integration scheme across the section at a given number of cross section points and along the element at a given number of integration points. Prior to the dynamic evaluation, the non – linear kinematic hardening rule for the plastic portion of the analytical material model was calibrated using a static push – over analysis. The material model calibration was based on actual in house material test stress – strain data collected during coupon testing of the pile material (see Figure A 41).

In order to utilize the combined material model, it was necessary to specify PIPE32 elements (3 node quadratic elements) which have specific formulations that allows for the use of the combined model as opposed the standard beam elements which only allow for the use of the kinematic hardening model. These elements also allow for the application internal pressure loading, although this option was not necessary or applicable to this dynamic analysis. Although the program default was specified as 8 cross section points for the integration of stresses over the pipe section, an investigation was conducted to determine whether a larger number of points was necessary to appropriately capture cross section plasticity. As shown in Figure 6.218, when subjected to a static pushover cap beam displacement, the force – deformation response of the pier system was shown to shift upward in the non – linear range when the number of section was increased from 8 to 16. However, no change in behavior was experienced by the model when the number of points was increased from 16 to 32. As a result, the decision to use 16 cross section points was made.

In addition to the specific modeling details that have been discussed, several other key aspects of the analysis should be noted. First, material level damping was included at a value of 3.5% and was specified as tangent stiffness proportion with no mass proportional damping included. Secondly, the analysis was conducted with a dynamic implicit formulation that used a Newton iterative solution technique and a maximum time step equal to the input record time step which, in all cases, was less than the elastic period of the structure divided by 20. Third, the analysis was conducted for an undamaged structure for each case considered. The resulting errors will be discussed where applicable in the following sections of this document. Lastly, although the model was capable of capturing the effects of material and geometric non – linearity, the model was not capable of capturing system strength loss due to local buckling of the pile walls as had been done with the quasi – static 3 dimensional models. This limitation had to be considered when reviewing the results of the analysis in order to select records to testing.

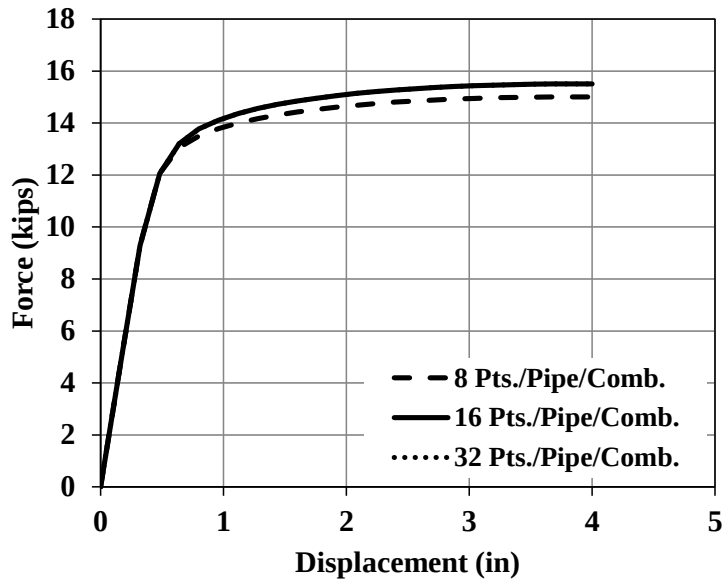

Figure 6.218 Push – Over Analysis Calibration of Dynamic Model

6.6.3 NLTHA Results and Record Selections for Shake Table Testing

Analytical results from the FEM were used to select 7 different ground motions that would be used for the first experimental shake table test. As detailed in Table 6.2, the selected acceleration time histories varied in event magnitude from 5.8 to 8.8 and PGA from 0.135 g to 1.92 g as shown in Figure 6.219 through Figure 6.225. The characteristics of the predicted displacement response histories to these events also varied as shown in Figure 6.226 through Figure 6.232. As shown, Mineral VA, El Centro, and Angol consisted of longer records with more displacement reversals, while Waimea, Pacoima Dam, Tarzana, and Kobe were shorter records more characteristic of velocity pulse style events. It should also be noted, that the records were all input into the analysis at a 1.0 acceleration scale factor to avoid manipulation of the time history and a time scale factor of 0.612 in order to maintain consistency with the similitude scaling that has been discussed in prior sections of this document.

The results of the analysis predicted maximum cap beam displacements ranging from 0.11 in. for the least demanding record Mineral VA, and a maximum cap beam displacement of 2.75 in. for the most demanding record, Kobe. Based on a centerline modeling technique that considers joint region flexibility, which is discussed in detail in subsequent chapters of this document, the predicted first yield displacement of the system was 0.641 in. resulting in a predicted effective yield displacement of 0.833 in. Considering this yield displacement magnitude, the analysis predicted a displacement ductility demand range of 0.13 to 3.29 as shown in Table 6.2.

Table 6.2 Analysis Input Records and $\mu_{\Delta max}$ Predictions

Event	M_W	Station	PGA (g)	Acc. Scale	Time Scale	$\mu_{\Delta max}$
Mineral, VA	5.8	Corbin	0.135	1.0	0.612	0.13
Imperial Valley	6.9	El Centro	0.359	1.0	0.612	0.57
Hawaii	6.7 (M_L)	Waimea	1.057	1.0	0.612	0.71
Maule, Chile	8.8	Angol	0.935	1.0	0.612	0.51
Northridge, CA	6.4	Pacoima Dam	1.530	1.0	0.612	1.46
Northridge, CA	6.4	Tarzana	1.920	1.0	0.612	2.11
Kobe	6.9	Not Known	0.821	1.0	0.612	3.29

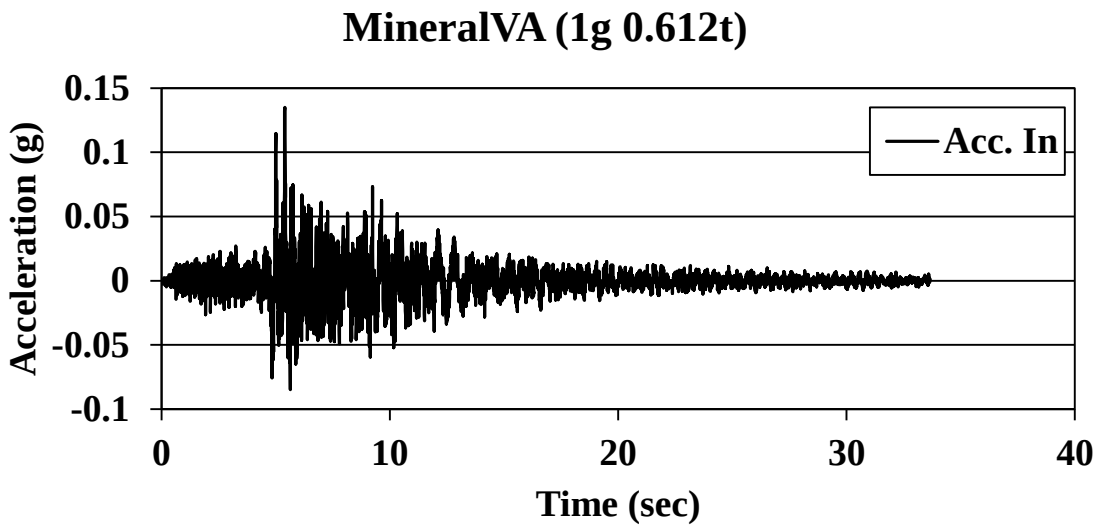

Figure 6.219 Mineral VA Acceleration Time History Input

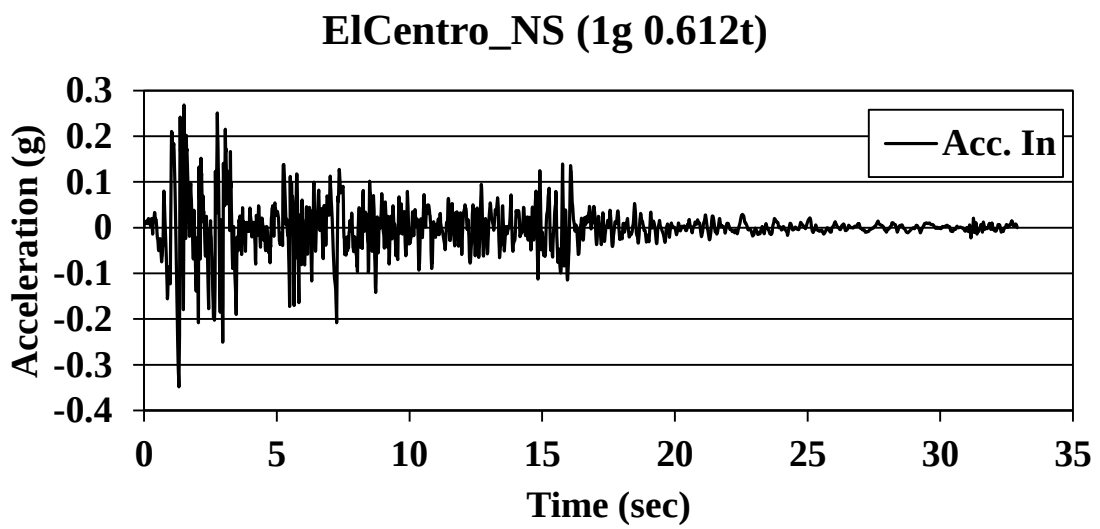

Figure 6.220 El Centro Acceleration Time History Input

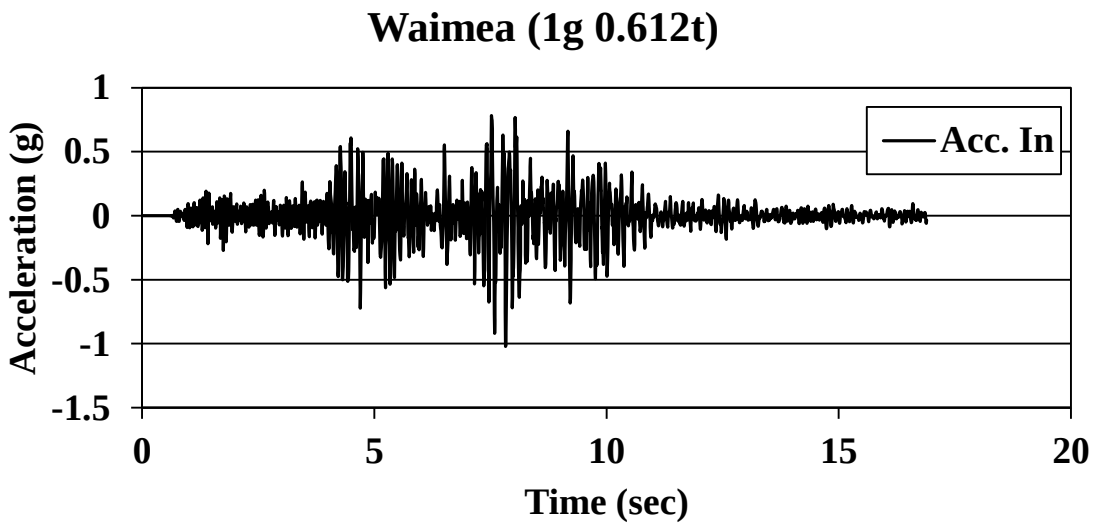

Figure 6.221 Waimea Acceleration Time History Input

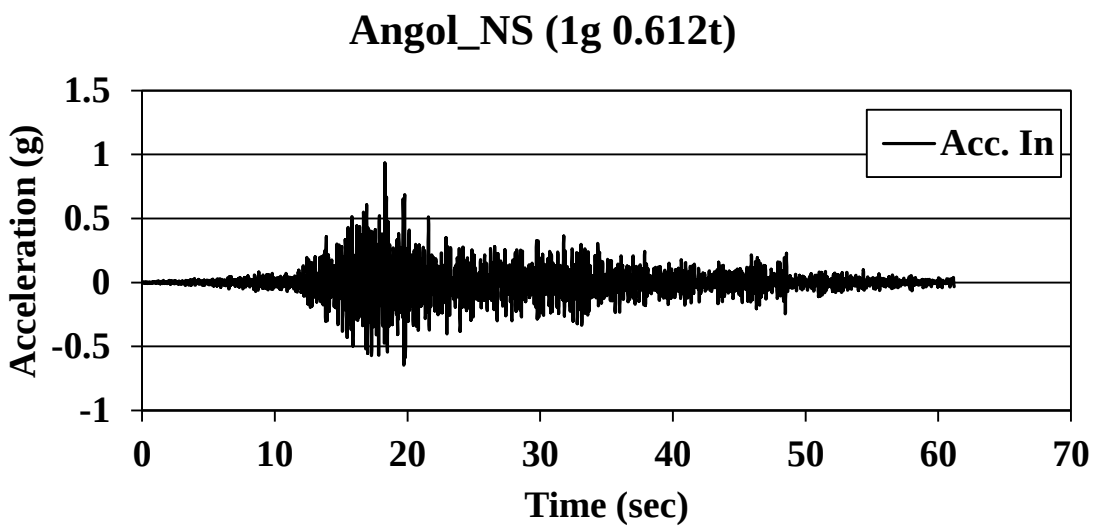

Figure 6.222 Angol Acceleration Time History Input

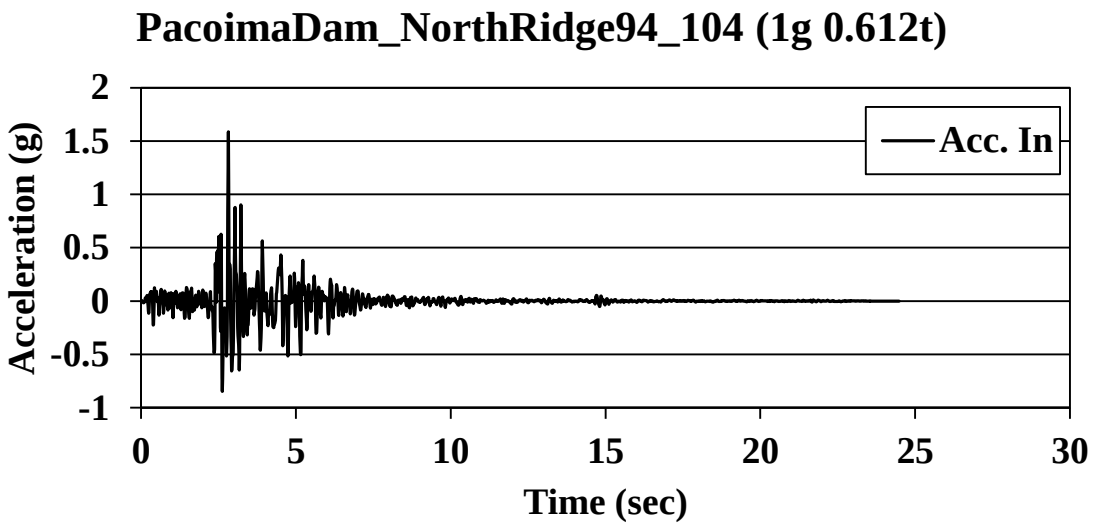

Figure 6.223 Pacoima Dam Acceleration Time History Input

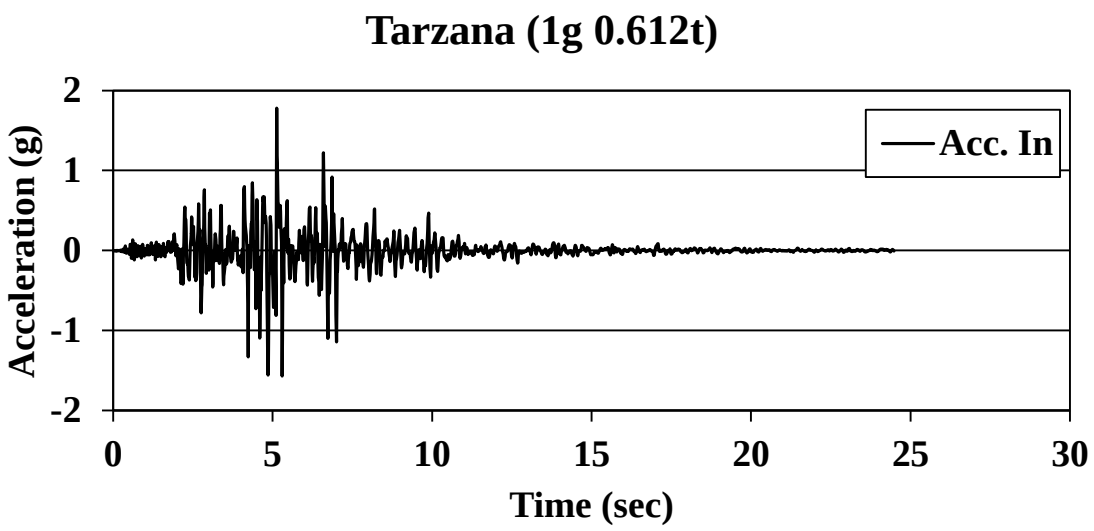

Figure 6.224 Tarzana Acceleration Time History Input

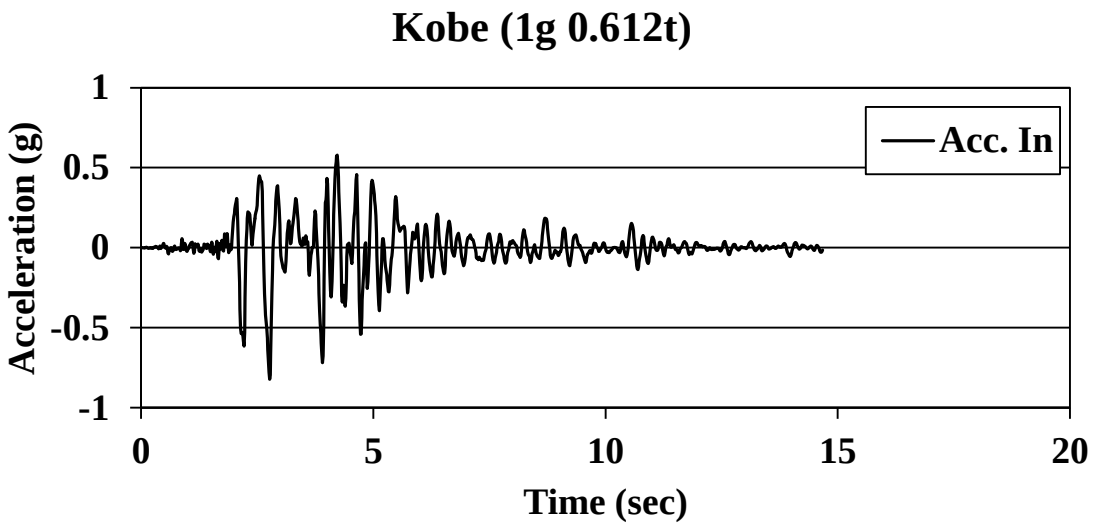

Figure 6.225 Kobe Acceleration Time History Input

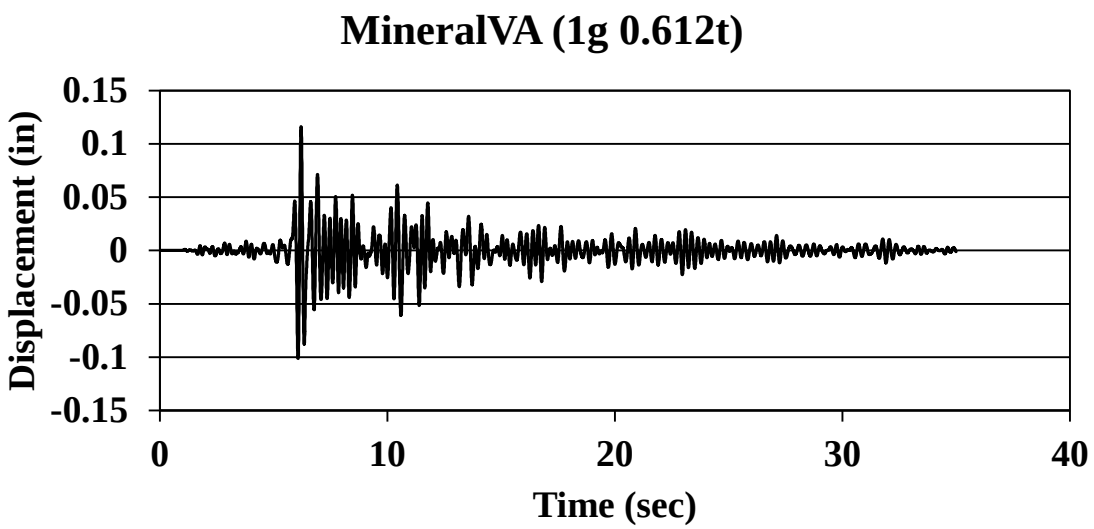

Figure 6.226 Mineral VA Predicted Cap Beam Displacement Response

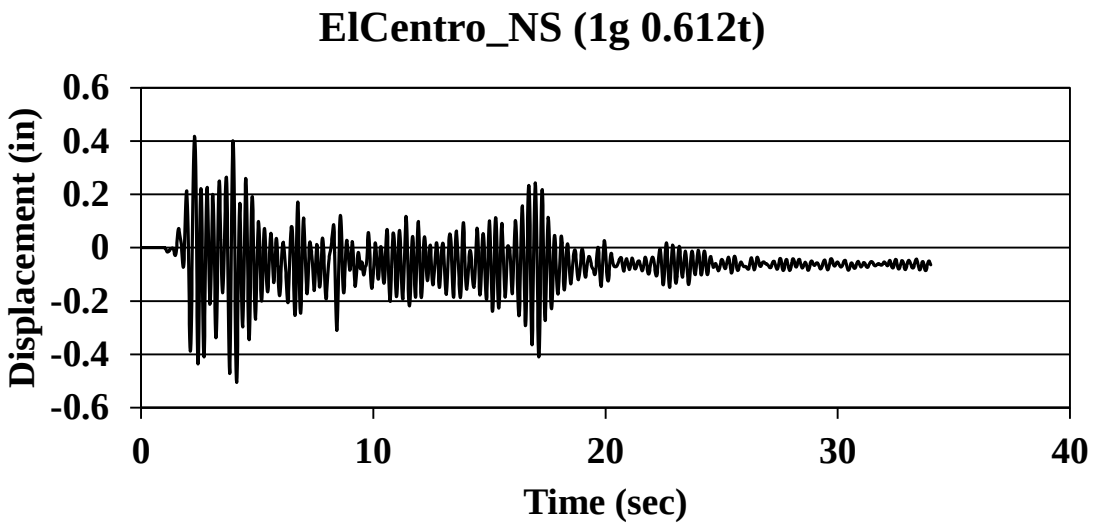

Figure 6.227 El Centro Predicted Cap Beam Displacement Response

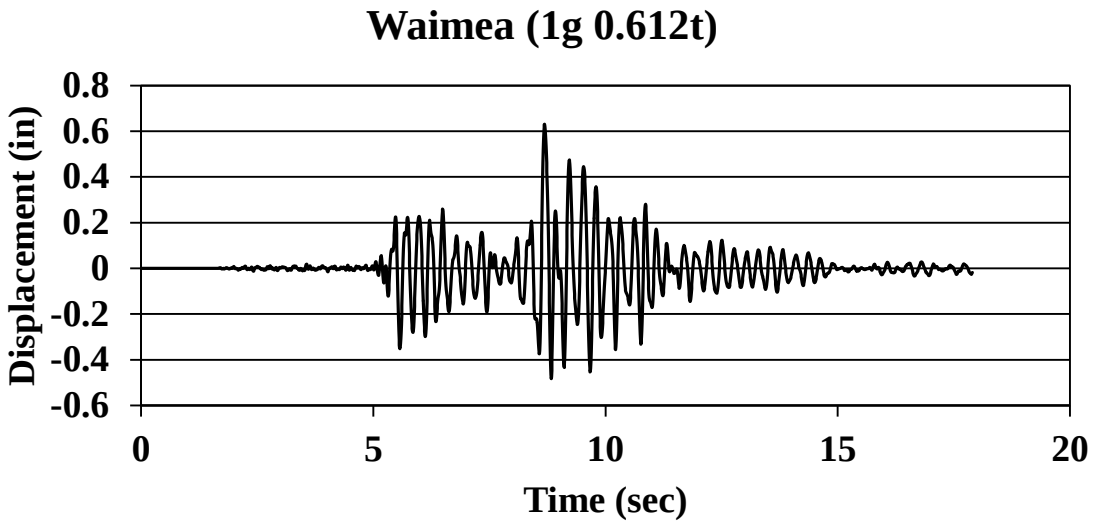

Figure 6.228 Waimea Predicted Cap Beam Displacement Response

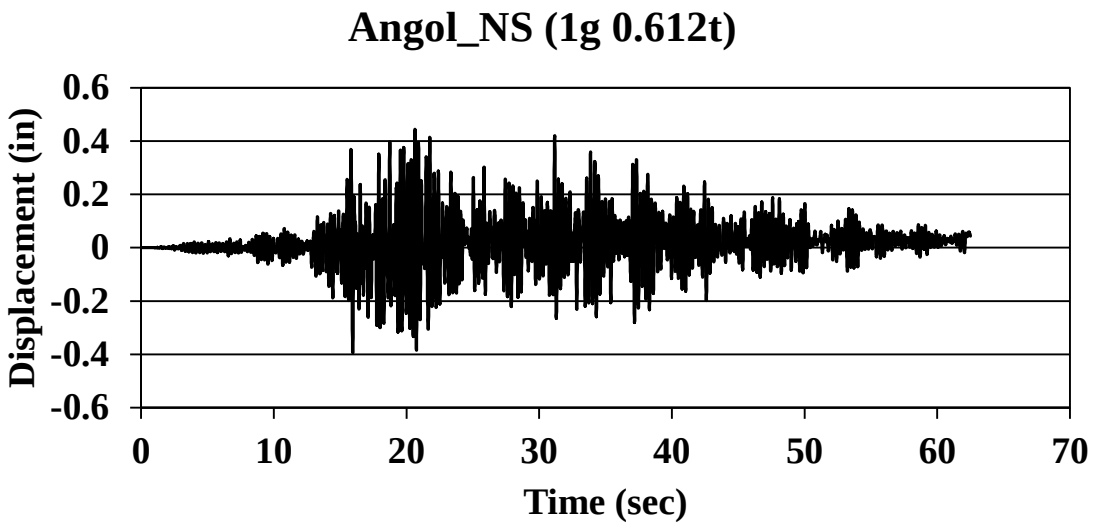

Figure 6.229 Angol Predicted Cap Beam Displacement Response

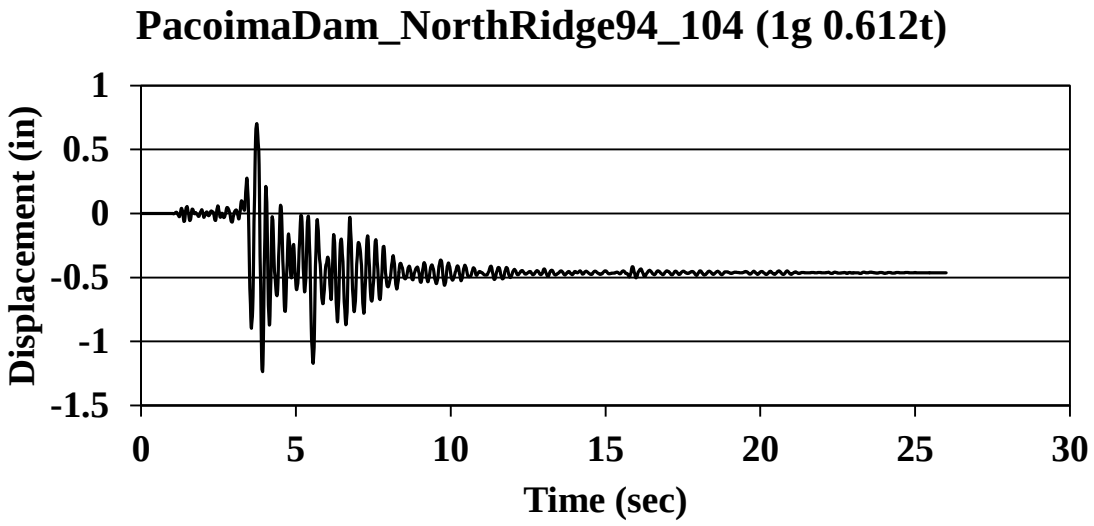

Figure 6.230 Pacoima Dam Predicted Displacement Time History

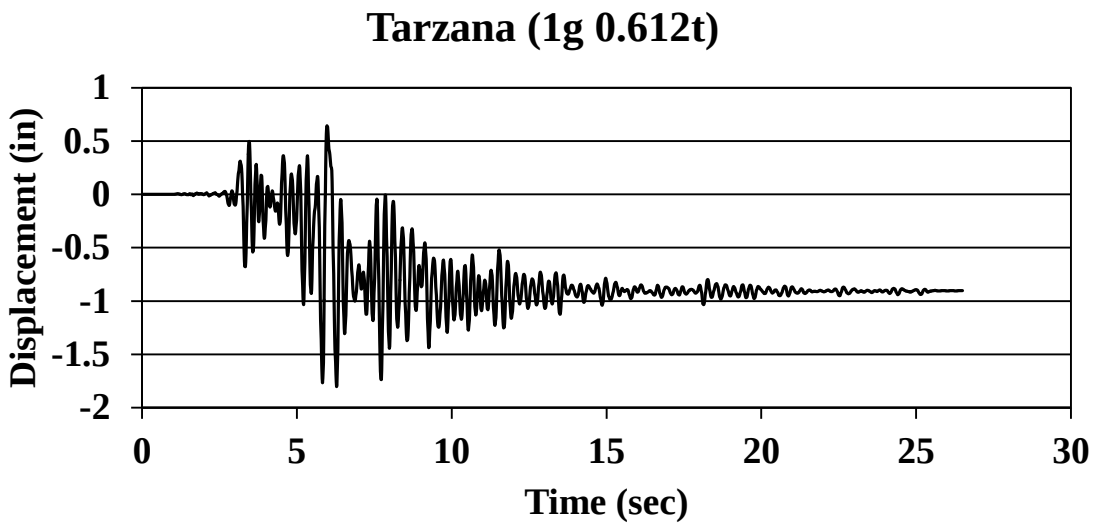

Figure 6.231 Tarzana Predicted Cap Beam Displacement Response

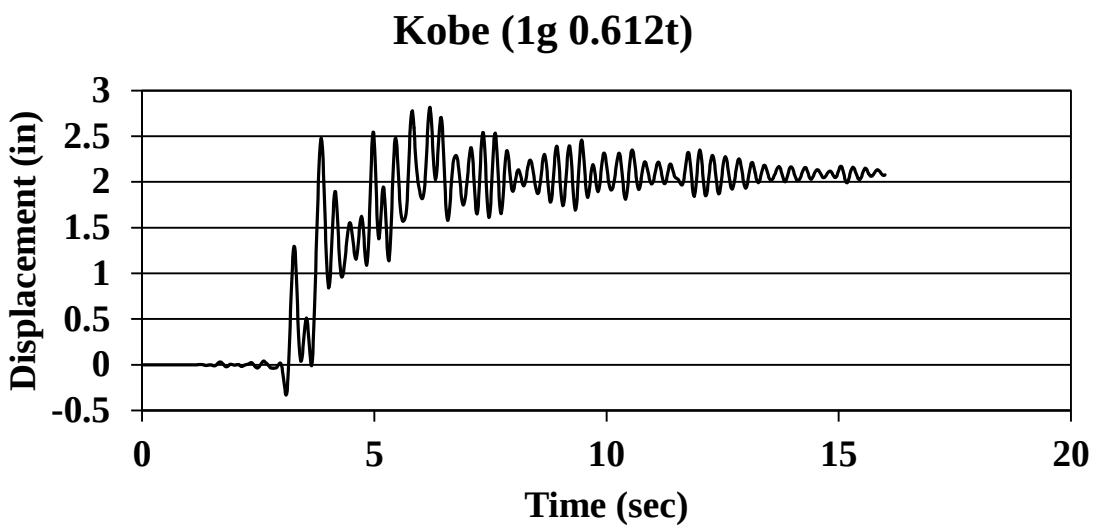

Figure 6.232 Kobe Predicted Cap Beam Displacement Response

Considering the experimental results of the large scale prototype test (phase 2 test 6), the scaled pier was expected to withstand a displacement ductility demand of 2 to 3 prior to significant local buckling occurring in the pile elements leading to system strength loss.

However, it should be noted that this prediction was based an experimental evaluation with a balanced full reversal three cycle set load history which may be conservative when compared to results of shake table testing. Consequently, it was anticipated that the 7 selected time histories, applied in increasing order of predicted ductility demand, would be capable of producing considerable local buckling in the critical region below the grouted shear stud connection. It was also anticipated that the Kobe record with a predicted ductility demand of 3.29 may be unnecessary.

6.6.4 Experimental Shake Table Testing Details

As has been noted, tuning of the shake table control system was based on conventional PID signal tuning to optimize control of the 3 stage servo valve used to operate the shake table hydraulic actuator. Prior to constructing the test specimen on the table, the suite of baseline corrected displacement records selected for the first shake table test, shown in Figure 6.233 through Figure 6.239, were conducted on an empty table and on the table with a 7.8 kip mass block to represent a reasonable level of base shear demand. As the displacement histories were conducted, table displacement data was recorded from the internal LVDT of the actuator as well as table acceleration data from accelerometers attached to the table. Processing of the recorded data allowed for comparison of the input displacement record to the output in effort to verify the table's capability to replicate the record. As shown in the example provided in Figure 6.240, the processed data indicated by observation that the output record was in good agreement with the input displacement history for each of the 7 records considered.

Although this suggested that the table was adequately tuned, it was unclear whether the sensitive nature of the resulting table acceleration history was in adequate agreement with that of the intended input. One potential option to evaluate resulting table accelerations was to compare the intended acceleration time histories to the output acceleration time histories

recorded by the accelerometers. However, by simple observation it was unclear whether the acceleration time histories were adequately replicated due to the high frequency content contained in typical accelerograms. As a result, the decision was made to generate and compare acceleration response spectrums (ARS) and displacement response spectrums (DRS) from both the input and output acceleration histories to evaluate the response characteristics of each. As shown in the examples provided in Figure 6.241 and Figure 6.242, it was found that for each record considered both the ARS and DRS matched well through the moderate period range prior to some separation beyond 2 – 2.5 seconds. It is possible that separation in the higher period ranges was due to incapability of the accelerometers used to capture the lower frequency content of the table that would tend to more significantly affect the response of higher period structures. Regardless, the scaled model specimen was expected to behave in the effective period range of 0.33 seconds to 0.75 seconds from the elastic range of response to a ductility 4 displacement level. Within this range, all records showed good agreement between the intended and output ARS and DRS. Although only examples of this comparison method have been provided here, the comparisons for each record conducted in both actual shake table tests are provided in the appendix of this document.

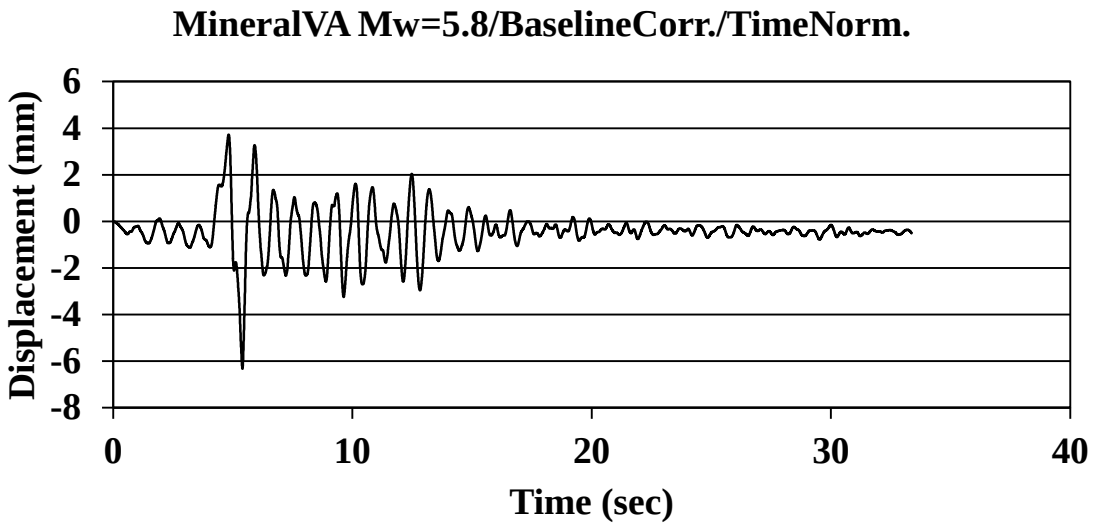

Figure 6.233 Mineral VA Input Displacement Time History

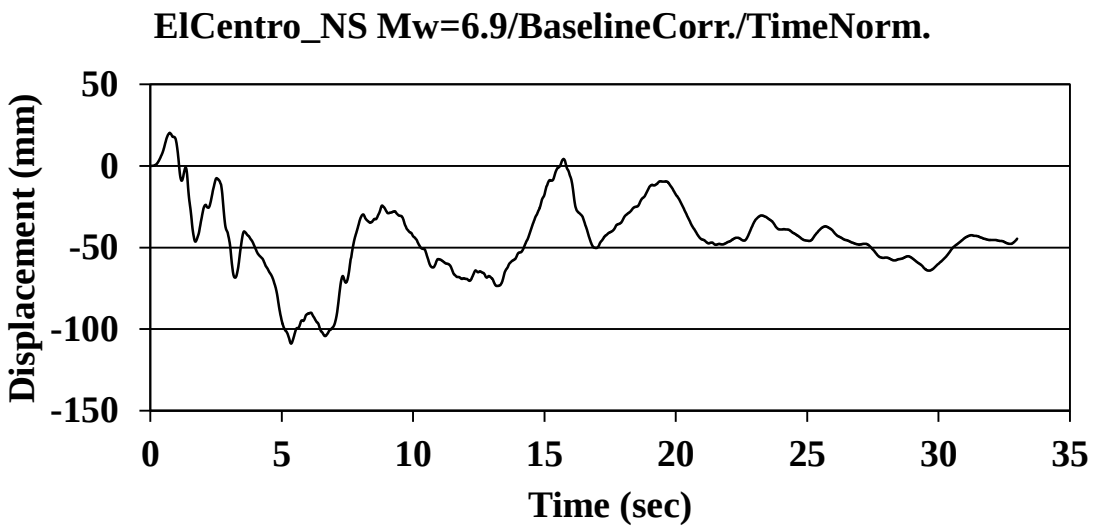

Figure 6.234 El Centro Input Displacement Time History

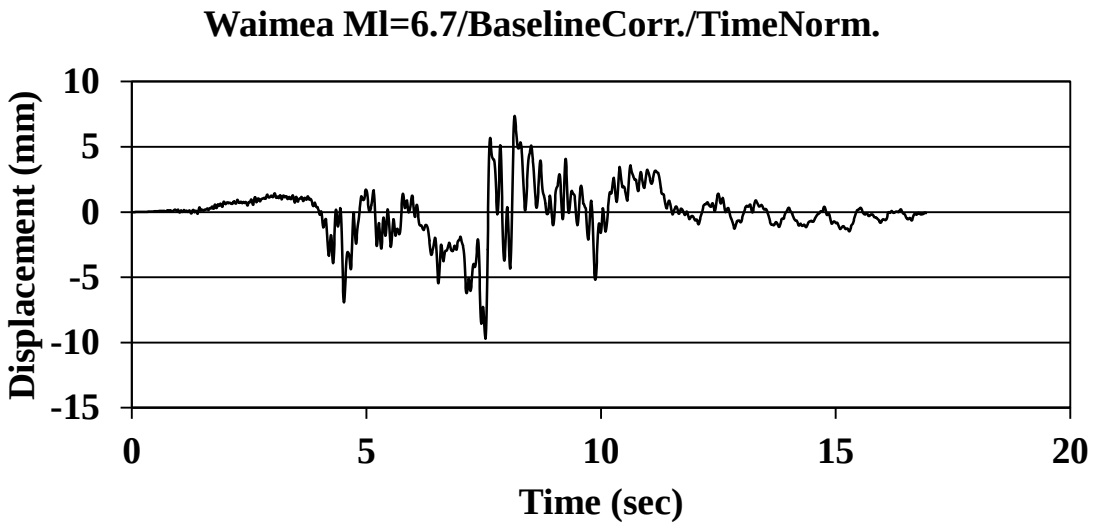

Figure 6.235 Angol Input Displacement Time History

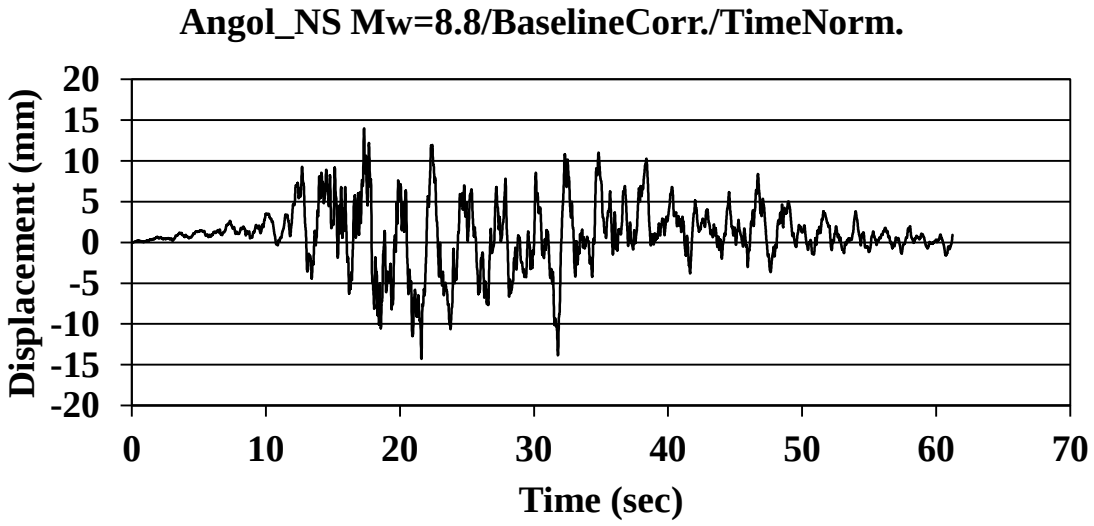

Figure 6.236 Angol Input Displacement Time History

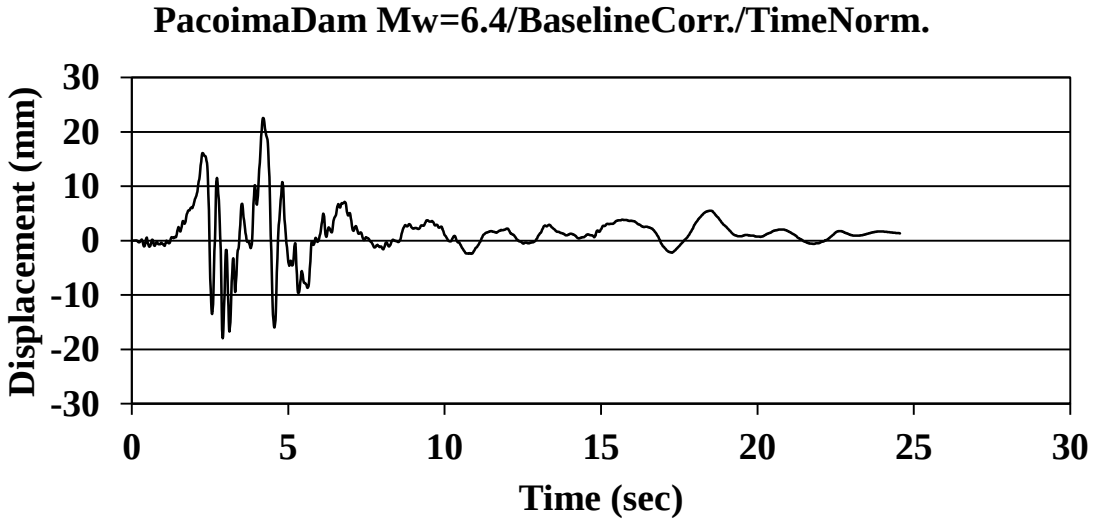

Figure 6.237 Pacoima Dam Input Displacement Time History

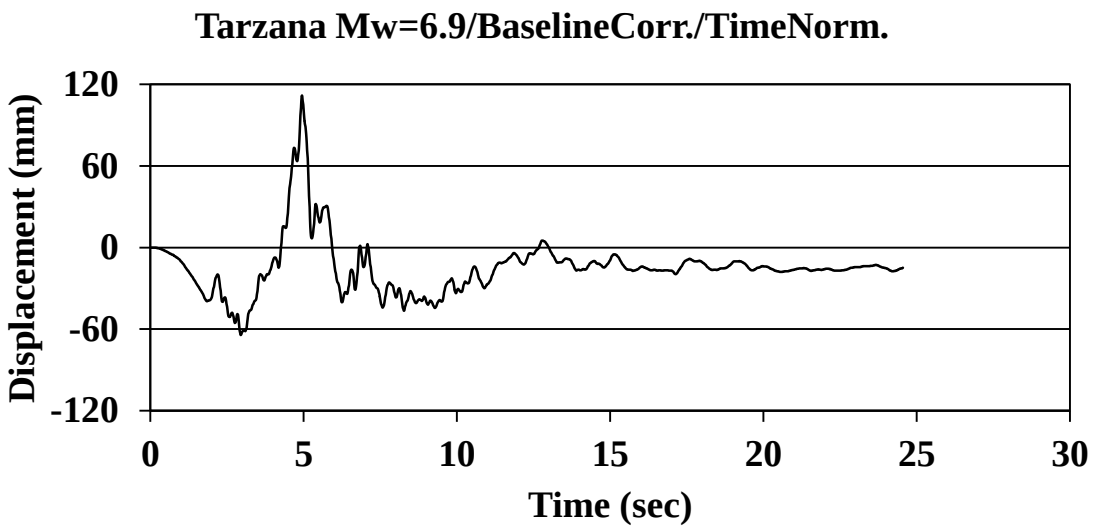

Figure 6.238 Tarzana Input Displacement Time History

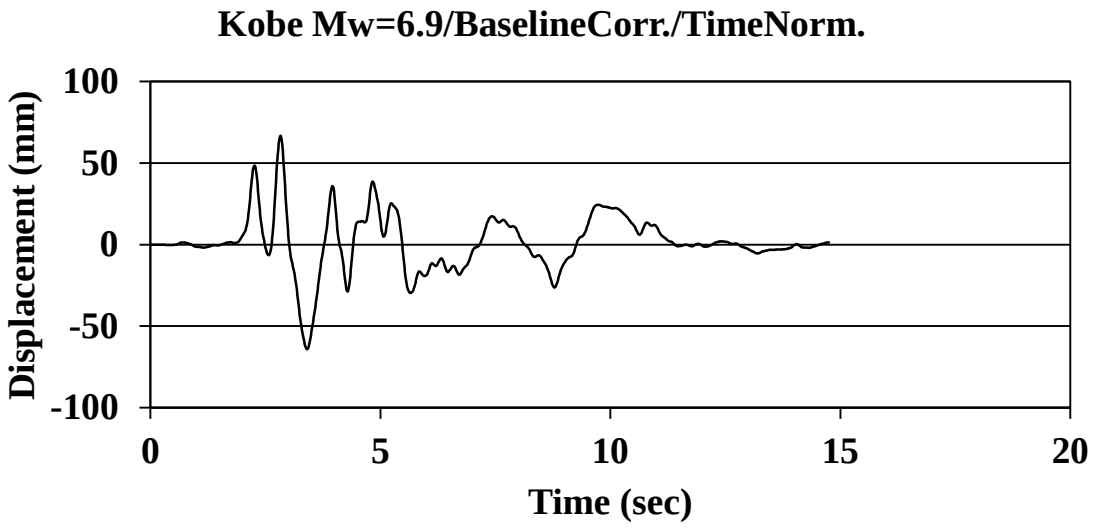

Figure 6.239 Kobe Input Displacement Time History

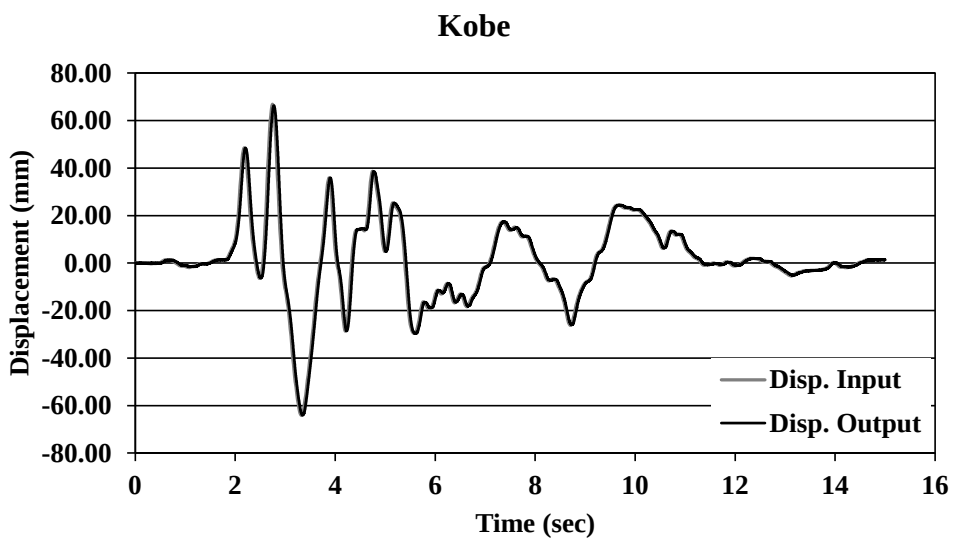

Figure 6.240 Example Displacement History Input / Output Comparison

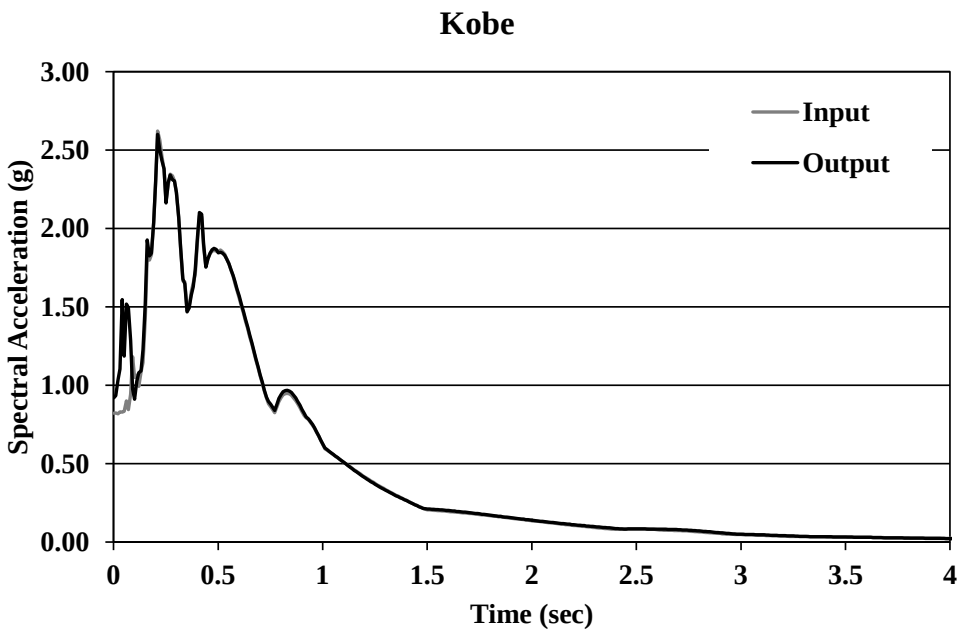

Figure 6.241 Example ARS Input / Output Comparison (ξ=5%)

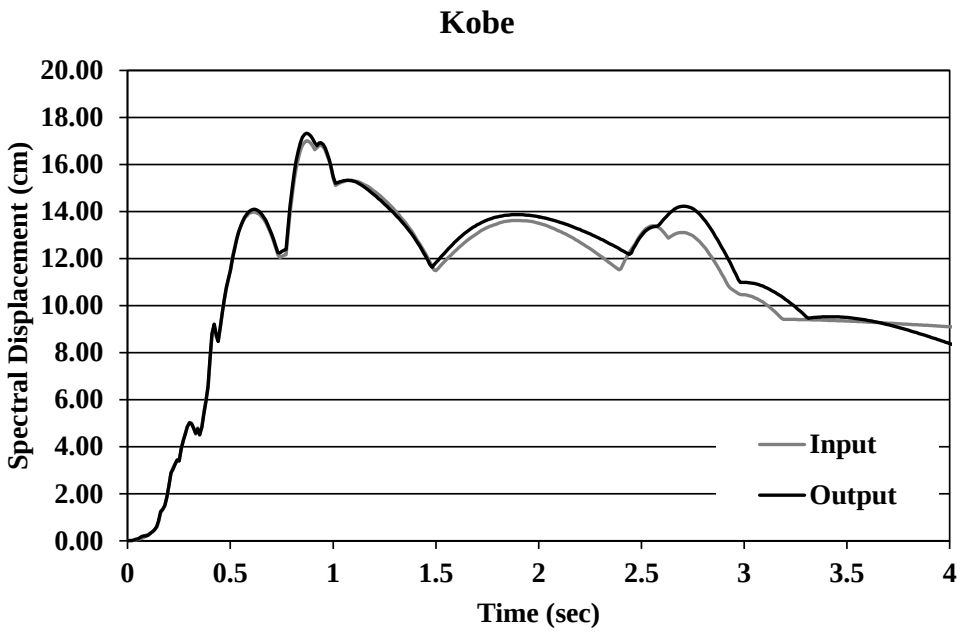

Figure 6.242 Example DRS Input / Output Comparison (ξ=5%)

As was the case with the large scale quasi – static testing conducted in this research project, both traditional laboratory instrumentation and the Optotrak system were used in the scaled shake table test. As shown in Figure 6.243 through Figure 6.245, accelerometers were placed on the shake table and at various locations on the mass block, string potentiometers were placed on the table and cap beam to measure total and relative displacements, and strain gauges were placed both in both critical and assumed non – critical locations on the pier system. The Optotrak marker instrumentation focused on one joint region both in the capacity protected pipe stub section and the critical pipe pile region. A lower number of LED markers were used in the dynamic shake table test than in the large scale quasi – static test due to the Optotrak's recording restrictions. The maximum recording frequency of the system is directly proportional to number of markers used in the experiment, resulting in a limited availability of markers to record at the desired 100 Hz frequency. Markers were also placed on the table to monitor table displacements.

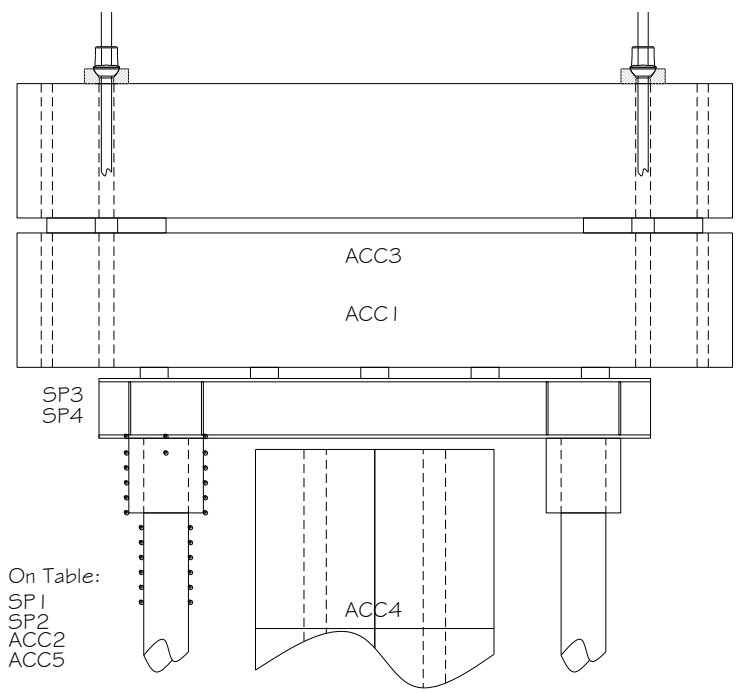

Figure 6.243 Phase 2 Tests 8 and 9 Instrumentation Layout

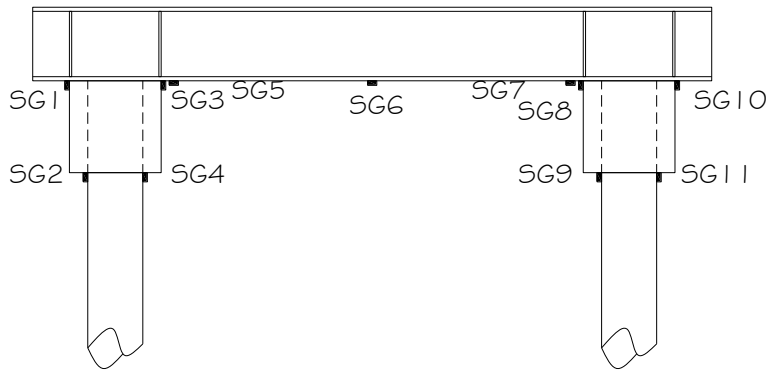

Figure 6.244 Phase 2 Test 8 (Table Test 1) Strain Gauge Layout

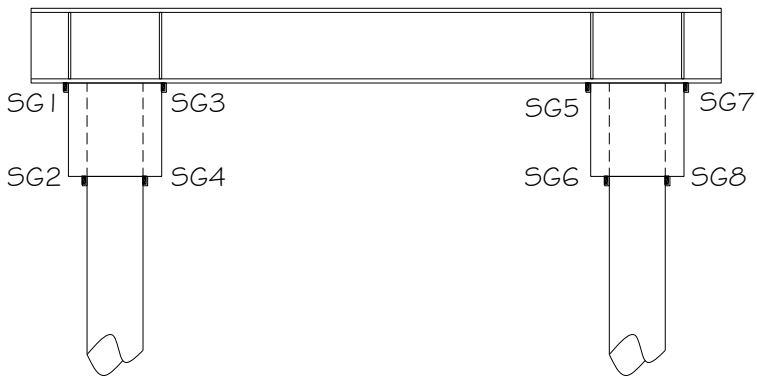

Figure 6.245 Phase 2 Test 9 (Table Test 9) Strain Gauge Layout

For each record considered in both the first and second shake table tests, the force – displacement response of the test piers was developed by post processing of the recorded test data. Structural displacement was determined using data recorded from Optotrak markers adhered to the cap beam and to the shake table by calculating the difference between the two markers. The corresponding system force at a given time during a record was determined by multiplying the recorded acceleration at the center of mass of the mass block system (ACC1) by the known attributable mass (22.5 kips/g). However as shown in Eq.(6.12), the basic equation of motion due to base excitation includes not only terms related to system force due to structural displacement (ku) and mass force due to total acceleration ($m\ddot{u}_t$), but also due damping forces ($c\dot{u}$) which arise from system velocity. Consequently, it should be

recognized the force – displacement responses generated from this method of data analysis also contain some level of damping forces which cannot be expressly calculated without known structural velocity. However, it should also be recognized that being a steel structure the associated material based viscous damping levels were likely small, in the range of 2 – 3%. In addition, it should also be noted that at the displacement response peaks, system velocity theoretically approaches zero as would the contribution of damping forces to the response of the system.

$$m\ddot{u}_t + c\dot{u} + ku = 0 \tag{6.12}$$

6.6.5 Shake Table Test 1 (Phase 2 Test 8) – Discussion and Results

The first experimental shake table record that was conducted was the Mineral VA time history with a PGA of 0.135 g. As shown in Figure 6.246 and Figure 6.247 the pier experienced multiple reversals loading exhibiting a relatively balanced displacement history as was predicted by NLTHA. The specimen exhibited a maximum displacement demand of 0.33 in. in both the positive and negative directions which corresponded to a maximum ductility demand of 0.40. This ductility demand was larger than that predicted by the NLTHA, 0.13, which may have been due to inaccuracy of the analysis or additional sources of displacement that were not considered in the analysis such as tolerance of the pinned base system and flexibility of the shake table. Should the discrepancy be due in part to additional sources of displacement, it is likely that the effect was most significant with the Mineral VA record which was the least demanding to the structure.

Regardless of the discrepancy in displacement ductility demand, the response was found to be in the elastic range of loading as shown in Figure 6.248. As is shown, the essentially elastic response resulted in no notable residual displacement and was found to be slightly less stiff than predicted by the analytical push – over analysis. Further, as shown in Figure 6.249,

the behavior of the connection region was shown to act as anticipated forcing the largest strain demands below the capacity protected region of the connection. However, no damage in the form of pile wall local buckling, material fracture, or grout loss was experienced during this record. As a result, the decision was made to continue the test with more demanding records.

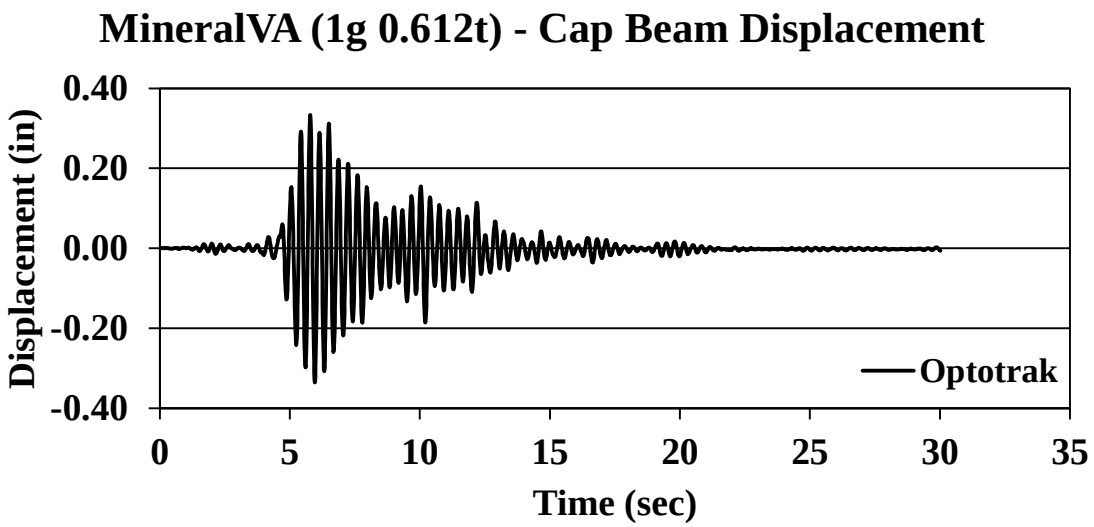

Figure 6.246 Shake Table Test 1 – Mineral VA Displacement History

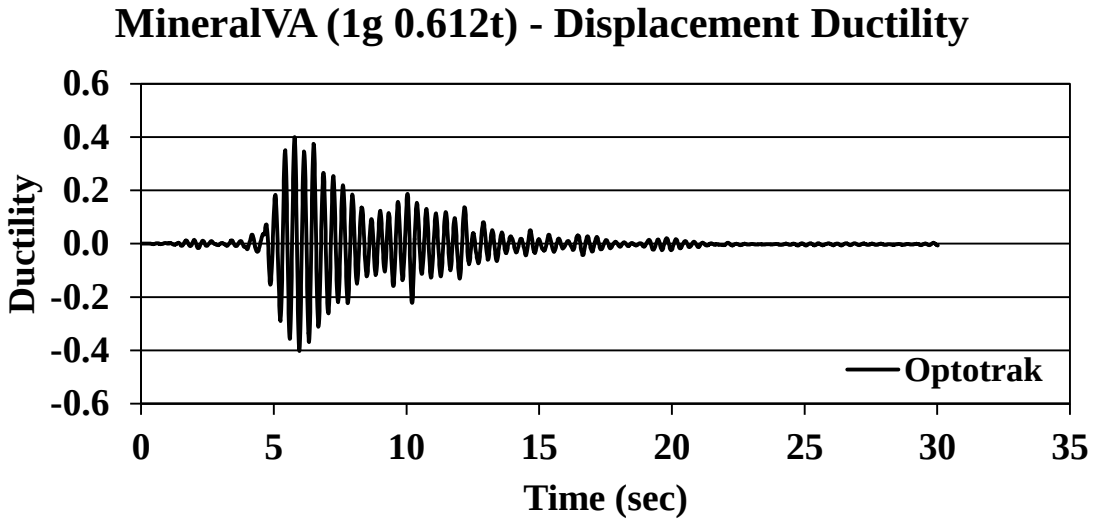

Figure 6.247 Shake Table Test 1 – Mineral VA Displacement Ductility History

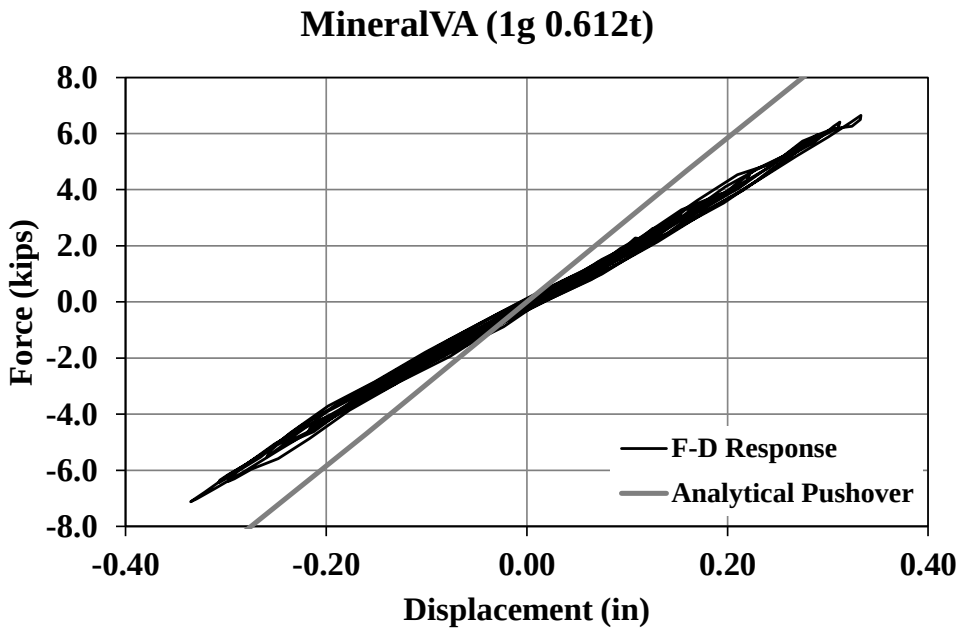

Figure 6.248 Shake Table Test 1 – Mineral VA Force – Displacement Response

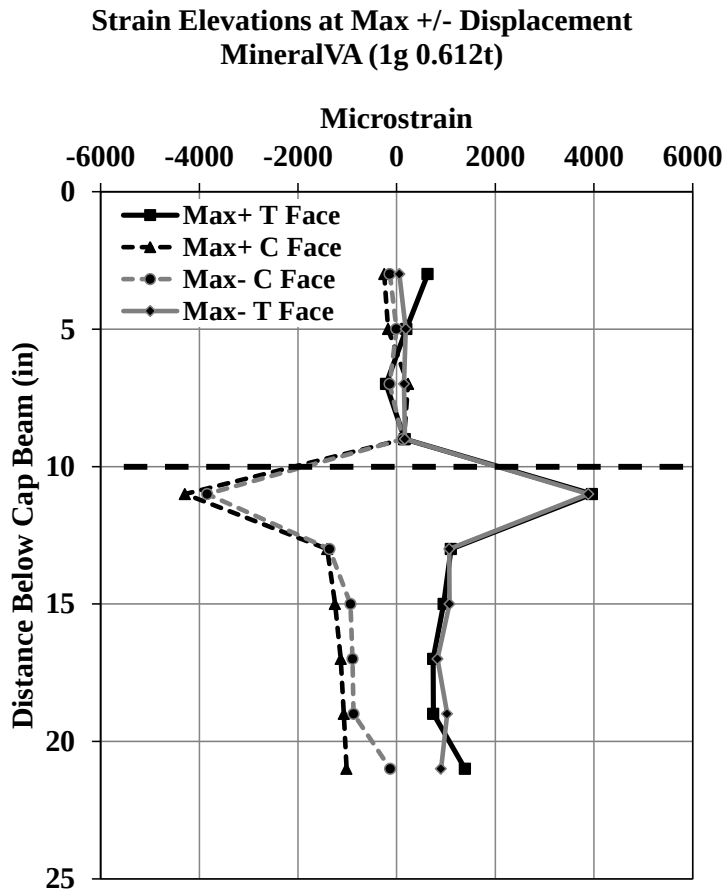

Figure 6.249 Shake Table Test 1 – Mineral VA Strain Elevations at Peak Disp.

The second record that was conducted was the El Centro time history with a PGA of 0.359 g. As shown in Figure 6.250 and Figure 6.251, the pier again experienced multiple reversals of loading exhibiting a relatively balanced displacement history as was predicted by NLTHA. The specimen experienced a maximum displacement demand of positive 1.03 in. and negative 0.69 in. corresponding to a maximum displacement ductility demand of 1.24. This ductility demand was again larger than that predicted by the NLTHA which was 0.57. As noted for the Mineral VA record, this discrepancy may have been due to inaccuracy of the analysis or additional sources of displacement that were not considered in the analysis.

The force – displacement response resulting from the El Centro record was shown to be relatively linear although experiencing slight inelasticity as would be expected for the displacement ductility demand of 1.24, as shown in Figure 6.252. This slight inelasticity resulted in a residual displacement of positive 0.125 in. at the completion of the record. The behavior of the connection region was again shown to perform as anticipated forcing the largest strain demands below the capacity protected region of the connection. As shown in Figure 6.253, approximately +/- 14000 με was experienced in the critical region immediately below the grouted shear stud connection. However, no damage in the form of pile wall local buckling, material fracture, or grout loss was experienced during this record suggesting larger demands could be placed on the system.

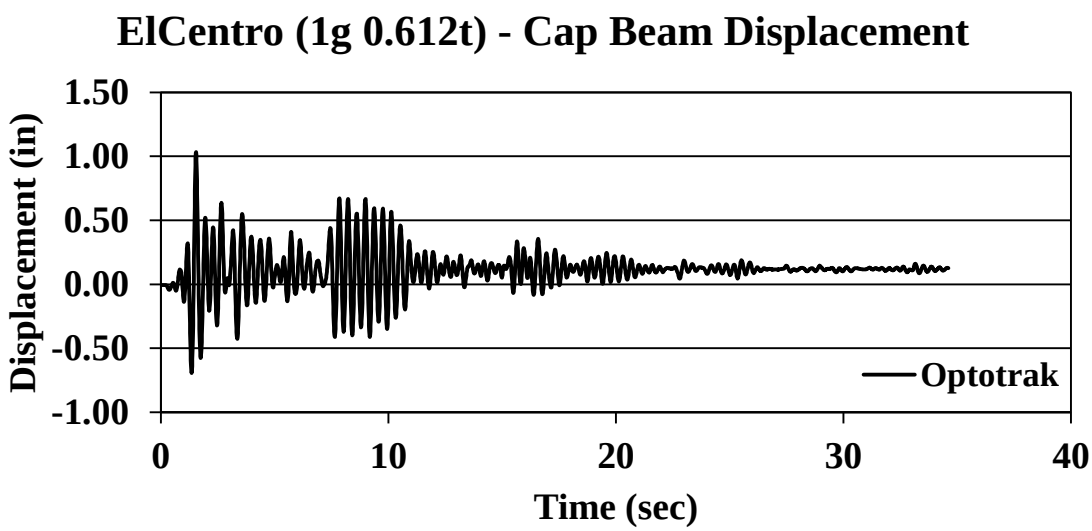

Figure 6.250 Shake Table Test 1 – El Centro Displacement History

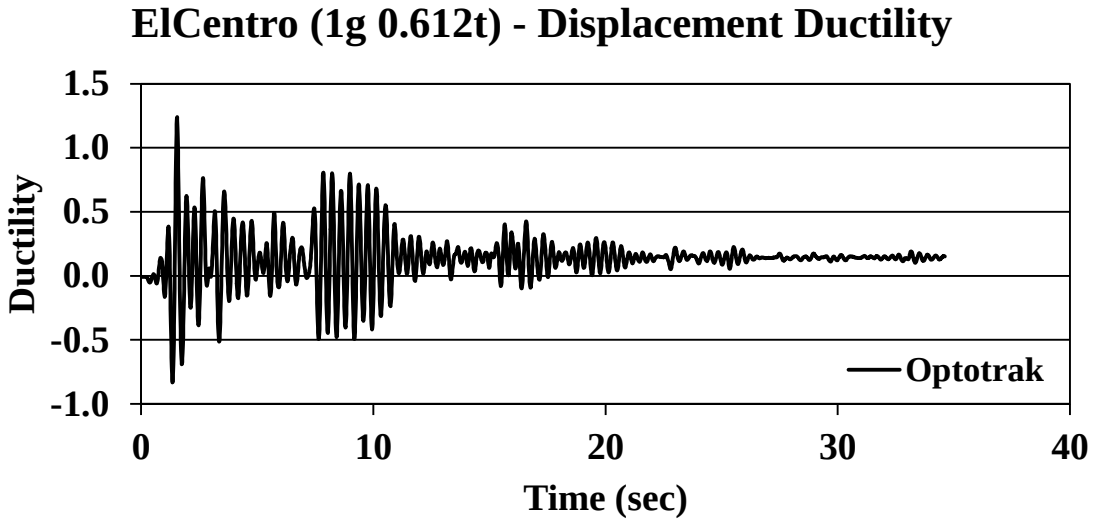

Figure 6.251 Shake Table Test 1 – El Centro Displacement Ductility History

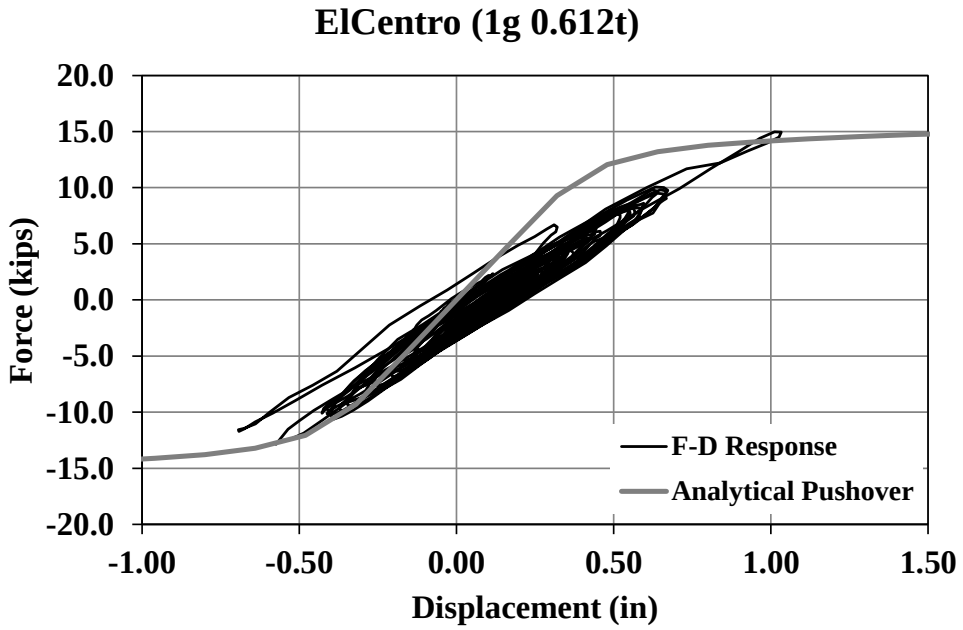

Figure 6.252 Shake Table Test 1 – El Centro Force – Displacement Response

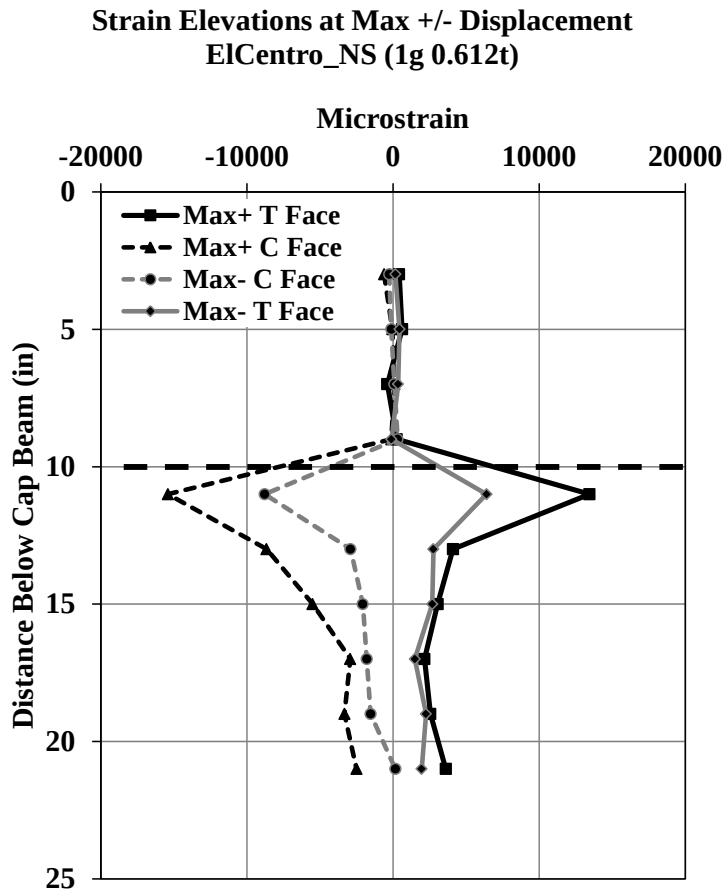

Figure 6.253 Shake Table Test 1 – El Centro Strain Elevations at Peak Displacements

The third record that was conducted was the Waimea time history with a PGA of 1.057 g and a predicted displacement ductility demand of 0.71 from NLTHA. As shown in Figure 6.254 and Figure 6.255, the pier again experienced multiple reversals of loading that were relatively balanced, although the duration of shaking was shorter than with the two prior records. The specimen exhibited a maximum displacement demand of positive 0.838 in. and negative 0.595 in. corresponding to a maximum ductility demand of 1.01. Although this ductility demand was again higher than predicted, the pier was subjected to an initial residual displacement of approximately 0.125 in. as has been noted. Considering the initial

displacement and the predicted ductility demand of 0.71, it appeared the NLTHA provided a better peak displacement demand prediction than with the prior two records.

The force – displacement response resulting from the Waimea record was shown to be essentially elastic with the pier oscillating around the approximate initial displacement of 0.125 in., as shown in Figure 6.256. Consequently, at the conclusion of the record only a minor increase to 0.140 in. of residual displacement was experienced. As was the case with the Mineral VA record, the essentially elastic response exhibited stiffness less than predicted the analytical push – over analysis. As shown in Figure 6.257, strain demands of approximately +/- 13000 με were experienced in the critical region immediately below the connection region which was similar to that experienced during the El Centro record. It is important to note, at this point in the testing series there was still no notable damage in the form of pile wall local buckling, material fracture, or grout loss.

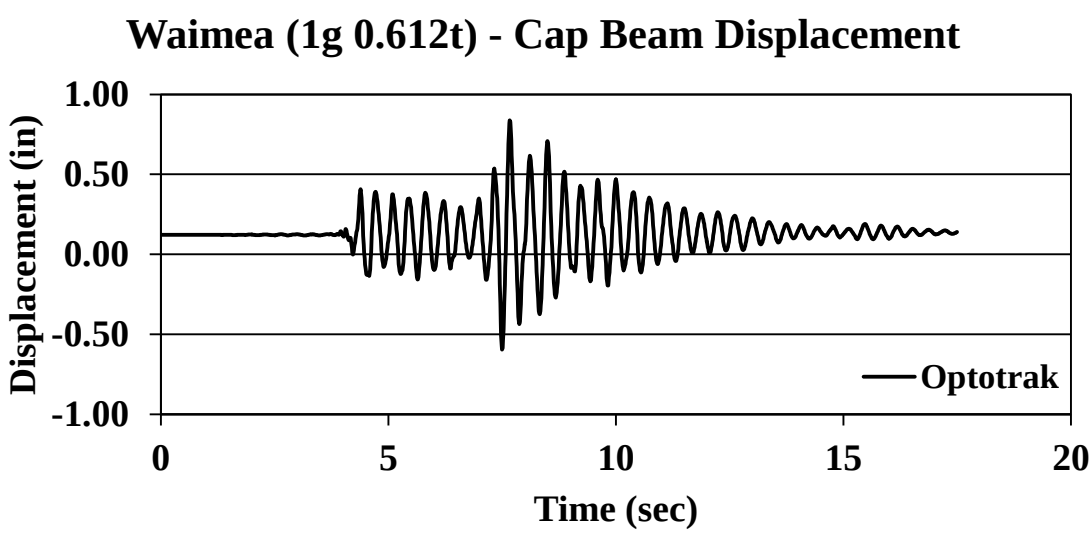

Figure 6.254 Shake Table Test 1 – Waimea Displacement History

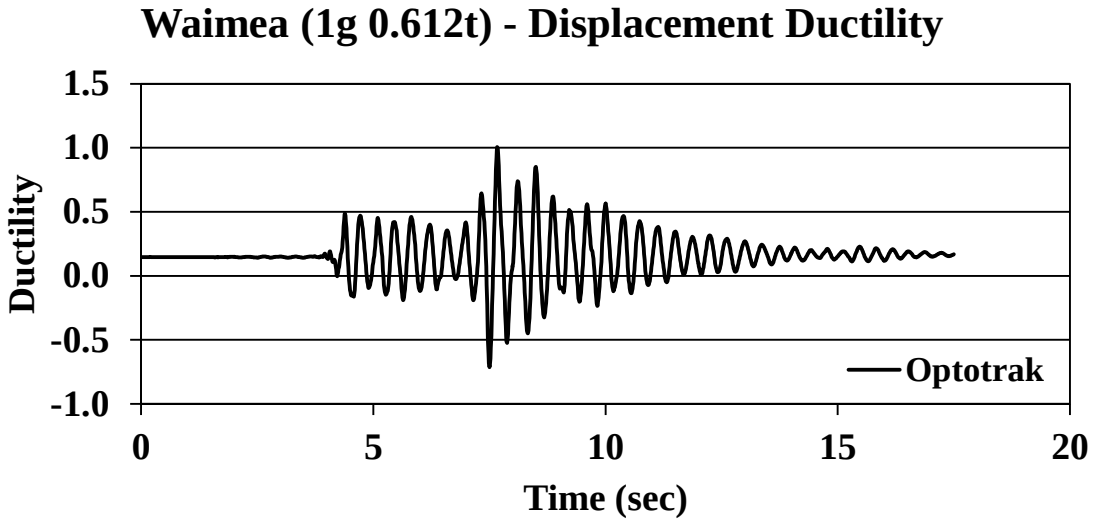

Figure 6.255 Shake Table Test 1 – Waimea Displacement Ductility History

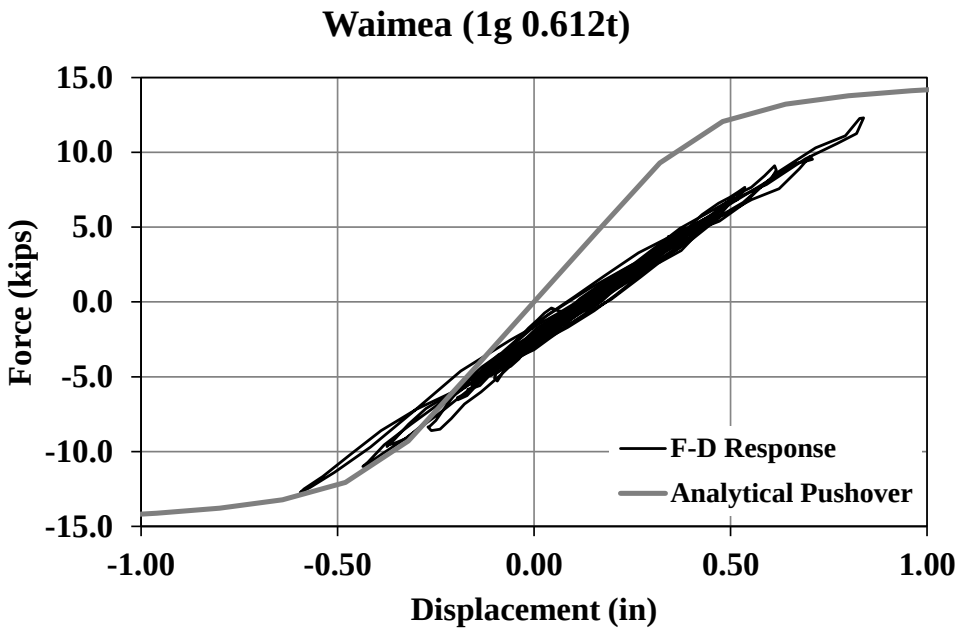

Figure 6.256 Shake Table Test 1 – Waimea Force – Displacement Response

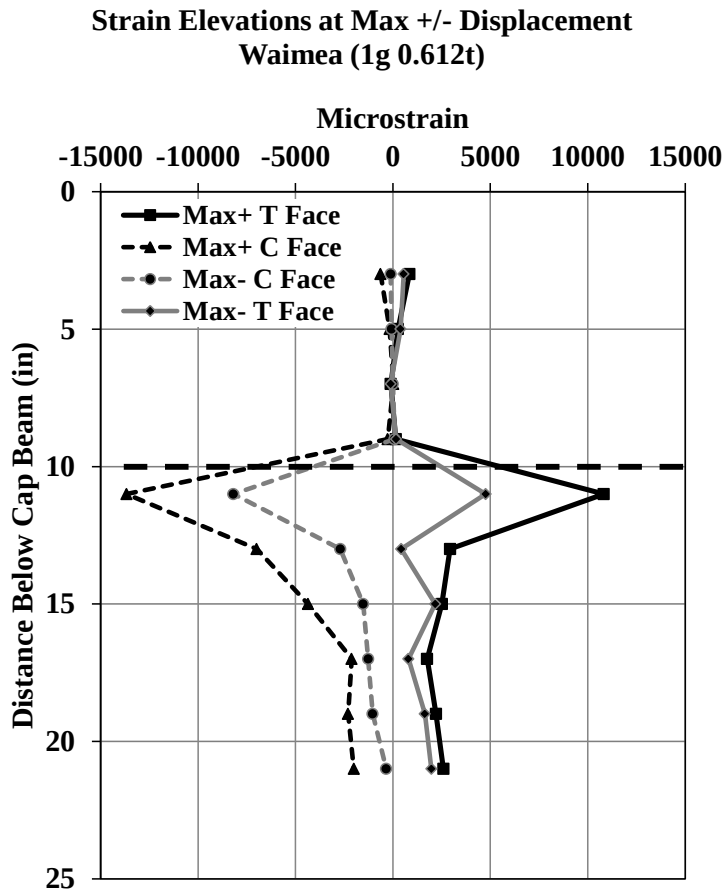

Figure 6.257 Shake Table Test 1 – Waimea Strain Elevations at Peak Displacements

The fourth record that was conducted was the Angol time history with a PGA of 0.935 g and a predicted displacement ductility demand of 0.51. Of the entire suite of records to be conducted, this record was the longest with the largest number of predicted reversals more representative of a subduction type event. As shown in Figure 6.258 and Figure 6.259, the pier experienced more reversals of loading than with any prior record as the pier was subjected to the longest duration of shaking. The displacement history was again relatively balanced suggesting an essentially elastic response. The specimen exhibited a maximum displacement demand of positive 0.814 in. and negative 0.572 in. corresponding to a maximum ductility demand of 0.98 which was similar to that of the Waimea record

regardless of the differences in overall response characteristics. Again the ductility demand was higher than predicted, but the pier was subjected to an initial residual displacement of approximately 0.140 in. which contributed to the experimental ductility demand value.

The force – displacement response resulting from the Angol record was found to be relatively linear with the pier oscillating around the approximate initial displacement of 0.140 in., as shown in Figure 6.260. At the conclusion of the record, the residual displacement had been reduced by a small amount to a value of positive 0.115 in. Interestingly, the hysteretic loops shown in the force – displacement response appear to be wider than that of the prior record, Waimea, regardless of the fact that the maximum displacement demands were essentially equal. One potential explanation for this observed characteristic may be the effects of damping forces becoming more significant with the higher number of reversals for the longer record. As has been discussed, the method used to calculate system force, recorded acceleration times known mass, includes damping force components to the overall equation of motion.

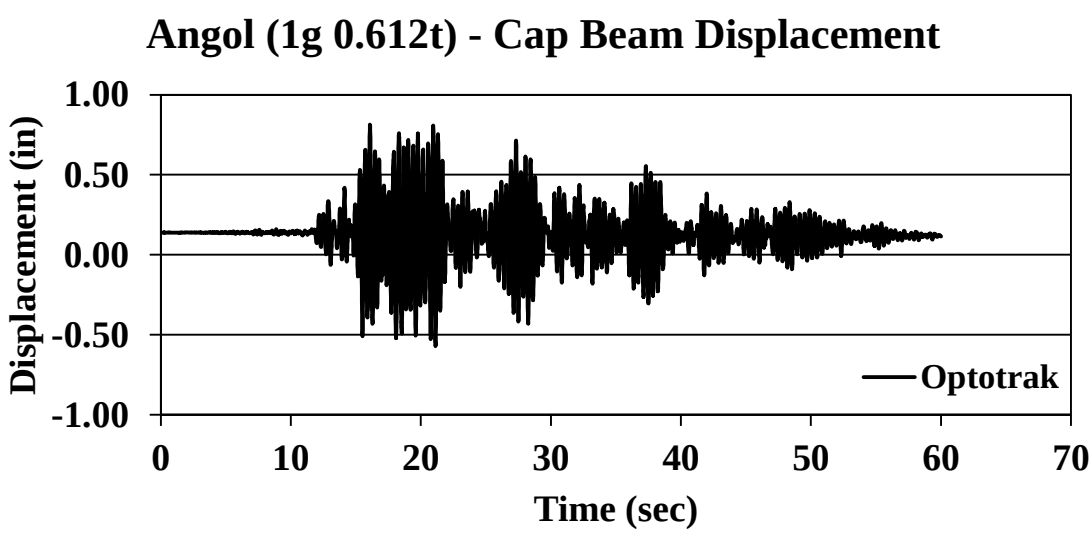

Figure 6.258 Shake Table Test 1 – Angol Displacement History

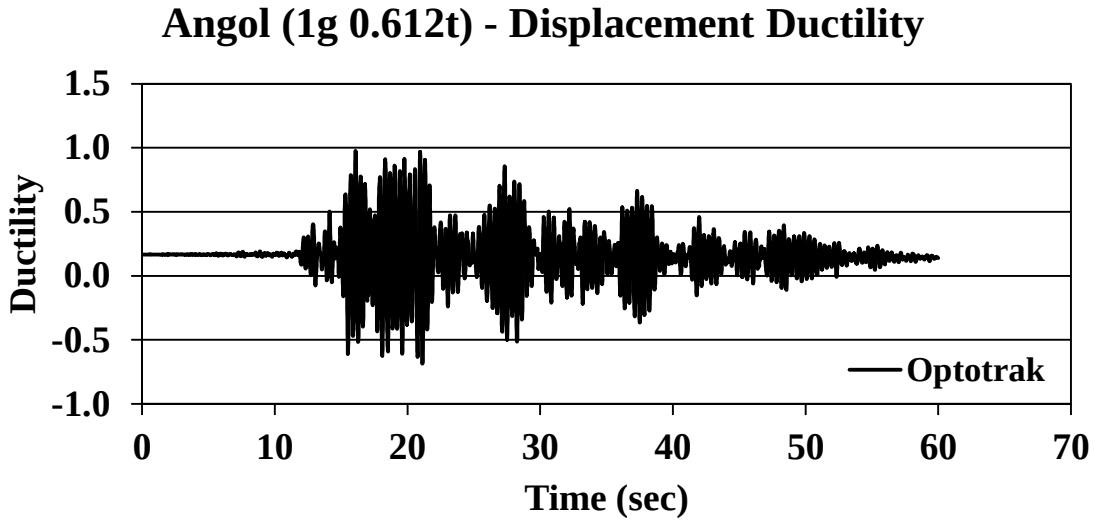

Figure 6.259 Shake Table Test 1 – Angol Displacement Ductility History

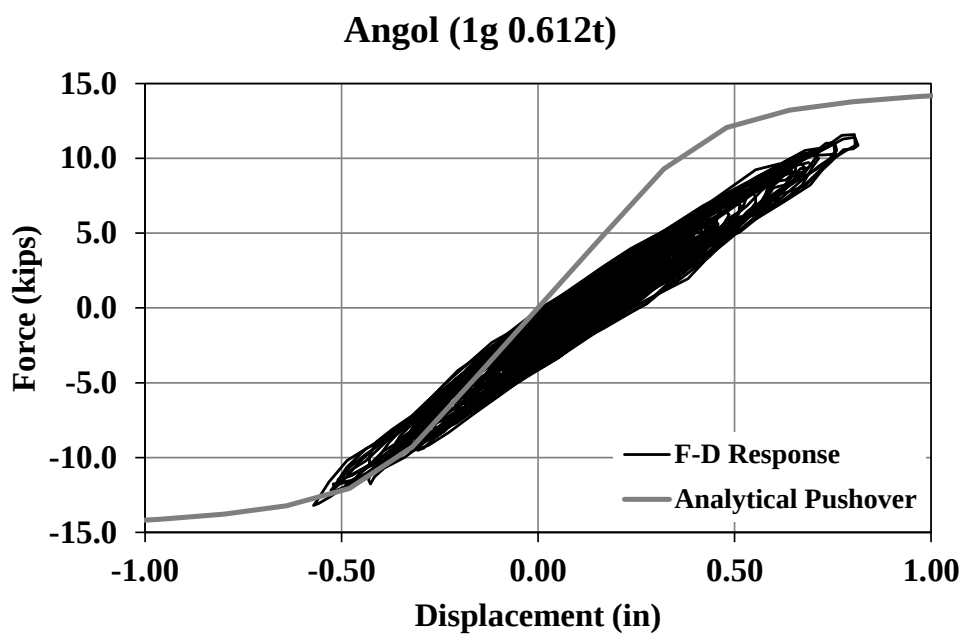

Figure 6.260 Shake Table Test 1 – Angol Force – Displacement Response

As shown in Figure 6.261, strain demands of approximately +10000 με and -13000 με were experienced in the critical region immediately below the connection region which was similar to that experienced during the prior Waimea record. This finding is reasonable given that the displacement demands were also similar. Again, at this point in the testing series there was still no notable damage in the form of pile wall local buckling, material fracture, or grout loss. Hence, more demanding records could be applied to the system.

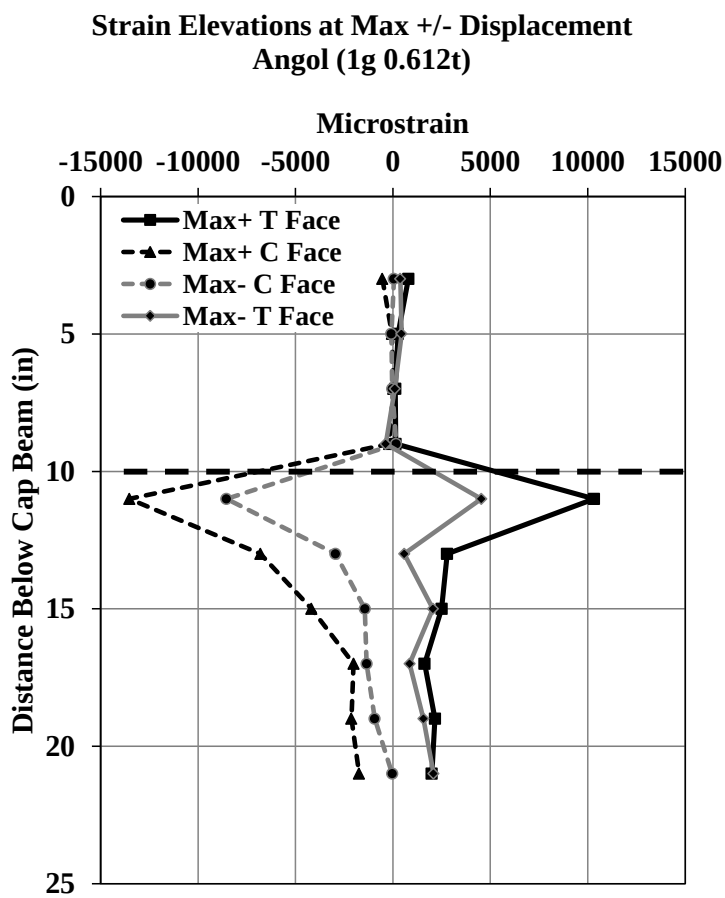

Figure 6.261 Shake Table Test 1 – Angol Strain Elevations at Peak Displacements

The fifth record that was conducted was the Pacoima Dam time history with a PGA of 1.530 g and a predicted displacement ductility demand of 1.46. This record represented a velocity pulse type event and was the first to demand considerable inelastic action from the

test specimen. As shown in Figure 6.262 and Figure 6.263, the pier experienced a shorter duration of shaking with cycles beyond the ductility 1 range in both directions of loading generating a reasonably balanced response. The specimen exhibited a maximum displacement demand of positive 1.61 in. and negative 1.00 in. corresponding to a maximum ductility demand of 1.93. Regardless of the inelastic action experienced, particularly in the positive direction, the residual displacement was increased by only a marginal amount of 0.13 in. to a total of 0.23 in. in the positive direction.

The force – displacement response resulting from the Pacoima Dam record displayed noticeable opening of the hysteretic loops indicative of inelastic action in the system, as shown in Figure 6.264. Beyond the elastic range of response, the force – displacement characteristics of the system were found to be in good agreement with the analytical push – over prediction. As shown, the hysteretic behavior of the actual system appears to show a yield plateau developing near the region predicted by the push – over analysis for the larger cycles of loading experienced during the record.

As shown in Figure 6.265, increased strain demands of approximately +/- 25000 $\mu\varepsilon$ were experienced in the critical region immediately below the capacity protected region of the connection. The strain data did not appear to indicate the onset of local buckling in this region which typically generates an illogical shape in the strain elevation such as compression strain on what should be a tensile extreme fiber. However, questionable regions of potential slight local buckling were visually observed on the south faces (negative direction) of each pile. Although difficult to distinguish, small amounts of pile wall distortion appeared to be developing in the region immediately below the grouted connection. At this point in the testing series, there was still no notable damage in the form of material fracture, grout loss, or system strength loss, only the possible onset of local buckling.

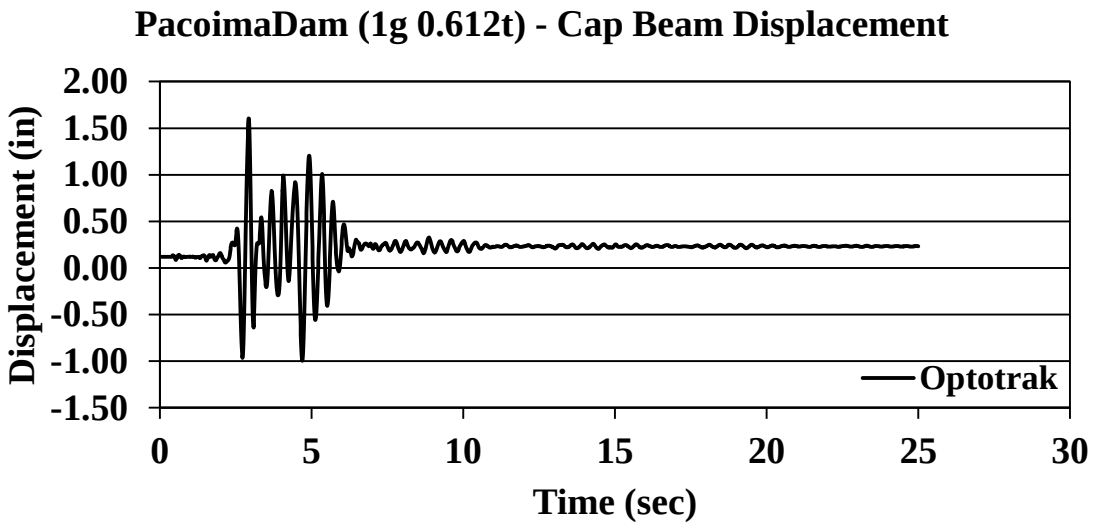

Figure 6.262 Shake Table Test 1 – Pacoima Dam Displacement History

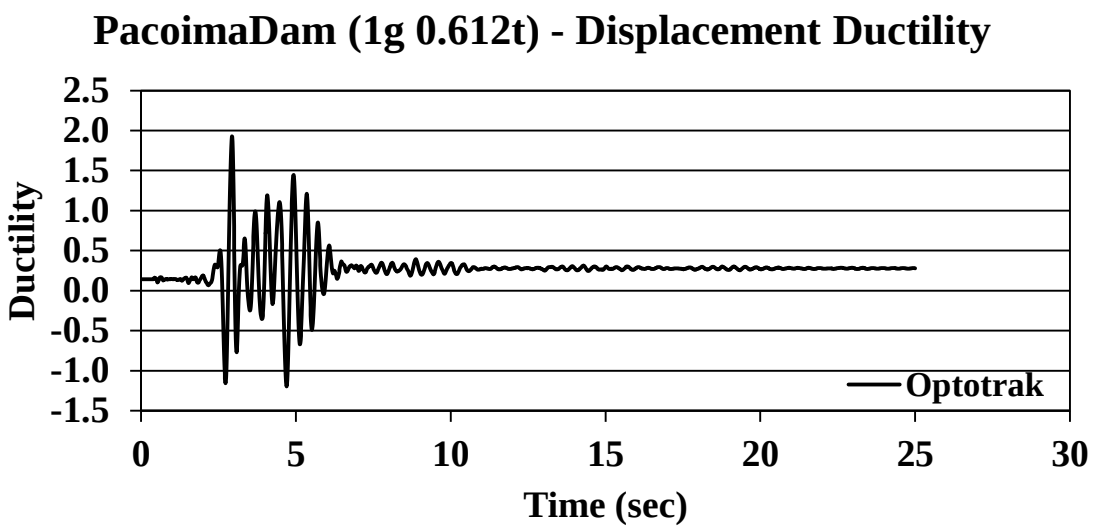

Figure 6.263 Shake Table Test 1 – Pacoima Dam Displacement Ductility History

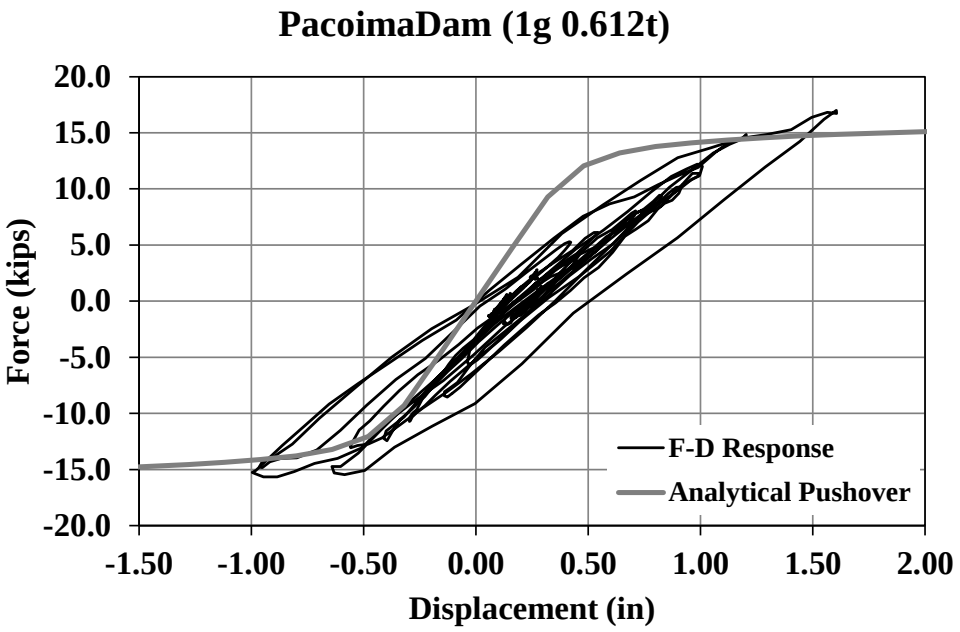

Figure 6.264 Shake Table Test 1 – Pacoima Dam Force – Displacement Response

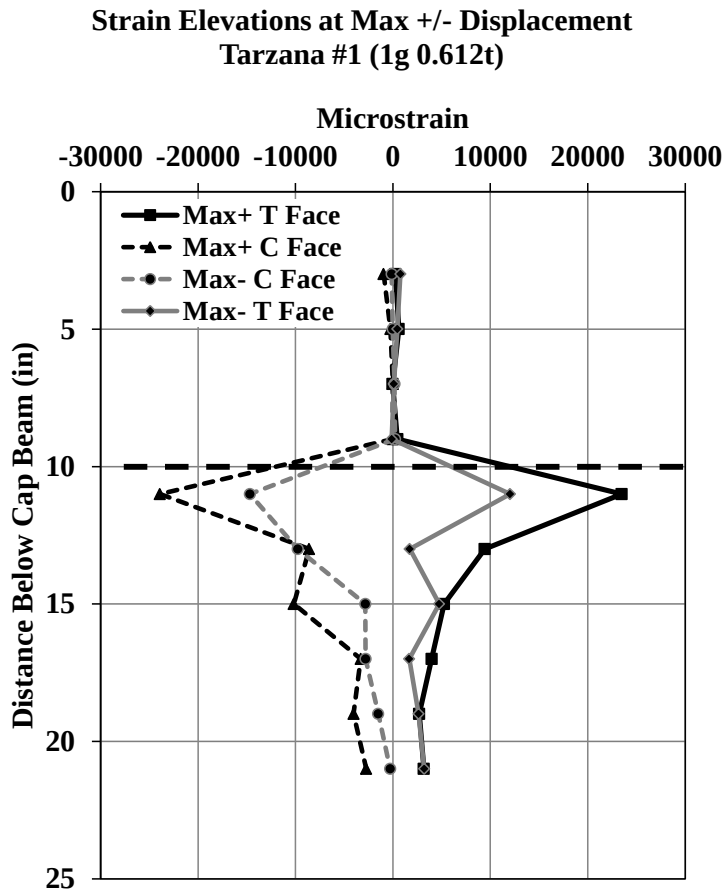

Figure 6.265 Shake Table Test 1 – Pacoima Dam Strain Elevations at Peak Disp.

Following the Pacoima Dam record, the sixth record that was conducted was the Tarzana time history with a PGA of 1.920 g and a predicted displacement ductility demand of 2.11. This record again represented a velocity pulse type event and produced further inelastic action in the test specimen. As shown in Figure 6.266 and Figure 6.267, the pier experienced a slightly longer duration of shaking than with the Pacoima Dam record, and the behavior was dominated by one large reversal at approximately 5 seconds into the record. The specimen exhibited a maximum displacement demand of positive 1.62 in. and negative 2.92 in. corresponding to a maximum ductility demand of 3.50. As had been the case with prior records, this ductility demand was higher than that predicted by NLTHA. However, it is

important to note that the analysis was conducted with a structure that had acquired no previous inelastic action.

The force – displacement response resulting from the Tarzana record displayed considerable yielding along the predicted push – over curve, particularly in the negative direction as shown in Figure 6.268. Hence, the force – displacement characteristics of the system continued to be in good agreement with the analytical push – over prediction in the inelastic range of loading. Unlike the previous records, the response of the system to the Tarzana record produced a large total residual displacement of negative 1.54 in. as shown in Figure 6.269.

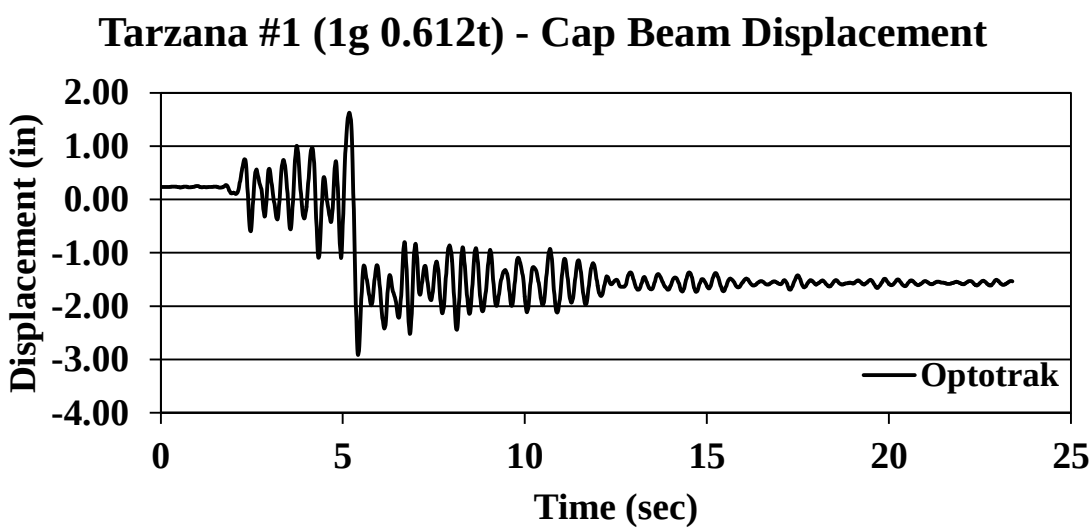

Figure 6.266 Shake Table Test 1 – Tarzana #1 Displacement History

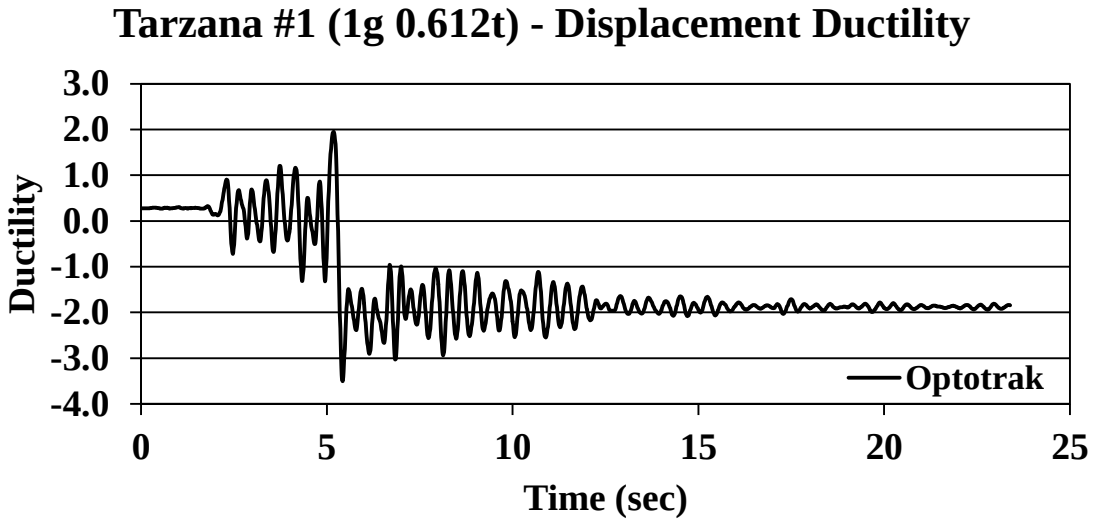

Figure 6.267 Shake Table Test 1 – Tarzana #1 Displacement Ductility History

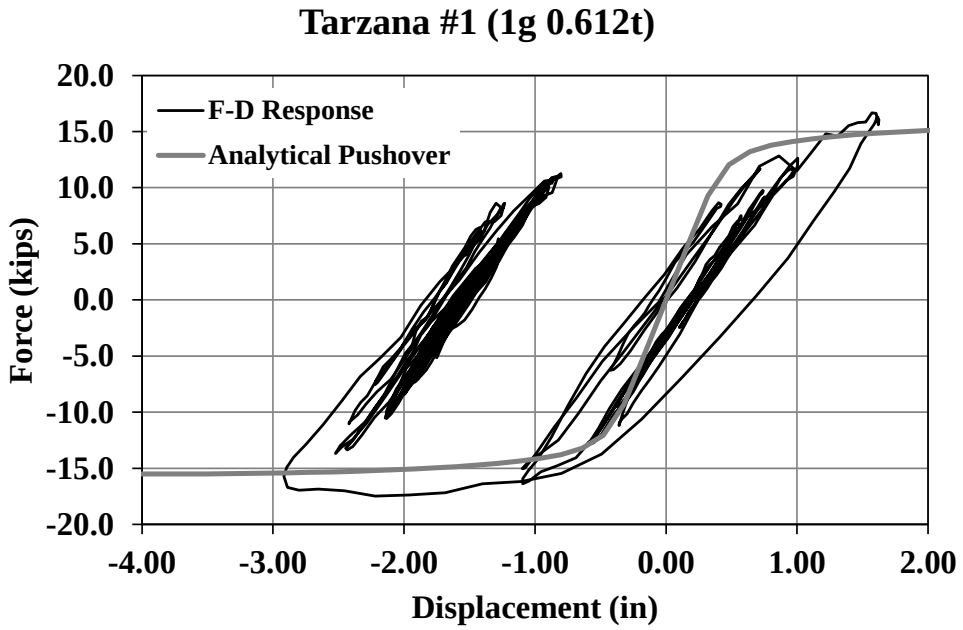

Figure 6.268 Shake Table Test 1 – Tarzana #1 Force – Displacement Response

Figure 6.269 Shake Table Test 1 – Tarzana #1 -2.54 in. Residual Displacement

As shown in Figure 6.270, increased strain demands of approximately +50000 με and -40000 με were experienced in the critical region immediately below the connection. In addition to increased strain demands in the critical region, local buckling was visually noted to develop during this record on the north face (positive direction) of both piles as shown in Figure 6.271. Although there was still no notable damage in the form of material fracture or grout loss and only moderate levels of local buckling had developed, a large residual displacement equal to a ductility demand of approximately 2 had developed in the negative direction. As a result, the decision was made to run the Tarzana record again in the inverse direction as the seventh record, in an effort to return the specimen closer to zero residual displacement prior to continuing to the most demanding record, Kobe.

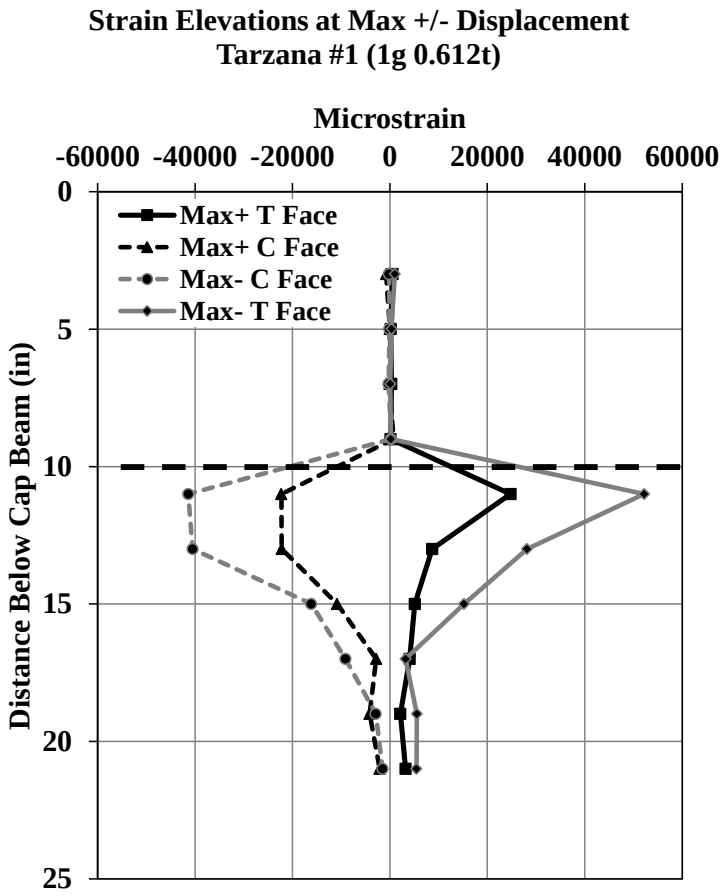

Figure 6.270 Shake Table Test 1 – Tarzana #1 Strain Elevations at Peak Displacements

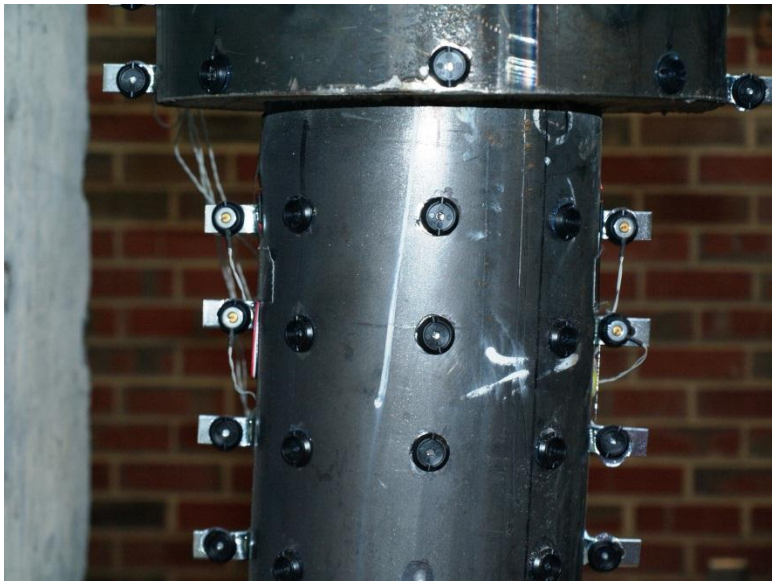

Figure 6.271 Shake Table Test 1 – Tarzana #1 Minor Local Buckling

The inverse Tarzana record (referred to as Tarzana #2 Inverse) was again dominated by a single reversal at approximately 5 seconds into the record. As shown in Figure 6.272 and Figure 6.273, this reversal generated a maximum positive displacement of 1.78 in. and a maximum negative displacement of 2.81 in. Most notably, the inverse record produced a residual displacement of positive 0.405 in. which essentially corrected the negative 2.54 in. of residual displacement experienced during the initial Tarzana record as is shown in Figure 6.274. The force – displacement response produced by the inverse record, provided in Figure 6.275, again showed yielding to occur reasonably close to the predicted push – over response. However, in this case, the yielding occurred in the positive direction which is consistent with the observed behavior correcting the prior negative residual displacement. Having returned the specimen to a lower residual displacement, the decision was made to continue with the more demanding Kobe record.

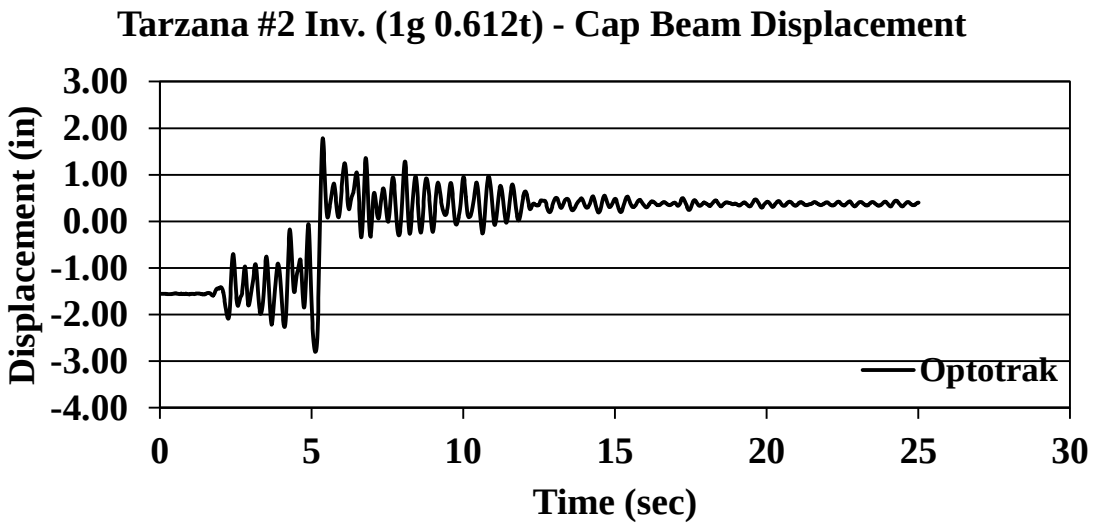

Figure 6.272 Shake Table Test 1 – Tarzana #2 Inverse Displacement History

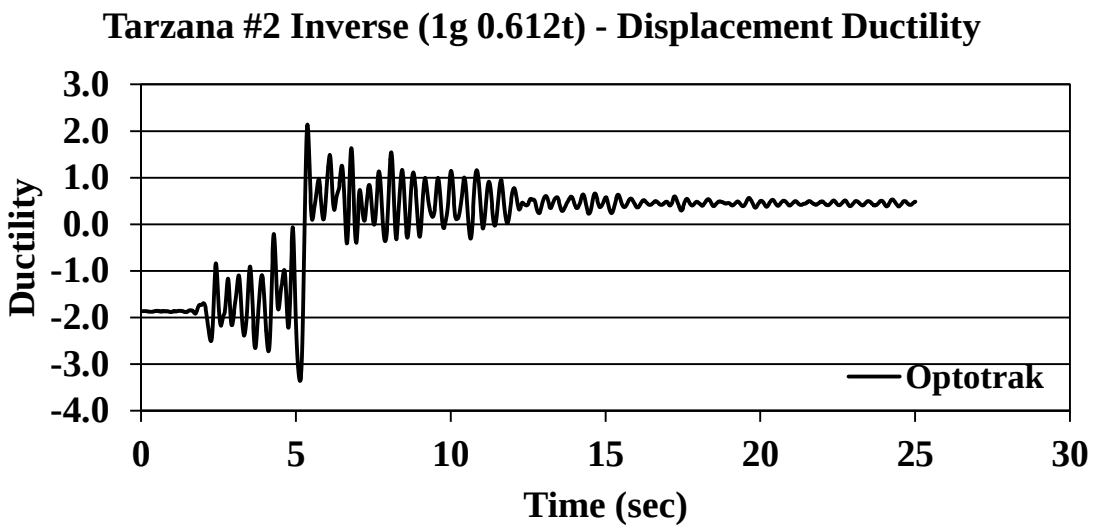

Figure 6.273 Shake Table Test 1 – Tarzana #2 Inverse Displacement Ductility History

Figure 6.274 Shake Table Test 1 – Tarzana #2 Inverse 0.405 in. Residual Displacement

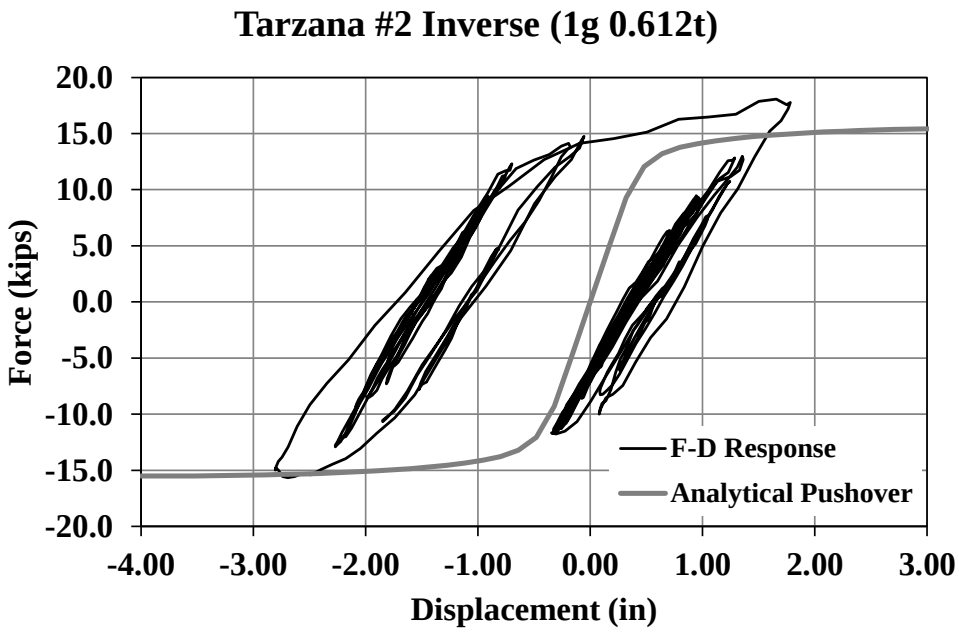

Figure 6.275 Shake Table Test 1 – Tarzana #2 Inverse Force – Displacement Response

The eighth record that was conducted was the Kobe time history with a PGA of 0.821 g and a predicted displacement ductility demand of 3.29. As has been noted, this was predicted to be the most demanding record and, although representative of a velocity pulse type event, was predicted to have more reversals of inelastic action than the Tarzana or Pacoima Dam records. As shown in Figure 6.276 and Figure 6.277, when subjected to the Kobe time history the pier was subjected to approximately 10 seconds of notable shaking and experienced a maximum displacement demand of positive 3.67 in. and negative 0.90 in. corresponding to a maximum ductility demand of 4.40. The large displacement pulse in the positive direction during the record resulted in a residual displacement of positive 2.15 in. as shown in Figure 6.278. The force – displacement response resulting from the Kobe record displayed considerable yielding along the predicted push – over curve, in this case particularly in the positive direction as shown in Figure 6.279. However, one negative cycle of loading also indicated yielding along the predicted curve prior to the large positive displacement cycle.

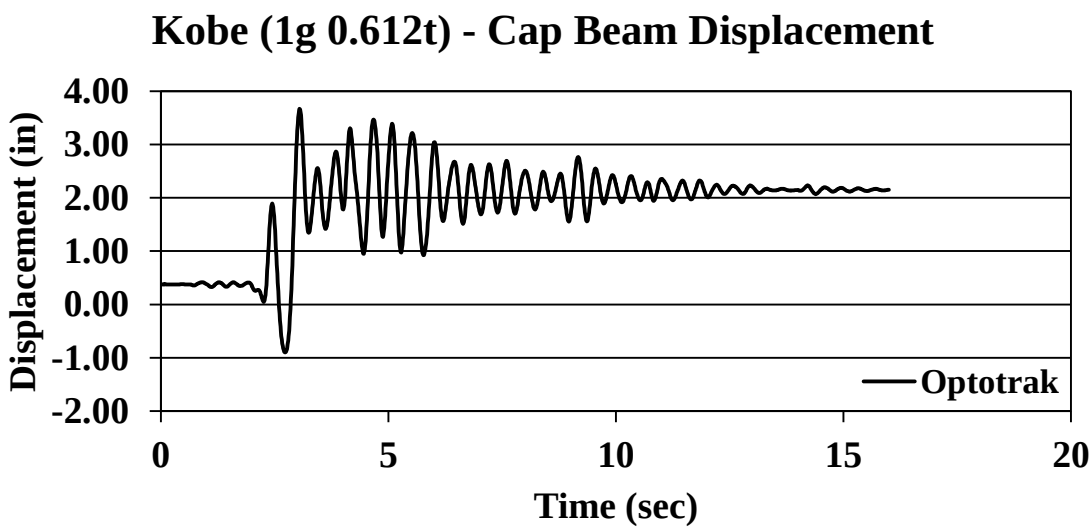

Figure 6.276 Shake Table Test 1 – Kobe Displacement History

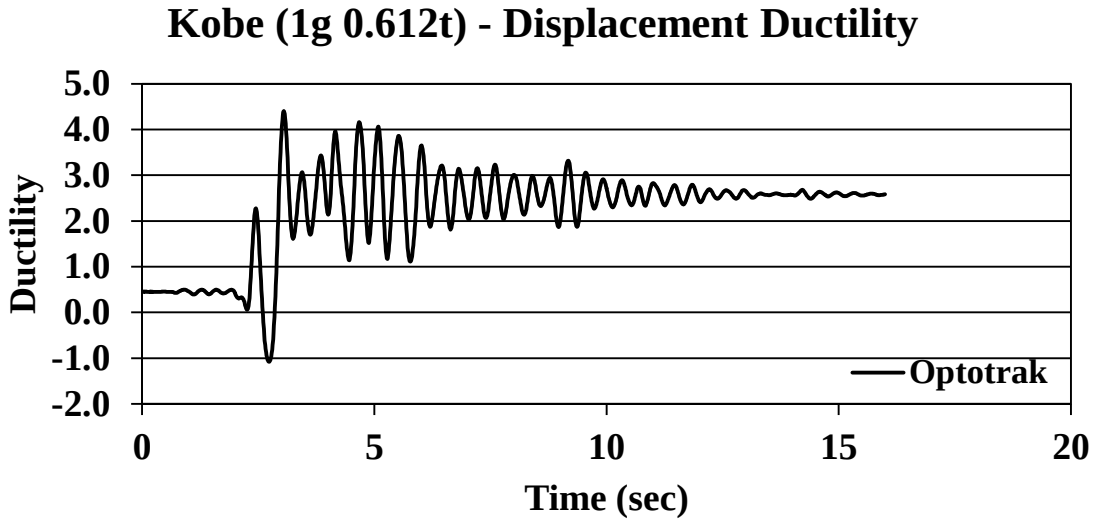

Figure 6.277 Shake Table Test 1 – Kobe Displacement Ductility History

Figure 6.278 Shake Table Test 1 – Kobe Force – 2.15 in. Residual Displacement

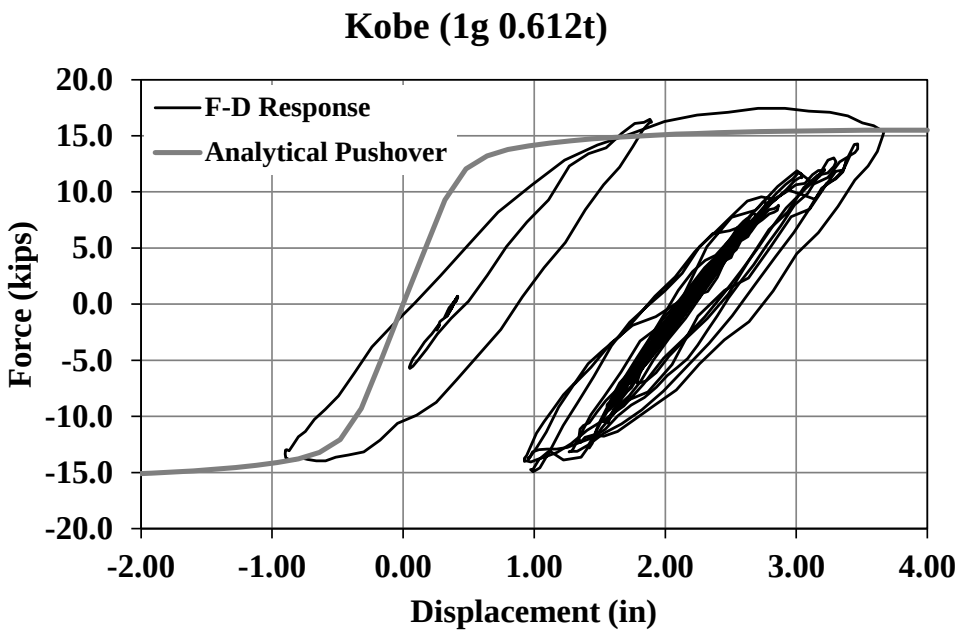

Figure 6.279 Shake Table Test 1 – Kobe Force – Displacement Response

As shown in Figure 6.280, strain demands in the critical region were found to decrease to approximately +25000 με and -35000 με regardless of the increased displacement demands. However, at the completion of the record large amounts of local buckling had developed on the south face (negative direction) of both piles immediately below the connection region as shown in Figure 6.281 and Figure 6.282. Although there was still no damage in the form of material fracture, buckling of the pile walls had become pronounced and the decision was made to not a run a larger record. Given the amount of mass applied directly to the system, concern existed that a collapse failure may occur if material fracture at the buckled region was generated. Further, the Kobe displacement record was the most demanding without using a scale factor greater than 1.0 to manipulate a record. Consequently, the decision was made run multiple smaller records in an effort to evaluate the post buckling strength capacity and behavior of the system while attempting to reduce the residual displacement produced by the Kobe record.

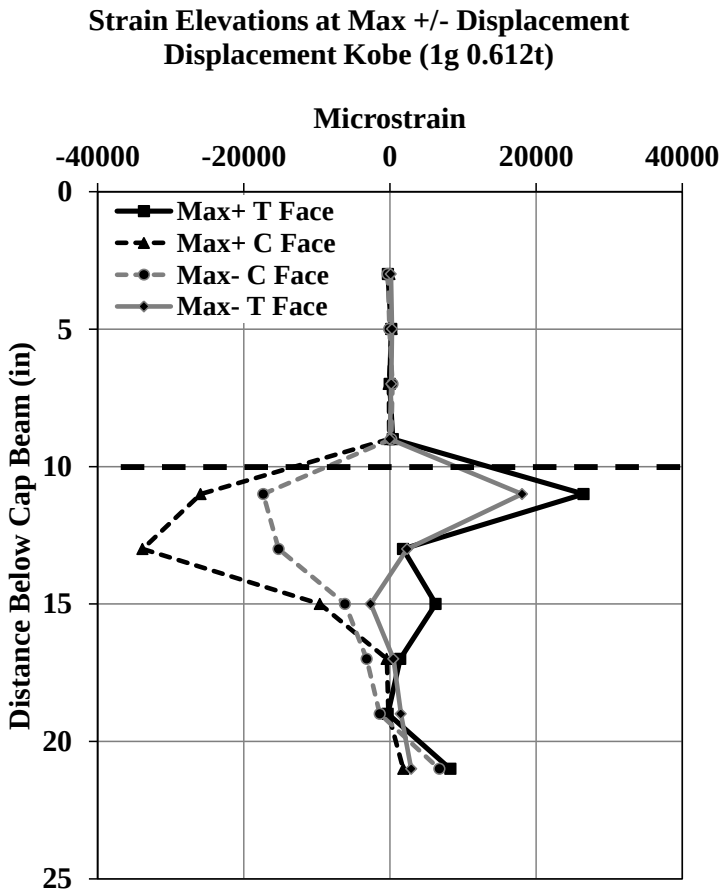

Figure 6.280 Shake Table Test 1 – Kobe Strain Elevations at Peak Displacements

Figure 6.281 Shake Table Test 1 – Kobe – Pile Buckling North Column

Figure 6.282 Shake Table Test 1 – Kobe – Pile Buckling South Column

Following the Kobe record, two repeated Tarzana records were conducted at 1.0 scale factors as well as the Angol displacement record at a scale factor of 1.5. As shown in Figure 6.283 through Figure 6.285, it was found that the strength of the system was reduced by

approximately 25% - 30% in the positive direction, but no notable strength degradation in the negative direction was experienced. This is most notable in the Tarzana #4 response which displays yielding in both directions of loading with a maximum strength of approximately 12 kips in the positive direction and approximately 16 kips in the negative direction. This affect was most likely due to the presence of local buckling on the south side of both columns which serve as the compression faces in the positive direction of loading and as the tension faces in the negative direction of loading. Regardless of the reduced strength capacity, the pier was capable of withstanding the entire displacement history, shown in Figure 6.286, while experiencing no material fracture or other undesirable failure mode.

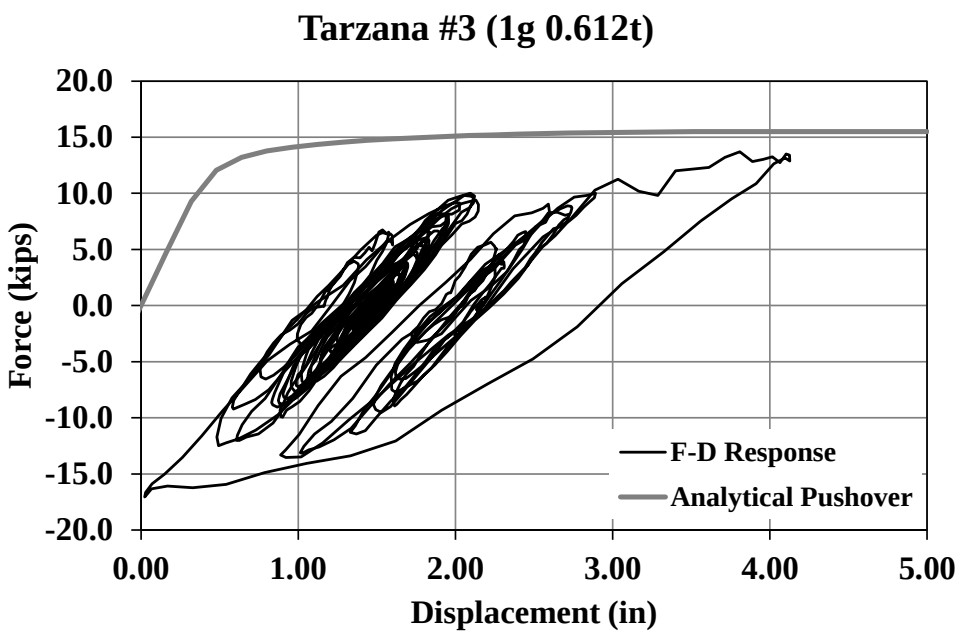

Figure 6.283 Shake Table Test 1 – Tarzana #3 Force – Displacement Response

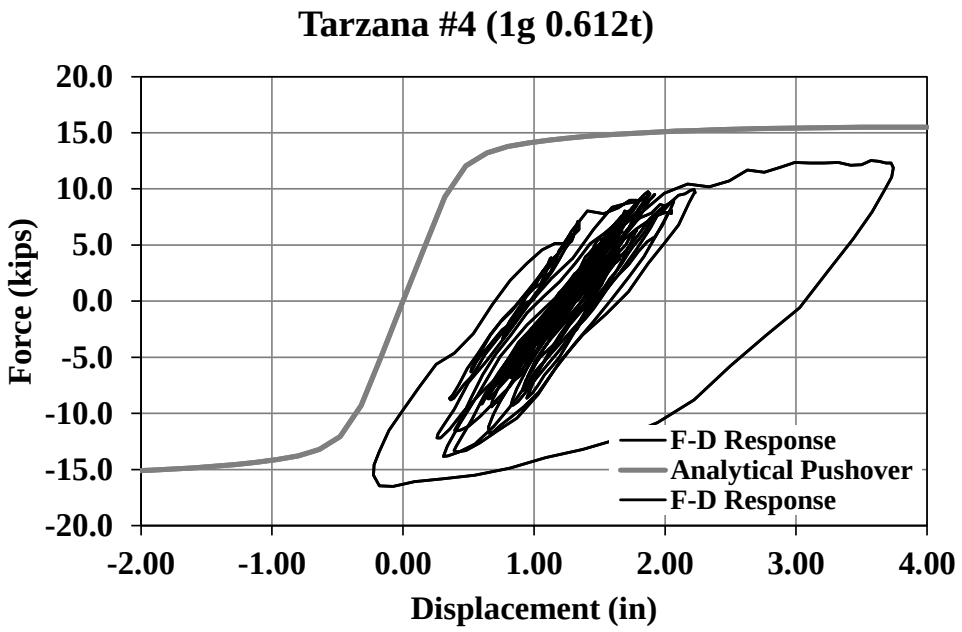

Figure 6.284 Shake Table Test 1 – Tarzana #4 Force – Displacement Response

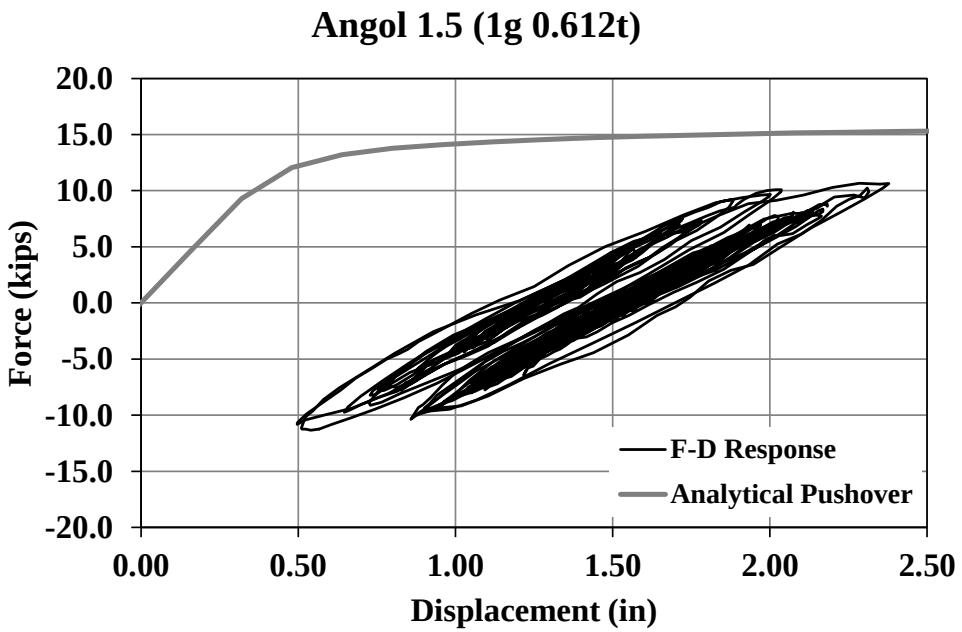

Figure 6.285 Shake Table Test 1 – Angol S.F. = 1.5 Force – Displacement Response

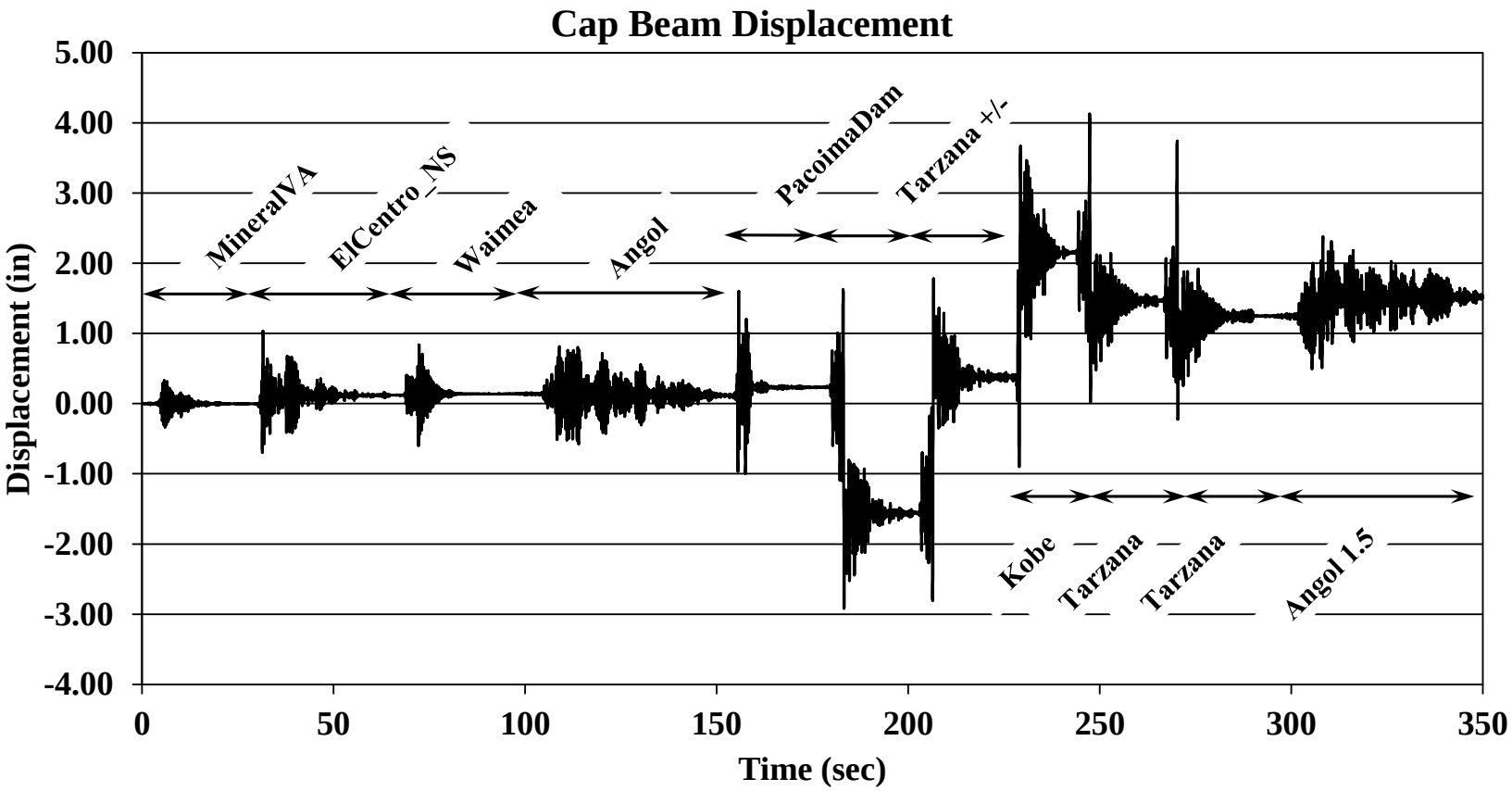

Figure 6.286 Shake Table Test 1 – Full Displacement History

6.6.6 Shake Table Test 2 (Phase 2 Test 9) – Discussion and Results

Following the first shake table test, the decision was made to run the second shake table test with no accumulation of damage prior to a "maximum" considered event in an effort to conduct a brief study on the effects of load history on the pile buckling limit state. As has been discussed, having subjected the first test specimen to a series of ground motions resulted in the accumulation of damage over multiple records. Potential small amounts of local buckling were first observed in the Pacoima Dam record, followed by larger amounts of local buckling which developed during the first and second inverse Tarzana records. The largest amount of local buckling then developed during the Kobe record which experienced the largest displacement demands. Although no apparent strength loss was noted during the Kobe record, strength loss was shown to exist in subsequent less demanding records.

Consequently, the second shake table test (phase 2 test 9) aimed to evaluate whether or not the accumulation of yielding and damage over multiple increasing demand level records, affected the response and behavior of the system to the most demanding event, Kobe. In order to study this, the decision was made not to conduct a suite of ground motions as had been done in test 1 but instead to conduct Kobe at a scale factor of 1.0 as the initial record. Based on the response of the specimen, the Kobe record could then either be scaled up or down as necessary to evaluate the remaining capacity of the pier. In this evaluation, Kobe was the only record considered such that the only variable between ground motion applications would be the scale factor.

As shown in Figure 6.287 and Figure 6.288, when initially subjected to the Kobe record the nominally identical second specimen experienced a maximum displacement of positive 3.16 in. which corresponded to a displacement ductility demand of 3.79. The response was dominated by a large reversal from the maximum negative displacement to the maximum positive displacement at approximately 3 seconds into the record. The maximum displacement is also shown in Figure 6.289, which provides a photograph of the pier taken by

high speed photography at approximately the maximum displacement of 3.79 in. With the response dominated by a positive maximum displacement, 1.53 in. of residual displacement existed at the completion of the record.

The force – displacement response of the Kobe record, shown in Figure 6.290, indicated yielding occurred in both directions of loading with the positive direction extending into the yield plateau range. The response was again shown to follow the predicted push – over analytical prediction well in the non – linear range. The pier exhibited an ultimate strength of approximately 17 kips in the positive direction. Alternatively, the pier experienced a maximum force of approximately 15 kips in the negative direction, which likely does not coincide with the ultimate strength in the negative direction as significant yielding did not occur. The connection region was again shown to behave appropriately as a modified weld protected connection by forcing the largest strain demands below capacity protected region of the connection as shown in Figure 6.291.

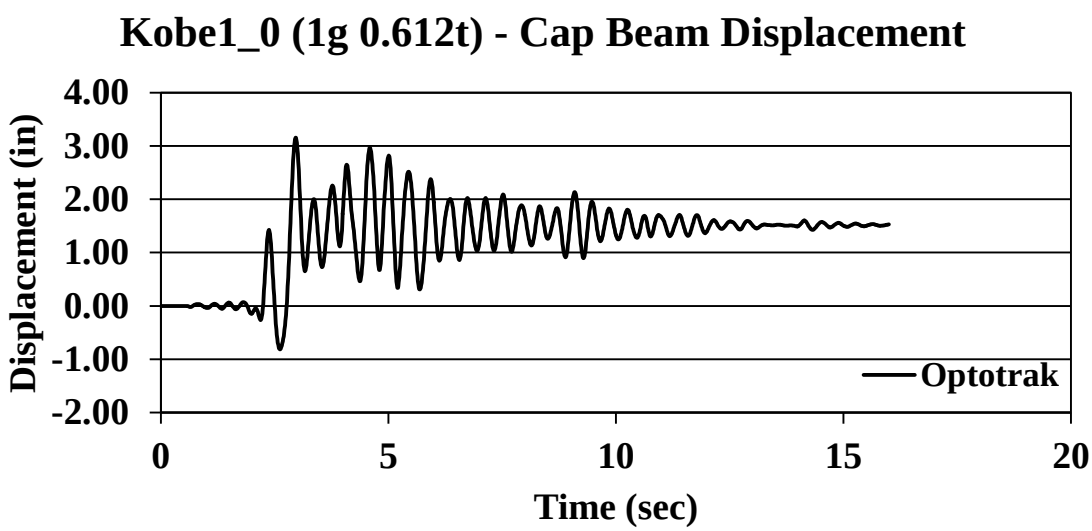

Figure 6.287 Shake Table Test 2 – Kobe #1 Displacement History

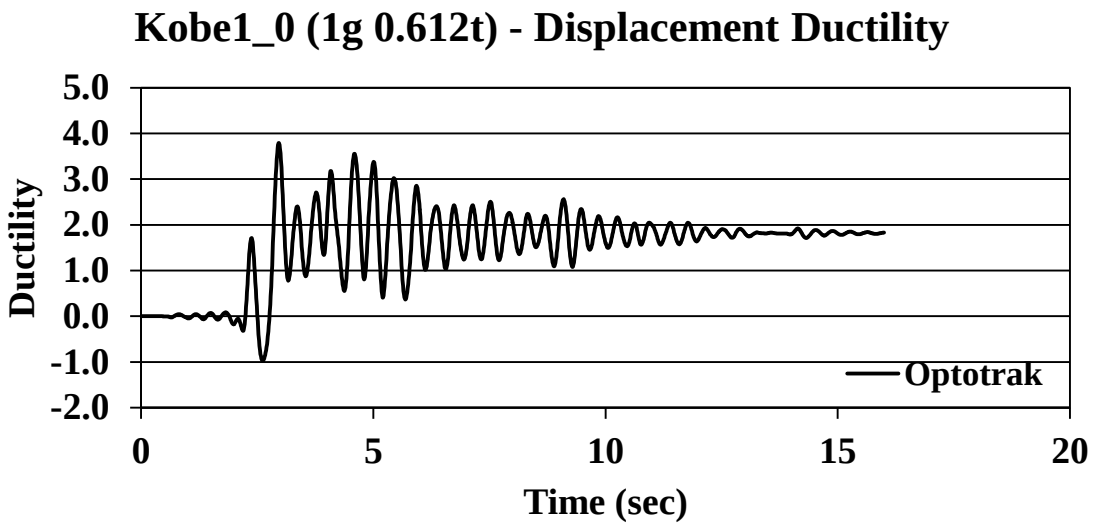

Figure 6.288 Shake Table Test 2 – Kobe #1 Displacement Ductility History

Figure 6.289 Shake Table Test 2 – Kobe #1 In – Motion Approx. Peak Disp.

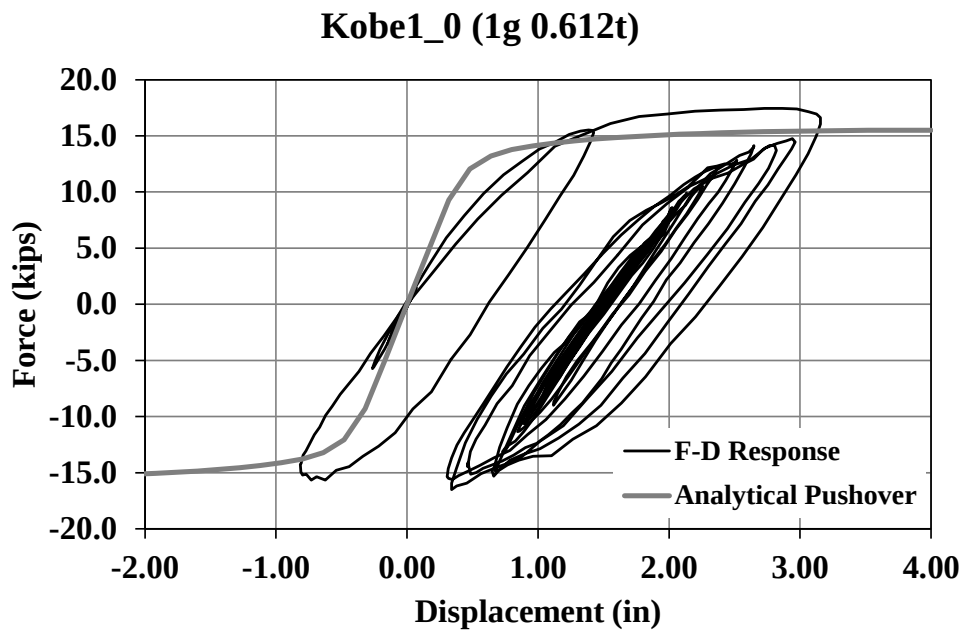

Figure 6.290 Shake Table Test 2 – Kobe #1 Force – Displacement Response

Considering the main goal of the second shake table test was to evaluate the effects of accumulation of damage over multiple records prior to the maximum demand event, comparisons have been made between the response of the first shake table test subjected to the Kobe record and that of the second. As shown in Figure 6.292 and Figure 6.293, both the displacement time histories and the force – displacement responses were shown to be similar in their characteristics. The only notable difference was that the response of the first test was offset by the initial residual positive displacement of 0.405 in. which was developed in the records prior Kobe. As shown in Figure 6.294, when the response of the first test is reduced by this initial displacement, the two evaluations show considerable similarity suggesting the dynamic behavior was essentially the same with the exception of the initial displacement. Further, comparison indicates that the accumulation of damage over multiple records did not impact the ultimate strength capacity of the system that was developed during the Kobe event in both the first and second shake table test.

Regardless of the similarity in response characteristics, it is important to note that the observed levels of local buckling that developed in the piles during the Kobe event, was less severe in the second test than that of the first. As shown in Figure 6.295 and Figure 6.296, only a small magnitude of local buckling was found to develop on the south face (negative direction) of the piles in the second test as opposed to the first which developed more pile wall deformation during the Kobe event as shown in Figure 6.281 and Figure 6.282. This observation suggests that although the response comparisons to the Kobe record were similar for that event, the second test specimen may not exhibit the strength loss that was shown to develop for the first specimen when subjected to less demanding subsequent records.

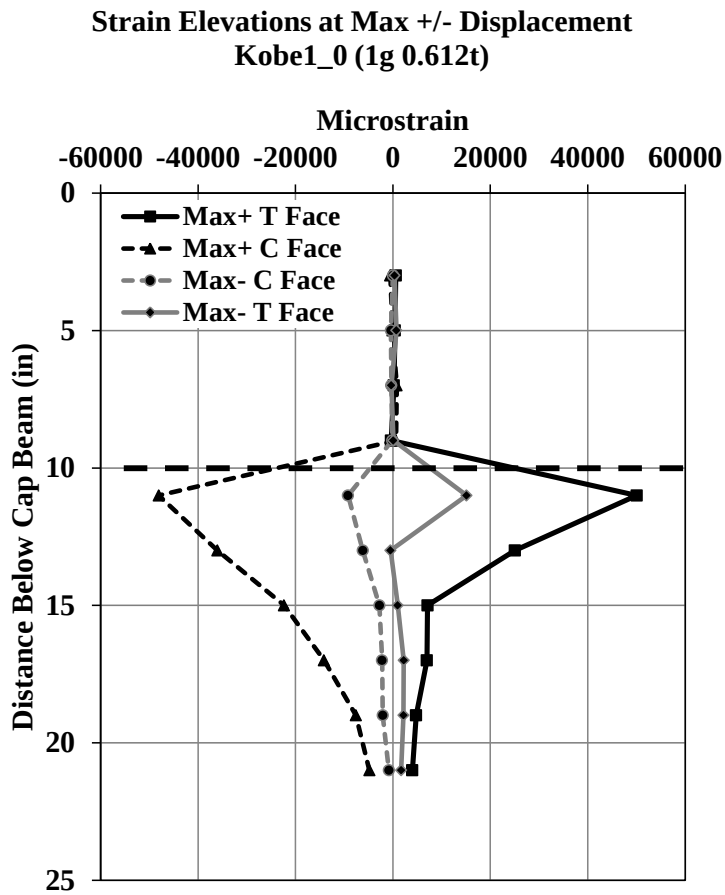

Figure 6.291 Shake Table Test 2 – Kobe #1 Strain Elevations at Peak Displacements

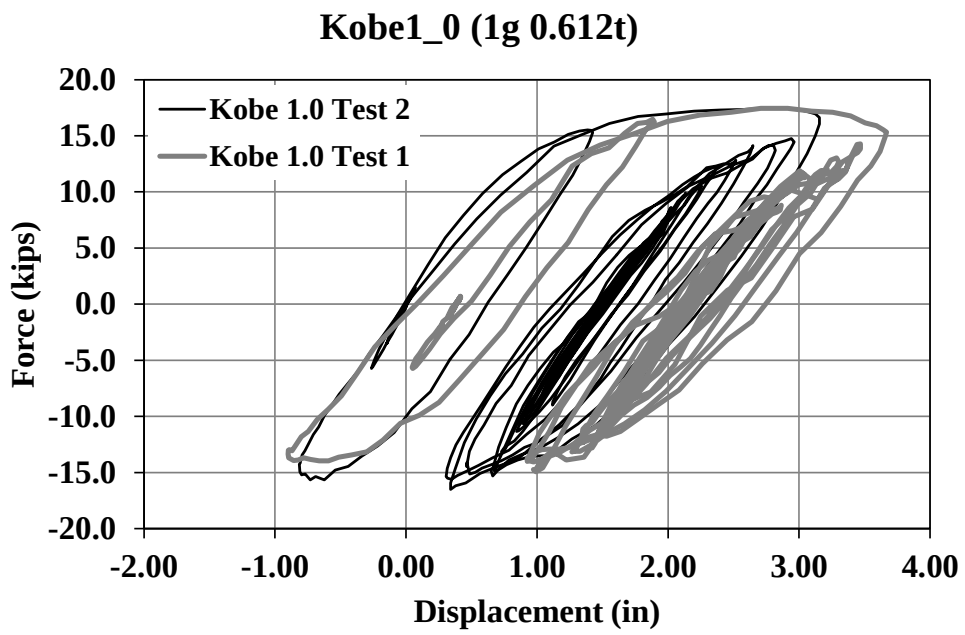

Figure 6.292 Shake Table Test 1 vs. 2 – Kobe Force – Displacement Response

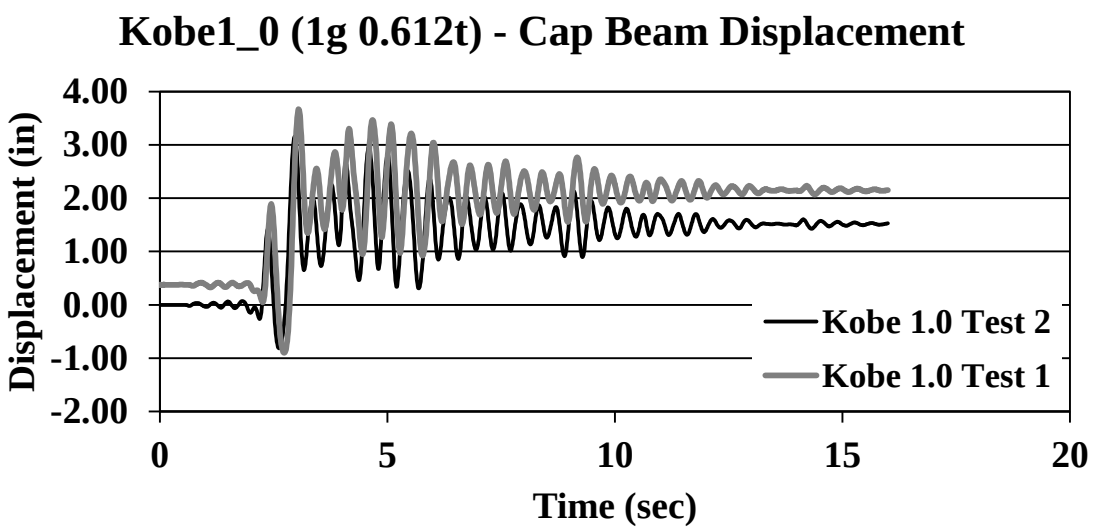

Figure 6.293 Shake Table Test 1 vs. 2 – Kobe Displacement History

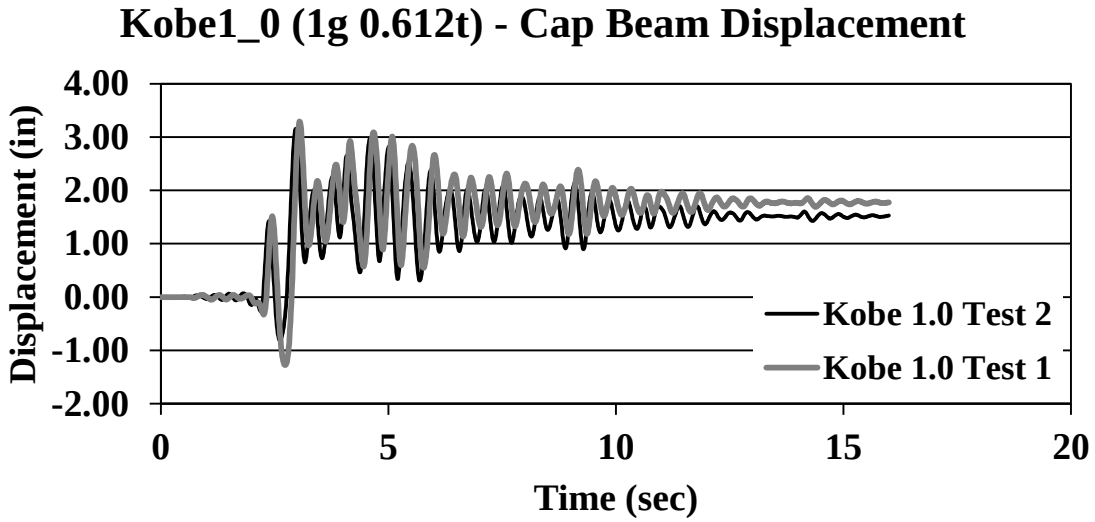

Figure 6.294 Shake Table Test 1 (Normalized) vs. 2 – Kobe Displacement History

Figure 6.295 Shake Table Test 2 – Kobe #1 North Column Joint Region

Figure 6.296 Shake Table Test 2 – Kobe #1 South Column Joint Region

Following the first Kobe record, the pier had been subjected to a residual displacement of 1.53 in. although local buckling of the pile walls had not become pronounced. The decision was made to apply a more demanding record to the pier by applying a larger scale factor to the Kobe displacement history. However, before doing so the Kobe record at a scale of 1.0 was run the inverse direction in attempt to correct the residual displacement experienced during the first record. As shown in Figure 6.297 and Figure 6.298, the inverse record exhibited a maximum positive displacement of 2.75 in., corresponding to a ductility demand of 3.29, and a maximum negative displacement of 1.81 in. As shown in Figure 6.299, the application of the record in the inverse direction produced considerable yielding in the negative direction which was consistent with the goal of correcting the residual displacement. However, at the completion of the record a residual displacement of positive 0.51 in. remained as shown in Figure 6.300. Further, the inverse record did not produce any additional notable buckling of the pile walls. Consequently, the decision was made to apply a larger scale factor to the Kobe record to produce further local buckling. Given that only 2/3

of the residual displacement had been corrected, the decision was made to run the larger record in the inverse direction.

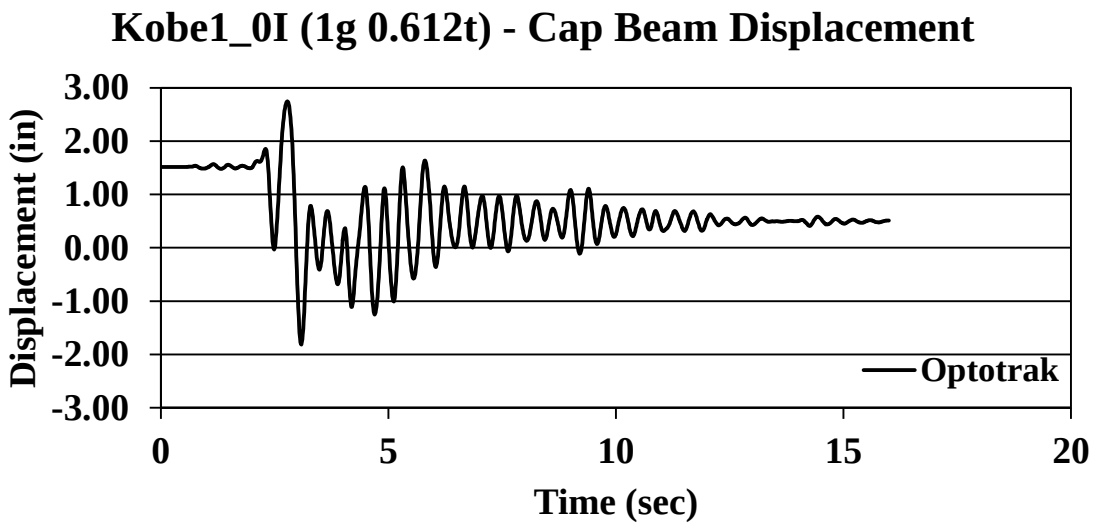

Figure 6.297 Shake Table Test 2 – Kobe #2 Inverse Displacement History

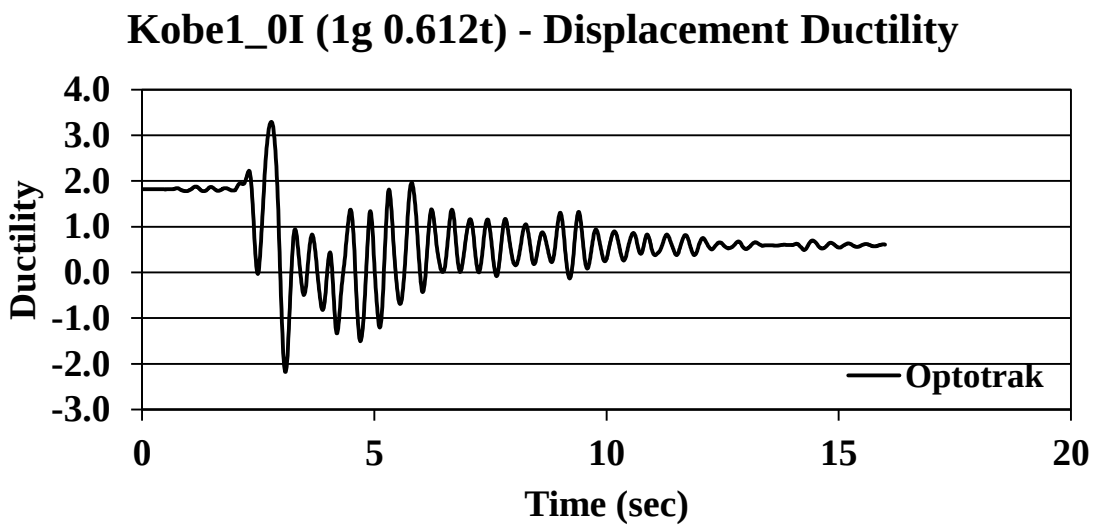

Figure 6.298 Shake Table Test 2 – Kobe #2 Inverse Displacement History

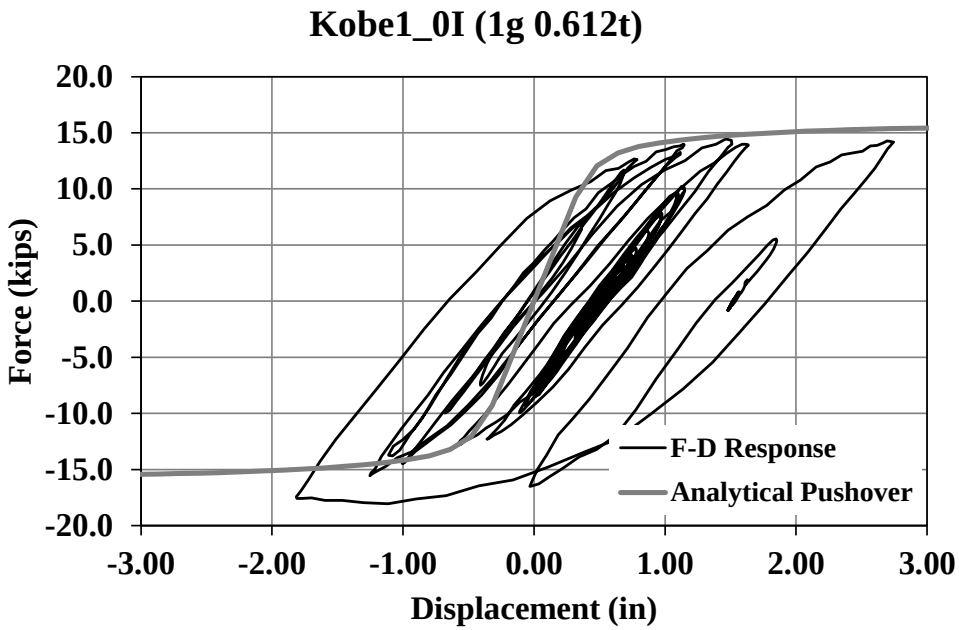

Figure 6.299 Shake Table Test 2 – Kobe #2 Inverse Force – Displacement Response

Figure 6.300 Shake Table Test 2 – Kobe #2 Inv. 0.51 in. Residual Displacement

Following the Kobe 1.0 inverse record, the final record that the second specimen was subjected to was the Kobe record in the inverse direction this time at a displacement history scale factor of 1.3. Although no analytical prediction at this scale factor had been conducted, this was thought to be a reasonable increase in the demand level to presumptively produce further pile wall local buckling. As shown in Figure 6.301 and Figure 6.302, the application of the record at this scale factor produced a maximum positive displacement of 2.06 in. and a maximum negative displacement of 4.68 in. which coincided with a maximum displacement ductility demand of 5.62. With the response dominated by a large reversal, as was the case at a 1.0 scale factor, the specimen was subjected to a residual displacement of negative 3.46 in.

The force – displacement response, shown in Figure 6.303, indicated yielding occurred initially in the positive direction along the predicted analytical push – over curve not indicating any significant strength loss in the positive direction nor the negative direction. The response further showed a larger amount of yielding in the negative direction with the force – displacement curve falling marginally higher than the predicted response, again suggesting no loss in strength in this direction of loading had occurred prior to reaching the maximum displacement. The condition of the pier and the south joint region approximately at the maximum displacement demand are shown in Figure 6.304 and Figure 6.305 which were both taken with high speed photography.

Following the application of the record, through visual observation it was found that local buckling of the pile walls in the critical region had propagated with the magnitude of pile wall distortion becoming severe as shown in Figure 6.306. As a result of the severity of local buckling, as well as the residual drift of negative 3.46 in., the decision was made to apply no other records to the test specimen. Although considerable damage in the form of pile wall local buckling had developed constituting an ultimate limit state, the pier was capable of withstanding the entire displacement history, shown in Figure 6.307, while experiencing no material fracture or other undesirable failure mode.

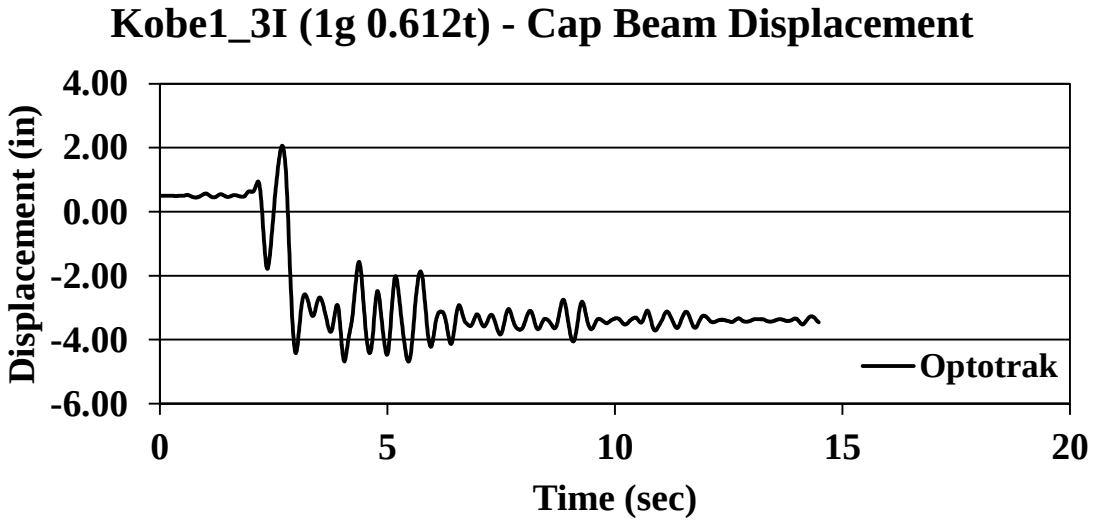

Figure 6.301 Shake Table Test 2 – Kobe 1.3 Inverse #3 Displacement History

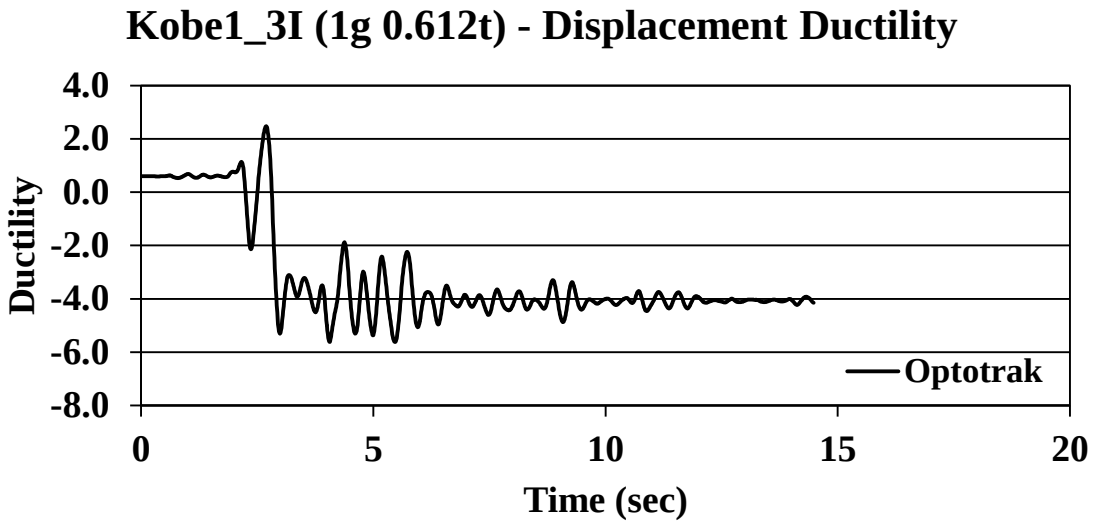

Figure 6.302 Shake Table Test 2 – Kobe 1.3 Inverse #3 Displacement Ductility History

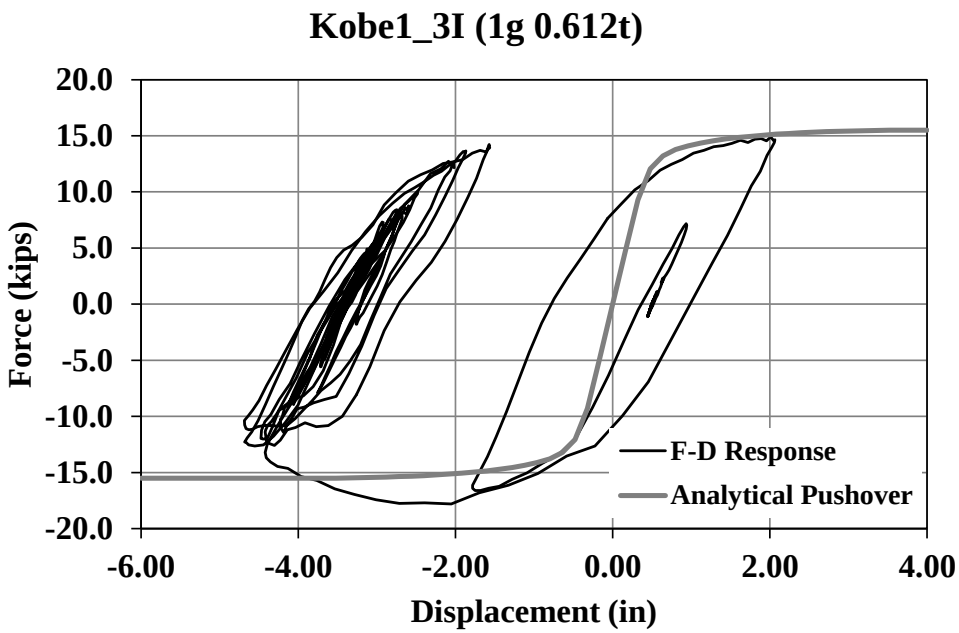

Figure 6.303 Shake Table Test 2 – Kobe 1.3 Inverse #3 Force – Displacement Response

Figure 6.304 Shake Table Test 2 – Kobe #3 Inv. In – Motion Approx. Peak Disp.

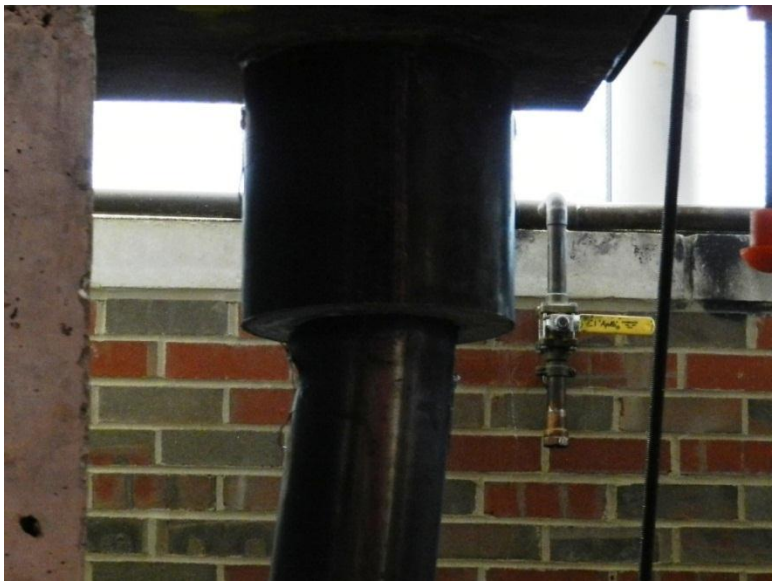

Figure 6.305 Shake Table Test 2 – Kobe #3 Inv. In – Motion Approx. Peak Disp.

Figure 6.306 Shake Table Test 2 – Kobe #3 Inv. South Column Joint Region

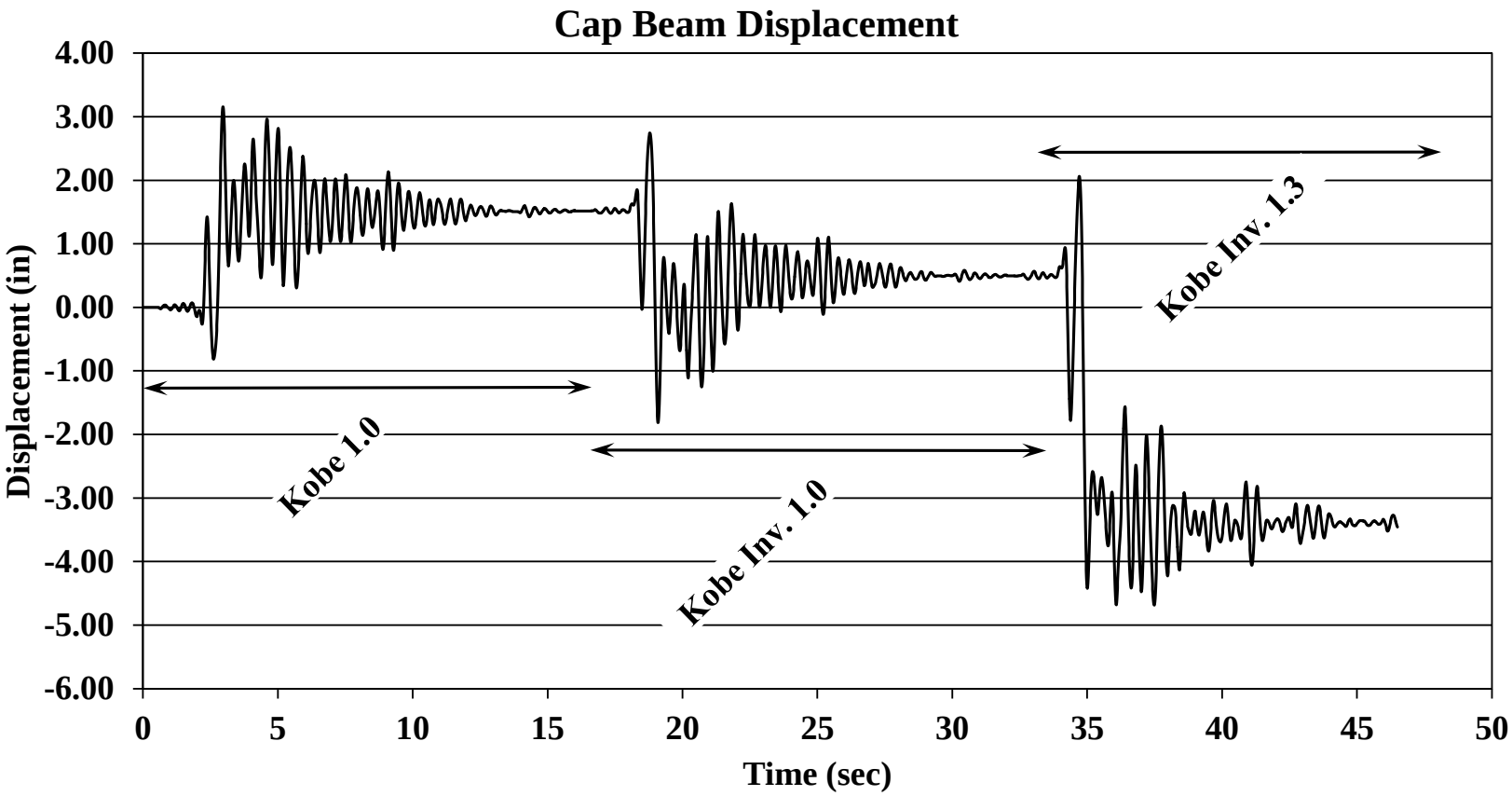

Figure 6.307 Shake Table Test 2 – Full Displacement History

6.6.7 DDBD Inverse Evaluation

The results of both the first and second shake table tests were used to inversely evaluate the accuracy of a Direct Displacement – Based Design (DDBD) procedure at predicting the maximum displacement demand of the steel pier system to a given acceleration time history. The DDBD procedure, aims to design a structure for a specific displacement limit state by providing a calculated strength to the structure which corresponds to an effective period at a maximum response associated with the secant stiffness of the structure. However, the procedure requires that total Equivalent Viscous Damping (EVD, ξ_{eq}) related to energy released from inelastic demands placed on the structure be considered when designing the structure for a maximum inelastic response with an elastic design displacement response spectrum. Further details of the procedure are provided in (Priestley, et. al., 2007).

One option to consider the inelastic action of the structure in a DDBD procedure is to calculate total EVD with calibrated design equation that are based a given hysteretic rule and a design displacement ductility demand. The calculated total EVD ratio can then be used with calibrated spectral reduction factor relationships (SRF, R_ξ) to determine values by which a design elastic DRS can be reduced when executing the DDBD procedure. It is recommended by (Priestley, et. al., 2007), that for steel structures the total EVD ratio be determined by the relationship calibrated for a Ramberg – Osgood hysteretic behavior as shown in Eq.(6.13). One option also recommended by (Priestley, et. al., 2007), is to use Eurocode spectral reduction factor relationships to determine appropriate levels of R_ξ for any given hysteretic rule. In the relationship for R_ξ provided in Eq.(6.14), the α factor accounts for the type of expected event when designing the structure. It is recommended that this factor be taken as 0.5 for far field events and 0.25 for near field events which accounts for the reduced energy dissipation that may be expected in a velocity pulse type of record which is generally dominated by a lower number of cyclic inelastic reversals.

$$\xi_{eq,RO} = 0.05 + 0.577\left(\frac{\mu_\Delta - 1}{\pi\mu_\Delta}\right) \tag{6.13}$$

$$R_\xi = \left(\frac{0.07}{0.02 + \xi_{eq}}\right)^\alpha \tag{6.14}$$

To evaluate the appropriateness of these recommendations in regards to the scaled G.S.C. test specimens, an inverse DDBD procedure was conducted for each record applied to the specimen. To conduct this procedure, data recorded during testing was used to calculate system strength and the associated secant stiffness and corresponding effective period at the maximum displacement response for each record conducted. The ductility demand associated with the maximum response was used to determine the associated total ξ_{eq} and R_ξ in accordance with Eq.(6.13) and Eq.(6.14). As opposed to reducing a spectral response, the calculated R_ξ was used to amplify the recorded maximum displacement of the structure during testing, which along with the calculated effective period was plotted as a single data point on the elastic 5% damped DRS determined from the acceleration time history recorded during testing. It is important to note, in this evaluation the Mineral VA, El Centro, and Angol records were considered far field events and α was taken as 0.5, while Waimea, Pacoima Dam, Tarzana, and Kobe were considered near field events with α taken as 0.25.

As shown in Figure 6.308 through Figure 6.317, the results of this analysis technique showed the calculated inverse DDBD response to be in good agreement with the elastic displacement response spectrum found from testing. In each case, the amplified maximum displacement response and associated effective period based on secant stiffness fell reasonably close to the elastic DRS. This finding suggest that both the EVD model and the SRF model, discussed in (Priestley, et. al., 2007), were applicable to the response of the scaled G.S.C. test pier. Interestingly, in all cases the inverse DDBD predictions were closer in test 1, which was subjected to multiple records, than in test 2 which was subjected to an

initial "maximum" considered event. Regardless, all cases were in reasonable agreement with the DDBD predictions.

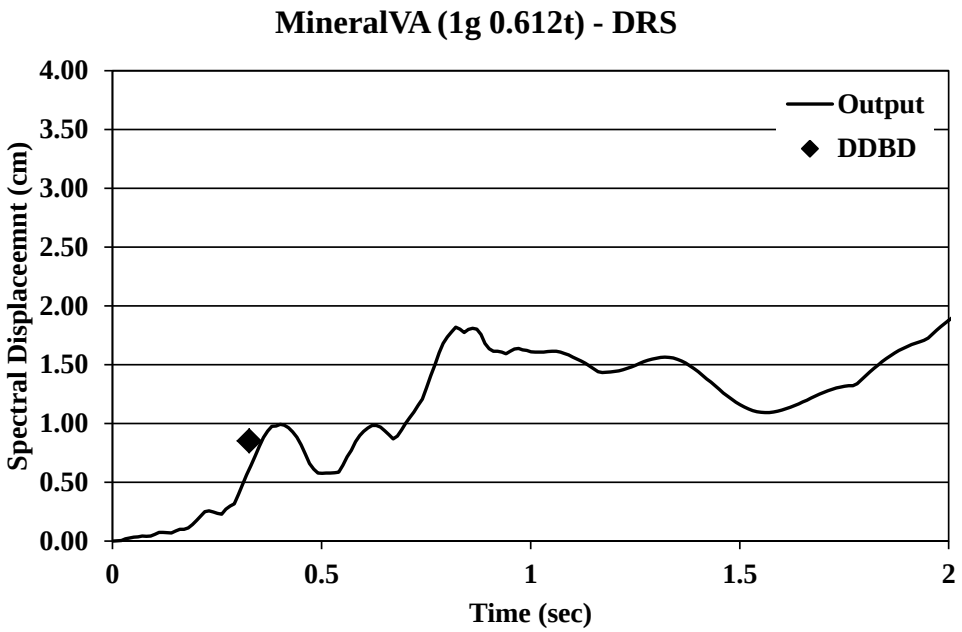

Figure 6.308 Shake Table Test 1 – Mineral VA – Inverse DDBD Results (ξ=5%)

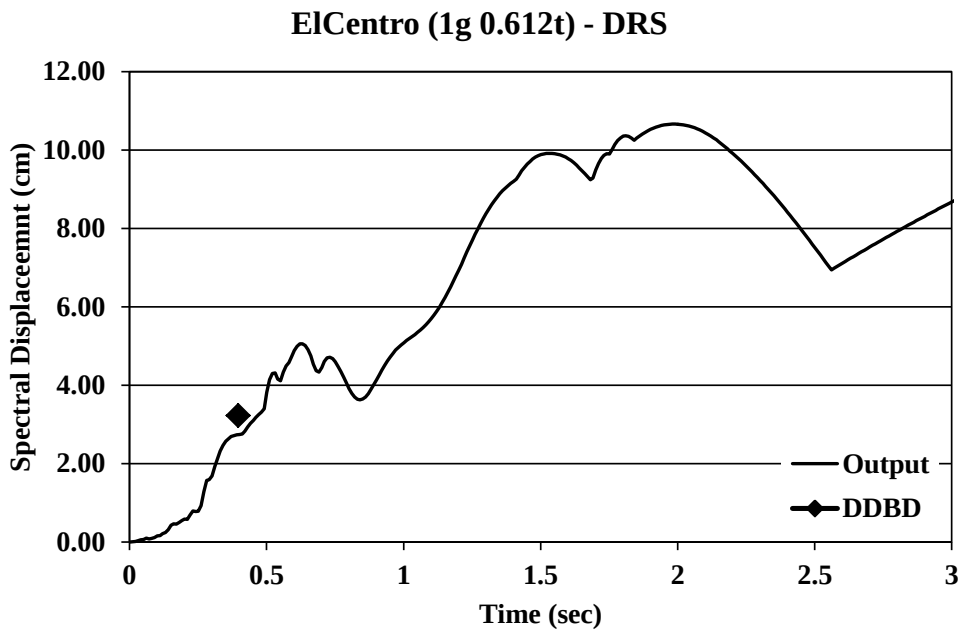

Figure 6.309 Shake Table Test 1 – El Centro – Inverse DDBD Results (ξ=5%)

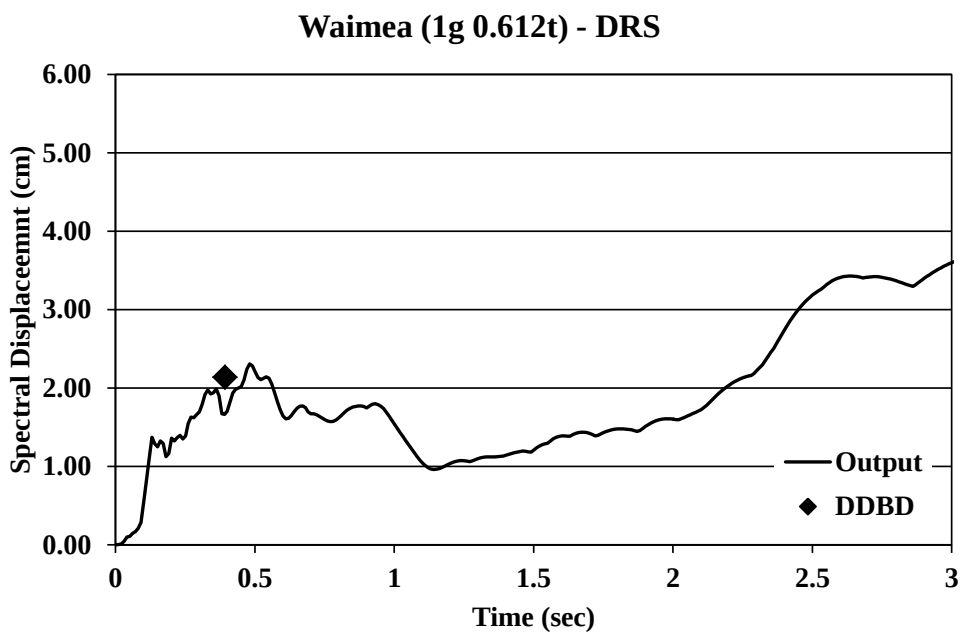

Figure 6.310 Shake Table Test 1 – Waimea – Inverse DDBD Results (ξ=5%)

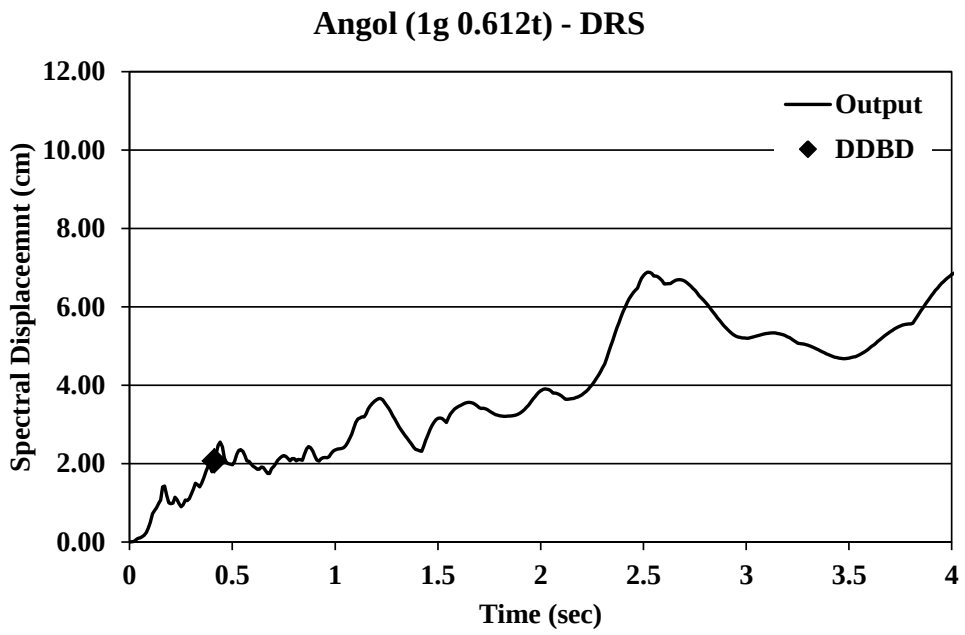

Figure 6.311 Shake Table Test 1 – Angol – Inverse DDBD Results (ξ=5%)

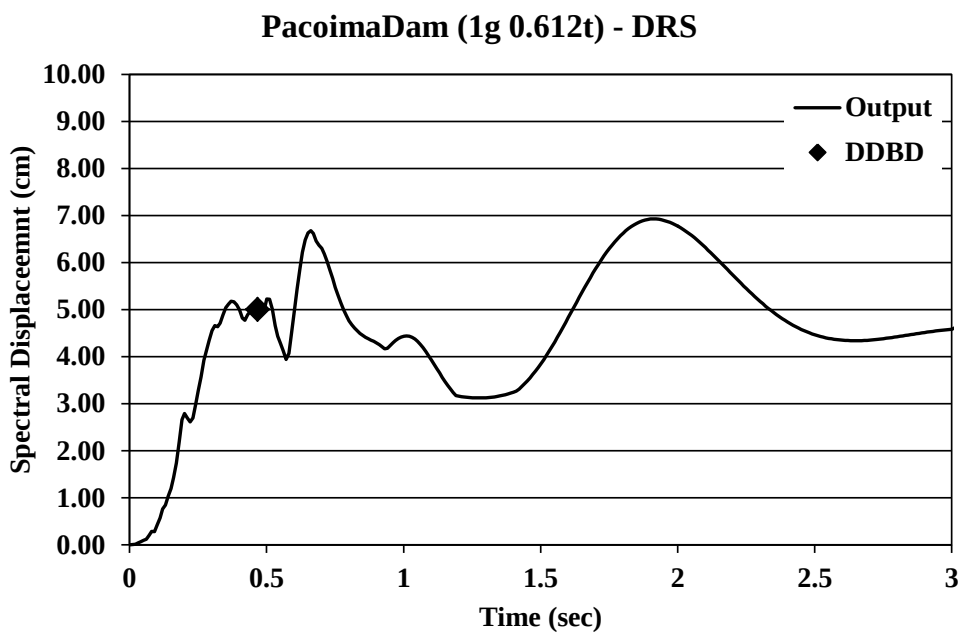

Figure 6.312 Shake Table Test 1 – Pacoima Dam – Inverse DDBD Results (ξ=5%)

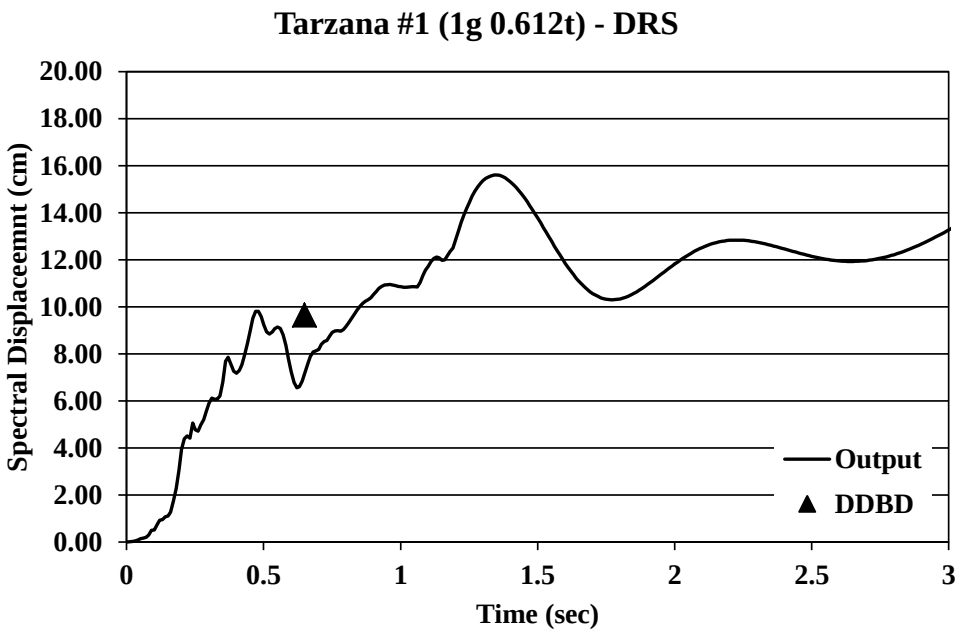

Figure 6.313 Shake Table Test 1 – Tarzana #1 – Inverse DDBD Results (ξ=5%)

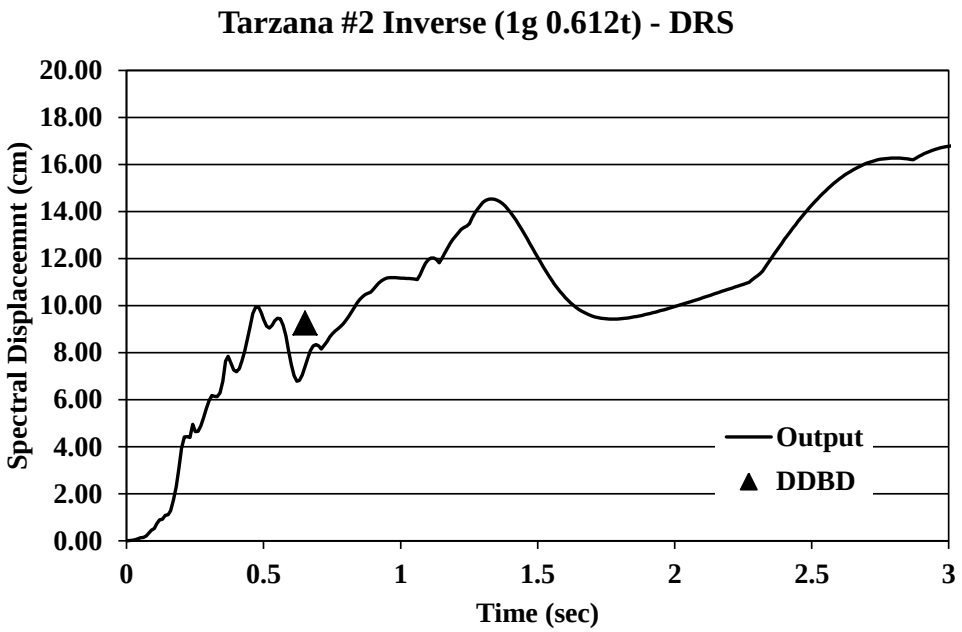

Figure 6.314 Shake Table Test 1 – Tarzana Inverse #2 – Inverse DDBD Results (ξ=5%)

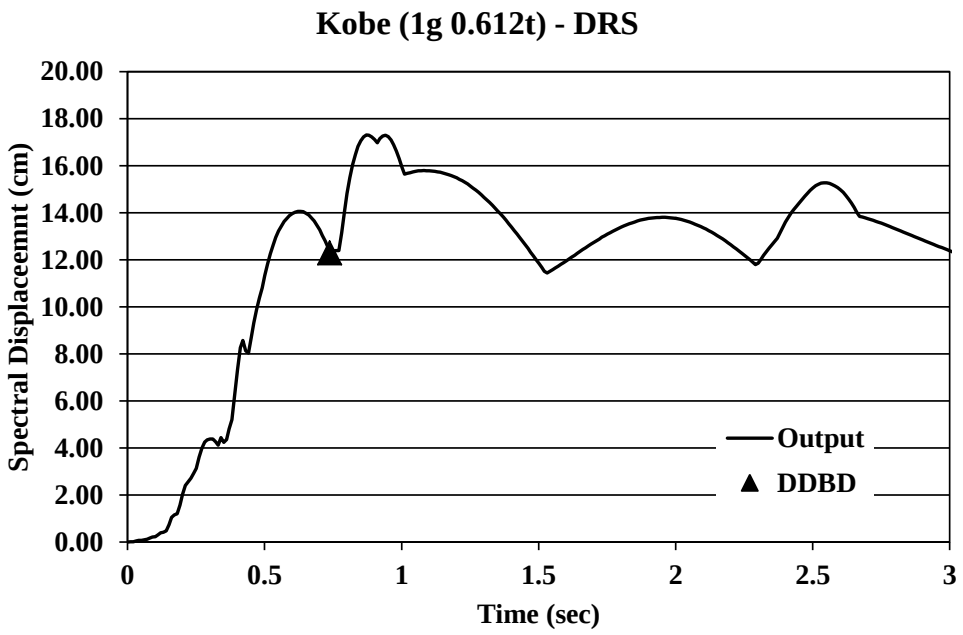

Figure 6.315 Shake Table Test 1 – Kobe – Inverse DDBD Results (ξ=5%)

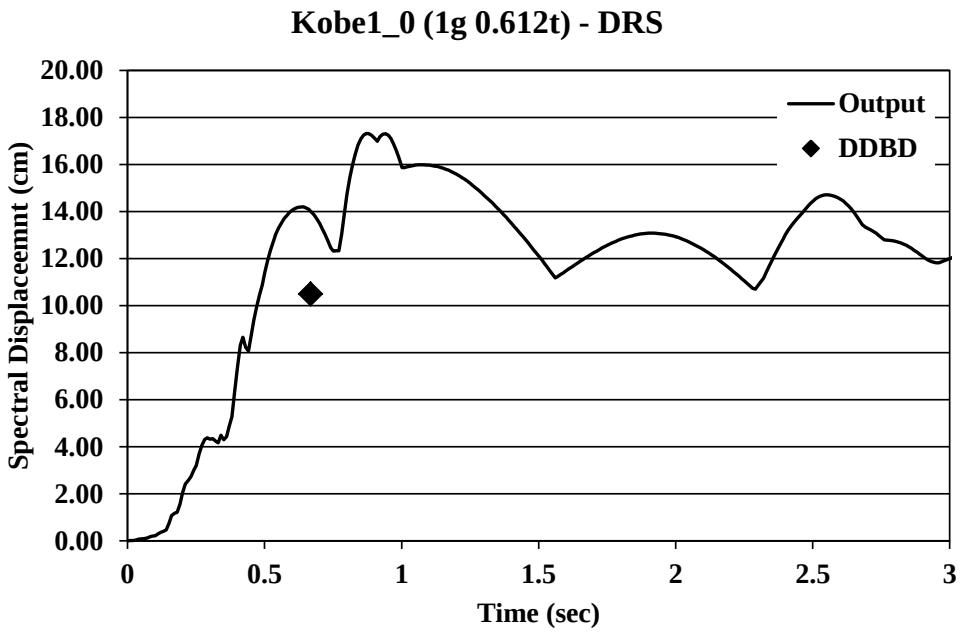

Figure 6.316 Shake Table Test 2 – Kobe #1– Inverse DDBD Results (ξ=5%)

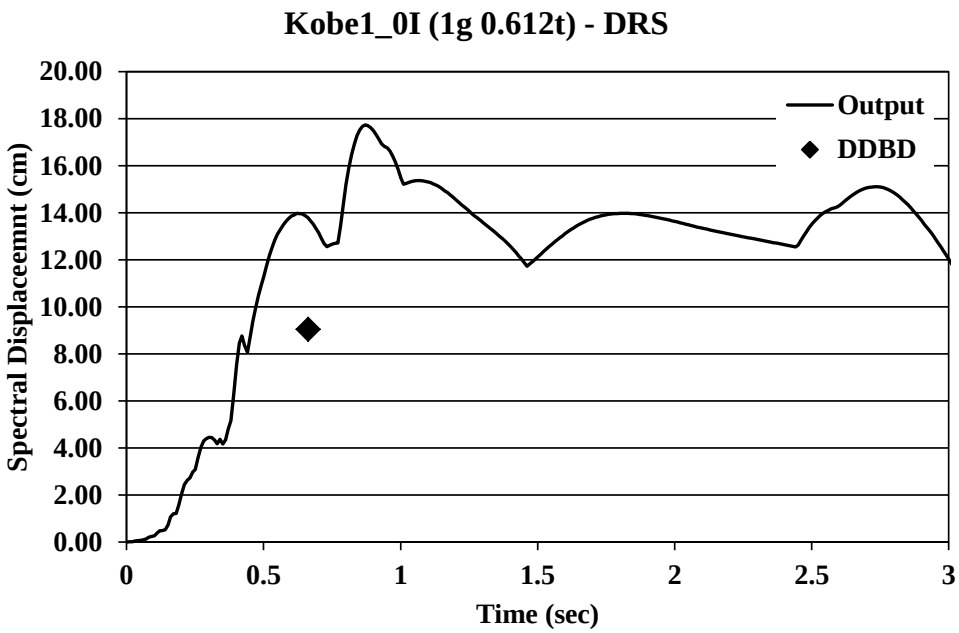

Figure 6.317 Shake Table Test 2 – Kobe Inverse #2 – Inverse DDBD Results (ξ=5%)

6.6.8 Shake Table Testing Conclusions

The results of the two experimental shake table tests conducted which are summarized in Table 6.3, provided four key conclusions that were of importance to this research project. First and most important, the grouted shear stud connection configuration that was developed was shown to adequately behave as a modified weld protected connection when subjected to dynamic loading replicating actual earthquake ground motions. As was the case with large scale quasi – static testing, the connection configuration was able to mitigate any undesirable failure modes by properly locating damage in the form of pile wall local buckling in the intended critical demand region below the capacity protected portion of the connection. Although this was shown to be the case with quasi – static large scale testing, as has been noted, the results of the shake table tests help mitigate any uncertainties regarding the capabilities of the connection to behave as anticipated when subjected to actual seismic loading.

Table 6.3 Shake Table Test Peak Response Results

Test #	Record	M_W	PGA (g)	Max Disp. (in)	Max Drift (%)	$\mu_{\Delta max}$
1	Mineral VA	5.8	0.135	0.33	0.62	0.40
1	El Centro	6.9	0.359	1.03	1.94	1.24
1	Waimea	6.7 (M_L)	1.057	0.84	1.58	1.01
1	Angol	8.8	0.935	0.84	1.58	0.98
1	Pacoima Dam	6.4	1.530	1.61	3.04	1.93
1	Tarzana #1	6.4	1.920	2.92	5.51	3.50
1	Tarzana #2 Inv.	6.4	1.920	2.81	5.30	3.37
1	Kobe	6.9	0.821	3.67	6.92	4.40
2	Kobe	6.9	0.821	3.16	5.96	3.79
2	Kobe Inverse	6.9	0.821	2.75	5.19	3.29
2	Kobe 1.3 Inverse	6.9	0.821	4.68	8.83	5.82

Secondly, since the design of the grouted shear stud connection region differed (beyond the 3/8 scale factor) from that of the large scale prototype specimen, but remained within the confines of the recommended design model, the tests also served as a validation of these recommendations. The explicit requirements and limitations of this design model are discussed in detail in subsequent sections of this document.

Third, it was found that the shake table test piers were capable of withstanding larger deformation demands than the large scale prototype specimen which was evaluated in phase 2 test 6. As has been noted, the large scale specimen subjected to the balanced reverse cyclic three cycle set load history was capable of withstanding a ductility demand of 2 – 3 prior to the development of significant local buckling of the pile elements resulting in system strength loss. Contrarily, the first shake table specimen was capable of withstanding a displacement ductility demand of 4.40, and the second 5.82 prior to the development of significant local buckling which occurred during the Kobe record in both cases. Also in both cases, strength loss was not noted to occur as these maximum displacement ductility demands were developed. This finding likely suggests that the three cycle set load history is more demanding than actual seismic loading which may contain less displacement reversals

and that results obtained from the large scale tests with balanced load histories are likely conservative.

Lastly, it was found applying a series of displacement records to the first specimen allowing cumulative yielding and damage to occur produced severe local buckling with a less demanding record than when an initial “maximum” event was conducted in the second test. However, the comparison also showed the force – displacement response characteristics of the two tests to be essentially the same with the exception of an initial residual displacement in the first test. This may suggest the development of local buckling has a larger effect on subsequent records than the record during which the buckling occurs. As has been discussed, less demanding records applied after Kobe 1.0 in the first evaluation displayed strength loss, while a more demanding record following Kobe 1.0 in the second evaluation did not.

Chapter 7: Steel Truss Pier Evaluation

7.1 General Discussion

Unlike the other tests in the first and second phase of the steel pier project at NCSU, one experimental evaluation in this research project did not focus on developing or evaluating a steel pipe pile to cap beam moment resisting connection. Alternatively, the test was aimed at evaluating the global hysteretic performance and controlling failure modes of a truss style steel pier specimen subjected to lateral loading. The truss style pier, shown in Figure 7.1, was designed to be a full scale prototype of existing piers which were used by AKDOT in the Gustavus-Causeway Replacement project. The intention of the experimental and analytical evaluations that were conducted was to evaluate the performance of the existing system as opposed to developing improvements for future construction. Consequently, the test specimen was designed to be nominally identical to that of the two column pier layout shown in the shop drawings of the causeway replacement project which were provided by AKDOT to NCSU and are included in the appendix of this document. In addition to the lateral load placed on the pier in the experimental evaluation, vertical dead load representative of superstructure weight was also applied to the specimen to accurately model the behavior of the system when subjected to seismically induced forces which would of course occur under the presence of superstructure dead load.

Figure 7.1. Truss Style Steel Pier Specimen

7.2 Truss Pier Design and Construction

The experimental specimen was designed to essentially be a copy of existing truss style piers in Alaska as has been mentioned. Consequently, no engineering design work was conducted by the researchers in order to develop the specimen configuration which was modeled after provided shop drawings. However, it was necessary to choose a pile length that could be accommodated in the laboratory. Pinned base connections, shown in Figure 7.2, were used as physical boundary conditions in the experimental set up as was done for other tests in the project. The pinned bases were intended to mimic the point of inflection which would occur in the bending moment gradient along the piles of an actual driven pile system subjected to double bending. Since the distance from the cap beam to the point of

inflection in the bending moment gradient of an actual system can be variable depending on depth of fixity and soil stiffness conditions, a reasonable assumption of pile length for the specimen was made with the assistance of AKDOT engineers. A pile length of 17 ft. – 2 in. from the point of inflection to the center of loading was chosen as a reasonable dimension that could be accommodated in the laboratory.

Figure 7.2 Truss Pier with Laboratory Pinned Base Connection

As shown in Figure 7.3, the design utilized an ASTM A572 Gr. 50 triple wide HP12x53 cap beam with ASTM A36 C9x15 bracing elements and 24 in. x 0.500 in. piles manufactured to the material specifications of ASTM A500 Gr. B or better. In addition, ASTM A572 Gr. 50 cap beam stiffeners and ASTM A36 gusset plates, shown in Figure 7.4, were used in the design and were connected to the main elements of the pier with 1/4 in. shop fillet welds. All welds connecting the bracing elements to the gusset plates were detailed as 1/4 in. and were field welded. In addition, the piles were connected to the cap beam soffit with 1/2 in. fillet

welds also placed in field conditions in an overhead position. Although the weld sizes were detailed to match that of the existing system, the field welding procedure may have differed from the standard practice of AKDOT should all welds be placed in shop conditions and the truss assembly shipped as one piece in the construction of the actual structure. However, laboratory restrictions required that the frame be pieced together inside the lab, requiring field welding of the bracing elements to the gussets and the piles to the cap beam. As a result, some welds were oversized at the completion of the construction process as is shown in Figure 7.5. Any effects of this variance from the existing structure, assuming welds were correctly sized on the existing structure, will be discussed where necessary in this document. Documentation regarding welding of the truss pier specimen including welder certifications, inspector certifications, visual inspection reports, magnetic particle test reports, and shop weld ultrasonic testing reports are included in the appendix of this document.

It should be noted that one potentially impactful variation between the existing structure and the test specimen, was the exclusion of the full penetration splice weld below the truss system in the experimental specimen. The shop drawings of the existing structure indicated that splice welds of the 24 in. piles would be placed 1 ft. – 9 in. below the lower two work points of the truss system. The decision was made by the researchers to exclude this weld from the test specimen since it is widely accepted and has been shown in past research (Gonzalez, et. al., 2008) at NCSU that splice welds in plastic hinge regions or other regions of high strain demand can result in a brittle undesirable failure mode of weld cracking. Considering this knowledge and the desire to test the unknown behavior of the truss system, not the ductility of a pipe splice weld, the decision was made not to include these welds in the specimen design. The last variation to note was the decision to place notches in the outside transverse stiffeners of the cap beam to allow post-tensioning bars to extend along the length of the cap beam resting in the notch as part of the loading system, as is discussed in subsequent sections of this document. The presence of this notch was expected to have negligible impact on the performance of the system.

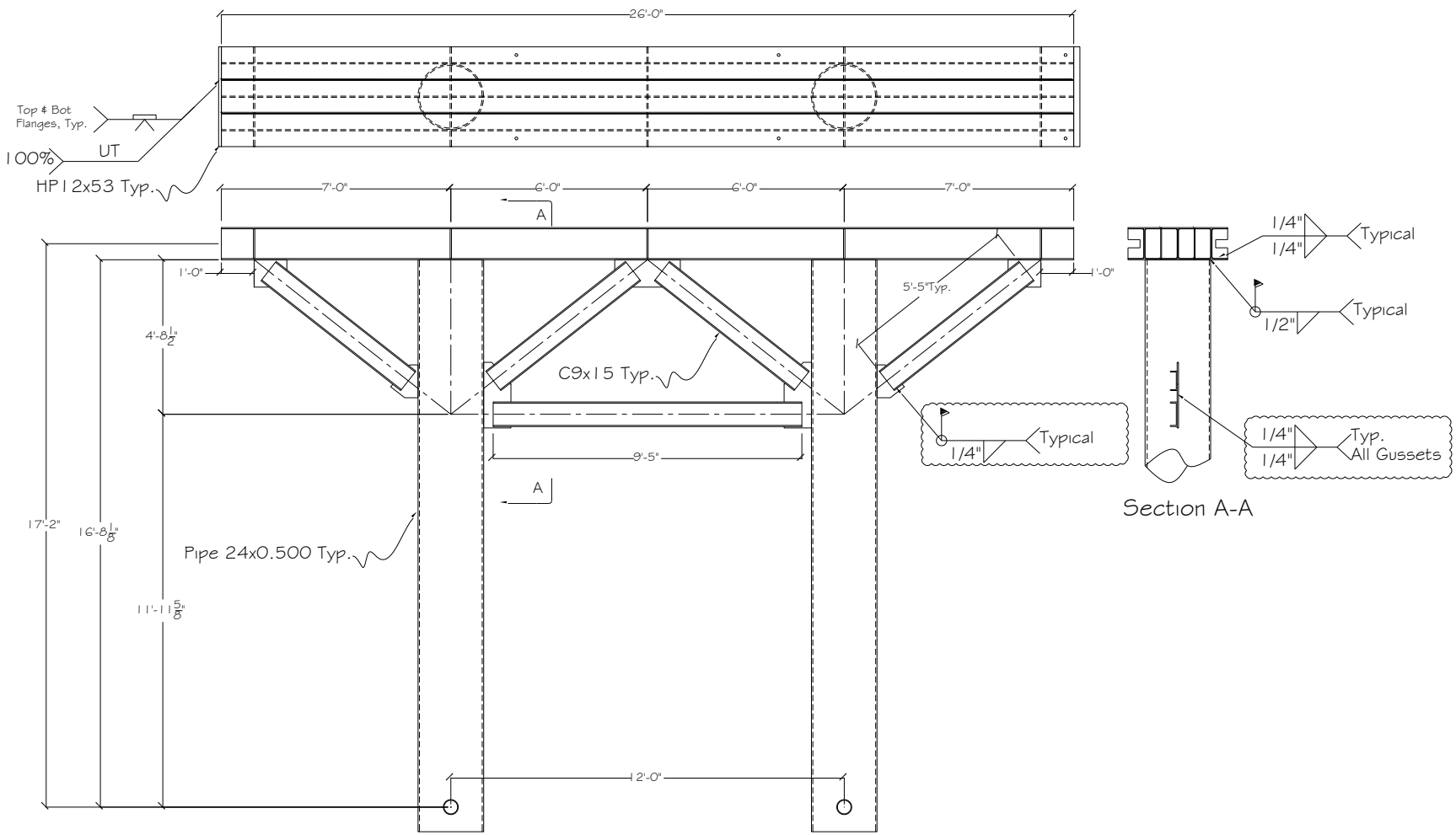

Figure 7.3 Steel Truss Pier Specimen Configuration

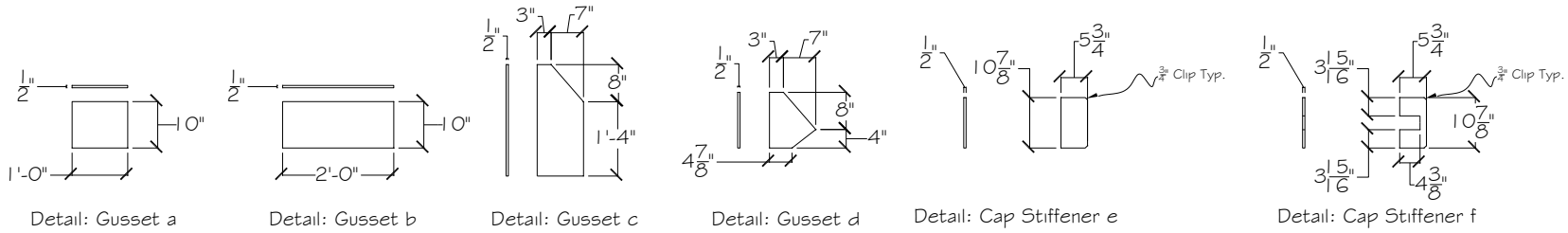

Figure 7.4 Gusset Plate and Cap Beam Stiffener Details

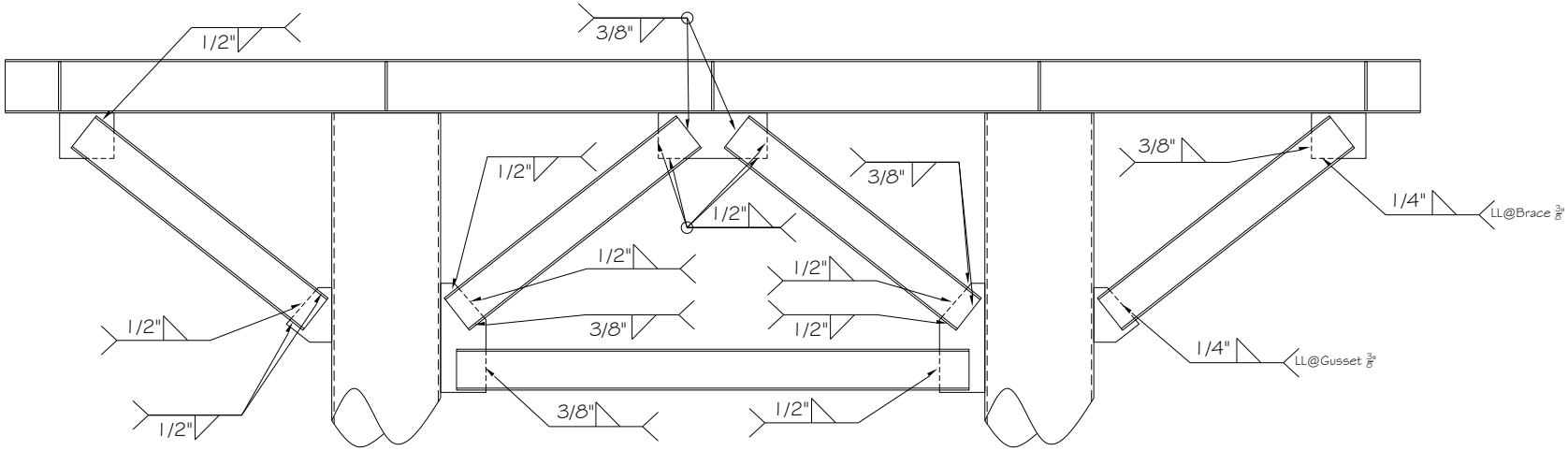

Figure 7.5 Steel Truss Pier As-Built Fillet Weld Sizes (Sizes Not Shown are Correct 1/4")

7.3 Finite Element Analysis Details Specific to the Truss Style Pier

In an effort to predict the hysteretic behavior and controlling failure modes of the truss style steel pier, detailed three dimensional Finite Element Analysis was conducted prior to the experimental investigation, as shown in Figure 7.6. The model contained 3 and 4-node shell elements with a kinematic bi-linear hardening material models which considered the expected stress strain behavior of the materials listed in Table 4.2. In this case, no actual stress strain data from the experimental materials was available so expected material properties were utilized. Geometric non-linearity was also considered in order to capture P-Delta effects, brace buckling (as was done with local buckling for other models), and other possible occurrences of local buckling throughout the system. As is subsequently discussed, the FEA was used not only to predict the cyclic hysteretic response of the system, but in this case also to develop the experimental cyclic loading procedure from the results of a monotonic loading analysis.

As with other Finite Element Models, the analysis used mesh independent tie definitions to define connectivity between the various elements of the system such as the brace to gusset plate connections. As has been noted in prior chapters, this method of defining connectivity restricts nodes on independent parts within a specified spatial tolerance to conform to the same displacements and rotations during the analysis. Although this method of modeling makes the analysis easier to conduct since welds are not required to be modeled, the associated limitations and assumptions should be noted. The most prominent of these limitations is the inability of this modeling procedure to capture the potential limit state of weld cracking, or base material cracking, since no welds were included and no cracking models were defined. Additionally, since no extreme convergence study was conducted in the gusset plate regions, any stress and strain concentrations in very small areas (edges of the gussets for example) should be understood to be of questionable accuracy. However, this basic modeling procedure has shown for pasts tests to capture local buckling, connection

behavior, global behavior, and stress and strain concentrations over reasonably sized regions in a manner comparable to that of the experimental investigations.

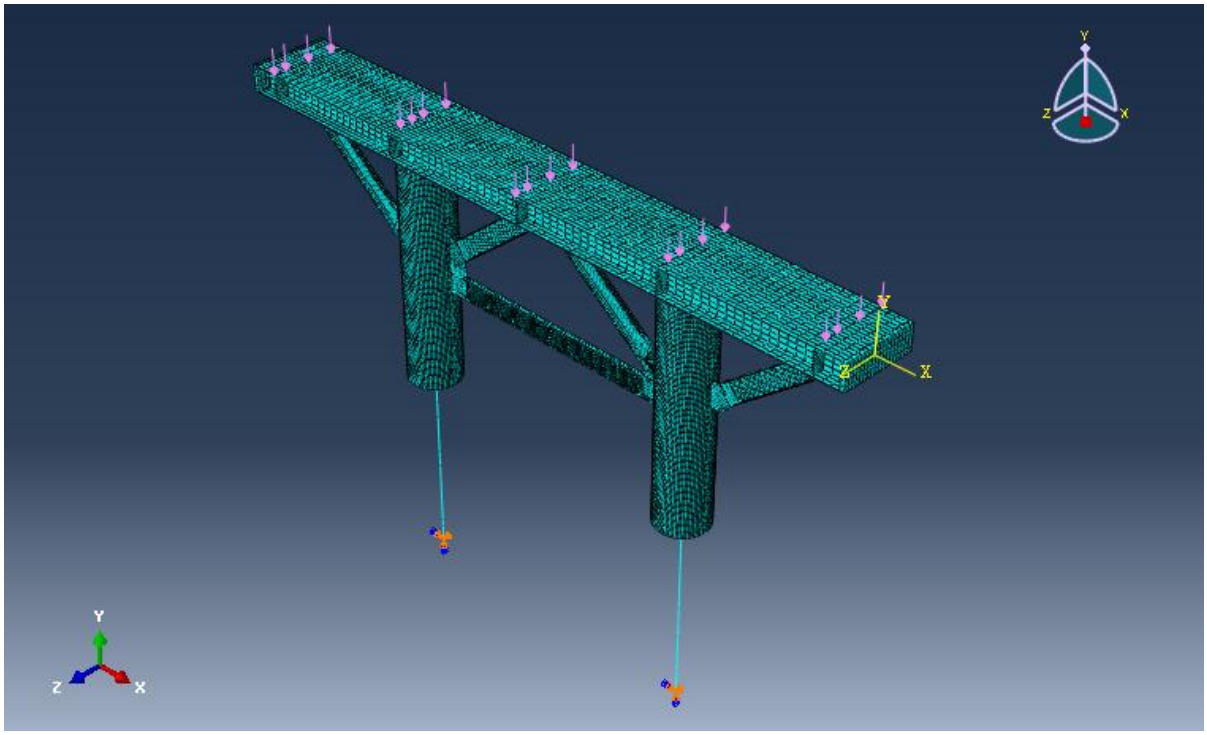

Figure 7.6 Truss Pier Three Dimensional FEM with Vertical Dead Loads

7.4 Lateral Load History and Instrumentation Specific to the Truss Style Pier

The test specimen was laterally loaded using a 440 kip MTS hydraulic servo-controlled actuator attached to a reaction wall as shown in Figure 7.7 similar to that of other test in this project although at a higher level on the reaction wall. However, the definition of the applied lateral displacement history differed from the three cycle set history used in othre tests which has been described in detail in prior chapters of this document. As has been noted, a critical assumption in the definition of a three cycle set load history is that a plastic hinge section

forms in the pile elements and that the rest of the system remains in the elastic range of response. In the case of the truss style pier, FEA conducted prior to testing that included the effects of vertical dead load, as is discussed in subsequent sections, showed that when subjected to a monotonic push-over displacement history the system experienced plastic behavior at loads lower than that calculated by (4.1) for a pile hinging mechanism. As shown in Figure 7.8, the analysis predicted a considerable degradation of tangent stiffness below the calculated first yield force of 168 kips assuming a pile hinging mechanism immediately below the truss assembly and an expected material yield stress of 58.8 ksi based on *ANSI/AISC 341-10* (AISC, 2010) and "AASHTO Guide Specifications for LRFD Seismic Bridge Design" (AASHTO, 2009) material over strength R_y values. The change in stiffness appeared to be an effect of buckling of the interior compression brace at 3.9 in. of displacement as shown in Figure 7.9 through Figure 7.11. These figures relate the cap beam displacement (U1 output) to the out of plane displacement of the brace (U3 output) at subsequent analysis increments as brace hinging began to form. In addition, local areas of inelasticity were shown to develop near the gusset plates in the pile, as shown in Figure 7.12, which may have also contributed to the reduction in stiffness.

As a result of the multiple sources of inelasticity, the decision was made to define the first yield displacement as 3.9 in. which coincides with initiation of compression brace buckling (defined as a loss of load carrying capacity of the member). Note that the internal compression brace had already experienced over 1 in. of out of plane displacement at this point in the analysis prior to the formation of a hinge. Having determined a yield displacement, the cyclic load history was then defined with single 1/4 increments of this yield displacement until a full cycle at 3.9 in. was conducted. This was followed by typical 3 cycle sets of displacement ductility increments where the ductility 1 was determined to be 5.08 in. by extrapolating the first yield displacement by the ratio of maximum system strength to the system strength at the first yield displacement as determined by FEA. This ratio was found to 1.303 from FEA predictions which resulted in the load and displacement histories shown in Figure 7.13 and Figure 7.14 respectively.

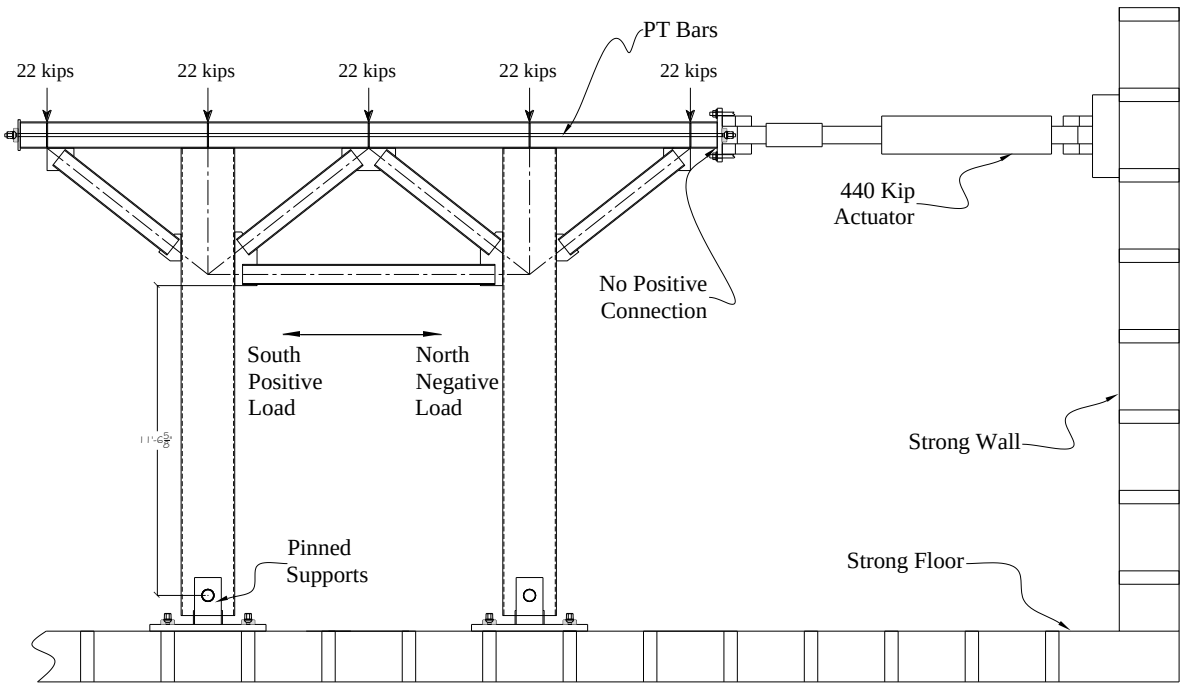

Figure 7.7 Truss Pier Laboratory Experimental Set Up

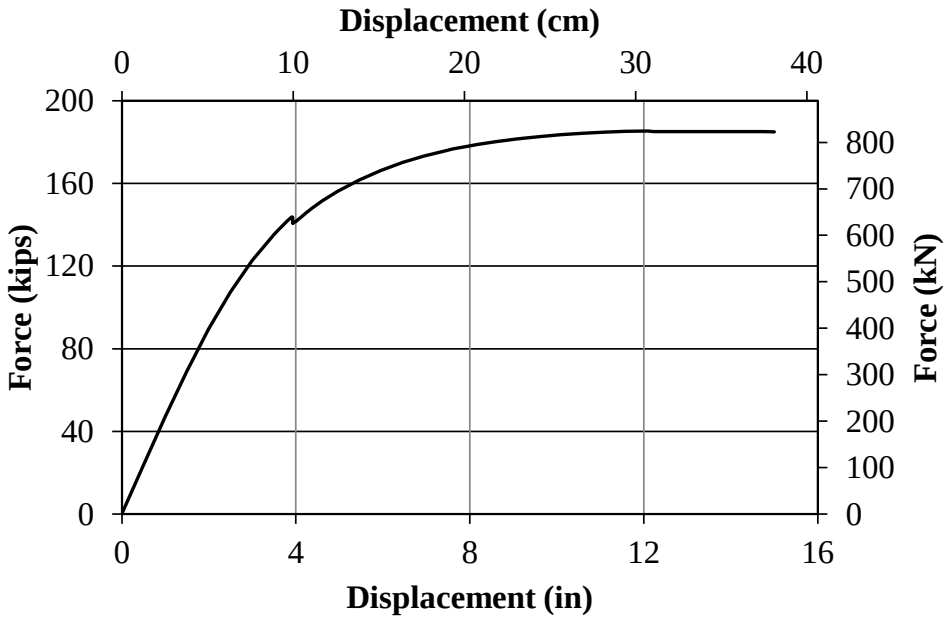

Figure 7.8 Truss Pier Monotonic Force-Displacement FEA Prediction

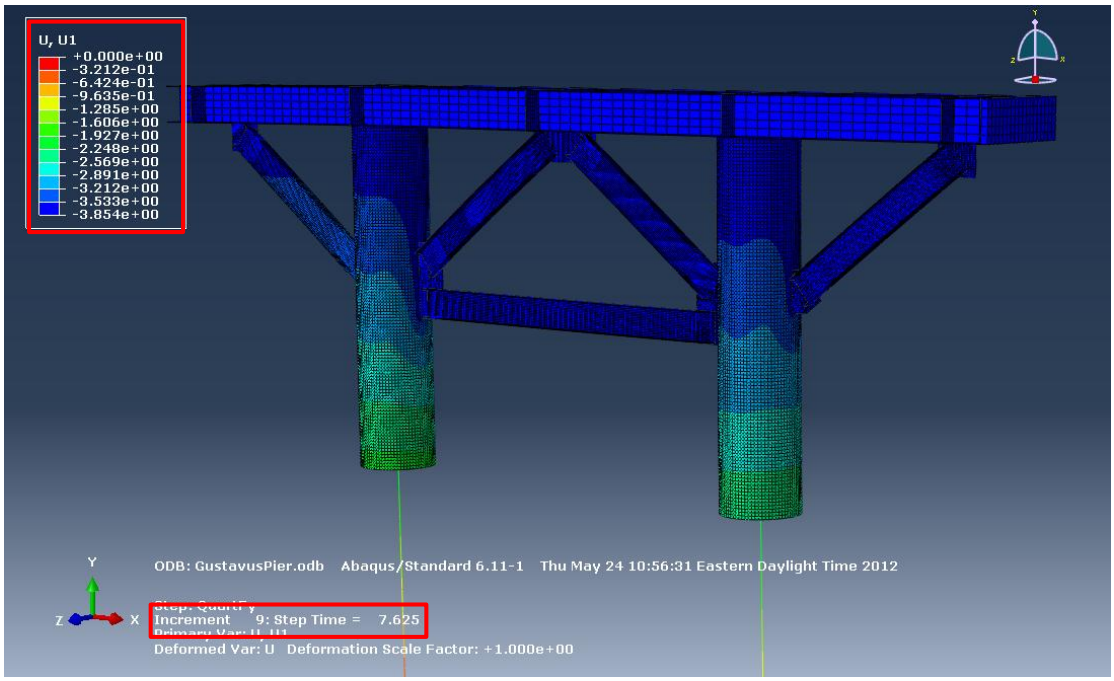

Figure 7.9 FEA – Monotonic Loading Displaced to 3.9 in (U1)

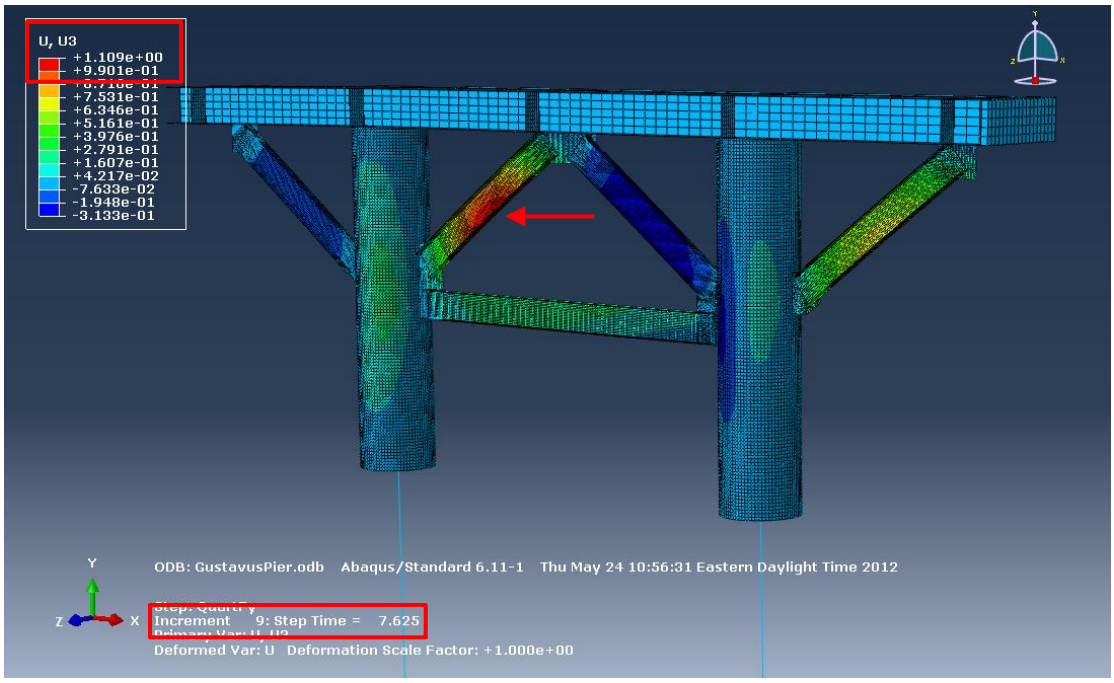

Figure 7.10 FEA - Buckling of Compression Brace (U3) at 3.9 in (U1)

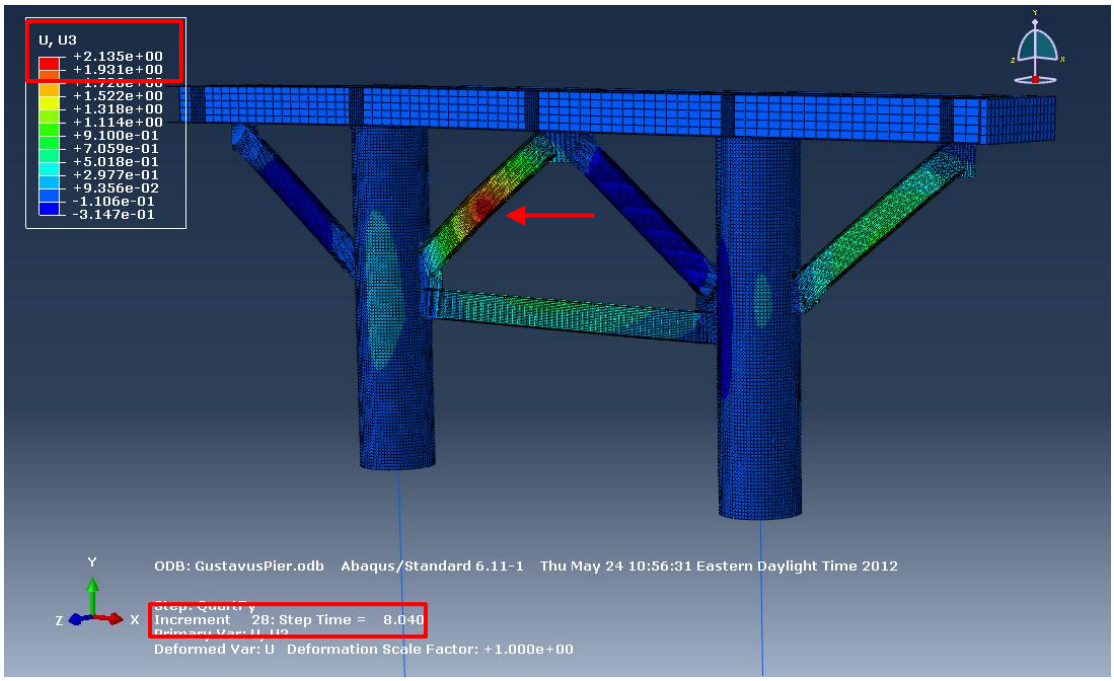

Figure 7.11 FEA - Propogation of Buckling of Compression Brace (U3) Past 3.9 in (U1)

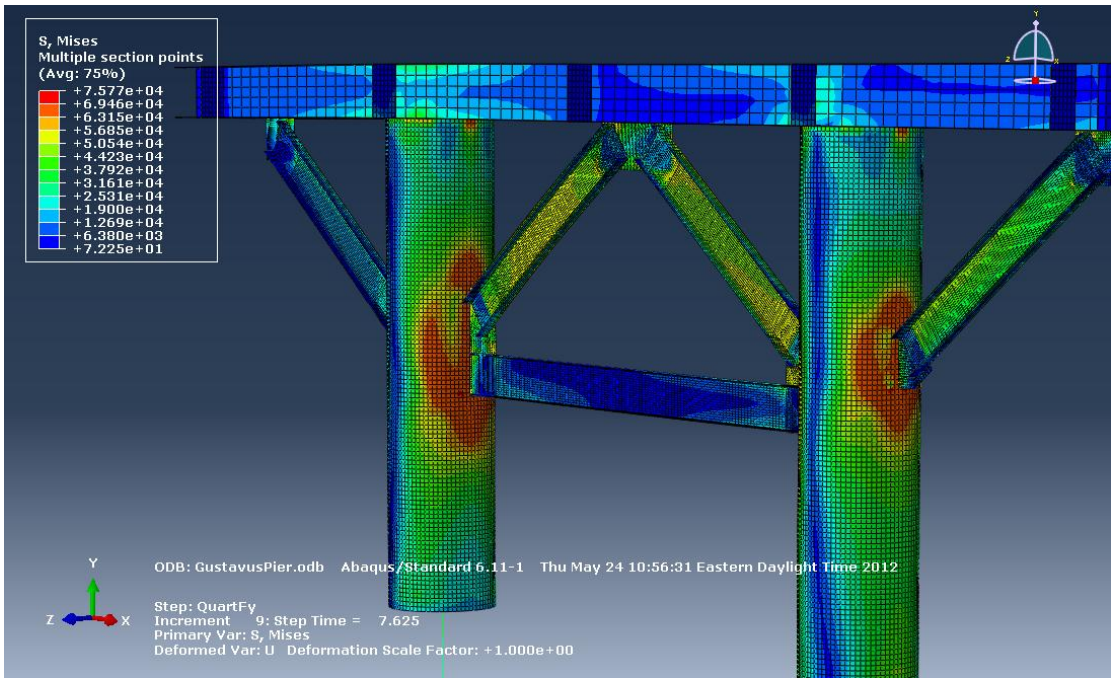

Figure 7.12 FEA - Locations Local of Inelasticity

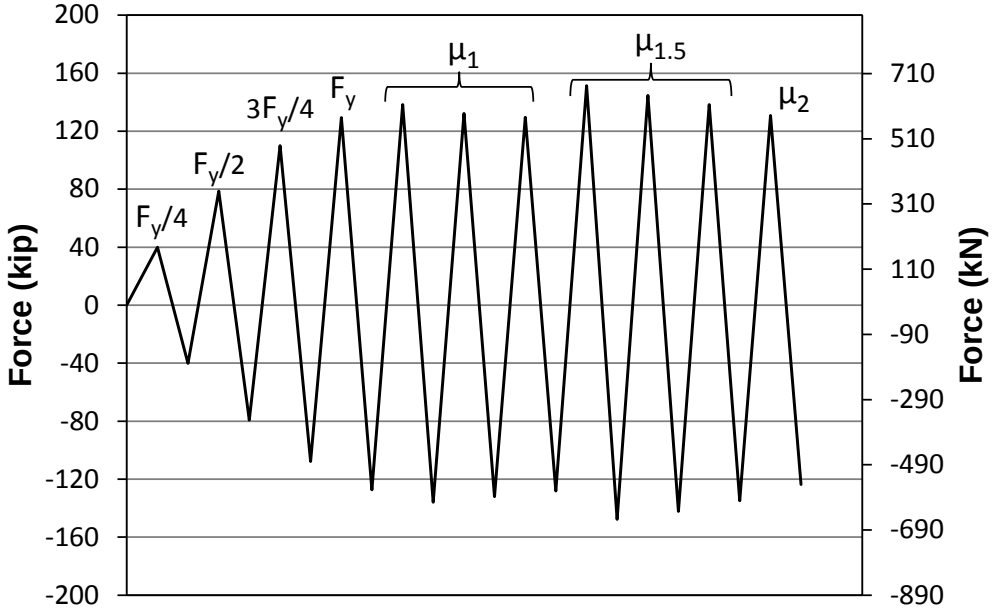

Figure 7.13 Truss Pier – Experimental Load History

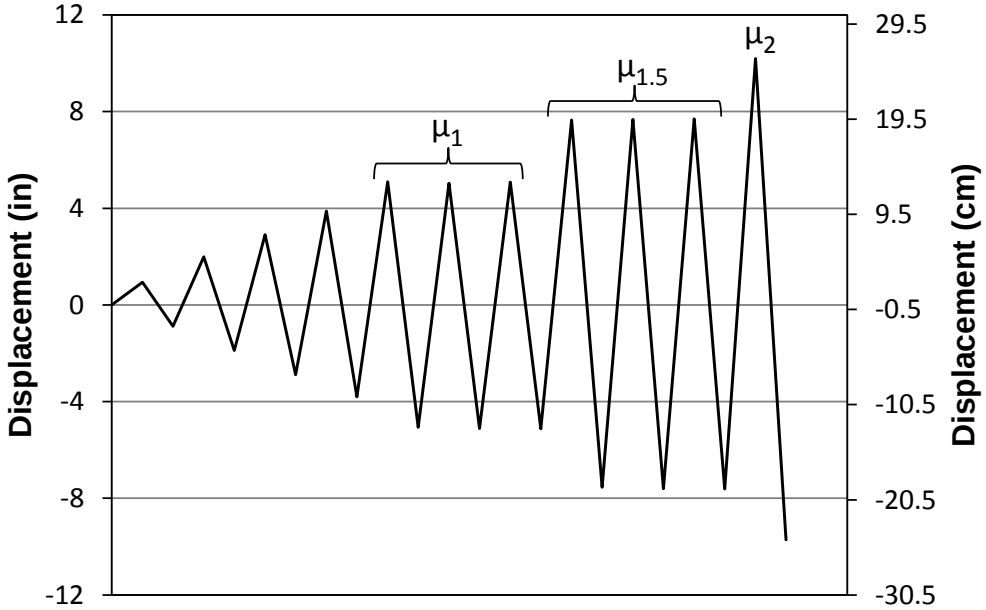

Figure 7.14 Truss Pier – Experimental Displacement History

The physical application of the lateral load in the experimental evaluation differed from other tests in this project because of a concern that due to buckling of brace members, pushing and pulling the specimen from a loading plate welded to one side of the pier may not produce a symmetric loading pattern. In an actual system, lateral load would be transferred to the pier system by the superstructure girders when superstructure shaking occurs due to seismic excitation. Replicating this condition in the experimental evaluation was considered but was found to be difficult due to laboratory restrictions. As an alternative compromise, it was decided that the pier would be pushed from both sides to produce a symmetrical loading condition which would more accurately represent the actual system loading. This was achieved by employing loading plates on both ends with post-tensioning bars traveling the length of the specimen, as shown in Figure 7.7, and providing no positive connection at the actuator end of the specimen between the loading plate and the pier. Hence, the actuator would push the specimen when in compression and pull the specimen from the opposite end of the pier with the post-tensioning bars when in tension. This design ensured that the specimen would be pushed from one end and then the other to produce the desired symmetric loading pattern.

The instrumentation used in experimental evaluation consisted of traditional laboratory instrumentation as well as the Optotrak motion sensing system which tracks the location of LED markers adhered to the specimen. The traditional equipment consisted partially of string potentiometers to measure cap beam displacement (SP1-2), any unanticipated pinned base assembly movement (SP3-6), and brace out of plane displacement (SP7-11) as shown in Figure 7.15. In addition, the traditional measurement equipment also consisted of electrical resistance strain gauges to monitor axial strains in the braces, longitudinal pile strains, cap beam bending strains, and gusset plate strains along the brace axis as is also shown in Figure 7.16.

In addition to the traditional instrumentation, a 2” spaced grid of Optotrak LED markers was placed on the east face of each pile at both the cap beam and truss point locations as

shown in Figure 7.16. Marker grids were also placed at the centerline of the internal braces, connection region of the external braces, and on the gusset plates. LED markers placed on the bottom flange of the cap beam at the centerline of the system were used to track cap beam displacement for comparison to string potentiometers 1 and 2 which were oriented along the cap beam axis.

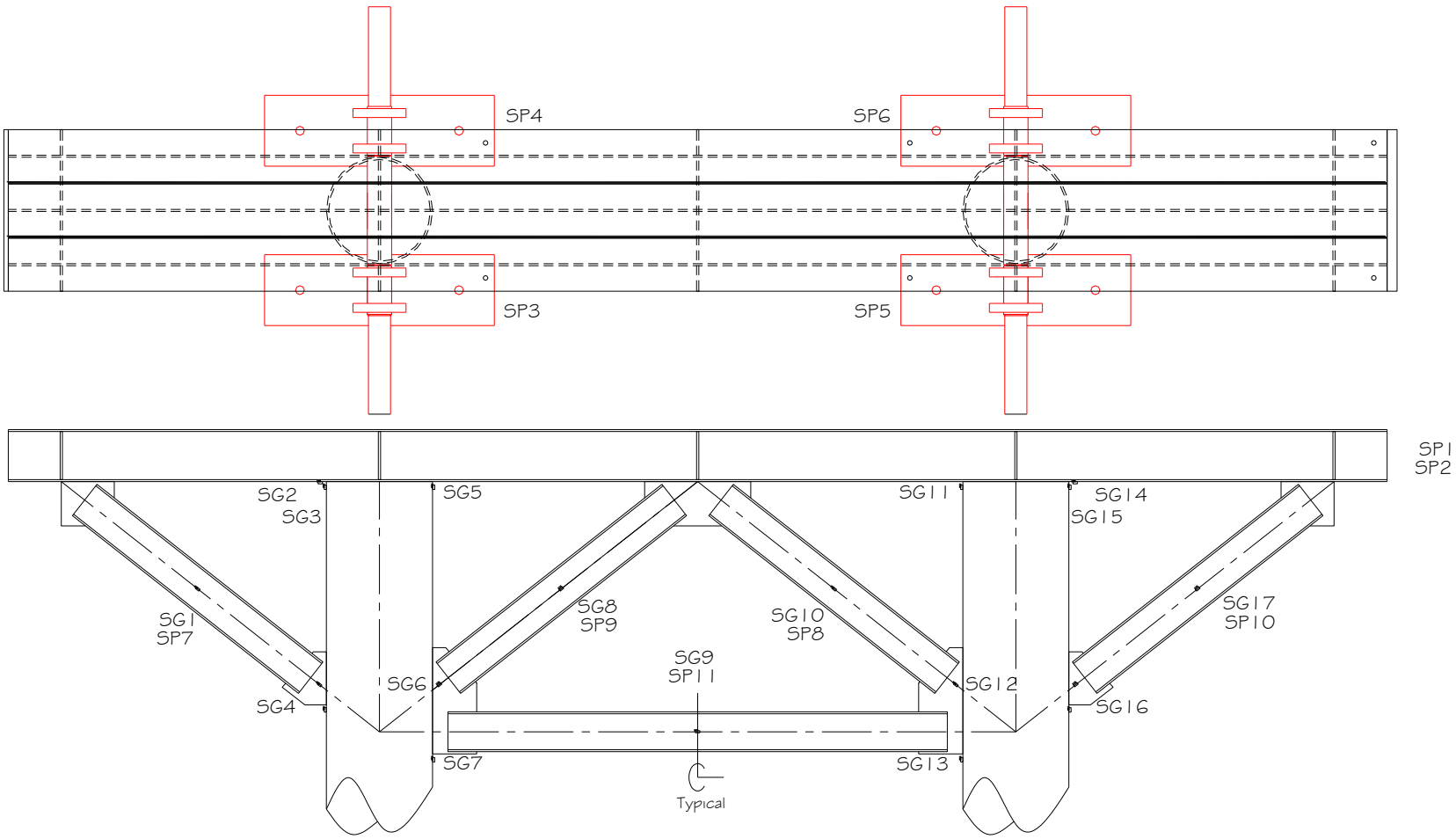

Figure 7.15 Truss Pier Traditional Instrumentation Layout

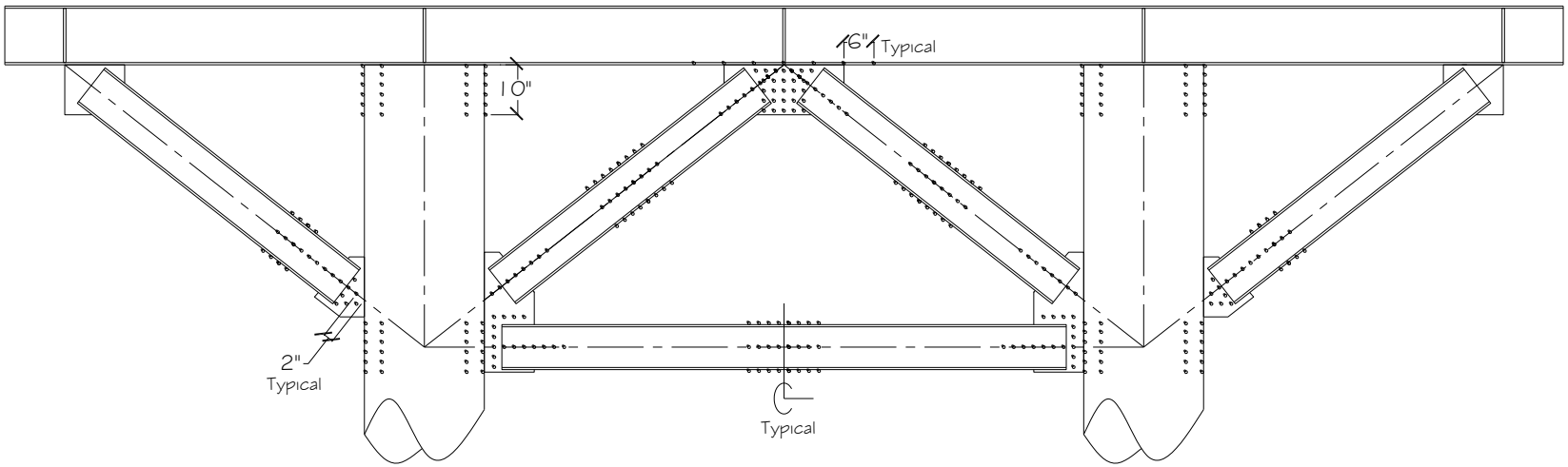

Figure 7.16 Truss Pier Optotrak Grid Layout (2 in. Spacing Typical)

7.5 Vertical Dead Load Considerations

In the case of the truss pier evaluation, the actual calculated dead loads for the Gustavus-Causeway Replacement project, which were provided by AKDOT to NCSU and are included in the appendix of this document, were used to determine the magnitude of vertical load that would be applied to the test pier. The calculations indicated a typical dead load of 108 kips for the entire pier or approximately 21.6 kips per girder location which were intended to be directly over the truss points and piles for a total of 5 girder reactions. Consideration was given to neglecting the effects of the vertical dead load on the hysteretic performance of the pier to ease laboratory set up requirements.

However, FEA conducted prior to testing indicated that strength degradation of the system could be affected and produce non-conservative testing results should the dead load be neglected, particularly at the displacement ductility levels of 3 and 4 should the pier be capable of reaching that level of response. As shown in Figure 7.17 through Figure 7.19, FEA conducted with the cyclic loading history discussed in prior sections, indicated a separation of the force-displacement envelopes in each cycle between the models with and without the inclusion of vertical dead load. Consequently, the decision was made to apply vertical dead to the experimental specimen at what would be the five girder locations in the actual system.

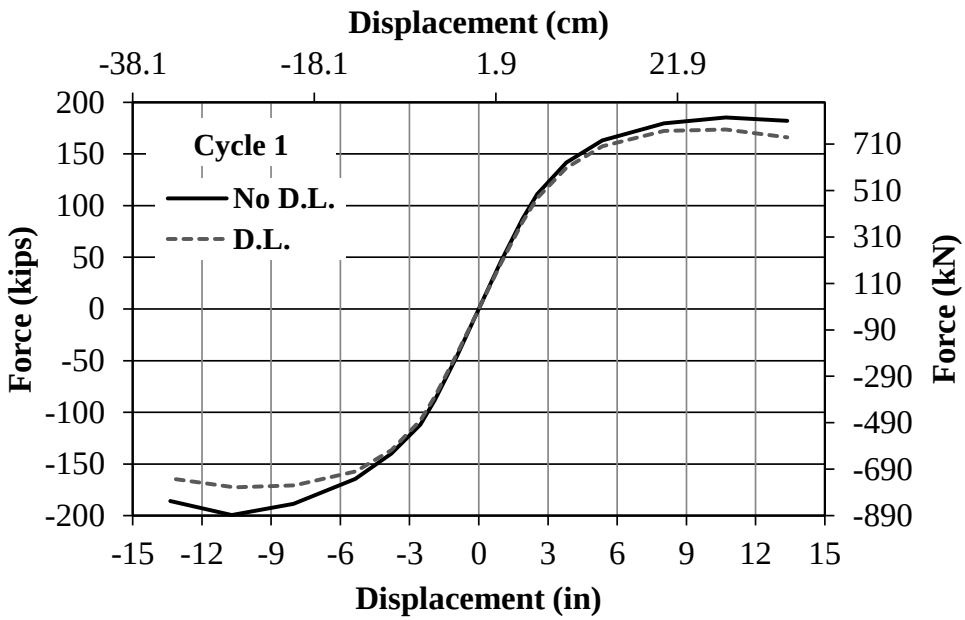

Figure 7.17. Force-Displacement Envelopes No D.L vs. D.L. FEA – Cycle 1

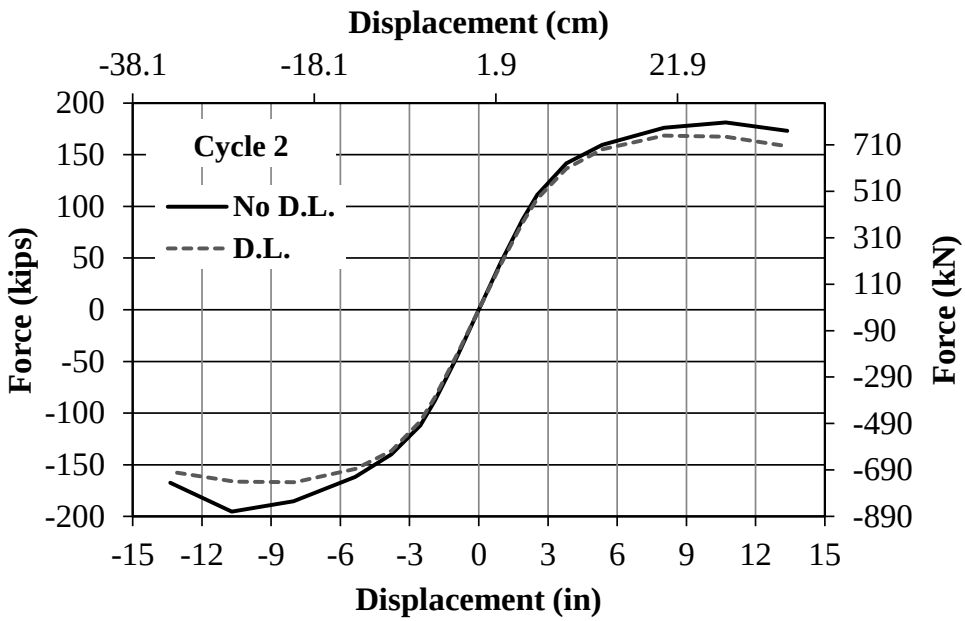

Figure 7.18 Force-Displacement Envelopes No D.L vs. D.L. FEA – Cycle 2

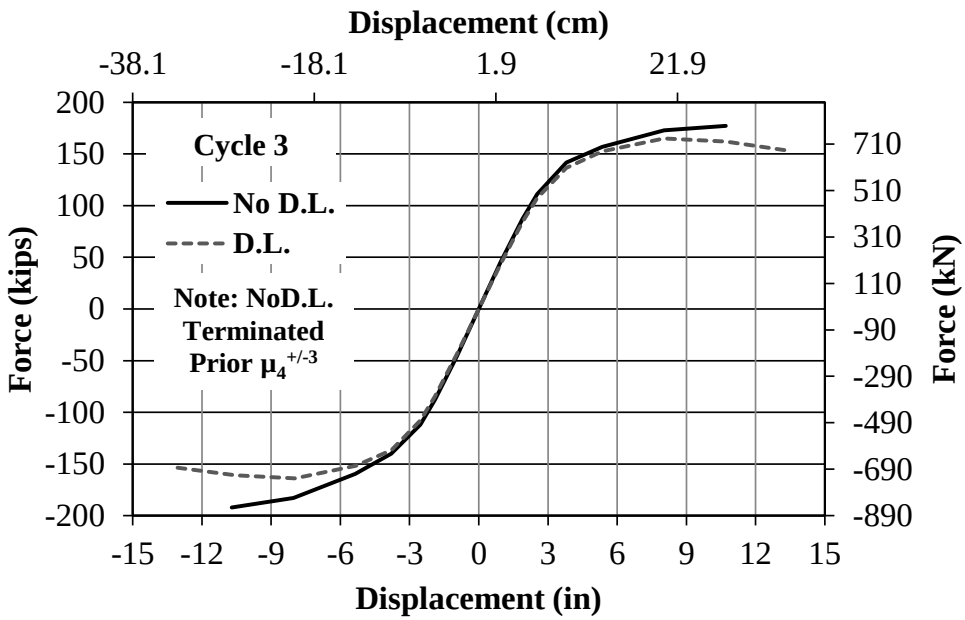

Figure 7.19 Force-Displacement Envelopes No D.L vs. D.L. FEA – Cycle 3

The dead load set up was designed with 5 back-to-back channel section spreader beams, one placed at each girder location, along with 10 twenty ton hydraulic jacks and 5/8 in. diameter post tensioning bars to produce a 21.6 kip reaction at each location as shown in Figure 7.20. To produce the necessary 10.8 kip force from each of the ten jacks, a closed loop hydraulic system was constructed with a manifold that split flow from a hydraulic pump to the ten individual jacks as shown in Figure 7.21. The closed loop hydraulic system also included a nominal 1 gallon pre-charged accumulator intended to accommodate necessary extension and retraction of the jacks due to vertical specimen displacements from lateral loading and system damage, while maintaining a reasonably constant force. The use of the manifold with a single source of hydraulic oil pressure (electric hydraulic pump) allowed the load to be monitored on a single bar with a load cell since the pressure would equalize across all jacks. The results provided from the load cell, shown in Figure 7.22, indicate that a reasonably constant load of approximately 10.8 kips per bar was achieved with the accumulation system with the exception of two peaks which reached approximately 15 kips.

Although it cannot be conclusively confirmed, it is likely that this was a result of the outer bar being monitored which had been shown in FEA to require the largest magnitude of outward stroke from the jack as the external compression brace began to buckle. Consequently this jack was provided the lowest amount of retraction stroke prior to pressurizing the system and may have fully retracted at the peak of a cycle prior to buckling of the external brace. This would allow the load to increase past that provided hydraulic pressure resistance.

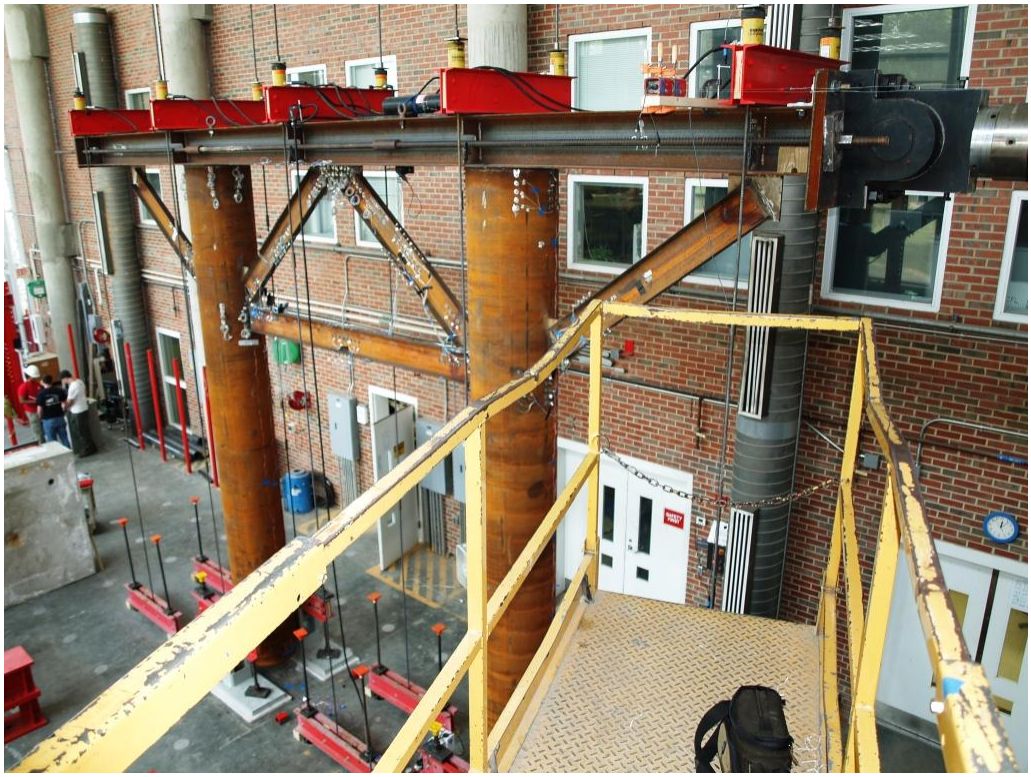

Figure 7.20 Truss Pier Application of Vertical Dead Load with 5 Spreader Beams

Figure 7.21 Truss Pier Vertical Dead Load Manifold System with Accumulator

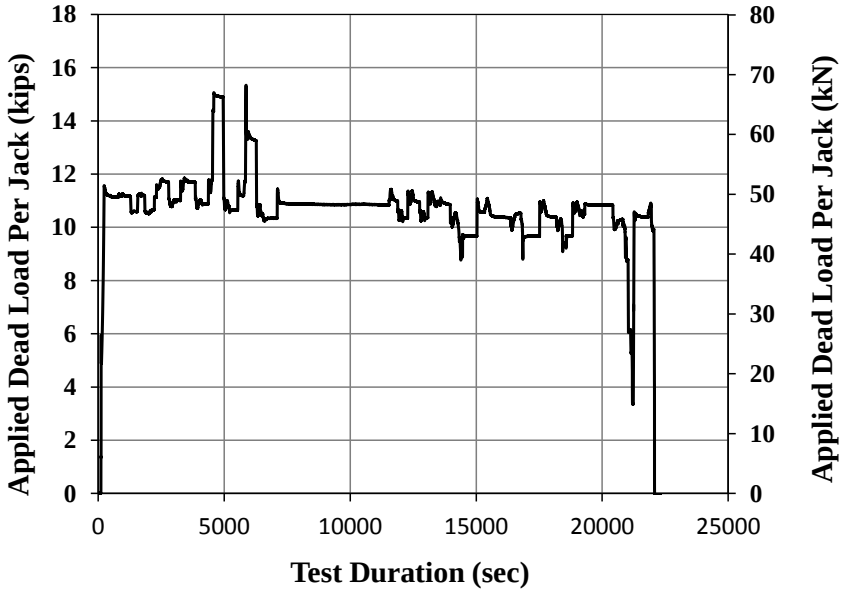

Figure 7.22 Truss Pier Applied Vertical Dead Load

7.6 Elastic Force Distribution

Figure 7.23 and Figure 7.24 provided in this section, display the elastic axial force distribution and moment distribution patterns throughout the system when lateral and vertical loads are applied to the pier. Although the majority of the discussion throughout this chapter will focus on behavior in the inelastic range which will of course alter the axial force and moment patterns, the elastic distribution patterns are provided here to assist the reader in understanding the basic behavior of the system. Force distributions such as compression braces versus tension braces for a given direction of loading may not be as immediately apparent as in the cases of typical two column piers with no bracing.

The line element model used to determine the distribution patterns considered the actual member properties and assumed fully fixed end conditions for all members. Although this may over estimate some of the connection stiffnesses, it is assumed to be reasonable for a basic understanding of system behavior. Additionally, the lateral load (110 kips) was arbitrarily selected as a reasonable magnitude as it was anticipated to be in the linear range of loading. It should also be noted, the program output indicates axial tension with a purple color and negative values and axial compression with a green color and positive values.

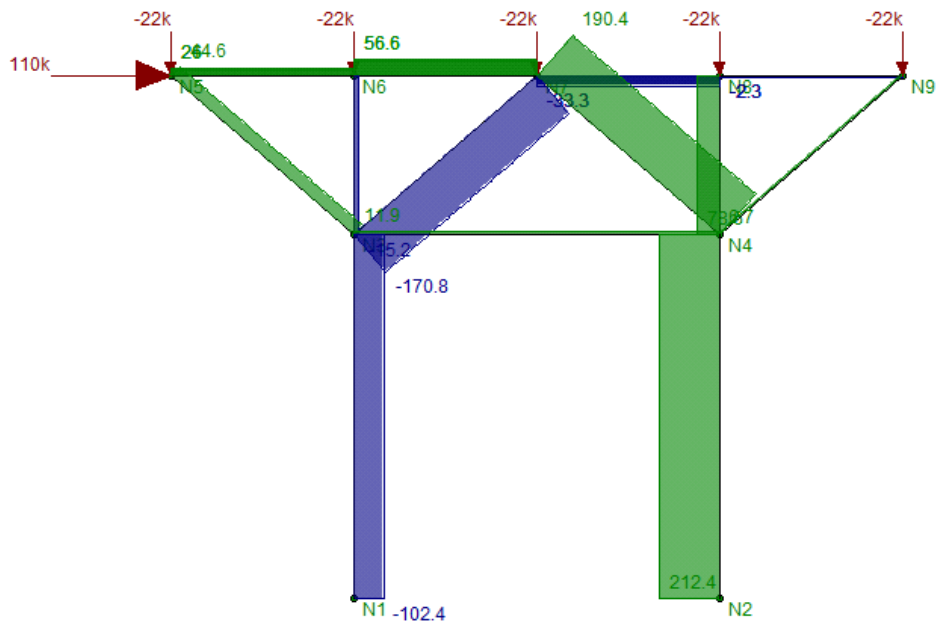

Figure 7.23. Truss Pier Elastic Axial Force Distribution Under Arbitrary Lateral Load

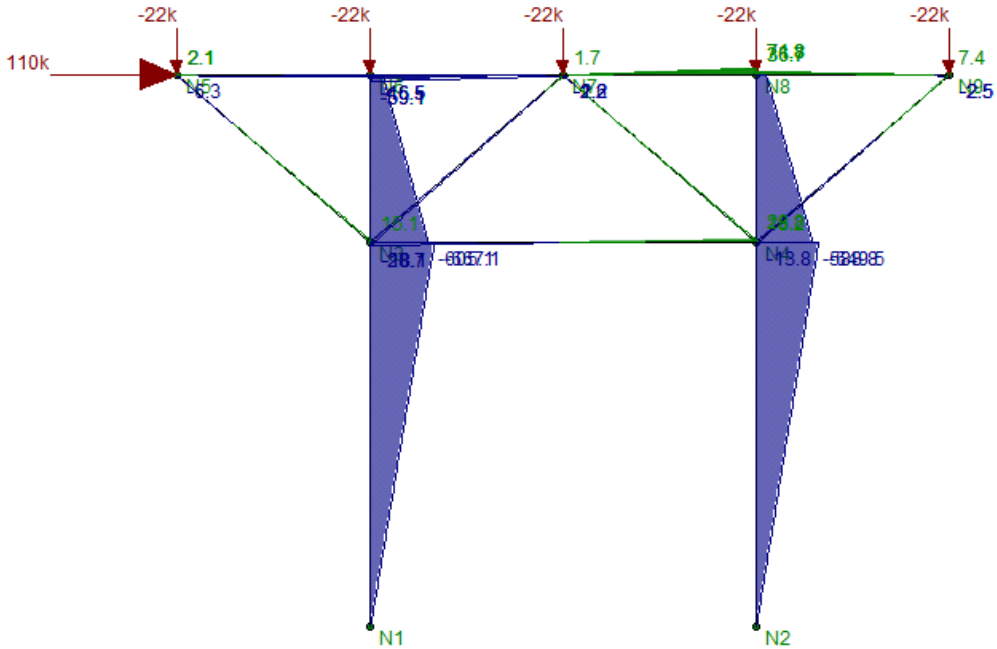

Figure 7.24 Truss Pier Elastic Moment Distribution Under Arbitrary Lateral Load

7.7 Cyclic Finite Element Predictions

In addition to the use of FEA to estimate the effects of vertical dead load on the response of the system and to develop the cyclic load history from a monotonic prediction, the analysis was also used to predict the general cyclic behavior of the pier and to identify potential limit states. The model was subjected to the same cyclic loading protocol that was developed for the experimental evaluation as has been discussed. The results of the analysis showed the behavior to be dominated by buckling of all diagonal braces throughout the cyclic history, again noting the model did not have the capability to predict weld or base material fracture. As is shown in Figure 7.25, the formation of a hinge due to buckling of the interior compression brace was visually noted to begin developing as early as the first cycle of ductility 1. Progression of brace hinging was shown to occur throughout subsequent cycles, as shown in Figure 7.26 and Figure 7.27, eventually reaching magnitudes of out of plane displacement in the ductility 2 level which would likely be unattainable in the experimental test based on engineering judgment.

It is important to note that the analysis predicted residual brace buckling to exist in what was the compression brace as the pier was forced past zero displacement and was subjected to a reversal of loading once brace hinging had developed, as shown in Figure 7.28. As the model was displaced towards the reversal peak the brace tended to straighten and carry an increasing amount of tensile load. It appears that this behavior is what generated the positive change in tangent stiffness that is shown in hysteretic response, Figure 7.29, toward the loading peaks. This effect resulted in a pinched hysteretic behavior compared to that of other piers tested in this project which produce a hysteretic behavior more typical of a Ramberg-Osgood response. However, regardless of the pinched behavior which shows considerable reduced strength at zero displacement, the analysis did predict that the pier would regain strength as it was displaced to the loading peaks of the displacement history.

Although it may be expected that the pier would act to some degree as a moment resisting frame when brace hinging occurred since the piles are welded to the cap beam, the analysis indicated that the system was incapable of developing significant bending resistance in the piles as shown in Figure 7.30 by the lack of significant longitudinal strain development in the pile member. Based on the displaced shape of the model, which depicted warping and prying of the cap beam bottom flange around the pile region, it is likely that the absence of cap beam transverse stiffeners at the extreme fibers of the pile precluded the connection from being able to develop the moment capacity of the piles. As has been noted, stiffeners were placed only at the pile centerline to resist loads from the girder reactions as was the case it the actual system.

Again, the analysis showed that regardless brace buckling the pier was able to regain strength at the peaks of the loading cycle, which indicated that global strength loss due to brace hinging may not be the controlling failure mode. This potential conclusion suggested that brace fracture due to low cycle fatigue in the hinge region or weld/gusset plate fracture may constitute the controlling failure modes. Although these modes of failure were not captured by the FEA, the results did show these regions experienced significant stress and strain demands. For example, the interior gusset at the south pile was shown to experience an area of stress concentration at the top of the gusset to pile weld region as shown in Figure 7.31. In addition, these modes of failure constituted the most likely outcome based on engineering judgment.

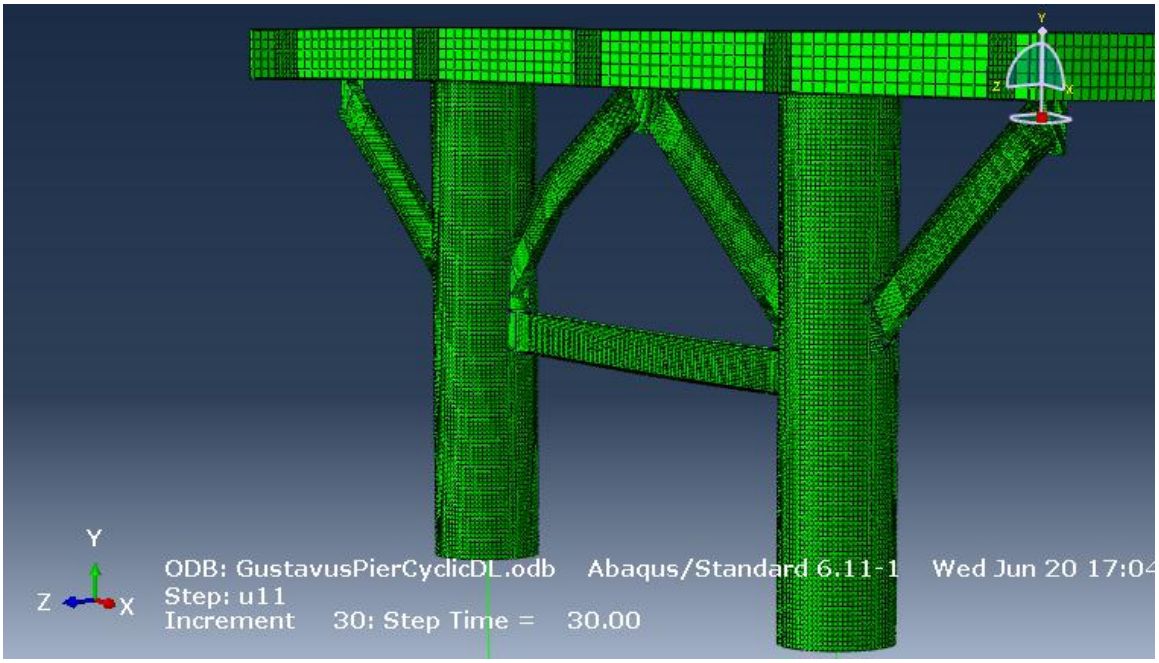

Figure 7.25. FEA - Ductility 1 Cycle 1 (Def. S.F. = 1.0) – Formation of Brace Hinge

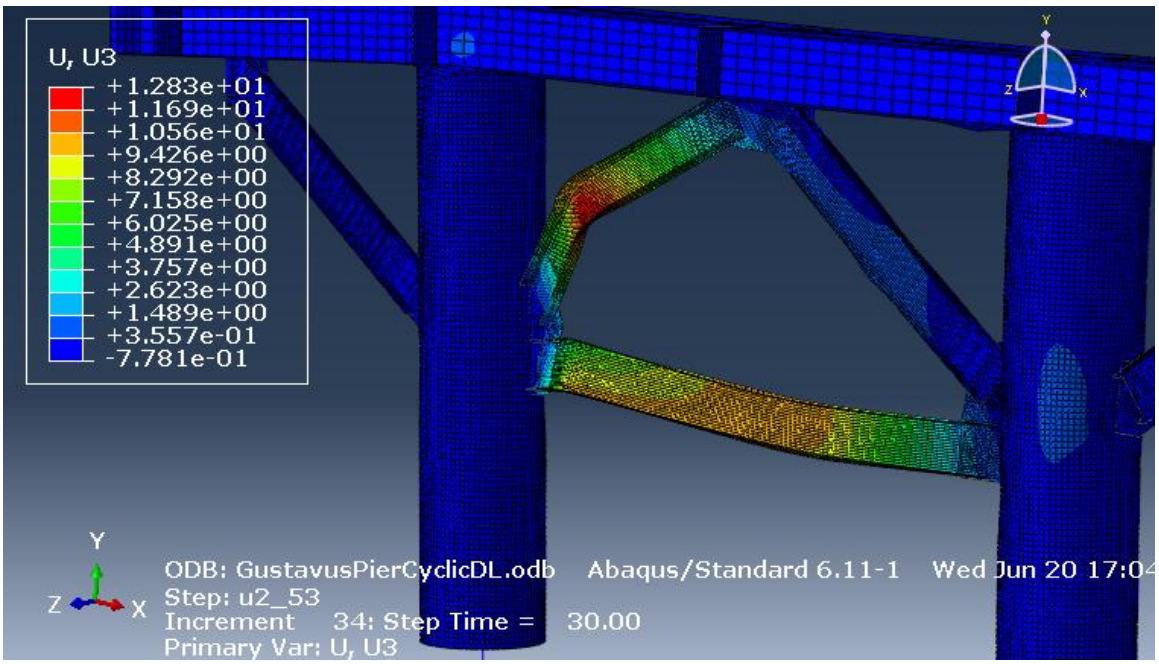

Figure 7.26 FEA - Ductility 2 Cycle 3 – U3 Out of Plane Disp. (in) (Def. S.F. = 1.0)

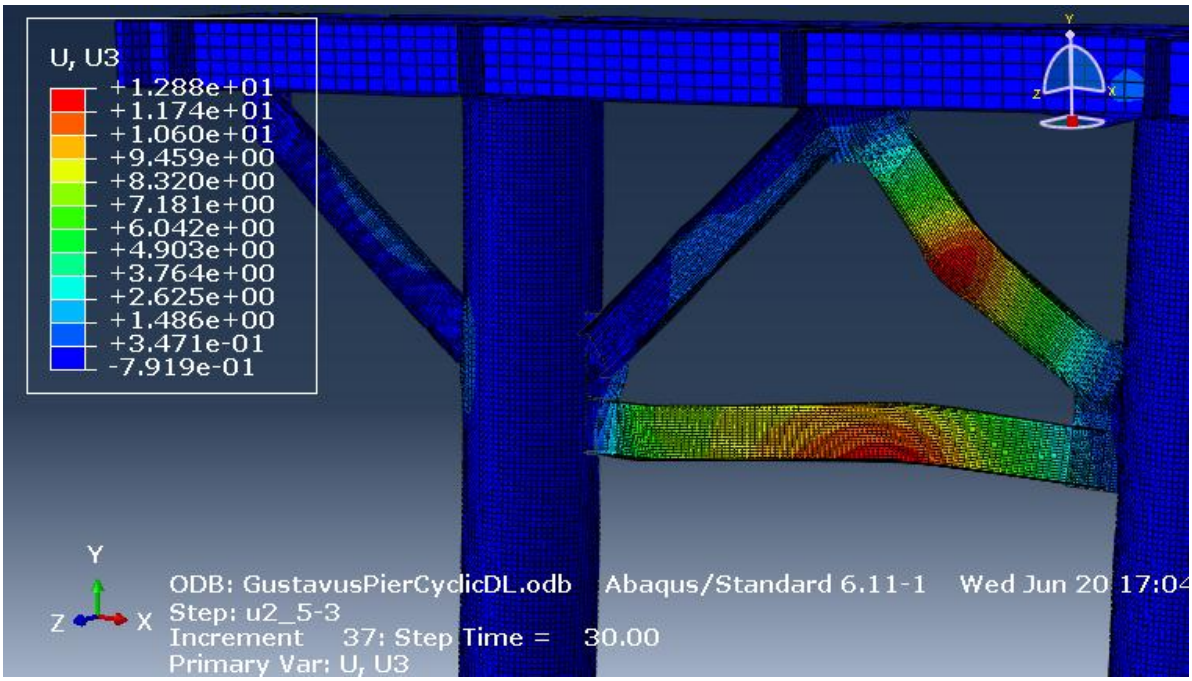

Figure 7.27 FEA - Ductility 2 Cycle -3 – U3 Out of Plane Disp. (in) (Def. S.F. = 1.0)

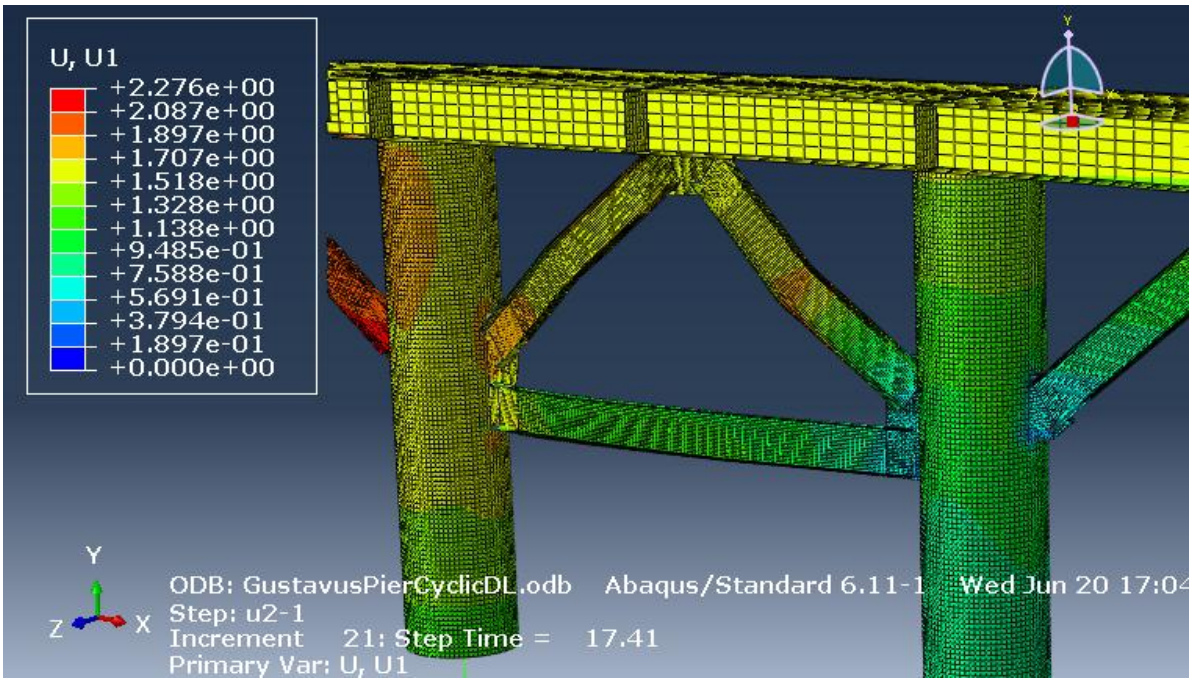

Figure 7.28 FEA Progressing to Ductility 2 Cycle -1 (Def. S.F. = 1.0)

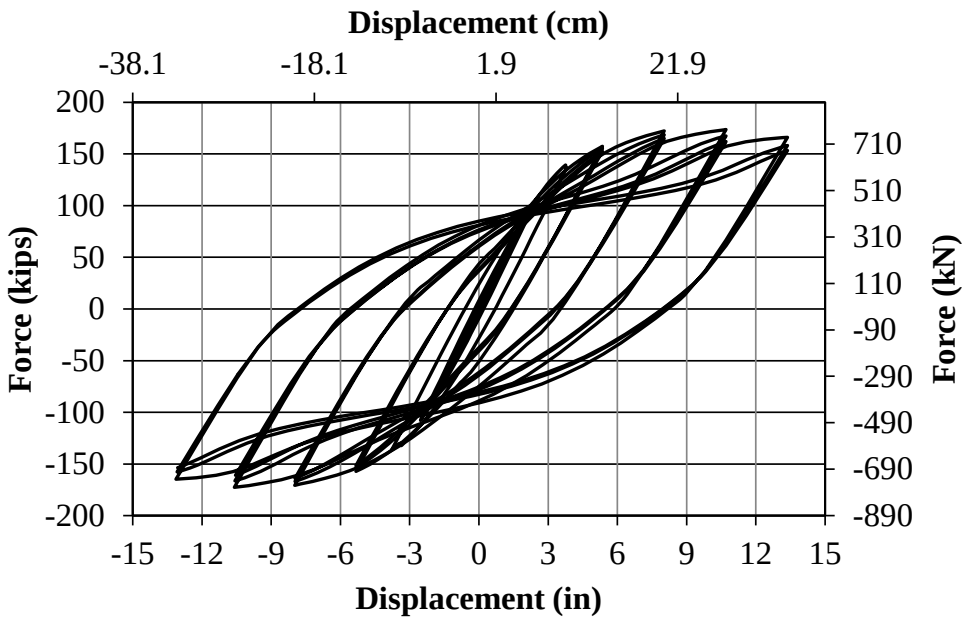

Figure 7.29 Truss Pier FEA – Force Displacement Response

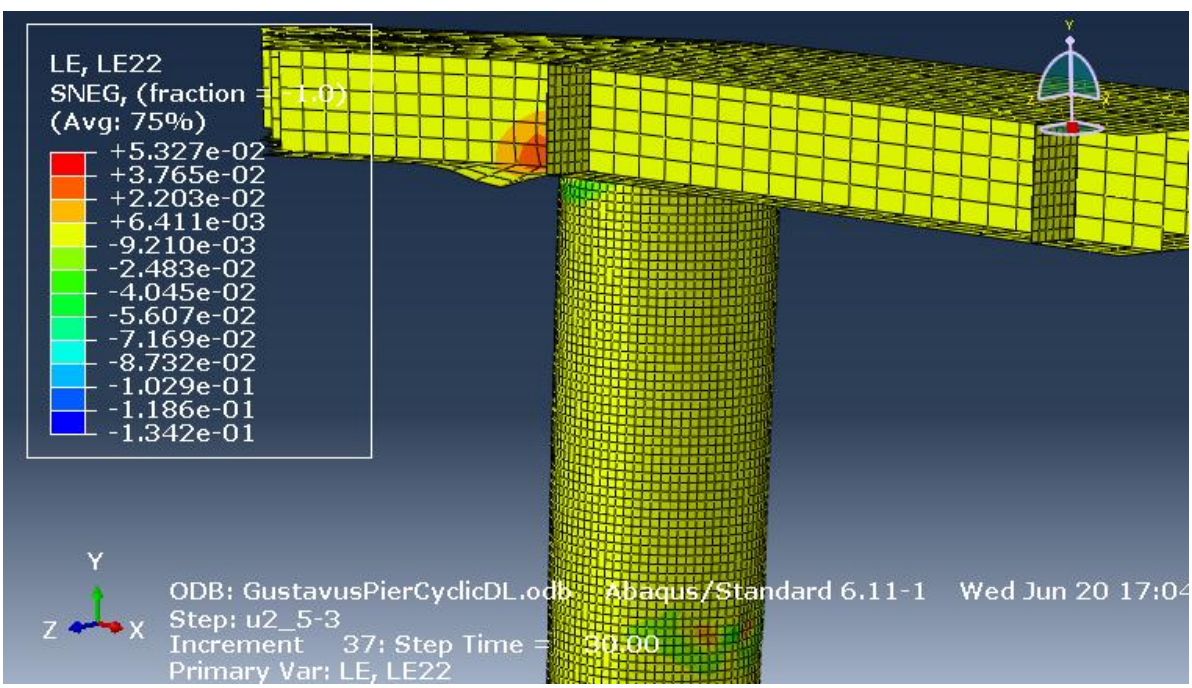

Figure 7.30 FEA - Ductility 2 Cycle -3 – Longitudinal Pile Strains (Def. S.F. = 1.0)

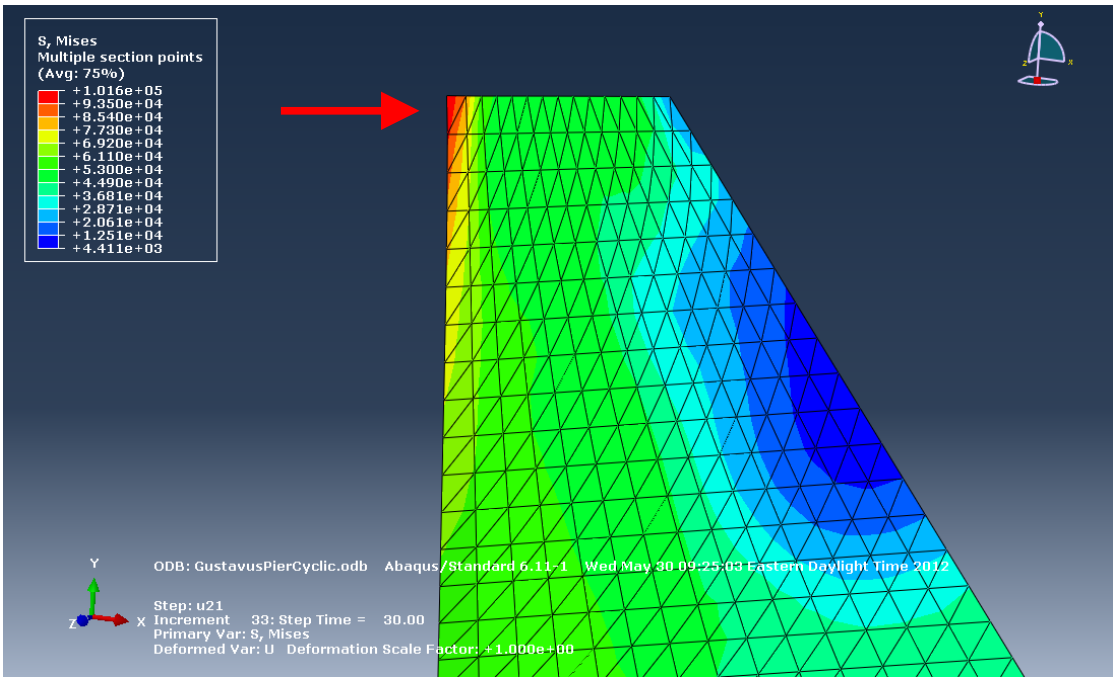

Figure 7.31 Von Mises Stresses (ksi) – Interior Gusset – Ductility 2 Cycle 1

7.8 Experimental Evaluation Summary

The experimental test behaved as predicted by the FEA throughout the elastic portion of the displacement history and through the first positive and negative cycles of the ductility 1.5 level which corresponded to 7.62 in. of cap beam displacement, as shown in Figure 7.32 and Figure 7.33. As was expected, brace buckling dominated the behavior of the system up to this level of loading which was assumed to be the cause of the observed pinched hysteretic behavior that regained strength at the loading peaks as shown in Figure 7.34 and Figure 7.35. Other than the observed brace buckling, no other signs of negative performance, including strength degradation, were observed at this point in the test.

The general hysteretic behavior of the system matched that of the FEA reasonably well as is shown in Figure 7.36, which helps to validate the accuracy of the modeling results.

Although the magnitude of brace buckling was pronounced at the ductility 1.5 level, measurable out of plane displacements were experienced as early as the +/- 1/2 F_y cycles where the internal compression braces experienced approximately 1/2 in. of out of plane displacement. Although generally at smaller magnitudes, the external compression braces also experienced considerable buckling beginning in the elastic cycles and increasing throughout the remainder of the test. The buckling behavior of the braces is summarized in Figure 7.37 through Figure 7.40 and Table 7.1 which provide the out of plane displacement history of each brace in both figure and tabular form. It should also be noted that gapping developed between the cap beam and the actuator end load plate during the test, indicating that the loading system was correctly pushing from both ends of the pier to generate the desired symmetrical loading pattern.

Post processing of test data was conducted to further evaluate the behavior of the braces. As has been noted, strain gauges were placed at the centerline of each brace to monitor axial strains in addition to Optotrak markers on the interior braces which were also oriented to capture axial strain at the brace centerline. As shown in Figure 7.41 and Figure 7.42, both the left and right interior braces appear to have experienced a relatively linear strain history through the elastic range of loading, +/- 3.9 in. of cap beam displacement. This is particularly notable in the strain gauge readings which are terminated due to gauge failure prior to the ductility 1.5 level as opposed to the Optotrak results which span the entire test duration.

Figure 7.32 Truss Pier – Ductility 1.5, Cycle 1, 7.62" Displacement, 151 kips

Figure 7.33 Truss Pier – Ductility 1.5, Cycle 1, 7.62" Displacement, 151 kips

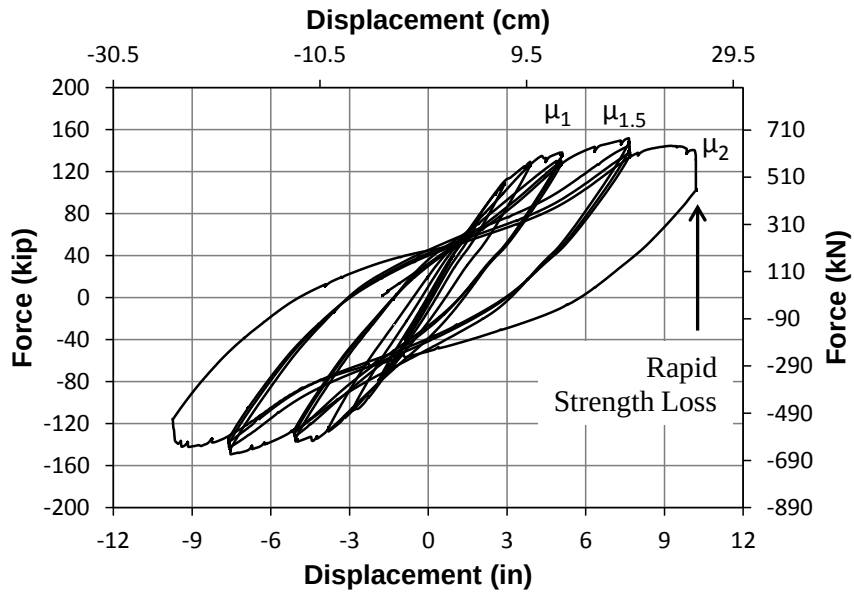

Figure 7.34 Truss Pier – Force Displacement Hysteresis

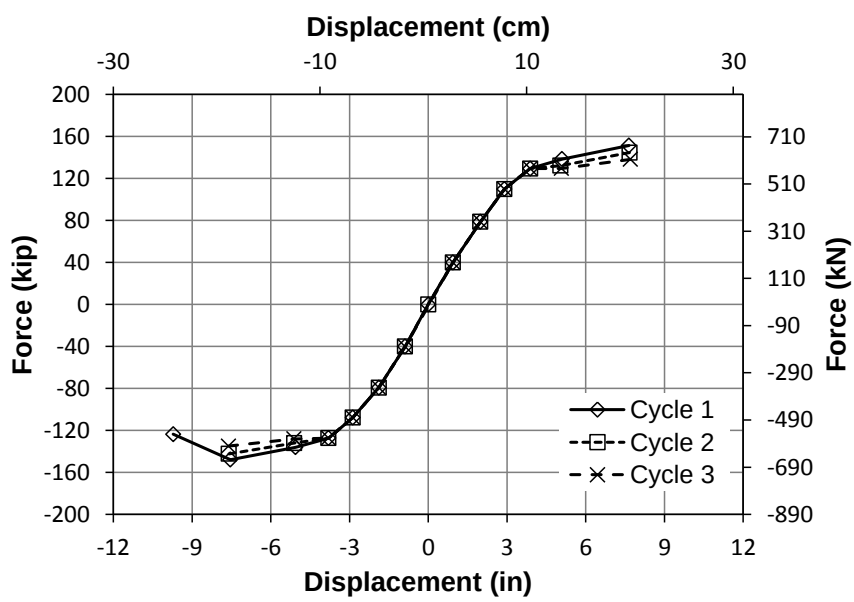

Figure 7.35 Truss Pier – Force Displacement Envelopes

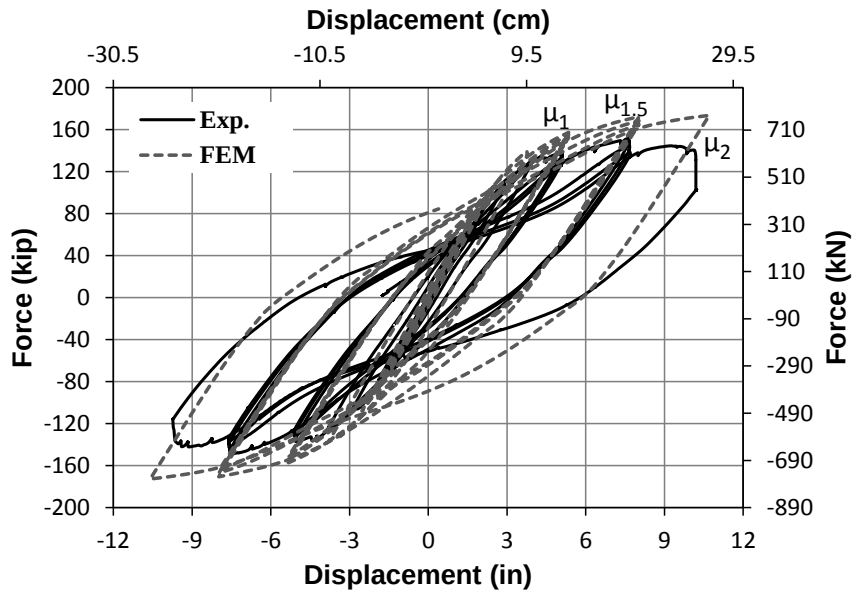

Figure 7.36 Truss Pier - FEM vs Experimental Force Displacement Hysteresis

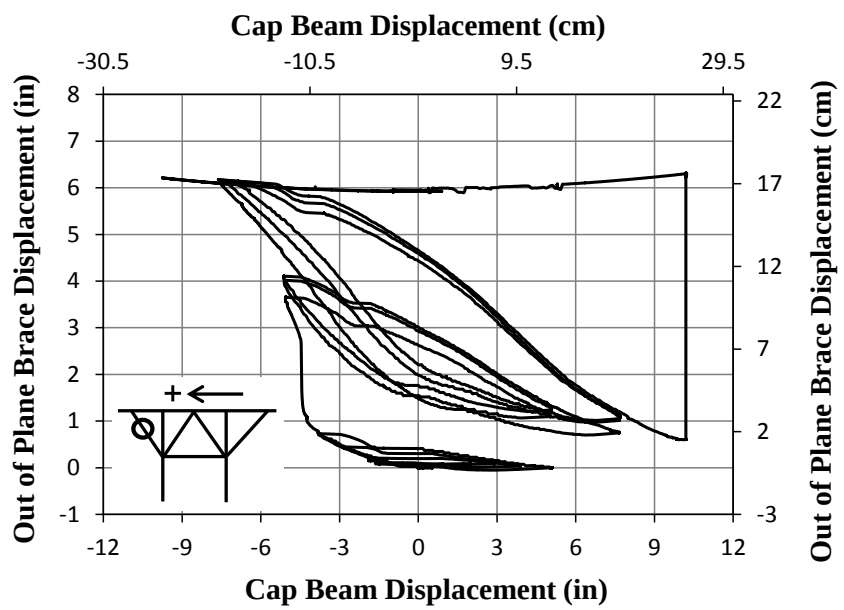

Figure 7.37 Out of Plane Behavior of Left External Brace

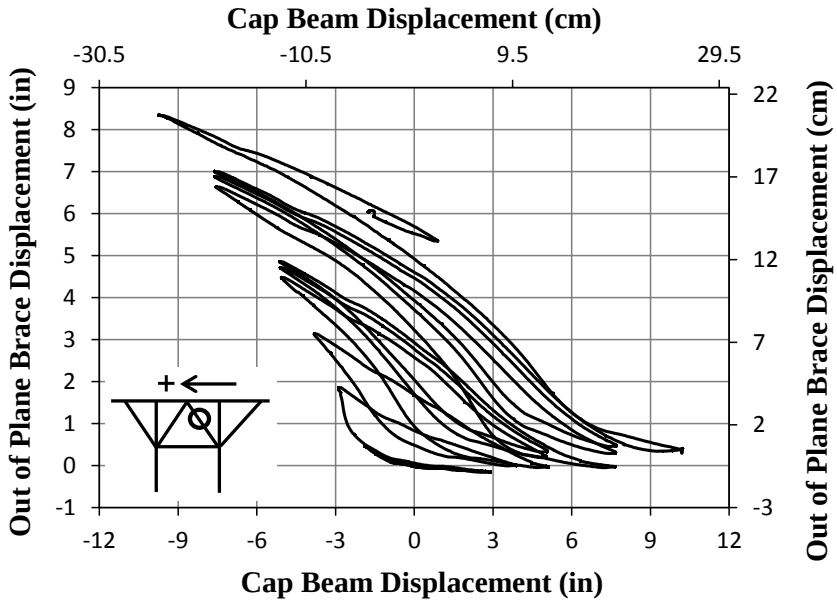

Figure 7.38 Out of Plane Behavior of Left Internal Brace

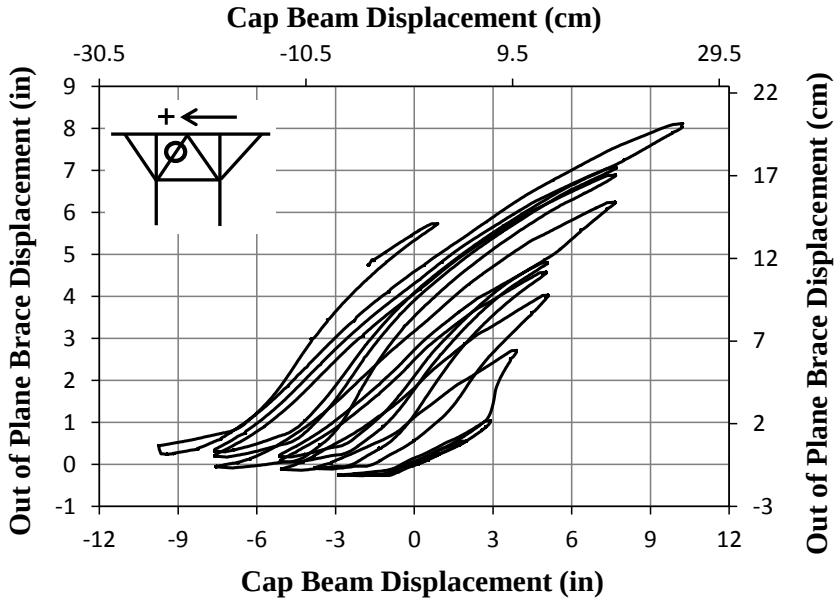

Figure 7.39 Out of Plane Behavior of Right External Brace

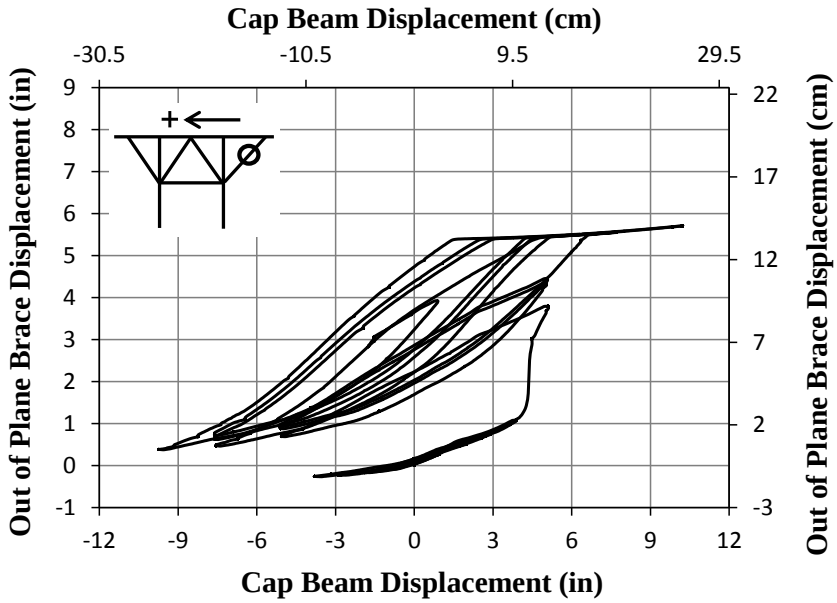

Figure 7.40 Out of Plane Behavior of Right Internal Brace

The first positive and negative cycles of ductility 1, corresponding to 5.08 in. of displacement, showed the strain history of both internal braces to continue in a relatively linear pattern in tension and plateau in compression suggesting inability of the brace to carry additional axial compression force, hence the formation of brace hinging. Interestingly, in the second cycle of ductility 1 the strain histories show both internal braces to rapidly gain tension strain, when subjected to tension force, indicating that the braces were able to yield in tension prior to significant buckling in compression. Alternatively, the external brace strain histories indicate that they experienced significant buckling prior to yielding in tension. As shown in Figure 7.43, the external braces also follow a relatively linear strain history in the elastic region, prior to a rapid gain in tension strain as the specimen was loaded to the ductility 1 level. In the case of the external braces, this gain in tension strain occurred as the brace was subjected to compressive forces and compressive strains. Noting that the strain gauges were placed on the front of the braces which would correspond to the tension face of the buckled brace, the rapid reversal from compressive strain to tension strains is likely

representative of significant brace buckling, which in this case appeared to occur prior to tension yielding.

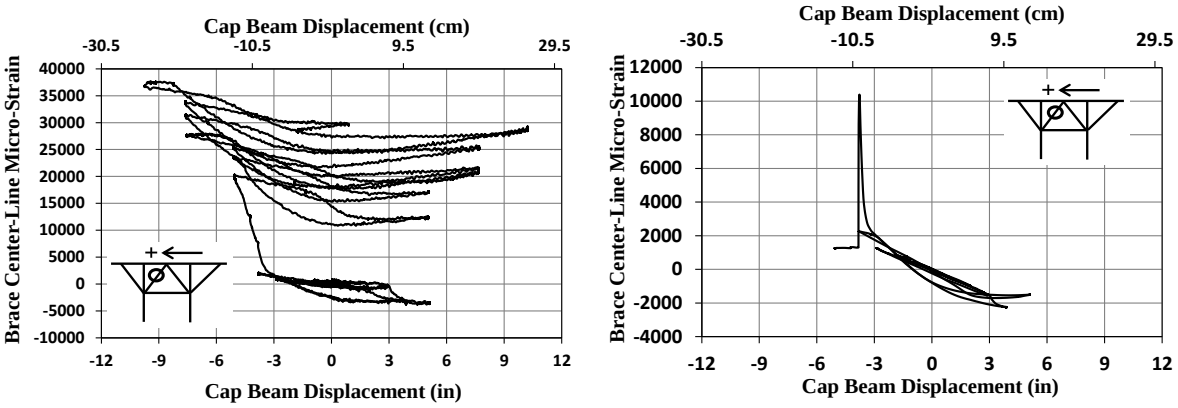

Figure 7.41 Left Internal Brace Strain Hysteresis (Left: Optotrak – Right: Strain Guage)

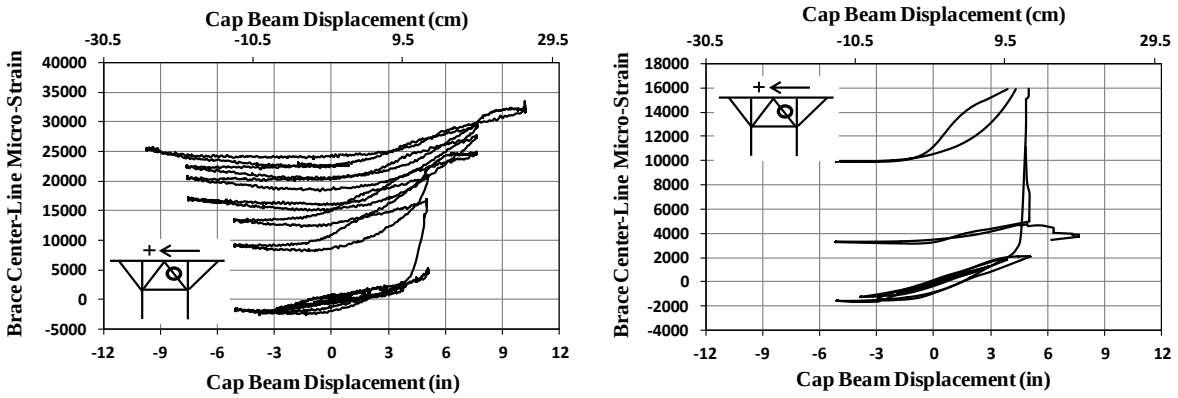

Figure 7.42 Right Internal Brace Strain Hysteresis (Left: Optotrak – Right: Strain Guage)

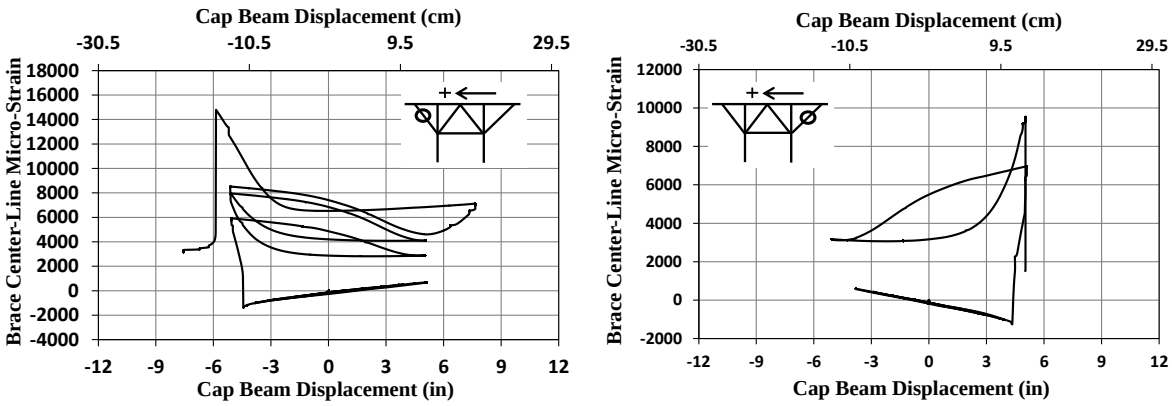

Figure 7.43 External Brace Strain Gauge Hysteresis (Left: Left Brace – Right: Right Brace)

Following the first positive and negative cycles of the ductility 1.5 level, the test was continued as no potential limit states had been observed with the exception of progressive brace buckling. At the completion of the second positive cycle of ductility 1.5, corresponding to 7.62 in. of displacement, three locations of weld cracking were visually noted. The first was an approximate 1 in. crack at the bottom of the double sided fillet weld connecting the north interior gusset plate to the pile. The second was in the same location on the south interior pile gusset but was approximately 1/2 in. in length. Lastly, a crack approximately 3 in. long at the south side of the fillet weld connecting the north pile to the cap beam was noted. This crack extended not only along the weld but also approximately 2 in. into the bottom flange of the cap beam along either side of the web of the center HP12x53. It is possible that the extension of the crack into the cap beam flange is the result of the absence of transverse cap beam stiffeners at the extreme fibers of the pile.

Although cracking had been noted, no significant strength loss had been experienced so the test was continued. The conclusion of the second negative cycle of ductility 1.5 led to the development of several additional weld cracks. First, the approximate 1/2 in. crack at the bottom of the south interior gusset to pile weld was noted to increase to approximately 1 in. in length. Second, a crack developed on the north side of south pile in the pipe to cap beam

fillet weld extending into the cap beam similar to that in north pile. Third, a crack on the north side of the double sided fillet weld connecting the centerline gusset plate to the cap beam soffit was noted. Lastly, cracking on the north side of the north pile to cap beam fillet weld was noted again extending into the cap beam flange. However, there was still no significant strength degradation at the peak of loading and the test was continued. At the completion of the third positive cycle of ductility 2, additional cracks were noted at the south centerline gusset plate to cap beam fillet weld similar to that of the north side, and at the south side of the fillet weld connecting the south pile to the cap beam. The accompanying third negative cycle produced no new cracks but did produce some propagation of the existing cracks.

As the specimen was loaded to the first positive cycle of ductility 2, which corresponded to 10.16 in. of displacement, no additional cracking was noted prior to the completion of the cycle. However, while statically holding the pier at the ductility 2 displacement, complete rupture of the double sided fillet weld connecting the south exterior gusset plate to the south pile occurred in a rapid and violent manner. This resulted in an immediate loss in strength of approximately 25% as shown in the force displacement response provided in Figure 7.34. As would be expected, the exterior south brace connected to this gusset plate was in tension in the positive direction of loading. No cracks were noted in this weld prior to rupture. Also while holding, propagation of the crack at the north pile to interior gusset weld began to occur, which required the specimen to be unloaded.

Regardless of the obvious upper bound limit state that had occurred, an attempt was made to conduct the first negative cycle of ductility 2. Although the full displacement was achieved, rapid propagation of the south interior gusset to pile weld was noted while holding at the negative ductility 2 displacement of -10.16 in. For safety concerns, the specimen was unloaded and the test concluded. Throughout the inelastic cycles of the test, cap beam damage in form of bottom flange warping and prying was observed as shown in Figure 7.54. This result was similar to that predicted by FEA and further indicates that the welded pipe to

cap beam connection was likely not acting as a rigid moment resisting connection due to the absence of stiffeners at the extreme fibers of the piles. After re-centering the specimen and removing any applied load, significant residual out of plane buckling displacement existed in all braces as shown in Figure 7.55. A summary of all noted cracking and applicable figures is provided in Table 7.2.

Table 7.1 Summary of Brace Buckling Out of Plane Displacements

Ductility	Cycle	SP7 (in)	SP8 (in)	SP9 (in)	SP10 (in)	SP11 (in)
$0.25F_y$	N/A	0.076	-0.053	0.237	0.272	-0.043
$-0.25\ F_y$	N/A	0.075	0.079	-0.191	-0.089	-0.044
$0.5\ F_y$	N/A	0.083	-0.112	0.552	0.512	-0.179
$-0.5\ F_y$	N/A	0.151	0.464	-0.255	-0.163	-0.161
$0.75\ F_y$	N/A	0.086	-0.154	1.011	0.748	-0.350
$-0.75\ F_y$	N/A	0.431	1.797	-0.253	-0.222	-0.633
F_y	N/A	0.040	0.013	2.669	1.069	-1.181
$-\ F_y$	N/A	0.707	3.115	-0.079	-0.256	-1.371
1	1	0.001	-0.026	4.002	3.728	-2.261
1	-1	3.588	4.469	-0.111	0.702	-2.644
1	2	1.114	0.224	4.558	4.299	-2.561
1	-2	3.948	4.707	0.096	0.914	-2.664
1	3	1.276	0.353	4.794	4.420	-2.581
1	-3	4.058	4.849	0.212	0.960	-2.639
1.5	1	0.764	-0.023	6.219	5.551	-3.643
1.5	-1	6.116	6.626	-0.045	0.491	-4.107
1.5	2	1.081	0.321	6.879	5.558	-3.924
1.5	-2	6.166	6.874	0.223	0.679	-4.115
1.5	3	1.121	0.491	7.055	5.561	-3.959
1.5	-3	6.175	7.001	0.324	0.740	-4.118
2	1	0.607	0.380	8.036	5.705	-5.492
2	-1	6.210	8.345	0.353	0.385	-7.040

Table 7.2 Truss Pier – Noted Cracking Summary

Crack #	Ductility	Cycle	Cracking Description	Reference
1	1.5	2	Cracking at Bottom of Interior Gusset to Pile Weld, North Pile, Approximately 1 in.	Figure 7.44
2	1.5	2	Cracking at Bottom of Interior Gusset Weld to Pile, South Pile, Approximately 1/2 in.	N/A
3	1.5	2	Cracking at Pile to Cap Fillet Weld Extreme Fiber, North Column South Face, Approx. 3 in., Extended into Cap Along Web	Figure 7.45
4	1.5	-2	Cracking at Bottom of Interior Gusset to Pile Weld, South Pile, Propagate to Approximately 1 in.	Figure 7.46
5	1.5	-2	Cracking at Pile to Cap Fillet Weld Extreme Fiber, South Column North Face, Approx. 1 in., Extended into Cap Along Web	Figure 7.47
6	1.5	-2	Cracking at Pile to Cap Fillet Weld Extreme Fiber, North Column North Face, Approx. 1 in., Extended into Cap Along Web	Figure 7.48
7	1.5	-2	Cracking on North End of Centerline Gusset to Cap Beam Weld	Figure 7.49
8	1.5	3	Cracking on South End of Centerline Gusset to Cap Beam Weld	Figure 7.50
9	1.5	3	Cracking at Pile to Cap Fillet Weld Extreme Fiber, South Column South Face, Approx. 1 in., Extended into Cap Along Web	Figure 7.51
10	2	1	Rupture of Entire Exterior Gusset to Pile Weld, South Pile, Occurred While Holding at Displacement Peak	Figure 7.52
11	2	1	Propogation (unzipping) of Inside Gusset to Pile Weld, North Pile	Figure 7.53
12	2	-1	Propogation (unzipping) of Inside Gusset to Pile Weld, South Pile	N/A

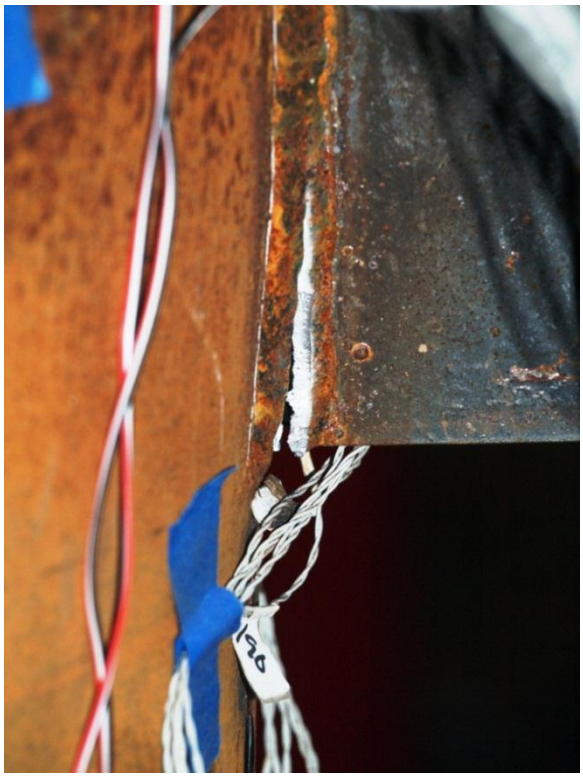

Figure 7.44 Crack #1

Figure 7.45 Crack#3

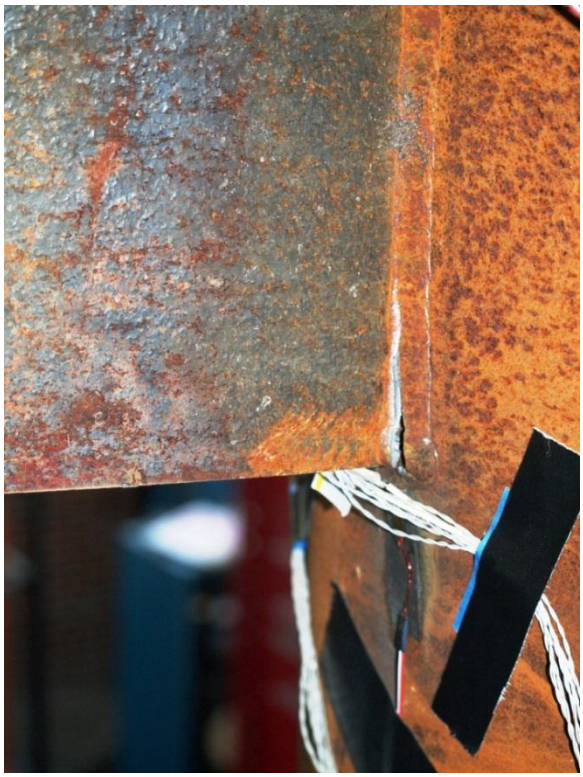

Figure 7.46 Crack #4

Figure 7.47 Crack #5

Figure 7.48 Crack #6

Figure 7.49 Crack #7

Figure 7.50 Crack #8

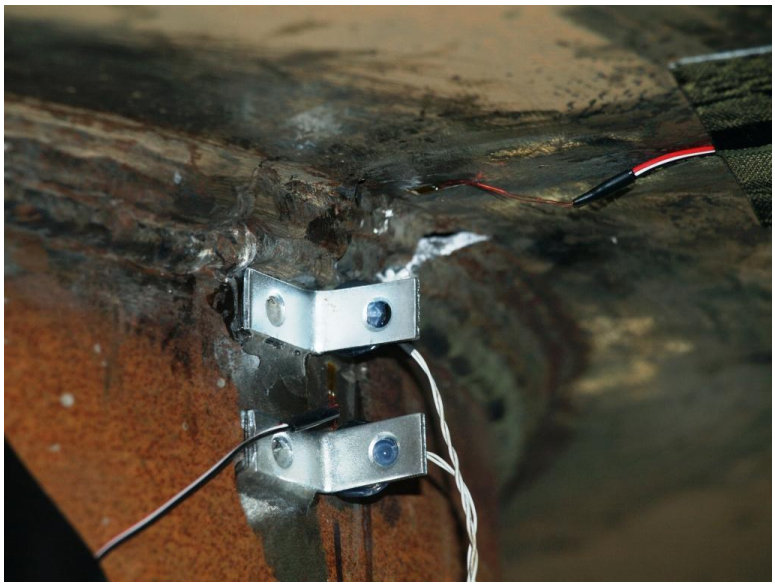

Figure 7.51 Crack #9

Figure 7.52 Crack #10

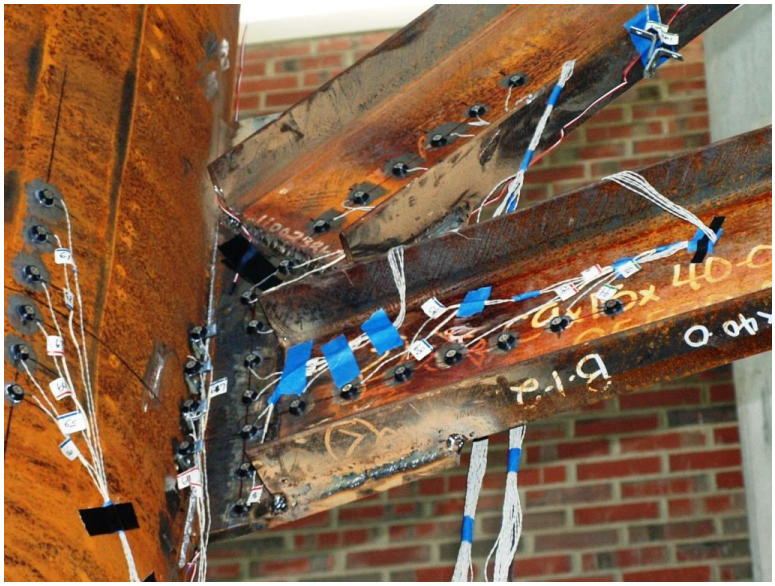

Figure 7.53 Crack #11

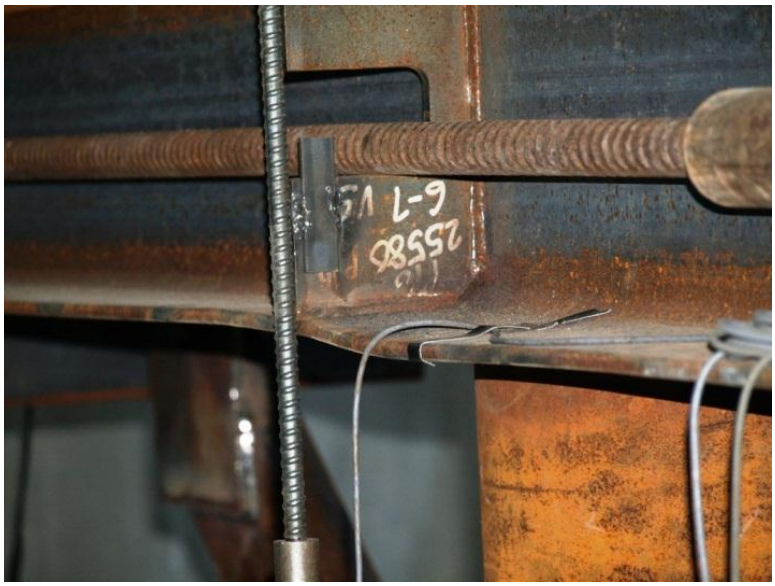

Figure 7.54 Cap Beam Damage at Pile

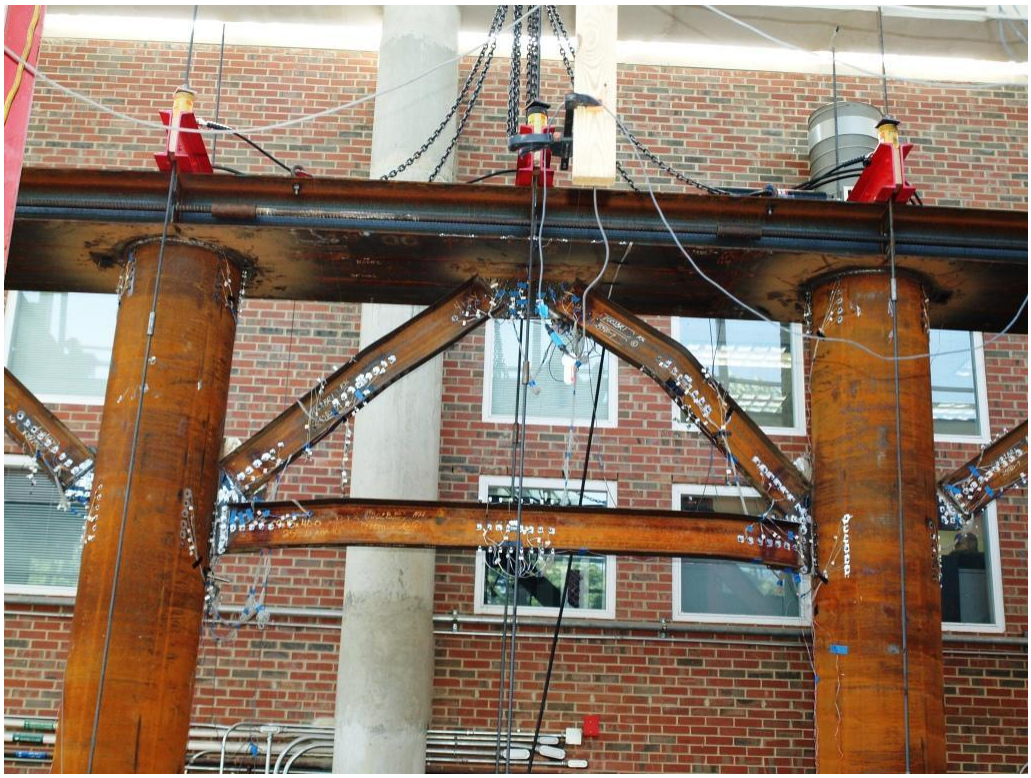

Figure 7.55 Residual Damage at Conclusion of Test

7.9 Comparison of Truss Style Pier with Typical Ductile Steel Pier

A brief discussion is provided here to elaborate upon the differences between the global hysteretic performance of the truss style steel pier and that of a typical driven pile steel pier with moment resisting pipe pile to cap beam connections. As shown in Figure 7.56, the most obvious difference is the general hysteretic shape. A typical steel pier exhibits a hysteretic shape similar to that of a Ramberg-Osgood curve which has notably wide hysteretic loops as is shown with the grouted shear stud connection (G.S.C.) pier response which was evaluated in test 6 of the second phase of this project and was subjected to vertical dead loads in addition to the lateral loading. It should be noted this hysteretic shape is common for ductile steel frames as is discussed in many text including (Priestly, et. al., 2007).

Contrarily, the truss style pier exhibits more pinched hysteretic loops which is likely the effect of the brace buckling mechanism that has been discussed. The differences between the two behaviors do not necessarily provide a distinct preferable choice in terms of hysteretic shape. The wide loops of the G.S.C. pier provide larger magnitudes of equivalent viscous damping which is a function hysteretic loop area and can reduce the required design strength capacity of a system for a given spectral displacement demand. However, this behavior is also associated with larger magnitudes of residual displacement which could be disadvantageous when seismic loading occurs. The truss style pier with pinched hysteretic loops would be less susceptible to residual displacements but also have less equivalent viscous damping for a given drift limit.

The second difference between the two styles of steel piers is the reliable displacement ductility capacity as is also notable in Figure 7.56. The results of prior testing, showed the grouted shear stud connection pier to have a reliable displacement ductility capacity of 3, depending on the exact definition of allowable strength loss that an engineer may choose. As has been discussed, the truss style pier would have a reliable displacement ductility capacity

of 1.5 due to the brittle gusset weld fracture at the ductility 2 level, assuming the cracking experienced at the ductility 1.5 level was acceptable as no strength loss was experienced. Hence, ductility 1.5 would be a maximum upper bound of potential reliable displacement capacity. However, it is important to note, that ductility of the typical style pier is highly dependent upon connection detailing as it has been shown in this research project that some connection styles, such as directly welded steel pipe pile to steel cap beam connections, possess limited ductility capacity due to weld cracking similar to that of the truss style pier.

The final difference between the two styles of piers that will be discussed is the controlling type of failure mechanism. The truss style pier was controlled by an ultimate limit state of gusset weld fracture which is considered a brittle and typically undesirable failure mode. As was shown in the hysteretic response, no considerable strength degradation was developed prior to the fracture of the exterior gusset plate weld which was associated with rapid strength loss. In addition, other forms of damage existed in every other element of the system including weld cracking, cap beam flange damage, and brace buckling. Most lateral load resisting systems are designed with a reliable single ductile mode of failure as discussed in (Priestly, et. al., 2007). It has been shown in this research project that with proper detailing, a typical driven pile steel pier can be designed with a definable ductile failure mode of pile hinging in the form of local buckling. It is possible that with further study, this could also be achieved with modification to the truss style pier. However, as currently detailed a single definable failure was shown to not exist for the truss style system.

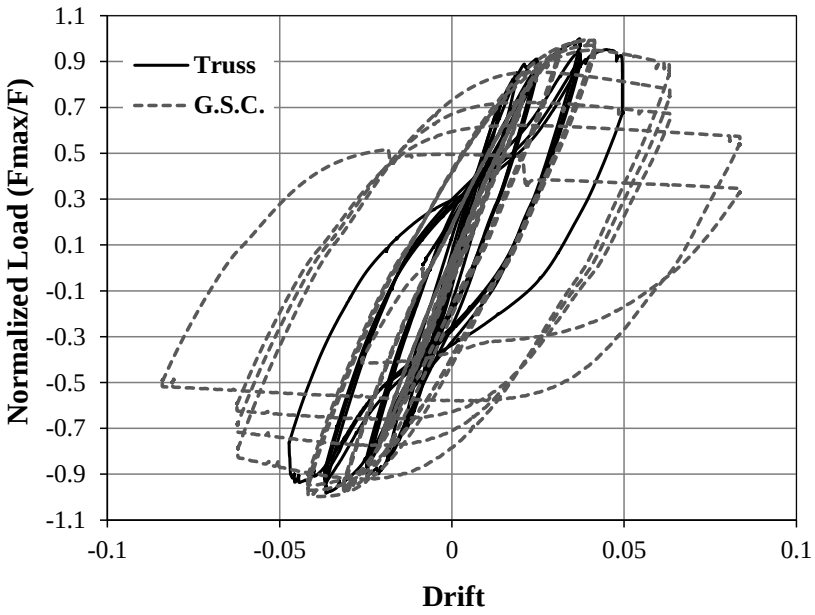

Figure 7.56. Truss vs G.S.C. Force-Displacement Response

7.10 General Conclusions in Regards to the Truss Style Steel Pier

The combination of analytical and experimental results discussed in this chapter indicate that the truss style steel pier under evaluation would likely be judged as inadequate to serve as a lateral load resisting system in areas of high seismicity as currently designed. The three main problematic issues regarding the system's performance are the limited displacement ductility capacity, the undesirable brittle failure mode of weld rupture, and multiple sources of inelasticity and damage. Although a considerable amount of discussion has been provided regarding the pinched hysteretic shape of the force displacement response, this did not appear to constitute negative performance; only a difference from that of a typical steel pier. The expected brace buckling mechanism that dominated the system's behavior prior to cracking

and weld rupture did not appear to directly constitute any negative performance criteria. Although straightening of the buckled braces was required upon loading reversals, the pier was able to regain strength towards the peak of each cycle, further no brace fracturing was experienced. However, it is possible that the brace buckling mechanism which placed rotational demands on the gusset plates was to some degree responsible for the weld cracking and rupture that was experienced.

Although the test specimen was able to sustain all three cycles of loading at the ductility 1.5 level with negligible strength loss, multiple sources of weld and base metal cracking were observed at this ductility level as has been discussed. Defining a reliable ductility capacity of this type of system is subjective to an exact definition of reliable response and would vary depending on an engineer's definition of allowable damage. However, it is likely that most designers would not consider cracking as an allowable form of damage regardless of the magnitude of associated strength loss. With this definition, the truss style specimen under evaluation would have a reliable displacement ductility capacity of 1 due to cracking noted to occur in several locations at the ductility 1.5 level. It is important to note when making conclusions regarding displacement ductility capacity of the system, results are related to a specific definition of yield displacement which in this case was based on initial buckling of the compressive braces. Therefore, it may also be beneficial to consider the drift associated with the ultimate reliable displacement ductility capacity of 1 which is independent of a yield definition and in the case the test pier was 2.29% considering a span from the pinned supports to the center of loading.

Chapter 8: Grouted Shear Stud Connection: Parametric Study

8.1 Introduction to the Parametric Study

As was concluded in prior chapters, the results of experimental testing of the grouted shear stud connection configuration with and without the inclusion of vertical dead load representative of superstructure weight indicated that the displacement ductility capacity of the pier may be impacted by the magnitude of applied vertical load. As was discussed, the nominally identical piers of tests 2, which included no applied vertical load, and test 6, which included a total of 146 kips of applied vertical load, exhibited different displacement capacities based on a given strength loss limit state. It was found that the inclusion of the vertical load reduced the displacement ductility capacity by approximately 1 level. It is worth noting that due to the cap beam shear force that develops due to lateral loading, axial forces in the columns are of course developed.

In the case of no applied vertical load, the experimental pier was capable of reaching a reliable displacement ductility of 3 corresponding to 6.31% drift for a limit state of 20% strength loss. When 146 kips of vertical load was included in the experimental investigation, which represented a reasonable upper bound of superstructure weight, the pier was capable of reaching a displacement ductility capacity of 2 corresponding to a drift of 4.21% drift for a limit state of 20% strength loss. As a result of this outcome, the decision was made to conduct a parametric study that would take into account variable vertical dead load magnitudes to investigate the effects on allowable displacement ductility capacity. In addition, it should be noted that the displacement capacity of pier is likely also a function of D/t ratio of the piles which are subjected to the local buckling mechanism. Consequently, D/t ratio was also taken into account as a variable in parametric study. The goal of the

parametric study was to generate a relationship between displacement ductility capacity ($\mu_{\Delta all}$), (defined by variable levels of allowable system strength loss (F_{loss})), as a function of D/t_{des} ratio of the pile members and axial load ratio (ALR) (defined by Eq.(8.1)). In this equation, (D) represents the total dead load on the pier, (n) the total number of piles, (A_g) the gross area of each pile, and (f_{ymin}) the minimum specified ASTM yield stress of the pile material.

$$ALR = \frac{D}{nA_g f_{y\min}} \tag{8.1}$$

Given the number of analyses that were necessary to correlate the four variables under consideration, experimental testing to achieve the goal was not viable. However, as has been discussed in prior chapters, the detailed Finite Element Models which had been developed for the grouted shear stud connection piers had shown good agreement with the experimental tests when calibrated with appropriate material test data. As shown in Figure 8.1 through Figure 8.5, both the full Force – Displacement hysteresis as well as the cycle by cycle back – bone envelopes show good agreement between the experimental evaluation and the analytical simulation for the case of with no applied vertical dead load. Additionally, this is also shown to be the case in the evaluation with applied vertical dead load which corresponded to an ALR of 7.66% in the experimental tests. As shown in Figure 8.6 through Figure 8.10, the analytical simulation was shown to capture the associated strength loss related to the formation of the local buckling mechanism between ductility levels as well as in the cycles of loading which is a key component of the parametric study. Consequently, the decision was made to utilize the FEM procedure to conduct the necessary analysis associated with the parametric study.

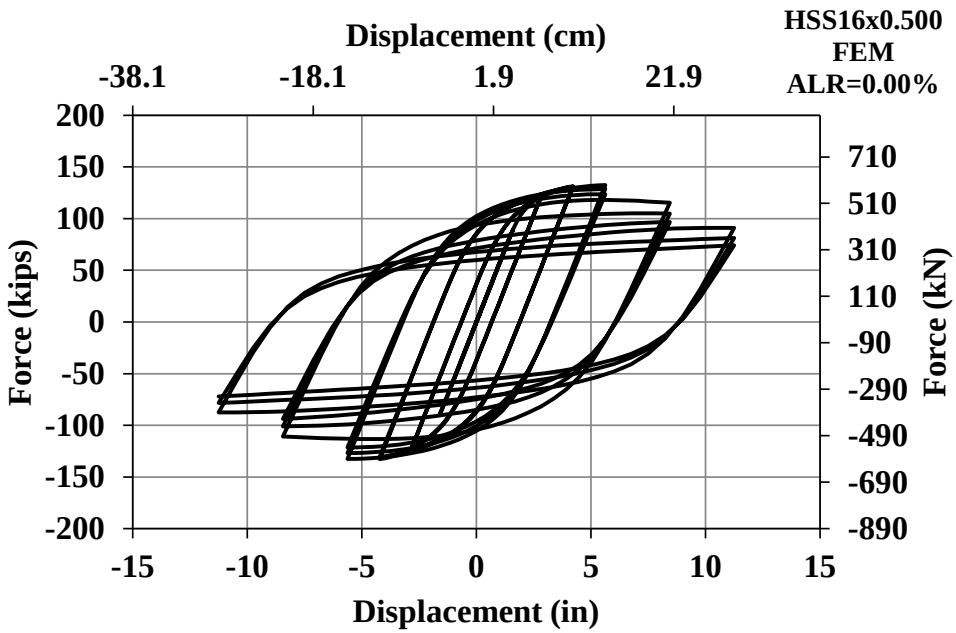

Figure 8.1 FEM Force – Displacement Response/HSS16x0.500/ALR=0.00%

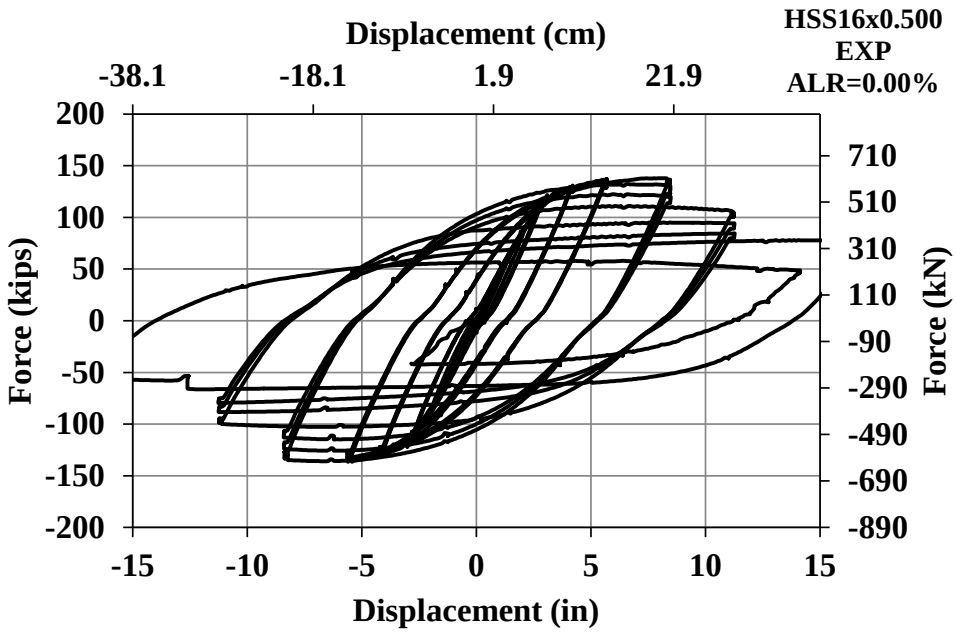

Figure 8.2 Experimental Force – Displacement Response/HSS16x0.500/ALR=0.00%

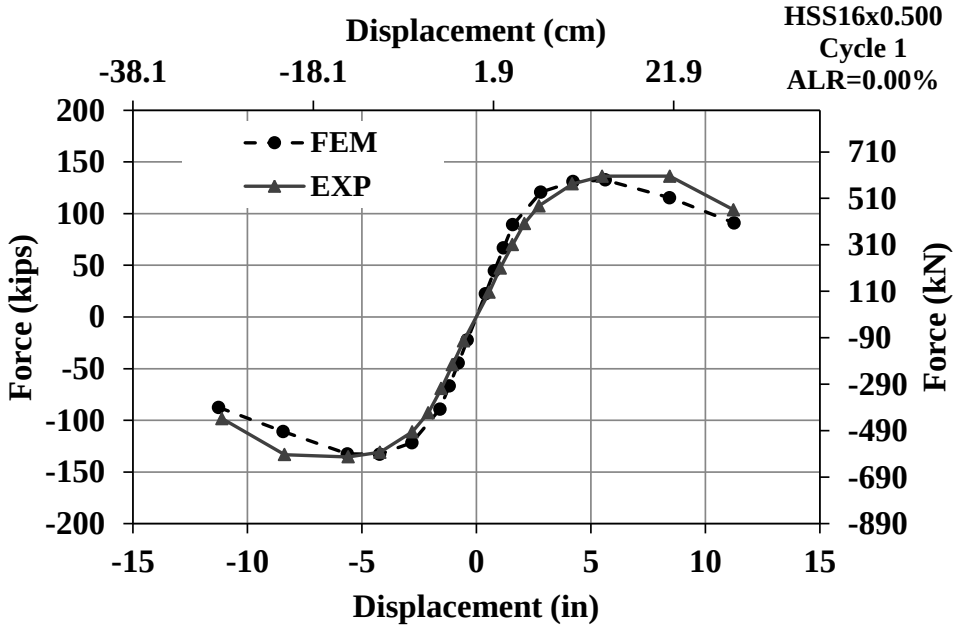

Figure 8.3 Cycle 1 Comparison – HSS16x0.500/ALR=0.00%

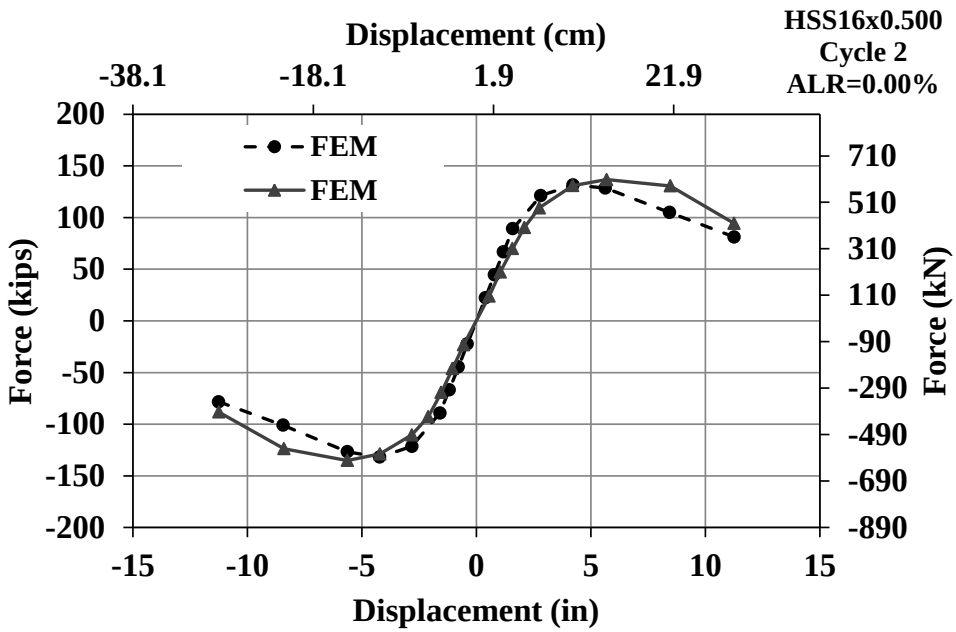

Figure 8.4 Cycle 2 Comparison – HSS16x0.500/ALR=0.00%

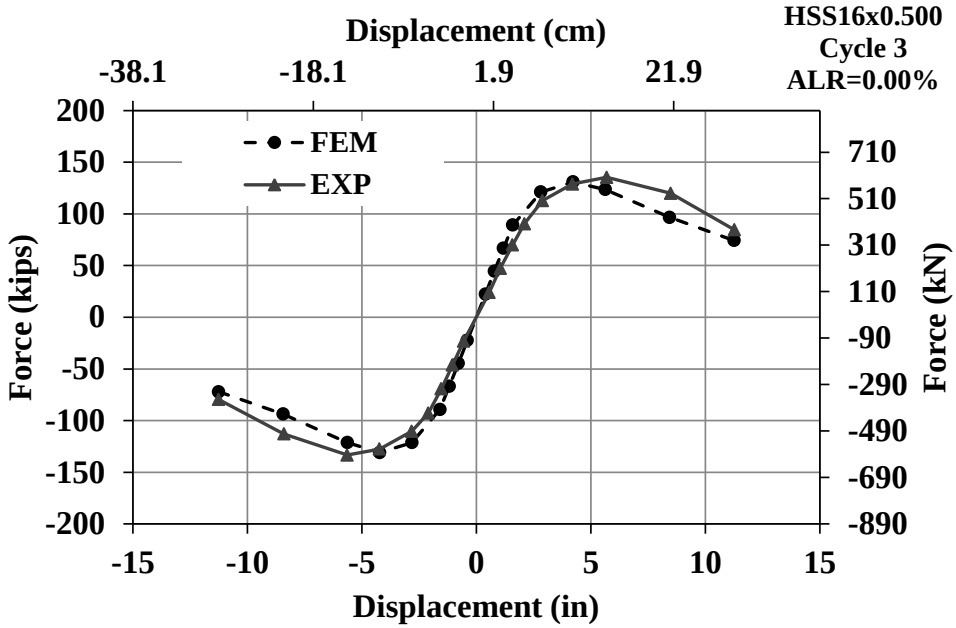

Figure 8.5 Cycle 3 Comparison – HSS16x0.500/ALR=0.00%

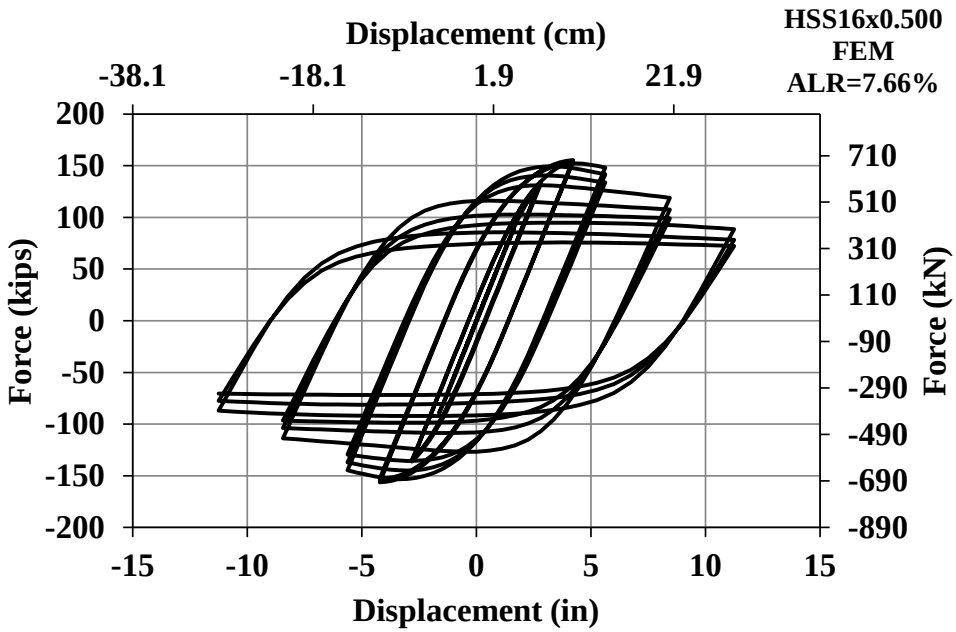

Figure 8.6 FEM Force – Displacement Response/HSS16x0.500/ALR=7.66%

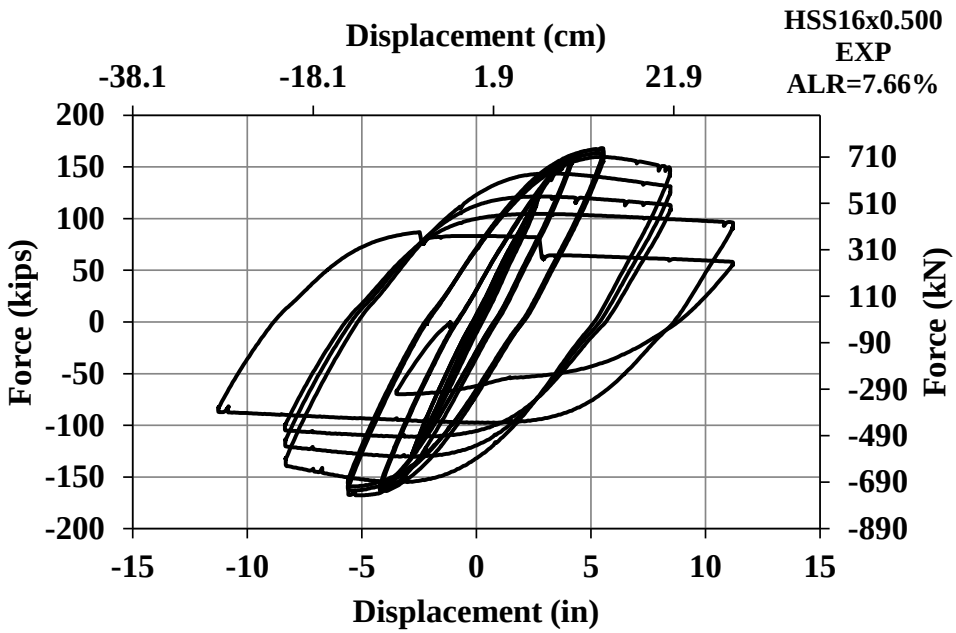

Figure 8.7 Experimental Force – Displacement Response/HSS16x0.500/ALR=7.66%

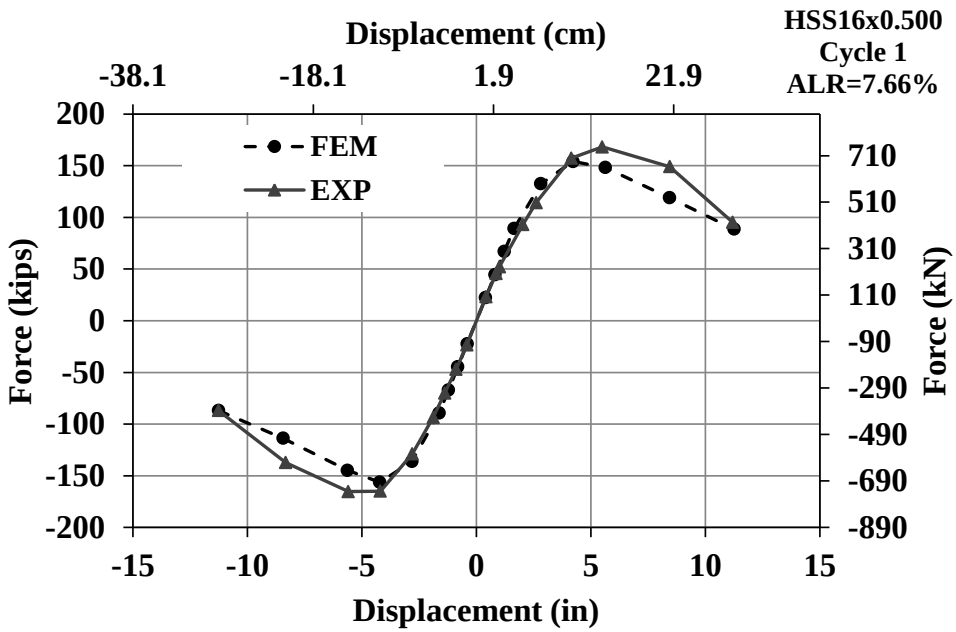

Figure 8.8 Cycle 1 Comparison – HSS16x0.500/ALR=7.66%

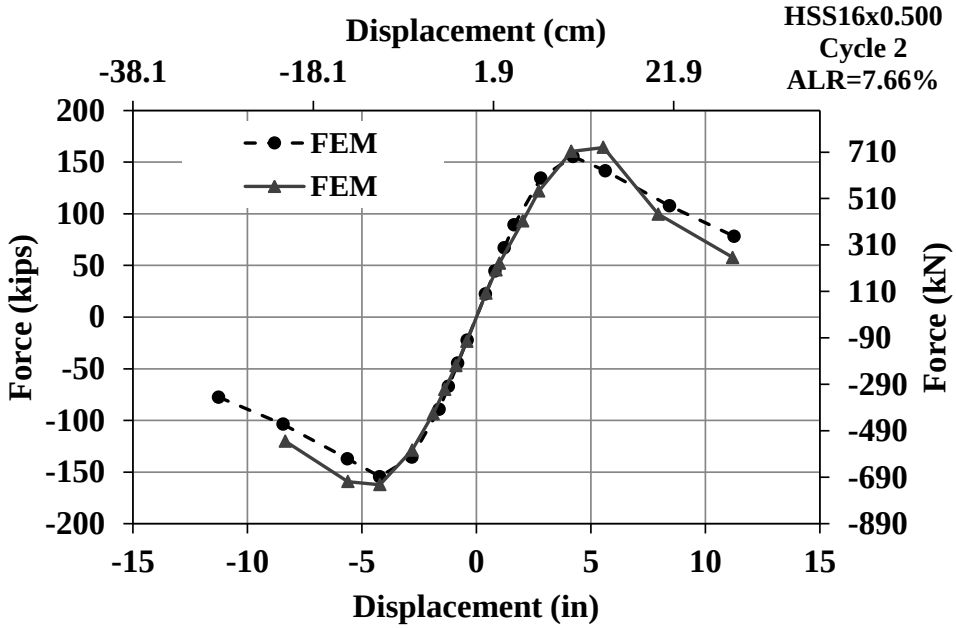

Figure 8.9 Cycle 2 Comparison – HSS16x0.500/ALR=7.66%

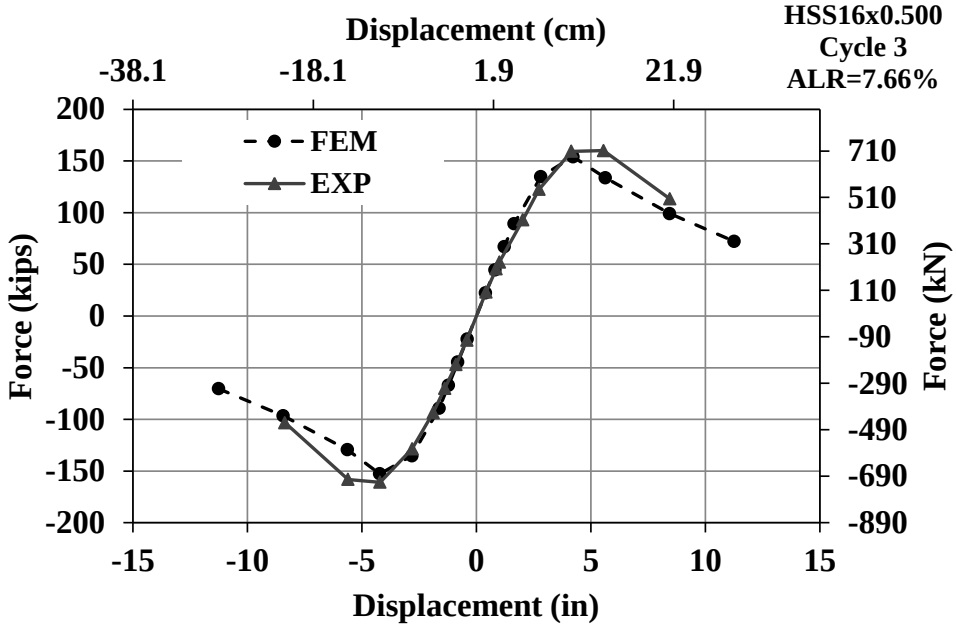

Figure 8.10 Cycle 3 Comparison – HSS16x0.500/ALR=7.66%

8.2 Line Model Method for First Yield Displacements

In order to conduct the parametric study and in order for the resulting relationships to be suitable for design, a simple method for determining first yield displacements of grouted shear stud connection piers with various pile sizes was needed. Through a trial and error process, it was found that elastic two dimensional centerline modeling appeared to capture the first yield displacement of the system reasonably well when compared to the experimental results. However, one modification to the standard centerline modeling procedure was necessary to appropriately model the system. Through the trial and error process, it was found that cap beam flexibility, shear deformations, secondary effects, and connection region flexibility all needed to be considered.

Cap beam flexibility, shear deformations, and secondary effects can all be handled with basic centerline modeling programs such as RISA (RISA Technologies, 2011) which was used in this research work. However, connection region flexibility was found to be impactful and to be more difficult to model with line elements. The use of rigid end offsets over the connection length which can be handled by most modeling programs was explored, however it was found to under predict the first yield displacement. Conversely, it was found that ignoring the connection stiffness, as may be done in typical centerline modeling, over predicted the first yield displacement. The most appropriate method of representing connection region stiffness was to represent composite action of the inner pipe pile member and the outer pipe pile stub member over the connection length.

More specifically, the centerline modeling procedure was found to be most accurate when the two pile pier, shown in Figure 8.11, was modeled with a total of 6 centerline representative nodes as shown in Figure 8.12. In the line element model, elements representative of the HSS16x0.500 piles span from node 1 to node 5 and node 3 to node 6, while elements representative of both the HSS16x0.500 piles and the 24x0.500 pipe stubs

span from node 5 to node 2 and node 6 to node 4. Hence, two line elements span these regions. An element representative of the double HP14x117 spans from node 2 to node 5.

With this modeling procedure, two members are modeled between nodes 5 and 2 as well as nodes 6 and 4. These members are subjected to the same end rotations and translations, and consequently the same displacements along the member, although different resulting forces will be generated. In this procedure, the distance from nodes 1 and 3 to nodes 2 and 4 is the centerline height of the pier from the pinned base which is representative of the point of contraflexure in an actual system. The distance from nodes 5 and 6 to nodes 2 and 4 is representative of the length of the connection region, (23 in. in this case) shifted upward by 1/2 the depth of the cap beam section. Lastly, the horizontal distance between nodes is the centerline spacing between piles.

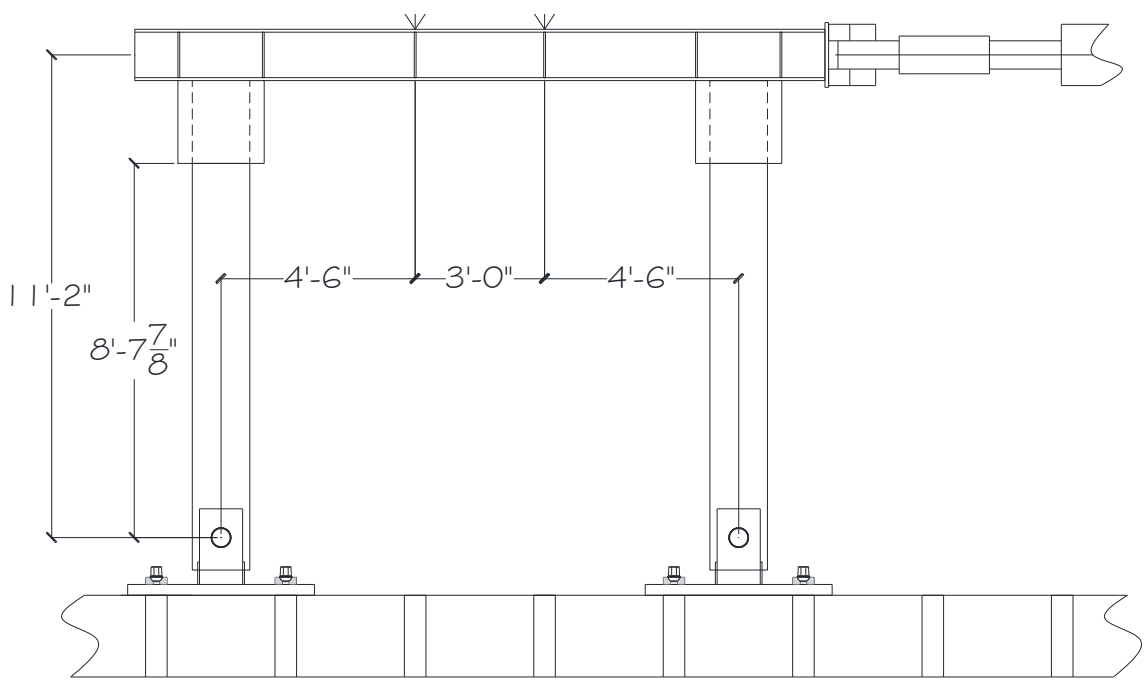

Figure 8.11 Experimental Grouted Shear Stud Connection Pier Configuration

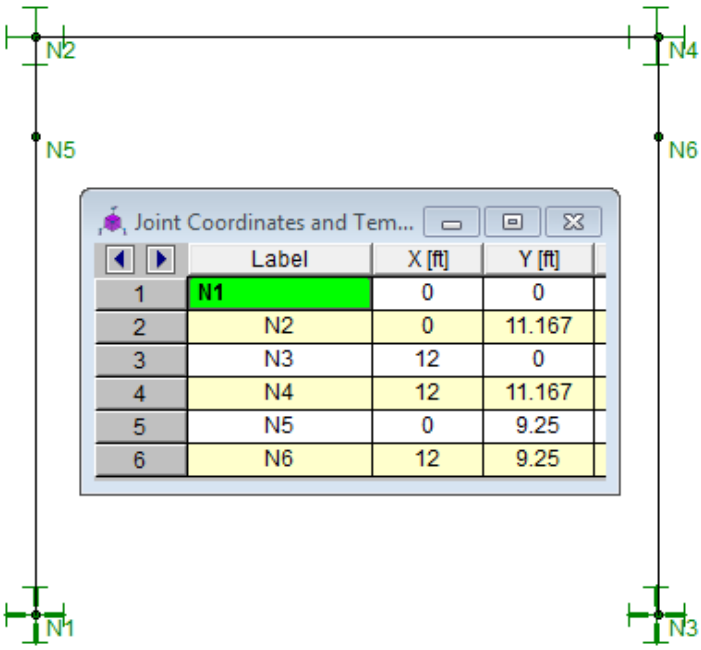

	Label	X [ft]	Y [ft]
1	N1	0	0
2	N2	0	11.167
3	N3	12	0
4	N4	12	11.167
5	N5	0	9.25
6	N6	12	9.25

Figure 8.12 Representative Centerline Model Configuration

Although a centerline modeling procedure is recommended to define the geometry of the pier, the calculation of the first yield force to apply to the model must consider the actual geometry of the system. It is recommended that the first yield force be based on the first yield moment capacity of the pile elements, assuming a critical cross section develops at the base of the connection region and that shears are assumed to be distributed equally between the two piles. It should be noted that this will not be the case with piers containing more than two columns, where internal columns will typically reach first yield prior to exterior columns.

Applying this method with an anticipated material yield stress of 58.8 ksi (AISC, 2010) (AASHTO, 2009), along with the cross sectional properties of the HSS16x0.500 members and a shear span of 8 ft – 8-7/8 in., resulted in a first yield force of 97.3 kips. Applying this force to the line element model along with an assumed modulus of elasticity of 29000 ksi, resulted in a predicted first yield displacement of 2.10 in. This value was found to be

comparable to the 4 experimentally determined average first yield displacements of 2.15 in., 2.11 in., 1.96 in., and 1.95 in. suggesting that the model is a reasonable approach to determining first yield displacements.

As has been noted, the modeling procedure should include the effects of cap beam flexibility as well as secondary effects in addition to the modifications for joint rigidity. The inclusion of cap beam flexibility can be achieved by including the cross sectional properties of the cap beam element. The issue of secondary effects in an elastic analysis is handled differently by different analyses codes. For this parametric study, P-Delta effects arising from global equilibrium induced axial loads was considered with the stiffness reduction method described in (AISC, 2005). It should also be noted that vertical dead loads were not considered when calculating first yield displacements in this parametric study. This was done to reduce the number of load/displacement histories that needed to be modeled, such that for a given pile size a single load/displacement history could be defined regardless of ALR. Further, this allows for direct comparisons of drift or displacement capacity for a given pile size with varying ALR and allowable strength loss.

8.3 Parametric Study Details and Matrix

As has been noted, Finite Element Analysis simulations were conducted to evaluate the correlation between allowable displacement ductility, allowable system strength loss, ALR, and D/t ratio. In order to evaluate these 4 parameters, the analysis matrix described in Table 8.1, was developed which considers 5 D/t_{des} levels ranging from 21.5 to 51.7, each subjected to three different levels of ALR (10%, 7.66%, and 5%) for a total of 15 analyses. The variable bounds chosen were considered to be reasonable ranges that would be likely to be utilized in design. As will be discussed in detail in subsequent sections of this chapter, the use of final design recommendations resulting from this parametric study should remain within the bounds of the variable ranges considered.

The 15 models that were developed all considered the same ideal global geometry shown in Figure 8.13. The differences between the models included load/displacement history (constant for a given pile size), pile and stub pile thickness, magnitude of applied vertical dead load, and configuration of the shear stud connectors. As was the case with prior models, the shear studs generating connection between the grout and pipe elements were modeled with fastener definitions to join appropriate areas of each mesh which negated the need to actually model the geometry of the shear stud connector. It is important to note that due to the variability in the actual stress strain response of ASTM A500 Gr. B material, the non-linear portion of the steel constitutive model used in the parametric study did not consider any actual tensile test data. The material model considered in all of the analyses was based on expected yield and ultimate stress values determined from the over-strength provisions of (AISC, 2010) (AASHTO, 2009). Although this may not appropriately predict the ultimate force capacity of a particular pier with known material properties, the FEM procedure had been shown between tests 2 and 6 to appropriately capture strength loss magnitudes regardless of varying ultimate strength conditions due to varying material properties. Hence, the need to only consider strength loss as a parameter normalized by ultimate strength capacity of a particular pier allowed for use of expected material properties to calibrate a bi – linear kinematic hardening rule for these analyses.

For each of the 5 pile sizes considered in the parametric study, it was necessary to determine a predicted first yield displacement in order to calibrate the three cycle set load history that would be used in the analytical quasi-static evaluations. The line model method which considered cap beam flexibility, secondary effects, and joint region flexibility as has been discussed was used to determine the necessary 5 first yield displacements. These values, which are shown in the seventh column of Table 8.2, were found to slightly increase as the pile thickness increased resulting in a higher first yield force. Although typical cantilever column first yield displacements have been shown to be independent of first yield force (Priestly, et. al., 2007), this was shown to not be the case with this type of pier system that is comprised of multiple displacement components.

It appeared from the line model analyses, the most influential additional displacement mechanism was cap beam flexibility which was a reasonable result based upon the fact that the same cap beam was used for all 5 models which were of course subjected to different levels of first yield force. It should be noted, in all cases the cap beam remained as a capacity protected member

In order to quantify the effects of cap beam flexibility, the analyses were subsequently conducted with rigid end offsets over the connection region and the differential displacements between the systems remained effectively constant as can be seen in the ninth column of Table 8.2. However, when a rigid cap beam was considered, and when a rigid cap beam and no secondary effects were considered, the predicted first yield displacements of all 5 models were nearly identical as can be seen in the eleventh and thirteenth column of Table 8.2. The analyses indicated that it is necessary to consider cap beam flexibility, connection region flexibility, and secondary effects to most accurately predict first yield displacements.

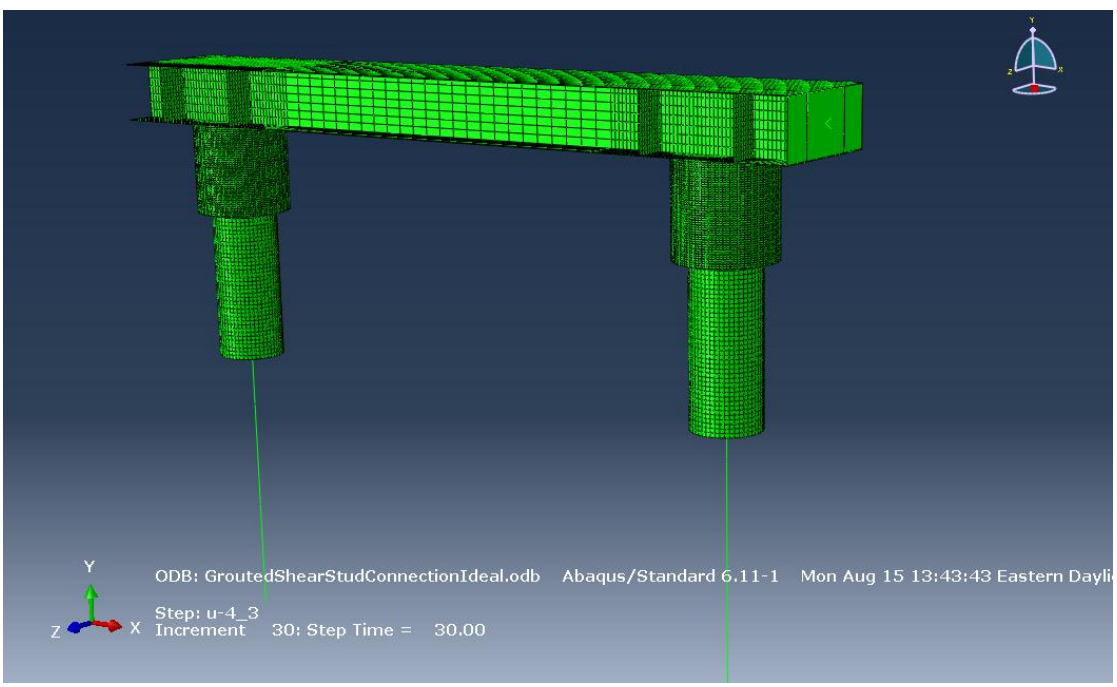

Figure 8.13 Parametric Study Finite Element Model

Table 8.1 Grouted Shear Stud Parametric Study Matrix

Pile Size	D/t	D/t_{des} (5)	t_{des} (5) (in)	A_g (in^2)	ALR (2) (%)	D (k)	F'_y (k)	Δ'_y (3) (in)	Studs (4)	Stub Pile
HSS16x0.800 (1)	20.0	21.5	0.744	35.7	5	150	147.7	2.303	120 - 7/8" Dia.	24x0.875 (6)
					7.66	229				
					10	300				
HSS16x0.625	25.6	27.5	0.581	28.1	5	119	119.0	2.190	96 - 7/8" Dia.	24x0.625
					7.66	182				
					10	238				
HSS16x0.500	32.0	34.4	0.465	22.7	5	96	97.3	2.097	96 - 3/4" Dia.	24x0.500
					7.66	147				
					10	192				
HSS16x0.375	42.7	45.8	0.349	17.2	5	72	74.7	2.000	96 - 3/4" Dia.	24x0.375
					7.66	111				
					10	145				
HSS16x0.333 (1)	48.0	51.7	0.310	15.3	5	64	66.7	1.944	96 - 5/8" Dia.	24x0.375
					7.66	99				
					10	129				

Table 8.1 Footnotes:

(1)Pile size likely unavailable; used to generate desired D/t value.

(2)Axial Load Ratio based on ASTM A500 Gr.B specified minimum yield stress of 42 ksi.

(3)Elastic first yield displacement based on line model method.

(4)Required number of ASTM A108 shear studs per connection (pile and pipe stub) assuming a minimum 6 ksi grout strength.

(5)Design wall thickness based a 93% of specified wall thickness.

(6)Pile size likely unavailable; used for conceptual design.

Table 8.2 Line Model Method First Yield Displacements for Parametric Study Matrix

Pile Size	D/t	D/t_{des} (5)	t_{des} (5) (in)	F'_y (k)	Stub Pile Size	Δ'_y (in)		Δ'_y (in)		Δ'_y (in)		Δ'_y (in)
HSS16x0.800	20.0	21.5	0.744	147.7	24x0.875	**2.30**	Rigid End Offsets Over Connection	1.85	Rigid Cap and Rigid End Offsets Over Connection	1.28	Rigid Cap and Rigid End Offsets Over Connection	1.06
HSS16x0.625	25.6	27.5	0.581	119.0	24x0.625	**2.19**		1.72		1.27		1.04
HSS16x0.500	32.0	34.4	0.465	97.3	24x0.500	**2.10**		1.63		1.25		1.03
HSS16x0.375	42.7	45.8	0.349	74.7	25x0.375	**2.00**		1.53		1.24		1.02
HSS16x0.333	48.0	51.7	0.310	66.7	24x0.375	**1.94**		1.49		1.24	No P-Delta Consideration (2)	1.01

Table 8.2 Footnotes:

(1) Design wall thickness based a 93% of specified wall thickness.

(2) wyL2/3=[(58.8ksi/29000ksi)(103.5in)2]/[(8in)(3)]=0.95in (note: shear displacements neglected in this calculation)

8.4 Parametric Study Results

As would be expected, it was found from the results of the 15 simulations that, in general, system strength loss due to local buckling of the pile walls increased as ALR increased and as D/t ratio increased for a given displacement ductility level. In no cases was an opposite trend experienced. Further, it appeared that the D/t variable was more influential in terms of strength loss experienced by the system than was ALR. These two basic trends can be seen in Figure 8.14 through Figure 8.43 which provide the cycle by cycle Force-Displacement envelopes and associated strength loss at the positive and negative peaks of loading for all three ALRs of each D/t value considered.

It should be noted when reviewing this data set that some of the strength loss values reported become considerably large (as high as 60%) particularly for the higher D/t values. Although these strength loss values are outside the bounds of what would likely be used for design purposes, the decision was made to include these values in the calibration of a design expression. This was done in order to expand the coverage of the regression analysis used to generate design equations, such that the model could be used for retrofit/evaluation of existing structures which may be subjected to higher anticipated strength loss values. However, it should be noted that the analyses used in the study did not consider fracture of pile material following the formation of local buckling regardless that this was shown experimentally to occur after significant strength degradation. It should therefore be understood that the higher levels of strength loss may not be attainable without fracture of pile material.

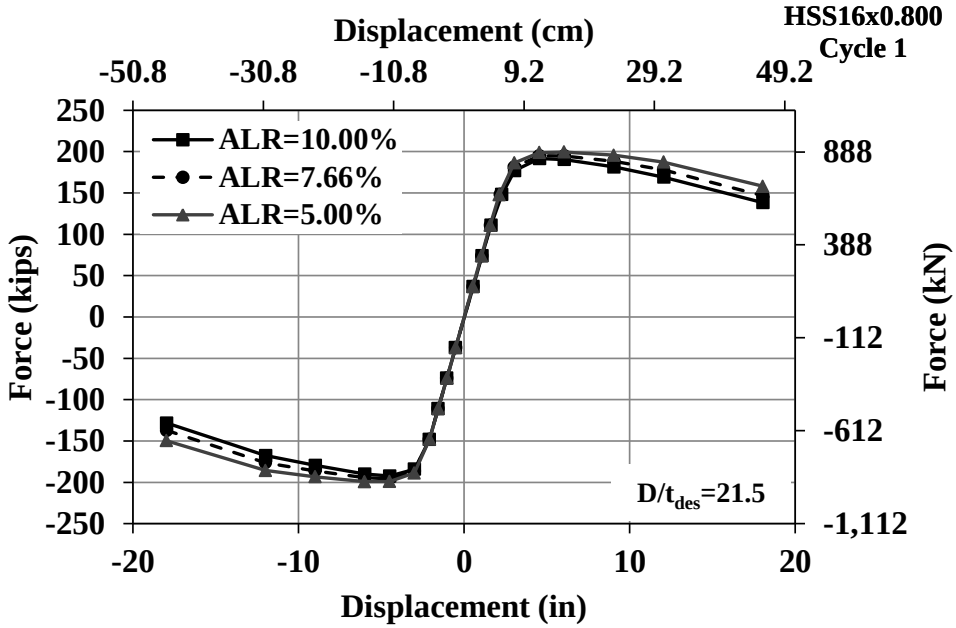

Figure 8.14 Cycle 1 Comparison – HSS16x0.800 D/t_{des}=21.5

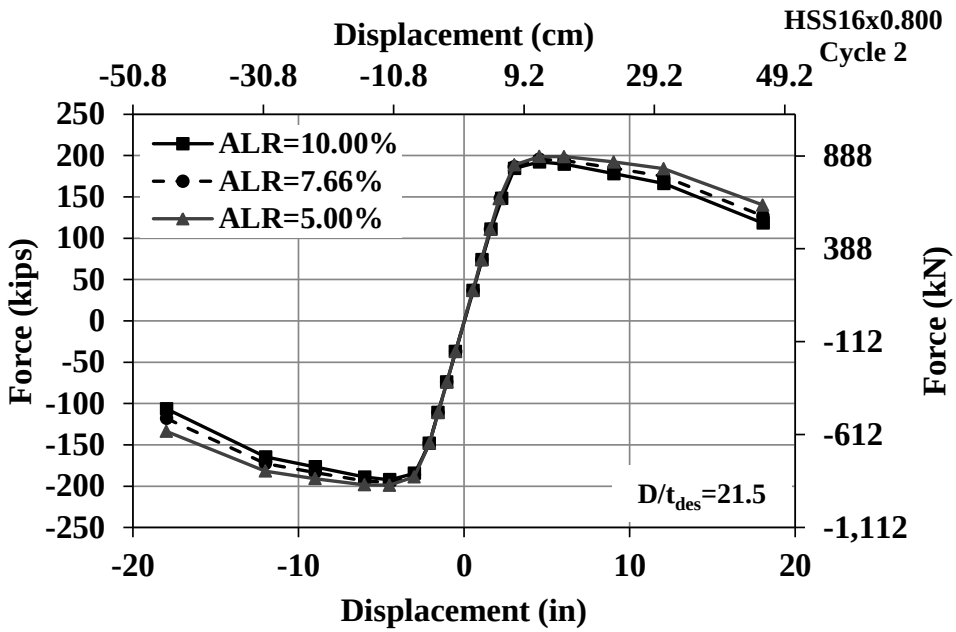

Figure 8.15 Cycle 2 Comparison – HSS16x0.800 D/t_{des}=21.5

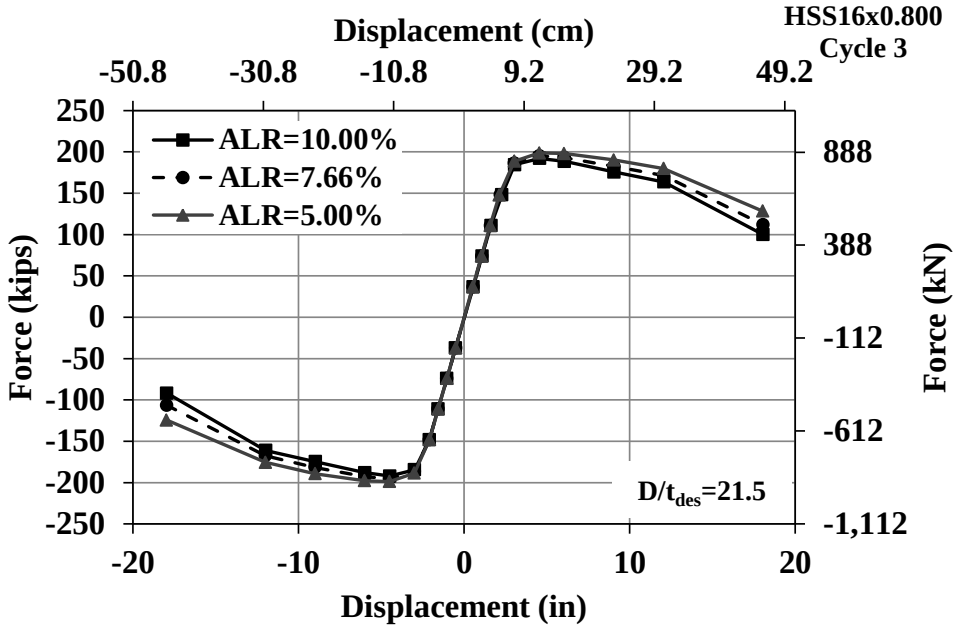

Figure 8.16 Cycle 3 Comparison – HSS16x0.800 D/t_{des}=21.5

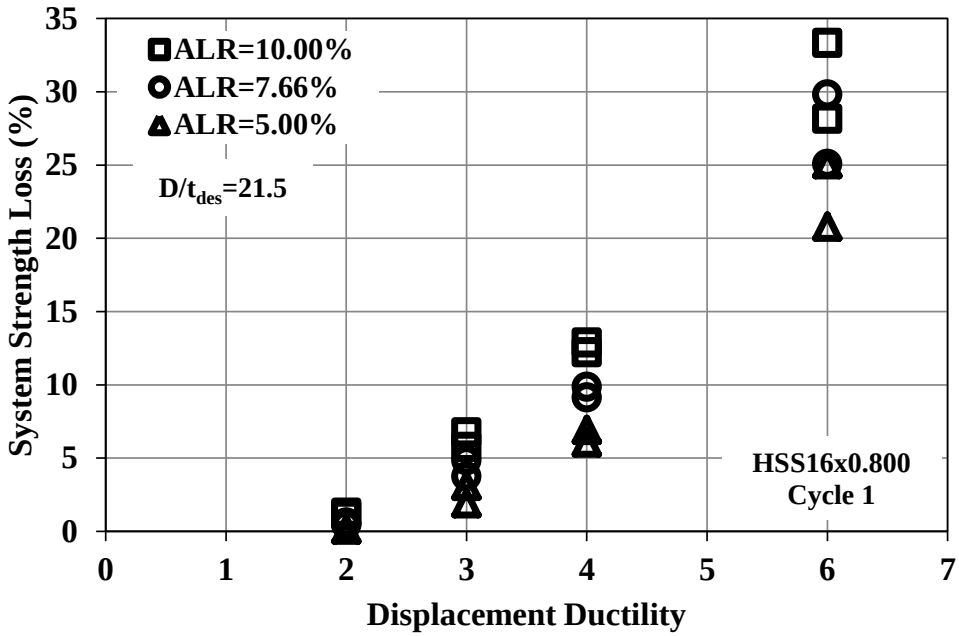

Figure 8.17 Cycle 1 Strength Loss Comparison – HSS16x0.800 D/t_{des}=21.5

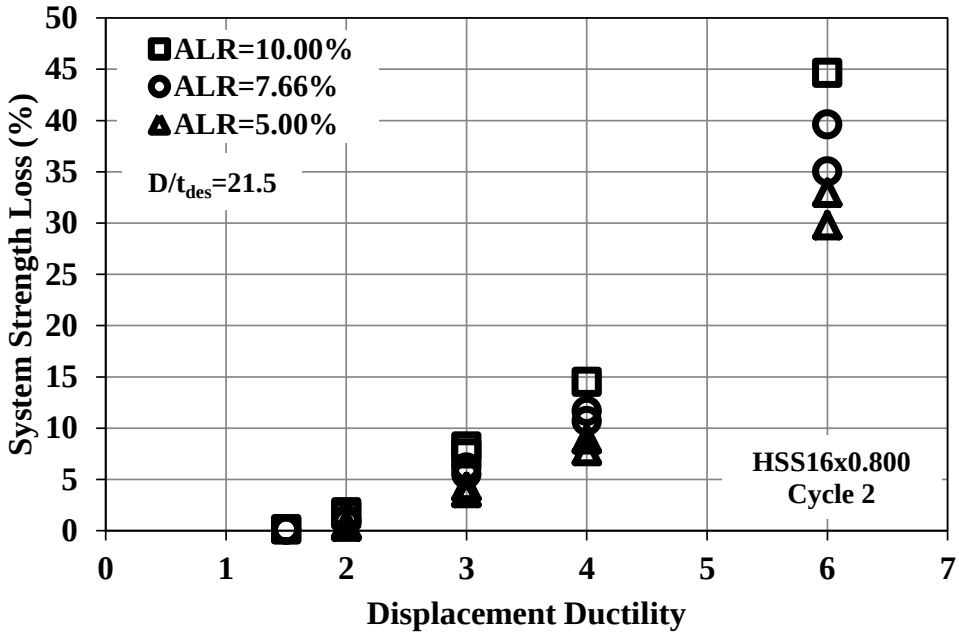

Figure 8.18 Cycle 2 Strength Loss Comparison – HSS16x0.800 D/t_{des}=21.5

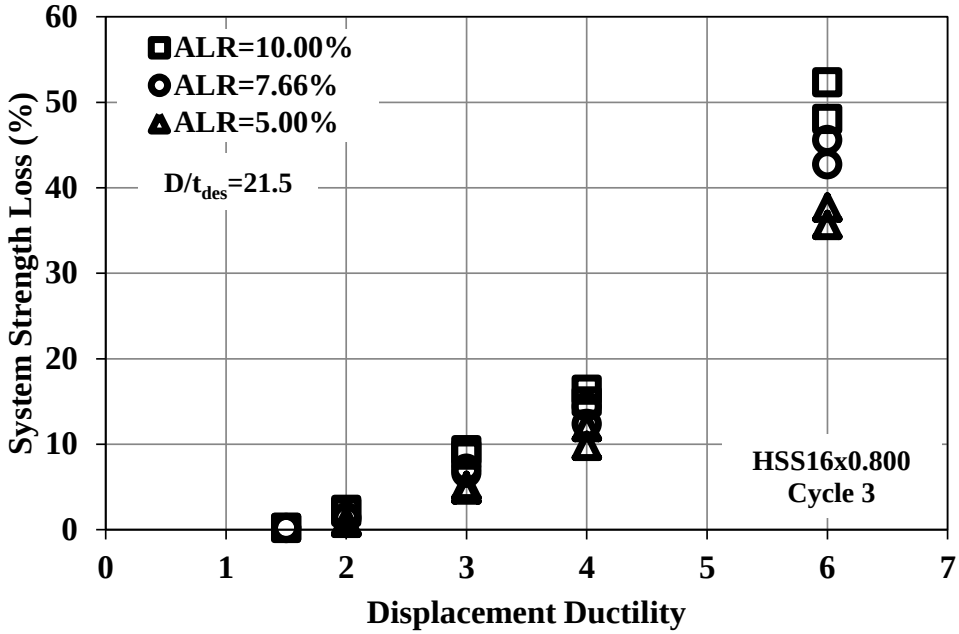

Figure 8.19 Cycle 3 Strength Loss Comparison – HSS16x0.800 D/t_{des}=21.5

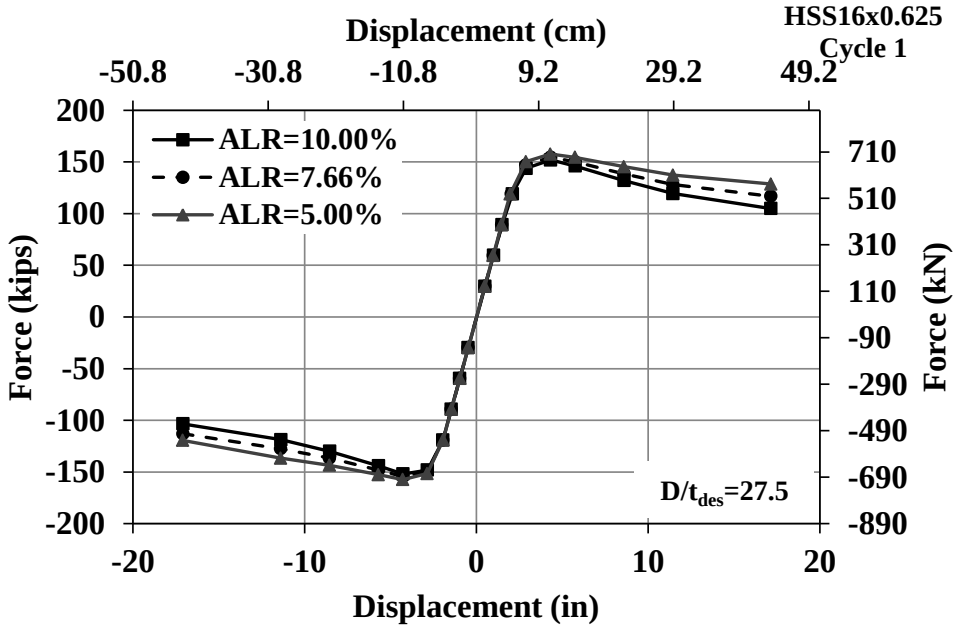

Figure 8.20 Cycle 1 Comparison – HSS16x0.625 D/t_{des}=27.5

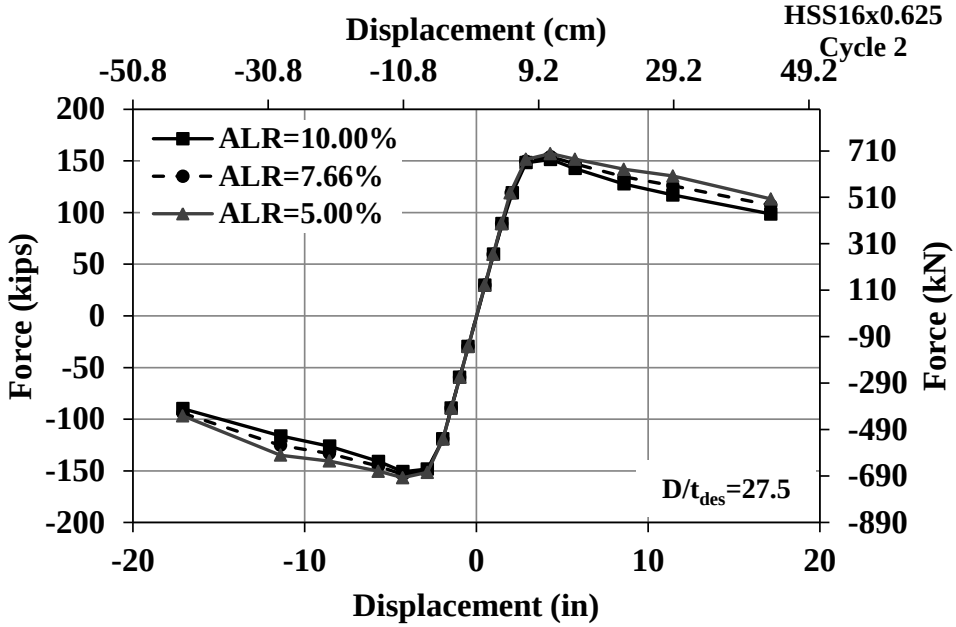

Figure 8.21 Cycle 2 Comparison – HSS16x0.625 D/t_{des}=27.5

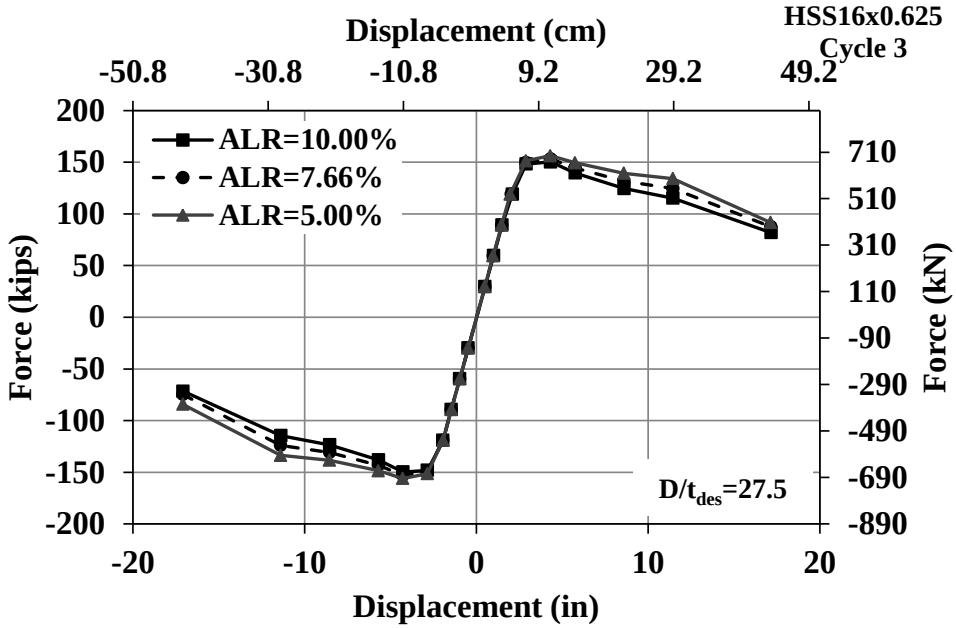

Figure 8.22 Cycle 3 Comparison – HSS16x0.625 D/t_{des}=27.5

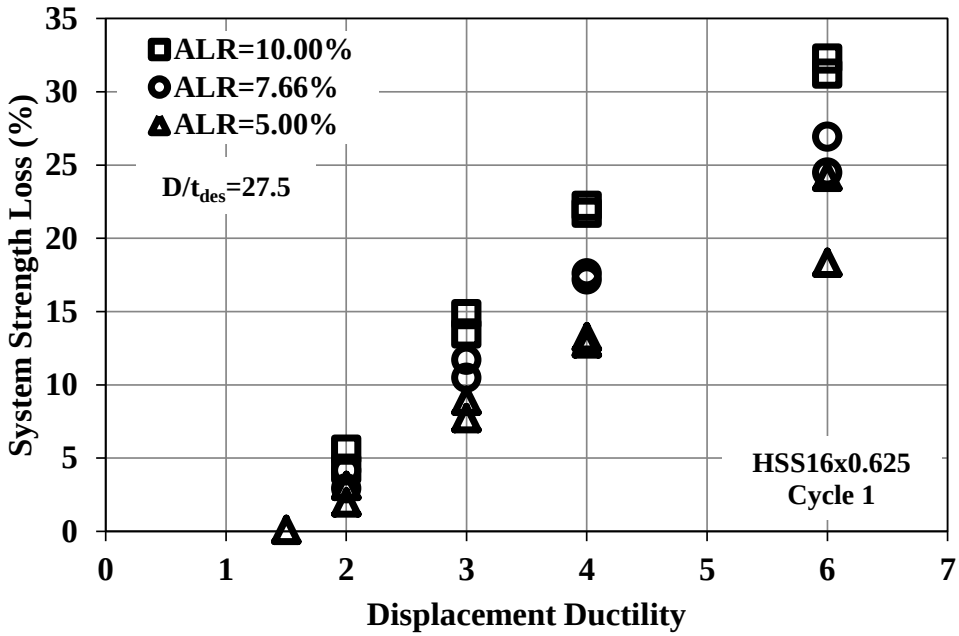

Figure 8.23 Cycle 1 Strength Loss Comparison – HSS16x0.625 D/t_{des}=27.5

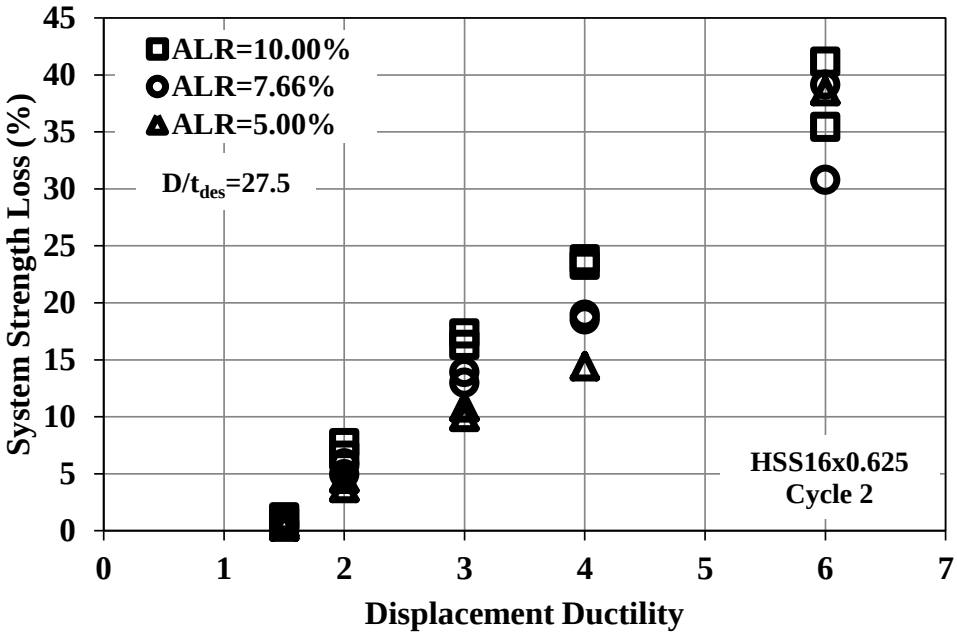

Figure 8.24 Cycle 2 Strength Loss Comparison – HSS16x0.625 D/t_{des}=27.5

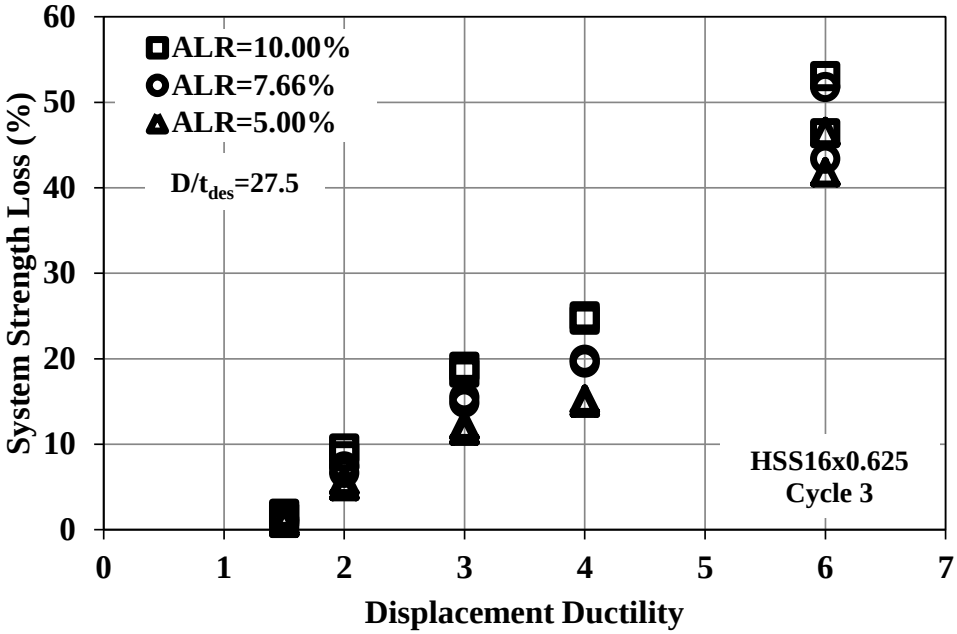

Figure 8.25 Cycle 3 Strength Loss Comparison – HSS16x0.625 D/t_{des}=27.5

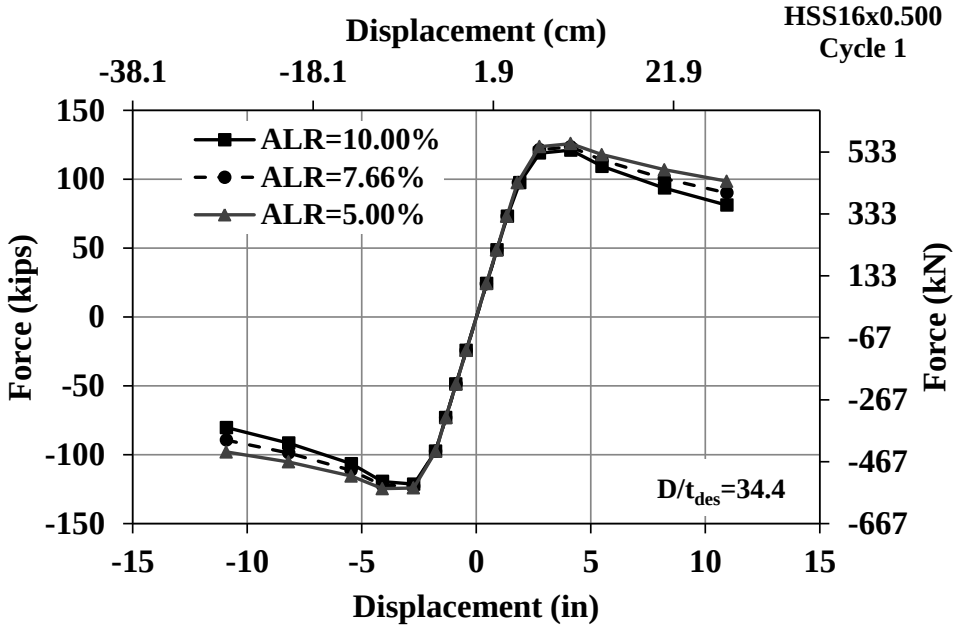

Figure 8.26 Cycle 1 Comparison – HSS16x0.500 D/t_{des}=34.4

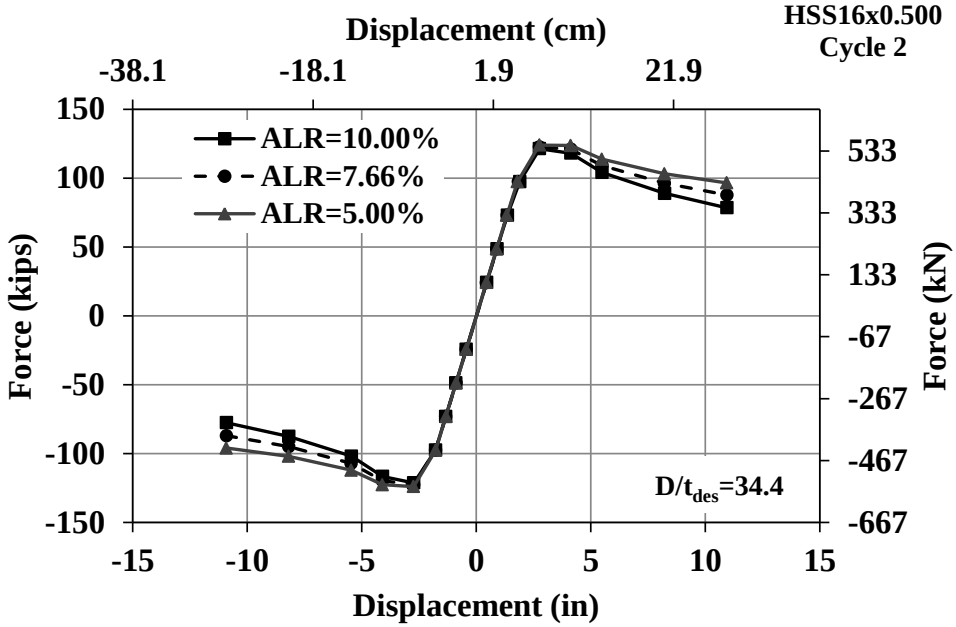

Figure 8.27 Cycle 2 Comparison – HSS16x0.500 D/t_{des}=34.4

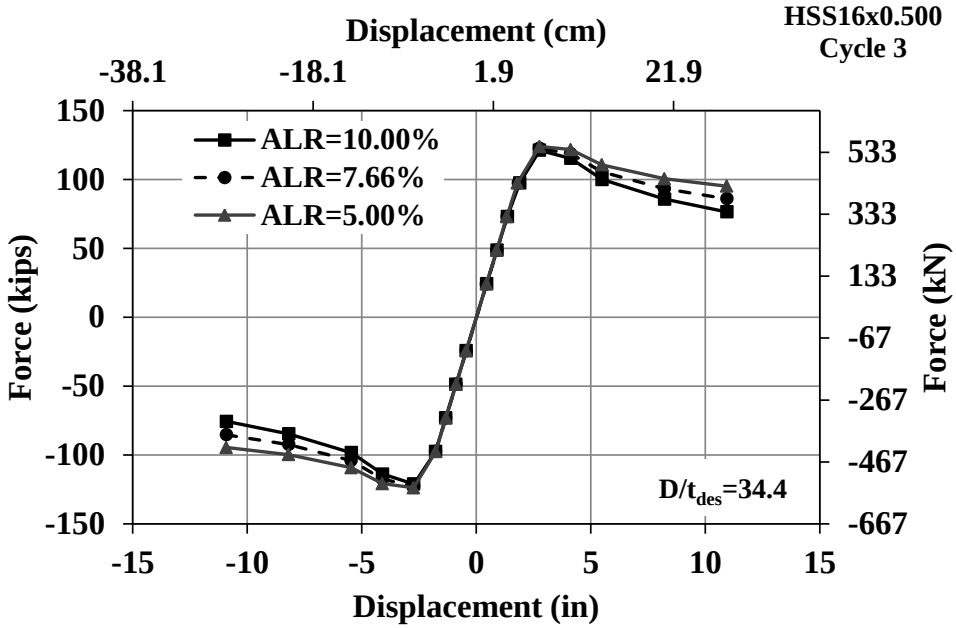

Figure 8.28 Cycle 3 Comparison – HSS16x0.500 D/t_{des}=34.4

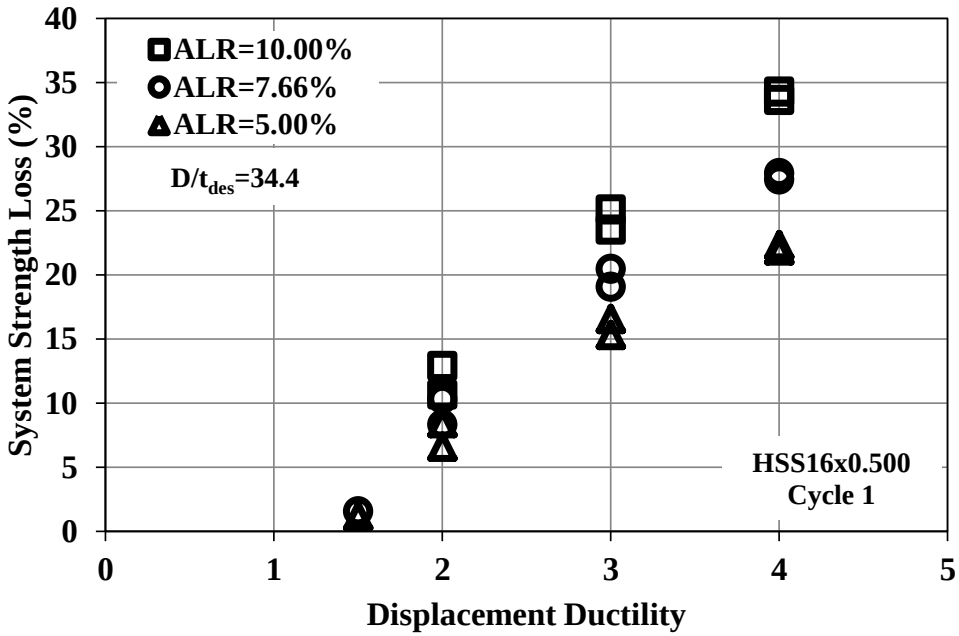

Figure 8.29 Cycle 1 Strength Loss Comparison – HSS16x0.500 D/t_{des}=34.4

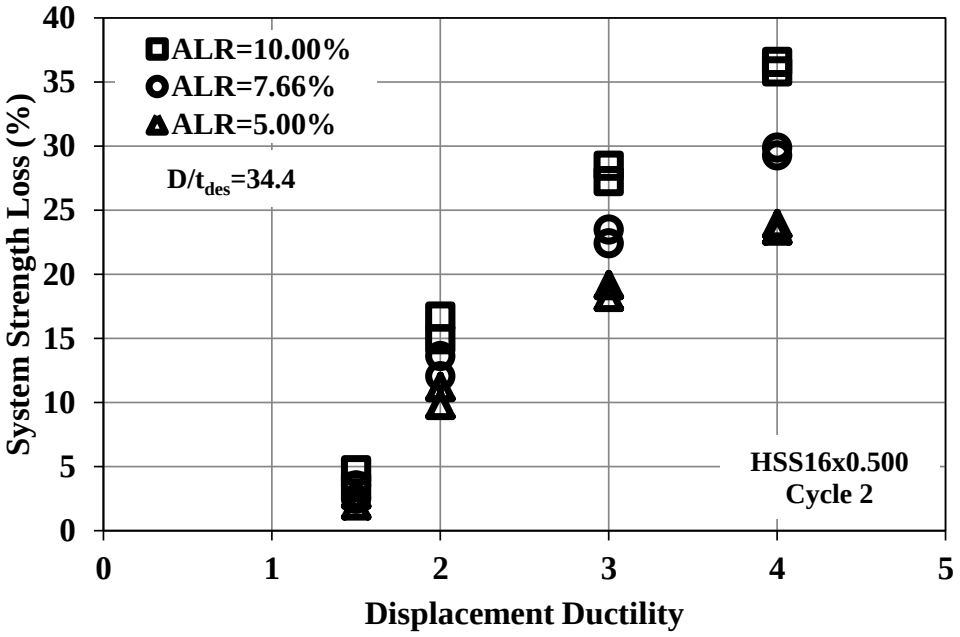

Figure 8.30 Cycle 2 Strength Loss Comparison – HSS16x0.500 D/t_{des}=34.4

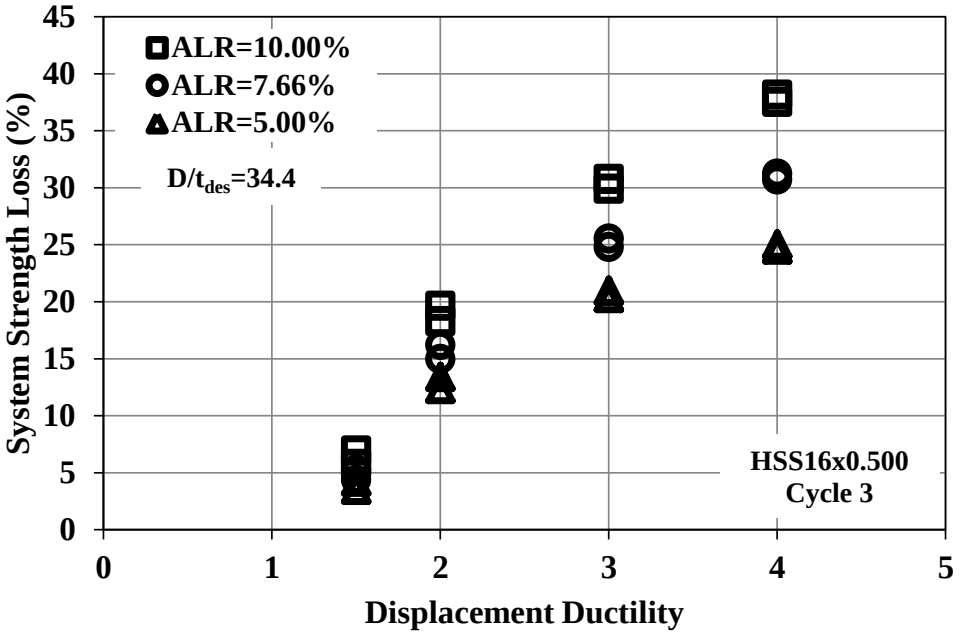

Figure 8.31 Cycle 3 Strength Loss Comparison – HSS16x0.500 D/t_{des}=34.4

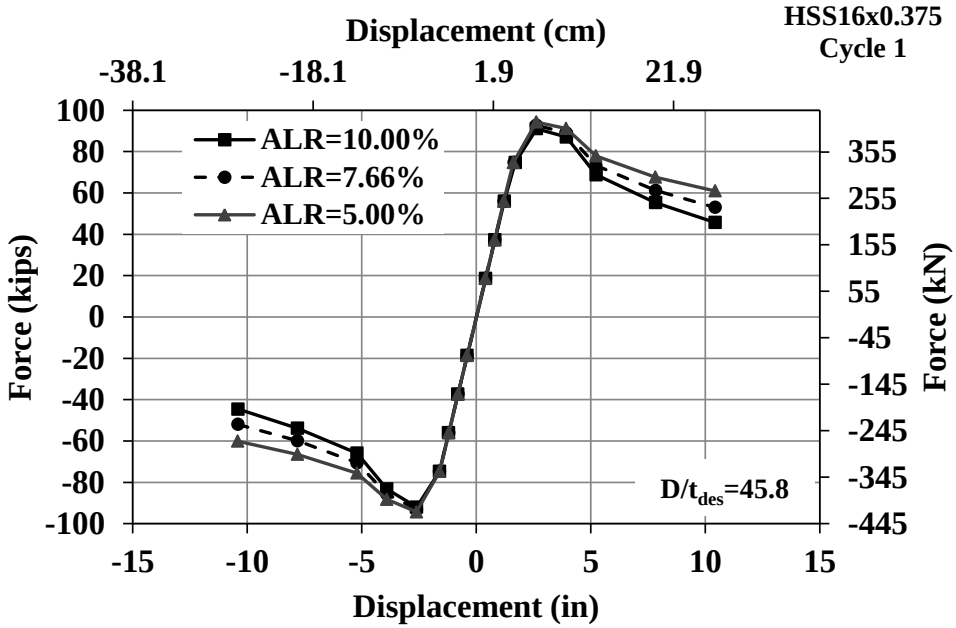

Figure 8.32 Cycle 1 Comparison – HSS16x0.375 D/t_{des}=45.8

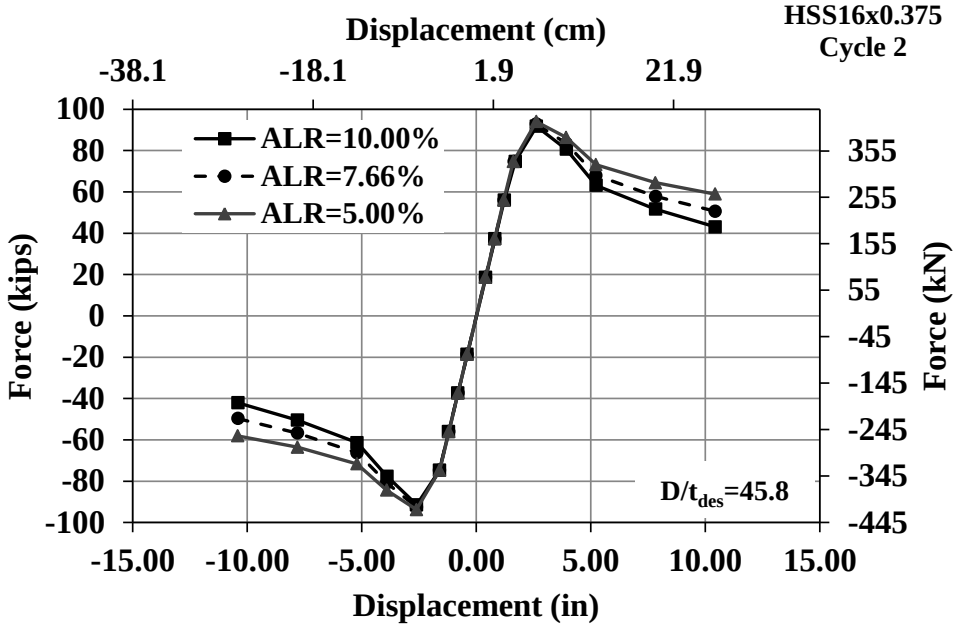

Figure 8.33 Cycle 2 Comparison – HSS16x0.375 D/t_{des}=45.8

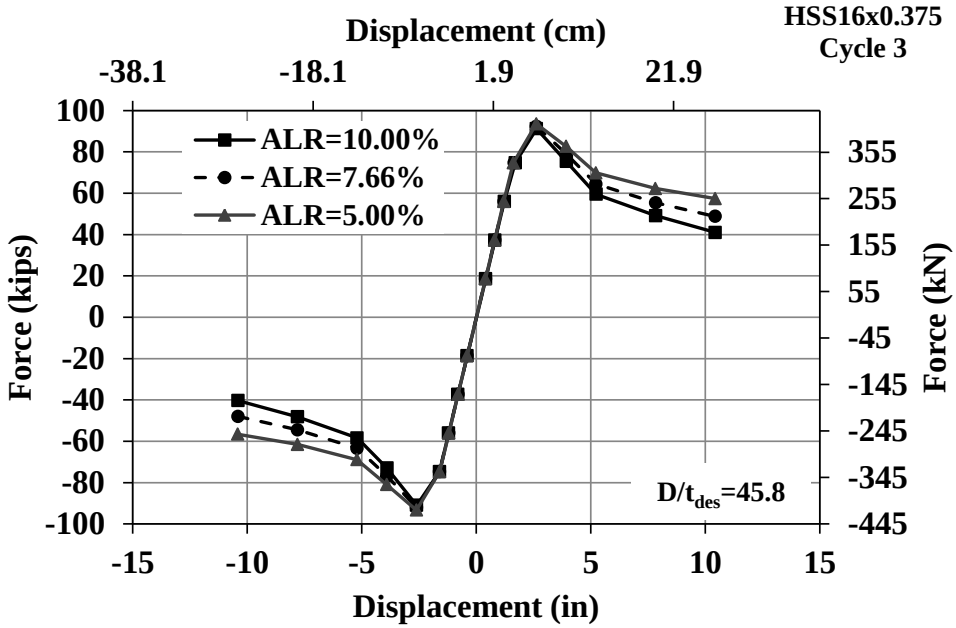

Figure 8.34 Cycle 3 Comparison – HSS16x0.375 D/t_{des}=45.8

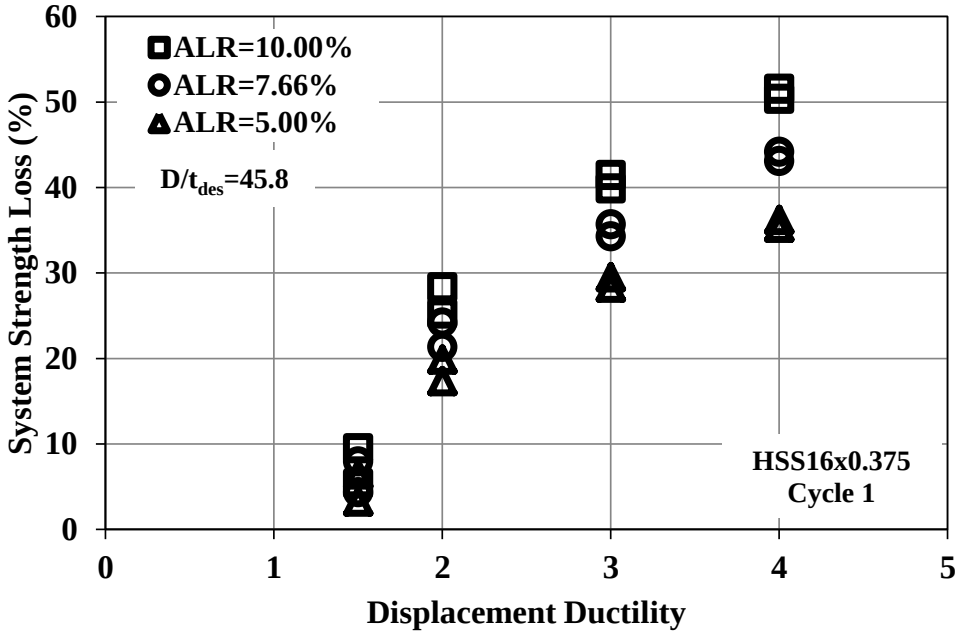

Figure 8.35 Cycle 1 Strength Loss Comparison – HSS16x0.375 D/t_{des}=45.8

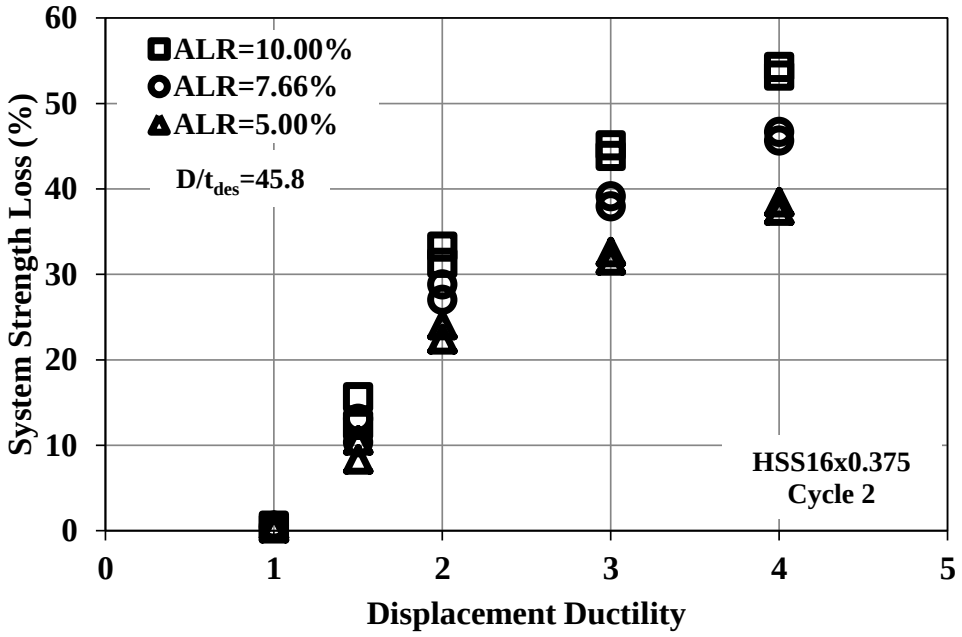

Figure 8.36 Cycle 2 Strength Loss Comparison – HSS16x0.375 D/t_{des}=45.8

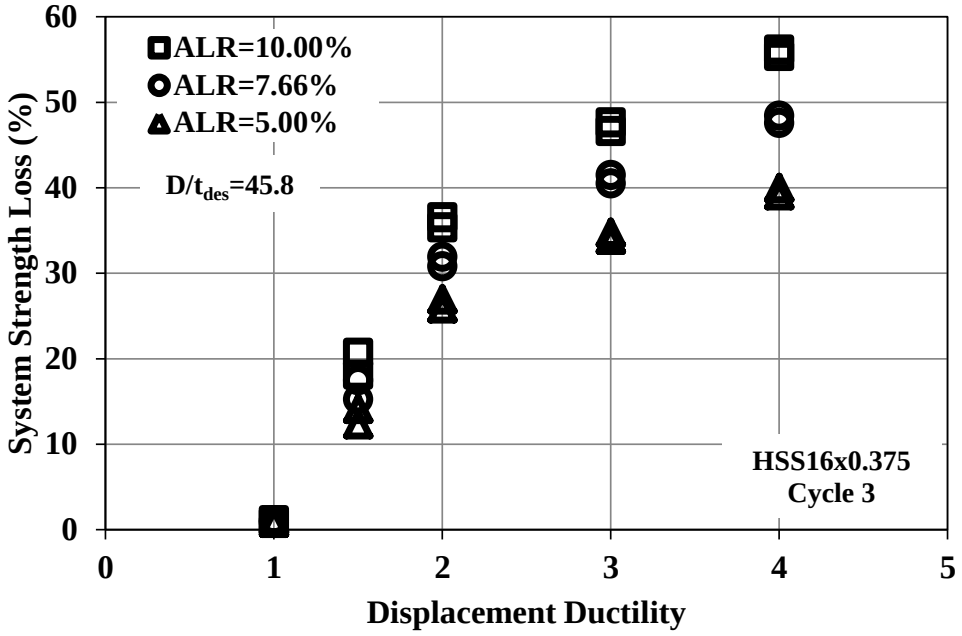

Figure 8.37 Cycle 3 Strength Loss Comparison – HSS16x0.375 D/t_{des}=45.8

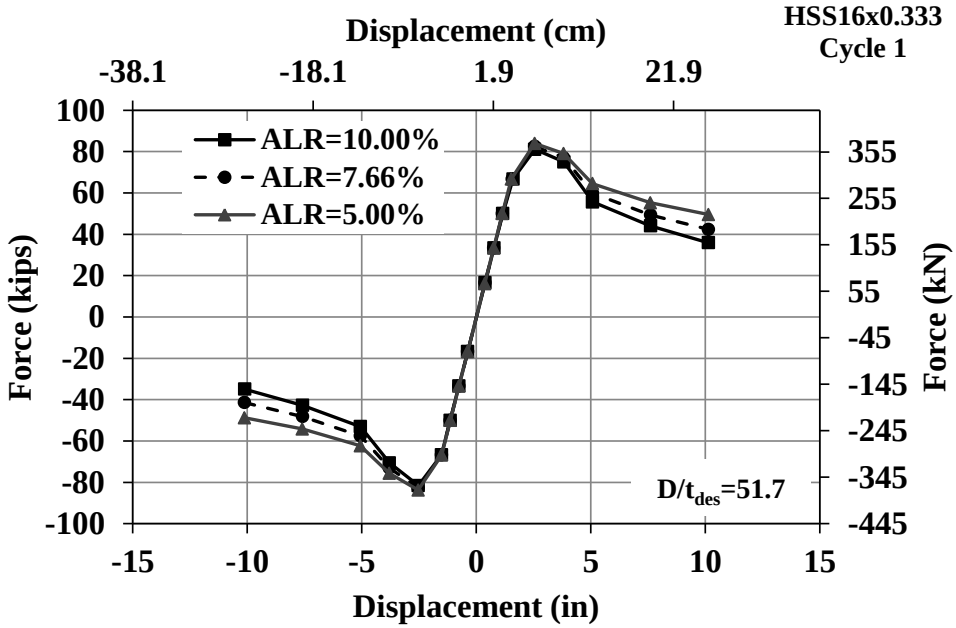

Figure 8.38 Cycle 1 Comparison – HSS16x0.333 D/t_{des}=51.7

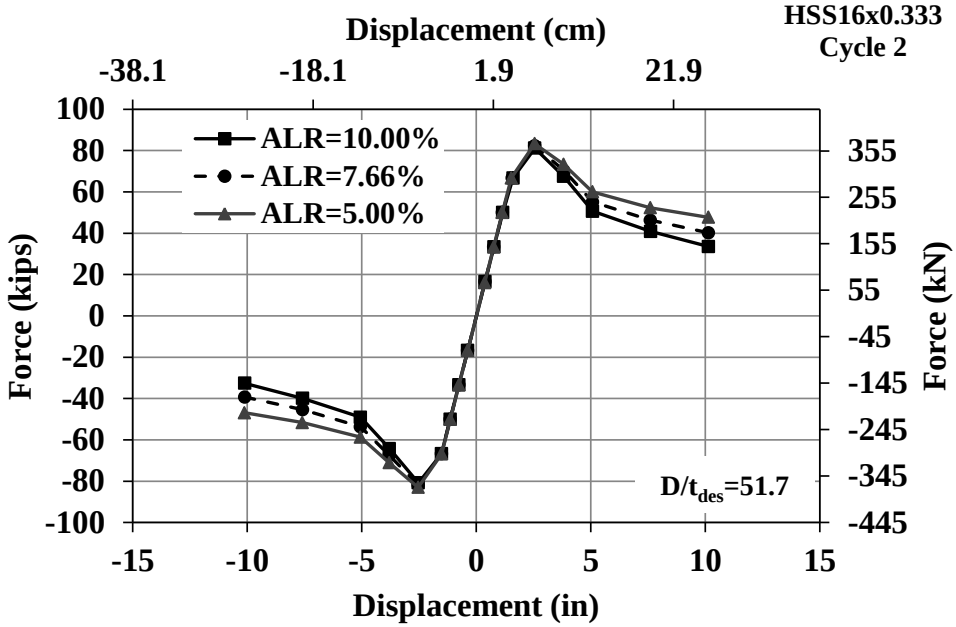

Figure 8.39 Cycle 2 Comparison – HSS16x0.333 D/t_{des}=51.7

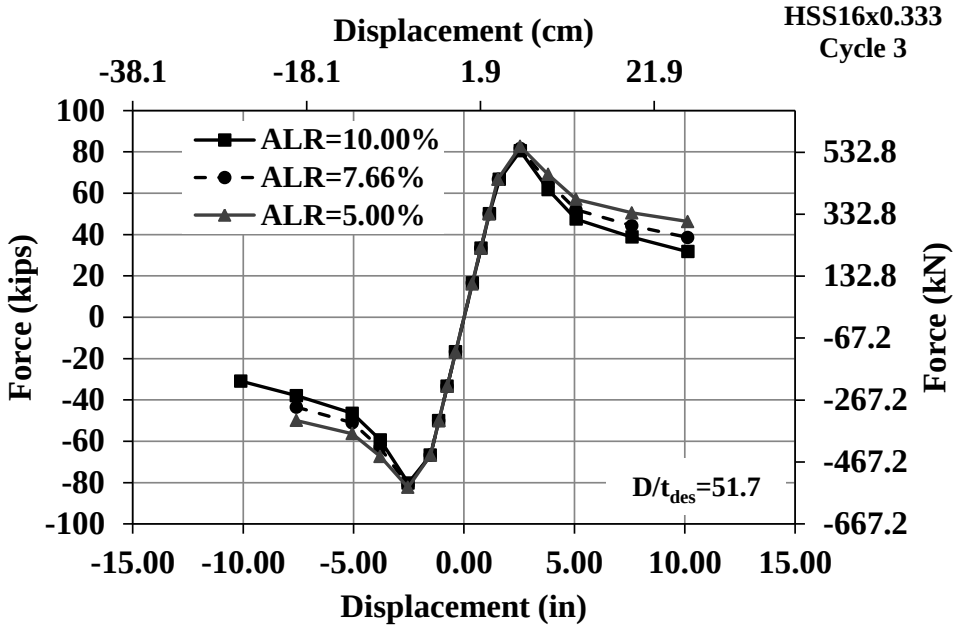

Figure 8.40 Cycle 3 Comparison – HSS16x0.333 D/t_{des}=51.7

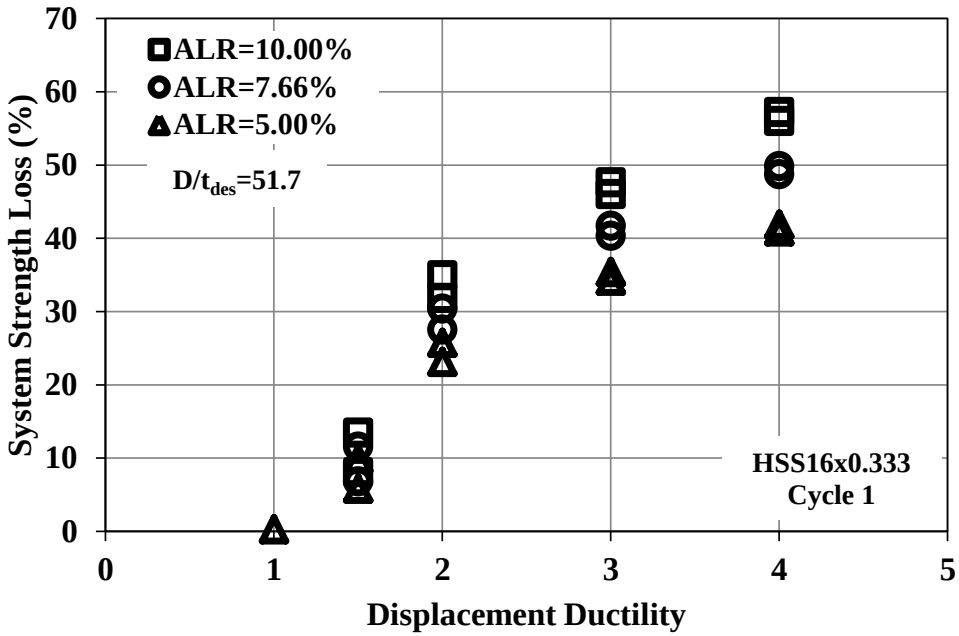

Figure 8.41 Cycle 1 Strength Loss Comparison – HSS16x0.333 D/t_{des}=51.7

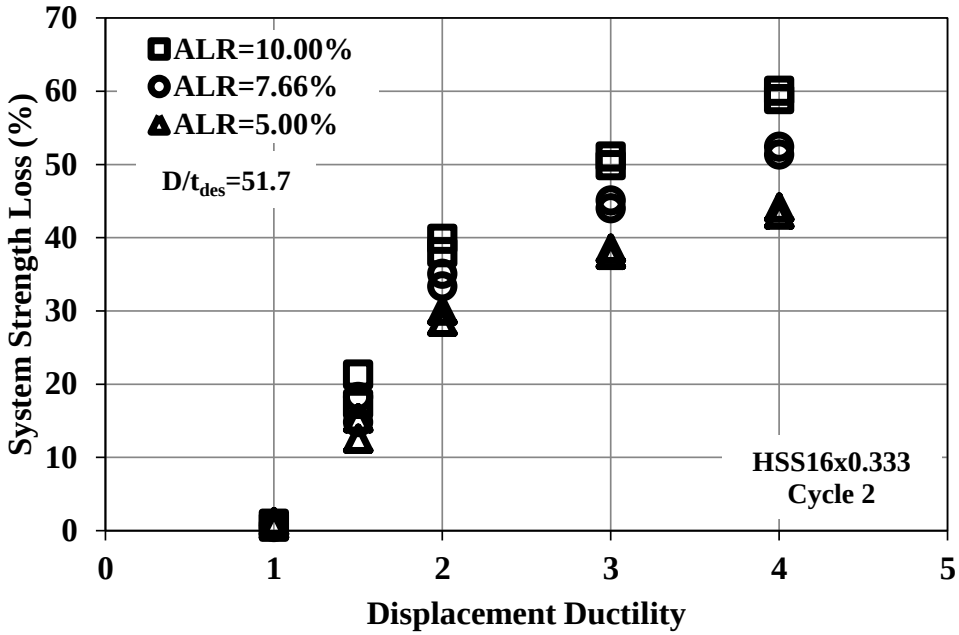

Figure 8.42 Cycle 2 Strength Loss Comparison – HSS16x0.333 D/t_{des}=51.7

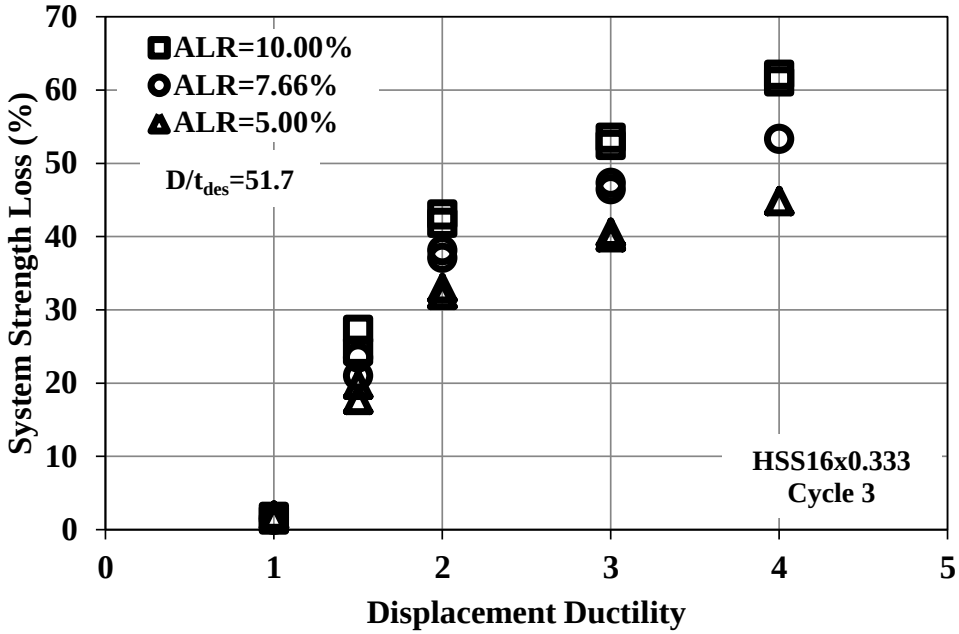

Figure 8.43 Cycle 3 Strength Loss Comparison – HSS16x0.333 D/t_{des}=51.7

8.5 Design Model Recommendation and Limitations

8.5.1 Design Model Development and Calibration

Following the development of the data set presented in the prior section, multivariate polynomial regression analysis, using a least – squares technique, was conducted in Mathcad (Parametric Technology Corporation, 2010) in effort to generate a design equation to calculate allowable displacement ductility capacity as a function of ALR, D/t_{des} ratio, and allowable system strength loss. The initial attempt at the regression analysis considered a first degree polynomial equation. This generated a function with four terms in the form of [$\mu_{all} = a_0ALR + a_1D/t_{des} + a_2F_{loss} + a_3$] which was considered reasonable as a design calculation.

In order to graphically evaluate the effectiveness of the first degree polynomial regression results, the linear regression lines were plotted against the parametric study strength loss data for a given ALR and D/t_{des} ratio. Figure 8.44 through Figure 8.48 display the results of this approach for the first cycles of loading of the three cycle sets. Note, cycles 2 and 3 produced similar results and are not shown for brevity. As is graphically indicated , the regression analysis was successful at capturing the general trends experienced in the data set, primarily increasing strength loss with increasing ductility capacity, ALR and D/t_{des} ratio. However, it appeared there were two problematic areas where the regression results and the actual data set tended to disagree. The first region of considerable disagreement was the ductility 1.5 to 2 region for the higher 2 D/t_{des} ratios and the second, was the ductility 4 to 6 range for the higher 2 D/t_{des} ratios. The particular issue regarding these 2 regions of disagreement was that both occurred in the general range of 10%-25% strength loss which would likely correspond to the most applicable region for design. Based on this result, it was decided that a different form of the regression would be necessary to appropriately model the data set.

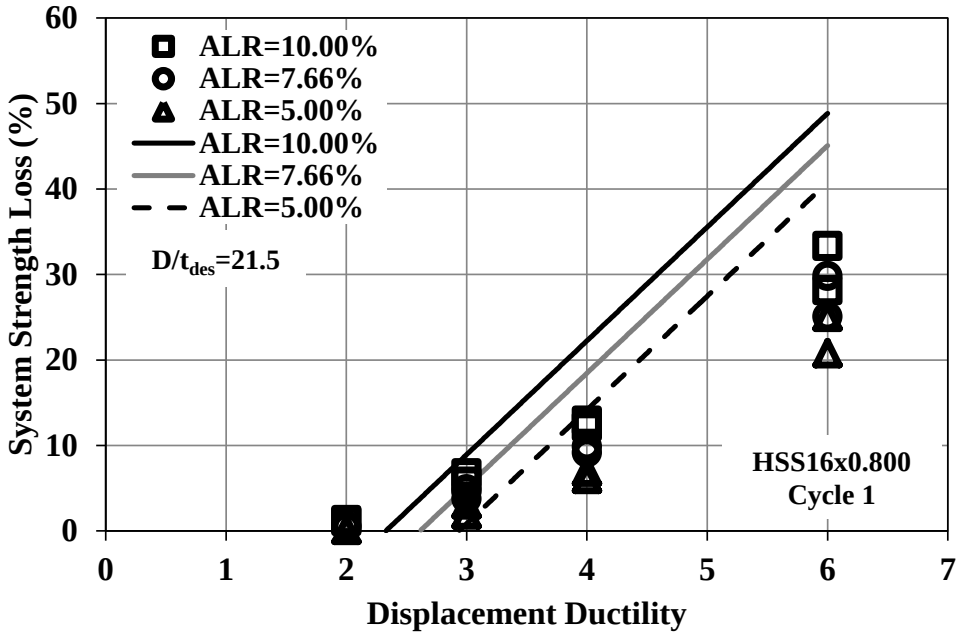

Figure 8.44 FIRST Degree Regression Analysis Results – D/t_{des}=21.5

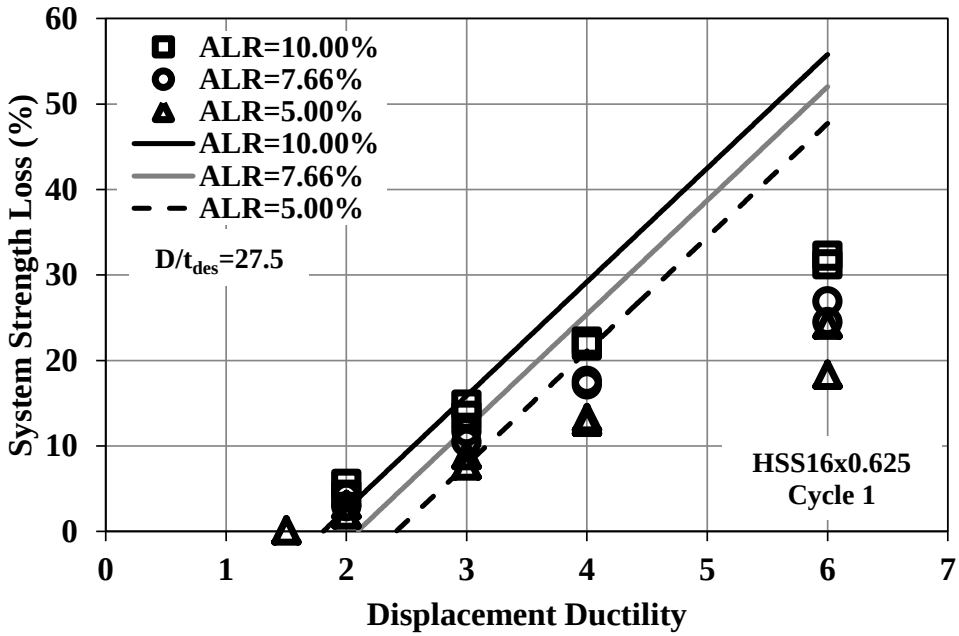

Figure 8.45 FIRST Degree Regression Analysis Results – D/t_{des}=27.5

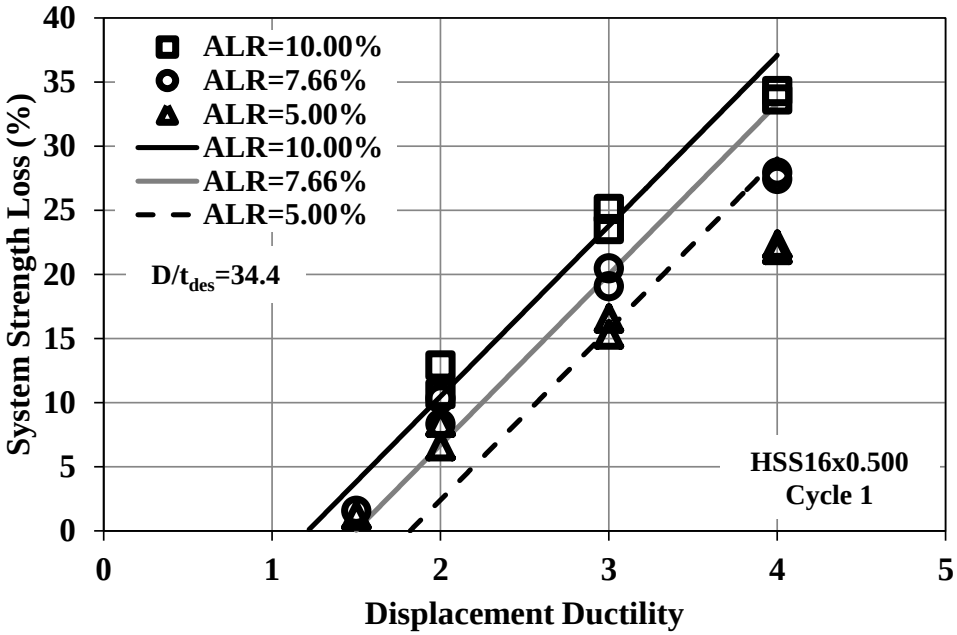

Figure 8.46 FIRST Degree Regression Analysis Results – D/t_{des}=34.4

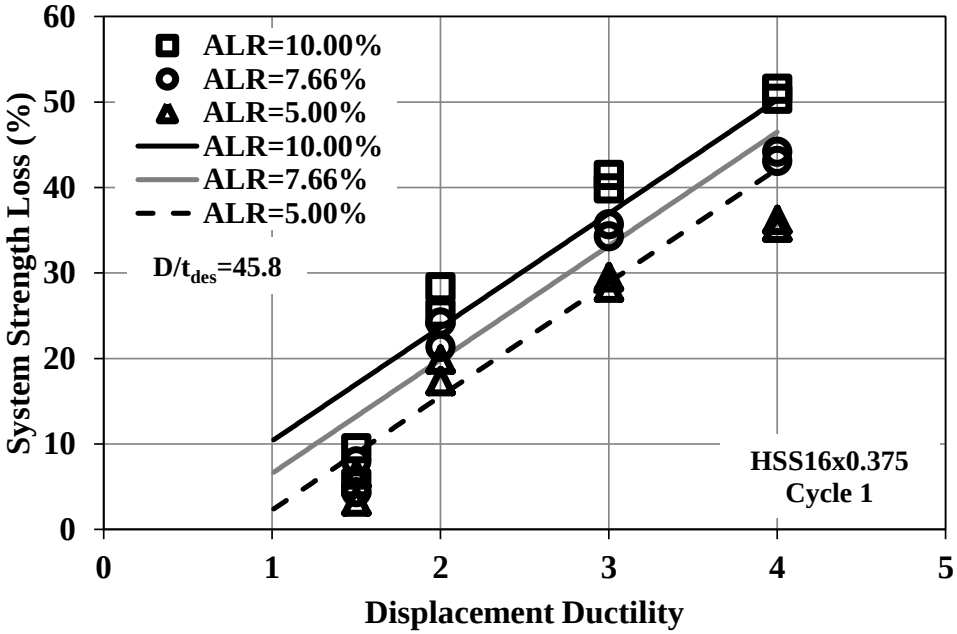

Figure 8.47 FIRST Degree Regression Analysis Results – D/t_{des}=45.8

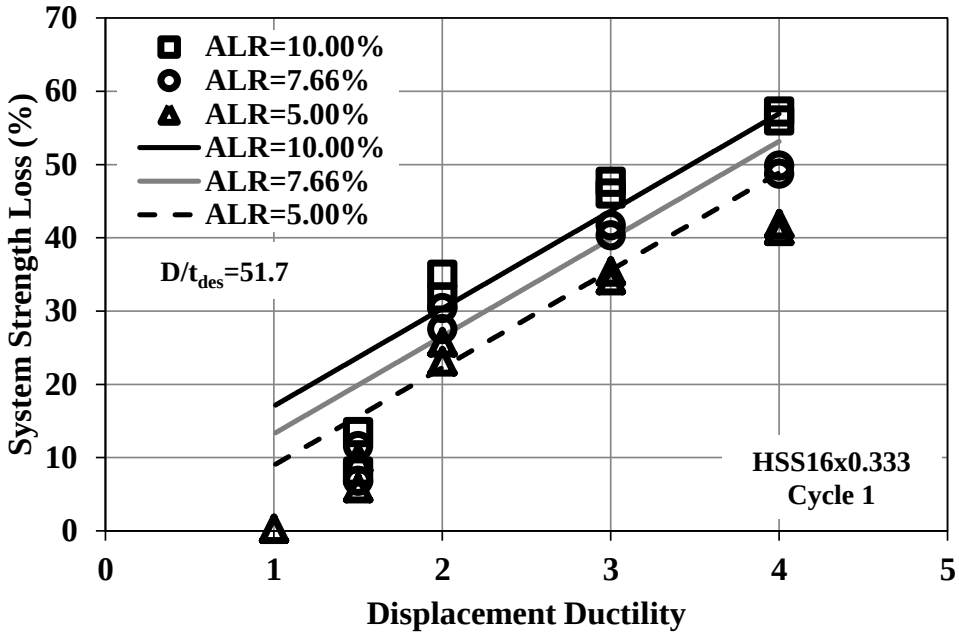

Figure 8.48 FIRST Degree Regression Analysis Results – D/t_{des}=51.7

On option for modifying the regression analysis in an effort to better capture the behavior of the data set was to increase the order of the polynomial considered in the least squares regression. Increasing the order of the regression analysis from a first degree polynomial to a second degree polynomial resulted in a function to calculate reliable ductility capacity that had 10 total terms. Although this clearly was not as simple as the 4 term equation generated by the first order regression, it was felt that it may still be manageable for design should it appropriately capture trends of the data set.

As shown in Figure 8.49 through Figure 8.53, this form of the regression appeared to better agree through the ductility 2 to 4 region for all cases, and showed some slight improvement at the ductility 6 level of the lower 2 D/t_{des} ratios. However, the regression showed little improvement in the ductility 1.5 to 2 range for the lower 2 D/t_{des} ratios which corresponded again to a strength loss range of 10% - 20%. Again, this was assumed to be an important combination of strength loss and D/t_{des} ratio for design purposes, indicating that it

may be necessary to improve the regression analysis. Further, the improvement from the first order case to the second order case was found to be only marginal for the significant increase in complexity of the design equation.

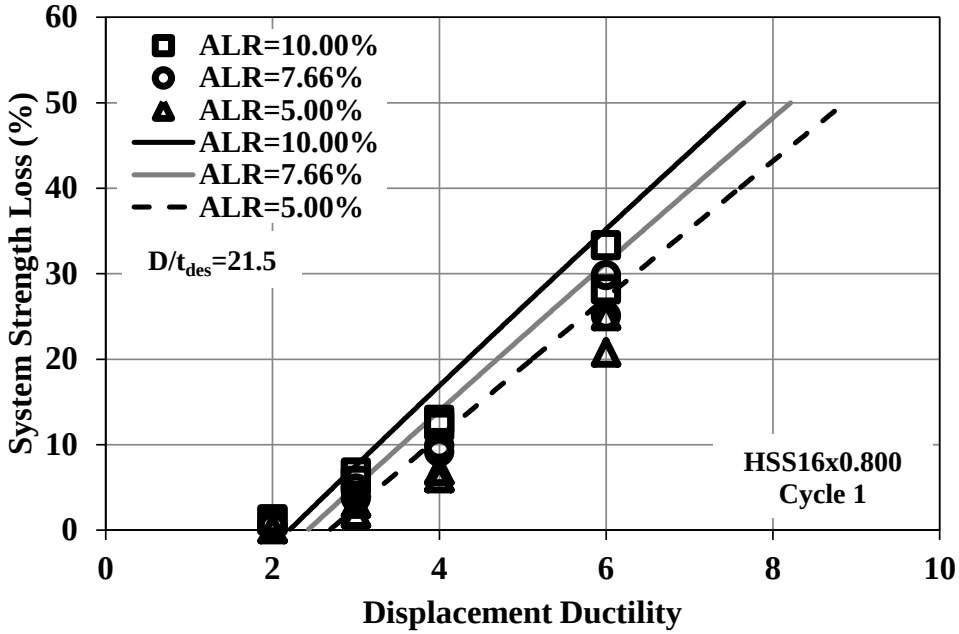

Figure 8.49 SECOND Degree Regression Analysis Results – D/t_{des}=21.5

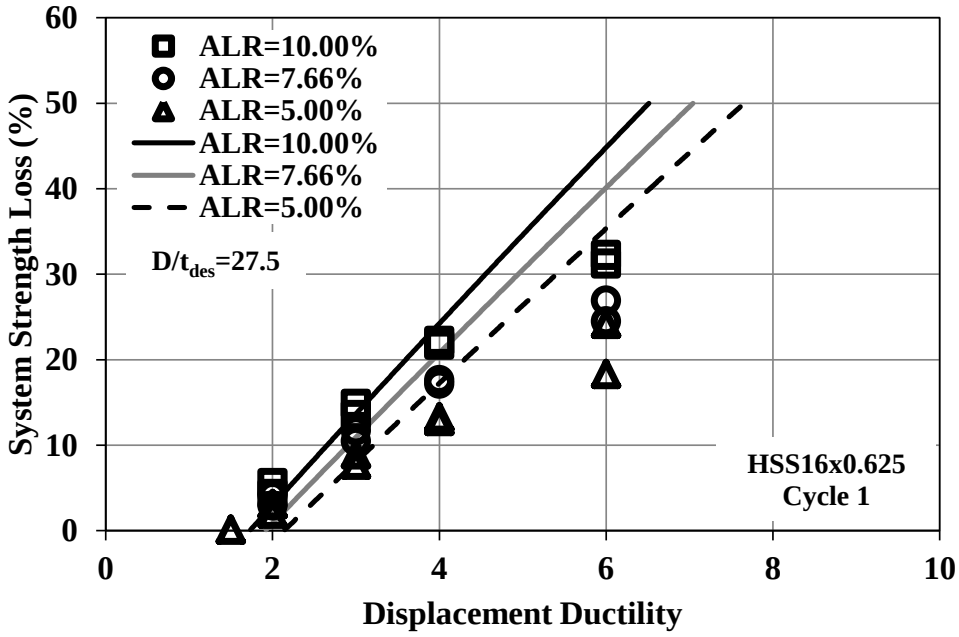

Figure 8.50 SECOND Degree Regression Analysis Results – D/t_{des}=27.5

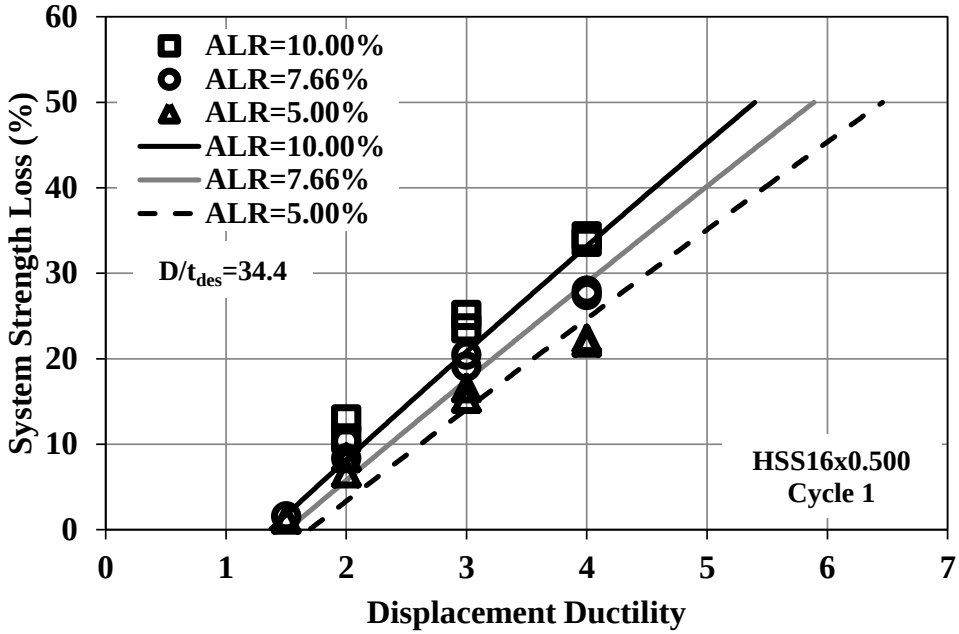

Figure 8.51 SECOND Degree Regression Analysis Results – D/t_{des}=34.4

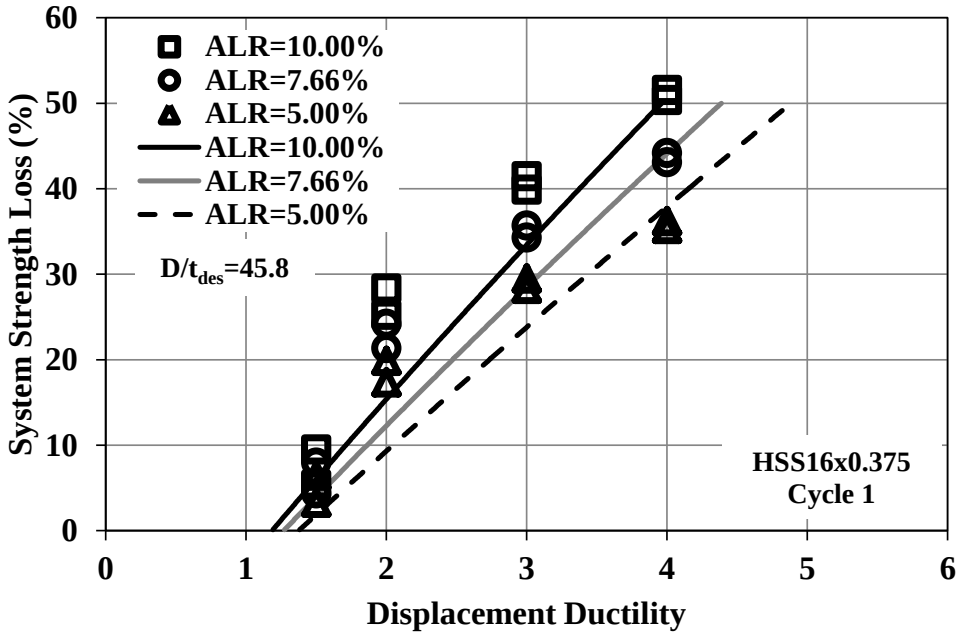

Figure 8.52 SECOND Degree Regression Analysis Results – D/t_{des}=45.8

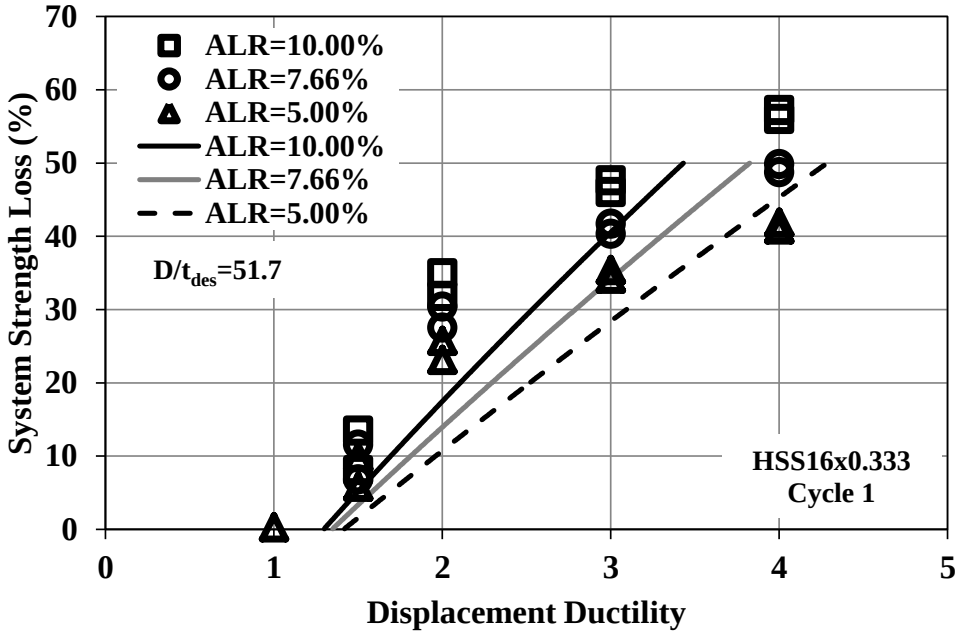

Figure 8.53 SECOND Degree Regression Analysis Results – D/t_{des}=51.7

Following the attempt at a second order polynomial regression, one possible option to further improve the accuracy of the design model was to again increase the order of the polynomial associated with the multivariate regression analysis to the third order. However, this increased the number of terms associated with the design equation to 20, which would likely render solution by hand impractical. The complexity associated with this equation would likely require some form of an accompanying program should the method be recommended. Regardless, the decision was made to investigate the option.

As shown Figure 8.54 through Figure 8.58, the third order multivariate regression analysis appeared to generate nonlinearity associated with the F_{loss} parameter which had appeared to remain linear in the first and second order cases. As is shown, the third order polynomial design equation indicates good agreement within the ductility 2 to 4 range, and good agreement in the case D/t_{des}=21.5 at the ductility 6 level. However, the equation again fails to appropriately capture the ductility 1.5 to 2 range for the lower D/t_{des} ratios. In this case, it appeared that the higher order terms associated with the F_{loss} variable caused the regression curves to invert towards the lower ductility levels, as shown in Figure 8.57 and Figure 8.58, which not only does not capture the behavior of the data set but further is illogical based on the behavior of actual piers. It is worth noting, similar behavior was observed past the ductility 6 level which is also illogical, but with the model limited to a ductility level of 6, this problem may be mitigated. Given the complexity of the design equation, illogical behavior at lower ductility levels, and lack of overall improvement, the design equation associated with the third degree multivariate regression is not recommended.

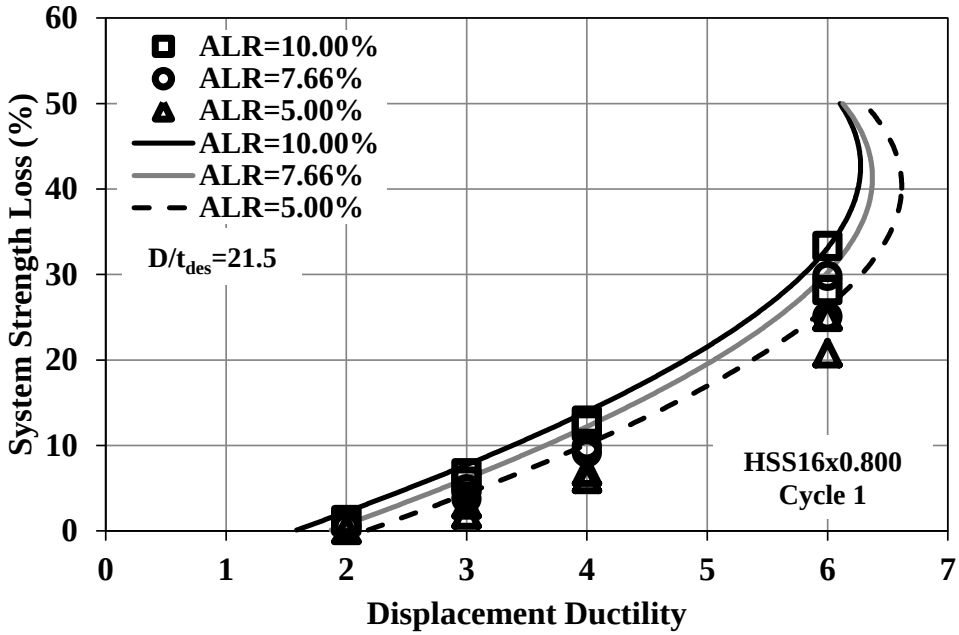

Figure 8.54 THIRD Degree Regression Analysis Results – D/t_{des}=21.5

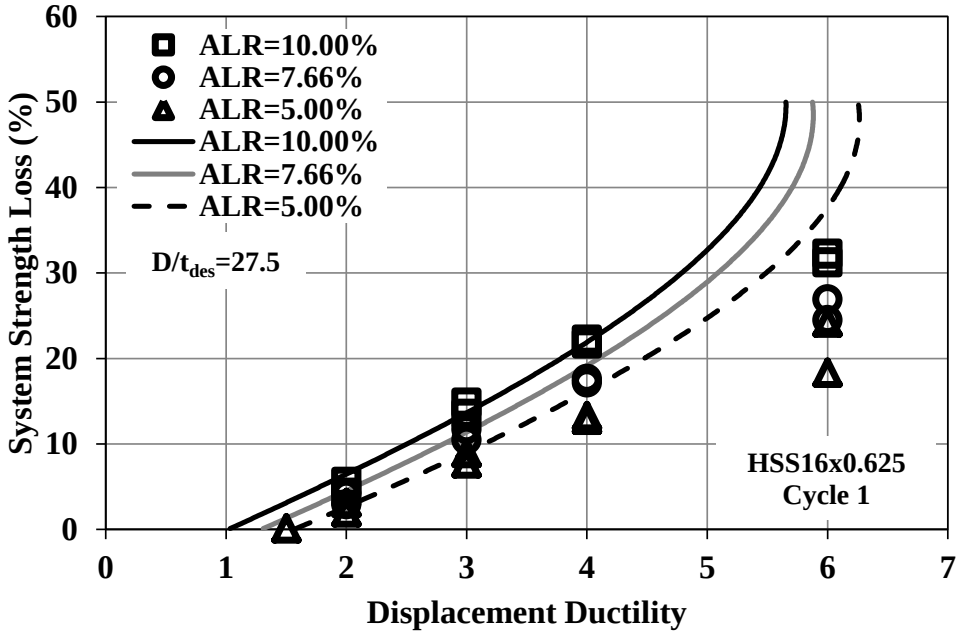

Figure 8.55 THIRD Degree Regression Analysis Results – D/t_{des}=27.5

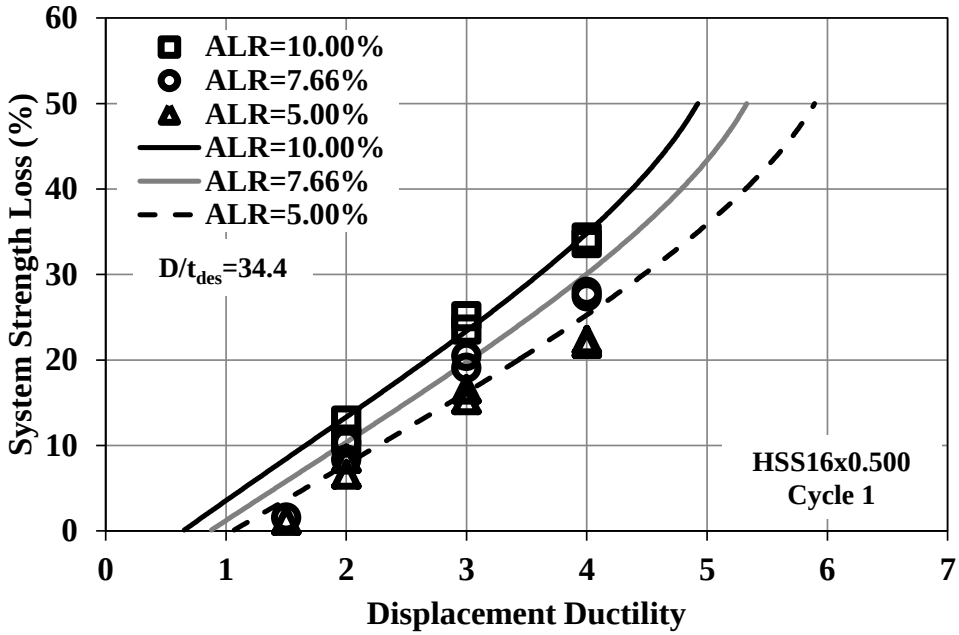

Figure 8.56 THIRD Degree Regression Analysis Results – D/t_{des}=34.4

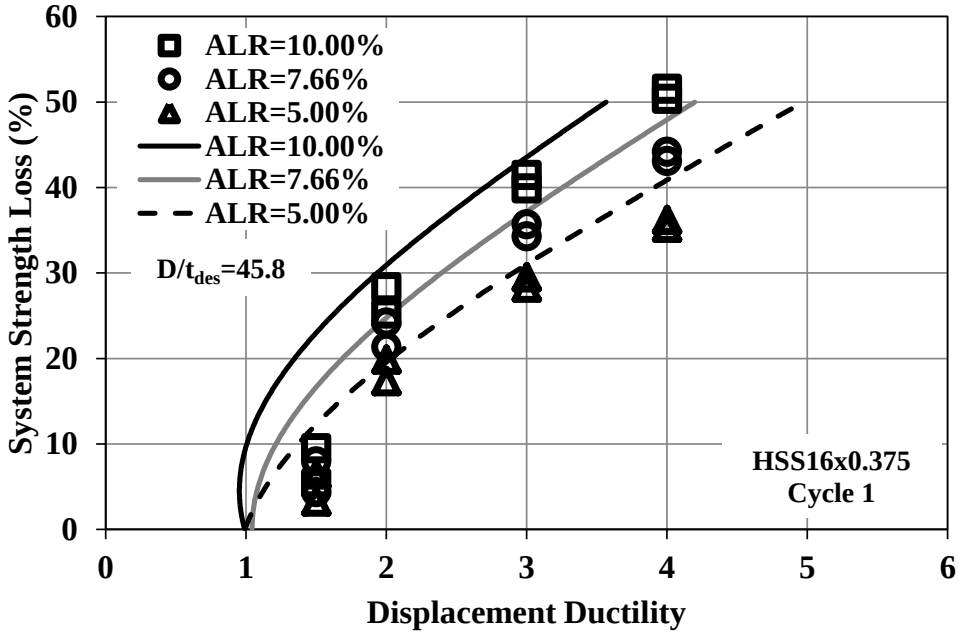

Figure 8.57 THIRD Degree Regression Analysis Results – D/t_{des}=45.8

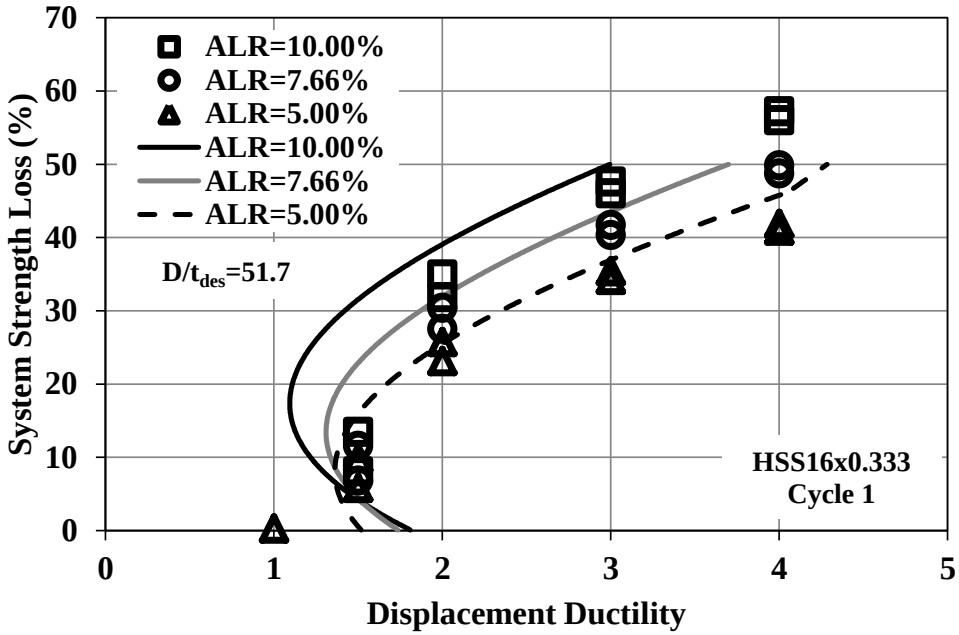

Figure 8.58 THIRD Degree Regression Analysis Results – D/t_{des}=51.7

Noting that the higher power polynomial multivariate regression analyses were more complex and did not adequately capture the behavior of the data set, the decision was made to attempt developing a multi-linear polynomial multivariate model. Reviewing the strength loss results from the data set, it appeared for the cases with lower D/t_{des} ratios that a relatively linear variation existed between the data in the ductility 1 to 2 range, and a linear variation in the 2 to 4 range with a different slope. Likewise, with the higher D/t_{des} ratios, there seemed to be a relatively linear variation in the ductility 2 to 4 range, and also in the 4 to 6 range with a different slope. Hence, there appeared to be two applicable pivot points, one at ductility 2 and one at ductility 4. This behavior is schematically depicted in Figure 8.59. However, it should be noted that this figure is only for schematic purposes to illustrate the behavior of the entire data set. In general only two of the three trends were noted for a single D/t_{des} ratio.

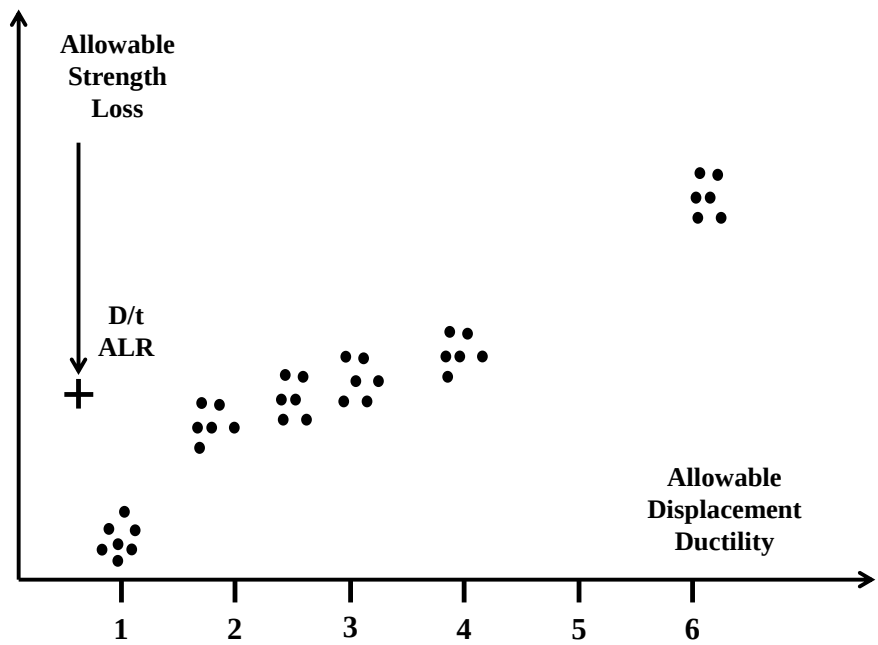

Figure 8.59 Strength Loss vs. Displacement Ductility Schematic

In an effort to calibrate the design equation, the data set was lumped into three overlapping groups. These groups included data in the displacement ductility range 1 to 2, the range 2 to 4, and the range 4 to 6 as shown in Figure 8.60. For each of the three data sets, a first order multivariate least-squares regression analysis was conducted, resulting in 3 separate design equations each in the form of [$\mu_{all} = a_0ALR + a_1D/t_{des} + a_2F_{loss} + a_3$]. These analytical regression lines are schematically shown in Figure 8.60 as lines 1, 2, and 3 which essentially define a backbone tri-linear regression curve.

The intention of the design model was that for a given ALR, D/t_{des} ratio, and allowable strength loss (F_{loss}), one of the three curves would control the ultimate displacement ductility capacity of the system. As illustrated in Figure 8.61, entering the vertical strength loss axis of the graph provides 3 possible solutions. The first possible option (shown by lowest dashed arrow), involves passing the 2 curve and proceeding to the applicable 1 curve for the ductility 1 to 2 range. The second possible option (shown by the middle dashed arrow), involves

passing the 1 curve and proceeding to the applicable 2 curve for the ductility 2 to 4 range. Lastly, the third option (shown by the highest dashed arrow), involves passing the 1 curve and stopping at the applicable 3 curve prior to reaching the 2 curve, for the ductility range 4 to 6.

This process essentially forms the backbone curve show by the heavy trace in Figure 8.62 and is mathematically defined as shown in Figure 8.63. As shown, the model is not forced to pivot at ductility 2 and 4, but instead pivots near these regions at a value that is determined from the calibration of the design equations. The three design equations are split into two regions, one for ductility range 1-3, and one for ductility range 3-6. Although this was conceptually unnecessary, doing so ensures that the 3 curve does not interfere within the ductility 1 to 2 range which is mathematically unclear. Lastly, the model should be bounded by ductility levels 1 and 6 as this is what was considered in the data set.

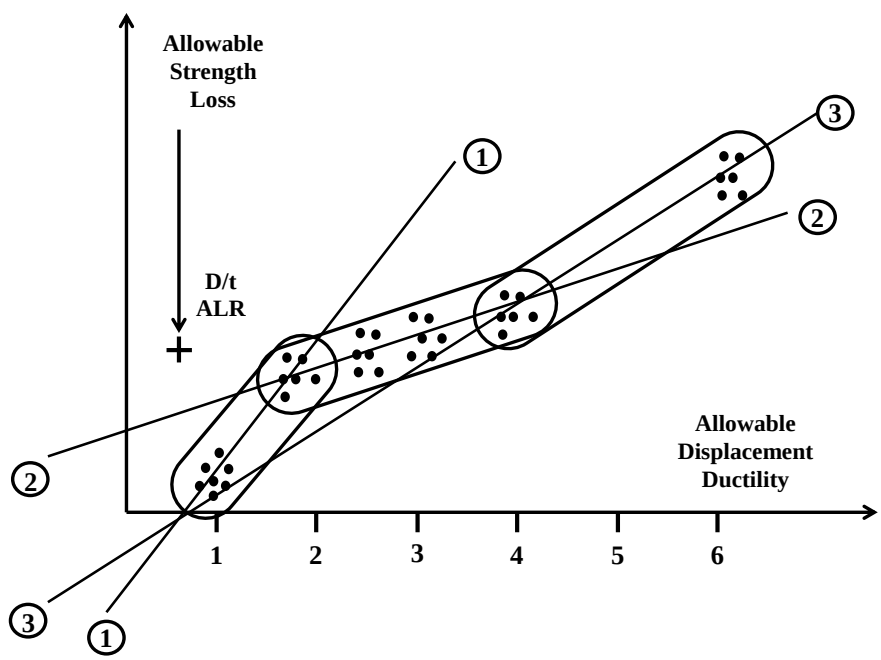

Figure 8.60 Schematic of 3 Individual Regressions

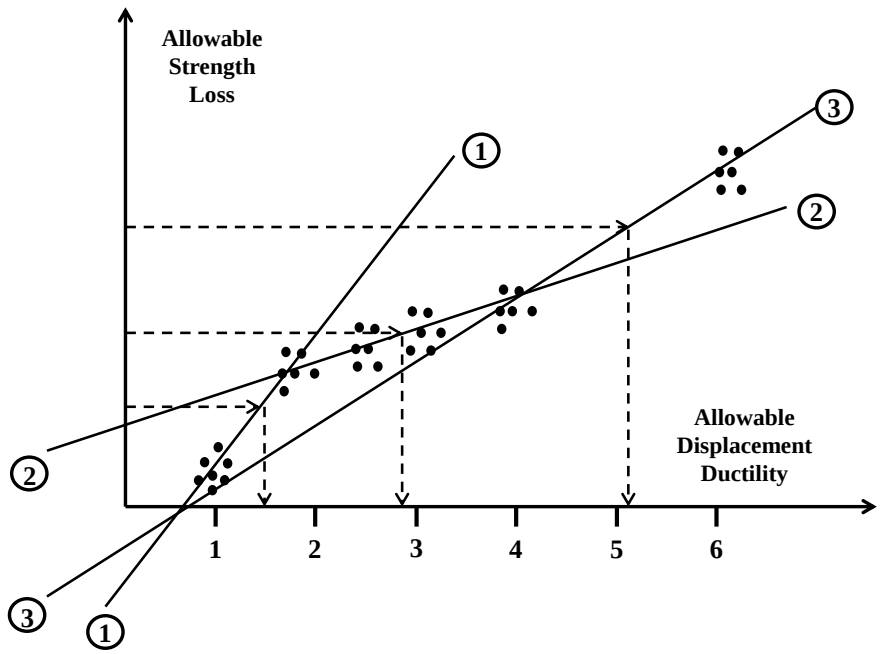

Figure 8.61 Schematic Use of 3 Part Design Equation

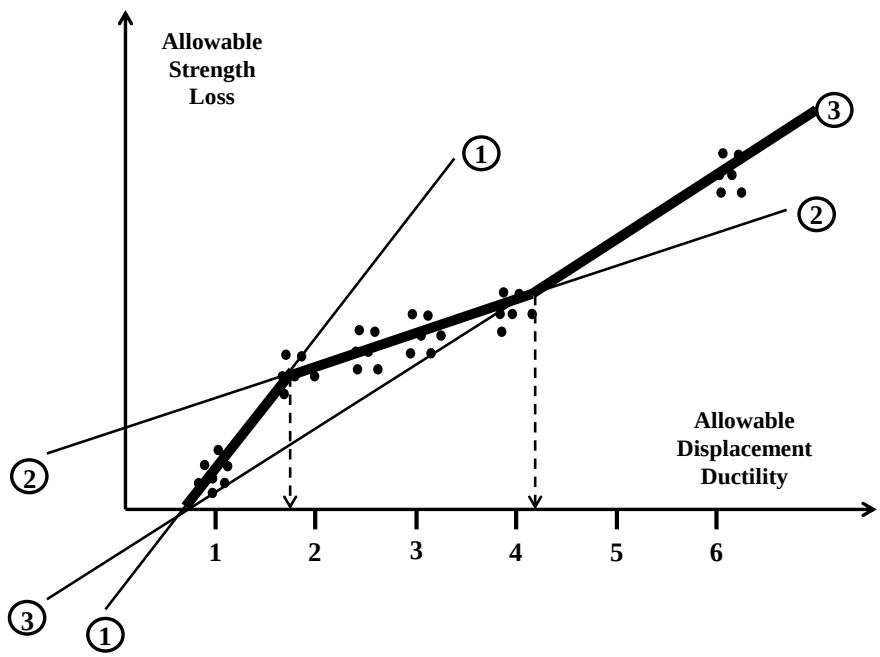

Figure 8.62 Schematic of Design Equation Backbone Curve

$\mu_{\Delta all}$ = ② ≥ ① For: $\mu_{\Delta all}$ = 1-3

$\mu_{\Delta all}$ = ② ≤ ③ For: $\mu_{\Delta all}$ = 3-6

Where: ①, ②, ③ are f(ALR, D/t_{des}, F_{loss})

Figure 8.63 Multi-Linear Design Model Concept

First order multivariate regression analysis with the data sets discussed produced the design equations shown in Eq.(8.2) and Eq.(8.3), where the coefficients are considered to 5 decimal places. The data sets used, consisted of ALR, D/t_{des}, and F_{loss} values from all three cycles of loading with no distinction between cycles. Configuring the data sets in this manner inherently assumed that sustaining strength throughout multiple cycles of loading at a given ductility level would be a design requirement when determining allowable ductility capacities.

The set of design equations that were generated were used to calculate the allowable displacement ductility values for the input data set of ALR, D/t_{des}, and F_{loss} values, and the results were compared to the corresponding ductility values input into the regression analysis. From this comparison, the design model resulted in an an allowable displacement ductility RMS error of 0.5095. Reducing the number of significant figures of the coefficients allowed for simplification of the design equation set to that given in Eq.(8.4) and Eq.(8.5). This simplification increased the allowable displacement ductility RMS error by an insignificant amount to 0.5347 and had no other observable effects on the comparisons to the data set that will be subsequently discussed. It should also be noted, the design model has been calibrated for the input variables to be in the form of a decimal for ALR (i.e. 0.0766 for 7.66%), integer values for D/t_{des} (i.e. 34.4), and F_{loss} as integer values (i.e. 25 for 25%).

For $\mu_{\Delta all}$=1-3: $$\mu_{\Delta all} = 6 \geq [6.32684 - 16.6213ALR - 0.11407D/t_{des} + 0.08974F_{loss}] \geq \\ .....[2.69139 - 2.76687ALR - 0.02944D/t_{des} + 0.03113F_{loss}] \geq 1 \quad (8.2)$$

For $\mu_{\Delta all}$=3-6: $$\mu_{\Delta all} = 6 \geq [6.32684 - 16.6213ALR - 0.11407D/t_{des} + 0.08974F_{loss}] \leq \\ .....[6.49541 - 11.78241ALR - 0.07937D/t_{des} + 0.0493F_{loss}] \geq 1 \quad (8.3)$$

For $\mu_{\Delta all}$=1-3: $$\mu_{\Delta all} = 6 \geq [6.3 - 16.6ALR - 0.114D/t_{des} + 0.0897F_{loss}] \geq \\ .....[2.7 - 2.8ALR - 0.029D/t_{des} + 0.0311F_{loss}] \geq 1 \quad (8.4)$$

For $\mu_{\Delta all}$=3-6: $$\mu_{\Delta all} = 6 \geq [6.3 - 16.6ALR - 0.114D/t_{des} + 0.0897F_{loss}] \leq \\ .....[6.5 - 11.8ALR - 0.079D/t_{des} + 0.0493F_{loss}] \geq 1 \quad (8.5)$$

In order to support the use of the multi-linear regression analysis design model, the regression traces of strength loss vs. displacement ductility, for each ALR and D/t_{des} ratio, have been plotted against the values provided by the 15 analyses. As shown in Figure 8.64 through Figure 8.78, this has been done for all cycles of loading such that comparisons with the cyclic strength degradation that was experienced can be made. However, it should be noted that the design model is cycle independent and consequently the traces are constant between cycles.

As is shown, by allowing the multi-linear design model to pivot around the ductility 2 and 4 regions, the model appeared to adequately capture the behavior of higher D/t_{des} ratios in the ductility 1 to 2 range and the lower D/t_{des} ratios in in the ductility 4 to 6 range. In addition, the model also appeared to capture behavior in the intermediate ductility 2 to 4 range. By doing so, the model was able to predict with reasonable accuracy, the strength loss behavior in the range important to design (10%-30%) as well as at higher levels that may be useful in the evaluation of an existing structure.

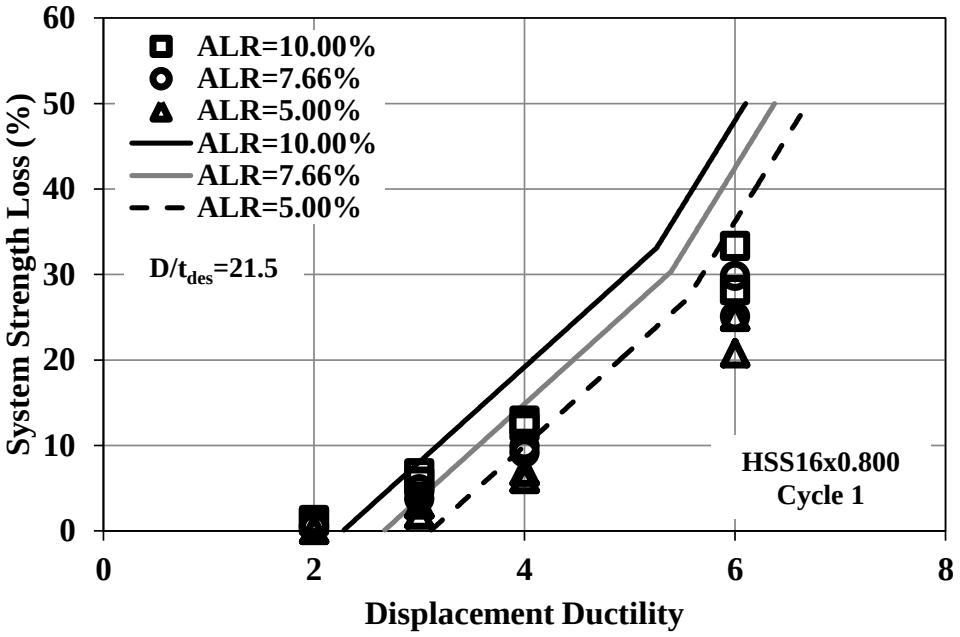

Figure 8.64 Multi-Linear Regression Analysis Results – Cycle 1 – D/t_{des}=21.5

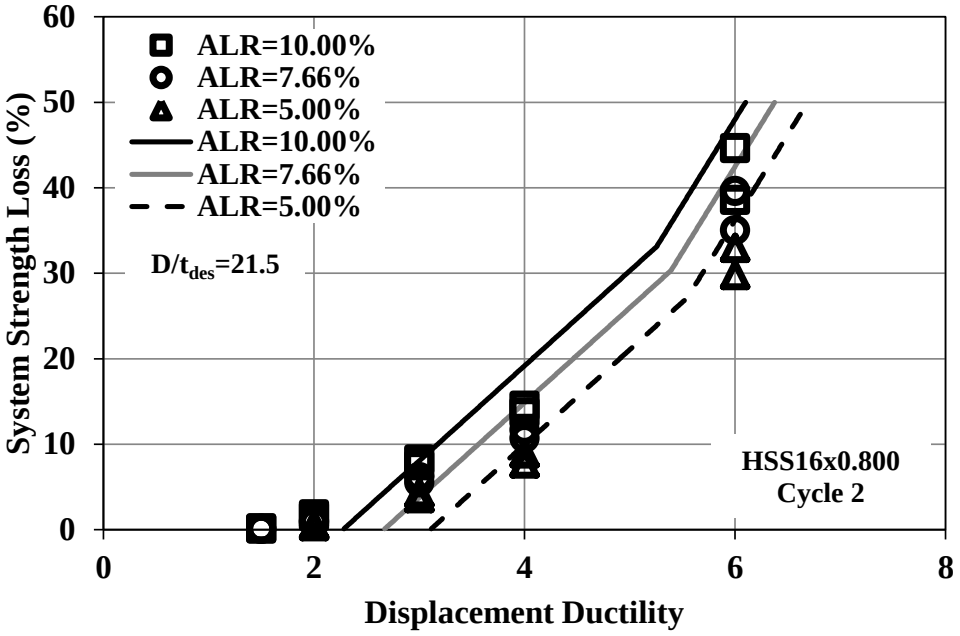

Figure 8.65 Multi-Linear Regression Analysis Results – Cycle 2 – D/t_{des}=21.5

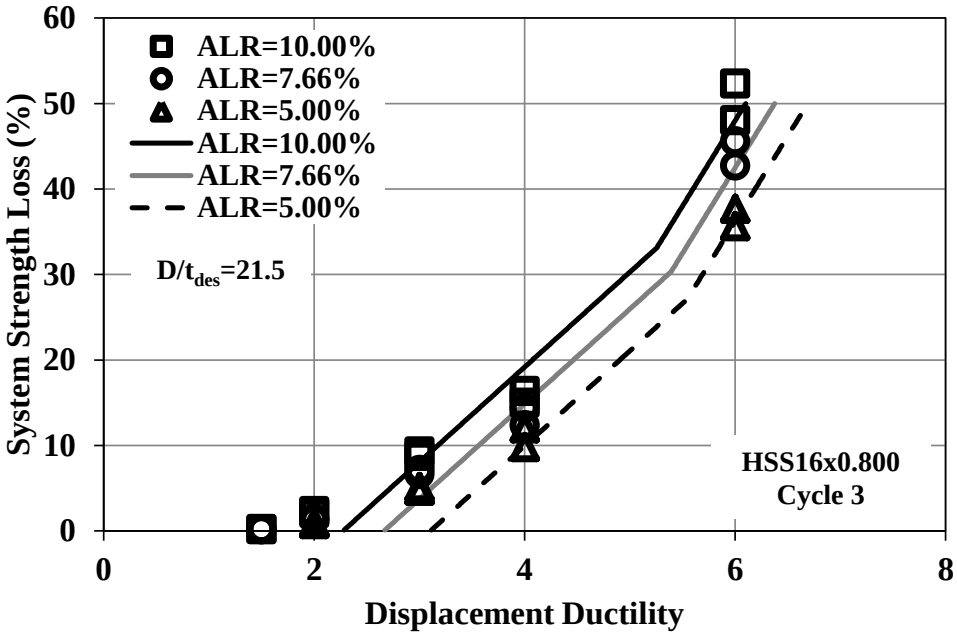

Figure 8.66 Multi-Linear Regression Analysis Results – Cycle 3 – D/t_{des}=21.5

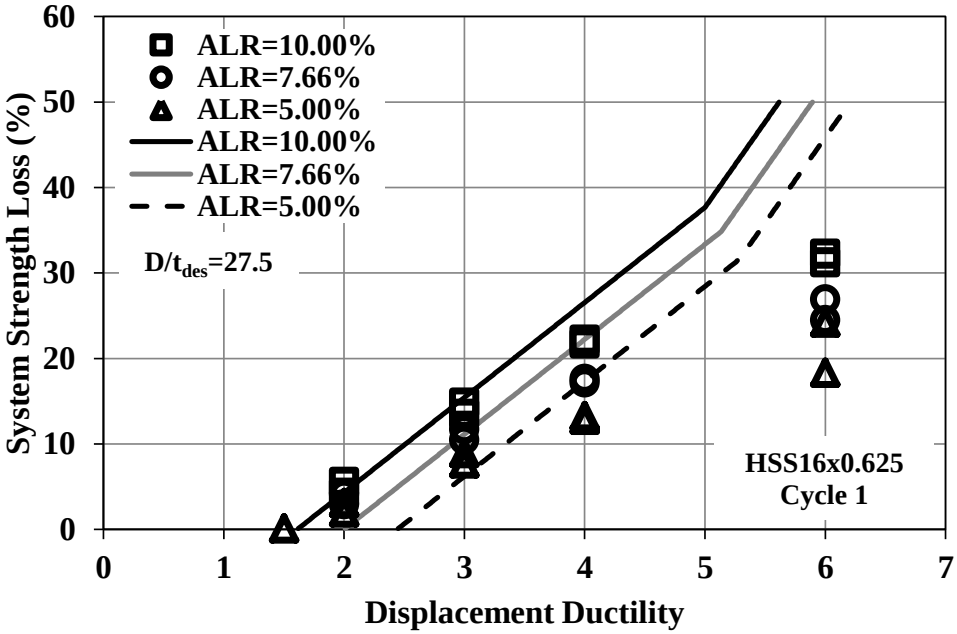

Figure 8.67 Multi-Linear Regression Analysis Results – Cycle 1 – D/t_{des}=27.5

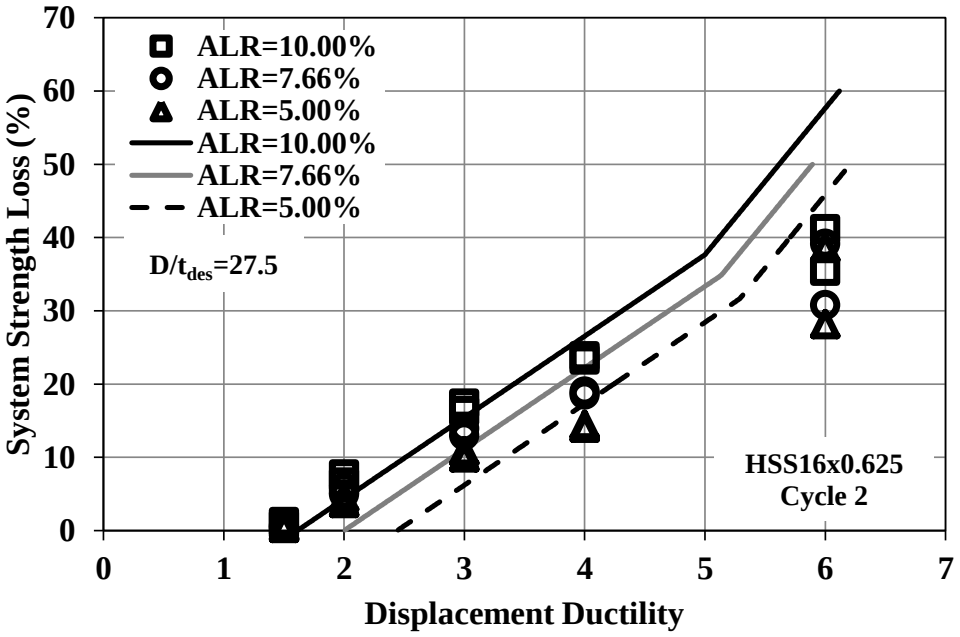

Figure 8.68 Multi-Linear Regression Analysis Results – Cycle 2 – D/t_{des}=27.5

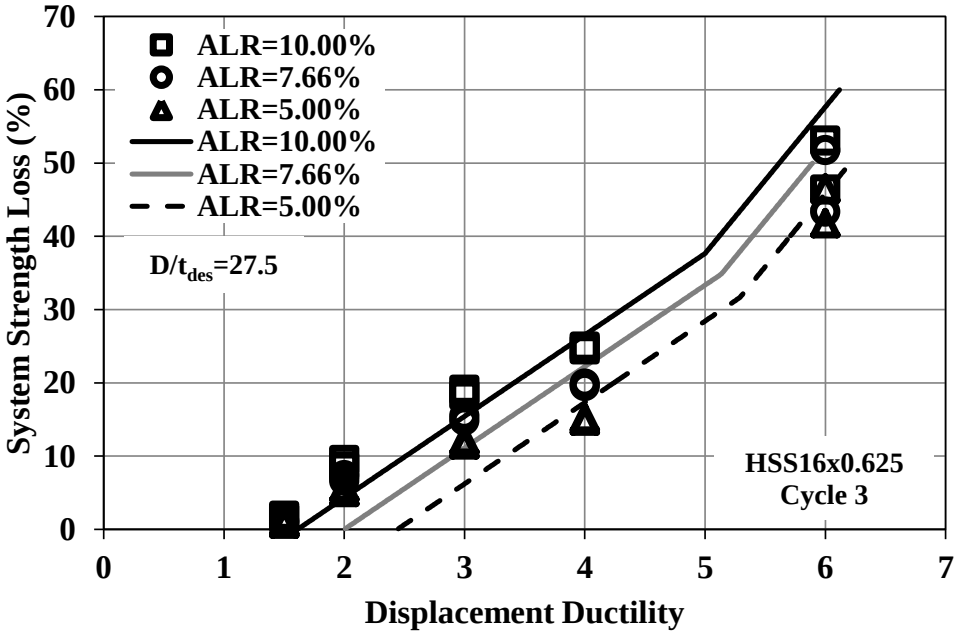

Figure 8.69 Multi-Linear Regression Analysis Results – Cycle 3 – D/t_{des}=27.5

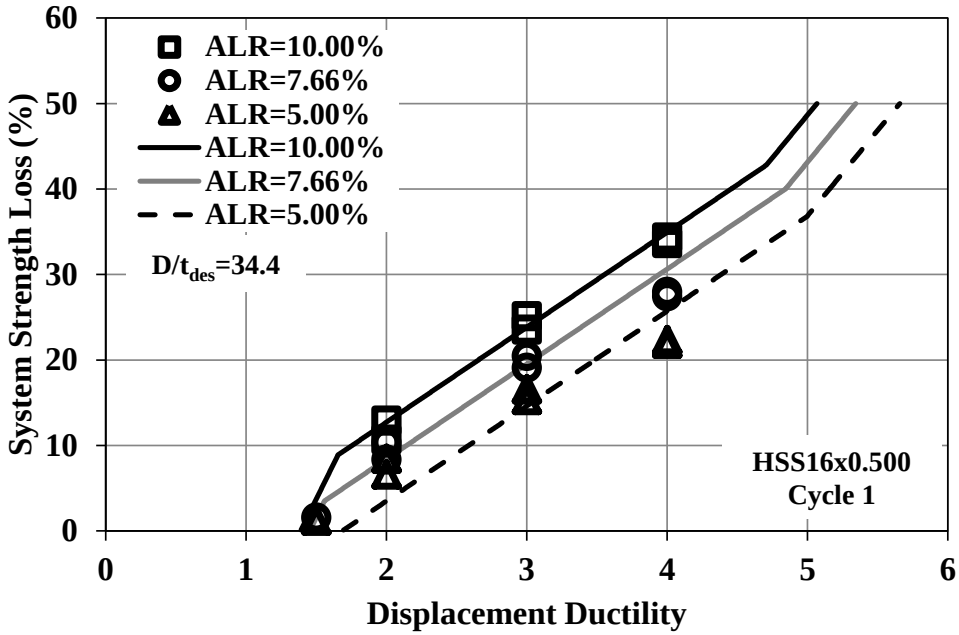

Figure 8.70 Multi-Linear Regression Analysis Results – Cycle 1 – D/t_{des}=34.4

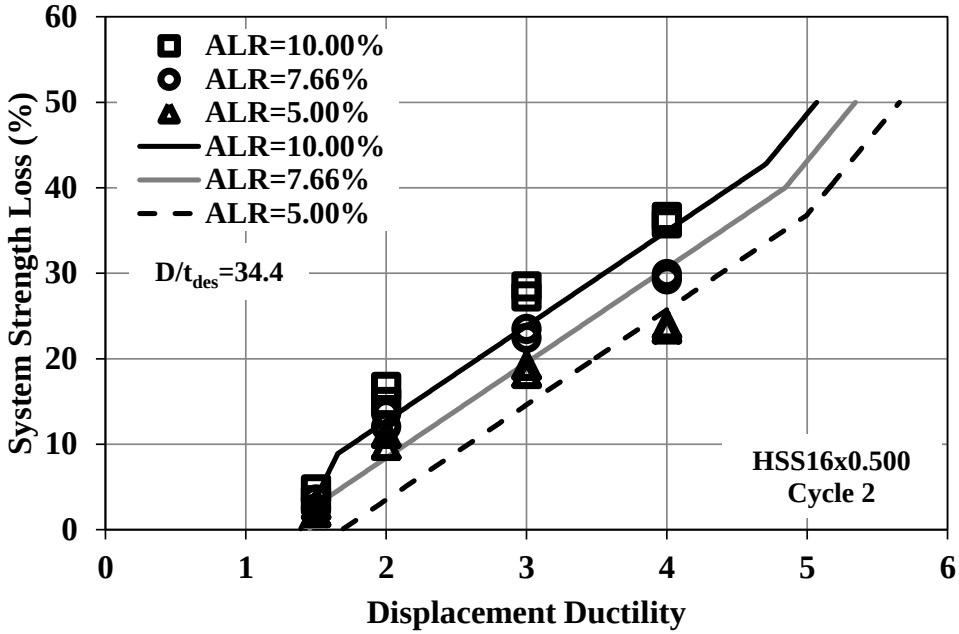

Figure 8.71 Multi-Linear Regression Analysis Results – Cycle 2 – D/t_{des}=34.4

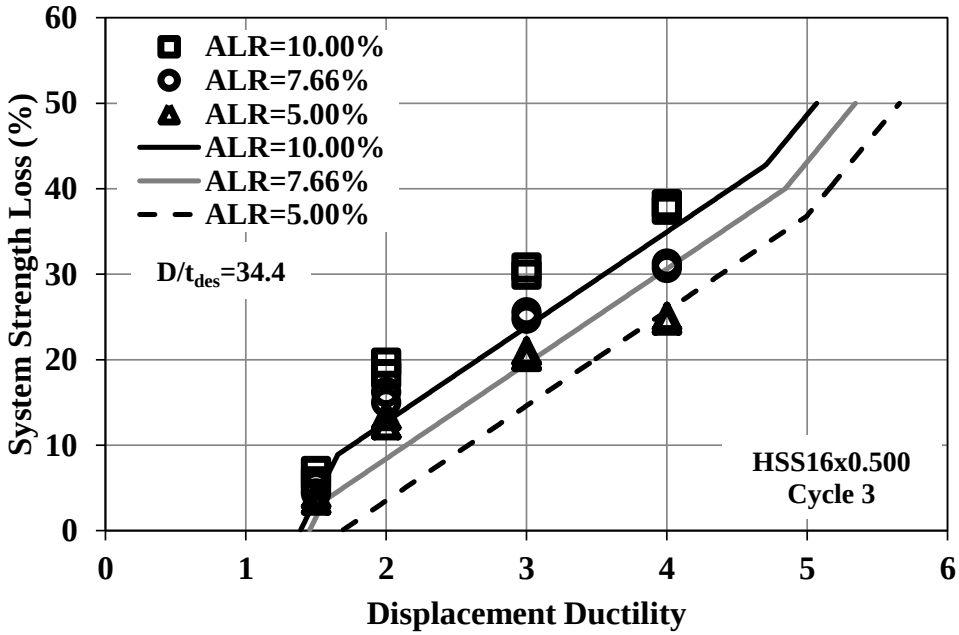

Figure 8.72 Multi-Linear Regression Analysis Results – Cycle 3 – D/t_{des}=34.4

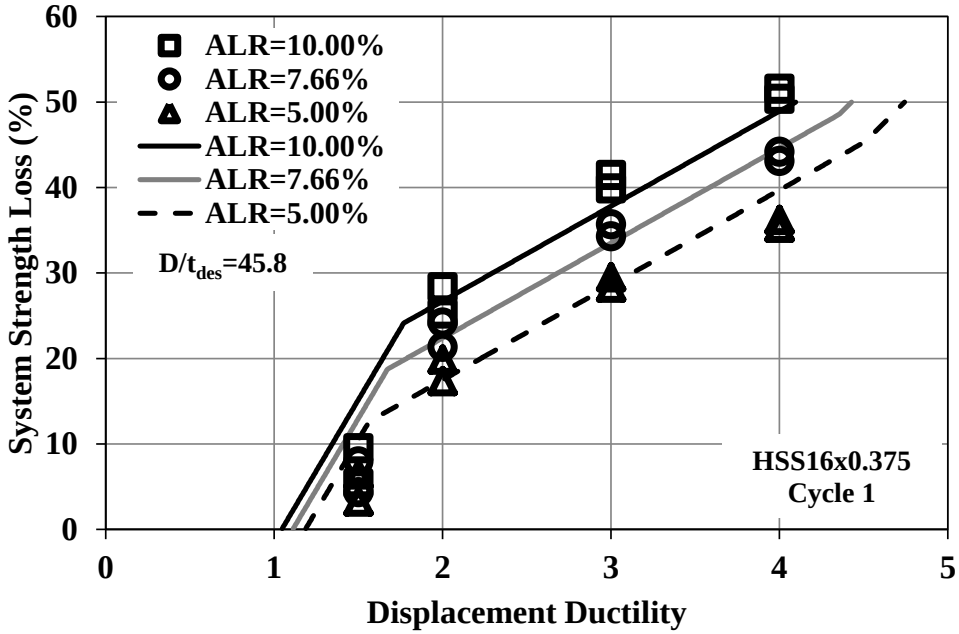

Figure 8.73 Multi-Linear Regression Analysis Results – Cycle 1 – D/t_{des}=45.8

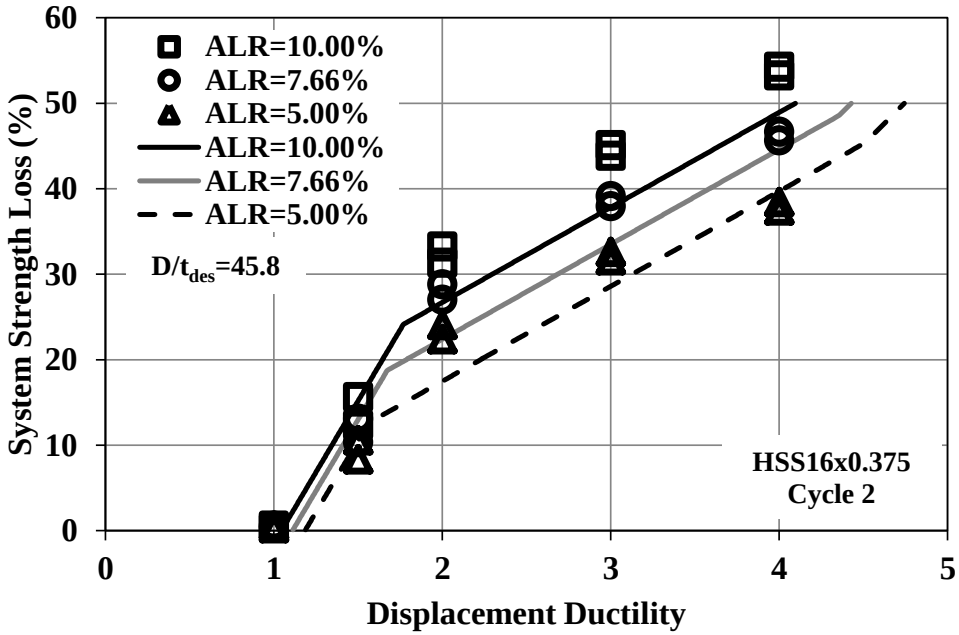

Figure 8.74 Multi-Linear Regression Analysis Results – Cycle 2 – D/t_{des}=45.8

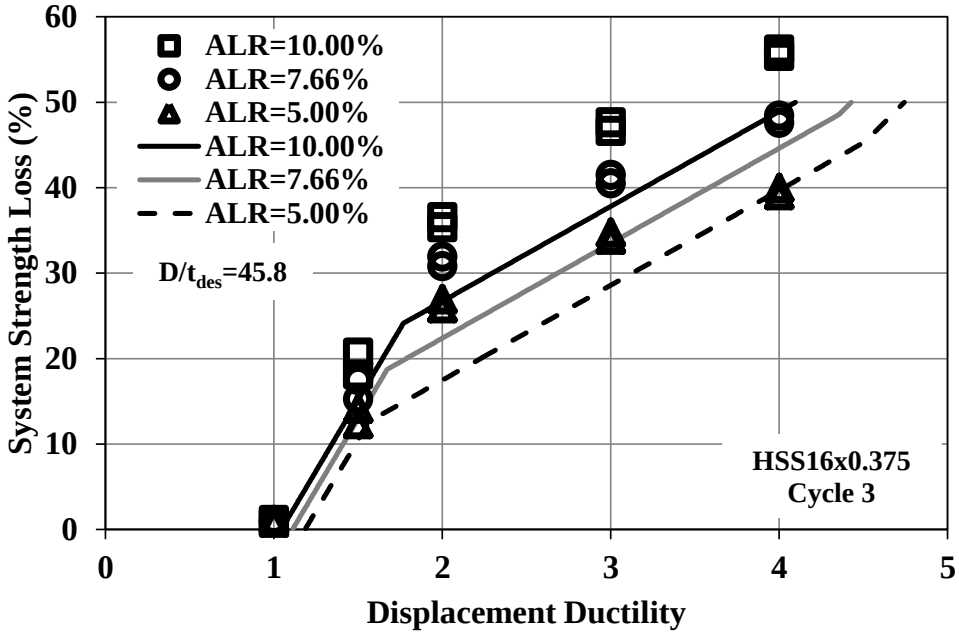

Figure 8.75 Multi-Linear Regression Analysis Results – Cycle 3 – D/t_{des}=45.8

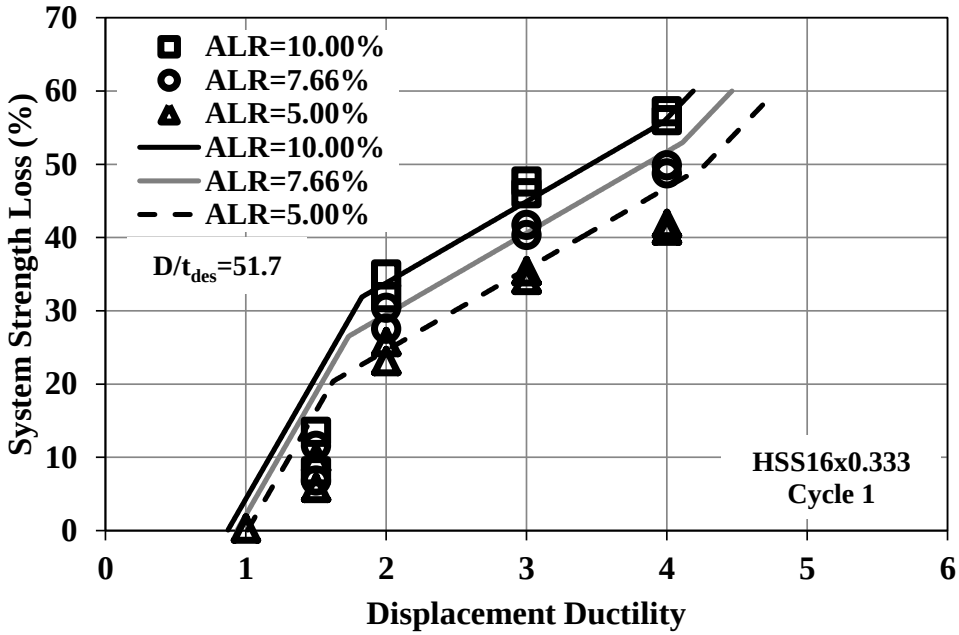

Figure 8.76 Multi-Linear Regression Analysis Results – Cycle 1 – D/t_{des}=51.7

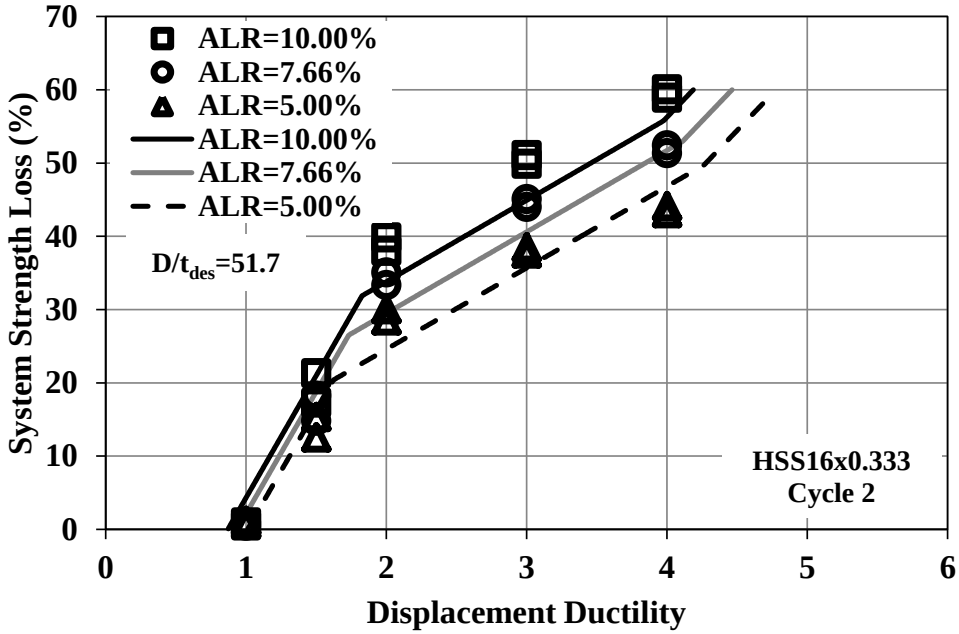

Figure 8.77 Multi-Linear Regression Analysis Results – Cycle 2 – D/t_{des}=51.7

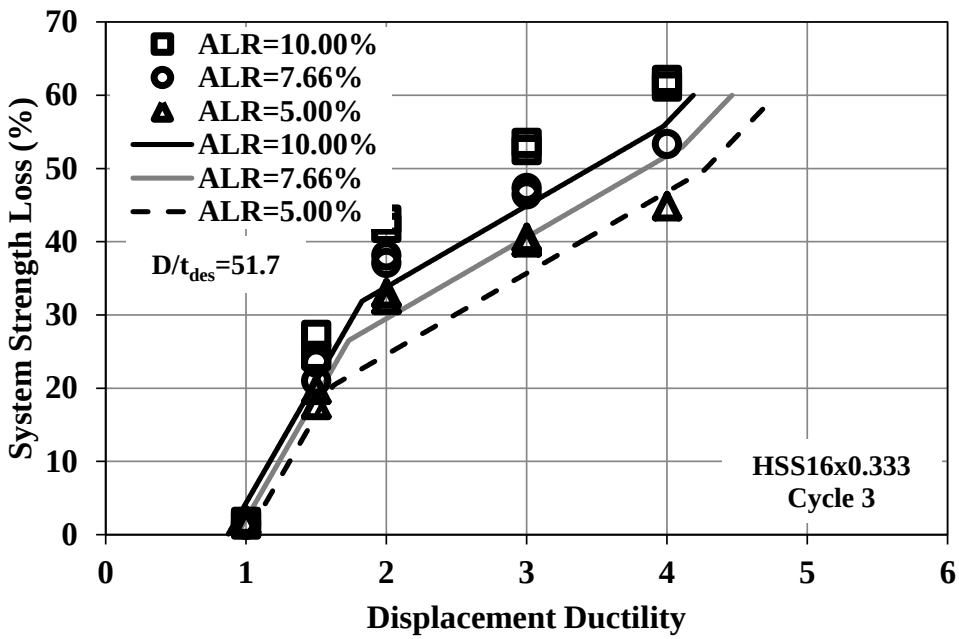

Figure 8.78 Multi-Linear Regression Analysis Results – Cycle 3 – D/t_{des}=51.7

In addition to the graphical comparisons that have been shown, the multi-linear design model was used to calculate allowable displacement ductility values, and corresponding drift capacities, for each of the 15 models considered in the parametric study for allowable strength loss values of 20% and 30%. As shown in Table 8.3, these allowable ductility values range from 4.81 for the lowest D/t_{des} and ALR combination, to 1.54 for the highest D/t_{des} and ALR in the case of at a 20% strength loss limit state. As would be expected, when a 30% strength loss limit state is considered, these values increased to 5.69 and 1.86. The general trend through all 15 combinations appeared to be reasonable when compared to the FEM results which have presented through this chapter.

Table 8.3 Calculated $\mu_{\Delta all}$ and Drift Capacities for 20% and 30% F_{loss} Limit States

Pile Size	D/t_{des}	t_{des} (in)	ALR (%)	$\mu_{\Delta all}$ @ 20% Loss L.S.	Drift @ 20% Loss L.S.	$\mu_{\Delta all}$ @ 30% Loss L.S.	Drift @ 30% Loss L.S.
HSS16x0.800	21.5	0.744	0.0500	**4.81**	**0.083**	**5.690**	**0.098**
			0.0766	**4.37**	**0.075**	**5.268**	**0.091**
			0.1000	**3.98**	**0.068**	**4.879**	**0.084**
HSS16x0.625	27.5	0.581	0.0500	**4.12**	**0.067**	**5.022**	**0.082**
			0.0766	**3.68**	**0.060**	**4.580**	**0.075**
			0.1000	**3.29**	**0.054**	**4.192**	**0.069**
HSS16x0.500	34.4	0.465	0.0500	**3.34**	**0.052**	**4.238**	**0.066**
			0.0766	**2.90**	**0.045**	**3.797**	**0.059**
			0.1000	**2.51**	**0.039**	**3.408**	**0.053**
HSS16x0.375	45.8	0.349	0.0500	**2.04**	**0.030**	**2.935**	**0.044**
			0.0766	**1.78**	**0.027**	**2.493**	**0.037**
			0.1000	**1.71**	**0.026**	**2.105**	**0.031**
HSS16x0.333	51.7	0.310	0.0500	**1.68**	**0.024**	**2.271**	**0.033**
			0.0766	**1.61**	**0.023**	**1.920**	**0.028**
			0.1000	**1.54**	**0.022**	**1.855**	**0.027**

8.5.2 Design Model Limitation

The applicable limitations and bounds to the recommended multi-linear regression design model should be clearly noted and considered when utilizing these recommendations. First, the model is bounded by allowable displacement ductility levels of 1 and 6 as has been mathematically mandated in design equation set. Secondly, the model should only be used for ALRs of 5% - 10% and D/t_{des} ratios from 51.7 – 21.5 as these were the bounds of the parametric study matrix and resulting data set. Lastly, the model should only be used with piers containing grouted shear stud connections that are expected to effectively form a flexural hinging mode of failure by inducing pile wall local buckling. It should clearly be noted that the design equation set was calibrated to capture the behavior of the parametric

study data set as closely as possible, with no explicit factor of safety being considered. Hence, the recommended model is intended to serve as an estimate of actual displacement capacity and any factors of safety felt to be applicable by a designer, needs to be subsequently applied.

In addition to these limitations, three points of interest should be noted that are not necessarily limitations to the model, but may require more study to fully understand. First the parametric study considered only 2 pile piers and second, the aspect ratio (L/D) to the inflection point in all models was 8.375. It is not expected that either of these parameters would impact the results, as the mechanism which induces strength loss is local buckling of the pipe walls which, by definition, is a local phenomenon. Nonetheless, caution should be used when deviating from the parameters used in the analytical results presented. The use of a significantly higher aspect ratio may impact the displacement capacity of the pier system.

Lastly, the piers considered in the study were subjected to single bending, while actual driven pile systems would be subjected to double bending with a non-linear moment gradient below the soil level with the potential to form in – ground hinges. Therefore, it should be recognized that the displacement capacity calculated by the design model corresponds to the relative displacement capacity between the point of contraflexure and the cap beam centerline which would not be equal to the total displacement capacity of the system. This approach would require the relative deflection at the point of contraflexure be calculated in order to determine the total displacement capacity of the pier.

Chapter 9: Conclusions and Design Recommendations

9.1 General Discussion

This chapter is intended to serve as a collection of conclusive results discussed throughout this document in order to provide design recommendations in one concise chapter. In the case of all conclusions made, it should be recognized that the resulting recommendations are bounded by the limitations of the experimental and analytical work that comprised the research project. Specific instances of limitations resulting from such bounds of the research work will be noted where applicable throughout this chapter. Although minimal levels of explanation will be provided as to what results led to the recommendations made in this chapter, the reader is referred to the prior chapters of this document for detailed discussion of the research work considered throughout this project.

9.2 Standard Welded Connection Recommendations

Standard welded connections have been defined in this project as any circular pipe pile to cap beam welded moment resisting connection configuration that does not specifically relocate damage away from the cap beam interface and protect critical welded regions as the pier is subjected to lateral loading. The configurations which fall into this category that were considered in the first phase of steel pier testing at NCSU included a fillet weld, a complete joint penetration weld (CJP), a complete joint penetration weld with an exterior full depth reinforcing fillet, and a complete joint penetration weld with both interior and exterior full depth reinforcing fillets. Although the piers containing CJP welds with reinforcing fillets exhibited greater levels of displacement capacity compared to the piers with fillet welds or CJP welds with no reinforcing fillets, all cases were shown to ultimately be controlled by the limit state of connection region cracking as is summarized in Table 9.1.

Table 9.1 Standard Welded Connection Experimental Results

Configuration	Failure Ductility	Failure Description	Reliable Ductility	Reliable Drift
3/4" Fillet	2	South Column North-Mid Face Crack at Weld Toe in Base Metal	1	0.028
45° CJP	3	Multiple Cracks in Both Columns at Weld Toe in Base Metal and Through Weld	1.5-2	0.035 - 0.047
45° CJP w/ 3/4" Ext. Backer Fillet (#1)	4	South Column North Face Crack at Weld Toe In Base Metal	3	0.070
45° CJP w/ 3/4" Ext. Backer Fillet (#2)	3	South Column South Face Crack at Weld Toe in Base Metal	2-3	0.049 - 0.072
45° CJP w/ 3/4" Ext./Int Backer Fillet	3	South Column South Face Crack at Weld Toe in Base Metal	2-3	0.548 – 0.081

In some cases, minor levels of local buckling of the pile walls was experienced, but in no case was propagation of the buckled region leading to a strength loss limit state experienced prior to crack formation in the joint region. Finite Element Modeling conducted to better understand the connection behavior showed that a local buckling failure mode would be likely to control the response of the system should cracking be mitigated. However, the model which was representative of systems containing any type of standard welded connection also showed a region of elevated strain concentration to develop immediately below the cap beam soffit. As shown in Figure 9.1, this region was located near what would be the weld toe region of an actual system, which is where the experimental tests experienced the undesirable cracking mode of failure.

Although the reliable drift capacities associated with piers containing CJP welds with reinforcing fillets are of reasonable magnitudes, as shown in Table 9.1, the apparent

controlling failure mechanism of joint region cracking prior to the development of the more desirable pile wall local buckling limit state was experienced regardless of the weld configuration. For this reason, the use of standard welded connections is not recommended for design when a non – linear response beyond displacement ductility of 1.5 is required. However, it should be noted in all cases the standard welded connection configurations considered in this research experienced no signs of inadequate behavior in the elastic range of loading.

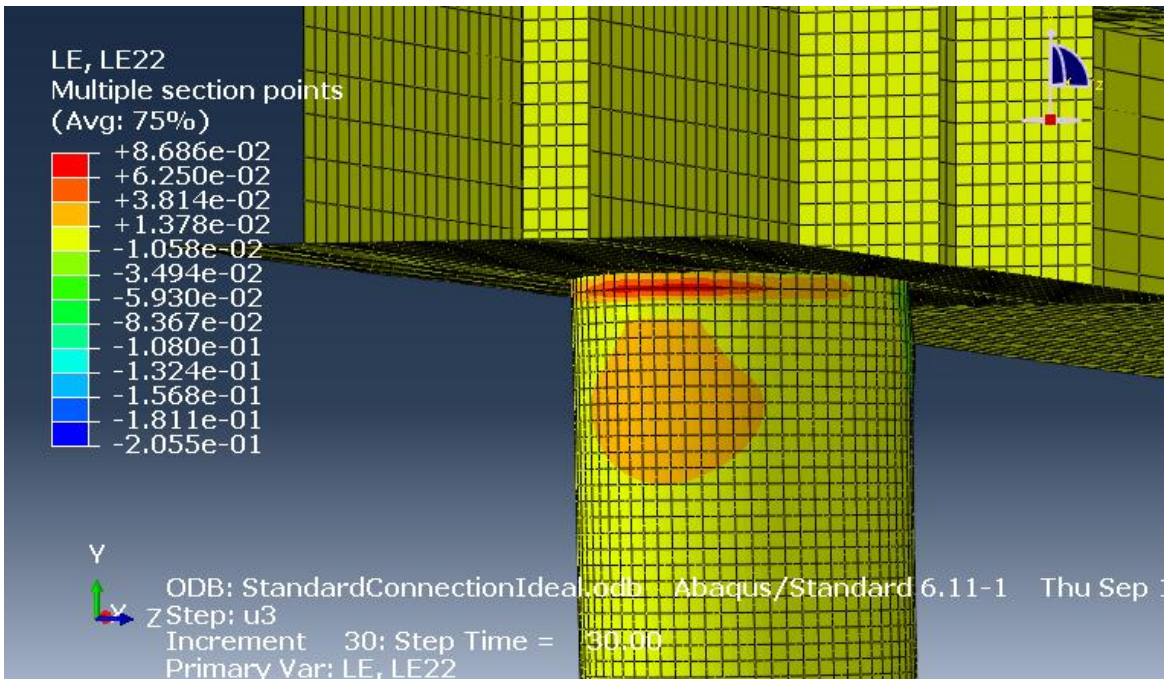

Figure 9.1 FEM – Local Tension Strain Concentration at Weld Toe Region

9.3 Modified Welded Connection Recommendations

9.3.1 General Recommendations

As a result of the standard welded connections' seeming inability to avoid the undesirable failure mode of joint region cracking, the concept of modified weld protected connections was developed. As the name suggests, the intention of modified weld protected connections was to explicitly protect critical welded joint regions by relocating damage in an effort to encourage the more desirable failure mode of pile wall local buckling. Application of a basic capacity design philosophy to the development of modified weld protected connections led to the concept of hinge relocation to improve the response of the pier.

As shown in Figure 9.2, the hinge relocation design intention aimed to move damage down the pile away from the cap beam soffit and critical welded regions. However, relocation of the hinge increases the bending moment demand in the joint region protected zone as the full over – strength bending moment capacity associated with flexural hinging of the piles in the hinge zone is linearly extrapolated to the protected zone. This extrapolation is considered in the basic hinge relocation equation, Eq.(9.1), where (H) represents the distance from the point of contraflexure to the cap beam soffit, (X_d) the design depth of hinging, (Z_{hinge}) the plastic modulus of the hinge region, (S_{pz}) the elastic modulus of the protected zone, and (O) applicable strain hardening over-strength factors. Thus, in order to effectively protect the critical welded regions of the steel pipe pile to cap beam connection, two key criteria had to be met.

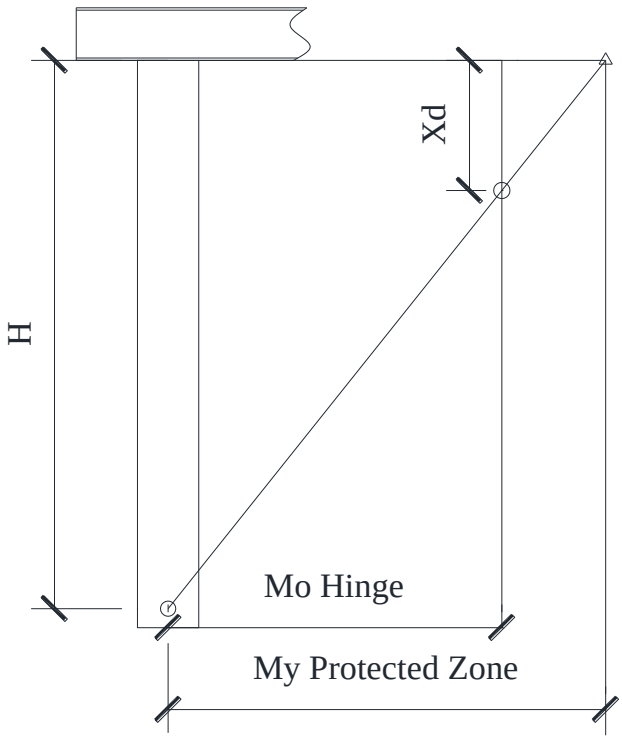

Figure 9.2 Flexural Hinge Relocation Concept

$$\frac{H - X_d}{f_{y,\exp} Z_{hinge} O} = \frac{H}{f_{y,\min} S_{pz}} \tag{9.1}$$

First, the location of damage in the pile element would be moved below the welded region as has been mentioned and secondly, the welded region would be strengthened to remain in the elastic range of response taking into account the increased bending moment demand. It was postulated by the researchers that following these two key criteria would allow the more desirable failure mode of flexural hinging, in the form of pile wall local buckling, to control the ultimate limit state of the system given that welded connections had been shown to avoid cracking in the elastic range of loading in past research. The flexural

hinge relocation method for protecting critical welded regions is, in general, recommended for design purposes. This general recommendation is based upon the results of specific modified weld protected connections that were developed and are subsequently discussed in this chapter.

9.3.2 Kerf Connection Recommendations

One potential modified weld protected connection that was developed was a cruciform gusset plate style connection. The connection consisted of gusset plates located in the joint zone oriented longitudinally and transversely to the cap beam as shown in the detail provided in Figure 9.3. This particular connection configuration required the use of an alternate cap beam configuration (opposed to the standard double HP cap beam) which had a centerline web directly over the longitudinal gusset plates. This resulted in the use of a built-up I shape cap beam for this particular connection configuration.

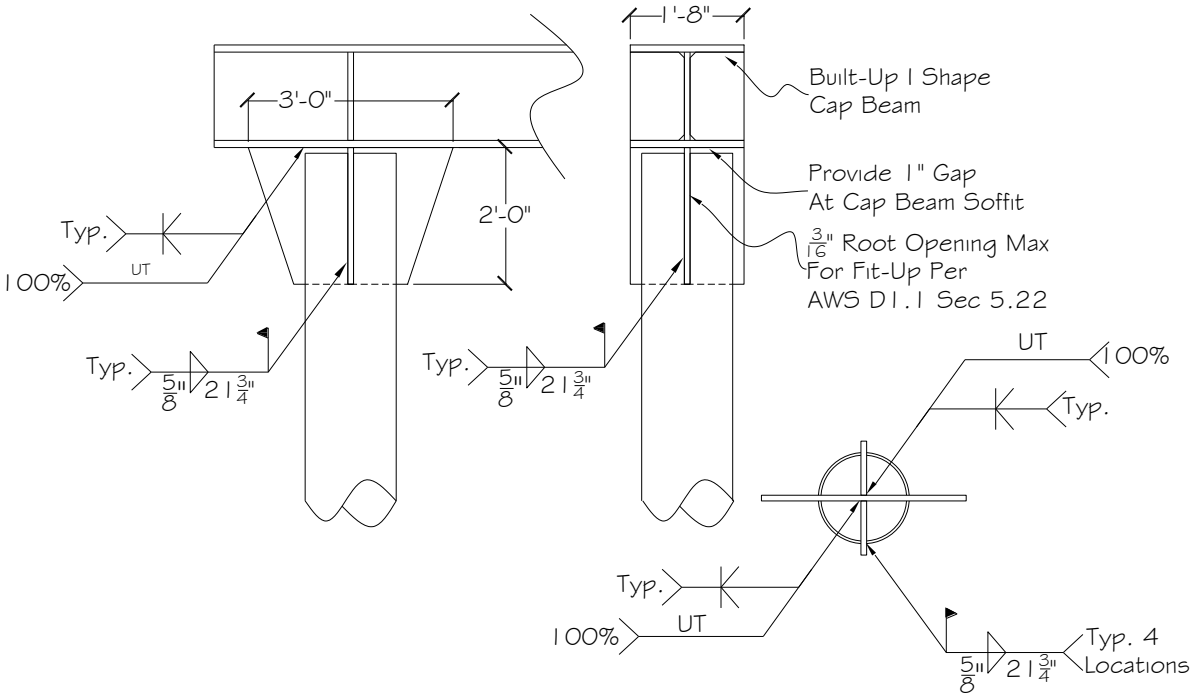

Figure 9.3 Kerf Connection Detail

In an effort to achieve the goals of a modified weld-protected connection, the longitudinal gusset plates forming the connection were designed to remain in the elastic range of response when subjected to the flexural demands associated with hinging of the pile elements and were joined to the built up I section cap beam with complete joint penetration welds. It was assumed that the longitudinal plates would act as narrow rectangular sections in strong axis bending at the cap beam interface. From the over-strength pile hinging moment capacity, the extrapolated flexural demands at the cap beam interface was determined and the necessary length of gusset plate for the cross section to remain elastic was calculated as 36 in. for a 1 in. wide plate.

The gusset plates were joined to the HSS16x0.500 piles, which were field slotted by torching to allow for gusset plate insertion, with 5/8 in. fillet welds longitudinal to the pile axis. The welds were assumed to act in shear along the length of the weld in order to produce a moment couple that would resist the flexural demands associated with pile hinging. The necessary length of welding, which controlled the necessary depth of the gusset plate, was determined from the over-strength pile hinging demand. Although the gusset plates oriented transverse to the cap beam were not assumed to carry any load as the pier was displaced longitudinally, they would be necessary should the pier be subjected double bending in the longitudinal direction of the bridge. Further, by inspection the transverse gussets are likely necessary to stabilize the longitudinal gusset in the out of plane direction.

The results of experimental testing, as well as Finite Element Analysis, showed an area of strain concentration to develop at the base of the longitudinal gusset plate in the slotted region of the pile. Consequently, circumferential pile wall cracking developed at the end of the slotted region and propagated around the cross section as shown in Figure 9.4. This cracking was experienced on each of the 4 extreme fibers in the experimental evaluation at the ductility 2 level, prior to the development of any significant buckling limit state. Based on the experimental results, the kerf connection configuration would likely be limited to a displacement ductility capacity of 2.

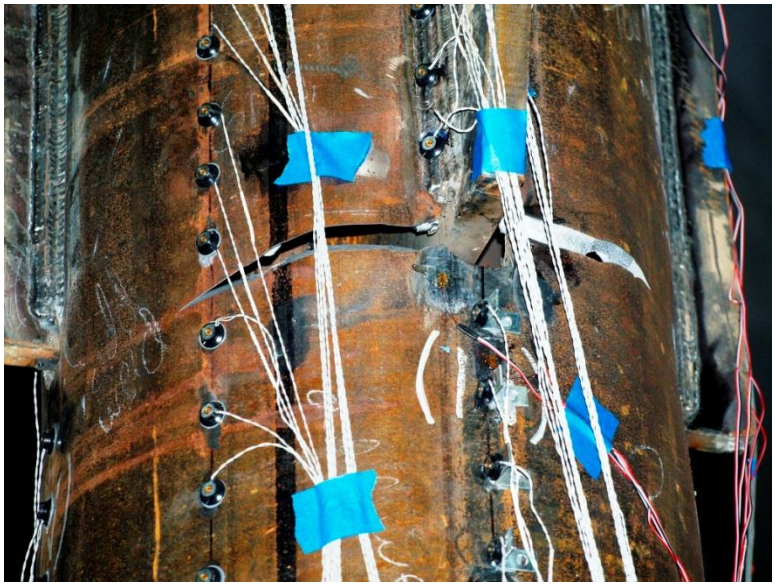

Figure 9.4 Circumferential Cracking at Base of Gusset Assembly

Although the connection configuration was able to locate damage away from the cap beam interface and was able of capacity protecting critical welds, which were the two key criteria of modified weld protected connections, the geometry of the configuration did not allow for the desirable failure mechanism of pile wall local buckling too develop. This resulted in an arguably low ductility capacity and an associated brittle failure mechanism. Consequently, use of the kerf connection configuration is not recommended for design, without further consideration for controlling pile wall cracking at the base of the assembly.

9.3.3 Column Capital Connection Recommendations

A second potential modified weld protected connection configuration that was developed was the flared column capital connection assembly. The initial attempt at developing a capital assembly for this type of connection, resulted in a rolled and welded circular pipe section formed from ASTM A572 Gr. 50 plate material which had a thicker upper region than that of the HSS16x0.500 piles intended to capacity protect the critical welded interface region between the capital and cap beam soffit. More specifically, the

assembly shown in Figure 9.5 was fabricated by rolling plate into two 180 degree sections which were then welded together with CJP welds. After welding the plates, the lower 8 in. of the assembly was machined to reduce the thickness of the fabricated pipe section to match the dimensions of the HSS16x0.500 piles. This turned-down section was intended to behave as a buckling region to isolate damage away from any welded regions, noting that no welding between the upper thick section and lower thinner section existed.

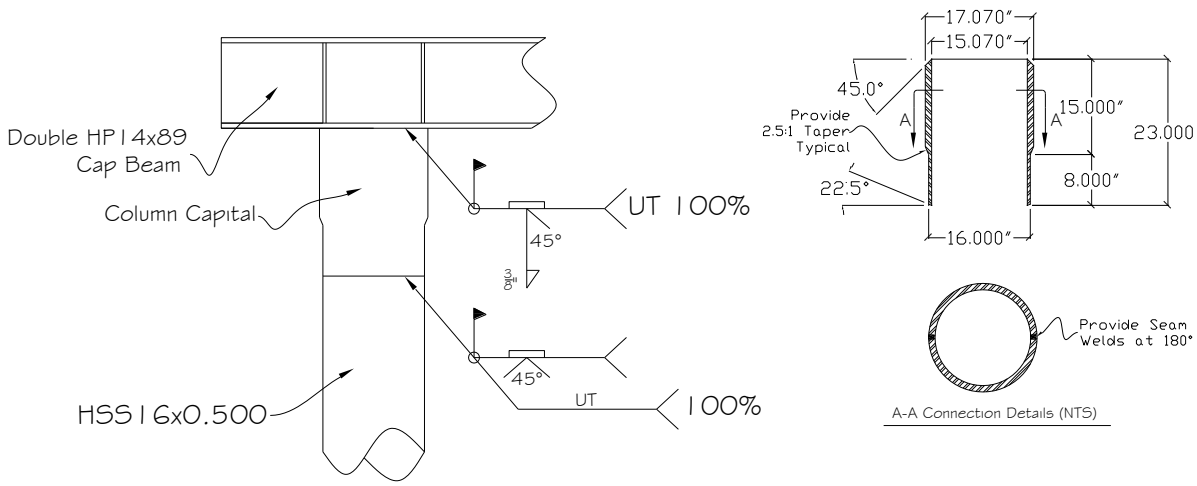

Figure 9.5 Column Capital Connection Detail

The design of this system was based on the principle that the critical section of the flared column capital (adjacent to the cap beam flange) should remain elastic as the full plastic flexural over – strength moment capacity at the intended hinge region just below the flared section was developed. Taking into account the moment demand extrapolated from the hinging region to critical welded region at the top of the assembly, a maximum depth of flared section (X_m) could be determined for a given flared section thickness as shown in Eq.(9.2). The assembly was then detailed with a depth of flared section (X_d) less than the maximum calculated value which, in the case of the test pier, resulted in a 15 in. deep flared section for a 1 in. flared section wall thickness.

$$X_d \leq X_m = H - \frac{Hf_y Z_{hinge} O}{f_y S_{pz}} \tag{9.2}$$

The results of experimental testing showed the configuration to be capable of both protecting the critical column capital to cap beam welded region, as well as relocating damage away from this interface by inducing the desired local buckling mode of failure. The system would likely be assigned a reliable ductility capacity of 3 or 4 depending on the chosen definition of allowable strength loss. Although, this connection configuration was shown to fulfill the specific requirements that have been defined for modified weld protected connections, the location of observed local buckling was not shown to develop in the intended region of the capital assembly. Local buckling developed in the experimental test in the HSS16x0.500 pile section below the capital assembly to pile splice weld, potentially endangering this welded region. Although no negative effects were experienced due to the location of local buckling, the design behavior was not fully induced.

In an effort to explicitly induce the local buckling failure mode in the intended region, a modified form of the flared column capital assembly was developed. More specifically, to ensure that a capacity protected region existed at the column to cap beam interface, and that pile hinging in the form of local buckling was properly located at the desired location, a specific reduced thickness section with a higher D/t ratio than the remainder of the capital assembly and HSS pile section was developed as shown in Figure 9.6. The design intent was similar in nature to a reduced section I beam which also protects critical welded regions by isolating damage away from welds. It should be noted, the length of the reduced thickness section, as well as the thicker lower section were chosen based on engineering judgment. Additionally the use of thicker wall pile (HSS16x0.625) was necessary to have a reasonable D/t ratio in the reduced thickness section.

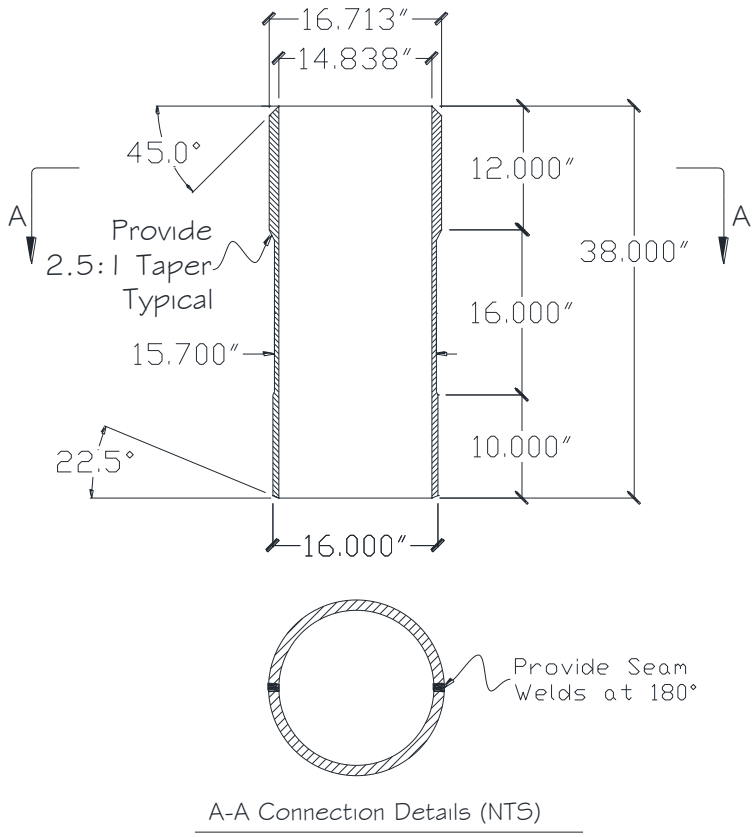

Figure 9.6 Modified Column Capital Details

The experimental results, as well as those of data analysis and Finite Element Modeling, indicated that the modified reduced section column capital did effectively relocate damage, in the form of flexural hinging, away from the capital to cap beam interface. No signs of brittle weld failure were experienced as the preferable failure mode of pile wall local buckling was developed. Ultimately, cracking of the assembly material at the buckled regions occurred in displacement ductility 4 level, resulting in a reliable displacement ductility level of 3 which corresponded to a reliable displacement of 6.43 in. or a drift of 4.3%. By specifically locating damage in the desired region while protecting critical welded regions, the assembly fully achieved its design intention.

Following testing, material tests were conducted to evaluate the effects of the forming and machining process on material behavior of the capital assemblies. It was found that both the 2% offset yield stress and the ultimate stress of the material was increased by approximately 15% after fabrication. FEM that utilized the post – fabrication material test data, predicted the buckling to occur in the HSS16x0.500 pile when the standard column capital configuration was used. This likely indicates that the increased mechanical material properties were the reason for the observed location of local buckling with the standard configuration, and suggests that the modified version is necessary. As a result, the modified form of the flared column capital connection configuration could be recommended for design purposes. Although the results of this research indicate that that the modified assembly is capable of behaving successfully as a modified weld protected connection, further study would be required to fully quantify the configurations reliable displacement capacity which would likely be a function of the reduced section D/t ratio.

9.3.4 Grouted Shear Stud Connection Design Recommendations

The third and final modified weld protected connection configuration that was developed in this research project, consisted of a composite grouted pocket style configuration shown in Figure 9.7. More specifically, the connection consisted of a 24 in. x 0.500 in. stub pipe pile section that was connected to a double HP14x117 cap beam with CJP and 3/8 in. reinforcing fillet welds. The inner diameter of the stub pile contained 12 lines of welded 3/4 in. diameter 2-1/2 in. long shear stud connectors located at 30 degrees on center around the inside of the pipe with 4 shear studs in a given line. Similarly the top of the HSS16x0.500 pile section had 12 lines of 4 matching shear studs welded at 30 degrees on center around the cross section offset by 15 degrees radially and 2-1/2 in. vertically from the studs inside the larger stub pile. The shear stud pocket was grouted from bottom to top using a non-shrinking flowable grout material, after the piles had been inserted into the stub pipe section to complete the moment resisting connections of the pier. This configuration allowed for +/- 1 in. of construction

tolerance. Further, it should be noted that the configuration dictates of minimum shear stud overlap of 1/2 in. should a full construction tolerance offset exist.

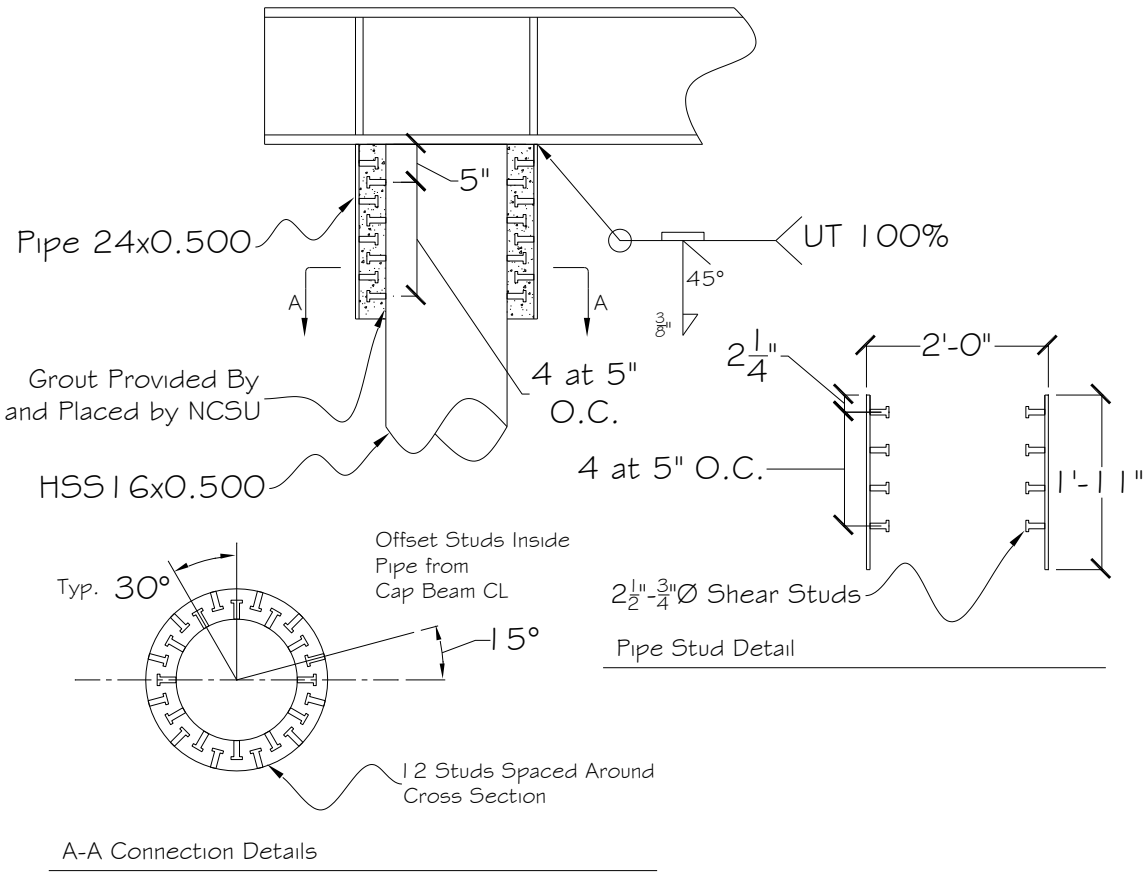

Figure 9.7 Grouted Shear Stud Connection Details

The design of the composite connection was based on the assumption that the total nominal strength of the shear stud connectors, on the pile side, should be capable of developing yielding of the HSS16x0.500 gross cross section. From known, or anticipated, material properties, a required number of 3/4 in. diameter shear studs could be determined and distributed around the cross section in an even pattern at 30 degrees on center. A matching number of studs were then placed on the stub pile side to facilitate load transfer in a truss like mechanism between the studs on either side of the connection. The nominal capacity of a single shear stud was determined utilizing the provisions of "AASHTO LRFD

Bridge Design Specifications" (AASHTO, 2007) Section 6.10.10.4.3 as well as the ANSI/AISC 360-05 (AISC, 2005) Section I3 both of which provide similar models shown in Eq.(9.3) through Eq.(9.5). As indicated in these equations, the model is a function of concrete compressive strength as well as the cross sectional area of the shear stud with an upper bound of stud shear rupture. Although the model is intended for use (in both codes) for composite construction between beams and a slab or bridge deck, it has been assumed conservative for use in this design given the highly confined nature of the annular grout pocket maintaining a logical upper bound of shear stud rupture.

$$Q_n = 0.5A_{sc}\left(f_c^{'}E_c\right)^{0.5} \leq A_{sc}F_u \qquad \textit{units: psi} \tag{9.3}$$

$$E_c = 1746\sqrt{f_c^{'}} \qquad \textit{units: psi} \text{ (AISC, 2005)} \tag{9.4}$$

$$E_c = 1820\sqrt{f_c^{'}} \qquad \textit{units: psi} \text{ (AASHTO, 2005)} \tag{9.5}$$

Utilizing this model, along with expected material properties of the grout and specified material properties of ASTM A108 shear stud connectors, it was found that a minimum of 47 shear stud connectors were necessary based on an anticipated yield stress of 58.8 ksi for the HSS16x0.500 ASTM A500 Gr. B piles. This anticipated yield stress was based on the recommendation (AASHTO, 2009) (AISC, 2010) of $1.4F_y$ where F_y is the ASTM minimum specified yield stress of 42 ksi. To generate a symmetrical condition, 12 lines of 4 shear studs at 30 degrees on center were used providing 48 shear studs on the pile side or 96 total per connection. It should also be noted that the 24 in. x 0.500 in. stub pile section, acting non – compositely at the cap beam connection, was designed to remain elastic as the full flexural over strength moment capacity of the piles was developed in order to fulfill the two key criteria of modified weld protected connection; damage relocation and protection of critical welded regions.

The ability of the connection configuration to act effectively as a modified weld protected connection was evaluated using both experimental and analytical methods. Three experimental tests were conducted with one considering nominally ideal geometry, one considering full construction tolerance offsets, and one considering nominally ideal geometry with applied vertical dead load representative of superstructure weight. In the case with construction tolerance offsets, the cap beam was displaced full possible amount (1 in.) along the longitudinal axis of the pier such that minimum shear stud overlap (1/2 in.) existed on one extreme fiber, and maximum overlap (2-1/2 in.) on the other. It was anticipated that this would place the largest possible demand on the grout material to transfer load from one set of shear studs to the other on the minimum overlap extreme fiber.

In all three cases, the grouted shear stud configuration was shown to fulfill all design intentions of modified weld protected connections. In each case, damage in the form of pile wall local buckling was shown to develop immediately below the connection region, leading to a strength loss ultimate limit state which developed over multiple cycles of loading and multiple ductility levels. Further, the critical stub pipe pile to cap beam welded connection was shown to be capacity protected by remaining in the elastic range of response.

The behavior of the specimens with and without construction tolerance offsets was nominally identical, suggesting that a designer can be assured adequate performance under to the presence of full construction tolerance offsets. In the two cases without applied vertical dead loads, the piers exhibited reliable displacement ductility levels of 3 or 4 depending on the exact considered allowable level of strength loss. These limit states, corresponded to 8.44 in. and 11.28 in. of lateral displacement, respectively, or 6.3% and 8.4% drift at the cap beam level. As has been noted, under the presence of applied vertical dead loads the connection configuration again properly located damage below the connection region and protected critical welded regions. However, the experimental specimen was shown to be limited to an ultimate displacement ductility capacity of 2 or 3 depending on the exact allowable level of strength degradation. These limit states correspond to 5.63 in. and 8.44 in.

of lateral displacement, respectively, or 4.2% and 6.3% drift which is one ductility level less than the piers not subjected to dead load. This result was the effect of the development and propagation of local buckling occurring at an earlier ductility level, which may be due to increased P-Delta demands. The behavior and results discussed here were also verified with Finite Element Analysis which was subsequently used to investigate the effects of varying axial load magnitudes and D/t ratios.

In addition, the results of two experimental shake table tests showed the grouted shear stud connection configuration to adequately behave as a modified weld protected connection when subjected to dynamic loading replicating actual earthquake ground motions. As was the case with large scale quasi – static testing, the connection configuration was able to mitigate any undesirable failure modes by properly locating damage in the form of pile wall local buckling in the intended critical demand region below the capacity protected portion of the connection. Although this was shown to be the case with quasi – static large scale testing, as has been noted, the results of the shake table tests help mitigate any uncertainties regarding the capabilities of the connection to behave as anticipated when subjected to actual seismic loading. Further, the scaled shake table specimens were shown to be capable of withstanding larger displacement ductility demands prior to the development of system strength loss when subjected to ground motions, than was the case with the large scale quasi – static tests which were subjected to the three cycle set balanced load history.

Based on the results of experimental and analytical investigations, the grouted shear stud configuration is recommended for design purposes. It is recommended that Eq.(9.3) through Eq.(9.5) are used to determine the required number of pile side ASTM A108 shear stud connectors, which should be spaced radially at 30 degrees on center around the cross section with no less than 4 shear stud connectors in a given line. The spacing between shear studs should be no less than two times the length of the shear stud. A matching set of shear stud connectors should be placed on the stub piles side of the connection offset radially by 15 degrees and vertically by 1/2 the distance between shear studs.

The length of the stub pipe pile should be sized to accommodate the necessary number of shear stud connectors, and the diameter to provide the desired maximum construction tolerance for a chosen shear stud length. However, design dimensions should ensure a minimum shear stud overlap of 1/2 in. Lastly, the thickness of stub pipe pile should be sized for a minimum elastic modulus such that the protected zone at the top of the connection remains elastic as the over – strength flexural moment capacity of the hinge zone is developed. This can be evaluated by calculating a minimum elastic modulus in accordance with Eq.(9.6), which represents a re-arranged form of the basic hinge relocation equation where X_d represents the length of the connection region.

$$S_{pz,\min} = \frac{Hf_{y,\exp}Z_{hinge}O}{f_{y,\min}(H - X_d)} \tag{9.6}$$

Lastly, the arrangement of the shear stud connectors can allow the bottom shear stud of each line to be either on the pile side or on the stub pipe side of the connection. As shown in Figure 9.7, the arrangement utilized in this research project had the bottom row of shear stud connectors on the pile side of the connection, and the configuration was shown to perform adequately. It is possible that should the bottom row of shear studs be located on the stub pile side of the connection, the cover grout layer may be protected and experience less spalling. This may be considered advantageous by reducing the need for any repair. However, it may also be considered advantageous to allow spalling to occur as was done in the tests, which would provide a visual indicator following a seismic that considerable demands were placed on a pier.

As has been noted, results produced by internal strain gauges as well as the results of the FEM simulation, it is not immediately apparent that a reduction in the number of shear connectors or the overall size of the connection should be reduced. Hence, the design

methodology of developing the axial yield capacity of the pile to determine the required number shear stud connectors appears to be adequate and no optimization options are immediately evident. Although the inclusion of bond stress capacity between the HSS16x0.500 pile and the grout block, to develop the axial yield capacity of the pile could be considered, the resulting effect on the required number of shear connectors would likely be minimal. For example, considering a reasonable bond stress capacity of 0.8 MPa (116 psi) over the length of the connection would induce a reduction in required shear connectors of approximately 10% for the configuration considered in the experimental tests. This would correspond to approximately 5 shear studs which likely not affect most designs as the required number must be rounded up to generate a symmetrical pattern. Further, the complicated action occurring within the connection would make it difficult to verify the assumed 0.8 MPa bond stress or to estimate an alternate value.

The allowable displacement ductility capacity resulting from this connection configuration appeared to be influenced by the presence of vertical dead loads. Consequently, a parametric study was conducted that considered axial load magnitude, D/t ratio, and allowable strength loss to develop a design equation to determine allowable displacement ductility. The results of this study will be subsequently discussed in this chapter.

9.3.5 Buckling Restrained G.S.C. Design Recommendations

An alternative modified version of the grouted shear stud connection configuration was developed in an effort to mitigate post – buckling strength degradation that was shown to be associated with the pile wall local buckling limit state. More specifically, an additional 10 in. of length was provided in the connection design which was used to generate a 1/2 in. annular block – out around the HSS16x0.500 pile as the connection was grouted as shown in Figure 9.8. The intention of the design was for the grout block to provide restraint against propagation of pile wall local buckling, associated with pile flexural hinging, in an effort to

mitigate post buckling strength degradation. The concept was partially influenced by the work of (Nishikawa, K., et. al., 1998) which focused on strengthening existing structures with steel restraining rings as was discussed in the literature review section of this document. As in that past study, specific consideration was given in the design process to avoid altering system behavior prior to local buckling by avoiding premature contact of the pile wall as will be subsequently discussed.

Both FEM results, which were used to size the annular gap, as well as experimental testing results, showed pile wall local buckling to develop in the block – out region as was intended. Further, the configuration was shown to enhance post buckling behavior by generating a positive change in tangent stiffness as the buckled pile wall contacted the restraint block. The positive change in stiffness, allowed the pier to regain some of the strength loss that had been experienced as the system was displaced towards the loading peaks. Although this result was obvious in the Force – Displacement hysteretic behavior, the associated magnitudes of regained system strength were marginal when compared to the standard grouted shear stud configuration. Ultimately, pile wall cracking was experienced at the displacement ductility 4 level, resulting in a reliable displacement ductility of 3 (6.3% drift) as was the case with the standard configuration. Based on these results, the modified buckling restrained grouted shear stud configuration is not recommended for design, based on the additional labor and materials, as well as the marginal improvement in performance.

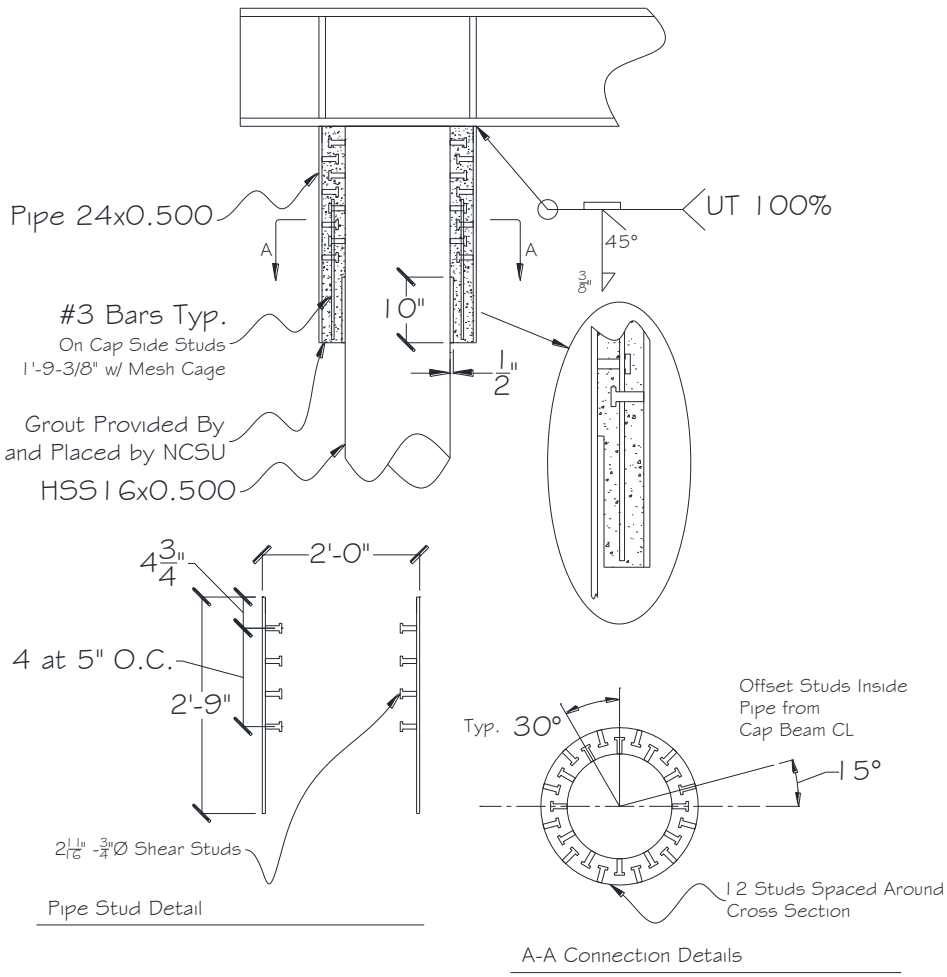

Figure 9.8 B.R. Grouted Shear Stud Connection Details

9.3.6 Displacement Capacity of Grouted Shear Stud Connection Piers

As has been mentioned, a parametric study was conducted in order to generate a design equation to estimate the allowable displacement capacity of piers containing grouted shear stud connections. The design equation for allowable displacement ductility ($\mu_{\Delta all}$) as a function of allowable system strength loss (F_{loss}), D/t_{des} ratio of the pile members, and axial load ratio (ALR) as defined by Eq.(9.7). In this equation, (D) represents the total dead load on the pier, (n) the total number of piles, (A_g) the gross area of each pile, and (f_{ymin}) the

minimum specified ASTM yield stress of the pile material. In order to develop the relationship, the parametric study considered 15 combinations of ALR and D/t_{des} ratio ranging from 5% to 10% and 51.7 to 21.5 respectively. Given the large number of required combinations, experimental evaluations were not possible. Consequently, Finite Element Analysis which had been shown to produce comparable results to the experimental tests was used to evaluate the 15 combinations.

$$ALR = \frac{D}{nA_g f_{y\min}} \tag{9.7}$$

In order to conduct the parametric, study and in order for the resulting relationships to be usable in a design scenario, a simple method for determining first yield displacements of grouted shear stud connection piers with various pile sizes was needed. Through a trial and error process, it was found that elastic 2 – dimensional centerline modeling appeared to capture first yield the displacement of a system reasonably well when compared to the experimental results found from laboratory testing. However, one modification to the standard centerline modeling procedure was necessary to appropriately model the connection region flexibility. Additionally, it was found that cap beam flexibility, shear deformations, P-Delta effects all needed to be considered.

As has been noted, connection region flexibility was found to be impactful and is not inherently considered with line elements. One option explored, was the possibility of using rigid end offsets over the connection length which can be handled by most modeling programs. However, this was found to under predict the first yield displacement by over predicting connection rigidity. Conversely, it was found that ignoring the connection stiffness as may be done in typical centerline modeling, over predicted the first yield displacement. The most appropriate method of representing connection region stiffness was

found to be representing composite action of the inner pipe pile member and the outer pipe pile stub member used to form the grouted shear stud connection.

More specifically, the centerline modeling procedure was found to be most accurate when the two pile pier was modeled with a total of 6 centerline nodes as shown in Figure 9.9. In the line element model, elements representative of the HSS16x0.500 piles span from node 1 to node 5 and node 3 to node 6, while elements representative of both the HSS16x0.500 piles and the 24x0.500 pipe stubs span from node 5 to node 2 and node 6 to node 4. Hence, two line elements span these regions. An element representative of the double HP14x117 spans from node 2 to node 5.

With this modeling procedure, two members are modeled between nodes 5 and 2 as wells as nodes 6 and 4. These members are subjected same end rotations and translations, and consequently the same displacements along the member although different resulting member forces will be generated. In this procedure, the distance from nodes 1 and 3 to nodes 2 and 4 is the centerline height of the pier from the pinned base which is representative of the point of contraflexure in an actual system. The distance from nodes 5 and 6 to nodes 2 and 4 is representative of the length of the connection region, (23 in. in this case) shifted upward by 1/2 the depth of the cap beam section. Lastly, the horizontal distance between nodes is the centerline spacing between piles.

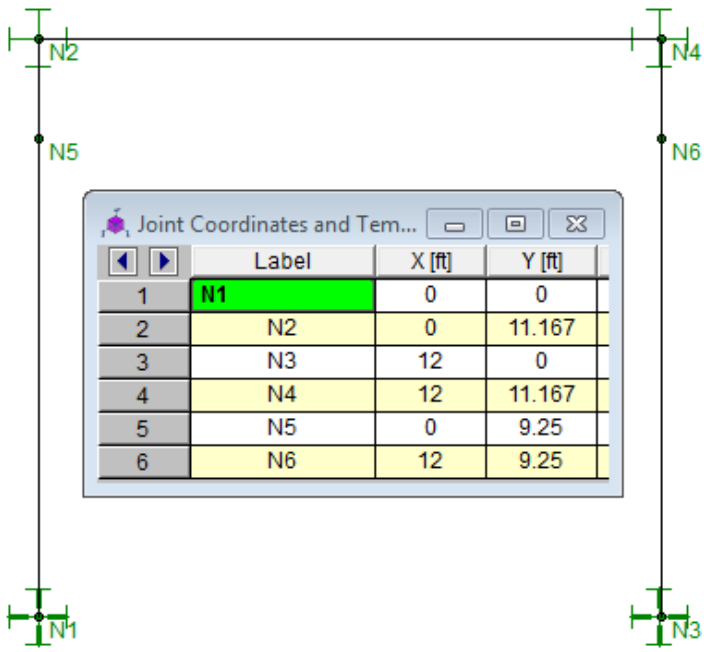

	Label	X [ft]	Y [ft]
1	N1	0	0
2	N2	0	11.167
3	N3	12	0
4	N4	12	11.167
5	N5	0	9.25
6	N6	12	9.25

Figure 9.9 Modified Centerline Model

Although a centerline modeling procedure is recommended to define the geometry of the pier, the calculation of a first yield force to apply to the model must consider the actual geometry of the system. It is recommended that the first yield force be based on the first yield moment capacity of the pile elements, assuming a critical cross section develops at the base of the connection region and that shears are assumed to be distributed equally between the two piles. It should be noted however, this will not be the case with piers containing more than two columns, where internal columns will typically reach first yield prior to exterior columns.

Applying this method to model piers that had been experimentally tested, along with an assumed modulus of elasticity of 29000 ksi, resulted in a predicted first yield displacement of 2.10 in. This value was found to be comparable to the 4 experimentally determined average first yield displacements of 2.15 in., 2.11 in., 1.96 in., and 1.95 in. suggesting that the model is a reasonable approach to determining first yield displacement magnitudes. It should also

be noted, vertical dead loads were not considered when calculating first yield displacements due to lateral forces in this parametric study. This was done to reduce the number of load/displacement histories that needed to be modeled, such that for a given pile size a single load/displacement history could be defined regardless of ALR. Further, this allows for direct comparisons of drift or displacement capacity for a given pile size with varying ALR and allowable strength loss.

Each of the 15 Finite Element Models, which considered expected material properties determined from the over-strength provisions of (AISC, 2010) (AASHTO, 2009), was subjected to the three cycle set load history used throughout this project. Force – Displacement data output from each analysis was used to evaluate the relationship between displacement ductility, strength loss, ALR, and D/t_{des} ratio. As would be expected, it was found that, in general, system strength loss due to local buckling of the pile walls increased as ALR increased and as D/t ratio increased for a given displacement ductility level. In no cases was an opposite trend experienced. Further, it appeared that the D/t_{des} variable was more influential in terms of strength loss experienced by the system than was ALR. These two basic trends can be seen in the examples provided in Figure 9.10 through Figure 9.13 which provide Force – Displacement envelopes and associated strength loss magnitudes at the positive and negative peaks of loading for all three ALRs of two example D/t_{des} values.

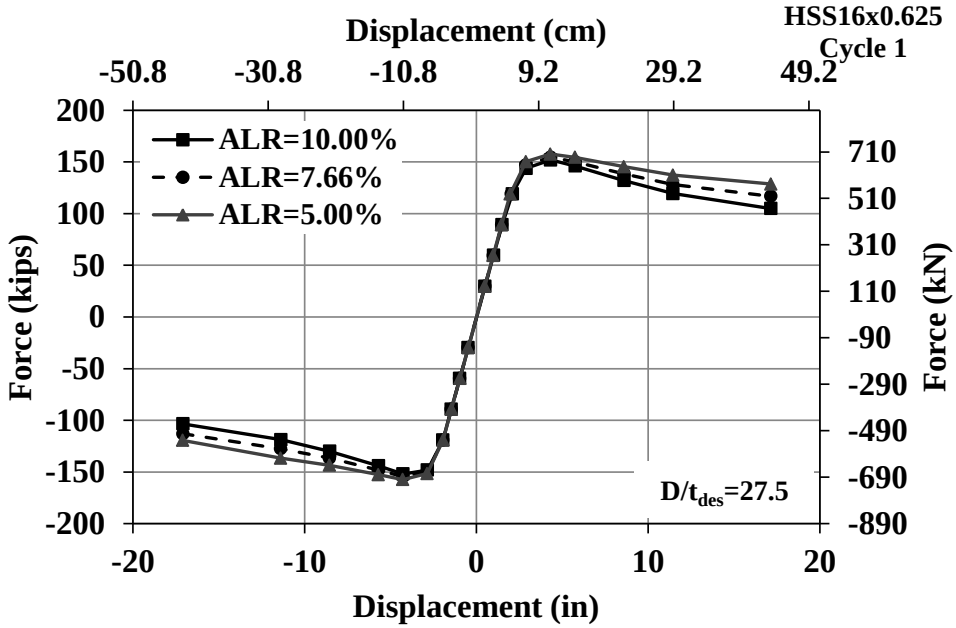

Figure 9.10 Cycle 1 Comparison – HSS16x0.625 D/t_{des}=27.5

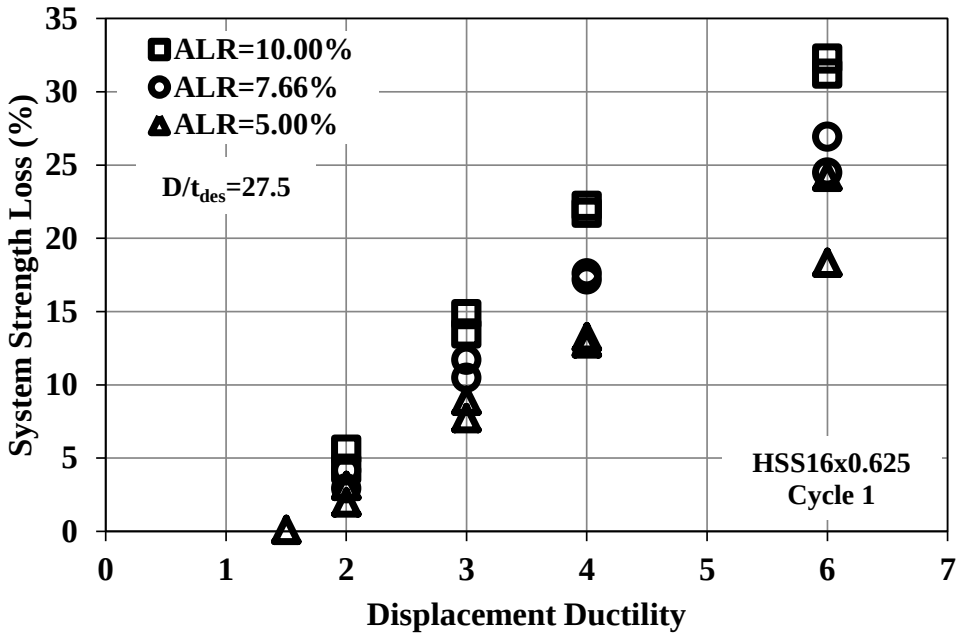

Figure 9.11 Cycle 1 Strength Loss Comparison – HSS16x0.625 D/t_{des}=27.5

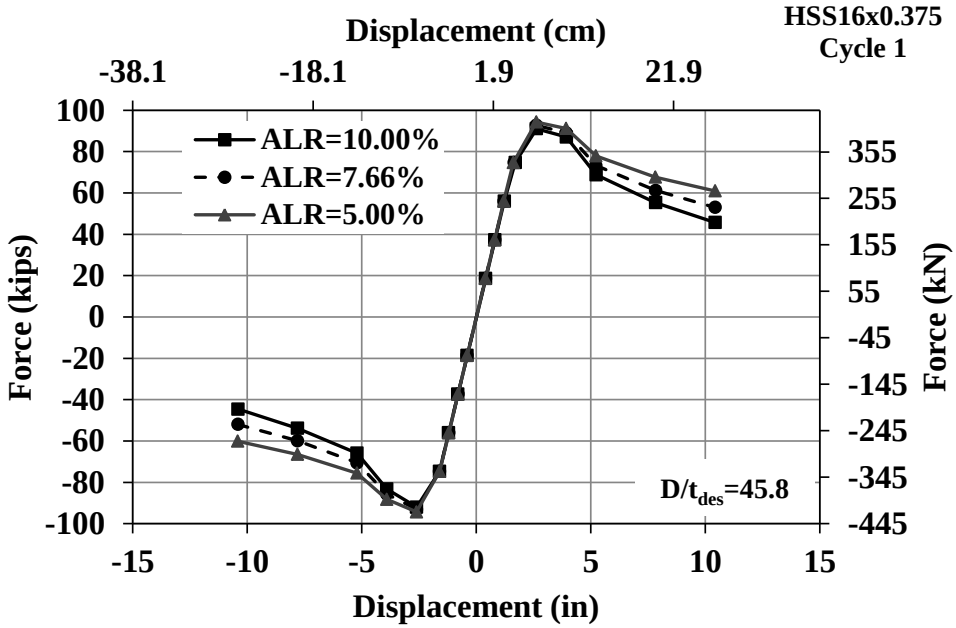

Figure 9.12 Cycle 1 Comparison – HSS16x0.375 D/t_{des}=45.8

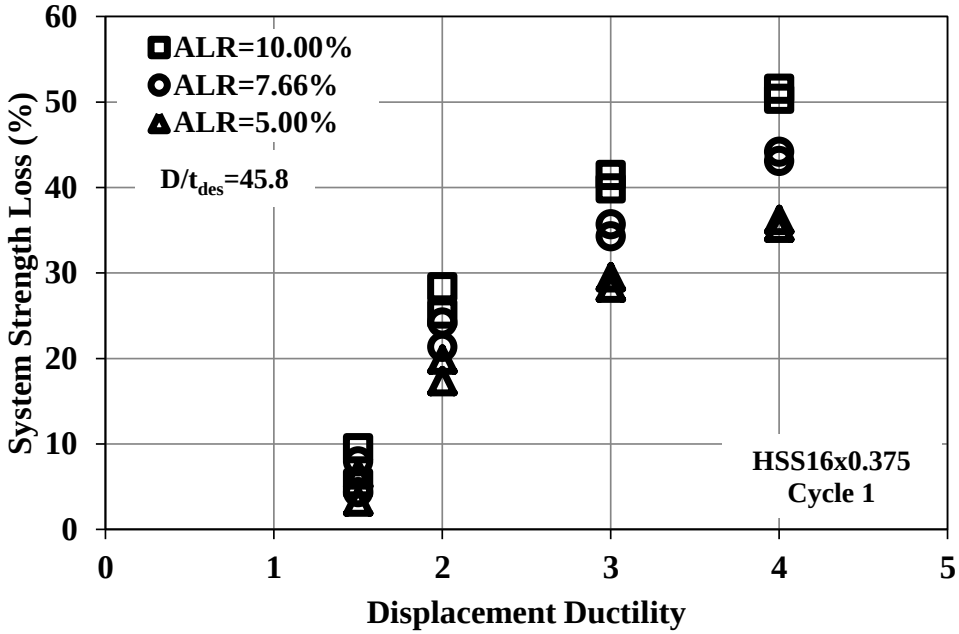

Figure 9.13 Cycle 1 Strength Loss Comparison – HSS16x0.375 D/t_{des}=45.8

The resulting data set of corresponding μ_{Δ}, F_{loss}, D/t_{des}, and ALR values, was used to conduct a multivariate least – squares polynomial regression analysis to generate a design equation to calculate $\mu_{\Delta all}$ as a function of the other three variables. The analysis was initially conducted as a first order polynomial which was shown to inappropriately predict $\mu_{\Delta all}$, in two general regions of the data set. An attempt was made to mitigate the problem by increasing the order of the considered polynomial to the second and eventually third degree. However, these attempts showed only marginal improvements and introduced other problem in the case of the third degree polynomial. Additionally, the complexity of the design equation was increased with each increase in polynomial order.

Reviewing the strength loss results from the data set, it appeared for the cases with lower D/t_{des} ratios that a relatively linear variation existed between the data in the ductility 1 to 2 range, and a linear variation in the 2 to 4 range with a different slope. Likewise, with the higher D/t_{des} ratios, there seemed to be a relatively linear variation in the ductility 2 to 4 range, and also in the 4 to 6 range with a different slope. Hence, there appeared to be two applicable pivot points, one at ductility 2 and one at ductility 4. This behavior is schematically depicted in Figure 9.14. However, it should be noted that this figure is only for schematic purposes to illustrate the behavior of the entire data set. In general only two of the three trends were noted for a single D/t_{des} ratio.

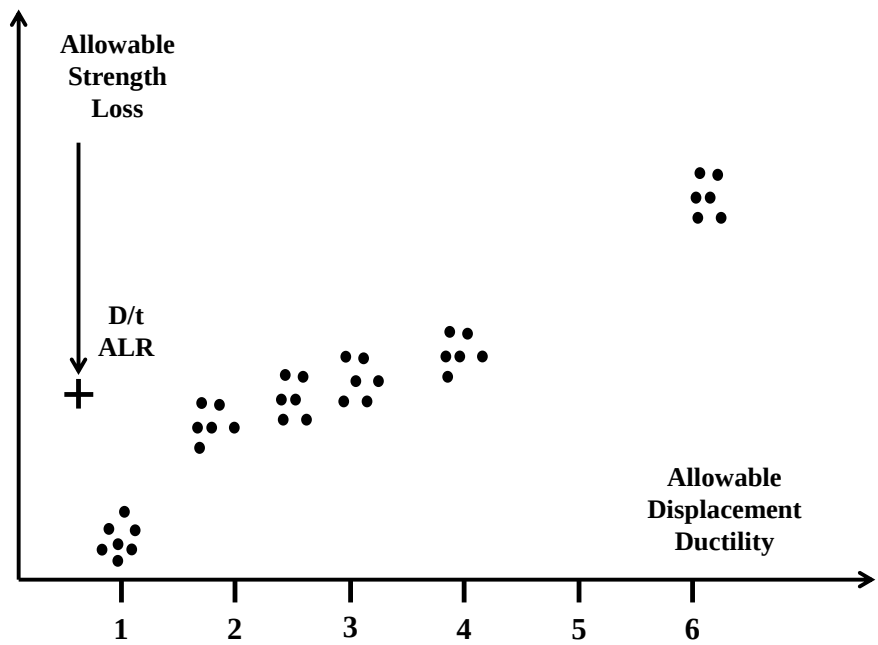

Figure 9.14 Strength Loss vs. Displacement Ductility Schematic

In an effort to calibrate the design equation, the data set was lumped into three overlapping groups. These groups included data in the displacement ductility range 1 to 2, the range 2 to 4, and the range 4 to 6 as shown in Figure 9.15. For each of the three data sets, a first order multivariate least-squares regression analysis was conducted, resulting in 3 separate design equations each in the form of [$\mu_{all} = a_0ALR + a_1D/t_{des} + a_2F_{loss} + a_3$]. These analytical regression lines are schematically shown in Figure 9.16 as lines 1, 2, and 3 which essentially define a backbone tri – linear regression curve.

The intention of the design model was that for a given ALR, D/t_{des} ratio, and allowable strength loss (F_{loss}), one of the three curves would control the ultimate displacement ductility capacity of the system. As illustrated in Figure 9.16, entering the vertical strength loss axis of the graph provides 3 possible solutions. The first possible option (shown by lowest dashed arrow), involves passing the 2 curve and proceeding to the applicable 1 curve for the ductility 1 to 2 range. The second possible option (shown by the middle dashed arrow), involves

passing the 1 curve and proceeding to the applicable 2 curve for the ductility 2 to 4 range. Lastly, the third option (shown by the highest dashed arrow), involves passing the 1 curve and stopping at the applicable 3 curve prior to reaching the 2 curve, for the ductility range 4 to 6.

This process essentially forms the backbone curve shown by the heavy trace in Figure 9.17. As shown, the model is not forced to pivot at ductility 2 and 4, but instead pivots near these regions at an exact value that is determined from the calibration of the design equations. The three design equations are split into two logical tests, one for ductility range 1-3, and one for ductility range 3-6. Although this was conceptually unnecessary, doing so ensures that the 3 curve does not interfere with the ductility 1 to 2 range which is mathematically unclear. Lastly, the model should be bounded by ductility levels 1 and 6 as this is what was considered in the data set.

Although the process which has been graphically described may seem cumbersome for design, it can actually be reduced to three mathematical relationships grouped into two logical tests. As shown in Eq.(9.8) and Eq.(9.9), using this set of design equations will generate two different allowable displacement ductility values, one will fall in the correct range and should be used for design while one will not and should be disregarded. It should also be noted, the design equation set has been calibrated for the input variables to be in the form of a decimal for ALR (i.e. 0.0766 for 7.66%), integer values for D/t_{des} (i.e. 34.4), and F_{loss} as integer values (i.e. 25 for 25%).

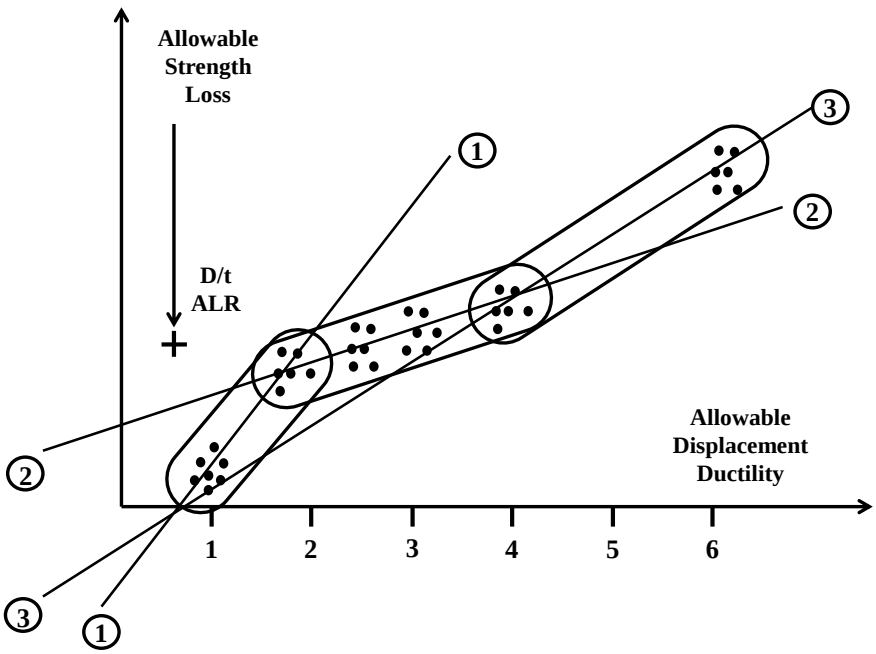

Figure 9.15 Schematic of 3 Individual Regressions

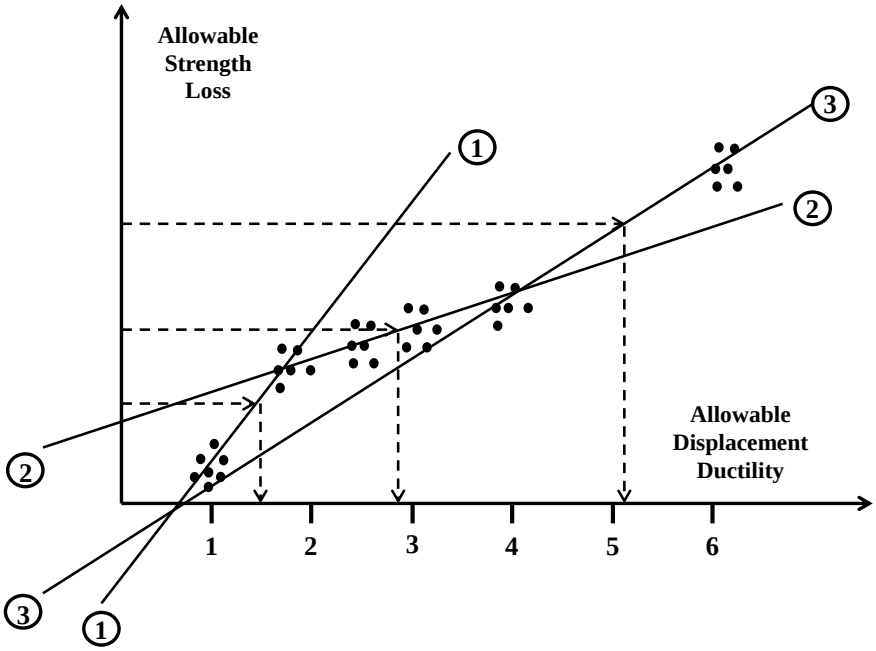

Figure 9.16 Schematic Use of 3 Part Design Equation

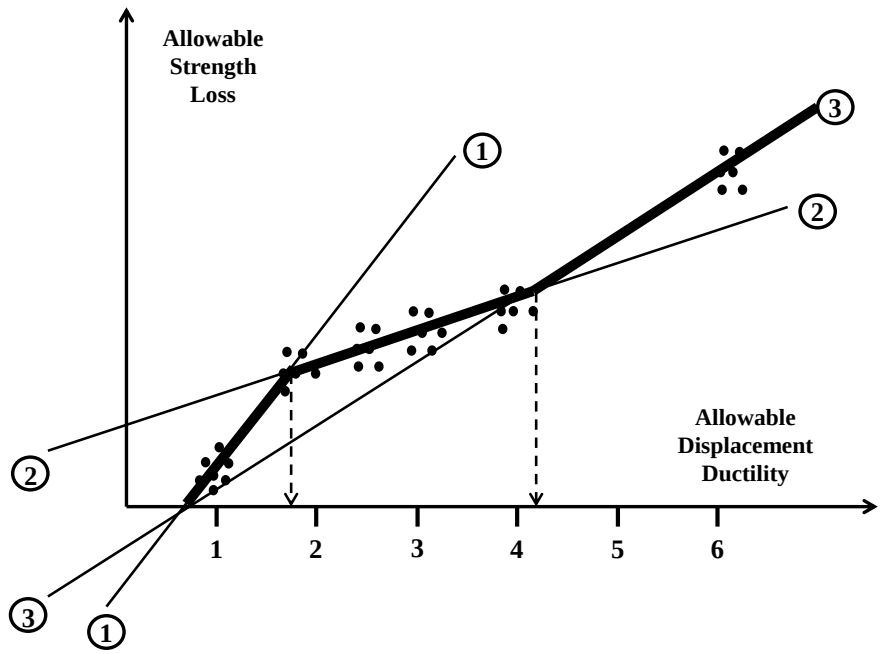

Figure 9.17 Schematic of Design Equation Backbone Curve

For $\mu_{\Delta all}$=1-3:

$$\mu_{\Delta all} = 6 \geq [6.3 - 16.6ALR - 0.114D/t_{des} + 0.0897F_{loss}] \geq \\ .....[2.7 - 2.8ALR - 0.029D/t_{des} + 0.0311F_{loss}] \geq 1 \quad (9.8)$$

For $\mu_{\Delta all}$=3-6:

$$\mu_{\Delta all} = 6 \geq [6.3 - 16.6ALR - 0.114D/t_{des} + 0.0897F_{loss}] \leq \\ .....[6.5 - 11.8ALR - 0.079D/t_{des} + 0.0493F_{loss}] \geq 1 \quad (9.9)$$

When compared to the data set from the 15 analyses, the recommended design model equation set shows relatively good agreement. As shown in the examples of Figure 9.18 and Figure 9.19, allowing the multi – linear design model to pivot around the ductility 2 and 4 regions, the model appeared to adequately capture the behavior of higher D/t_{des} ratios in the ductility 1 to 2 range and the lower D/t_{des} ratios in in the ductility 4 to 6 range. In addition,

the model also appeared to capture behavior in the intermediate ductility 2 to 4 range. By doing so, the model was able to predict with reasonable accuracy, the strength loss behavior in the range important to design (10%-30%) as well as at higher levels that may be useful in the evaluation of an existing structure. Ultimately, when comparing μ_Δ values calculated with the design model to those that existed in the data set, the design model was shown to be associated with an allowable displacement ductility RMS error of 0.5347.

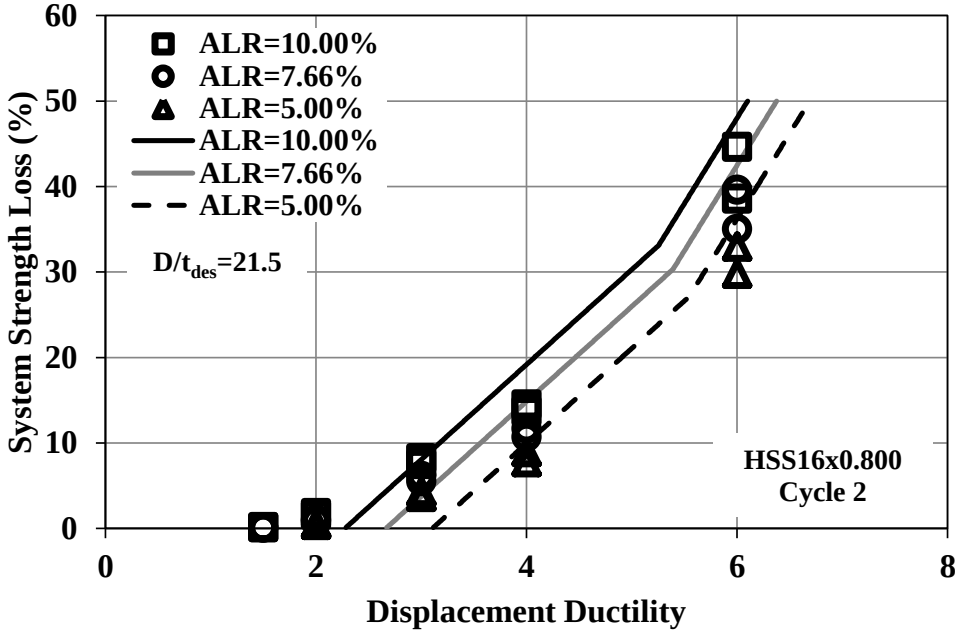

Figure 9.18 Multi-Linear Regression Analysis Results – Cycle 2 – D/t_{des}=21.5

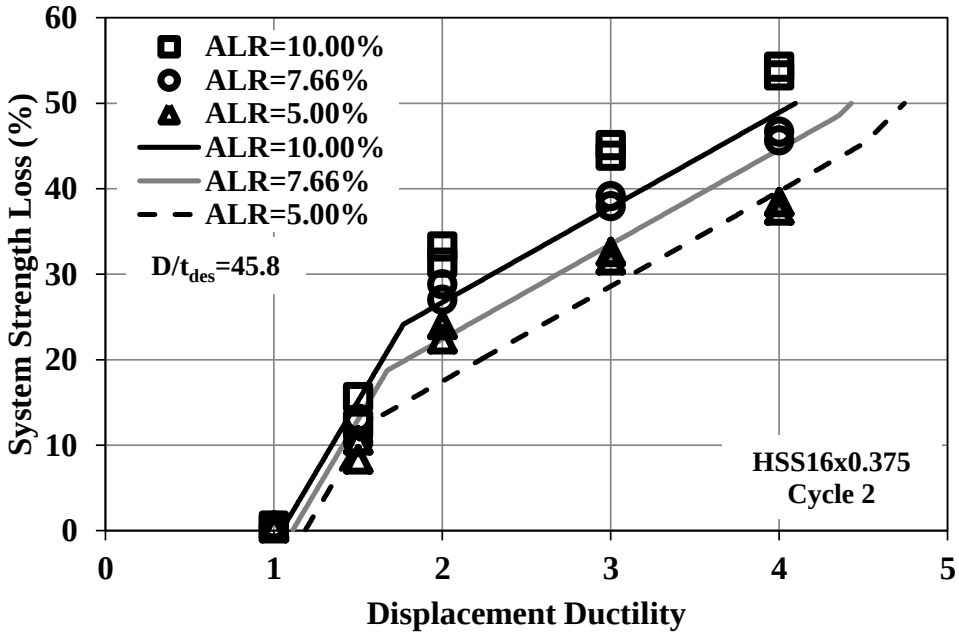

Figure 9.19 Multi-Linear Regression Analysis Results – Cycle 2 – D/t_{des}=45.8

Based on the findings of the parametric study, the design model equation set provided by Eq.(9.8) and Eq.(9.9), is recommended for estimating the allowable displacement ductility capacity of steel piers containing grouted shear stud connections. However, several applicable limitations and bounds to the recommended multi-linear regression design model should be clearly noted and considered when utilizing these recommendations. First, the model is bounded by allowable displacement ductility levels of 1 and 6 as has been mathematically mandated in design equation set. Secondly, the model should only be used for ALRs of 5% - 10% and D/t_{des} ratios from 51.7 – 21.5 as these were the bounds of the parametric study matrix and resulting data set. Lastly, it should clearly be noted that the design equation set was calibrated to capture the behavior of the parametric study data set as closely as possible, with no explicit factor of safety being considered. Hence, the recommended model is intended to serve as an estimate of actual displacement capacity and any factors of safety felt to be applicable by a designer, needs to be subsequently applied.

It should also be noted, the piers considered in the study were subjected to single bending, while actual driven pile systems would be subjected to double bending with a non-linear moment gradient below the soil level with the potential to form in – ground hinges. Therefore, it should be recognized that the displacement capacity calculated by the design model corresponds to the relative displacement capacity between the point of contraflexure and the cap beam centerline which would not be equal to the total displacement capacity of the system. This approach would require the relative deflection at the point of contraflexure be calculated in order to determine the total displacement capacity of the pier.

9.4 Truss Style Steel Pier Recommendations

Unlike the other tests in the first and second phase of the steel pier project at NCSU, one experimental evaluation in this research project did not focus on developing or evaluating a steel pipe pile to cap beam moment resisting connection. Alternatively, the test was aimed at evaluating the global hysteretic performance and controlling failure mode(s) of a truss style steel pier specimen subjected to lateral loading. The experimental specimen was nominally identical to that of existing piers used by AKDOT in the Gustavus – Causeway Replacement project.

The specimen was comprised of a triple wide HP12x53 cap beam, 24x0.500 in. pipe piles, and C9x15 truss elements. Detailed Finite Element Analysis was conducted prior to the experimental evaluation and found from a monotonic loading procedure, that the behavior of the pier was dominated by brace buckling that began at 3.9 in. of cap beam displacement. This was subsequently defined as the first yield displacement. Further, it was found that a pile hinging mode of failure was unlikely. Both experimental and analytical results from the cyclic loading procedure showed the pier to experience out of plane brace buckling which resulted in a pinched hysteretic shape compared to that of typical steel moment frame piers. However, the brace buckling behavior appeared not to be associated

with any negligible strength loss as the pier was able to regain load carrying capacity toward the cyclic loading peaks.

Multiple sources of weld and base material cracking developed at the ductility 1.5 stage of loading, but also were not associated with any negligible strength loss. Ultimately, complete rupture of the fillet weld connecting the exterior south pile gusset plate to the pile wall occurred in the first cycle of ductility 2, as shown in Figure 9.20. This fracture was associated with a rapid loss of strength of approximately 25%. This failure mechanism resulted in a reliable displacement ductility of 1 which was associated with 2.29% drift capacity.

Figure 9.20 Gusset Plate Weld Cracking

As a result of the multiple sources of inelasticity, and more importantly multiple sources of weld cracking and eventual rapid weld rupture, the truss style steel pier as currently

detailed is not recommended for use when a reliable ductile non – linear response is expected. Further, with the lack of a definable failure mechanism it is likely not possible to define a reliable displacement capacity of the system. However, it may be possible to develop a similar system that exhibits a reliable response and definable failure mechanism should items such as gusset plate sizing, weld sizing, and connection region detailing be considered. Further study would of course be required to determine if this is possible and what changes would be required if so.

9.5 Design Recommendations Summary

Throughout this chapter, numerous design recommendations have been outlined which are the result of the work conducted in this research project. This section is intended to serve as a brief conclusive summary of these design recommendations. The various limitations and uncertainties associated with these recommendations have been discussed throughout this chapter and further throughout this entire document. These limitations and uncertainties should be considered when utilizing these recommendations.

- Standard welded connections are not recommended for design when a displacement ductility capacity beyond 1.5 is required.
- The flexural hinge relocation method for protecting critical welded regions is, in general, recommended for design purposes.
- Use of the kerf connection configuration is not recommended for design, without further consideration for controlling the development pile wall cracking at the base of the assembly.
- The modified form of the flared column capital connection configuration could be recommended for design purposes. Although the results of this research indicate that that the modified assembly is capable of behaving successfully as a

modified weld protected connection, further study would be required to fully quantify the configurations reliable displacement ductility capacity.

- The grouted shear stud configuration is recommended for design purposes with the quantitative design recommendations made in prior sections.
- The modified buckling restrained grouted shear stud configuration is not recommended for design, based on the additional labor and materials as well as the arguably marginal associated improvement in performance.
- Based on the findings of the parametric study, the design model equation set provided by Eq.(9.8) and Eq.(9.9), is recommended for estimating the allowable displacement ductility capacity of steel piers containing grouted shear stud connections. Several bounds and limitations, however, are applicable and are listed in prior sections. Further, the modified elastic line element modeling procedure for determine first yield displacements is recommended.
- As a result of the multiple sources of inelasticity, and more importantly multiple sources of weld cracking and eventual rapid weld rupture, the truss style steel pier as currently detailed is not recommended for use when a reliable ductile non – linear response is expected. Further, with the lack of a definable failure mechanism it is likely not possible to define a reliable displacement capacity of the system.

REFERENCES

American Association of State Highway and Transportation Officials (AASHTO) [2009] "AASHTO Guide Specifications for LRFD Seismic Bridge Design" 1st Edition, Washington, DC.

American Institute of Steel Construction (AISC) [2010] "Seismic Provisions for Structural Steel Buildings", *ANSI/AISC 341-10*, Chicago.

American Welding Society (AWS) [2008] "Structural Welding Code" *AWS D1.1M/D1.1:2008*, Miami, FL.

Boresi, A.P.; Schmidt, R.J. [2003] *Advanced Mechanics of Materials*, 6th Edition, John Wiley & Sons, USA.

Bruneau, M, Uang, C.M., Whittaker, A. [1998] *Ductile Design of Steel Structures*, McGraw – Hill, New York, NY.

Cookson, K. A. [2009] "Seismic Performance of Steel Bridge Bent Welded Connections" M.S. thesis, Department of Civil Construction and Environmental Engineering, North Carolina State University, Raleigh.

Fulmer, S.J., Kowalsky, M.J., Nau, J.M., and Hassan, T. [2010] "Ductility of Welded Steel Pile to Steel Cap Beam Connections" Proc. of the SEI Structures Congress, Orlando, Florida, USA, pp. 216-227.

Fulmer, S.J., Kowalsky, M.J., Nau, J.M., Hassan, T. [2010] "Ductility of Welded Steel Column to Steel Cap Beam Connections" North Carolina State University Constructed Facilities Laboratory Technical Research Report No. RD-09-06.

Gonzalez, L.A.; Kowalsky, M.J.; Nau, J.M.; and Hassan. T. [2008] "Reversed Cyclic Testing of Full Scale Pipe Piles", North Carolina State University Constructed Facilities Laboratory Technical Report No. IS-08-13.

Jacobsen, L.S. [1930] "Steady forced vibrations as influenced by damping" ASME Transactione 52(1), 169–181.

Paulay, T., Priestley, M.J.N. [1992] *Seismic Design of Reinforced Concrete and Masonry Buildings*, Wiley, New York, pp. 686.

Parametric Technology Corporation (PTC) [2010] "Matcad 15.0 (15.0.0.436 [006041742])" Needham, MA, USA.

Priestley, M.J.N., Calvi, G.M. and Kowalsky, M.J. [2007] *Direct Displacement-Based Seismic Design of Structures*, IUSS Press, Pavia, Italy.

Montejo, L. A., Kowalsky M.J., and Hassan T. [2008] "Seismic Behavior of Reinforced Concrete Bridge Columns at Sub-Freezing Temperatures" North Carolina State University Constructed Facilities Laboratory Technical Research Report No. RD-08-01.

RISA Technologies, LLC [2011] "RISA-3D Demonstration Version 9.1.1"

Nishikawa, K., Yamamoto, S., Natori, T., Terao, K., Yaunami, H., Terada, M. [1998] "Retrofitting for seismic upgrading of steel bridge columns", Engineering Structures 20(4-6), 540-551.

Steunenburg, M., Sexsmith, R.G., Stiemer, S.F. [1998] "Seismic Behavior of Steel Pile to Precast Concrete Cap Beam Connections", ASCE Journal of Bridge Engineering 3(4), 177-188.

APPENDIX 1: Material Certifications and In-House Material Tests Data

TENSION TEST OF MATERIALS

(In accordance with ASTM A370-08)

Test Designation:	AKDOT-Phase 1- HSS16x500
Specimen Identification:	2
Date:	10/24/2010
Material Grade:	A500 Gr. B/C
Gage length (in.):	2.012
Total length (in.):	12.0
Length between shoulders (in.):	2.0
Thickness (in.):	0.462
Width (in.):	1.491

Test Setup:		
Procedure:	Tensile Test	
Range 1	Rate:	0.025 in./min
	End Level:	Sample Yield
Range 2	Rate:	0.2 in./min
	End Level:	Sample Break

Test Data:	
.1% Offset Yield:	54300 psi
.2% Offset Yield:	**56100 psi**
.5 in/in Yield:	56100 psi
Ulimate Strength:	69400 psi
Modulus of elasticity:	19.2 x1000ksi
% Elongation:	37%
Average Poisson's Ratio:	-0.369

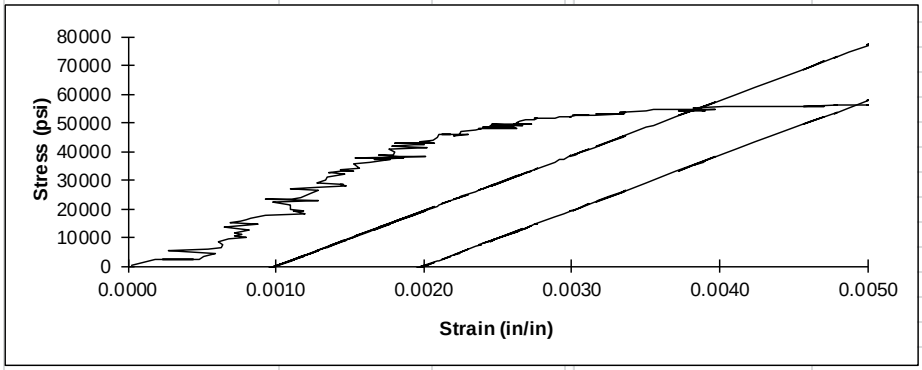

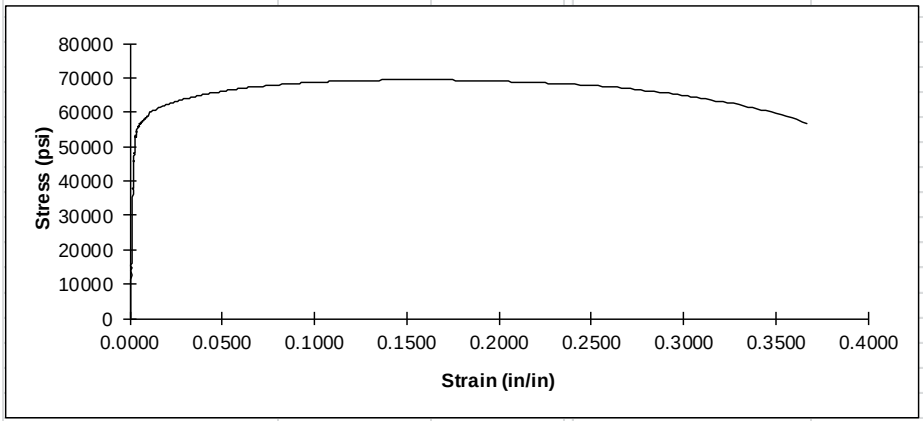

Figure A 1 Phase 1 Test 5 and 6 ASTM A500 Gr. B HSS16x0.500 Tension Test

SteelFab
PO Box 19289, 28219 Charlotte NC 28214
704-394-5376 Fax: 704-393-1400

Purchase Order 24725ABM-1 This number must appear on all invoices and shipping papers

ISSUED TO:
TUBULAR STEEL, INC.
1031 Executive Parkway Dr.

ST. LOUIS,, MO 63141-6351
TEL (800)388-7203 FAX 314-851-9336
Attn: Diane Jones

DELIVER TO:
SteelFab
8623 Old Dowd Road

Charlotte, NC 28214

Ship via
FOB Point:

Issued 01-21-08 Deliver by: 02-04-08 A.M.
Terms

[x] Material Test Reports Required

Please provide prices and delivery schedule before shipping. Notify us immediately if shipping schedule cannot be met.

No.	Qty	Type	Size	Grade	Length	Weight	Unit Cost	Extended Cost
/	12	HSS	16x.500	A500-B	11' 7-3/8"	11,536#	$61.2200 /LF	$8,532.54
	Mark T							
			Square Cut 2 Ends allocate 12 to 24725-1-1 RCVD.12 01/29@Y-1					

11,536#	Mat'l Cost	$8,532.54
	Freight	
	Sales Tax	
	Cut Charges	
	Total	$8,532.54

Figure A 2 Phase 1 Test 5 and 6 Material Certifications (1)

Atlas Tube Canada ULC
200 Clark St.
Harrow, Ontario, Canada
N0R 1G0
Tel: 519-738-3541
Fax: 519-738-3597

Atlas TUBE

MATERIAL TEST REPORT

Ref.B/L: 80255184
Date: 09.04.2007
Customer: 193

Sold to

Tubular Steel
1031 Executive Parkway
ST.LOUIS MO 63141
USA

Shipped to

Tubular Steel
950 Bunker Hill Rd.
STAUNTON IL 62088
USA

Material: 10.750x250x50'1"0(2x1)NMH Material No: R10750250 Made in: Canada
Sales order: 323849 Purchase Order: 3050

Heat No	Pcs	C	Mn	P	S	Si	Al	Cu	Cb	Mo	Ni	Cr	V
894321	2	0.200	0.790	0.007	0.006	0.020	0.038	0.020	0.004	0.002	0.008	0.019	0.000

Bundle No	Yield	Tensile	Eln.2in	Certification
M200469368	055891 Psi	066500 Psi	30.8 %	ASTM A500-03A GRADE B&C

Material Note:
Sales Or.Note:

Material: 16.000x500x42'0"0(2x1)NMH Material No: R16000500 Made in: Canada
Sales order: 321369 Purchase Order: 2895

Heat No	Pcs	C	Mn	P	S	Si	Al	Cu	Cb	Mo	Ni	Cr	V
480876	2	0.180	0.790	0.010	0.002	0.150	0.039	0.056	0.006	0.005	0.018	0.040	0.000

Bundle No	Yield	Tensile	Eln.2in	Certification
M200469737	054363 Psi	068010 Psi	39.0 %	ASTM A500-03A GRADE B&C

Material Note:
Sales Or.Note:

Material: 16.000x500x42'0"0(2x1)NMH Material No: R16000500 Made in: Canada
Sales order: 321369 Purchase Order: 2895

Heat No	Pcs	C	Mn	P	S	Si	Al	Cu	Cb	Mo	Ni	Cr	V
480876	2	0.180	0.790	0.010	0.002	0.150	0.039	0.056	0.006	0.005	0.018	0.040	0.000

Bundle No	Yield	Tensile	Eln.2in	Certification
M200469738	054363 Psi	068010 Psi	39.0 %	ASTM A500-03A GRADE B&C

Material Note:
Sales Or.Note:

ALL INCLUDED ROUNDS MEET A500 GRADE B/C AND A53 NON-HYDRO-TESTED

Authorized by Quality Assurance:

The results reported on this report represent the actual attributes of the material furnished and indicate full compliance with all applicable specification and contract requirements.

Steel Tube Institute OF NORTH AMERICA

Page : 3 Of 3

Metals Service Center Institute

Certs Received by

Figure A 3 Phase 1 Test 5 and 6 Material Certifications (2)

Atlas Tube Canada ULC
200 Clark St.
Harrow, Ontario, Canada
N0R 1G0
Tel: 519-738-3541
Fax: 519-738-3537

Ref.B/L: 80276234
Date: 01.19.2008
Customer: 193

Atlas TUBE

MATERIAL TEST REPORT

Sold to

Tubular Steel
1031 Executive Parkway
ST.LOUIS MO 63141
USA

Shipped to

Tubular Steel
950 Bunker Hill Rd.
STAUNTON IL 62088
USA

Material: 7.000x260x21'0"0(7x1).
Sales order: 362468
Material No: R07000250
Purchase Order: 1319-cut order
Made in: Canada

Heat No	Pcs	C	Mn	P	S	Si	Al	Cu	Cb	Mo	Ni	Cr	V
482380		0.190	0.810	0.012	0.008	0.015	0.051	0.057	0.006	0.002	0.011	0.029	0.000

Bundle No	Yield	Tensile	Ein.2in	Certification
M100704317	053017 Psi	065370 Psi	35.7 %	ASTM A500-03A GRADE B&C

Material Note:
Sales Or.Note:

Material: 16.000x500x50'0"0(2x1)NMH
Sales order: 360283
Material No: R16000500
Purchase Order: 1072
Made in: Canada
Cust Material #: 1072-103

Heat No	Pcs	C	Mn	P	S	Si	Al	Cu	Cb	Mo	Ni	Cr	V
482577	2	0.200	0.800	0.010	0.004	0.150	0.040	0.032	0.005	0.002	0.013	0.039	0.000

Bundle No	Yield	Tensile	Ein.2in	Certification
M200505808	053872 Psi	067910 Psi	38.3 %	ASTM A500-03A GRADE B&C

Material Note:
Sales Or.Note:

Material: 16.000x500x50'0"0(2x1)NMH
Sales order: 360283
Material No: R16000500
Purchase Order: 1072
Made in: Canada
Cust Material #: 1072-103

Heat No	Pcs	C	Mn	P	S	Si	Al	Cu	Cb	Mo	Ni	Cr	V
482577	2	0.200	0.800	0.010	0.004	0.150	0.040	0.032	0.005	0.002	0.013	0.039	0.000

Bundle No	Yield	Tensile	Ein.2in	Certification
M200505806	053872 Psi	067910 Psi	38.3 %	ASTM A500-03A GRADE B&C

Material Note:
Sales Or.Note:

ALL INCLUDED ROUNDS MEET A500 GRADE B/C AND A53 NON-HYDRO-TESTED

Authorized by Quality Assurance:

The results reported on this report represent the actual attributes of the material furnished and indicate full compliance with all applicable specification and contract requirements.

Steel Tube Institute OF NORTH AMERICA

Page : 3 Of 3

Metals Service Center Institute

Certs Received by

Figure A 4 Phase 1 Test 5 and 6 Material Certifications (3)

BILL OF LADING NO. 222691

STRAIGHT BILL OF LADING - SHORT FORM
ORIGINAL - NOT NEGOTIABLE

Page 1

RECEIVED: subject to the classification and tariff in effect on the date of the issue of this Bill of Lading

FROM: NUCOR STEEL - HERTFORD **TELEPHONE** 252/358-3700
AT: 1505 River Road **DATE** 01/16/2009
Cofield, NC

BOL No. 222691

Freight Term
F.O.B. PREPAID

egrant
(Signature of Consignor)

SHIP TO: ONEAL STEEL INC GREENSBORO (DOORS 7 & 8)
105 EAST FLORIDA STREET
G2 DOORS 7 & 8
GREENSBORO, NC 27406

SOLD TO: ONEAL STEEL INC
P O BOX 98
BIRMINGHAM, AL 35201

ROUTE:

CARRIER: TENNESSEE STEEL HAULERS

CAR OR VEHICLE NO. L/R# : 224420 / Vehicle :TRL 95-7594
Ticket# : 766307 / Gross Wt:74,940.00 lbs
211 miles

Master Plate	Pieces	Customer PO	Product	Order / Line	Weight (lbs)
9100114-09	1	2182063OP	PLATE - 1" x 96" x 240" Grade: ASTM A36-08/ASTM A709 Grade 36-08/ASME SA36-03a Cust Part#: 808915 MARKING:808915	69232 / 1	6,534.14

Heat	C	Mn	P	S	Si	Cu	Ni	Cr	Mo	Sn	Al	V	Nb	N	Ti	B	Ca
9100114	0.17	0.82	0.013	0.008	0.16	0.30	0.10	0.09	0.01	0.024	0.018	0.005	0.001	0.0000	0.003	0.0000	0.0020

Master Plate	Pieces	Customer PO	Product	Order / Line	Weight (lbs)
9100232-03	2	2182063OP	PLATE - 1" x 96" x 240" Grade: ASTM A36-08/ASTM A709 Grade 36-08/ASME SA36-03a Cust. Part#: 808915 MARKING:808915	69232 / 1	13,068.29

Heat	C	Mn	P	S	Si	Cu	Ni	Cr	Mo	Sn	Al	V	Nb	N	Ti	B	Ca
9100232	0.18	0.84	0.012	0.003	0.19	0.27	0.09	0.10	0.02	0.008	0.004	0.004	0.001	0.0000	0.003	0.0000	0.0020

Master Plate	Pieces	Customer PO	Product	Order / Line	Weight (lbs)
9100184-02	3	2182063OP	PLATE - 1.25" x 96" x 240" Grade: ASTM A572 Grade 50-07/ASTM A709 Grade 50-08/AASHTO M270-50 Type 2 Cust. Part#: 809803 MARKING:809803	69232 / 2	24,503.04

This one

Line Note COLOR CODE PLATES: GREEN/YELLOW

Heat	C	Mn	P	S	Si	Cu	Ni	Cr	Mo	Sn	Al	V	Nb	N	Ti	B	Ca
9100184	0.17	1.20	0.012	0.005	0.21	0.22	0.07	0.06	0.02	0.009	0.030	0.040	0.001	0.0000	0.003	0.0000	0.0010

Ship To Notes : "DO NOT SHIP WITH TESTS PENDING."DO NOT MIX WITH ONEAL STEEL INC. GREENSBORO3 ORDERS ON SAME TRUCK" MON-FRI 8 AM - 5PM COILS RECVD 6-7:30 AM/5-10PM ONLY 336-601-1106 BOBBY ELDER EXT. 106 OR 102 FOR APPOINTMENTS (8 APPTS. PER DAY MAX) MAX LIFT 15000# GROUP LIKE SIZES AND LIKE GRADES TOGETHER·NOTE: ALL SURFACE.CRITICAL MATERIAL IS ORDERED IN TRUCKLOAD QUANTITIES - MAKE EVERY EFFORT TO SHIP AS ORDERED (FULL TRUCKLOADS PER S.O.)SEND SHIPPING NOTICES AND FOREIGN/RAIL REPORTS TO: 105 EAST FLORIDA STR GREENSBORO NC 27420INVOICE TO BILLING ADDRESSSEND ALL OTHER CORESPONDENCE TO: PO BOX 2623 BIRMINGHAM AL 35202-2623

NUCOR STEEL - HERTFORD
P.O. Box 279
Winton, NC 27986

Permanent post office address of shipper

SHIPPER'S SIGNATURE:

CARRIER'S SIGNATURE:

Figure A 5 Phase 1 Test 6 Column Capital Plate Material Certifications

TENSION TEST OF MATERIALS

(In accordance with ASTM A370-08)

Test Designation:	AKDOT-Phase 2- HSS16x500
Specimen Identification:	1
Date:	10/24/2010
Material Grade:	A252 Gr. 3
Gage length (in.):	2.051
Total length (in.):	12.0
Length between shoulders (in.):	2.0
Thickness (in.):	0.457
Width (in.):	1.503

Test Setup:		
Procedure:	Tensile Test	
Range 1	Rate:	0.025 in./min
	End Level:	Sample Yield
Range 2	Rate:	0.2 in./min
	End Level:	Sample Break

Test Data:	
.1% Offset Yield:	55900 psi
.2% Offset Yield:	**58400 psi**
.5 in/in Yield:	59200 psi
Ulimate Strength:	71200 psi
Modulus of elasticity:	30.1 x1000ksi
% Elongation:	16%

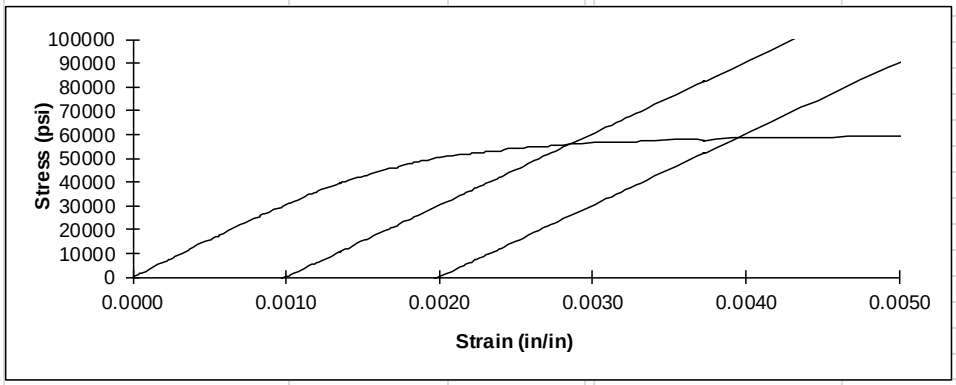

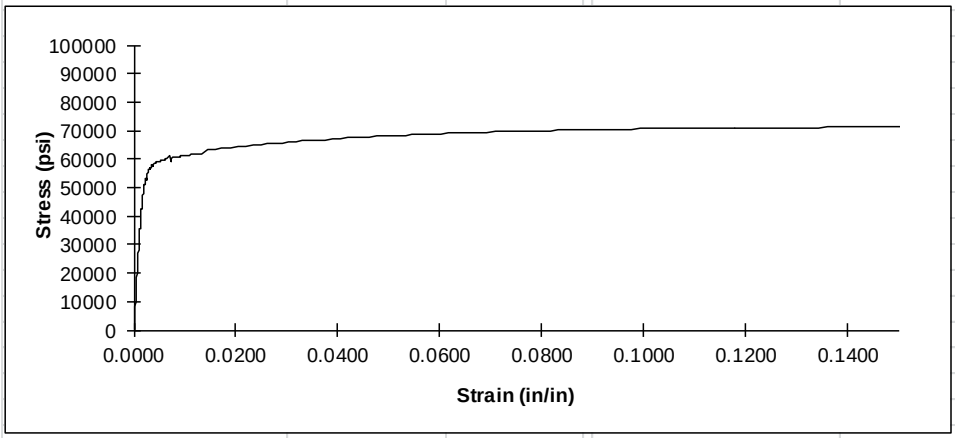

Figure A 6 Phase 2 Test 1 ASTM A500 Gr. B HSS16x0.500 Tension Test (1)

TENSION TEST OF MATERIALS

(In accordance with ASTM A370-08)

Test Designation:	AKDOT-Phase 2- HSS16x500
Specimen Identification:	2
Date:	10/24/2010
Material Grade:	A500 Gr. B/C
Gage length (in.):	1.998
Total length (in.):	12.0
Length between shoulders (in.):	2.0
Thickness (in.):	0.457
Width (in.):	1.532

Test Setup:		
Procedure:	Tensile Test	
Range 1	Rate:	0.025 in./min
	End Level:	Sample Yield
Range 2	Rate:	0.2 in./min
	End Level:	Sample Break

Test Data:	
.1% Offset Yield:	49700 psi
.2% Offset Yield:	**54200 psi**
.5 in/in Yield:	55800 psi
Ulimate Strength:	71900 psi
Modulus of elasticity:	26.4 x1000ksi
% Elongation:	41%
Average Poisson's Ratio:	-0.373

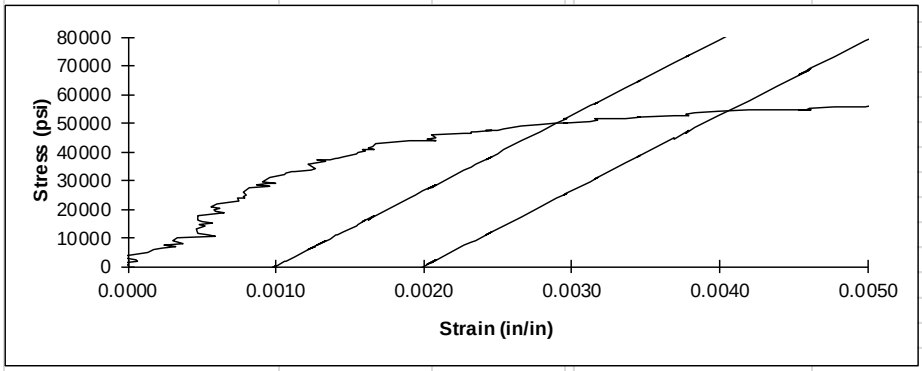

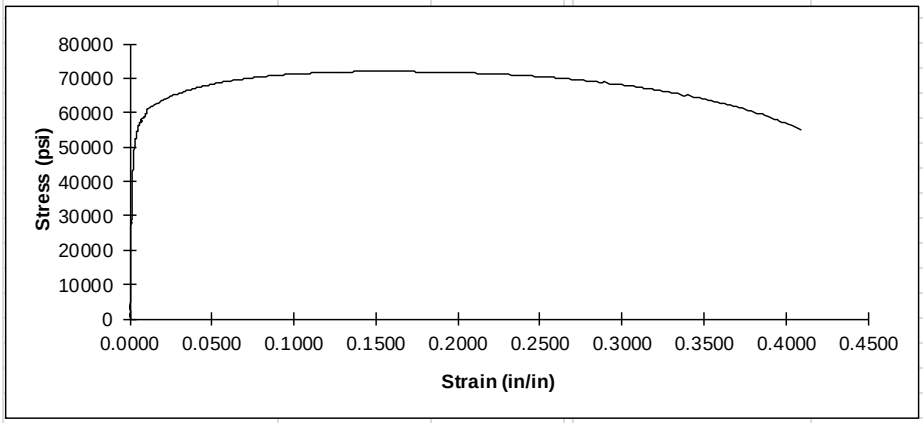

Figure A 7 Phase 2 Test 1 ASTM A500 Gr. B HSS16x0.500 Tension Test (2)

TENSION TEST OF MATERIALS

(In accordance with ASTM A370-08)

Test Designation:	AKDOT-Phase 2- Plate
Specimen Identification:	C1
Date:	10/24/2010
Material Grade:	A572 Gr. 50/A709 Gr. 50
Gage length (in.):	2.068
Total length (in.):	12.0
Length between shoulders (in.):	2.0
Thickness (in.):	0.211
Width (in.):	0.494

Test Setup:		
Procedure:	Tensile Test	
Range 1	Rate:	0.025 in./min
	End Level:	Sample Yield
Range 2	Rate:	0.2 in./min
	End Level:	Sample Break

Test Data:	
.1% Offset Yield:	56200 psi
.2% Offset Yield:	**57000 psi**
.5 in/in Yield:	57300 psi
Ulimate Strength:	82200 psi
Modulus of elasticity:	25.8 x1000ksi
% Elongation:	25%

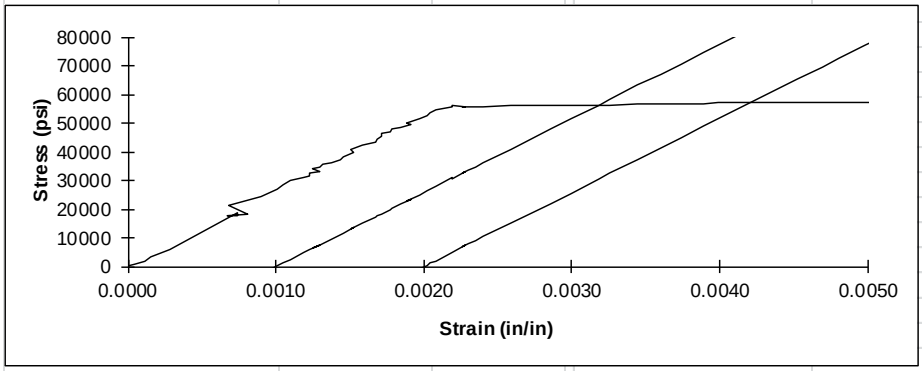

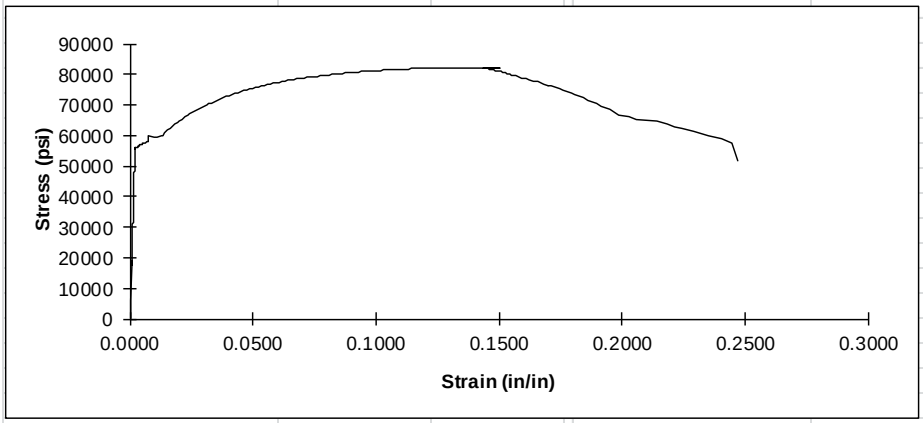

Figure A 8 Phase 2 Test 1 ASTM A572 Gr. 50 Plate Tension Test (1)

TENSION TEST OF MATERIALS

(In accordance with ASTM A370-08)

Test Designation:	AKDOT-Phase 2- Plate
Specimen Identification:	C2
Date:	10/24/2010
Material Grade:	A572 Gr. 50/A709 Gr. 50
Gage length (in.):	2.069
Total length (in.):	12.0
Length between shoulders (in.):	2.0
Thickness (in.):	0.172
Width (in.):	0.493

Test Setup:		
Procedure:	Tensile Test	
Range 1	Rate:	0.025 in./min
	End Level:	Sample Yield
Range 2	Rate:	0.2 in./min
	End Level:	Sample Break

Test Data:	
.1% Offset Yield:	56400 psi
.2% Offset Yield:	**56700 psi**
.5 in/in Yield:	56800 psi
Ulimate Strength:	80900 psi
Modulus of elasticity:	30.9 x1000ksi
% Elongation:	24%

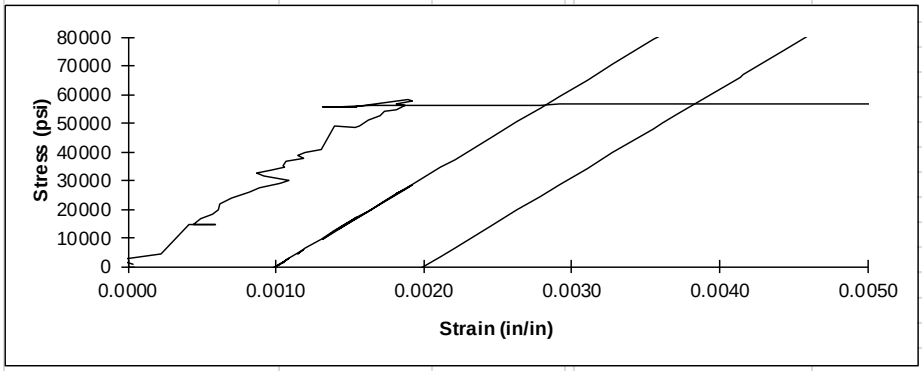

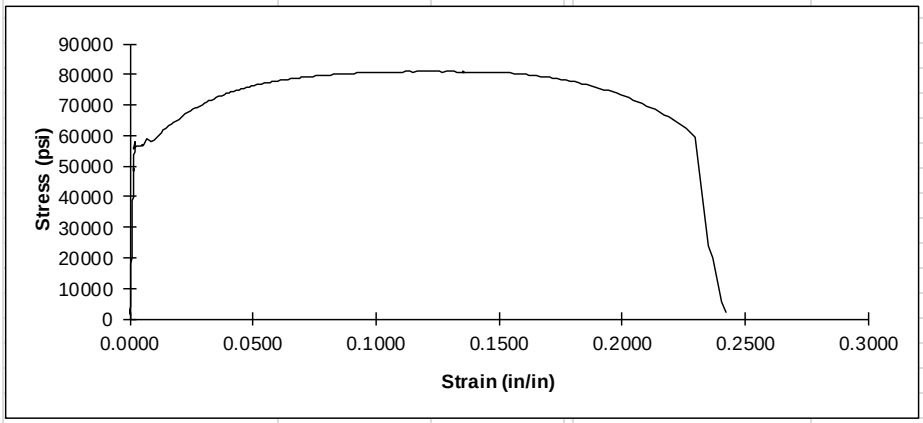

Figure A 9 Phase 2 Test 1 ASTM A572 Gr. 50 Plate Tension Test (2)

Atlas Tube Canada ULC
200 Clark St.
Harrow, Ontario, Canada
N0R 1G0
Tel: 519-733-3541
Fax: 519-733-3537

Atlas TUBE

Ref.B/L: 80382016
Date: 05.07.2010
Customer: 78

MATERIAL TEST REPORT

Sold to
Infra-Metals Corporation
580 Middletown Blvd-Suite
LANGHORNE PA 19047
USA

Shipped to
Infra-Metals Corporation
4601 Curtis Ave
BALTIMORE MD 21226
USA

Material: 10.750x385x35'0"0(2x1). Material No: R10750385 Made in: Canada
Sales order: 546018 Purchase Order: 18600 Melted in: Canada

Heat No	C	Mn	P	S	Si	Al	Cu	Cb	Mo	Ni	Cr	V	Ti	B	N
743990	0.180	0.930	0.009	0.008	0.009	0.040	0.000	0.005	0.000	0.000	0.000	0.002	0.002	0.000	0.000

Bundle No	Yield	Tensile	Elo.2in	Certification
M200988460	059530 Psi	074310 Psi	23.9 %	ASTM A500-07 GRADE B&C

CE: 0.32
Material Note:
Sales Or.Note:

Material: 10.750x385x50'0"0(2x1). Material No: R10750385 Made in: Canada
Sales order: 546018 Purchase Order: 18600 Melted in: Canada

Heat No	C	Mn	P	S	Si	Al	Cu	Cb	Mo	Ni	Cr	V	Ti	B	N
743990	0.180	0.930	0.009	0.008	0.009	0.040	0.000	0.009	0.000	0.000	0.000	0.002	0.002	0.000	0.000

Bundle No	Yield	Tensile	Elo.2in	Certification
M200988484	059530 Psi	074310 Psi	23.9 %	ASTM A500-07 GRADE B&C

CE: 0.32
Material Note:
Sales Or.Note:

Material: 16.000x600x50'0"0(2x1). Material No: R16000600 Made in: Canada
Sales order: 546018 Purchase Order: 18600 Melted in: USA

Heat No	C	Mn	P	S	Si	Al	Cu	Cb	Mo	Ni	Cr	V	Ti	B	N
L52187	0.190	0.860	0.014	0.009	0.012	0.060	0.000	0.005	0.000	0.000	0.000	0.001	0.000	0.000	0.000

Bundle No	Yield	Tensile	Elo.2in	Certification
M200984221	052020 Psi	067460 Psi	28.1 %	ASTM A500-07 GRADE B&C

CE: 0.33
Material Note:
Sales Or.Note:

63897

Authorized by Quality Assurance:
The results reported on this report represent the actual analysis of the material furnished and indicate full compliance with all applicable specifications and contract requirements.
Chemical analysis was performed using D1.5 method.

Steel Tube Institute of North America

Page : 4 Of 4

Metals Service Center Institute

Figure A 10 Phase 2 Test 1 ASTM A500 Gr. B HSS16x0.500 Material Certifications

NUCOR
PLATE MILL

P.O.Box 279
Winton, NC 27986
(252) 356-3700

Mill Test Report
Page 1

NUCOR It's our Nature

Issuing Date : 09/21/2010 B/L No. : 272996 Load No. : 274583 Our Order No. : 84945/4 Cust. Order No. : STK-4385

Vehicle No: ANDERSON BROS. 819

Specification : 1.0000" x 96.000" x 240.000"
ASTM A572 Grade 50/345-07/A709 Grade 50-09a/ AASHTO M270 50 97
Type 2

Sold To : STEELFAB INC
PO BOX 18289, 28219
CHARLOTTE,NC 28214

Ship To : STEELFAB INC
8623 OLD DOWD ROAD
CHARLOTTE,NC 28214

Marking :

Heat No	C	Mn	P	S	Si	Cu	Ni	Cr	Mo	Al(tot)	V	Nb	Ti	N	Ca	B	Sn	CEQ	PCM
0506617	0.19	1.17	0.025	0.003	0.19	0.24	0.10	0.16	0.02	0.028	0.043	0.002	0.002		0.0016	0.0003	0.011	0.45	0.28

Tensile Test								Charpy Impacts												
Plate Serial No	Pieces	Tons	Dir.	(psi) Yield	(psi) Tensile	Elongation % in 2"	Elongation % in 8"	Dir.	1	(%) shear	2	(%) shear	3	(%) shear	Ave.	(%) shear	Size	Temp	Min Ave.
0506617-02	7	22.66	T	60,500	84,100		19.9												
			T	53,200	80,900		20.6												

CERTS RECEIVED BY
SV

Manufactured to fully killed fine grain practice by Electric Arc Furnace. Welding or weld repair was not performed on this material. Mercury has not been used in the direct manufacturing of this material. Produced as continuous cast discrete plate as-rolled, unless otherwise noted in Specification.
Yield by 0.5EUL method unless otherwise specified. Ceq = C+(Mn/6)+((Cr+Mo+V)/5)+((Cu+Ni)/15)
Pcm = C+(Si/30)+(Mn/20)+(Cu/20)+(Ni/60)+(Cr/20)+(Mo/15)+(V/10)+5B
Melted and manufactured in the USA. ISO 9001-2000 certified (#008461) by SRI Quality System Registrar (#0995-09). PED 97/23/EC 7/2 Annex 1, Para. 4.3 Compliant. DIN 50049 3.1.B/EN 10204 3.1B(2004), DIN EN 10204 3.1(2005) compliant. For ABS grades only. Quality Assurance certificate 06-MMPQA-363

We hereby certify that the contents of this report are accurate and correct. All test results and operations performed by the material manufacturer are in compliance with the applicable specifications, including customer specifications.

T. A. Dagnetto, Metallurgist

09/21/2010 12:02:29 PM

Figure A 11 Phase 2 Test 1 ASTM A572 Gr. 50 Material Certifications

TENSION TEST OF MATERIALS

(In accordance with ASTM A370-10)

Test Designation:	Phase 2 Test 2,3
Specimen Identification:	1
Date:	4/15/2011
Material Grade:	A500 Gr. B/C
Gage length (in.):	2.065
Total length (in.):	12.0
Length between shoulders (in.):	2.5
Thickness (in.):	0.485
Width (in.):	1.320

Test Setup:		
Procedure:	Tensile Test	
Range 1	Rate:	0.025 in./min
	End Level:	Sample Yield
Range 2	Rate:	0.2 in./min
	End Level:	Sample Break

Test Data:	
.1% Offset Yield:	58400 psi
.2% Offset Yield:	**59100 psi**
.5 in/in Yield:	60200 psi
Ulimate Strength:	76500 psi
Modulus of elasticity:	40.2 x1000ksi
% Elongation:	38%

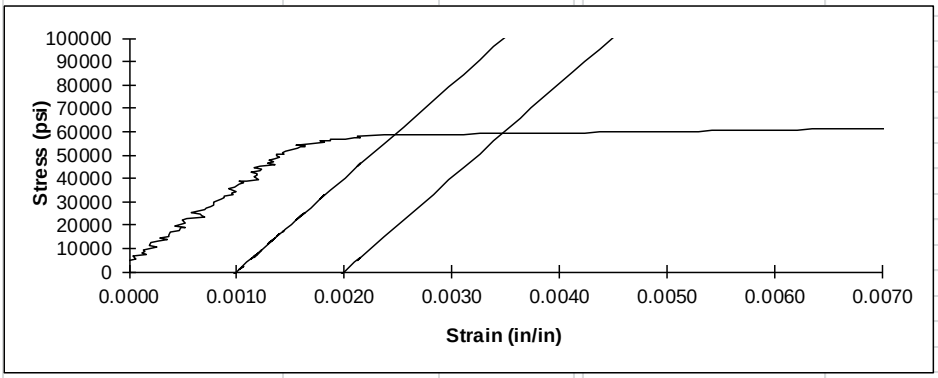

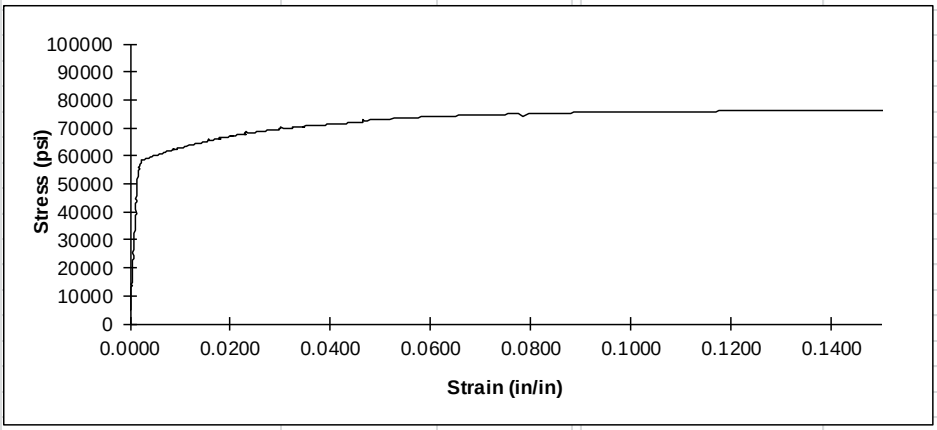

Figure A 12 Phase 2 Test 2 ASTM A500 Gr. B HSS16x0.500 Tension Test (1)

TENSION TEST OF MATERIALS

(In accordance with ASTM A370-10)

Test Designation:	Phase 2 Test 2,3
Specimen Identification:	2
Date:	4/15/2011
Material Grade:	A500 Gr. B/C
Gage length (in.):	2.016
Total length (in.):	12.0
Length between shoulders (in.):	2.5
Thickness (in.):	0.487
Width (in.):	1.272

Test Setup:		
Procedure:	Tensile Test	
Range 1	Rate:	0.025 in./min
	End Level:	Sample Yield
Range 2	Rate:	0.2 in./min
	End Level:	Sample Break

Test Data:	
.1% Offset Yield:	52200 psi
.2% Offset Yield:	**54300 psi**
.5 in/in Yield:	55500 psi
Ulimate Strength:	73700 psi
Modulus of elasticity:	32.8 x1000ksi
% Elongation:	39%

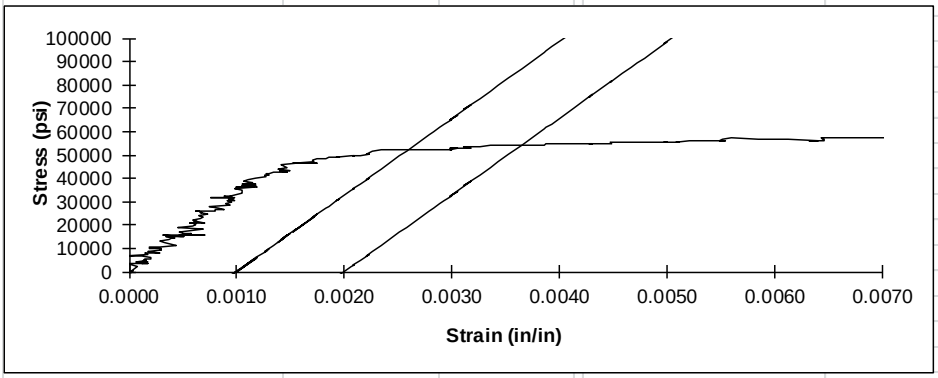

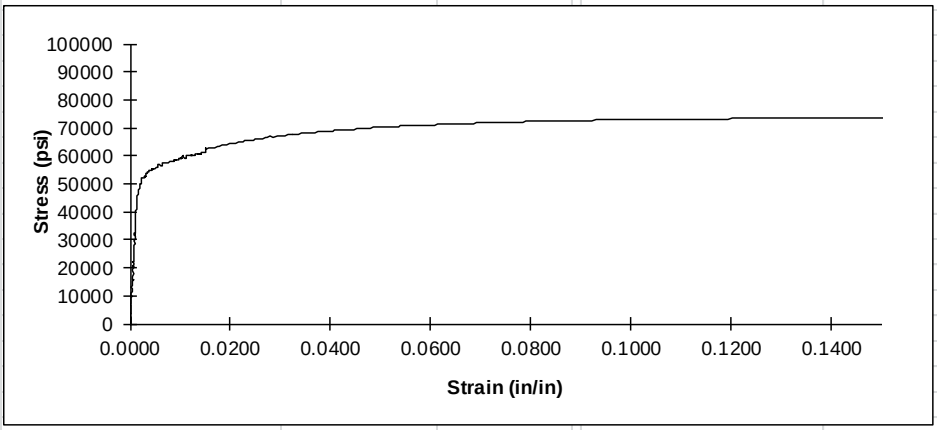

Figure A 13 Phase 2 Test 2 ASTM A500 Gr. B HSS16x0.500 Tension Test (2)

ISO 9001:2000 CERTIFIED

AMERICAN STEEL PIPE
A division of American Cast Iron Pipe Co.,
P.O. Box 2727, Birmingham, AL 35202-2727
QUALIFICATION REPORT OF SHIPMENT

DATE: 09/SEP/2008

CUSTOMER ADDRESS: SAGINAW PIPE INCORPORATED
P O BOX 8
SAGINAW AL 35137

Customer Order Number 35049

MFG Order Number S108488

LINE	PIECES	FOOTAGE	SIZE	WALL	SHIPMENT DESCRIPTION SHIP. NO 1-2	SPECIFICATIONS	GRADE
1	27	1088.3	24.00	.500	ERW STEEL PIPE	ASTM A500	C B

All tests are from the body of the pipe in the transverse direction unless otherwise noted.
Standard tensile gage length 1-1/2" x 2".

HEAT	C	MN	P	S	CB	SI	TI	CU	NI	MO	CR	V	AL	B	N	C.E.	Coil Pipe
13380	* LINE 1						EDITION REFERENCE 4				YEAR 2008 Yield Strength by Strap						
H=	0.070	1.130	0.010	0.004	0.052	0.196	0.020	0.020	0.010	0.010	0.030	0.004	0.046	.0002	.0055	0.269	0036
P=	0.070	1.079	0.013	0.006	0.056	0.181	0.016	0.022	0.013	0.007	0.034	0.009	0.035	.0000	.0000	0.262	08/16
M=Weld Ten. 86.5 ksi Ten. 89.0 ksi Yield 71.0 ksi %EL 37.0 RB Hydro: Psi RUN: 44-8																	
Y/T RATIO = 0.80																	
13380	* LINE 1						EDITION REFERENCE 4				YEAR 2008 Yield Strength by Strap						
H=	0.070	1.130	0.010	0.004	0.052	0.196	0.020	0.020	0.010	0.010	0.030	0.004	0.046	.0002	.0055	0.269	0037
P=	0.070	1.066	0.013	0.006	0.054	0.173	0.017	0.022	0.013	0.006	0.035	0.009	0.039	.0000	.0000	0.260	/
M=Weld Ten. 00.0 ksi Ten. 00.0 ksi Yield 00.0 ksi %EL 00.0 RB Hydro: Psi RUN: 44-8																	
Y/T RATIO = 0.00																	

PAGE 1
Continued

Issue No.: 6

Form Date: 10/18/2004

QD-AW3F05

CERTS RECEIVED BY
SV

Figure A 14 Phase 2 Test 2 ASTM A500 Gr. B HSS16x0.500 Material Certifications (1)

ISO 9001:2000 CERTIFIED

CUSTOMER NAME: SAGINAW PIPE INCORPORATED

Customer Order Number 35049

Date: 09/SEP/2008
MFG Order Number S108488

HEAT	C	MN	P	S	CB	SI	TI	CU	NI	MO	CR	V	AL	B	N	C.E.	Coil Pipe
13394	* LINE 1						EDITION REFERENCE 4				YEAR 2008		Yield Strength by Strap				
H=	0.060	1.090	0.014	0.004	0.046	0.235	0.018	0.030	0.010	0.010	0.030	0.004	0.037	.0002	.0035	0.253	0027
P=	0.059	1.083	0.014	0.006	0.042	0.192	0.014	0.058	0.017	0.006	0.037	0.009	0.030	.0000	.0000	0.255	/
M=Weld Ten.		00.0 ksi		Ten.	00.0 ksi		Yield	00.0 ksi		%EL 00.0	RB		Hydro:		Psi	RUN:	44-8
Y/T RATIO = 0.00																	
25236	* LINE 1						EDITION REFERENCE 4				YEAR 2008		Yield Strength by Strap				
H=	0.060	1.050	0.012	0.005	0.045	0.184	0.017	0.030	0.010	0.010	0.030	0.003	0.027	.0002	.0050	0.246	0091
P=	0.061	1.038	0.013	0.006	0.044	0.173	0.014	0.037	0.016	0.008	0.033	0.002	0.023	.0000	.0000	0.246	08/16
M=Weld Ten.		84.5 ksi		Ten.	85.0 ksi		Yield	71.5 ksi		%EL 38.0	RB		Hydro:		Psi	RUN:	44-8
Y/T RATIO = 0.84																	
25236	* LINE 1						EDITION REFERENCE 4				YEAR 2008		Yield Strength by Strap				
H=	0.060	1.050	0.012	0.005	0.045	0.184	0.017	0.030	0.010	0.010	0.030	0.003	0.027	.0002	.0050	0.246	0092
P=	0.061	1.028	0.012	0.006	0.042	0.173	0.015	0.038	0.016	0.007	0.034	0.002	0.022	.0000	.0000	0.245	/
M=Weld Ten.		00.0 ksi		Ten.	00.0 ksi		Yield	00.0 ksi		%EL 00.0	RB		Hydro:		Psi	RUN:	44-8
Y/T RATIO = 0.00																	
13381	* LINE 1						EDITION REFERENCE 4				YEAR 2008		Yield Strength by Strap				
H=	0.070	1.070	0.012	0.004	0.045	0.184	0.019	0.020	0.010	0.010	0.030	0.003	0.040	.0002	.0032	0.259	0054
P=	0.064	1.052	0.014	0.006	0.040	0.174	0.015	0.022	0.010	0.006	0.037	0.007	0.034	.0005	.0000	0.251	08/16
M=Weld Ten.		85.5 ksi		Ten.	86.5 ksi		Yield	70.5 ksi		%EL 36.0	RB		Hydro:		Psi	RUN:	44-8
Y/T RATIO = 0.82																	

PAGE 7
Continued

Issue No.: 6 Form Date: 10/18/2004 QD-AW3F05

CERTS RECEIVED BY

Figure A 15 Phase 2 Test 2 ASTM A500 Gr. B HSS16x0.500 Material Certifications (2)

ISO 9001:2000 CERTIFIED

CUSTOMER NAME: SAGINAW PIPE INCORPORATED

Customer Order Number 35049

Date: 09/SEP/2008
MFG Order Number S108488

CERTS RECEIVED BY
SV

Legend Analyses:

A-Z - Additional Testing	R - Retest	Hydrostatic Test: OK
H - Heat Analysis	L - Longitudinal	Flattening Test: OK
P - Product Analysis	T - Transitional	
M- Mechanical Properties	W - Weld Line	

EDITION REFERENCE 1: API 5L 41ST EDITION 4/1/1995
EDITION REFERENCE 2: API 5L 42ND EDITION 7/1/2000
EDITION REFERENCE 3: API 5L 43RD EDITION 10/4/2004
EDITION REFERENCE 4: ASTM/ASME ANNUAL BOOK OF STANDARDS SECT.1, VOL 01.01

* Manufactured and Melted in the USA.

We hereby certify that the above figures are correct as contained in the records of this company, and th the pipe were manufactured, tested and inspected in compliance with the Latest edition of the applicable specification, in Birmingham, Alabama, U.S.A.

Noel A. Gordon

Noel A. Gordon
Manager of Quality Assurance - Steel Pipe

PAGE 10
End Of Report

Issue No.: 6 Form Date: 10/18/2004 QD-AW3F055

Figure A 16 Phase 2 Test 2 ASTM A500 Gr. B HSS16x0.500 Material Certifications (3)

Atlas ABC Corp (Atlas Tube Chicago)
1855 East 122nd Street
Chicago, Illinois, USA
60633
Tel: 773-646-4500
Fax: 773-646-6126

Atlas Tube
JMC STEEL GROUP

Ref.B/L: 80406699
Date: 11.11.2010
Customer: 547

MATERIAL TEST REPORT

Sold to

Saginaw Pipe Co., Inc.
PO Box 8
SAGINAW AL 35137
USA

Shipped to

Saginaw Pipe Co., Inc.
Highway 31 South
SAGINAW AL 35137
USA

Material: 16.000x500x50'0'0(1x1). Material No: R16000500 Made in: USA
Melted in: USA

Sales order: 593337 Purchase Order: 39148

Heat No	C	Mn	P	S	Si	Al	Cu	Cb	Mo	Ni	Cr	V	Ti	B	N
M07072	0.180	0.790	0.012	0.007	0.015	0.053	0.020	0.005	0.002	0.010	0.030	0.001	0.001	0.000	0.000

Bundle No	PCs	Yield	Tensile	Elo.2in	Certification
M900368865	1	073070 Psi	076320 Psi	41 %	ASTM A500-07 GRADE B&C

CE: 0.32

Material Note:
Sales Or.Note:

Material: 16.000x500x50'0'0(1x1). Material No: R16000500 Made in: USA
Melted in: USA

Sales order: 593337 Purchase Order: 39148

Heat No	C	Mn	P	S	Si	Al	Cu	Cb	Mo	Ni	Cr	V	Ti	B	N
M07072	0.180	0.790	0.012	0.007	0.015	0.053	0.020	0.005	0.002	0.010	0.030	0.001	0.001	0.000	0.000

Bundle No	PCs	Yield	Tensile	Elo.2in	Certification
M900368866	1	073070 Psi	076320 Psi	41 %	ASTM A500-07 GRADE B&C

CE: 0.32

Material Note:
Sales Or.Note:

CERTS RECEIVED BY
SV

Figure A 17 Phase 2 Test 2 ASTM A500 Gr. B HSS16x0.500 Material Certifications (4)

Atlas Tube Canada ULC
200 Clark St.
Harrow, Ontario, Canada
N0R 1G0
Tel: 519-738-3541
Fax: 519-738-3537

Ref.B/L: 80341987
Date: 06.01.2009
Customer: 1806

MATERIAL TEST REPORT

Sold to
Infra-Metals Corporation
1900 Bessmer Road
PETERSBURG VA 23805
USA

Shipped to
Steel Fab
8623 Old Dowd Road
CHARLOTTE NC 28214
USA

Material: 16.000x625x21'0"O(2x1). Material No: R16000625 Made in: Canada
Sales order: 467828 Purchase Order: A1959 ! after jun1

Heat No	C	Mn	P	S	Si	Al	Cu	Cb	Mo	Ni	Cr	V	Ti
286777	0.210	0.770	0.011	0.002	0.023	0.031	0.080	0.000	0.007	0.030	0.030	0.001	0.003

Bundle No	Yield	Tensile	Eln.2in	Certification	CE: 0.36
M200605408	051780 Psi	066400 Psi	33.8 %	ASTM A500-07 GRADE B&C	

Material Note:
Sales Or.Note:

Material: 16.000x625x40'6"O(2x1). Material No: R16000625 Made in: Canada
Sales order: 467828 Purchase Order: A1959 ! after jun1

Heat No	C	Mn	P	S	Si	Al	Cu	Cb	Mo	Ni	Cr	V	Ti
286777	0.210	0.770	0.011	0.002	0.023	0.031	0.080	0.000	0.007	0.030	0.030	0.001	0.003

Bundle No	Yield	Tensile	Eln.2in	Certification	CE: 0.36
M200605413	051780 Psi	066400 Psi	33.8 %	ASTM A500-07 GRADE B&C	

Material Note:
Sales Or.Note:

Material: 16.000x625x40'6"O(2x1). Material No: R16000625 Made in: Canada
Sales order: 467828 Purchase Order: A1959 ! after jun1

Heat No	C	Mn	P	S	Si	Al	Cu	Cb	Mo	Ni	Cr	V	Ti
286777	0.210	0.770	0.011	0.002	0.023	0.031	0.080	0.000	0.007	0.030	0.030	0.001	0.003

Bundle No	Yield	Tensile	Eln.2in	Certification	CE: 0.36
M200605412	051780 Psi	066400 Psi	33.8 %	ASTM A500-07 GRADE B&C	

Material Note:
Sales Or.Note:

Material: 16.000x625x21'0"O(2x1). Material No: R16000625 Made in: Canada
Sales order: 467828 Purchase Order: A1959 ! after jun1

Heat No	C	Mn	P	S	Si	Al	Cu	Cb	Mo	Ni	Cr	V	Ti
286777	0.210	0.770	0.011	0.002	0.023	0.031	0.080	0.000	0.007	0.030	0.030	0.001	0.003

Bundle No	Yield	Tensile	Eln.2in	Certification	CE: 0.36
M200605409	051780 Psi	066400 Psi	33.8 %	ASTM A500-07 GRADE B&C	

Material Note:
Sales Or.Note:

Certs Received by

Authorized by Quality Assurance:
The results reported on this report represent the actual attributes of the material furnished and indicate full compliance with all applicable specification and contract requirements.
Certified to AWS D1.1 method.

Steel Tube Institute

Page : 2 Of 2

Metals Service Center Institute

Figure A 18 Phase 2 Test 3 ASTM A500 Gr. B HSS16x0.625 Material Certifications (1)

Atlas Tube Canada ULC
200 Clark St.
Harrow, Ontario, Canada
N0R 1G0
Tel: 519-738-3541
Fax: 519-738-3537

Atlas TUBE

Ref.B/L: 80341987
Date: 06.01.2009
Customer: 1806

MATERIAL TEST REPORT

Sold to

Infra-Metals Corporation
1900 Bessmer Road
PETERSBURG VA 23805
USA

Shipped to

Steel Fab
8623 Old Dowd Road
CHARLOTTE NC 28214
USA

Material: 16.000x625x45'0"0(2x1). Material No: R16000625 Made in: Canada
Sales order: 467828 Purchase Order: A1959 ! after jun1

Heat No	C	Mn	P	S	Si	Al	Cu	Cb	Mo	Ni	Cr	V	Ti
286774	0.220	0.750	0.011	0.001	0.020	0.029	0.080	0.000	0.007	0.030	0.030	0.001	0.002

Bundle No	Yield	Tensile	Eln.2in	Certification	CE: 0.38
M200605415	055410 Psi	070050 Psi	36.2 %	ASTM A500-07 GRADE B&C	

Material Note:
Sales Or.Note:

Material: 16.000x625x45'0"0(2x1). Material No: R16000625 Made in: Canada
Sales order: 467828 Purchase Order: A1959 ! after jun1

Heat No	C	Mn	P	S	Si	Al	Cu	Cb	Mo	Ni	Cr	V	Ti
286777	0.210	0.770	0.011	0.002	0.023	0.031	0.080	0.000	0.007	0.030	0.030	0.001	0.003

Bundle No	Yield	Tensile	Eln.2in	Certification	CE: 0.36
M200605415	051780 Psi	066400 Psi	33.8 %	ASTM A500-07 GRADE B&C	

Material Note:
Sales Or.Note:

Material: 16.000x625x40'5"0(2x1). Material No: R16000625 Made in: Canada
Sales order: 467828 Purchase Order: A1959 ! after jun1

Heat No	C	Mn	P	S	Si	Al	Cu	Cb	Mo	Ni	Cr	V	Ti
286777	0.210	0.770	0.011	0.002	0.023	0.031	0.080	0.000	0.007	0.030	0.030	0.001	0.003

Bundle No	Yield	Tensile	Eln.2in	Certification	CE: 0.36
M200605414	051780 Psi	066400 Psi	33.8 %	ASTM A500-07 GRADE B&C	

Material Note:
Sales Or.Note:

Material: 16.000x625x30'0"0(2x1). Material No: R16000625 Made in: Canada
Sales order: 467828 Purchase Order: A1959 ! after jun1

Heat No	C	Mn	P	S	Si	Al	Cu	Cb	Mo	Ni	Cr	V	Ti
286777	0.210	0.770	0.011	0.002	0.023	0.031	0.080	0.000	0.007	0.030	0.030	0.001	0.003

Bundle No	Yield	Tensile	Eln.2in	Certification	CE: 0.36
M200605411	051780 Psi	066400 Psi	33.8 %	ASTM A500-07 GRADE B&C	

Material Note:
Sales Or.Note:

Certs Received by

Authorized by Quality Assurance:
The results reported on this report represent the actual attributes of the material furnished and indicate full compliance with all applicable specification and contract requirements.
Chemical analysis by the AWS D1.1 method.

Steel Tube Institute OF NORTH AMERICA

Page : 1 Of 2

Metals Service Center Institute

Figure A 19 Phase 2 Test 3 ASTM A500 Gr. B HSS16x0.625 Material Certifications (2)

TENSION TEST OF MATERIALS

(In accordance with ASTM A370-10)

Test Designation:	AKDOT-Phase 2-Test 3-Capital
Specimen Identification:	1
Date:	6/9/2011
Material Grade:	A572 Gr. 50/A709 Gr. 50
Gage length (in.):	2.020
Total length (in.):	12.0
Length between shoulders (in.):	2.5
Thickness (in.):	0.216
Width (in.):	0.499

Test Setup:		
Procedure:	Tensile Test	
Range 1	Rate:	0.025 in./min
	End Level:	Sample Yield
Range 2	Rate:	0.2 in./min
	End Level:	Sample Break

Test Data:	
.1% Offset Yield:	42100 psi
.2% Offset Yield:	**48500 psi**
.5 in/in Yield:	52400 psi
Ulimate Strength:	79600 psi
Modulus of elasticity:	35.2 x1000ksi
% Elongation:	27%

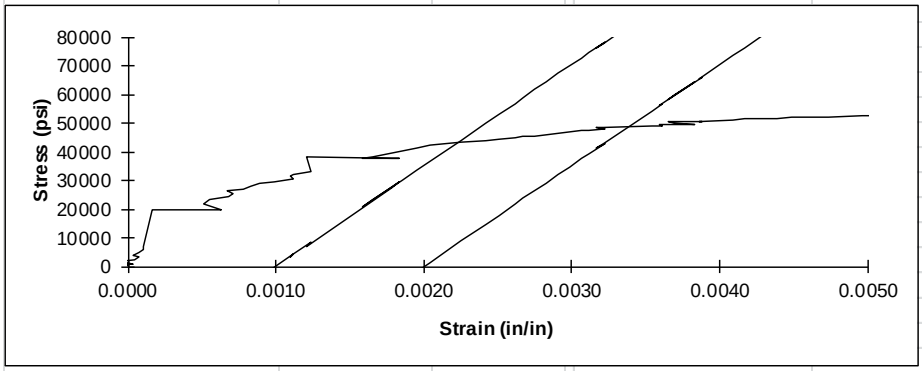

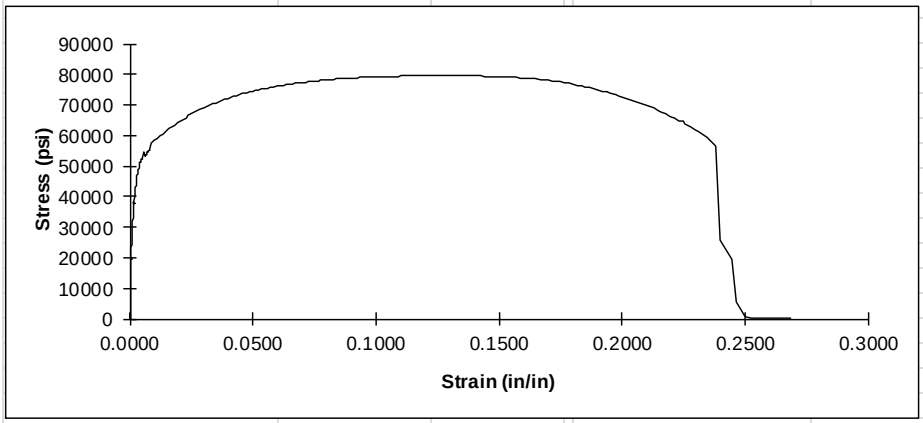

Figure A 20 Phase 2 Test 3 Modified Capital ASTM A572 Gr. 50 Plate Tension Test (1)

TENSION TEST OF MATERIALS

(In accordance with ASTM A370-10)

Test Designation:	AKDOT-Phase 2-Test 3-Capital
Specimen Identification:	2
Date:	6/9/2011
Material Grade:	A572 Gr. 50/A709 Gr. 50
Gage length (in.):	1.981
Total length (in.):	12.0
Length between shoulders (in.):	2.5
Thickness (in.):	0.269
Width (in.):	0.486

Test Setup:		
Procedure:	Tensile Test	
Range 1	Rate:	0.025 in./min
	End Level:	Sample Yield
Range 2	Rate:	0.2 in./min
	End Level:	Sample Break

Test Data:	
.1% Offset Yield:	54100 psi
.2% Offset Yield:	**53700 psi**
.5 in/in Yield:	53200 psi
Ulimate Strength:	79700 psi
Modulus of elasticity:	27.0 x1000ksi
% Elongation:	26%

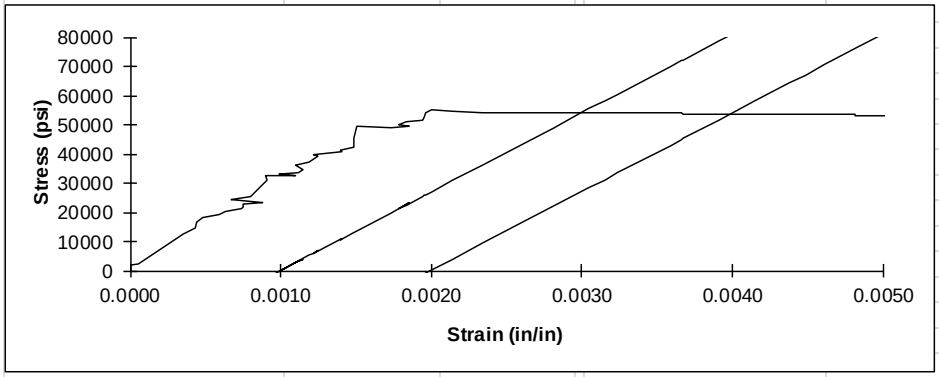

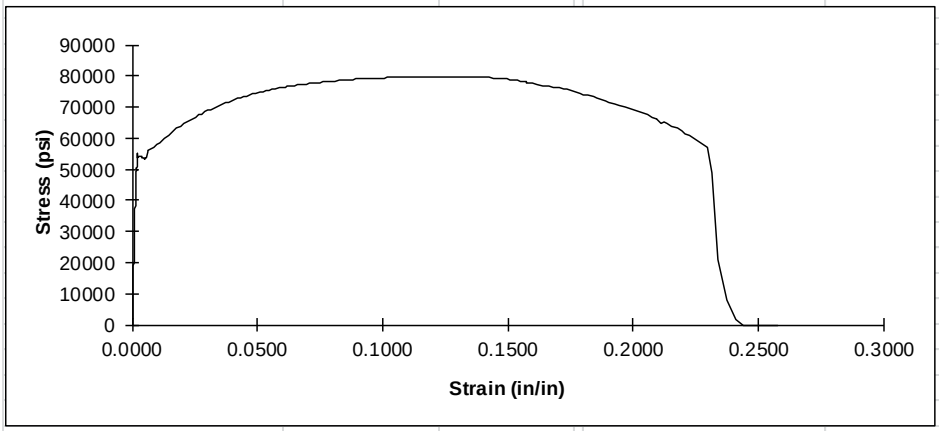

Figure A 21 Phase 2 Test 3 Modified Capital ASTM A572 Gr. 50 Plate Tension Test (2)

TENSION TEST OF MATERIALS

(In accordance with ASTM A370-10)

Test Designation:	AKDOT-Phase 2-Test 3-Capital
Specimen Identification:	3
Date:	6/9/2011
Material Grade:	A572 Gr. 50/A709 Gr. 50
Gage length (in.):	-2.002
Total length (in.):	12.0
Length between shoulders (in.):	2.5
Thickness (in.):	0.196
Width (in.):	0.499

Test Setup:		
Procedure:	Tensile Test	
Range 1	Rate:	0.025 in./min
	End Level:	Sample Yield
Range 2	Rate:	0.2 in./min
	End Level:	Sample Break

Test Data:	
.1% Offset Yield:	53300 psi
.2% Offset Yield:	**53500 psi**
.5 in/in Yield:	53300 psi
Ulimate Strength:	78600 psi
Modulus of elasticity:	36.1 x1000ksi
% Elongation:	27%

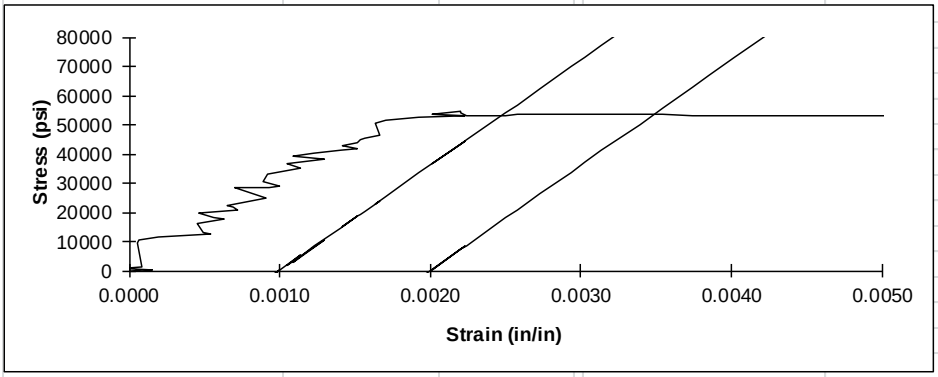

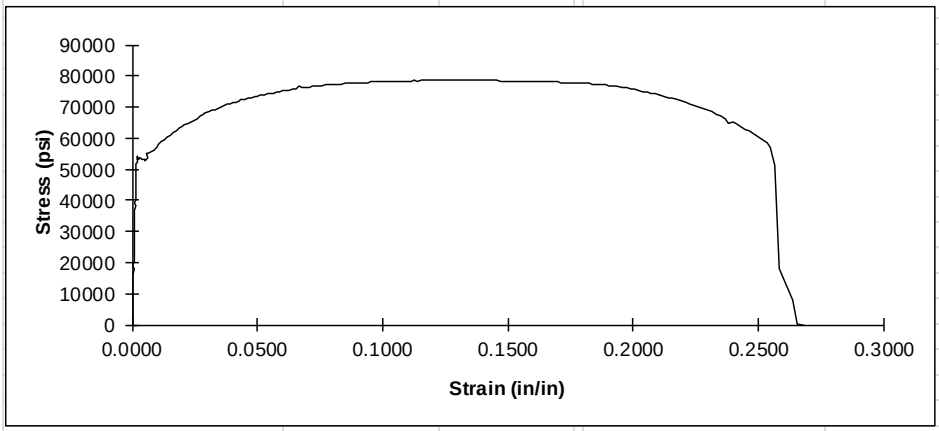

Figure A 22 Phase 2 Test 3 Modified Capital ASTM A572 Gr. 50 Plate Tension Test (3)

TENSION TEST OF MATERIALS

(In accordance with ASTM A370-10)

Test Designation:	AKDOT-Phase 2-Test 3-Capital
Specimen Identification:	4
Date:	6/9/2011
Material Grade:	A572 Gr. 50/A709 Gr. 50
Gage length (in.):	1.020
Total length (in.):	12.0
Length between shoulders (in.):	1.5
Thickness (in.):	0.260
Width (in.):	0.269

Test Setup:		
Procedure:	Tensile Test	
Range 1	Rate:	0.025 in./min
	End Level:	Sample Yield
Range 2	Rate:	0.2 in./min
	End Level:	Sample Break

Test Data:	
.1% Offset Yield:	53200 psi
.2% Offset Yield:	**52900 psi**
.5 in/in Yield:	54200 psi
Ulimate Strength:	79900 psi
Modulus of elasticity:	30.6 x1000ksi
% Elongation:	35%

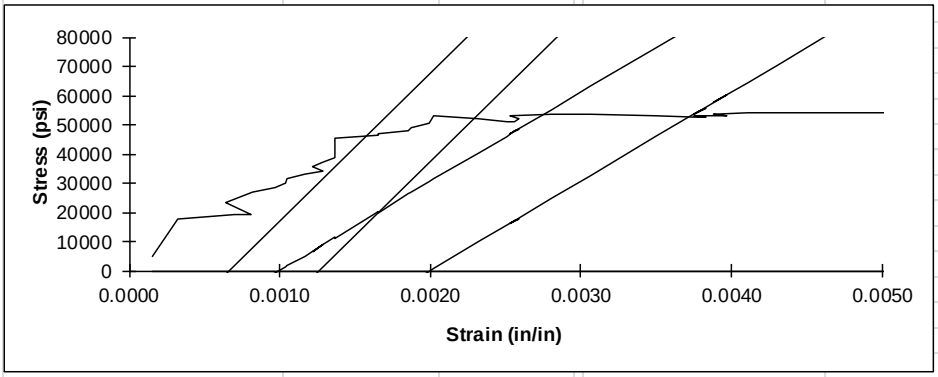

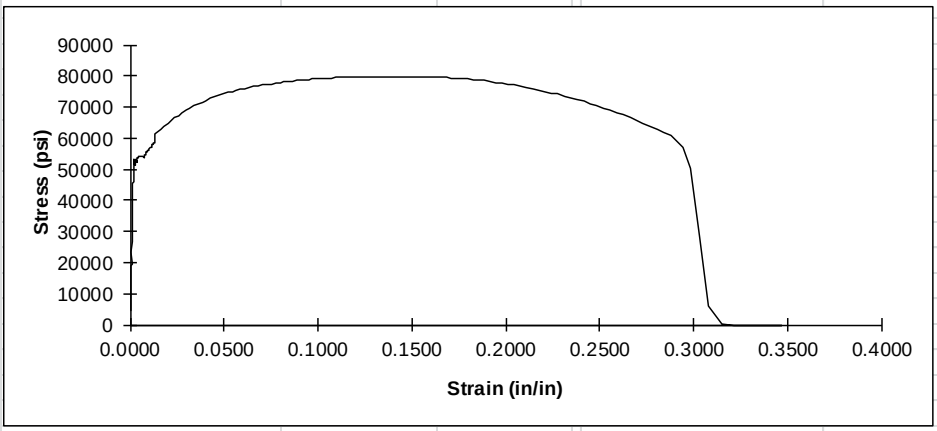

Figure A 23 Phase 2 Test 3 Modified Capital ASTM A572 Gr. 50 Plate Tension Test (4)

TENSION TEST OF MATERIALS

(In accordance with ASTM A370-10)

Test Designation:	AKDOT-Test 3-Capital Rolled
Specimen Identification:	1
Date:	11/9/2011
Material Grade:	A572 Gr. 50/A709 Gr. 50
Gage length (in.):	-2.037
Total length (in.):	12.0
Length between shoulders (in.):	2.5
Thickness (in.):	0.597
Width (in.):	1.530

Test Setup:		
Procedure:	Tensile Test	
Range 1	Rate:	0.025 in./min
	End Level:	Sample Yield
Range 2	Rate:	0.25 in./min
	End Level:	Sample Break

Test Data:	
.1% Offset Yield:	62400 psi
.2% Offset Yield:	**65000 psi**
.5 in/in Yield:	66500 psi
Ulimate Strength:	87300 psi
Modulus of elasticity:	36.9 x1000ksi
% Elongation:	37%

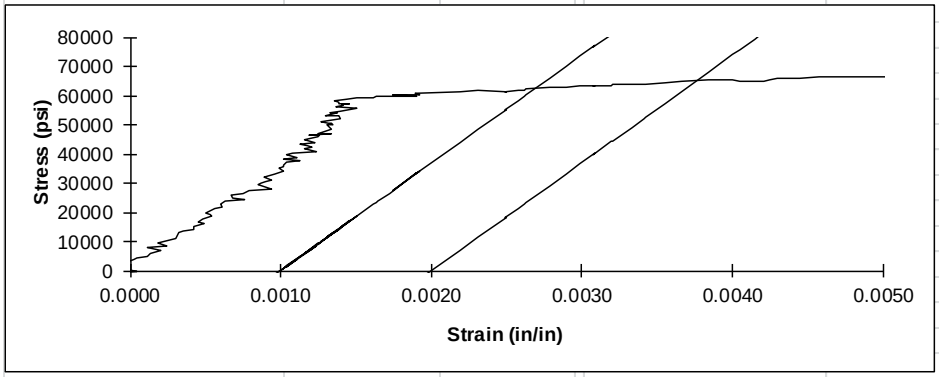

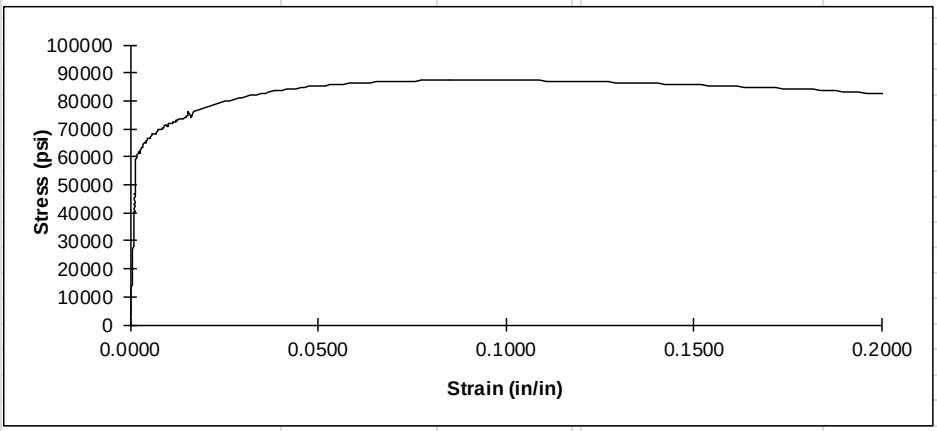

Figure A 24 Phase 2 Test 3 Modified Capital Tension Test After Rolling (1)

TENSION TEST OF MATERIALS

(In accordance with ASTM A370-10)

Test Designation:	AKDOT-Test 3-Capital Rolled
Specimen Identification:	2
Date:	11/9/2011
Material Grade:	A572 Gr. 50/A709 Gr. 50
Gage length (in.):	2.018
Total length (in.):	12.0
Length between shoulders (in.):	2.5
Thickness (in.):	0.589
Width (in.):	1.500

Test Setup:		
Procedure:	Tensile Test	
Range 1	Rate:	0.025 in./min
	End Level:	Sample Yield
Range 2	Rate:	0.25 in./min
	End Level:	Sample Break

Test Data:	
.1% Offset Yield:	61400 psi
.2% Offset Yield:	**62900 psi**
.5 in/in Yield:	64900 psi
Ulimate Strength:	86600 psi
Modulus of elasticity:	35.3 x1000ksi
% Elongation:	36%

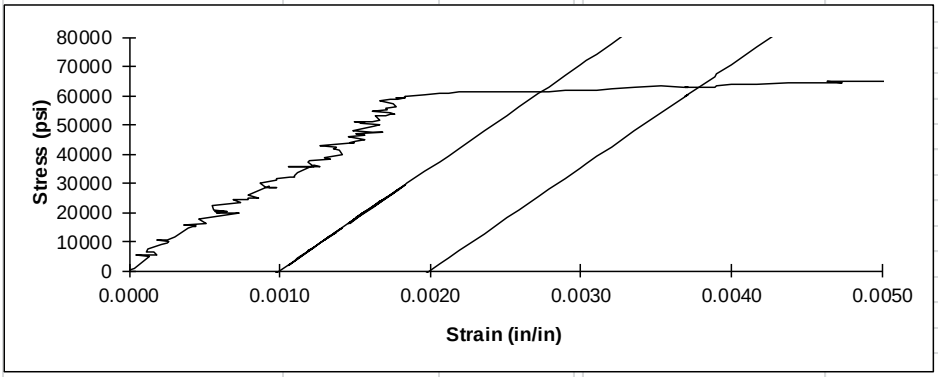

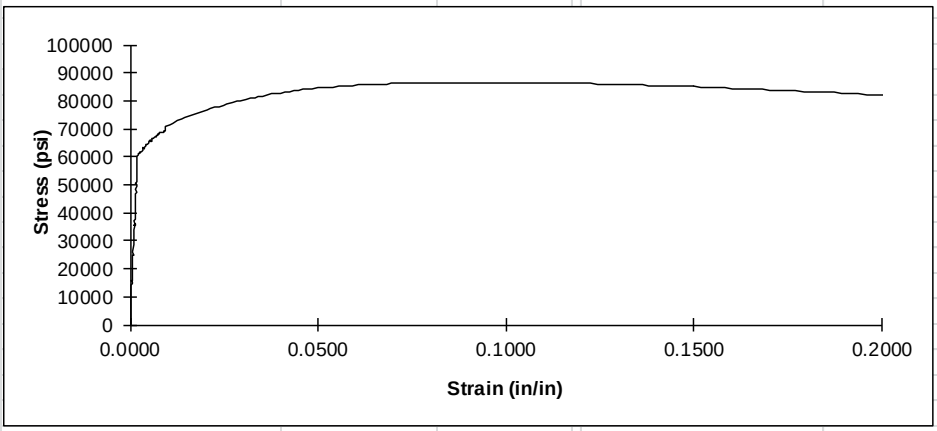

Figure A 25 Phase 2 Test 3 Modified Capital Tension Test After Rolling (2)

TENSION TEST OF MATERIALS

(In accordance with ASTM A370-10)

Test Designation:	AKDOT-Test 3-Capital Rolled
Specimen Identification:	3
Date:	11/9/2011
Material Grade:	A572 Gr. 50/A709 Gr. 50
Gage length (in.):	-2.019
Total length (in.):	12.0
Length between shoulders (in.):	2.5
Thickness (in.):	0.576
Width (in.):	1.504

Test Setup:		
Procedure:	Tensile Test	
Range 1	Rate:	0.025 in./min
	End Level:	Sample Yield
Range 2	Rate:	0.25 in./min
	End Level:	Sample Break

Test Data:	
.1% Offset Yield:	62800 psi
.2% Offset Yield:	**65700 psi**
.5 in/in Yield:	68200 psi
Ulimate Strength:	88000 psi
Modulus of elasticity:	39.7 x1000ksi
% Elongation:	44%

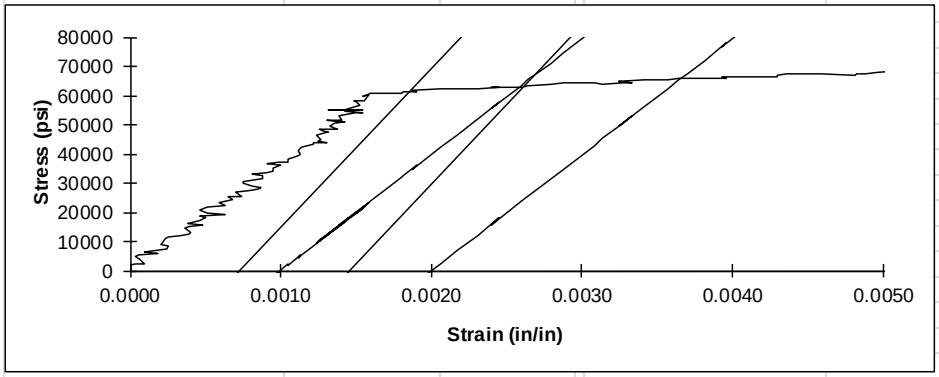

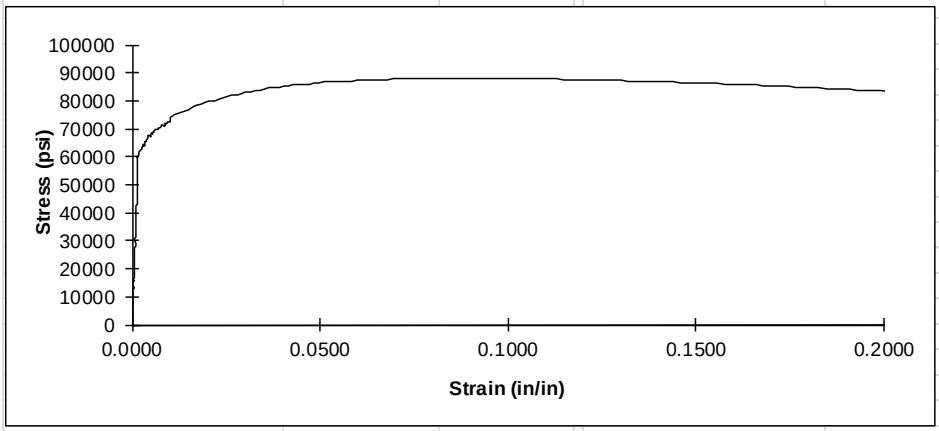

Figure A 26 Phase 2 Test 3 Modified Capital Tension Test After Rolling (3)

TENSION TEST OF MATERIALS

(In accordance with ASTM A370-10)

Test Designation:	AKDOT-Test 3-Capital Rolled
Specimen Identification:	4
Date:	11/9/2011
Material Grade:	A572 Gr. 50/A709 Gr. 50
Gage length (in.):	2.170
Total length (in.):	12.0
Length between shoulders (in.):	2.5
Thickness (in.):	0.576
Width (in.):	1.532

Test Setup:		
Procedure:	Tensile Test	
Range 1	Rate:	0.025 in./min
	End Level:	Sample Yield
Range 2	Rate:	0.25 in./min
	End Level:	Sample Break

Test Data:	
.1% Offset Yield:	65500 psi
.2% Offset Yield:	**67900 psi**
.5 in/in Yield:	69700 psi
Ulimate Strength:	89300 psi
Modulus of elasticity:	31.6 x1000ksi
% Elongation:	28%

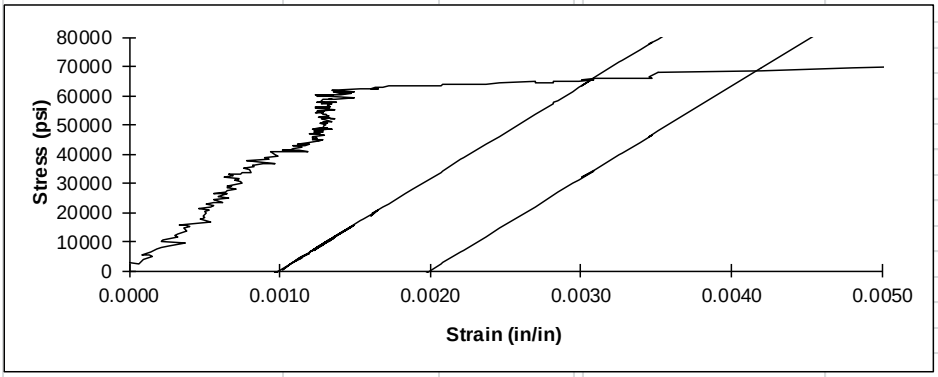

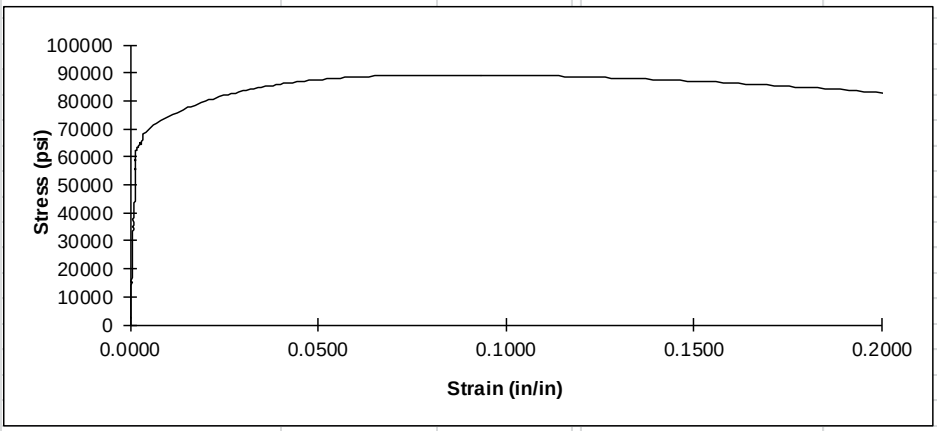

Figure A 27 Phase 2 Test 3 Modified Capital Tension Test After Rolling (4)

NUCOR
PLATE MILL

P.O.Box 279
Winton, NC 27986
(252) 356-3700

Mill Test Report

Page 1

NUCOR It's our Nature.

Issuing Date : 11/16/2010 B/L No. : 277618 Load No. : 279242 Our Order No. : 86918/4 Cust. Order No. : 2242099 OP

Vehicle No: 7406

Specification : 1.2500" x 96.000" x 240.000"
ASTM A572 Grade 50-07/ASTM A709 Grade 50-09a/AASHTO M270-50
Type 2

Sold To : ONEAL STEEL INC
P O BOX 98
BIRMINGHAM,AL 35201

Ship To : ONEAL STEEL INC GREENSBORO
(DOORS 7 & 8)
105 EAST FLORIDA STREET
G2 DOORS 7 & 8
GREENSBORO,NC 27405

Marking : 809803

Heat No	C	Mn	P	S	Si	Cu	Ni	Cr	Mo	Al(tot)	V	Nb	Ti	N	Ca	B	Sn	CEQ	PCM
0507913	0.17	1.22	0.017	0.002	0.20	0.25	0.08	0.12	0.02	0.012	0.042	0.002	0.002		0.0006	0.0002	0.011	0.43	0.26

Tensile Test

Plate Serial No	Pieces	Tons	Dir.	(psi) Yield	(psi) Tensile	Elongation % in 2"	Elongation % in 8"
0507913-04	5	20.41	T	56,600	82,400		22.2
			T	55,500	81,800		21.8

Charpy Impacts

Dir.	1	(%) shear	2	(%) shear	3	(%) shear	Ave.	(%) shear	Size	Temp	Min Ave.

RECEIVED
GREENSBORO
NOV 17 2010
BY

Manufactured to fully killed practice by Electric Arc Furnace. Welding or weld repair was not performed on this material. Mercury has not been used in the direct manufacturing of this material. Produced as continuous cast discrete plate as-rolled, unless otherwise noted in Specification.
Yield by 0.5EUL method unless otherwise specified. Ceq = C+(Mn/6)+((Cr+Mo+V)/5)+((Cu+Ni)/15)
Pcm = C+(Si/30)+(Mn/20)+(Cu/20)+(Ni/60)+(Cr/20)+(Mo/15)+(V/10)+5B
Melted and manufactured in the USA. ISO 9001:2008 certified (#008063) by SRI Quality System Registrar (#0995-09). PED 97/23/EC 7/2 Annex 1, Para. 4.3 Compliant. DIN 50049 3.1.B/EN 10204 3.1B(2004), DIN EN 10204 3.1(2005) compliant. For ABS grades only, Quality Assurance certificate 09-MMPQA-546

We hereby certify that the contents of this report are accurate and correct. All test results and operations performed by the material manufacturer are in compliance with the applicable specifications, including customer specifications.

T. A. Deprelis, Metallurgist

11/16/2010 12:36:37 PM

Figure A 28 Phase 2 Test 3 Modified Capital ASTM A572 Gr. 50 Material Certifications

Bill To:
STEELFAB INC
ACTS PAYABLE
PO BOX 19289
CHARLOTTE NC
28219 US

Ship To: 1
STEELFAB, INC.
8623 OLD DOWD ROAD
CHARLOTTE NC
28214 US

Order Date:03/02/2011
PO No:25580ABM-3
Mill Order No:3863890
Load No:1361917
Manifest No:2058535

CERTIFIED MATERIAL TEST REPORT
GERDAU AMERISTEEL
Petersburg Mill
GERDAU AMERISTEEL 25801 Hofheimer Way
Petersburg, VA 23803
(804)524-2855

SPECIFICATIONS	SIZE	GRADE	LENGTH	PRODUCT
ASTM A6-09, A572-07	HP 14 X 117# / HP 360 X 174	A572-50	35 FT / 10.668 M	H-PILE BEAMS

HEAT NO: 30509710

CHEMICAL ANALYSIS

C	Mn	P	S	Si	Cu	Ni	Cr	Mo	Sn	V	Al	Nb
.08	1.08	.010	.028	.26	.30	.10	.11	.017	.011	.002	.003	.017

PHYSICAL PROPERTIES

Yield Strength KSI	Yield Strength MPa	Tensile Strength KSI	Tensile Strength MPa	Specimen Area Sq In	Specimen Area Sq cm	Elongation %	Gage Length		Bend Test Dia. Result	ROA %
53.4	368.2	70.5	486.1	1.230	7.94	28.3	8 In	200 mm		
53.7	370.2	71.1	490.2	1.251	8.07	29.9	8 In	200 mm		

Remarks

Meets ASTM A709 & AASHTO M270 Grade 50 non-tension component requirements

CERTS RECEIVED BY
SV

All manufacturing processes of this product, including electric arc MELTING and continuous CASTING, occurred in the U.S.A.
CMTR complies with EN 10204 3.1

"I hereby certify that the contents of this report are correct and accurate. All tests and operations performed by this material manufacturer or its sub-contractors, when applicable, are in compliance with the requirements of the material specifications and applicable purchaser designated requirements."

Signed: Date: Mar. 05, 2011
Tom L. Harrington: Quality Assurance Manager

Signed: Date:
Notary Public (if applicable)

Page: 1 of 1

Figure A 29 Phase 2 Test 2, 3 ASTM A572 Gr. 50 HP14x117 Material Certifications

Atlas ABC Corp (Atlas Tube Chicago)
1855 East 122nd Street
Chicago, Illinois, USA
60633
Tel: 773-646-4500
Fax: 773-646-6128

Atlas Tube JMC STEEL GROUP

Ref.B/L: 80427975
Date: 05.17.2011
Customer: 547

MATERIAL TEST REPORT

Sold to
Saginaw Pipe Co., Inc.
PO Box 8
SAGINAW AL 35137
USA

Shipped to
Saginaw Pipe Co., Inc.
Highway 31 South
SAGINAW AL 35137
USA

Material: 16.000x500x40'0"0(1x1).A2523 **Material No:** R160005004000-A252 **Made in:** USA **Melted in:** USA

Sales order: 632540 **Purchase Order:** 40109 RO

Heat No	C	Mn	P	S	Si	Al	Cu	Cb	Mo	Ni	Cr	V	Ti	B	N
M24724	0.210	0.760	0.011	0.010	0.012	0.062	0.030	0.005	0.004	0.010	0.030	0.001	0.001	0.000	0.000

Bundle No	PCs	Yield	Tensile	Eln.2in	Certification	CE: 0.35
M900404899	1	069070 Psi	083110 Psi	37 %	ASTM A252-10 GR 3	

Material Note:
Sales Or.Note: Meets ASTM A500-10A Grade B&C

Material: 16.000x500x40'0"0(1x1).A2523 **Material No:** R160005004000-A252 **Made in:** USA **Melted in:** USA

Sales order: 632540 **Purchase Order:** 40109 RO

Heat No	C	Mn	P	S	Si	Al	Cu	Cb	Mo	Ni	Cr	V	Ti	B	N
M24724	0.210	0.760	0.011	0.010	0.012	0.062	0.030	0.005	0.004	0.010	0.030	0.001	0.001	0.000	0.000

Bundle No	PCs	Yield	Tensile	Eln.2in	Certification	CE: 0.35
M900404811	1	069070 Psi	083110 Psi	37 %	ASTM A252-10 GR 3	

Material Note:
Sales Or.Note: Meets ASTM A500-10A Grade B&C

Material: 16.000x500x40'0"0(1x1).A2523 **Material No:** R160005004000-A252 **Made in:** USA **Melted in:** USA

Sales order: 632540 **Purchase Order:** 40109 RO

Heat No	C	Mn	P	S	Si	Al	Cu	Cb	Mo	Ni	Cr	V	Ti	B	N
E22705	0.200	0.820	0.017	0.008	0.031	0.055	0.030	0.005	0.003	0.010	0.040	0.001	0.001	0.000	0.000

Bundle No	PCs	Yield	Tensile	Eln.2in	Certification	CE: 0.35
M900404853	1	055720 Psi	074800 Psi	40 %	ASTM A252-10 GR 3	

Material Note:
Sales Or.Note: Meets ASTM A500-10A Grade B&C

Certs Received by
TDC

Authorized by Quality Assurance:
The results reported on this report represent the actual attributes of the material furnished and indicate full compliance with all applicable specification and contract requirements.
D1.1 method.

Steel Tube Institute OF NORTH AMERICA

Page : 2 Of 5

Metals Service Center Institute

Figure A 30 Phase 2 Test 4 ASTM A500 Gr. B HSS 16x0.500 Material Certifications

COUPON TENSILE TEST ANALYSIS

In accordance with ASTM A370-10

Test Designation:	AKDOT-Phase2	
Specimen Identification:	5-1	
Date:	7/16/2012	
Material Grade:		
Gage length:	2.004	in
Total length:	12	in
Length between shoulders:	2.5	in
Thickness:	0.491	in
Width:	1.518	in

Test Setup:			
Procedure:	Tensile Test		
Range 1	Rate:	0.025	in/min
	End Level:	Sample Yield	
Range 2	Rate:	0.3	in/min
	End Level:	Sample Break	

Test Data:		
yield stress:	55400	psi
0.1% offset yield:	67100	psi
0.2% offset yield:	71500	psi
Ulimate strength:	79000	psi
Modulus of elasticity:	28.88	e6 psi
% elongation:	40.02%	

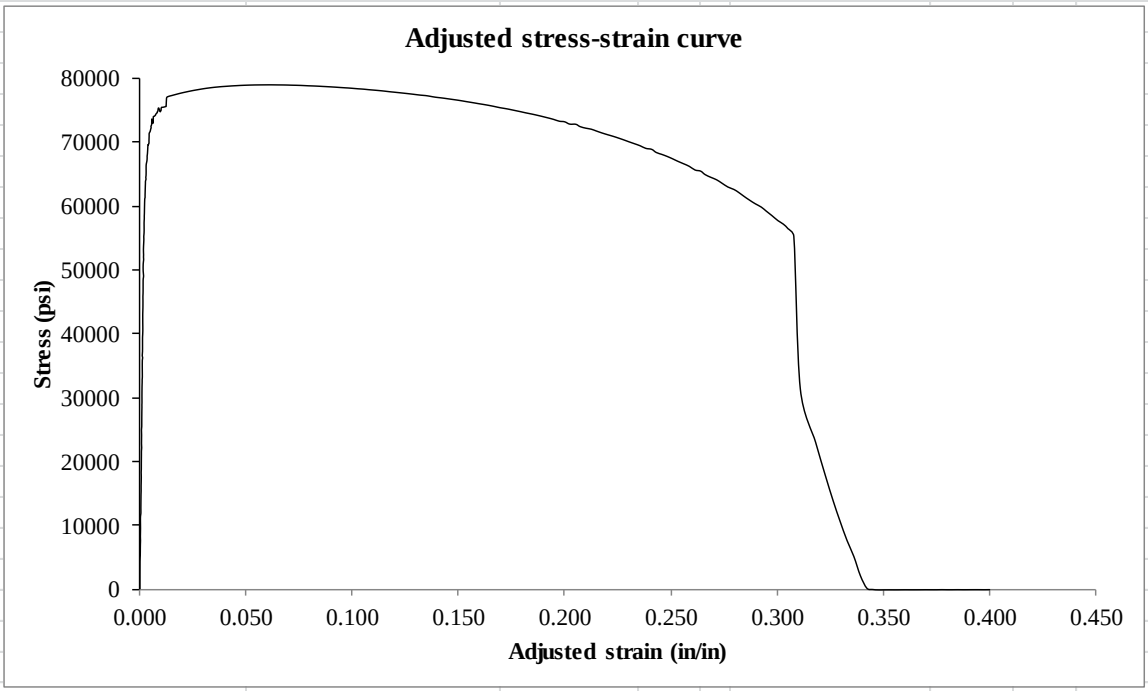

Figure A 31 Phase 2 Test 5 ASTM A500 Gr. B HSS16x0.500 Tensile Test (1)

COUPON TENSILE TEST ANALYSIS

In accordance with ASTM A370-10

Test Designation:	AKDOT-Phase2	
Specimen Identification:	5-2	
Date:	7/16/2012	
Material Grade:		
Gage length:	1.902	in
Total length:	12	in
Length between shoulders:	2.5	in
Thickness:	0.494	in
Width:	1.517	in

Test Setup:			
Procedure:	Tensile Test		
Range 1	Rate:	0.025	in/min
	End Level:	Sample Yield	
Range 2	Rate:	0.3	in/min
	End Level:	Sample Break	

Test Data:		
yield stress:	49400	psi
0.1% offset yield:	62600	psi
0.2% offset yield:	66700	psi
Ulimate strength:	78800	psi
Modulus of elasticity:	38.03	e6 psi
% elongation:	39.82%	

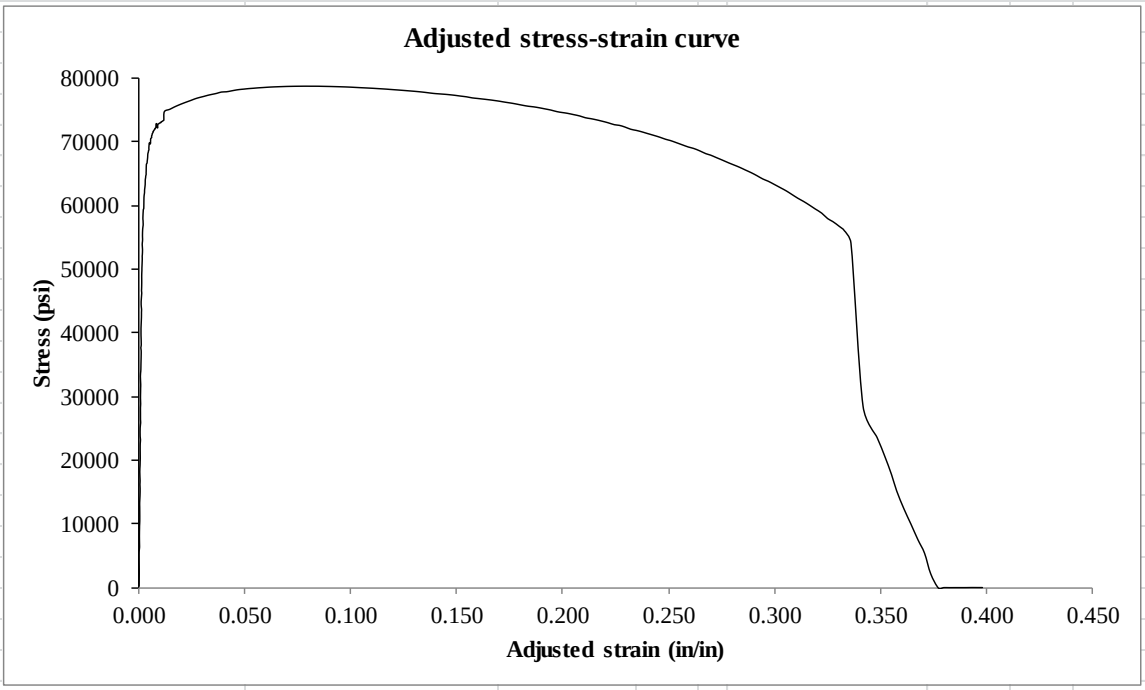

Figure A 32 Phase 2 Test 5 ASTM A500 Gr. B HSS16x0.500 Tensile Test (2)

Atlas ABC Corp (Atlas Tube Chicago)
1855 East 122nd Street
Chicago, Illinois, USA
60633
Tel: 773-646-4500
Fax: 773-646-6128

Atlas TUBE

Ref.B/L: 80380574
Date: 04.20.2010
Customer: 1806

MATERIAL TEST REPORT

Sold to
Infra-Metals Corporation
1900 Bessmer Road
PETERSBURG VA 23805
USA

Shipped to
STEEL FAB OF VA, INC.
1510 REESE STREET
EMPORIA VA 23847
USA

Material: 16.000x500x30'0"0(1x1).A2523 Material No: R16000500 Made in: USA
Melted in: USA
Sales order: 545215 Purchase Order: A3488 Cust Material #: TAG # 25450ABM-4

Heat No	C	Mn	P	S	Si	Al	Cu	Cb	Mo	Ni	Cr	V	Ti	B	N
C52325	0.210	0.880	0.012	0.005	0.030	0.033	0.080	0.000	0.020	0.050	0.050	0.005	0.001	0.000	0.000

Bundle No	Yield	Tensile	Ein.2in	Certification	CE: 0.39
MS00319469	068810 Psi	085570 Psi	37 %	ASTM A252-98 GR 3	

Material Note:
Sales Or.Note:

Material: 16.000x500x50'0"0(1x1).CTMIL Material No: R16000500 Made in: USA
Melted in: USA
Sales order: 545215 Purchase Order: A3488 Cust Material #: TAG # 25450ABM-4

Heat No	C	Mn	P	S	Si	Al	Cu	Cb	Mo	Ni	Cr	V	Ti	B	N
C52399	0.210	0.830	0.008	0.005	0.030	0.031	0.070	0.000	0.010	0.030	0.030	0.001	0.001	0.000	0.000

Bundle No	Yield	Tensile	Ein.2in	Certification	CE: 0.37
0002312564	067490 Psi	080490 Psi	37 %	ASTM A500-07 GRADE B&C	

Material Note:
Sales Or.Note:

Material: 16.000x500x50'0"0(1x1).CTMIL Material No: R16000500 Made in: USA
Melted in: USA
Sales order: 545215 Purchase Order: A3488 Cust Material #: TAG # 25450ABM-4

Heat No	C	Mn	P	S	Si	Al	Cu	Cb	Mo	Ni	Cr	V	Ti	B	N
C52399	0.210	0.830	0.008	0.005	0.030	0.031	0.070	0.000	0.010	0.030	0.030	0.001	0.001	0.000	0.000

Bundle No	Yield	Tensile	Ein.2in	Certification	CE: 0.37
0002312572	067490 Psi	080490 Psi	37 %	ASTM A500-07 GRADE B&C	

Material Note:
Sales Or.Note:

CERTS RECEIVED BY

Authorized by Quality Assurance:
The results reported on this report represent the actual attributes of the material furnished and indicate full compliance with all applicable specification and contract requirements.
Certified calculated using the AWS D1.1 method.

Steel Tube Institute OF NORTH AMERICA

Page : 5 Of 5

Metals Service Center Institute

Certs Received by
TDC

Figure A 33 Phase 2 Test 5 ASTM A500 Gr. B HSS 16x0.500 Material Certifications

Bill To:
STEELFAB INC
ACTS PAYABLE
PO BOX 19289
CHARLOTTE NC
28219 US

Ship To: 1
STEELFAB, INC.
8623 OLD DOWD ROAD
CHARLOTTE NC
28214 US

Order Date:10/03/2011
PO No:25580ABM-9
Mill Order No:3937515
Load No:1402174
Manifest No:2096855

CERTIFIED MATERIAL TEST REPORT
GERDAU AMERISTEEL
Petersburg Mill
GERDAU AMERISTEEL 25801 Hofheimer Way
Petersburg, VA 23803
(804)524-2855

SPECIFICATIONS	SIZE	GRADE	LENGTH	PRODUCT
ASTM A6-09, A572-07	HP 14 X 117# / HP 360 X 174	A572-50	35 FT / 10.668 M	H-PILE BEAMS

HEAT NO: 30543410

CHEMICAL ANALYSIS

C	Mn	P	S	Si	Cu	Ni	Cr	Mo	Sn	V	Al	Nb
.08	1.06	.017	.029	.19	.28	.09	.15	.015	.012	.001	.000	.017

PHYSICAL PROPERTIES

Yield Strength KSI	Yield Strength MPa	Tensile Strength KSI	Tensile Strength MPa	Specimen Area Sq In	Specimen Area Sq cm	Elongation %	Gage Length		Bend Test Dia. Result	ROA %
53.6	369.6	72.2	497.8	1.247	8.05	26.8	8 In	200 mm		
53.8	370.9	70.4	485.4	1.216	7.85	27.6	8 In	200 mm		

Remarks

Meets ASTM A709 & AASHTO M270 Grade 50 non-tension component requirements

CERTS RECEIVED BY
SV

All manufacturing processes of this product, including electric arc MELTING and continuous CASTING, occurred in the U.S.A.
CMTR complies with EN 10204 3.1

"I hereby certify that the contents of this report are correct and accurate. All tests and operations performed by this material manufacturer or its sub-contractors, when applicable, are in compliance with the requirements of the material specifications and applicable purchaser designated requirements."

Signed: Date: Oct. 08, 2011
Tom L. Harrington: Quality Assurance Manager

Signed: Date:
Notary Public (if applicable)

Page: 1 of 1

Figure A 34 Phase 2 Test 5 ASTM A572 Gr. 50 HP14x117 Material Certifications (1)

Bill To:
STEELFAB INC
ACTS PAYABLE
PO BOX 19289
CHARLOTTE NC
28219 US

Ship To: 1
STEELFAB, INC.
8623 OLD DOWD ROAD
CHARLOTTE NC
28214 US

Order Date:10/03/2011
PO No:25580ABM-9
Mill Order No:3937515
Load No:1402174
Manifest No:2096855

CERTIFIED MATERIAL TEST REPORT
GERDAU AMERISTEEL
Petersburg Mill
GERDAU AMERISTEEL 25801 Hofheimer Way
Petersburg, VA 23803
(804)524-2855

SPECIFICATIONS	SIZE	GRADE	LENGTH	PRODUCT
ASTM A6-09, A572-07	HP 14 X 117# / HP 360 X 174	A572-50	35 FT / 10.668 M	H-PILE BEAMS

HEAT NO: 30543410

CHEMICAL ANALYSIS

C	Mn	P	S	Si	Cu	Ni	Cr	Mo	Sn	V	Al	Nb
.08	1.06	.017	.029	.19	.28	.09	.15	.015	.012	.001	.000	.017

PHYSICAL PROPERTIES

Yield Strength KSI	Yield Strength MPa	Tensile Strength KSI	Tensile Strength MPa	Specimen Area Sq In	Specimen Area Sq cm	Elongation %	Gage Length		Bend Test Dia. Result	ROA %
53.6	369.6	72.2	497.8	1.247	8.05	26.8	8 In	200 mm		
53.8	370.9	70.4	485.4	1.216	7.85	27.6	8 In	200 mm		

Remarks

Meets ASTM A709 & AASHTO M270 Grade 50 non-tension component requirements

CERTS RECEIVED BY

All manufacturing processes of this product, including electric arc MELTING and continuous CASTING, occurred in the U.S.A.
CMTR complies with EN 10204 3.1

"I hereby certify that the contents of this report are correct and accurate. All tests and operations performed by this material manufacturer or its sub-contractors, when applicable, are in compliance with the requirements of the material specifications and applicable purchaser designated requirements."

Signed: Date: Oct. 08, 2011
Tom L. Harrington: Quality Assurance Manager

Signed: _____ Date: _____
Notary Public (if applicable)

Page: 1 of 1

Figure A 35 Phase 2 Test 5 ASTM A572 Gr. 50 HP14x117 Material Certifications (2)

COUPON TENSILE TEST ANALYSIS

In accordance with ASTM A370-10

Test Designation:	AKDOT-Phase2	
Specimen Identification:	6-1	
Date:	7/16/2012	
Material Grade:		
Gage length:	2.013	in
Total length:	12	in
Length between shoulders:	2.5	in
Thickness:	0.489	in
Width:	1.512	in

Test Setup:			
Procedure:	Tensile Test		
Range 1	Rate:	0.025	in/min
	End Level:	Sample Yield	
Range 2	Rate:	0.3	in/min
	End Level:	Sample Break	

Test Data:		
yield stress:	57000	psi
0.1% offset yield:	66900	psi
0.2% offset yield:	71200	psi
Ulimate strength:	79500	psi
Modulus of elasticity:	27.15	e6 psi
% elongation:	35.58%	

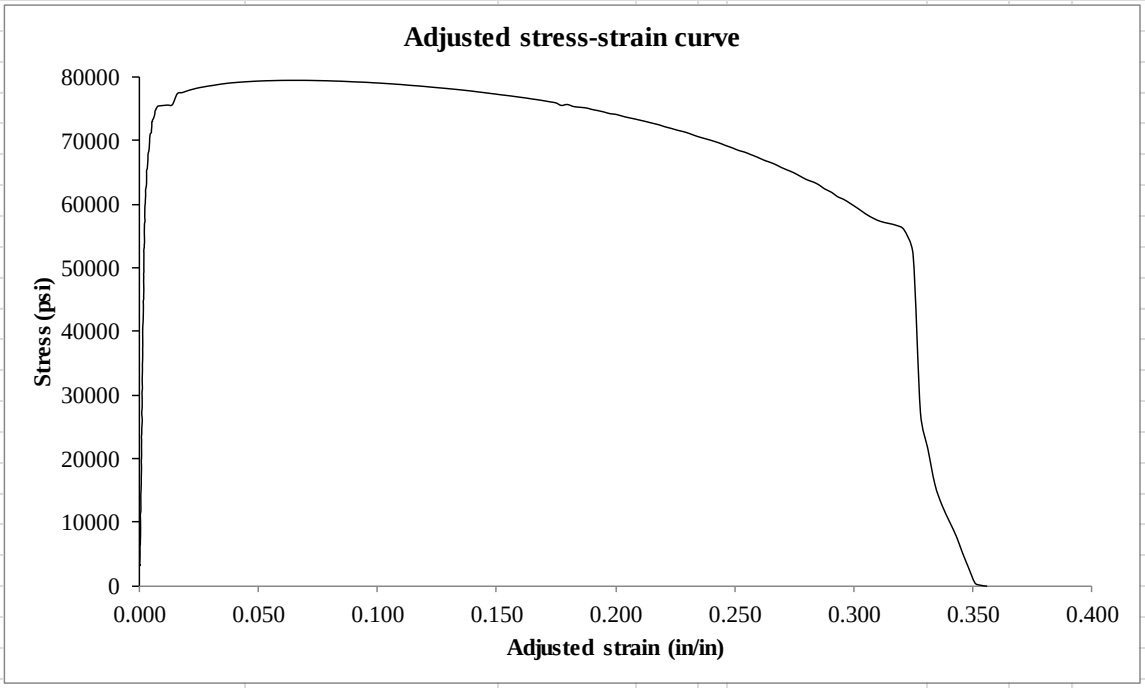

Figure A 36 Phase 2 Test 6 ASTM A500 Gr. B HSS16x0.500 Tensile Test (1)

COUPON TENSILE TEST ANALYSIS

In accordance with ASTM A370-10

Test Designation:	AKDOT-Phase2	
Specimen Identification:	6-3	
Date:	7/16/2012	
Material Grade:		
Gage length:	2.017	in
Total length:	12	in
Length between shoulders:	2.5	in
Thickness:	0.487	in
Width:	1.015	in

Test Setup:			
Procedure:	Tensile Test		
Range 1	Rate:	0.025	in/min
	End Level:	Sample Yield	
Range 2	Rate:	0.3	in/min
	End Level:	Sample Break	

Test Data:		
yield stress:	47200	psi
0.1% offset yield:	63400	psi
0.2% offset yield:	68600	psi
Ulimate strength:	77900	psi
Modulus of elasticity:	29.53	e6 psi
% elongation:	37.38%	

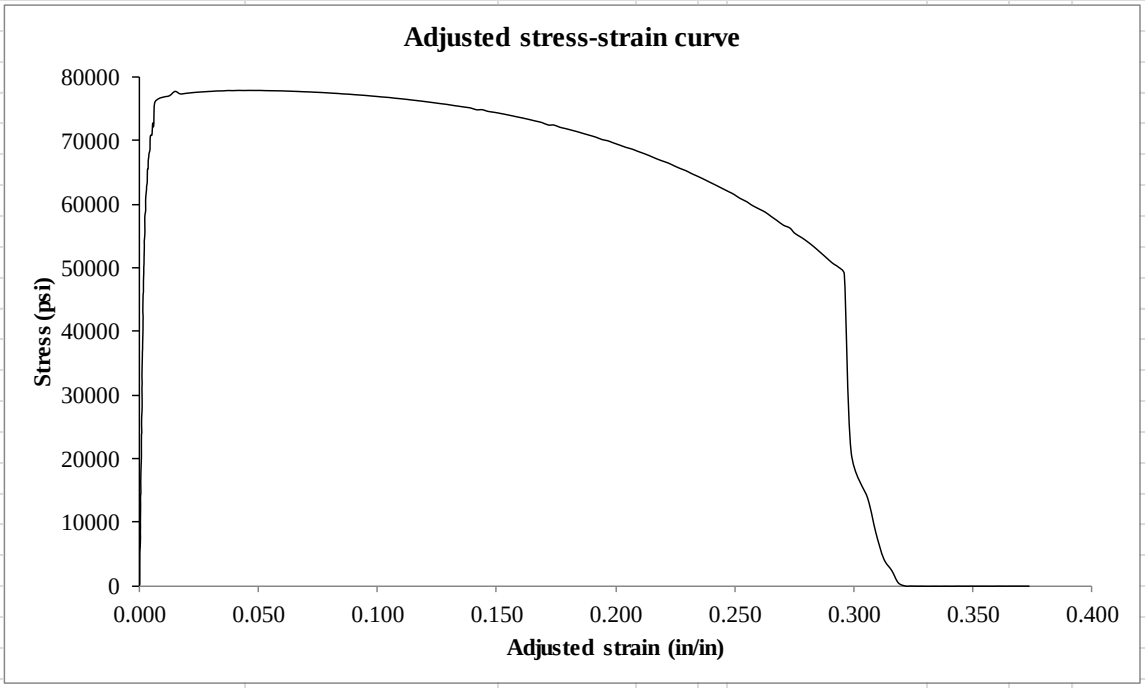

Figure A 37 Phase 2 Test 6 ASTM A500 Gr. B HSS16x0.500 Tensile Test (3)

Material Test Report

Page 3 of 4

Melted and Manufactured in the United States

C	Mn	P	S	Si	Al	Cu	Cb	Mo	Ni	Cr	V	Ti
0.200	0.770	0.012	0.008	0.010	0.051	0.050	0.004	0.004	0.020	0.060	0.000	0.001

Material	Material #	Sales Order	PO Number	Customer Material #
8.0x8.0x500x28'0"0(2x2).	000000000080080500	544675	A3488	TAG JOB # 25450ABM-4

Bundle #	Heat #	Yield	Tensile	Ein.2in	Certification	Made In	CE
M900325695	16778C	71930	83630	32	ASTM A500-07 GRADE B&C	USA	0.36

Melted and Manufactured in the United States

C	Mn	P	S	Si	Al	Cu	Cb	Mo	Ni	Cr	V	Ti
0.210	0.790	0.006	0.006	0.010	0.056	0.060	0.005	0.007	0.020	0.050	0.000	0.001

Material	Material #	Sales Order	PO Number	Customer Material #
8.0x8.0x500x28'0"0(3x2).	000000000080080500	544675	A3488	TAG JOB # 25450ABM-4

Bundle #	Heat #	Yield	Tensile	Ein.2in	Certification	Made In	CE
M900325696	16778C	71930	83630	32	ASTM A500-07 GRADE B&C	USA	0.36

Melted and Manufactured in the United States

C	Mn	P	S	Si	Al	Cu	Cb	Mo	Ni	Cr	V	Ti
0.210	0.790	0.006	0.006	0.010	0.056	0.060	0.005	0.007	0.020	0.050	0.000	0.001

Material	Material #	Sales Order	PO Number	Customer Material #
16.000x500x30'0"0(1x1).A2523	R16000500	545215	A3488	TAG # 25450ABM-4

Bundle #	Heat #	Yield	Tensile	Ein.2in	Certification	Made In	CE
M900319469	C62325	66810	85570	37	ASTM A252-98 GR 3	USA	0.39

Melted and Manufactured in the United States

C	Mn	P	S	Si	Al	Cu	Cb	Mo	Ni	Cr	V	Ti
0.210	0.880	0.012	0.005	0.030	0.033	0.080	0.000	0.020	0.050	0.050	0.005	0.001

Material	Material #	Sales Order	PO Number	Customer Material #
16.000x500x50'0"0(1x1).CTMIL	R16000500	545215	A3488	TAG # 25450ABM-4

Bundle #	Heat #	Yield	Tensile	Ein.2in	Certification	Made In	CE
0002312554	C62399	67490	80490	37	ASTM A500-07 GRADE B&C	USA	0.37

Melted and Manufactured in the United States

C	Mn	P	S	Si	Al	Cu	Cb	Mo	Ni	Cr	V	Ti
0.210	0.830	0.008	0.005	0.030	0.031	0.070	0.000	0.010	0.030	0.030	0.001	0.001

Material	Material #	Sales Order	PO Number	Customer Material #
16.000x500x50'0"0(1x1).CTMIL	R16000500	545215	A3488	TAG # 25450ABM-4

Bundle #	Heat #	Yield	Tensile	Ein.2in	Certification	Made In	CE
0002312572	C62399	67490	80490	37	ASTM A500-07 GRADE B&C	USA	0.37

RECEIVED
APR 28 2010

Melted and Manufactured in the United States

STEELFAB OF VIRGINIA

http://customer.atlastube.com/Deliveries/MaterialTestReport.aspx?id=80380574 4/23/2010

CHECKED/RECEIVED BY
SV

Figure A 38 Phase 2 Test 6 ASTM A500 Gr. B HSS16x0.500 Material Certifications

COUPON TENSILE TEST ANALYSIS

In accordance with ASTM A370-10

Test Designation:	AKDOT-Phase2	
Specimen Identification:	S-6	
Date:	7/17/2012	
Material Grade:		
Gage length:	1.741	in
Total length:	12	in
Length between shoulders:	2.5	in
Thickness:	0.177	in
Width:	0.767	in

Test Setup:			
Procedure:	Tensile Test		
Range 1	Rate:		in/min
	End Level:	Sample Yield	
Range 2	Rate:		in/min
	End Level:	Sample Break	

Test Data:		
yield stress:	33300	psi
0.1% offset yield:	51600	psi
0.2% offset yield:	51800	psi
Ulimate strength:	68700	psi
Modulus of elasticity:	38.51	e6 psi
% elongation:	34.11%	

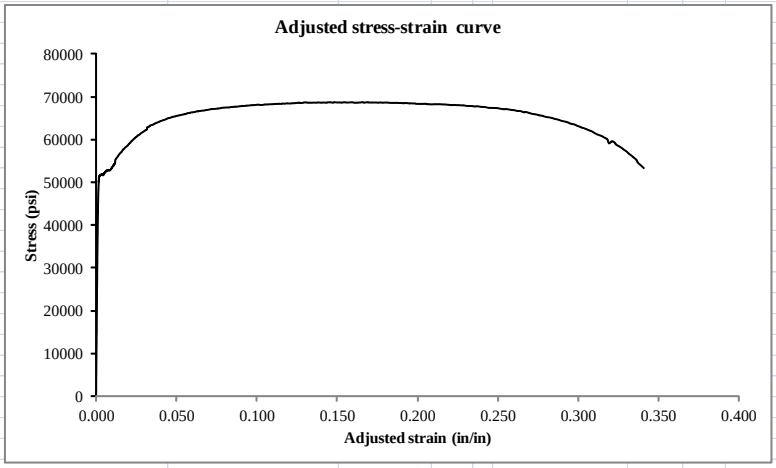

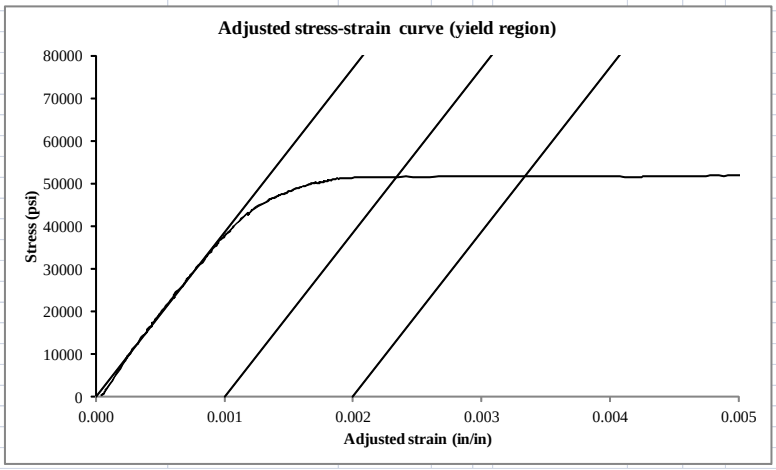

Figure A 39 Phase 2 Test 8, 9 ASTM A500 Gr. B HSS6x0.188 Tensile Test (1)

COUPON TENSILE TEST ANALYSIS

In accordance with ASTM A370-10

Test Designation:	AKDOT-Phase2	
Specimen Identification:	S-7	
Date:	7/17/2012	
Material Grade:		
Gage length:	1.734	in
Total length:	12	in
Length between shoulders:	2.5	in
Thickness:	0.175	in
Width:	0.763	in

Test Setup:			
Procedure:	Tensile Test		
Range 1	Rate:		in/min
	End Level:	Sample Yield	
Range 2	Rate:		in/min
	End Level:	Sample Break	

Test Data:		
yield stress:	24700	psi
0.1% offset yield:	46800	psi
0.2% offset yield:	50800	psi
Ulimate strength:	69700	psi
Modulus of elasticity:	33.80	e6 psi
% elongation:	34.82%	

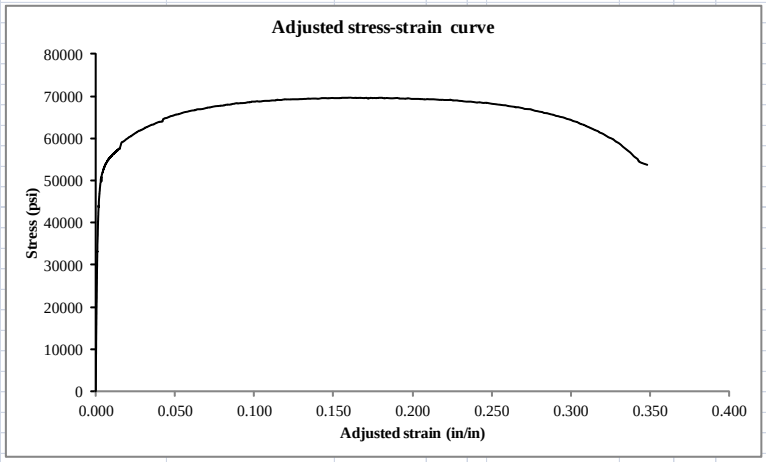

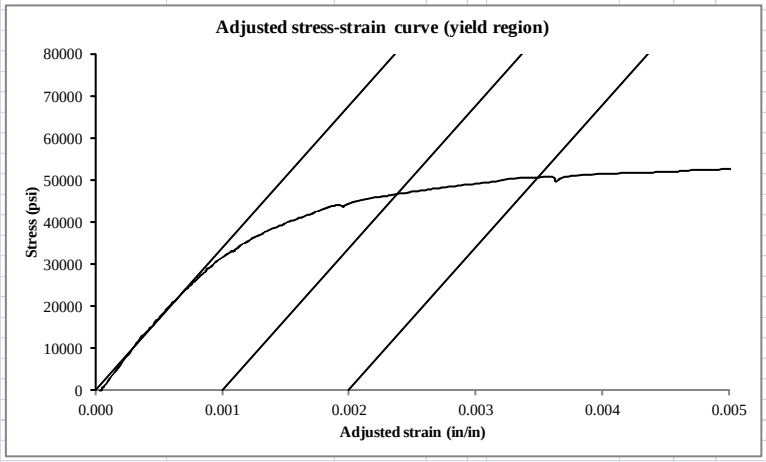

Figure A 40 Phase 2 Test 8, 9 ASTM A500 Gr. B HSS6x0.188 Tensile Test (2)

COUPON TENSILE TEST ANALYSIS

In accordance with ASTM A370-10

Test Designation:	AKDOT-Phase2	
Specimen Identification:	S-8	
Date:	7/17/2012	
Material Grade:		
Gage length:	1.735	in
Total length:	12	in
Length between shoulders:	2.5	in
Thickness:	0.177	in
Width:	0.763	in

Test Setup:			
Procedure:	Tensile Test		
Range 1	Rate:		in/min
	End Level:	Sample Yield	
Range 2	Rate:		in/min
	End Level:	Sample Break	

Test Data:		
yield stress:	25700	psi
0.1% offset yield:	46100	psi
0.2% offset yield:	49100	psi
Ulimate strength:	68700	psi
Modulus of elasticity:	35.87	e6 psi
% elongation:	36.22%	

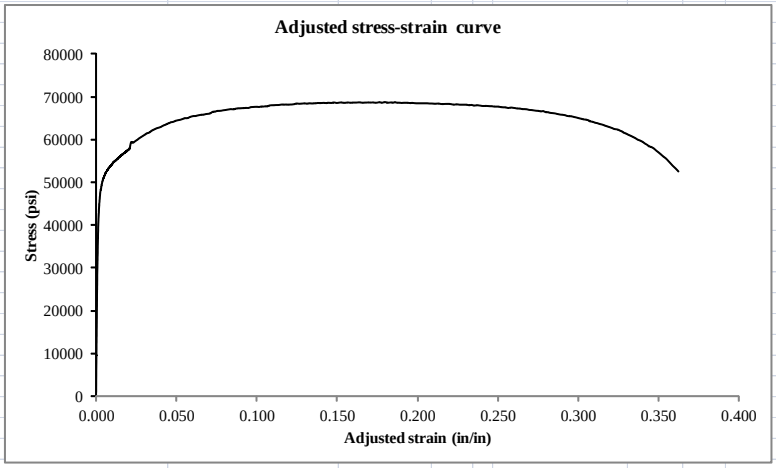

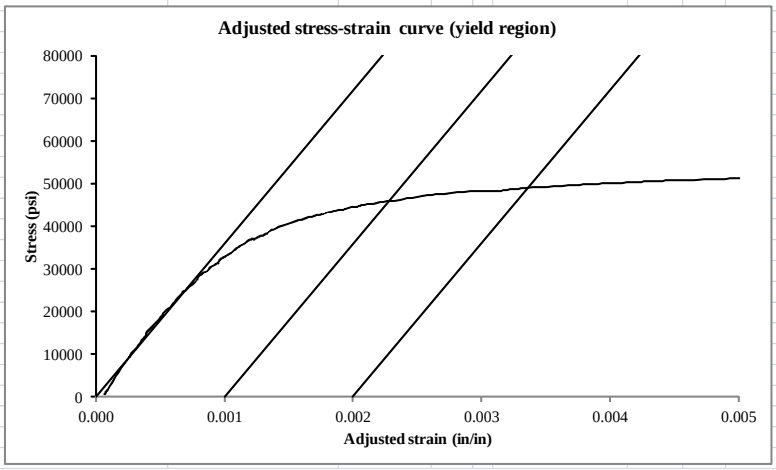

Figure A 41 Phase 2 Test 8, 9 ASTM A500 Gr. B HSS6x0.188 Tensile Test (3)

Independence Tube

6226 W. 74th St
Chicago, IL 60638
708-496-0380
Fax: 708-563-1950

independencetube.com
itctube.com
Certificate Number: CHI 822763

Sold By:
INDEPENDENCE TUBE CORPORATION
6226 W. 74th St.
Chicago, IL 60638
Tel: 708-496-0380
Fax: 708-563-1950

Sold To:
942 - INFRA-METALS
1900 BESSEMER ROAD
PETERSBURG, VA 23805

Purchase Order No: VA-42237
Sales Order No: CHI 195968 - 1
Bill of Lading No: CHI 113052 - 3
Invoice No:

Shipped: 10/6/2011
Invoiced:

Ship To:
1 - INFRA-METALS
1900 BESSEMER ROAD
800-435-0850
PETERSBURG, VA 23805

CERTIFICATE of ANALYSIS and TESTS
Customer Part No:

Certificate No: CHI 822763
Test Date: 10/5/2011

ROUND A500 GRADE B(C)
6.000"OD X .188" X 30'

Total Pieces	Total Weight
20	7,008

Heat Number: 132700

Bundle Tag	Yield, Tensile Strength, Elongation, Measurements	Y/T Ratio	Pieces	Weight
563637	YLD=59722/TEN=75213/ELG=31.57	0.7940	10	3,504
563638	YLD=59722/TEN=75213/ELG=31.57	0.7940	10	3,504

Heat Number
132700

*** Chemical Analysis ***
C=0.2000 Mn=0.8300 P=0.0100 S=0.0020 Si=0.0300 Al=0.0470 Cu=0.0200
Carbon Eq.=0.3383 Carbon Eq. = C + (Mn/6)

Certification:

I certify that the above results are a true and correct copy of records prepared and maintained by Independence Tube Corporation. Sworn this day, 10/5/2011

Annette Gorz, Test Report Clerk

WE PROUDLY MANUFACTURE ALL OF OUR HSS IN THE USA.
INDEPENDENCE TUBE PRODUCT IS MANUFACTURED, TESTED,
AND INSPECTED IN ACCORDANCE WITH ASTM STANDARDS.
****

CURRENT STANDARDS:
.....A500/A500M-10a
.....A513-07
.....A252-98 (2002)

Certs Received by
TDC

Page - 1

Figure A 42 Phase 2 Test 8, 9 ASTM A500 Gr. B HSS6x0.188 Material Certifications

Customer Name	Customer PO#	Shipper No	Heat Number
STEELFAB INC - CHARLOTTE	25580ABM-14	257409	803058

WELDED TUBE OF CANADA

101 RAYETTE ROAD
CONCORD, ONTARIO L4K 2S9
FAX: (905) 738-4070
TEL: (905) 669-1111
TOLL FREE: 1-800-565-TUBE (8823)

TEST REPORT
RAPPORT D'ESSAI

NUMBER/NUMERO : 693021

DATE (M/M D/J Y/A): 2/15/11

PAGE: 1

12237 DATHA METALS CO.
580 MIDDLETOWN BLVD.
LANGHORNE
PA 19047 USA

Customer P.O.	WTC BOL#	Ship Date	WTC Item# Description
VA-32053	373270	2/15/11	67349 ASTM A500-09 GR B & C,RNK,10.000-.250-250.000

CHEMICAL COMPOSITION

HEAT	TYPE	C	Mn	P	S	Si	Cu	Ni	Cr	Mo	Sn	V	Cb	Ti	N	B	Al	Ca	CE
835157	HEAT	.200	.740	.008	.003	.032	.050	.020	.010	.010	.002			.001	.003	.000	.050	.002	
757717	HEAT	.060	.570	.008	.009	.012	.050	.020	.029	.003	.003	.002	.034	.002	.007	.000	.042		.166
803058	HEAT	.060	.560	.010	.008	.014	.039	.014	.039	.004	.002	.002	.028	.002	.005	.000	.031		.163

CE = C + Mn/6 + (Si + Cu)/15 + (Cr + Mo + V)/5

TENSILE & HARDNESS PROPERTIES

HEAT	TYPE/SIZE	ORIENT	LOC	COND	YIELD (0.2% OFFSET) ksi	TENSILE ksi	ELONG % (2")
CRITERIA					MIN 46.0 MAX	MIN 62.0 MAX	MIN 23 MAX
835157	S-1.50"	L	B	AW	49.2	69.8	39
757717	S-1.50"	L	B	AW	64.3	76.7	34
803058	S-1.50"	L	B	AW	57.6	70.1	39

LEGEND S-STRIP L-LONGITUDINAL T-TRANSVERSE B-BODY W-WELD AW-AS WELDED N-NORMALIZED QT-QUENCHED AND TEMPERED SR-STRESS RELIEVED

Certs Received by
TDC

Figure A 43 Phase 2 Test 8, 9 ASTM A500 Gr. B HSS10x0.250 Material Certifications

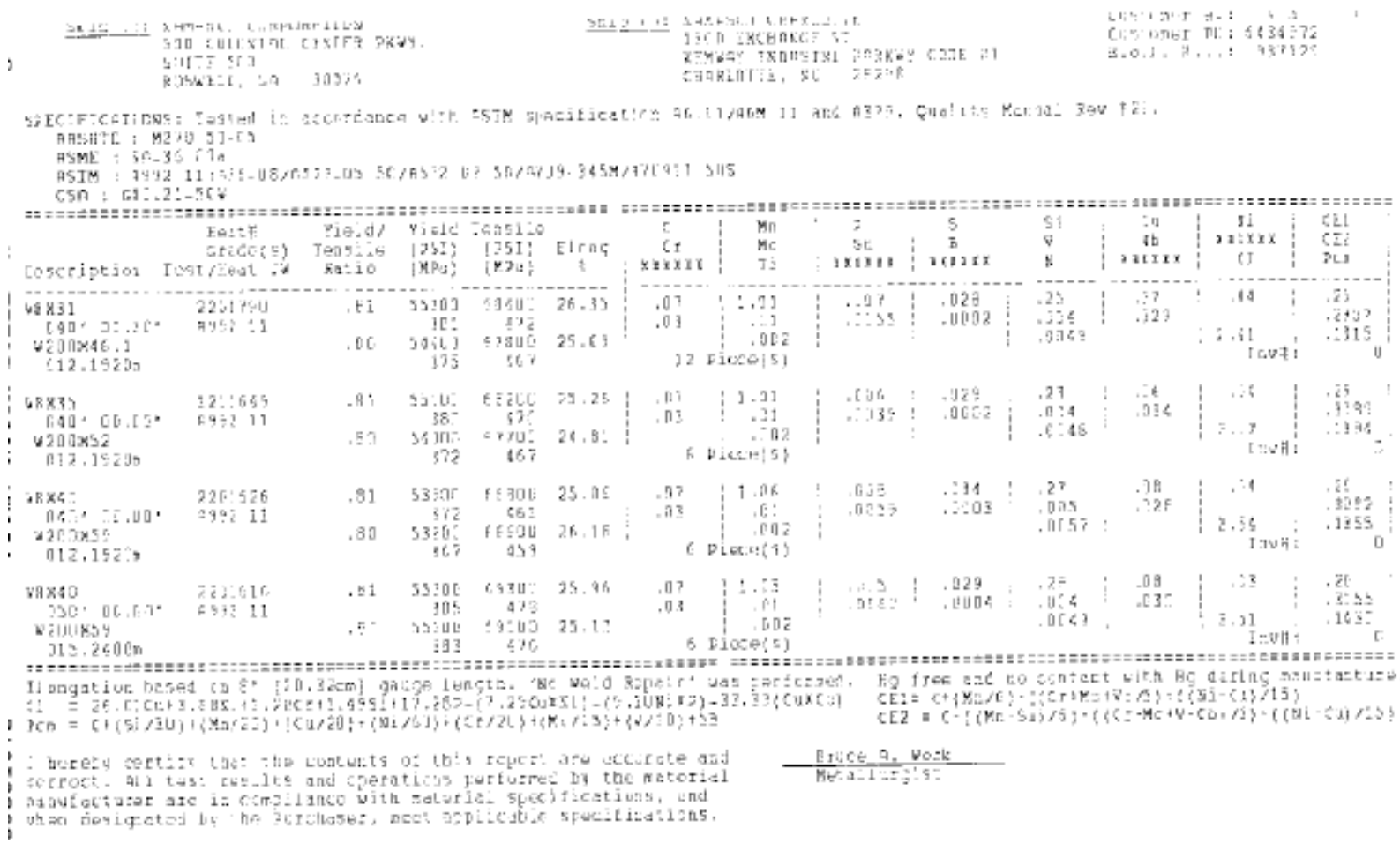

SPECIFICATIONS: Tested in accordance with ASTM specifications A6.11/A6M 11 and A370, Quality Manual Rev 121.
ASHTO : M270 50-05
ASME : SA-36 07a
ASTM : A992 11;A36-08/A572-05 50/A572 02 50/A709-345M/A709M 50S
CSA : G40.21-50W

Description	Test/Heat #	Field/ Tensile Ratio	Yield (PSI) (MPa)	Tensile (PSI) (MPa)	Elong %	C Cr	Mn Mo	P Ni	S B	Si V	Cu Nb	Al	CE1 CE2
W8X31	2201790	.81	55300	68400	26.30	.07	1.01	.007	.028	.25	.07	.44	.23
[40' 01.00']	A992 11		381	472		.03	.11	.0155	.0002	.034	.029		.2407
W200X46.1		.00	56100	67800	25.03		.002			.0049		2.41	.1315
[12.1920m]			393	467			12 Piece(s)					Inv#:	0
W8X35	2211665	.85	55100	68200	25.25	.01	1.01	.006	.029	.23	.04	.04	.25
[40' 00.00']	A992 11		387	470		.03	.31	.0139	.0002	.034	.034		.3190
W200X52		.80	56300	69700	24.81		.702			.0148		2.7	.1394
[12.1920m]			372	467			6 Piece(s)					Inv#:	0
W8X40	2201526	.81	53300	66300	25.05	.07	1.06	.035	.034	.27	.08	.04	.25
[40' 00.00']	A992 11		372	461		.03	.01	.0255	.0003	.035	.028		.3092
W200X59		.80	53600	66900	26.18		.002			.0057		2.56	.1355
[12.1920m]			369	459			6 Piece(s)					Inv#:	0
W8X40	2201610	.81	55300	69300	25.96	.07	1.05	.005	.029	.25	.08	.03	.20
[50' 00.00']	A992 11		385	478		.03	.01	.0162	.0004	.034	.030		.3255
W200X59		.87	55500	69500	25.12		.002			.0049		2.31	.1437
[15.2400m]			383	479			6 Piece(s)					Inv#:	0

Elongation based on 8" [20.32cm] gauge length. 'No Weld Repair' was performed. No free and no contact with Hg during manufacture.
CE1 = 26.0[C]+3.3[Mn]+1.2[Cu]+1.4[Ni]+17.2[P]-(7.2[Cu*Ni])-(5.1[Ni*P])-32.33[C*Cu] CE1= C+(Mn/6)+((Cr+Mo+V)/5)+((Ni+Cu)/15)
Pcm = C+(Si/30)+(Mn/20)+(Cu/20)+(Ni/60)+(Cr/20)+(Mo/15)+(V/10)+5B CE2 = C+[(Mn+Si)/6]+((Cr+Mo+V+Cu+Ni)/5)+((Ni+Cu)/15)

I hereby certify that the contents of this report are accurate and correct. All test results and operations performed by the material manufacturer are in compliance with material specifications, and when designated by the purchaser, meet applicable specifications.

Bruce A. Wood
Metallurgist

Figure A 44 Phase 2 Test 8, 9 ASTM A992 W8x40 Material Certifications

APPENDIX 2: Weld Inspection and Certification Documentation

Green's Welding

Welder Qualification Test Record

Page 1 of 1
Green, Justin

WQTR No. Green, Justin | Welder Name Justin Green | Welder Id

WPS No. Prequalified | Revision | Date 5/14/2008

Variables	Record Actual Values Used In Qualification	Qualification Range
Process (Table 4.10, Item (1))	FCAW	FCAW
Transfer Mode (GMAW): Short-Cir. ☐ Globular ☐ Spray ☐		Short-Circuiting ☐ Globular ☐ Spray ☐
Type Manual ☐ Machine ☐ Semi-Auto ☒ Auto ☐		Manual ☐ Machine ☐ Semi-Auto ☒ Auto ☐
Number of Electrodes Single ☒ Multiple ☐		Single ☒ Multiple ☐
Current/Polarity AC ☐ DCEP ☒ DCEN ☐ Pulsed ☐		AC ☐ DCEP ☒ DCEN ☐ Pulsed ☐
Position (Table 4.10, Item (4))	1G	Flat
Weld Progression: (Table 4.10, Item (6)) Up ☐ Down ☐		Up ☐ Down ☐
Backing [Table 4.10, Item (7)] Use Backing ☒		With Backing ☒ Without Backing ☒
Consumable Insert (GTAW) Use Insert ☐		With Insert ☐ Without Insert ☐
Material/Spec.	A-36 to A-36	Group 1 Material
Thickness (Plate): Groove (in)	1.0	0.125 - Unlimited in
Fillet ( )		Unlimited - Unlimited in
Thickness (Pipe/tube): Groove ( )		-
Fillet ( )		Unlimited - Unlimited in
Diameter(Pipe): Groove ( )		-
Fillet ( )		Unlimited - Unlimited in
Notes		
Filler Metal (Table 10, Item (2))		5/64" Tri-mark
Spec.	AWS A5.20	
Class.	E70T-4	
F-No.	6	
Gas/Flux Type (Table 4.10, Item (3))		
Other		

VISUAL INSPECTION (4.8.1) Acceptable Yes

GUIDED BEND TEST RESULTS (4.30.5)

Type	Result	Type	Result

Fillet Test Results (4.30.2.3 and 4.30.4.1)

Appearance | Fillet Size | Macroetch

Fracture Test Root Penetration | Description

Inspected By Leroy Spangler | Test No. 04-162 | Organization Triad NDT, Inc. | Date 4/7/2004

RADIOGRAPHIC TEST RESULTS (4.30.3.1)

Film Identification No.	Result	Remark
JG-1G	Satisfactory	

Interpreted By Leroy Spangler
Organization Triad NDT, Inc.
Test No. 04-162
Date 5/14/2008

We, the undersigned, certify that the statements in this record are correct and that the test welds were prepared, welded, and tested in accordance with the requirements of section 4 of ANSI/AWS D1.1, (2006) Structural Welding Code-Steel.

Manufacturer Green's Welding | Authorized By Justin Green | Date 5/14/2008

Figure A 45 Phase 1 Test 5 and 6 Welder Certification Report

Annex E/305

WELDER, WELDING OPERATOR OR TACK WELDER QUALIFICATION TEST RECORD

Type of Welder: WELDER
Name: Ralph Quick *Identification No.:* 244-88-2556
Welding Procedure Specification No.: CPB 1023 *Rev.:* *Date:* 6-27-08

Variables	Record Actual Values Used in Qualification	Qualification Range
Process/Type [Table 4.10, Item (2)]	fcaw	
Electrode (single or multiple) [Table 4.10, Item (9)	SINGLE	FCAW
Current/Polarity	DCEp	
Position [Table 4.10, Item (5)]	2G HORIZONTAL	FLAT HORIZONTAL
Weld Progression [Table 4.10, Item (7)]	N/A	
Backing (YES or NO) [Table 4.10, Item (8)]	YES	WITH BACKING ONLY
Material/Spec. [Table 4.10, Item (1)]	ASTM to A36	
Base Metal		
Thickness: (Plate)		1/8"
Groove	1" PLATE	UNLIMITED GROOVE & UNLIMITED FILLET
Fillet	N/A	
Thickness: (Pipe/tube)		
Groove	N/A	
Fillet	N/A	
Diameter: (Pipe)	N/A	
Groove	N/A	
Fillet	N/A	
Filler Metal [Table 4.10, Item (3)]		
Spec No. A	AWS A5.20	
Class E	AWS E70T-4	
F-No.		
Gas/Flux Type [Table 4.10, Item (4)]	NR-311	
Other		

VISUAL INSPECTION (4.8.1)
Acceptable YES or NO YES

Guided Bend Test Results (4.30.5)

Type	Result	Type	Result
2G1 SIDE	SATISFACTORY		
2G2 SIDE	SATISFACTORY		

Fillet Test Results (4.30.2.3 and 4.30.4.1)
Appearance _____ Fillet Size _____
Fracture Test Root Penetration _____ Macroetch _____
(Describe the location, nature, and size of any crack or tearing of the specimen.)

Inspected by JERRY CAGLE Test Number CPB 1023
Organization AWS Date 6-27-08

RADIOGRAPHIC TEST RESULTS (4.30.3.1)

Film Identification Number	Results	Remarks	Film Identification Number	Results	Remarks

Interpreted by _____ Test Number _____
Organization _____ Date _____

We, the undersigned, certify that the statements in this record are correct and that the test welds were prepared, welded, and tested in accordance with the requirements of section 4 of ANSI/AWS D1.1 (2006) Structural Welding Code-Steel
(year)

Manufacturer or Contractor ***C.P.BUCKNER STEEL*** ***Authorized by***
Form E-4 ***Date*** ***6-27-08***

AWS QC 1 JERRY W. CAGLE 97076011 CWI

Figure A 46 Phase 1 Test 5 Welder Certification Report

Annex E/305

WELDER, WELDING OPERATOR OR TACK WELDER QUALIFICATION TEST RECORD

Type of Welder: WELDER
Name: RALPH QUICK *Identification No.:* 244-88-2556
Welding Procedure Specification No.: CPB 1022 *Rev.:* *Date:* 6-7-08

Variables	Record Actual Values Used in Qualification	Qualification Range
Process/Type [Table 4.10, Item (2)]	SMAW	
Electrode (single or multiple) [Table 4.10, Item (9)	SINGLE	
Current/Polarity	DCEN	
Position [Table 4.10, Item (5)]	4G OVERHEAD 3G VERTICAL	FLAT HORIZONTAL VERTICAL OVERHEAD
Weld Progression [Table 4.10, Item (7)]		
Backing (YES or NO) [Table 4.10, Item (8)]	YES	
Material/Spec. [Table 4.10, Item (1)]	ASTM to A36	
Base Metal		
Thickness: (Plate)		UNLIMITED GROOVE & FILLET
Groove	1" PLATE	
Fillet	N/A	
Thickness: (Pipe/tube)		
Groove	N/A	
Fillet	N/A	
Diameter: (Pipe)	N/A	
Groove	N/A	
Fillet	N/A	
Filler Metal [Table 4.10, Item (3)]		
Spec No. A	AWS A5.1	
Class E	E-7018	
F-No.	F-4	
Gas/Flux Type [Table 4.10, Item (4)]	N/A	
Other		

VISUAL INSPECTION (4.8.1)
Acceptable YES or NO YES

Guided Bend Test Results (4.30.5)

Type	Result	Type	Result
3G1 SIDE	SATISFACTORY	4G1 SIDE	SATISFACTORY
3G2 SIDE	SATISFACTORY	4G2 SIDE	SATISFACTORY

Fillet Test Results (4.30.2.3 and 4.30.4.1)
Appearance _____ Fillet Size _____
Fracture Test Root Penetration _____ Macroetch _____
(Describe the location, nature, and size of any crack or tearing of the specimen.)

Inspected by JERRY CAGLE Test Number CPB 1022
Organization AWS D1.1 Date 6-7-08

RADIOGRAPHIC TEST RESULTS (4.30.3.1)

Film Identification Number	Results	Remarks	Film Identification Number	Results	Remarks

Interpreted by _____ Test Number _____
Organization _____ Date _____

We, the undersigned, certify that the statements in this record are correct and that the test welds were prepared, welded, and tested in accordance with the requirements of section 4 of ANSI/AWS D1.1 (2006) Structural Welding Code-Steel
(year)

Manufacturer or Contractor C.P.BUCKNER STEEL ***Authorized by***
Form E-4 ***Date*** 6-7-08

AWS QC1 JERRY W. CAGLE 97070011 CWI

Figure A 47 Phase 1 Test 5 Welder Certification Report

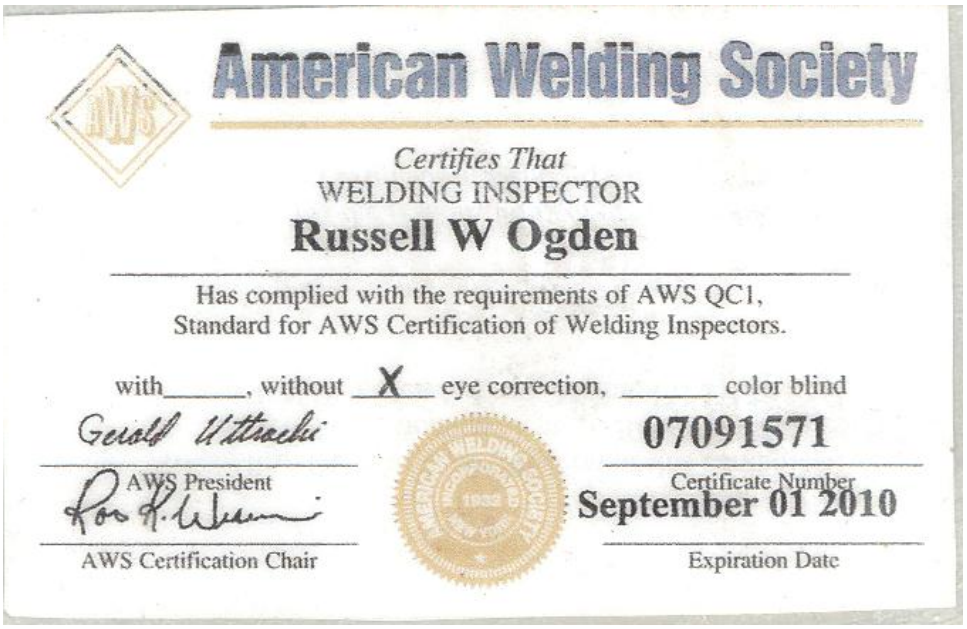

American Welding Society

Certifies That
WELDING INSPECTOR
Russell W Ogden

Has complied with the requirements of AWS QC1,
Standard for AWS Certification of Welding Inspectors.

with_____, without __X__ eye correction, _____ color blind

AWS President

AWS Certification Chair

07091571
Certificate Number

September 01 2010
Expiration Date

Figure A 48 Phase 1 Test 5 Weld Inspector Certification

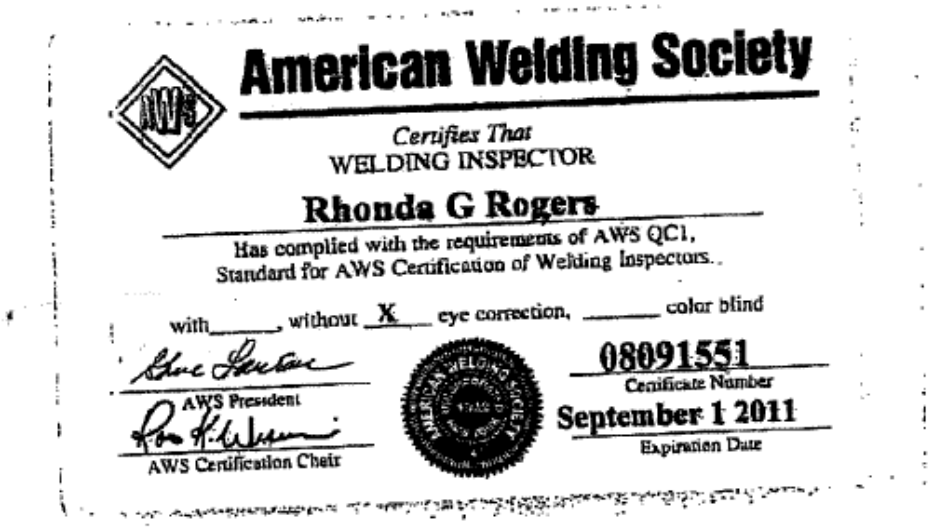

American Welding Society

Certifies That
WELDING INSPECTOR
Rhonda G Rogers

Has complied with the requirements of AWS QC1,
Standard for AWS Certification of Welding Inspectors.

with_____, without __X__ eye correction, _____ color blind

AWS President

AWS Certification Chair

08091551
Certificate Number

September 1 2011
Expiration Date

Figure A 49 Phase 1 Test 5 Weld Inspector Certification

ANNEX N

AWS D1.1/D1.1M:2006

WELDING PROCEDURE SPECIFICATION (WPS) Yes ☒
PREQUALIFIED ___X___ QUALIFIED BY TESTING _____
Or PROCEDURE QUALIFICATION RECORDS (PQR) Yes

Identification # CPB1015
Revision _____ Date _____ By _____
Authorized by Jerry Cagle Date 6-12-08
Type: Manual ☒ Semi-Automatic ☐
Machine ☐ Automatic ☐

Company Name Buckner Steel
Welding Process(es) SMAW
Supporting PQR No.(s) _____

JOINT DESIGN USED
Type: TC-U4A
Single ☐ Double Weld ☐
Backing: Yes ☒ No ☐
Backing Material: Steel A36 grade B
Root Opening 0.25 Root Face Dimension _____
Groove Angle: 45 Radius (J-U) _____
Backing Gouging: Yes ☐ No ☒ Method _____

BASE METALS
Material Spec. ASTM A53/ A572 Grade 50 for HP section
Type of Grade B
Thickness: Groove 1/2" Fillet _____
Diameter (Pipe) 16"

FILLER METALS
AWS Specification A 5.1
AWS Classification E7018

SHIELDING
Flux N/A Gas N/A
Composition _____
Electrode-Flux (Class) _____ Flow rate _____
Gas Cup Size _____

PREHEAT
Preheat temp., Min 70 (table 3.2 note A)
Interpass Temp., Min 70F Max 500F

POSITION
Position of groove Horizontal/Overhead Fillet Overhead
Vertical Position: Up ☐ Down ☐

ELECTRICAL CHARACTERISTICS
Transfer Mode (GMAW) Short-circuiting Globular spray
Current: AC ☐ DCEP ☒ DCEN ☐ Pulsed ☐
Other _____
Tungsten Electrode (GTAW)
Size _____
Type _____

TECHNIQUE
Stringer or Weave Bead: Stringer
Multi-pass or Single pass (per side) Multipass
Number of Electrodes: 1
Electrode Spacing Longitudinal N/A
Lateral N/A
Angle N/A

Contact Tube to Work Distance _____
Peening No
Interpass Cleaning: Wire brush, grinding or chipping

POSTWELD HEAT TREATMENT
Temp: N/A
Time: N/A

WELDING PROCEDURES

Pass or weld Layer(s)	Process	Filler Metals		Current		Volts	Travel Speed	Joint Details
		Class	Diam.	Type & Polarity	Amps or Wire Feed Speed			
12	SMAW	E7018	1/8"	DC+	100 – 130	20 – 24	5 to 7 in/min	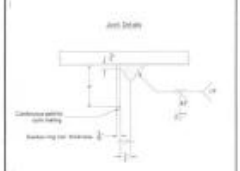

Form N-1 (Front)

Figure A 50 Phase 1 Test 5 WPS

S&ME
ENVIRONMENTAL SERVICES
ENGINEERING · TESTING

3201 Spring Forest Road
Raleigh, NC 27616
(919) 872-2660
(919) 876-3958

Field Report

Date 12-2-08	Job Number 1057-08-400
Project/Location NC State Constructed Facilities Lab	
Contractor	Weather/Temp Clear/50
Present at Site Russell Ogden	
Time 10	Mileage 30

To:

Services Performed

- ☐ Concrete Testing
- ☐ Cylinder Pickup
- ☐ Asphalt Testing
- Steel Testing
- ☐ Asphalt Coring
- ☐ Concrete Coring
- ☐ Undercut Evaluation
- ☐ Foundation Evaluation
- ☐ Proofrolling
- ☐ In-Place Density
- Other (Explain)

Observations/Remarks:

I. Examiner arrived on site and met with Steve and Kendra from NC state.
II. Examiner reviewed project specs and received copies of welding procedures and welder certification
For Justin Green of Green Welding Services.
III. Examiner has requested a copy of welder certification for Mr. Quick who is assisting Mr. Green.
IV. Examiner observed the beveling of the pipe connections to a 45 degree bevel.
V. Examiner observed the welding of the backing bar to the pipe. Weld was examined and was to spec.
VI. Examiner observed the root opening and fit up of the connection prior to welding.
VII. Examiner observed the preheating of the welded connection and the welding of the inner root pass
Of both pipe connection 1 and 2. Examiner noted no discrepancies in the root pass welds.
VIII. Rhonda Rodgers will return on 12-3-08 to continue the continuous examination of the welded
Connections.
IX. This examiner will return on 12-4-08 to continue examinations as needed.
No Further

On-Site Representative/Company

S&ME Personnel

Disclaimer: The presence of S&ME at the project site shall not be construed as an acceptance or approval of activities at the site. S&ME is at the project site to perform specific services and has certain responsibilities which are limited to those specifically authorized in our agreement with our client. In no event shall S&ME be responsible for the safety or the means and methods of other parties at the project site. **The information presented in this field report has not been reviewed by an engineer and is to be considered preliminary.**

PAGE ____ OF ____

Figure A 51 Phase 1 Test 5 QC Report

S&ME
ENVIRONMENTAL SERVICES
ENGINEERING · TESTING

3201 Spring Forest Road
Raleigh, NC 27616
(919) 872-2660
(919) 876-3958

Field Report

Date 12-03-08	Job No. 1057-08-400
Project/Location NC State Constructed Facilities Lab	
Contractor Buckner	Weather/Temp SUNNY 50F
Present at Site Rhonda Rogers	
Time	Mileage 30

To:
Steve, Kendra

Services Performed

- ☐ Concrete Testing
- ☐ Cylinder Pickup
- ☐ Asphalt Testing
- ■ Steel Testing
- ☐ Asphalt Coring
- ☐ Concrete Coring
- ☐ Undercut Evaluation
- ☐ Foundation Evaluation
- ☐ Proofrolling
- ☐ In-Place Density

Other (Explain)

Observations:

Subject: **Continuous Examination of CJP welded connections for bridge component testing.**

1) Examiner arrived on site. Met with Justin Green and Mr. Quick of Buckner Steel; Steve Fulmer and Kendra Cookson – NCSU.

2) Welder requested approval to use smaller diameter welding rod for outside root pass. Due to the specified 1/16" root opening, the 45 degree bevel, and the size of the 1/8" diameter rod, the shortest obtainable distance between the end of the rod and the base metal was excessive enough to cause long-arcing.

NOTE: Welder Certification for Mr. Quick has been faxed to SME Office Raleigh, NC.

3) Examiner observed preheating of welded components at each of the 2 connections.

4) Examiner observed back grinding of inner root pass at each of the 2 connections.

4) Examiner observed welding of inside diameter fillet welds at each of the 2 connections. Acceptable.

5) Kendra Cookson (NCSU) replied back that use of the smaller diameter welding rod for the outside root pass was acceptable.

6) Examiner observed welding and cleaning of the outside root pass at each of the 2 connections.

7) Examined outer root pass at each of the 2 connections.

8) Russ Ogden will return to continue examination 12-4-08.

END REPORT

Rhonda Rogers

Rhonda Rogers

On-Site Representative/Company **S&ME Personnel**

Disclaimer: The presence of S&ME at the project site shall not be construed as an acceptance or approval of activities at the site. S&ME is at the project site to perform specific services and has certain responsibilities which are limited to those specifically authorized in our agreement with our client. In no event shall S&ME be responsible for the safety or the means and methods of other parties at the project site. **The information presented in this field report has not been reviewed by an engineer and is to be considered preliminary.**

PAGE 1 OF 1

Figure A 52 Phase 1 Test 5 QC Report

S&ME
ENVIRONMENTAL SERVICES
ENGINEERING · TESTING

3201 Spring Forest Road
Raleigh, NC 27616
(919) 872-2660
(919) 876-3958

Field Report

Date 12-4-08	Job Number 1057-08-400
Project/Location NC State Constructed Facilities Lab	
Contractor	Weather/Temp Clear/50
Present at Site Russell Ogden	
Time 5	Mileage 30

To:

Services Performed

- ☐ Concrete Testing
- ☐ Cylinder Pickup
- ☐ Asphalt Testing
- Steel Testing
- ☐ Asphalt Coring
- ☐ Concrete Coring
- ☐ Undercut Evaluation
- ☐ Foundation Evaluation
- ☐ Proofrolling
- ☐ In-Place Density
- Other (Explain)

Observations/Remarks:

I. Examiner arrived on site to continue examination of welding

II. Examiner received copies of Mr. Quick's welding certifications

III. Examiner observed the completion of the full penetration Groove weld on the pipe to beam Connections.

IV. Examiner spoke with Perry Vezina of S&ME about conducting the UT examination. He is scheduled To conduct UT testing of the CJP welds on Monday morning.

V. Rhonda Rodgers will return on Monday to continue examination of multi pass fillet welds after UT Examination of the CJP welds has taken place.

VI. Examiner will return on Tuesday to continue examination.

No Further

On-Site Representative/Company **S&ME Personnel**

Disclaimer: The presence of S&ME at the project site shall not be construed as an acceptance or approval of activities at the site. S&ME is at the project site to perform specific services and has certain responsibilities which are limited to those specifically authorized in our agreement with our client. In no event shall S&ME be responsible for the safety or the means and methods of other parties at the project site. **The information presented in this field report has not been reviewed by an engineer and is to be considered preliminary.**

PAGE ____ OF ____

Figure A 53 Phase 1 Test 5 QC Report

S&ME
ENVIRONMENTAL SERVICES
ENGINEERING · TESTING

3201 Spring Forest Road
Raleigh, NC 27616
(919) 872-2660
(919) 876-3958

Field Report

Date 12-08-08	Job No. 1057-08-400
Project/Location NC State Constructed Facilities Lab	
Contractor Buckner	Weather/Temp SUNNY 27F
Present at Site Rhonda Rogers, Perry Vezina	
Time	Mileage 30

To:
Steve, Kendra

Services Performed

- ☐ Concrete Testing
- ☐ Cylinder Pickup
- ☐ Asphalt Testing
- ■ Steel Testing
- ☐ Asphalt Coring
- ☐ Concrete Coring
- ☐ Undercut Evaluation
- ☐ Foundation Evaluation
- ☐ Proofrolling
- ☐ In-Place Density

Other (Explain)

Observations:

Subject: **- Continuous Examination of CJP welded connections for bridge component testing.**
- UT of same contoured groove welded connections (pipe welded to top of beam).

1) Examiner arrived on site. Met with Justin Green, Mr. Quick of Buckner Steel; Steve Fulmer - NCSU.
2) Examined welded connections. **Excessive undercut** found on upper edge of inside weld of one connection. Notified welder. (Welder stated that repair will be made after UT of groove welds).
3) UT Examiner, Perry Vezina on site for Ultrasonic testing of the 2 connections. Perry pointed out that UT testing of the 2 connections *as they are* may result in "inconclusive" or "invalid" test results due to the following:
   - the construction sequence of the welded connection. (Inner fillet weld interferes with UT reading).
   - the lack of written procedure for UT of this particular set-up.
4) Decision was made to repair undercut and to clean up the welds today, and have an alternate Testing agency to come in to perform UT testing on Tuesday a.m. 12-9-08.
5) Examined preheating of connections to be welded/repaired.
6) Re-examined welds – undercut less than 1/32".
7) Examiner will return as requested.

END REPORT

Rhonda Rogers

On-Site Representative/Company | **S&ME Personnel**

Disclaimer: The presence of S&ME at the project site shall not be construed as an acceptance or approval of activities at the site. S&ME is at the project site to perform specific services and has certain responsibilities which are limited to those specifically authorized in our agreement with our client. In no event shall S&ME be responsible for the safety or the means and methods of other parties at the project site. **The information presented in this field report has not been reviewed by an engineer and is to be considered preliminary.**

PAGE 1 OF 1

Figure A 54 Phase 1 Test 5 QC Report

S&ME
ENVIRONMENTAL SERVICES
ENGINEERING · TESTING

3201 Spring Forest Road
Raleigh, NC 27616
(919) 872-2660
(919) 876-3958

Field Report

Date 12-09-08	Job No. 1057-08-400
Project/Location NC State Constructed Facilities Lab	
Contractor Buckner	Weather/Temp Partly cloudy 50F
Present at Site Rhonda Rogers	
Time	Mileage 30

To:
Steve, Kendra

Services Performed

- ☐ Concrete Testing
- ☐ Cylinder Pickup
- ☐ Asphalt Testing
- ■ Steel Testing
- ☐ Asphalt Coring
- ☐ Concrete Coring
- ☐ Undercut Evaluation
- ☐ Foundation Evaluation
- ☐ Proofrolling
- ☐ In-Place Density

Other (Explain)

Observations:

Subject: **- Continuous Examination of CJP welded connections for bridge component testing.**

1) Examiner arrived on site. Met with Justin Green, Mr. Quick of Buckner Steel.
2) Monitored welding of ¾" fillet welds on outside diameter of pipe at both connections of test assembly.
3) Examined fillet welds on each of the 2 connections according to AWS D1.5. Acceptable.
4) This section of the test assembly was relocated to inside "Constructed Facilities Lab" where J. Green, S. Fulmer, Kendra Cookson, and Mr. Quick made fit-up with 2 sections of 16" vertical pipes.
5) Examined fit-up of assembly. Acceptable according to detail and AWS D1.1. ¼" root opening. Tacked in place – J. Green.
6) Monitored welding of root pass for each of the groove welds on the vertical pipes. Welder J Green.
7) Examiner will return tomorrow (12-10-08) to examine root pass after cleanup.

END REPORT

Rhonda Rogers

On-Site Representative/Company **S&ME Personnel**

Disclaimer: The presence of S&ME at the project site shall not be construed as an acceptance or approval of activities at the site. S&ME is at the project site to perform specific services and has certain responsibilities which are limited to those specifically authorized in our agreement with our client. In no event shall S&ME be responsible for the safety or the means and methods of other parties at the project site. **The information presented in this field report has not been reviewed by an engineer and is to be considered preliminary.**

PAGE 1 OF 1

Figure A 55 Phase 1 Test 5 QC Report

S&ME
ENVIRONMENTAL SERVICES
ENGINEERING · TESTING

3201 Spring Forest Road
Raleigh, NC 27616
(919) 872-2660
(919) 876-3958

Field Report

Date 12-10-08	Job No. 1057-08-400
Project/Location NC State Constructed Facilities Lab	
Contractor Buckner	Weather/Temp Cloudy/misting rain 68F
Present at Site Rhonda Rogers	
Time	Mileage 30

To:
Steve, Kendra

Services Performed

- ☐ Concrete Testing
- ☐ Cylinder Pickup
- ☐ Asphalt Testing
- ■ Steel Testing
- ☐ Asphalt Coring
- ☐ Concrete Coring
- ☐ Undercut Evaluation
- ☐ Foundation Evaluation
- ☐ Proofrolling
- ☐ In-Place Density

Other (Explain)

Observations:

Subject: **- Continuous Examination of CJP welded connections for bridge component testing.**

- (NOTE: Examination - according to AWS D1.5 –Bridge welding code).

1) Examiner arrived on site. Met with Justin Green, Mr. Quick of Buckner Steel, S. Fulmer – NCSU.
2) Observed welders clean-up root pass on each of the groove welds for inspection.
3) Examined 1st root pass. Some slag left in 2 locations. Welder corrected. Acceptable.
4) Examined 2nd root pass. Incomplete fusion in 2 locations. Welder corrected. Acceptable.
5) Examiner observed welding of groove welds and the preparation of each weld for inspection.
6) Examined completed groove weld on each of the 2 connections. Acceptable.
7) Examiner will return as requested.

END REPORT

Rhonda Rogers

On-Site Representative/Company **S&ME Personnel**

Disclaimer: The presence of S&ME at the project site shall not be construed as an acceptance or approval of activities at the site. S&ME is at the project site to perform specific services and has certain responsibilities which are limited to those specifically authorized in our agreement with our client. In no event shall S&ME be responsible for the safety or the means and methods of other parties at the project site. **The information presented in this field report has not been reviewed by an engineer and is to be considered preliminary.**

PAGE 1 OF 1

Figure A 56 Phase 1 Test 5 QC Report

TRIAD N T

Triad Nondestructive Testing, Inc.
P.O. Box 2342
Kernersville, NC 27285-2342
(336) 996-2576

REPORT OF ULTRASONIC TESTING OF WELDS

Project ALASKA DOT #5 Job No. _____

Weld Identification SEE BELOW
Material Thickness 1/2"
Weld Joint AWS
Welding Process SMAW
Quality requirements - section no.
Remarks SPLICE WELD IN PIPE COLUMN

Line Number	Piece Number	Transducer Angle	From Face	Leg*	Indication Level a	Decibels: Reference Level b	Decibels: Attenuation Factor c	Decibels: Indication Rating d	Discontinuity: Length	Discontinuity: Angular distance (sound path)	Discontinuity: Depth from "A" surface	Discontinuity: Distance From X	Discontinuity: Distance From Y	Discontinuity Elevation	Remarks
1	1A	70°	A	1 & 2		63								ACCEPT	South
2	2A	70°	A	1 & 2		63								ACCEPT	North
3															
4															
5															
6															
7															
8															
9															

We, the undersigned, certify that the statements in this record are correct and that the welds were prepared and tested in accordance with the requirements of 6C of AWS D1.1, (2006 year) Structural Welding Code.

Test date 12/18/08
Manufacturer or Contractor NC STATE

Inspected by L. L. Spagle
Authorized by _____ Date _____

Figure A 57 Phase 1 Test 5 UT Inspection Report

Buckner Steel Erectors

Page 1 of 3

Welding Procedure Specification

CPB1015

WPS No. CPB1015 Revision _____ Date _____ By L. Leroy Spangler

Authorized By Jerry Cagle Date 3/12/2009 Prequalified ☒

Welding Process(es) SMAW _____ Type: Manual ☒ Machine ☐ Semi-Auto ☐ Auto ☐

Supporting PQR(s) _____

JOINT

Type T-Joint

Backing Yes ☒ No ☐ Single Weld ☒ Double Weld ☐

Backing Material A-36

Root Opening 1/4" Root Face Dimension 0" to 1/8"

Groove Angle 45 deg. Radius (J-U) _____

Back Gouge Yes ☐ No ☒

Method _____

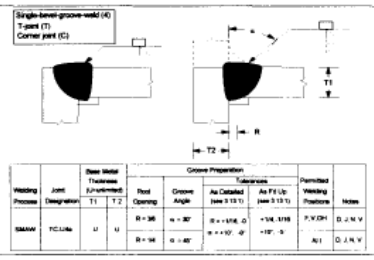

BASE METALS

Material Spec. ASTM A-500 to ASTM A-572

Type or Grade GR B to Gr 50

Thickness: Groove (in) 1.0 - Unlimited

Fillet (in) All - Unlimited

Diameter (Pipe, in) All - All

FILLER METALS

AWS Specification AWS A 5.1

AWS Classification E7018

SHIELDING

Flux _____ Gas _____

Composition _____

Electrode-Flux (Class) _____ Flow Rate _____

Gas Cup Size _____

PREHEAT

Preheat Temp., Min. 32 deg.

Thickness	Temperature
Up to 3/4"	32 deg.
Over 3/4" to 1-1/2"	150 deg.
Over 1-1/2" to 2-1/2"	225 deg.
Over 2-1/2"	300 deg.

Interpass Temp., Min. 32 deg. Max. 300 deg.

POSITION

Position of Groove All Fillet All

Vertical Progression: ☒ Up ☐ Down

ELECTRICAL CHARACTERISTICS

Transfer Mode (GMAW):

Short-Circuiting ☐ Globular ☐ Spray ☐

Current: AC ☐ DCEP ☒ DCEN ☐ Pulsed ☐

Other _____

Tungsten Electrode (GTAW):

Size _____ Type _____

TECHNIQUE

Stringer or Weave Bead Both

Multi-pass or Single Pass (per side) _____

Number of Electrodes 1

Electrode Spacing: Longitudinal _____

Lateral _____

Angle _____

Contact Tube to Work Distance _____

Peening None

Interpass Cleaning Mechanical

POSTWELD HEAT TREATMENT PWHT Required ☐

Temp. _____ Time _____

WELDING PROCEDURE

Layer/Pass	Process	Filler Metal Class	Diameter	Cur. Type	Amps or WFS	Volts	Travel Speed	Other Notes
1-15	SMAW	E7018	1/8"	DCEN	90 -130	20-24	5-7IPM	

Figure A 58 Phase 1 Test 6 WPS

Buckner Steel Erectors

Page 2 of 3

Welding Procedure Specification

CPB1015

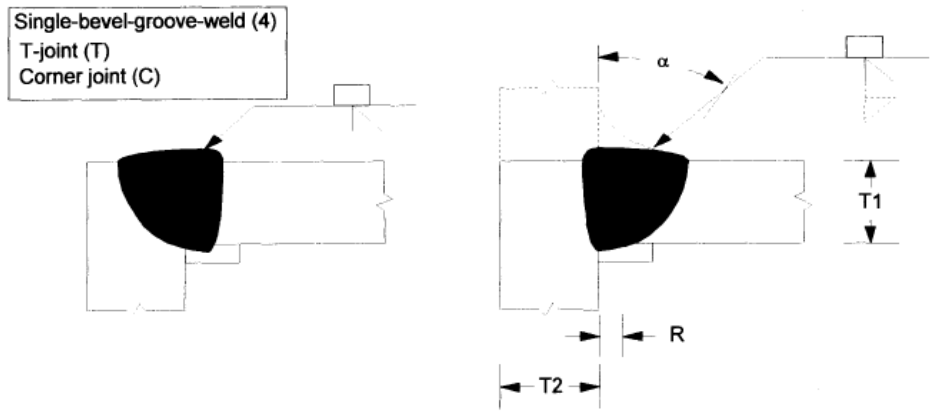

Welding Process	Joint Designation	Base Metal Thickness (U=unlimited)		Groove Preparation				Permitted Welding Positions	Notes
				Root Opening	Groove Angle	Tolerances			
		T1	T 2			As Detailed (see 3.13.1)	As Fit Up (see 3.13.1)		
SMAW	TC-U4a	U	U	R = 3/8	α = 30°	R = +1/16, -0 α = +10°, -0°	+1/4,-1/16 +10°, -5°	F,V,OH	D, J, N, V
				R = 1/4	α = 45°			All	D, J, N, V

MEMO

Figure A 59 Phase 1 Test 6 WPS

Page 3 of

Single-V-groove weld (2)
Butt joint (B)

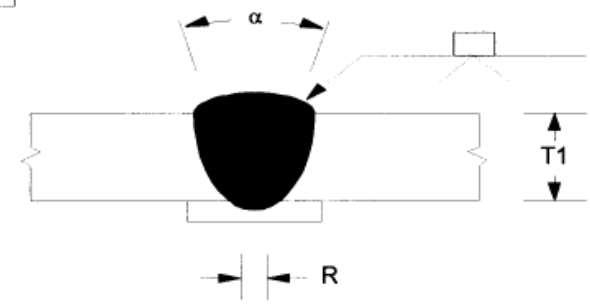

Welding Process	Joint Designation	Base Metal Thickness (U=unlimited)		Groove Preparation				Permitted Welding Positions	Notes
				Root Opening	Groove Angle	Tolerances			
						As Detailed (see 3.13.1)	As Fit Up (see 3.13.1)		
		T1	T 2						
SMAW	B-U2a	U	-	R=1/4	α = 45°	R = +1/16, -0 α = +10°, -0°	+1/4, -1/16 +10°, -5°	All	D, N
				R=3/8	α = 30°			F,V,OH	D, N
				R=1/2	α = 20°			F,V,OH	D, N

Figure A 60 Phase 1 Test 6 WPS

N
TRIAD
T

Triad
Nondestructive
Testing, Inc.
P.O. Box 2342
Kernersville, NC 27285-2342
(336) 996-2576

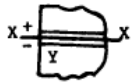

REPORT OF ULTRASONIC TESTING OF WELDS

Project ALASKA DOT

Job No. 08-114

Weld Identification SEE BELOW
Material Thickness 1"
Weld Joint AWS TC-U4a
Welding Process SMAW
Quality requirements - section no.
Remarks

Line Number	Piece Number	Transducer Angle	From Face	Leg*	Indication Level	Decibels: Reference Level	Decibels: Attenuation Factor	Decibels: Indication Rating	Discontinuity: Length	Discontinuity: Angular distance (sound path)	Discontinuity: Depth from "A" surface	Discontinuity: Distance From X	Discontinuity: Distance From Y	Discontinuity Elevation	Remarks
					a	b	c	d							
1	N	70°	A	1/2		60								ACCEPT	
2	S	70°	A	↓		↓								ACCEPT	
3															
4															
5															
6															
7															
8															
9															

We, the undersigned, certify that the statements in this record are correct and that the welds were prepared and tested in accordance with the requirements of 6C of AWS D1.1, (2008 year) Structural Welding Code.

Test date 3/18/09
Manufacturer or Contractor BUCKNER
Copy to Jerry Cagle - 03/23/09

Inspected by L. F. Spangler
Authorized by
Date

Figure A 61 Phase 1 Test 6 UT Inspection Report

METROLINA STEEL ERECTORS INC.

Page 1 of 2

Welding Procedure Specification

Metrolina 3G SMAW WPS

WPS No. **Metrolina 3G SMAW WPS** Revision **0** Date **11/10/2008** By **Troy Blackwell**

Authorized By **Barry Mitchell** Date **11/10/2008** Prequalified ☒

Welding Process(es) **SMAW** Type: Manual ☒ Machine ☐ Semi-Auto ☐ Auto ☐

Supporting PQR(s) **N/A** **N/A** **N/A** **N/A**

JOINT

Type **Butt**

Backing Yes ☒ No ☐ Single Weld ☒ Double Weld ☐

Backing Material **A 36**

Root Opening **1/4"** Root Face Dimension **N/A**

Groove Angle **45 Deg.** Radius (J-U) **N/A**

Back Gouge Yes ☐ No ☒

Method **N/A**

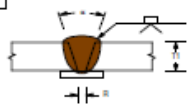

BASE METALS

Material Spec. **Group I or II** to **Group I or II**

Type or Grade **Group I or II** to **Group I or II**

Thickness: Groove ( ) **1/8"** - **Unlimited**

Fillet ( ) **N/A** - **N/A**

Diameter (Pipe,) **N/A** - **N/A**

POSITION

Position of Groove **Vertical** Fillet **N/A**

Vertical Progression: ☒ Up ☐ Down

FILLER METALS

AWS Specification **AWS A 5.1**

AWS Classification **E 7018**

ELECTRICAL CHARACTERISTICS

Transfer Mode (GMAW):

Short-Circuiting ☐ Globular ☐ Spray ☐

Current: AC ☐ DCEP ☒ DCEN ☐ Pulsed ☐

Other **N/A**

Tungsten Electrode (GTAW):

Size **N/A** Type **N/A**

SHIELDING

Flux **N/A**

Electrode-Flux (Class) **N/A**

Gas **N/A**

Composition **N/A**

Flow Rate **N/A**

Gas Cup Size **N/A**

TECHNIQUE

Stringer or Weave Bead **Both**

Multi-pass or Single Pass (per side) **Single**

Number of Electrodes **1**

Electrode Spacing: Longitudinal **N/A**

Lateral **N/A**

Angle **N/A**

Contact Tube to Work Distance **N/A**

Peening **N/A**

Interpass Cleaning **Chip & Brush Between Pass**

PREHEAT

Preheat Temp., Min. **32 Deg.**

Thickness	Temperature
Up to 3/4"	32 Deg.
Over 3/4" to 1-1/2"	50 Deg.
Over 1-1/2" to 2-1/2"	150 Deg.
Over 2-1/2"	225 Deg.

Interpass Temp., Min. **32 Deg.** Max. **550 Deg.**

POSTWELD HEAT TREATMENT PWHT Required ☐

Temp. **N/A** Time **N/A**

WELDING PROCEDURE

Layer/Pass	Process	Filler Metal Class	Diameter	Cur. Type	Amps or WFS	Volts	Travel Speed	Other Notes
All	SMAW	E 7018	3/32	DCEP	70-110		Manual	
All	SMAW	E 7018	1/8"	DCEP	90-160		Manual	
All	SMAW	E 7018	5/32"	DCEP	130-210		Manual	

Figure A 62 Phase 2 Test 1 WPS

METROLINA STEEL ERECTORS INC.

Page 2 of 2

Welding Procedure Specification

Metrolina 3G SMAW WPS

Single-V-groove weld (2)
Butt joint (B)

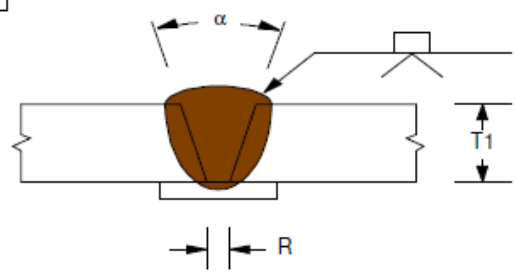

Welding Process	Joint Designation	Base Metal Thickness (U=unlimited)		Groove Preparation				Permitted Welding Positions	Notes
				Root Opening	Groove Angle	Tolerances			
						As Detailed (see 3.13.1)	As Fit Up (see 3.13.1)		
		T1	T 2						
SMAW	B-U2a	U	-	R=1/4	α = 45°	R = +1/16, -0	+1/4, -1/16	All	D, N
				R=3/8	α = 30°	α= +10°, -0°	+10°, -5°	F,V,OH	D, N
				R=1/2	α = 20°			F,V,OH	D, N

MEMO

1.) Weld axis is Vertical.

2.) When base metal is below 32 degrees F, preheat to 70 degrees minimum.

Figure A 63 Phase 2 Test 1 WPS

METROLINA STEEL ERECTORS INC.

Page 1 of 2

Welding Procedure Specification

Metrolina 4G SMAW WPS

WPS No. **Metrolina 4G SMAW WPS** Revision **0** Date **11/11/2008** By **Troy Blackwell**

Authorized By **Barry Mitchell** Date **11/11/2008** Prequalified ☒

Welding Process(es) **SMAW** Type: Manual ☒ Machine ☐ Semi-Auto ☐ Auto ☐

Supporting PQR(s) **N/A** **N/A** **N/A** **N/A**

JOINT

Type **Butt**

Backing Yes ☒ No ☐ Single Weld ☒ Double Weld ☐

Backing Material **A 36**

Root Opening **1/4"** Root Face Dimension **N/A**

Groove Angle **45 Deg.** Radius (J-U) **N/A**

Back Gouge Yes ☐ No ☒

Method **N/A**

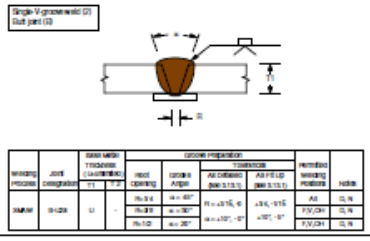

BASE METALS

Material Spec. **Group I or II** to **Group I or II**

Type or Grade **Group I or II** to **Group I or II**

Thickness: Groove ( ) **1/8"** - **Unlimited**

Fillet ( ) **N/A** - **N/A**

Diameter (Pipe,) **N/A** - **N/A**

POSITION

Position of Groove **Overhead** Fillet **N/A**

Vertical Progression: ☐ Up ☐ Down

FILLER METALS

AWS Specification **AWS A 5.1**

AWS Classification **E 7018**

ELECTRICAL CHARACTERISTICS

Transfer Mode (GMAW):

Short-Circuiting ☐ Globular ☐ Spray ☐

Current: AC ☐ DCEP ☒ DCEN ☐ Pulsed ☐

Other **N/A**

Tungsten Electrode (GTAW):

Size **N/A** Type **N/A**

SHIELDING

Flux **N/A**

Electrode-Flux (Class) **N/A**

Gas **N/A**

Composition **N/A**

Flow Rate **N/A**

Gas Cup Size **N/A**

TECHNIQUE

Stringer or Weave Bead **Both**

Multi-pass or Single Pass (per side) **Single**

Number of Electrodes **1**

Electrode Spacing: Longitudinal **N/A**

Lateral **N/A**

Angle **N/A**

Contact Tube to Work Distance **N/A**

Peening **N/A**

Interpass Cleaning **Chip & Brush Between Pass**

PREHEAT

Preheat Temp., Min. **32 Deg.**

Thickness	Temperature
Up to 3/4"	32 Deg.
Over 3/4" to 1-1/2"	50 Deg.
Over 1-1/2" to 2-1/2"	150 Deg.
Over 2-1/2"	225 Deg.

Interpass Temp., Min. **32 Deg.** Max. **550 Deg.**

POSTWELD HEAT TREATMENT

PWHT Required ☐

Temp. **N/A** Time **N/A**

WELDING PROCEDURE

Layer/Pass	Process	Filler Metal Class	Diameter	Cur. Type	Amps or WFS	Volts	Travel Speed	Other Notes
All	SMAW	E 7018	3/32	DCEP	70-110		Manual	
All	SMAW	E 7018	1/8"	DCEP	90-160		Manual	
All	SMAW	E 7018	5/32"	DCEP	130-210		Manual	

Figure A 64 Phase 2 Test 1 WPS

METROLINA STEEL ERECTORS INC.

Page 2 of 2

Welding Procedure Specification

Metrolina 4G SMAW WPS

Single-V-groove weld (2)
Butt joint (B)

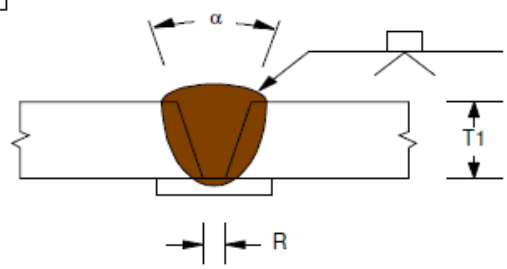

Welding Process	Joint Designation	Base Metal Thickness (U=unlimited)		Groove Preparation				Permitted Welding Positions	Notes
				Root Opening	Groove Angle	Tolerances			
						As Detailed (see 3.13.1)	As Fit Up (see 3.13.1)		
		T1	T 2						
SMAW	B-U2a	U	-	R=1/4	α = 45°	R = +1/16, -0 α= +10°, -0°	+1/4, -1/16 +10°, -5°	All	D, N
				R=3/8	α = 30°			F,V,OH	D, N
				R=1/2	α = 20°			F,V,OH	D, N

MEMO

1.) Weld axis is Over head.

2.) When base metal is below 32 degrees F, preheat to 70 degrees minimum.

Figure A 65 Phase 2 Test 1 WPS

Metrolina Steel Erectors Inc.

Page 1 of 1

Welder Qualification Test Record

Metrolina A Aguilar 3G4G

WQTR No. Metrolina A Aguilar 3G4G Welder Name Alex Aguilar Welder Id 8709

WPS No. Metrolina 3G4G SMAW Revision 0 Date 11/10/2008

Variables	Record Actual Values Used In Qualification	Qualification Range	
Process (Table 4.10, Item (1))	SMAW	SMAW	
Transfer Mode (GMAW): Short-Cir. ☐ Globular ☐ Spray ☐		Short-Circuiting ☐ Globular ☐ Spray ☐	
Type Manual ☒ Machine ☐ Semi-Auto ☐ Auto ☐		Manual ☒ Machine ☐ Semi-Auto ☐ Auto ☐	
Number of Electrodes Single ☒ Multiple ☐		Single ☒ Multiple ☐	
Current/Polarity AC ☐ DCEP ☒ DCEN ☐ Pulsed ☐		AC ☐ DCEP ☒ DCEN ☐ Pulsed ☐	
Position (Table 4.10, Item (4))	3G,4G	All	
Weld Progression: (Table 4.10, Item (6)) Up ☒ Down ☐		Up ☒ Down ☐	
Backing [Table 4.10, Item (7)] Use Backing ☒		With Backing ☐ Without Backing ☐	
Consumable Insert (GTAW) Use Insert ☐		With Insert ☐ Without Insert ☐	
Material/Spec.	A572 Grade 50 to A 572 Grade 50	Group I and II Steels	
Thickness (Plate): Groove (in)	1	1/8 - Unlimited	in
Fillet ( )	N/A	1/8 - Unlimited	in
Thickness (Pipe/tube): Groove ( )	N/A	N/A - N/A	
Fillet ( )	N/A	1/8 - Unlimited	in
Diameter(Pipe): Groove ( )	N/A	N/A - N/A	
Fillet ( )	N/A	1/8 - Unlimited	in
Notes			
Filler Metal (Table 10, Item (2))			
Spec.	SFA 5.1	EXX15,EXX16,EXX18,EXX15-X,EXX16-X,EXX18-X	
Class.	E 7018	EXX10,EXX11,EXX10-X,EXX11-X	
F-No.	4	EXX12,EXX13,EXX14,EXX13-X	
		EXX20,EXX27,EXX28,EXX20-X,EXX27-X	
Gas/Flux Type (Table 4.10, Item (3))	N/A	N/A	
Other	N/A	N/A	

VISUAL INSPECTION (4.8.1) Acceptable Yes

GUIDED BEND TEST RESULTS (4.30.5)

Type	Result	Type	Result
3G Side Bend	Meets Code Requirements.	3G Side Bend	Meets Code Requirements.
4G Side Bend	Meets Code Requirements.	4G Side Bend	Meets Code Requirements.

Fillet Test Results (4.30.2.3 and 4.30.4.1)

Appearance N/A Fillet Size N/A Macroetch N/A

Fracture Test Root Penetration N/A Description N/A

Inspected By Troy Blackwell Test No. 08-495/496 Organization Structural Evaluations Inc. Date 11/11/2008

RADIOGRAPHIC TEST RESULTS (4.30.3.1)

Film Identification No.	Result	Remark
N/A	N/A	N/A
N/A	N/A	N/A
N/A	N/A	N/A
N/A	N/A	N/A

Interpreted By N/A
Organization N/A
Test No. N/A
Date

We, the undersigned, certify that the statements in this record are correct and that the test welds were prepared, welded, and tested in accordance with the requirements of section 4 of ANSI/AWS D1.1, (2006) Structural Welding Code-Steel.

Manufacturer Metrolina Steel Erectors Inc. Authorized By Barry Mitchell Date 11/11/2008

Figure A 66 Phase 2 Test 1 and 3 Welder Certification Report

Welder, Welding Operator Or Tack Welder Qualification Test Record

Type of Welder: Welder [X] Tack Welder [ ] Operator [ ]
Name Calvin Stinson **Identification No.** CS
Welding Procedure Specification No. WP 1 **Revision** 0 **Date** 11/2/10

Variables	Record Actual Values Used In Testing	Qualification Range
Process/Type [Table 4.10, Item (1)]	SMAW	SMAW
Electrode (single or multiple) [Table 4.10, Item (8)]	Single	Single
Current/Polarity	DC+	
Position [Table 4.10, Item (4)]	3F	1F, 2F, 3F
Weld Progression [Table 4.10, Item (6)]	3F Up	3F, Up
Backing (Yes or No) [Table 4.10, Item (7)]	N/A	N/A
Material/Specification	A36 to A36	Any Group I Combination
Base Metal		
Thickness: (Plate)		
Groove	N/A	N/A
Fillet	1/2"	1/8"-1"
Thickness: (Pipe/Tube)		
Groove	N/A	N/A
Fillet	N/A	See Table 4.8
Diameter: (Pipe)	N/A	> 24"
Groove	N/A	N/A
Fillet	N/A	See Table 4.9
Filler Metal [Table 4.10, Item (3)]		
Specification Number	A5.1	
Classification	E7018	
F-Number [Table 4.10, Item (2)]	F-Number 4	F-Numbers 1-4
Gas/Flux Type [Table 4.10, Item (4)]	N/A	
Other	N/A	N/A

Visual Inspection (4.8.1)
Acceptable? Yes [x] No [ ] **Comments** Within acceptable tolerance of specifications

Guided Bend Test Results (4.30.5)

Type/Description	Result	Type/Description	Result
N/A			
N/A			

Fillet Test Results (4.30.2.3 and 4.30.4.1)

Appearance	N/A	Fillet Size	N/A
Fracture Test Root Penetration	N/A	Macro Etch	N/A

Describe the location, nature and size of any crack or tear of the specimen.
N/A

Inspected By: Randy Dempsey **Signature** Randy Dempsey **Test Number** AKDOT 1
Organization: NCDOT, Kernersville, NC **Date** 11/2/10

Radiographic Test Results (4.30.3.1)

Film Identification Number	Results	Remarks	Film Identification Number	Results	Remarks
N/A			N/A		
N/A			N/A		

Interpreted By **Signature** **Test Number**
Organization **Date**

We, the undersigned, certify that the statements in this record are correct and that the test welds were prepared, welded and tested in accordance with the requirements of section 4 of ANSI/AWS D1.1-2006 Structural Welding Code-Steel.

Certified Welding Inspector Randy Dempsey **Signature** Randy Dempsey **Date** 11/2/10
Manufacturer or Contractor Metrolina
Authorized By Steven Fulmer **Signature** **Date** 11/2/10

Figure A 67 Phase 2 Test 1 Welder Certification Report

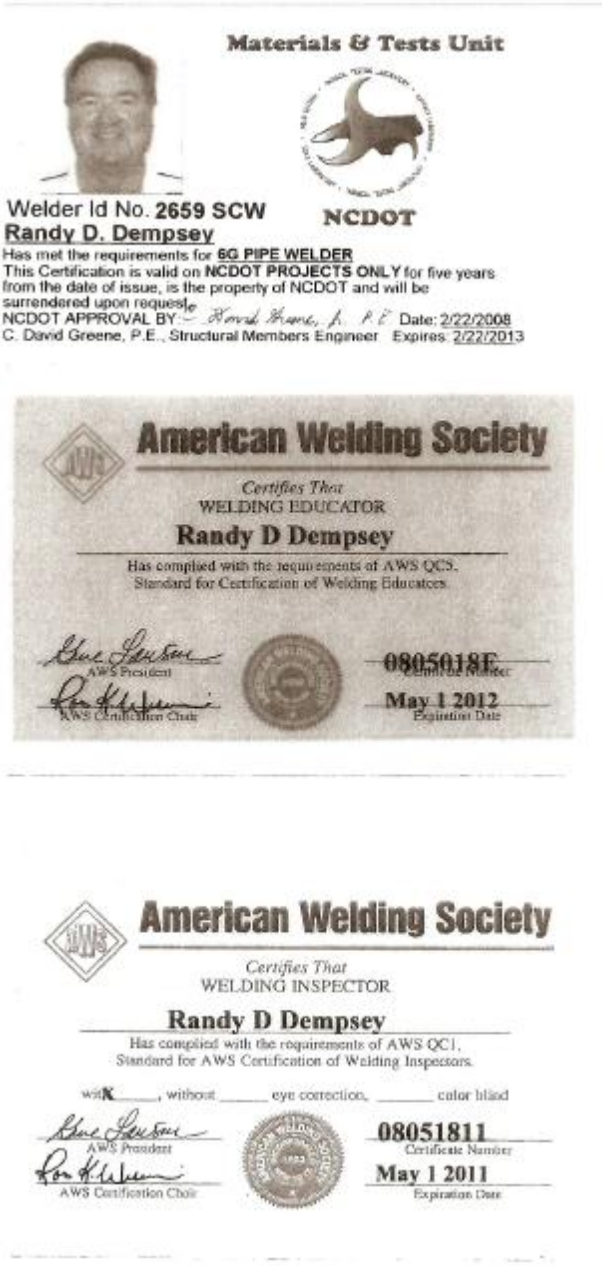

Materials & Tests Unit

NCDOT

Welder Id No. 2659 SCW
Randy D. Dempsey
Has met the requirements for 6G PIPE WELDER
This Certification is valid on NCDOT PROJECTS ONLY for five years from the date of issue, is the property of NCDOT and will be surrendered upon request.
NCDOT APPROVAL BY: David Greene, P.E. Date: 2/22/2008
C. David Greene, P.E., Structural Members Engineer Expires: 2/22/2013

American Welding Society
Certifies That
WELDING EDUCATOR
Randy D Dempsey
Has complied with the requirements of AWS QC5, Standard for Certification of Welding Educators.
AWS President
AWS Certification Chair
0805018E
Certificate Number
May 1 2012
Expiration Date

American Welding Society
Certifies That
WELDING INSPECTOR
Randy D Dempsey
Has complied with the requirements of AWS QC1, Standard for AWS Certification of Welding Inspectors.
with X, without ____ eye correction, ____ color blind
AWS President
AWS Certification Chair
08051811
Certificate Number
May 1 2011
Expiration Date

Figure A 68 Phase 2 Test 1 and 3 Weld Inspector Certifications

STEEL FAB, INC.
NONDESTRUCTIVE QUALIFICATION & CERTIFICATION OF
EXAMINATION PERSONNEL

NDE-PQC-001
Rev. 3 Page 19
Date 3-16-2005

Visual Acuity Examination Record

NAME Michael Lewis SSN Employee # 1752

ANNUAL VISUAL ACUITY EYE EXAMINATION FOR COMPLIANCE WITH :

STEELFAB, INC. "PROCEDURE for QUALIFICATION and CERTIFICATION OF NONDESTRUCTIVE EXAMINATION PERSONNEL"

An examination to assure [ ] natural or [ ] corrected near-distance vision has been administered using the standard *JAEGER* reading card for the minimum of J-2 size letter at not less than 12 inch distance.

An examination to assure the capability to distinguish and differentiate contrast among colors or shades of grey has been administered using *ISHIHARA* pseudo-isochromatic plates and was found to be [ ] capable or [ ] not capable.

Examination Administer

Examinee

Nov 4, 2009 Date of Exam

Figure A 69 Phase 2 Test 1 NDE Inspector Certifications

American Welding Society

Certifies That
WELDING INSPECTOR

Michael E. Lewis

Has complied with the requirements of AWS QC1, Standard for AWS Certification of Welding Inspectors.

with____ without X eye correction, ____ color blind

AWS President

AWS Certification Chair

03040281
Certificate Number

April 1 2012
Expiration Date

Figure A 70 Phase 2 Test 1 NDE Inspector Certifications

STEELFAB, INC.
CERTIFICATE OF PERSONNEL QUALIFICATIONS

NDT Method Magnetic Particle Level II
Certification Standard ASNT TC 1A

EMPLOYMENT/EDUCATION HISTORY

Name MIKE LEWIS Date Of Employment AUGUST 2005
High School Graduate Date 1999 Location Gastonia, NC
College NA Years Degree Year
Previous Nde Experience Or Technical/Scientific Study
JACKSON TUBE SERVICE ET, UT, MT

TRAINING

Classroom Hours 16 HRS Conducted By Bllanier / SteelFab
Laboratory Hours 250 hrs Conducted By Bllanier / SteelFab
Exam Grades: General 79 (23.7) Specific 89 (17.8) Practical 100 (50)
Composite Grade 91.5 (92)
Percentile Weights: General .3 Specific .2 Practical .5
Remarks

CERTIFICATION

Training Certified By Bllanier SFI Corporate Level III
Certification Examination Administered By Bllanier #21832 Level III
Date Of Certification 9-23-05

VISUAL ACUITY/COLOR PERCEPTION TEST

Date Of Test	Date Of Test	Date Of Test
9-1-2005	11-5-2008	
11-30-2006 ANS CWI	11-4-2007	
4-13-2051		

RECERTIFICATION

Date Of Recertification (3 Year) and Signature	Date of Recertification (3 Year) and Signature
9-1-2008	

I, the undersigned, verify the information contained on the Certificate of Personnel Qualifications form is true to the best of our knowledge. The examination scores, dates, names and signatures of qualified examiners were taken from original documents or copies of the original documents.

Bllanier/ASNT #21832/Sept 23, 2005 SteelFab, Inc.
Examiner/NDT Level/Date

Figure A 71 Phase 2 Test 1 NDE Inspector Certifications

North Carolina Department of Transportation	*QA Report 1*	Project Description
Materials & Tests Unit		**Alaska DOT Phase II Test 1 KERF CONNECTION**
	Part Description	Owner Representative: **Steven Fulmer**
		Project Location: **NCSU Construction Facilities Lab**
	Bridge Bent Test 1	Fabricator Name: **Metrolina Steel Erectors**
		Welder's Name: **Alex Aguilar/North Pile**
		Calvin Stinson/South Pile
NCDOT	Weld Location	QA Inspector: **Randy Dempsey, CWI/CWE**
	North & South Pipe Pile to gusset plates North, South, East and West	

	Date	Comments
Consumable Storage/Control	**11/1/10**	**see note 1**
Base Metal Preparation	**11/1/10**	**see note 2**
Joint Fit-Up	**11/2/10**	**see note 3**
Pre-Heat & Interpass Temperature Control	**11/2/10**	**see note 4**
Interpass Cleaning	**11/2/10**	**see note 5**
Visual Inspection of completed Fillet Weld	**11/3/10**	**see note 6**
Witness MT Testing of Fillet Weld	**11/3/10**	**see note 7**
Fillet Weld Repair after NDE		**N/A**
Follow-Up MT of Fillet Weld		**N/A**

note 1: The electrode oven was inspected and found to be in excellent working order. The electrodes were delivered in a hermetically sealed containers (Lincoln Excalibur E7018MR, 9 hour exposure limit). The rod oven was inspected daily.

note 2: The North and South pipe piles were slotted to accept the gusset plates that are welded to the bottom of the cap beam. A mechanical guide (straight edge) was used to improve the quality of the cut.

note 3: The cap beam was set with a 1" gap at the top in accordance with the engineer's drawing specifications. A 3/16" or smaller root opening was maintained in all areas except for 8" at the bottom of the East gusset, North side, North Pile, where the opening was 1/4". Due to the amount of rework that would be required to correct this deficiency, the engineer decided to continue without corrective action.

note 4: The 50° F preheat was not necessary due to the thickness of the material and the atmospheric conditions in the building being 71° to 73° F. Interpass temperatures between 240° and 255° F were recorded 1" from the toe of the weld using an infrared thermometer with a -58° to +932° F temperature range.

note 5: Several areas of excessive convexity on the root pass required grinding. The toe of the welds required light grinding to remove a small amount of entrapped slag. Other interpass cleaning included chipping and wire brushing. The weld size was increased where necessary to compensate for the root opening that was greater than 1/16".

note 6: Several discontinuities including arc strikes, excessive convexity and hammer marks were corrected on the completed weld. A few isolated areas of undercut was detectable but within acceptable tolerance of specifications.

note 7: A small area of incomplete fusion was found and repaired on the South Pile, South Gusset, West side at the start of the weld.

Figure A 72 Phase 2 Test 1 QC Report

Report of Magnetic-Particle Examination of Welds

SteelFab Project No.: 25580 **Name:** AK DOT
Quality Requirements – Section No.: NDE-MT-D1.1 2008 SOP
Reported To Client

Date	Piece Mark/ Weld Identification	Interpret Accept	Interpret Reject	Repairs Accept	Repairs Reject	Remarks
11-3-10	North Pile					
	North North West	✓				
	North North East	✓				
	North East North	✓				
	North East South	✓				
	North South East	✓				
	North South West	✓				
	North West North	✓				
	North West South	✓				

Weld Location and Identification Sketch

Pre Examination
Surface Preparation Wire brush

Equipment
Instrument Make: Parker Probe **Model:** DA-400 **S. No.:** 18305

Method of Inspection
☒ Dry ☐ Wet ☒ Visible ☐ Fluorescent
How Media Applied:
☐ Residual ☐ Continuos ☒ True Continuous
☒ AC ☐ DC ☐ Half Wave
☐ Prods ☒ Yoke ☐ Cable Wrap ☐ Other
Direction of Field: ☐ Circular ☒ Longitudinal

Strength of Field: 50-60 Hz 6 amps (fixed strength coil)
(Ampere turns, field density, magnetizing force, number and duration of force application)

Post Examination
Demagnetizing Technique (if required): N/A

Cleaning (if required): Marking Method:

We, the undersigned, certify that the statements in this record are correct and that the test welds were prepared and tested in accordance with the requirements of SteelFab SOP-NDE-MT-D1.

Inspector/Level Mike Lewis ASNT-TC-1A II Test Date 11/3/10

Figure A 73 Phase 2 Test 1 MT Report

Report of Magnetic-Particle Examination of Welds

SteelFab Project No.: 25580 **Name:** AKDOT
Quality Requirements – Section No.: NDE-MT-D1.1 2008 SOP
Reported To Client

Date	Piece Mark/ Weld Identification	Interpret Accept	Interpret Reject	Repairs Accept	Repairs Reject	Remarks
11-3-10	South Pile					
	South North West	✓				
	South North East	✓				
	South West North			✓		Bottom weld, LOF / repaired + Ground
	South West South	✓				
	South South East	✓				
	South South West	✓				
	South East North	✓				
	South East South	✓				

Weld Location and Identification Sketch

Pre Examination
Surface Preparation: Wire brush

Equipment
Instrument Make: Parker Probe **Model:** DA-400 **S. No.:** 18305

Method of Inspection
☒ Dry ☐ Wet ☒ Visible ☐ Fluorescent
How Media Applied:
☐ Residual ☐ Continuos ☒ True Continuous
☒ AC ☐ DC ☐ Half Wave
☐ Prods ☒ Yoke ☐ Cable Wrap ☐ Other
Direction of Field: ☐ Circular ☒ Longitudinal

Strength of Field: 50-60 Hz 6 amps (fixed strength coil)
(Ampere turns, field density, magnetizing force, number and duration of force application)

Post Examination
Demagnetizing Technique (if required): N/A

Cleaning (if required): Marking Method:

We, the undersigned, certify that the statements in this record are correct and that the test welds were prepared and tested in accordance with the requirements of SteelFab SOP-NDE-MT-D1.

Inspector/Level Mike Lewis ASNT-TC-1A II Test Date 11/3/10

Figure A 74 Phase 2 Test 1 MT Report

Metrolina Steel

AWS WELDER OR WELDING OPERATOR QUALIFICATION TEST (WQ)

(4C, AWS D1.1-2010, STRUCTURAL WELDING CODE – STEEL)

Welder Name Calvin Stinson **SSN** See MS Human Resources **Emp. No:** 0774
Welding Procedure Spec. No.: WPS-1 BU2a **Rev.:** 0 **Date:** 2000
Welding Process: Shielded Manual Arc Welding (SMAW) **Type:** Manual

Variables	Actual Values Used	Qualification Range
Backing Material/Type	Yes – Group I	With backing or backgouge 2nd side
Base Material Specification		
Group No.	A572-50 Group II	Group I, II, III AWS D1.1 with WPS
Thickness Table 4.9		
Groove	1.0"	1/8" to unlimited
Fillet	NA	1/8" to unlimited"
Diameter		
Groove	NA	Over 24" Diameter
Fillet	NA	Unlimited
Filler Metal		
Spec. No.	A5.1	A5.1, A5.5
Class	E7018	All 5.1 & 5.5 as E70XX or E60XX
F No.	F4	F1 thru F4
Deposited Weld Metal Thickness		
Groove	1.0"	1/8" to unlimited
Fillet	NA	1/8" to unlimited
Weld Position		
Orientation	3G & 4G	All plate PJP,CJP&Fillet-See below for more
Weld Progression	Uphill	Vertical uphill
Gas Type		
Shielding	NA	NA
Backing	NA	NA
Electrical Characteristics		
Current	Direct	Any current recommended by rod mfg.
Polarity	Reverse	Any polarity recommended by rod mfg.

Additional qualification ranges: Pipe-all PJP, CJP>24inch OD and all Fillet>30 degree, Pipe TYK PJP>24inch OD and greater than 30 degree. Box Tubing (HSS)-all CJP, PJP and all Fillet> 30 degree, PJP TYK> 30 degree slope. Plate Fillet > 30 degree slope.

GROOVE WELD TEST RESULTS

Visual Passed **Radiographic Results** NA

Guided Bend Test

Type and Figure No.	Results	Type and Figure No.	Results
(V) 5-16-11-1 Side - 4.13	Accept	(OH) 5-16-11-3 Side - 4.13	Accept
(V) 5-16-10-2 Side - 4.13	Accept	(OH) 5-16-11-4 Side – 4.13	Accept

Witnessed by: Reported as Metrolina Steel
Test Conducted by: SteelFab , Inc. Bruce L Lanier
Inspector: B L Lanier SCWI #04090028 Date: 5-16- 2011

We certify that the statements in this record are correct and that the test weld(s) were prepared, welded and tested in accordance with the requirements of Section 4, ANSI/AWS D1.1-2010.

Organization: Metrolina Steel
By:
Date:

Qualification Tests: SteelFab, Inc.
By: Bruce L Lanier AWS SCWI#04090028
Date: 5-16-2011

Bruce L Lanier SCWI 04090028 QC EXP. 8/1/2013

Page 1 of 1

Figure A 75 Phase 2 Test 3 Welder Certification Report

METROLINA STEEL ERECTORS INC.

Page 1 of 2

Welding Procedure Specification

Metrolina 4G SMAW WPS

WPS No. **Metrolina 4G SMAW WPS** Revision **0** Date **11/11/2008** By **Troy Blackwell**

Authorized By **Barry Mitchell** Date **11/11/2008** Prequalified ☒

Welding Process(es) **SMAW** Type: Manual ☒ Machine ☐ Semi-Auto ☐ Auto ☐

Supporting PQR(s) **N/A** **N/A** **N/A** **N/A**

JOINT

Type **Butt**

Backing Yes ☒ No ☐ Single Weld ☒ Double Weld ☐

Backing Material **A 36**

Root Opening **1/4"** Root Face Dimension **N/A**

Groove Angle **45 Deg.** Radius (J-U) **N/A**

Back Gouge Yes ☐ No ☒

Method **N/A**

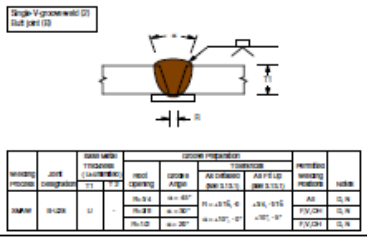

BASE METALS

Material Spec. **Group I or II** to **Group I or II**

Type or Grade **Group I or II** to **Group I or II**

Thickness: Groove ( ) **1/8"** - **Unlimited**

Fillet ( ) **N/A** - **N/A**

Diameter (Pipe,) **N/A** - **N/A**

FILLER METALS

AWS Specification **AWS A 5.1**

AWS Classification **E 7018**

SHIELDING

Flux **N/A** Gas **N/A**

Composition **N/A**

Electrode-Flux (Class) **N/A** Flow Rate **N/A**

Gas Cup Size **N/A**

PREHEAT

Preheat Temp., Min. **32 Deg.**

Thickness Up to 3/4" Temperature **32 Deg.**

Over 3/4" to 1-1/2" **50 Deg.**

Over 1-1/2" to 2-1/2" **150 Deg.**

Over 2-1/2" **225 Deg.**

Interpass Temp., Min. **32 Deg.** Max. **550 Deg.**

POSITION

Position of Groove **Overhead** Fillet **N/A**

Vertical Progression: ☐ Up ☐ Down

ELECTRICAL CHARACTERISTICS

Transfer Mode (GMAW):

Short-Circuiting ☐ Globular ☐ Spray ☐

Current: AC ☐ DCEP ☒ DCEN ☐ Pulsed ☐

Other **N/A**

Tungsten Electrode (GTAW):

Size **N/A** Type **N/A**

TECHNIQUE

Stringer or Weave Bead **Both**

Multi-pass or Single Pass (per side) **Single**

Number of Electrodes **1**

Electrode Spacing: Longitudinal **N/A**

Lateral **N/A**

Angle **N/A**

Contact Tube to Work Distance **N/A**

Peening **N/A**

Interpass Cleaning **Chip & Brush Between Pass**

POSTWELD HEAT TREATMENT

PWHT Required ☐

Temp. **N/A** Time **N/A**

WELDING PROCEDURE

Layer/Pass	Process	Filler Metal Class	Diameter	Cur. Type	Amps or WFS	Volts	Travel Speed	Other Notes
All	SMAW	E 7018	3/32	DCEP	70-110		Manual	
All	SMAW	E 7018	1/8"	DCEP	90-160		Manual	
All	SMAW	E 7018	5/32"	DCEP	130-210		Manual	

Figure A 76 Phase 2 Test 3 WPS

METROLINA STEEL ERECTORS INC.

Page 2 of 2

Welding Procedure Specification

Metrolina 4G SMAW WPS

Single-V-groove weld (2)
Butt joint (B)

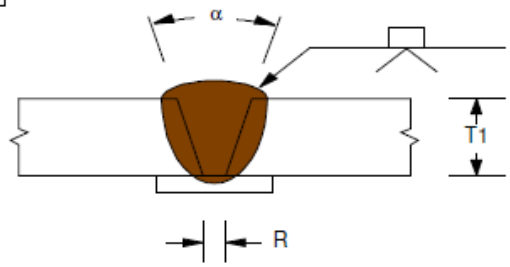

Welding Process	Joint Designation	Base Metal Thickness (U=unlimited)		Groove Preparation				Permitted Welding Positions	Notes
				Root Opening	Groove Angle	Tolerances			
						As Detailed (see 3.13.1)	As Fit Up (see 3.13.1)		
		T1	T 2						
SMAW	B-U2a	U	-	R=1/4	α = 45°	R = +1/16, -0	+1/4, -1/16	All	D, N
				R=3/8	α = 30°	α= +10°, -0°	+10°, -5°	F,V,OH	D, N
				R=1/2	α = 20°			F,V,OH	D, N

MEMO

1.) Weld axis is Over head.

2.) When base metal is below 32 degrees F, preheat to 70 degrees minimum.

Figure A 77 Phase 2 Test 3 WPS

North Carolina Department of Transportation	QA Report 1	Project Description
Materials & Tests Unit		Alaska DOT Phase II Test 3
		C1F-Column Capital Field Welding
	Part Description	Owner Representative: Steven Fulmer
		Project Location: NCSU Construction Facilities Lab
	Bridge Bent Test 3	Fabricator Name: Metrolina Steel Erectors
		Welder's Name: Alex Aguilar/North Pile
		Calvin Stinson/South Pile
NCDOT	Weld Location	QA Inspector: Randy Dempsey, CWI/CWE
	North & South Pipe Pile to Capital Column, Capital Column to Cap Beam	

	Date	Comments
Consumable Storage/Control	5/16/11	see note 1
Base Metal Preparation	5/17/11	see note 2
Joint Fit-Up	5/16/11	see note 3
Pre-Heat & Interpass Temperature Control	5/16/11	see note 4
Interpass Cleaning	5/16/11	see note 5
Visual Inspection of completed Butt Weld	5/17/11	see note 6
Visual Inspection of completed T-Joint	5/18/11	see note 7
Witness UT Testing		
Weld Repair after NDE		N/A
Follow-Up UT		N/A

note 1: The electrode oven was inspected and found to be in excellent working order. The electrodes were delivered in hermetically sealed containers (1/8" and 5/32" Lincoln Excalibur E7018MR, 9 hour exposure limit). The rod oven was inspected daily.

note 2: All mill scale was removed from the cap beam in accordance with ASW D1.1 guidelines for preparation of base metal for cyclically loaded structures.

note 3: The joint geometry of the capital column was inspected for accuracy and 1/4" plate was used to set the root opening. The mis-alignment of the butt joint was no greater than 10% of the thickness of the material (approximately 3/32"). The root opening of the backing bar to cap beam at the T-joint was no greater than 1/8"

note 4: The 50° F preheat was not necessary due to the thickness of the material and the atmospheric conditions in the building being 71° to 73° F. Interpass temperatures between 210° and 405° F were recorded 1" from the toe of the weld using an infrared thermometer with a -58° to +1022° F temperature range. The Capital Column was pre-heated to 150 degrees at the T-joint. Additional preheat in this area was required after the welders returned from lunch.

note 5: Any questionable area of weld metal of every pass was removed with a grinder before additional weld metal was applied. Other interpass cleaning included chipping and wire brushing.

note 6: A few discontinuities including excessive convexity of the weld reinforcement and poor transition from weld metal to base metal were corrected on the completed weld. A few isolated areas of undercut were detectable but within acceptable tolerance of specifications (less then 1/32").

note 7: A few discontinuities including porosity, underfill and undercut were repaired on the T-joint groove weld. A few areas of the fillet were undersize and required additional welding.

Additional Comments 1: The root pass of the T-joint was applied using 1/8" electrodes. To improve efficiency, all other passes of this joint were applied using 5/32" electrodes. The additional heat input from the larger diameter electrodes was inconsequential due to the 7/8" thick cap beam flange and the 1" thick material at the top of the capital column, which reduced interpass temperatures.

Additional Comments 2: Total man hours for day 1 of operations is 5x3=15, which includes 2 welders and 1 supervisor. The work included fit-up of the capital columns and approximately 60% completion of the butt welds.

Additional Comments 3: Total man hours for day 2 of operations is 10x3=30, which includes 2 welders and 1 supervisor. The work included completion of the butt welds, fit-up of the cap beam and approximately 80% completion of the 1" groove weld at the T-joint.

Additional Comments 4: Total man hours for day 3 of operations is 5x3=15, which includes 2 welders and 1 supervisor. The work included completion of the groove welds and the 3/8" reinforcing fillet welds at the T-joint.

Figure A 78 Phase 2 Test 3 QC Report

MISTRAS Services Division
A World of NDT Solutions

CERTIFICATE OF ULTRASONIC INSPECTION

Date: 4-5-11 Page: 1 of 1
PO Number: Verbal-Dwayne Job Number: N11-00451

Customer: Fabrication Associates Procedure: 100-UT-001 Rev. 2
Location: Charlotte, NC Code / Specification: ASME VIII
Project / System: W11-273 Acceptance: ASME VIII
Part Number: Description: 1.250 x 38.500" long seams

Inspection Method:

☐ Immersion	☐ Longitudinal wave	☐ Surface wave	Presentation: ☒ A-scan ☐ B-scan ☐ C-scan
☒ Contact	☒ Shear wave	☐ Thickness Measure	☐ Other:

Equipment:

Scope(s)			Transducer(s)			Wedge(s)
Model	Serial No.	Cal. Due Date	Frequency	Size	Serial No.	Angle
USN52R	OOP53X	05-20-11	2.25 MHz	5/8" x 3/4"	6473	45°
			2.25 MHz	5/8" x 3/4"	6473	60°
			2.25 MHz	5/8" x 3/4"	6473	70°

Calibration Standard:

Type:	ASME V	Serial No.:	503-014	Description:	1.5" Flat Block	Temp.:	60°F
Scanning Equipment:	N/A	**Couplant:**	Type:	Sonagel	Batch No.:	7724	

Setup Data:

Reflector	Metal Travel	Amplitude	Gate Level	DAC %	Other
3% Notch	5.500"	80%	40%	N/A	N/A

Scanning Speed (in/sec): 6"/Sec. Max.

Additional Information:

Test Results: Quantity Inspected: 4 Quantity Accepted: 4 Quantity Rejected: 0

4 ea. 1.250 x 38.500

Performed ultrasonic shear wave inspection on the above referenced final welds – No relevant indications at time of inspection.

☐ Attached Documentation:

Technician, Level & Date: 4-5-11 Michael A. Shearer Level II	Customer	Management Review

This report is not to be construed as a guaranty or warranty of the condition of the materials tested. Mistras Services is not liable for any misinterpretation of results or conditions, or for any claims or losses attributable to performance of a test. These services are rendered without any warranty. Any liability is limited to the amount paid for the services at issue. All orders are subject to Mistras Services Standard Terms and Conditions of Sale, which are available upon request.

Southeast Regional Office: 1721 Williams Road, Monroe NC 28110 Ph. (704) 291-2360 Fax. (704) 291-9536 Form 503-UT-001 Rev. 1, 06/04/2009

A World of NDT Solutions

Figure A 79 Phase 2 Test 3 Fabricated Column Capitals UT Report

GeoTechnologies, Inc.

3200 Wellington Court, Suite 108
Raleigh, North Carolina 27616
Phone: 919-954-1514 • Fax 919-954-1428

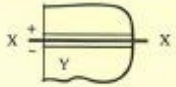

REPORT OF ULTRASONIC TESTING OF WELDS

Project Name: N.C. STATE
Project Number: STEEL BENT PHASE II TEST III
Weld Identification: SEE BELOW
Material Thickness: .625 .937
Weld Joint AWS: PRE QUALIFIED
Welding Process:: SMAW
Quality Requirements - Section No.:
Remarks: FULL PENETRATION WELDS

					Decibels				Discontinuity						
Line Number	Piece Number	Transducer Angle	From Face	Leg*	Indication Level a	Reference Level b	Attenuation Factor c	Indication Rating d	Length	Angular distance (sound path)	Depth from "A" Surface	Distance From X	Distance From Y	Discontinuity Elevation	Remarks
1	1	70°	A	1+2		60								ACCEPT	
2	2	↓	↓	↓		↓								↓	
3	3	↓	↓	↓		↓								↓	
4	4	↓	↓	↓		↓								↓	
5															
6															
7															
8															
9															

We, the undersigned, certify that the statements in this record are correct and that the weids were prepared and tested in accordance with the requirements of 6C of AWS D1.1 (2000 edition) Structural Welding Code.
year

Test Date: 5-23-11

Inspected by: [illegible] CWI 07091401

Manufacturer or Contractor:

Authorized by:

Date:

Figure A 80 Phase 2 Test 3 UT Inspection Report

Procedure 508 Exhibit 1- Final Inspection List

Job # 25580 Date 4-24-12 Inspector RBJ Initials Indicate 100% Weld Inspection/Piece

Emp. #	Piece Mark	Sequence	Quantity	WPS/PH	Rework Fillets	Rework Groove Weld	Rework Joint	Stop Error
1106	1131	1	2					
SUB-AA	(2103)							
2098								
2025	1P1	1	4					
SW	1C1	1	4					

CODES REWORK
DD = REPAIR BY ADDITIONAL WELD METAL
DU = GOUGE AND THEN REWELD
S= MISSED WELDS

CODES POOR FITUP
JOI = POOR JOINT GEOMETRY
GAP = GAPS AT FILLET WELDS
SEQ. = Weld Seq. Error

CODES-NCR
IMU-Incorrect Material
IWE-Incorrect Electrode

Figure A 81 Phase 2 Test 8, 9 Shop Weld UT Inspection Report (1)

SteelFab, Inc. — Ultrasonic Inspection Report

Job Name: Alaska D.O.T. Phase 2 — Job Number: 25580

Welding Process: FCAW (SAW) SMAW — Specifications: (AWS D1.1)

Type Material: (Carbon) Other — Section or Shape: Plate (Shape) Pipe

Piece Mark	Weld Number	Detail Mk	Face	Date	Transducer Angle	Defect No	A Reference Level	B Defect Level	C Atten. Factor	D Defect Rating	Leg	Length of Defect	Surface Distance	Length of Sound Patl	Depth From Surface	X Distance	Y Distance	Thickness	Type of Joint	Accepted	Rejected	Comments
							Decibels				Inches											
1B1	1	Flange 1	A	4/19/12	70°	1	42	49	0	+7	1	6"	.8"	.9"	.312	0	0	.5"	B-U2a-GF		✓	Welder # 2098
				4/19/12	70°	n/a	42	n/a	←							→	n/a	.5"	B-U2a-GF	✓		
	2	Flange 2	A	4/19/12	70°	n/a	42	n/a	←							→	n/a	.5"	B-U2a-GF	✓		
1B1	1	Flange 1	A	4/19/12	70°	n/a	42	n/a	←							→	n/a	.5"	B-U2a-GF	✓		
	2	Flange 2	A	4/19/12	70°	n/a	42	n/a	←							→	n/a	.5"	B-U2a-GF	✓		

Inspected By Craig Jeffers Level II

Figure A 82 Phase 2 Test 8, 9 Shop Weld UT Inspection Report (2)

APPENDIX 3: Truss Style Steel Pier Documentation

DEAD LOAD										
ITEM	WT/AREA (lbs/ft^2)	WT/LENGTH (lb/ft)	WT/EA (lb)	LENGTH (ft)	WIDTH (ft)	NUMBER (ea)	WEIGHT (lbs)	F (LBS)	L (FT)	M (FT.LB)
Decking:										
Open Grate	20			60	23.667		28400.4			
Concrete	46.6			60	4		11,184			
Girders:										
W40x167		167.00		60		5	50,100			
Diaphragms:										
W24x55		55.00		5.7		16	5,016			
Traffic Rail:										
Rail HSS 3x4x1/4		10.51		60		2	1,261			
Rail HSS 3x4x1/4		10.51		1.5		2	32			
Rail HSS 3x4x1/4		10.51		3			32			
Hand Rail:										
W6x20x2 rail post		20.00		2.58		10	516			
1.9" dia std wt. pipe		3.65		60		2	438			
1.9" dia std wt. pipe		3.65		2.5			9			
1.9" dia std wt. pipe		3.65		6			22			
1 1/2" dia extra strong pipe sleeve		3.63		0.7		2	5			
Exterior Rail:										
Post HSS3x3x1/4		8.81		4.75		10	418			
HSS 3x2x1/4		7.11		60		1	427			
HSS 3x2x1/4		7.11		1.18		2	17			
9 Guage Fence Fabric			4.2	60			252			
							98,129			
Welds, fasteners, etc 10%							9,813			
						DL (lbs) =	107,941			

Figure A 83 Typical Truss Style Pier Dead Loads (Provided by AKDOT)

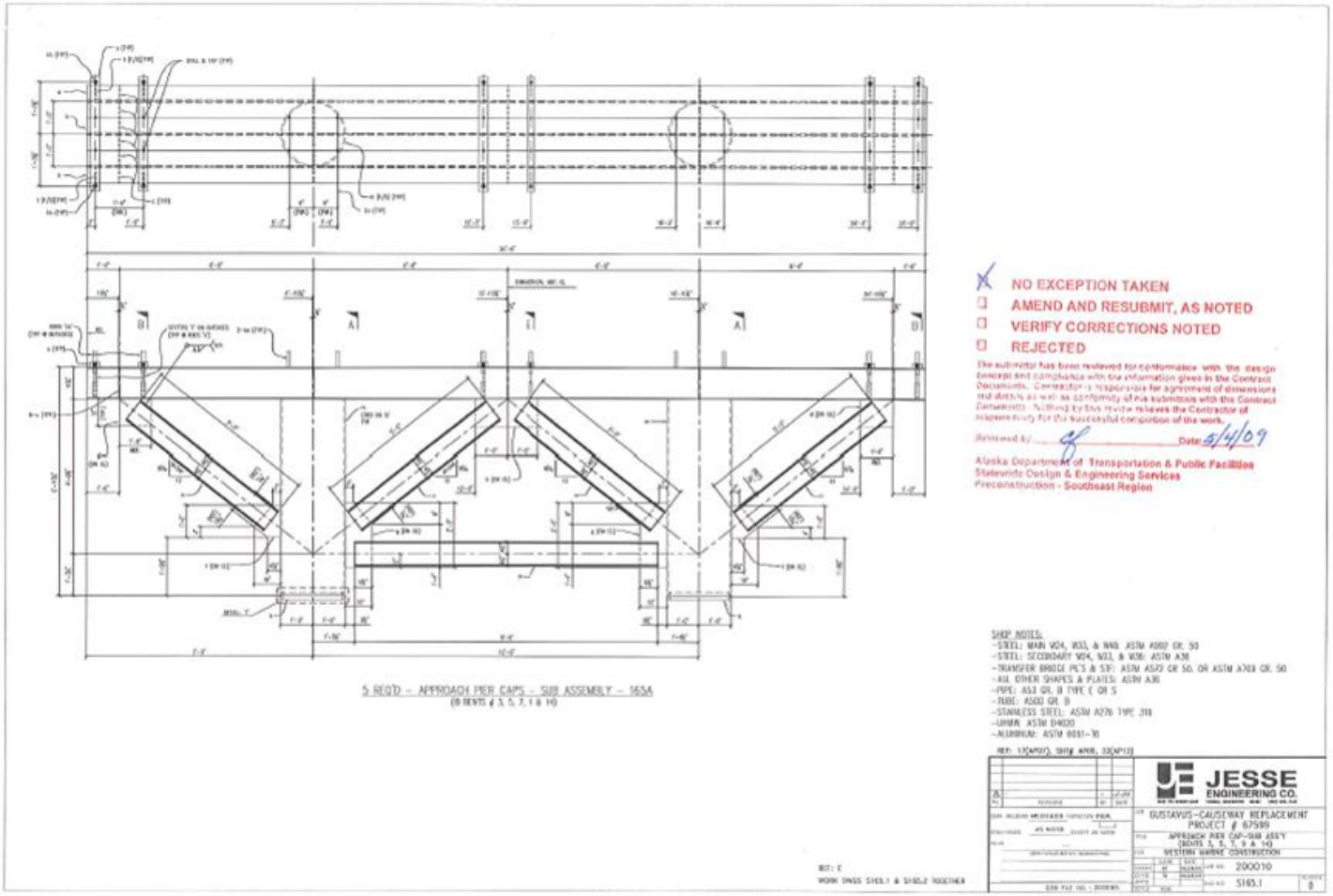

Figure A 84 Gustavus-Causeway Replacement Project Shop Drawings (Provided by AKDOT)

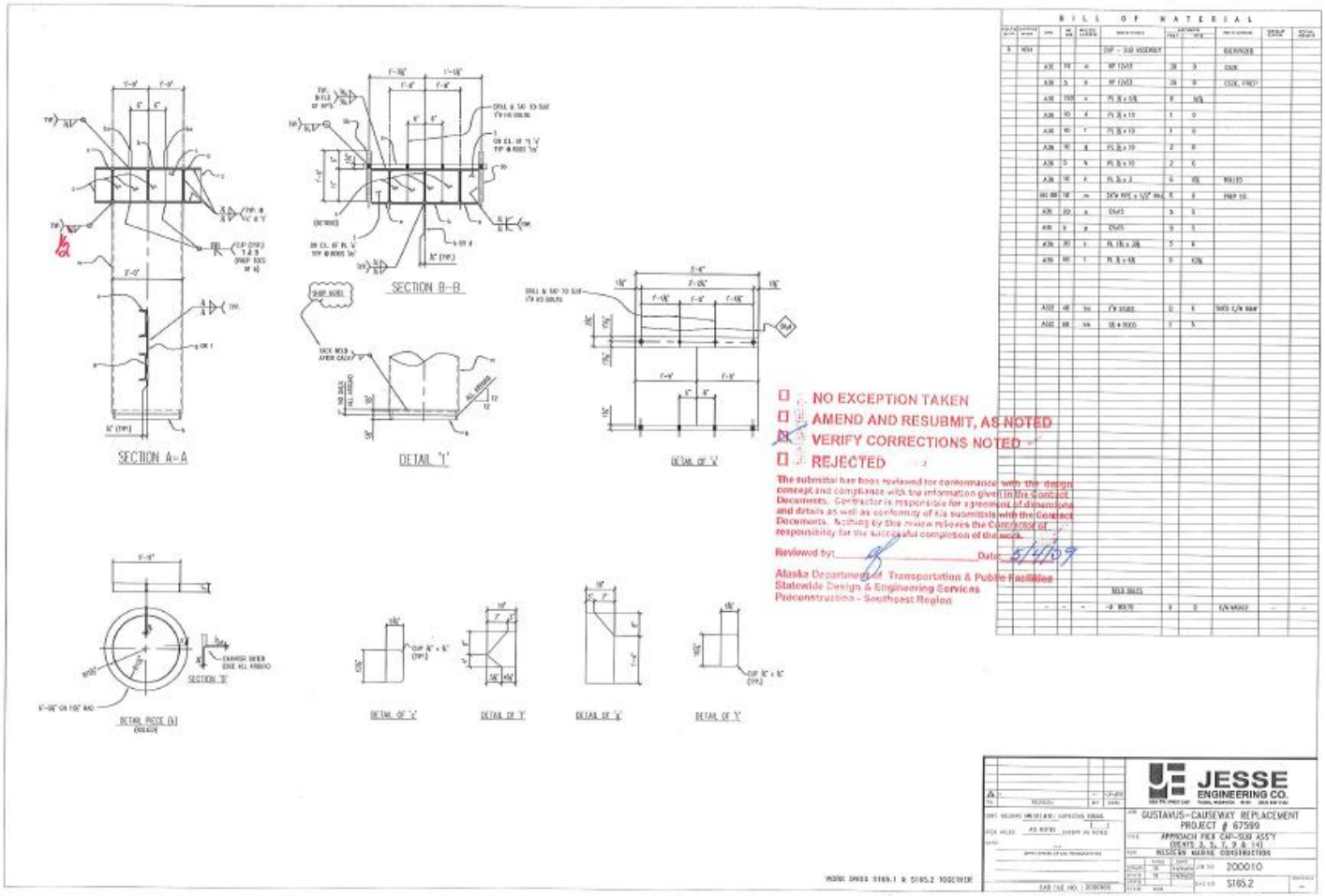

Figure A 85 Gustavus-Causeway Replacement Project Shop Drawings (Provided by AKDOT)

SteelFab, Inc. — Ultrasonic Inspection Report

Job Name: AKDOT Phase 2 Specimen 7 — Job Number: 25580

Welding Process: FCAW SAW SMAW — Specifications: AWS D1.1

Type Material: Carbon Other — Section or Shape: Plate Shape Pipe

Piece Mark	Weld Number	Detail Mk	Face	Date	Transducer Angle	Defect No	Reference Level (A)	Defect Level (B)	Atten. Factor (C)	Defect Rating (D)	Leg	Length of Defect	Surface Distance	Length of Sound Patl	Depth From Surface	X Distance	Y Distance	Thickness	Type of Joint	Accepted	Rejected	Comments
							Decibels				Inches											
1100181	1A	M3@1100181	A	2-17-12	70		55											7/8	B-U2A-GF	✓		1956 & 2103 @ 4W
	1B	M4@M3				1	55	58	0	+3	1	3 1/4	1.2	1.3	.47						X	
						2	55	57	0	+2	1	11 1/2	1.3	1.4	.48						X	
						3	55	60	0	+5	1	12"	1.3	1.4	.49						X	
						4	55	60	0	+5	1	4 3/8	1.1	1.2	.42						X	
						5	55	56	0	+1	1	11 3/4	1.1	1.2	.42						X	
						6	55	58	0	+3	1	3 1/2	1.2	1.3	.44						X	
						7	55	57	0	+2	1	6 1/2	1.21	1.29	.44						X	
						8	55	57	0	+2	1	2	1.20	1.28	.43						X	
						9	55	57	0	+2	1	5"	1.1	1.2	.42						X	
						10	55	57	0	+2	1	7 1/4	1.10	1.17	.40						X	
						11	55	59	0	+4	1	2 1/4	1.3	1.4	.46						X	
						12	55	60	0	+5	1	2 1/4	1.1	1.2	.41						X	
																						All UT Repairs DK
	2A	M3@1100181																		✓		
	2B	M4@M3																		✓		

Inspected By Robert Freeman Level II

Figure A 86 Truss Pier Cap Beam UT Report

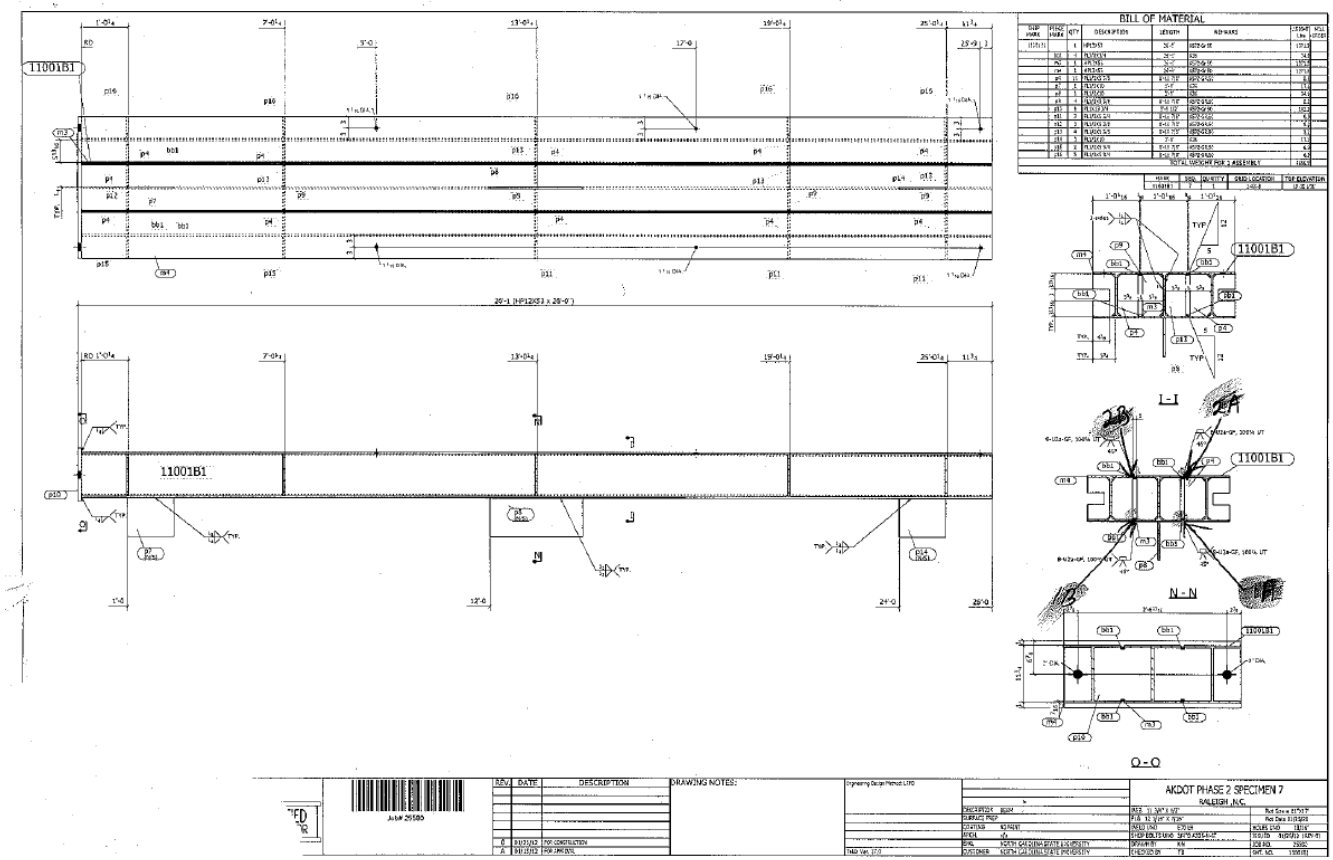

Figure A 87 Truss Pier Cap Beam UT Report (Continued)

ISO 9001:2000 CERTIFIED

CUSTOMER NAME: SAGINAW PIPE INCORPORATED

Customer Order Number 35049

MFG Order Number S108488

Date: 09/SEP/2008

HEAT	C	MN	P	S	CB	SI	TI	CU	NI	MO	CR	V	AL	B	N	C.E.	Coil Pipe
13340	* LINE 1						EDITION REFERENCE 4				YEAR 2008		Yield Strength by Strap				
H=	0.070	1.060	0.007	0.005	0.046	0.181	0.018	0.030	0.010	0.010	0.030	0.003	0.039	.0002	.0059	0.258	0076
P=	0.066	1.024	0.009	0.006	0.043	0.171	0.013	0.001	0.012	0.011	0.037	0.001	0.032	.0008	.0000	0.247	/
M=Weld Ten.		00.0 ksi	Ten.		00.0 ksi		Yield	00.0 ksi		%EL 00.0	RB		Hydro:		Psi	RUN:	44-8
Y/T RATIO = 0.00																	
13392	* LINE 1						EDITION REFERENCE 4				YEAR 2008		Yield Strength by Strap				
H=	0.060	1.110	0.012	0.007	0.046	0.190	0.017	0.040	0.010	0.010	0.040	0.004	0.036	.0002	.0054	0.259	0005
P=	0.065	1.095	0.016	0.008	0.039	0.178	0.014	0.042	0.014	0.006	0.041	0.009	0.025	.0000	.0000	0.262	07/16
M=Weld Ten.		84.5 ksi	Ten.		86.5 ksi		Yield	66.0 ksi		%EL 37.5	RB		Hydro:		Psi	RUN:	44-8
Y/T RATIO = 0.76																	
13392	* LINE 1						EDITION REFERENCE 4				YEAR 2008		Yield Strength by Strap				
H=	0.060	1.110	0.012	0.007	0.046	0.190	0.017	0.040	0.010	0.010	0.040	0.004	0.036	.0002	.0054	0.259	0006
P=	0.055	1.102	0.016	0.006	0.040	0.177	0.014	0.050	0.015	0.006	0.042	0.009	0.030	.0000	.0000	0.254	/
M=Weld Ten.		00.0 ksi	Ten.		00.0 ksi		Yield	00.0 ksi		%EL 00.0	RB		Hydro:		Psi	RUN:	44-8
Y/T RATIO = 0.00																	
13394	* LINE 1						EDITION REFERENCE 4				YEAR 2008		Yield Strength by Strap				
H=	0.060	1.090	0.014	0.004	0.046	0.235	0.018	0.030	0.010	0.010	0.030	0.004	0.037	.0002	.0035	0.253	0026
P=	0.057	1.079	0.015	0.006	0.043	0.191	0.014	0.043	0.016	0.007	0.038	0.010	0.031	.0000	.0000	0.252	08/16
M=Weld Ten.		85.5 ksi	Ten.		88.0 ksi		Yield	69.5 ksi		%EL 36.0	RB		Hydro:		Psi	RUN:	44-8
Y/T RATIO = 0.79																	

PAGE 6
Continued

Issue No.: 6 Form Date: 10/18/2004 QD-AW3F05

SV

Figure A 88 Truss Pier 24x0.500 Pile Material Mill Certifications

ISO 9001:2000 CERTIFIED

CUSTOMER NAME: SAGINAW PIPE INCORPORATED

Customer Order Number 35049

Date: 09/SEP/2008
MFG Order Number S108488

HEAT	C	MN	P	S	CB	SI	TI	CU	NI	MO	CR	V	AL	B	N	C.E.	Coil Pipe
13394	* LINE 1						EDITION REFERENCE 4				YEAR 2008		Yield Strength by Strap				
H=	0.060	1.090	0.014	0.004	0.046	0.235	0.018	0.030	0.010	0.010	0.030	0.004	0.037	.0002	.0035	0.253	0027
P=	0.059	1.083	0.014	0.006	0.042	0.192	0.014	0.058	0.017	0.006	0.037	0.009	0.030	.0000	.0000	0.255	/
M=Weld Ten.		00.0 ksi		Ten.		00.0 ksi	Yield	00.0 ksi		%EL 00.0	RB		Hydro:		Psi	RUN:	44-8
Y/T RATIO = 0.00																	
25236	* LINE 1						EDITION REFERENCE 4				YEAR 2008		Yield Strength by Strap				
H=	0.060	1.050	0.012	0.005	0.045	0.184	0.017	0.030	0.010	0.010	0.030	0.003	0.027	.0002	.0050	0.246	0091
P=	0.061	1.038	0.013	0.006	0.044	0.173	0.014	0.037	0.016	0.008	0.033	0.002	0.023	.0000	.0000	0.246	08/16
M=Weld Ten.		84.5 ksi		Ten.		85.0 ksi	Yield	71.5 ksi		%EL 38.0	RB		Hydro:		Psi	RUN:	44-8
Y/T RATIO = 0.84																	
25236	* LINE 1						EDITION REFERENCE 4				YEAR 2008		Yield Strength by Strap				
H=	0.060	1.050	0.012	0.005	0.045	0.184	0.017	0.030	0.010	0.010	0.030	0.003	0.027	.0002	.0050	0.246	0092
P=	0.061	1.028	0.012	0.006	0.042	0.173	0.015	0.038	0.016	0.007	0.034	0.002	0.022	.0000	.0000	0.245	/
M=Weld Ten.		00.0 ksi		Ten.		00.0 ksi	Yield	00.0 ksi		%EL 00.0	RB		Hydro:		Psi	RUN:	44-8
Y/T RATIO = 0.00																	
13381	* LINE 1						EDITION REFERENCE 4				YEAR 2008		Yield Strength by Strap				
H=	0.070	1.070	0.012	0.004	0.045	0.184	0.019	0.020	0.010	0.010	0.030	0.003	0.040	.0002	.0032	0.259	0054
P=	0.064	1.052	0.014	0.006	0.040	0.174	0.015	0.022	0.010	0.006	0.037	0.007	0.034	.0005	.0000	0.251	08/16
M=Weld Ten.		85.5 ksi		Ten.		86.5 ksi	Yield	70.5 ksi		%EL 36.0	RB		Hydro:		Psi	RUN:	44-8
Y/T RATIO = 0.82																	

PAGE 7
Continued

Issue No.: 6 Form Date: 10/18/2004 QD-AW3F05

SL

Figure A 89 Truss Pier 24x0.500 Pile Material Mill Certifications (Continued)

ISO 9001:2000 CERTIFIED

CUSTOMER NAME: SAGINAW PIPE INCORPORATED

Date: 09/SEP/2008

Customer Order Number	MFG Order Number
35049	S108488

Legend Analyses:

A-Z - Additional Testing	R - Retest	Hydrostatic Test:	OK
H - Heat Analysis	L - Longitudinal	Flattening Test:	OK
P - Product Analysis	T - Transitional		
M- Mechanical Properties	W - Weld Line		

SL

EDITION REFERENCE 1: API 5L 41ST EDITION 4/1/1995
EDITION REFERENCE 2: API 5L 42ND EDITION 7/1/2000
EDITION REFERENCE 3: API 5L 43RD EDITION 10/4/2004
EDITION REFERENCE 4: ASTM/ASME ANNUAL BOOK OF STANDARDS SECT.1, VOL 01.01

* Manufactured and Melted in the USA.

We hereby certify that the above figures are correct as contained in the records of this company, and th the pipe were manufactured, tested and inspected in compliance with the Latest edition of the applicable specification, in Birmingham, Alabama, U.S.A.

Noel A. Gordon

Noel A. Gordon
Manager of Quality Assurance - Steel Pipe

PAGE 10
End Of Report

Issue No.: 6 Form Date: 10/18/2004 QD-AW3F055

Figure A 90 Truss Pier 24x0.500 Pile Material Mill Certifications (Continued)

DATE	2/01/12
CUSTOMER NO.	3670
REQUEST ID	163759

NUCOR-YAMATO STEEL CO.
P.O. BOX 1228 ● BLYTHEVILLE,AR 72316

CERTIFIED MILL TEST REPORT
100% MELTED AND MANUFACTURED IN U.S.A.
All shapes produced by Nucor-Yamato Steel are cast and rolled to a fully killed and fine grain practice.
(Length May Not Be Traceable to Original Mill Cut)

SHIP TO:
SKYLINE STEEL
CAHABA PLACE, SUITE 200
4908 CAHABA RIVER ROAD
BIRMINGHAM, AL 35243

SPECIFICATIONS:
ASTM A572/A572M [illegible]
ASTM A709/A709M-[illegible]
ASTM A6/A6M-09

SOLD TO:
SKYLINE STEEL GEORGIA OFFICE
3250 PEACHTREE INDUS BLVD
SUITE 107
DULUTH, GA 30096

ITEM #	ITEM DESCRIPTION	QTY	HEAT #	MECHANICAL PROPERTIES: YIELD TO TENSILE RATIO	YIELD STRENGTH PSI / MPa	TENSILE STRENGTH PSI / MPa	ELONG % / %	CHARPY IMPACT TEMP °F / °C	CHARPY IMPACT ENERGY FT-LBS / JOULES	CHEMICAL PROPERTIES: C	Mn	P	S	Si	Cu	Ni	Cr	Mo / Sn	V / Pcm	Cb	CE / CI
1	HP12 - [illegible]	1	367606	.73	56000	77000	23			.16	.80	.017	.035	.15	.31	.12	[illegible]	[illegible]	.00	.014	[illegible]
	30'			.73	55000	75000	23											[illegible]			
	HP310x [illegible]				386	531	23														
	9.144 M				379	517	23														

CERTS RECEIVED BY
SL

CARBON EQUIVALENT: CE = CE(IIW) = C + Mn/6 + (Cr+Mo+V)/5 + (Ni+Cu)/15

Corrosion Index: CI=26.01(%Cu)+3.88(%Ni)+1.20(%Cr)+1.49(%Si)+17.28(%P)-7.29(%Cu)(%Ni)-9.10(%Ni)(%P)-33.39(%Cu)^2

ELONGATION BASED ON 8.00 INCH GAUGE LENGTH

I hereby certify that the contents of this report are accurate and correct. All test results and operations performed by this material manufacturer are in compliance with the requirements of the material specifications listed in the Specifications Block above.

Gary Lennell
QUALITY ASSURANCE

CUSTOMER COPY

STATE OF ARKANSAS COUNTY OF MISSISSIPPI
SWORN TO AND SUBSCRIBED BEFORE ME THIS 1 Day of 02/12
Charlene Wallis NOTARY PUBLIC
MY COMMISSION EXPIRES 10/21/2013
CHARLENE WALLIS MISSISSIPPI CO. ARKANSAS

Figure A 91. Truss Pier HP12x53 Material Mill Certifications

DATE	2/01/12
[redacted]	
CUSTOMER NO.	3670
REQUEST ID	163760

NUCOR-YAMATO STEEL CO.
P.O. BOX 1228 ● BLYTHEVILLE,AR 72316

CERTIFIED MILL TEST REPORT
100% MELTED AND MANUFACTURED IN U.S.A.
All shapes produced by Nucor-Yamato Steel are cast and rolled to a fully killed and fine grain practice.
(Length May Not Be Traceable to Original Mill Cut)

SHIP TO
SKYLINE STEEL
CAHABA PLACE, SUITE 200
4908 CAHABA RIVER ROAD
BIRMINGHAM, AL 35243

SPECIFICATIONS
ASTM A572/A572M [illegible]
ASTM A709/A709M [illegible]
ASTM A6/A6M-09

SOLD TO
SKYLINE STEEL GEORGIA OFFICE
3250 PEACHTREE INDUS BLVD
SUITE 107
DULUTH, GA 30096

ITEM #	ITEM DESCRIPTION	QTY	HEAT #	MECHANICAL PROPERTIES: YIELD TO TENSILE RATIO	YIELD STRENGTH PSI / MPa	TENSILE STRENGTH PSI / MPa	ELONG % / %	CHARPY IMPACT TEMP °F / °C	CHARPY IMPACT ENERGY FT-LBS / JOULES	CHEMICAL PROPERTIES: C	Mn	P	S	Si	Cu	Ni	Cr	Mo	V	Cb	CE
																		Sn	Pcm		CI
1	HP12 - 53.0	2	365733	.72	52000	72000	27			.08	1.13	.017	.032	.28	.31	.15	[illegible]	.04	.00	.016	[illegible]
	30'			.72	52000	72000	25											.01	.18		
	HP310x 79.0				359	496	27														
	9.144 M				359	496	25														

CERTS RECEIVED BY
SK

CARBON EQUIVALENT: CE = CE(IIW) = C + Mn/6 + (Cr+Mo+V)/5 + (Ni+Cu)/15 | Corrosion Index: CI=26.01(%Cu)+3.88(%Ni)+1.20(%Cr)+1.49(%Si)+17.28(%P)-7.29(%Cu)(%Ni)-9.10(%Ni)(%P)-33.39(%Cu)²

ELONGATION BASED ON 8.00 INCH GAUGE LENGTH

I hereby certify that the contents of this report are accurate and correct. All test results and operations performed by this material manufacturer are in compliance with the requirements of the material specifications listed in the Specifications Block above.

QUALITY ASSURANCE

CUSTOMER COPY

STATE OF ARKANSAS COUNTY OF MISSISSIPPI
SWORN TO AND SUBSCRIBED BEFORE ME THIS 1 Day of 02/12
Charlene Wallis NOTARY PUBLIC
MY COMMISSION EXPIRES 10/21/2019

CHARLENE WALLIS
NOTARY PUBLIC
MISSISSIPPI CO. ARKANSAS

Figure A 92. Test 7 HP12x53 Material Mill Certifications (Continued)

Metrolina Steel

AWS WELDER OR WELDING OPERATOR QUALIFICATION TEST (WQ)

(4C, AWS D1.1-2008, STRUCTURAL WELDING CODE – STEEL)

Welder Name V. Menendez **SSN** See MS Human Resources **Emp. No:** 8811
Welding Procedure Spec. No.: WPS-1 B1/2a **Rev.:** 0 **Date:** 2000
Welding Process: Shielded Manual Arc Welding (SMAW) **Type:** Manual

Variables	Actual Values Used	Qualification Range
Backing Material/Type	Yes – Group I	With backing or backgouge 2nd side
Base Material Specification		
Group No.	A572-50 Group II	Group I, II, III AWS D1.1 with WPS
Thickness Table 4.9		
Groove	3/8"	1/8" to 3/4"
Fillet	NA	1/8" to unlimited"
Diameter		
Groove	NA	Over 24" Diameter
Fillet	NA	Unlimited
Filler Metal		
Spec. No.	A5.1	A5.1, A5.5
Class	E7018	All 5.1 & 5.5 as E70XX or E60XX
F No.	F4	F1 thru F4
Deposited Weld Metal Thickness		
Groove	3/8"	1/8" to 3/4"
Fillet	NA	1/8" to unlimited
Weld Position		
Orientation	3G & 4G	All plate PJP,CJP&Fillet-See below for more
Weld Progression	Uphill	Vertical uphill
Gas Type		
Shielding	NA	NA
Backing	NA	NA
Electrical Characteristics		
Current	Direct	Direct
Polarity	Reverse	Reverse

Additional qualification ranges: Pipe-all PJP, CJP>24inch OD and all Fillet>30 degree, Pipe TYK PJP>24inch OD and greater than 30 degree. Box Tubing (HSS)-all CJP, PJP and all Fillet> 30 degree, PJP TYK> 30 degree slope. Plate Fillet > 30 degree slope.

GROOVE WELD TEST RESULTS

Visual Passed **Radiographic Results** NA

Guided Bend Test

Type and Figure No.	Results	Type and Figure No.	Results
(V) 5-18-10-1 Face - 4.12	Accept	(OH) 5-18-10-3 Root - 4.12	Accept
(V) 5-18-10-2 Root - 4.12	Accept	(OH) 5-18-10-4 Face – 4.12	Accept

Witnessed by: Reported as Barry Mitchell, Metrolina Steel
Test Conducted by: SteelFab , Inc. Bruce L Lanier
Inspector: B L Lanier SCWI #04000028 Date: 5-18-2010

We certify that the statements in this record are correct and that the test weld(s) were prepared, welded and tested in accordance with the requirements of Section 4, ANSI/AWS D1.1-2008.

Organization: Metrolina Steel
By:
Date:

Qualification Tests: SteelFab, Inc
By: Bruce L Lanier
Date: 5-18-2010

Page 1 of 1

Figure A 93 Truss Pier Welder Certifications

Metrolina Steel

AWS WELDER OR WELDING OPERATOR QUALIFICATION TEST (WQ)

(4C, AWS D1.1-2008, STRUCTURAL WELDING CODE – STEEL)

Welder Name R. Ibarra **SSN** See MS Human Resources **Emp. No:** 2191
Welding Procedure Spec. No.: WPS-1 BU2a **Rev.:** 0 **Date:** 2000
Welding Process: Shielded Manual Arc Welding (SMAW) **Type:** Manual

Variables	Actual Values Used	Qualification Range
Backing Material/Type	Yes – Group I	With backing or backgouge 2nd side
Base Material Specification		
Group No.	A572-50 Group II	Group I, II, III AWS D1.1 with WPS
Thickness Table 4.9		
Groove	3/8"	1/8" to 3/4"
Fillet	NA	1/8" to unlimited"
Diameter		
Groove	NA	Over 24" Diameter
Fillet	NA	Unlimited
Filler Metal		
Spec. No.	A5.1	A5.1, A5.5
Class	E7018	All 5.1 & 5.5 as E70XX or E60XX
F No.	F4	F1 thru F4
Deposited Weld Metal Thickness		
Groove	3/8"	1/8" to 3/4"
Fillet	NA	1/8" to unlimited
Weld Position		
Orientation	3G & 4G	All plate PJP,CJP&Fillet-See below for more
Weld Progression	Uphill	Vertical uphill
Gas Type		
Shielding	NA	NA
Backing	NA	NA
Electrical Characteristics		
Current	Direct	Direct
Polarity	Reverse	Reverse

Additional qualification ranges: Pipe-all PJP, CJP>24inch OD and all Fillet>30 degree, Pipe TYK PJP>24inch OD and greater than 30 degree. Box Tubing (HSS)-all CJP, PJP and all Fillet> 30 degree, PJP TYK> 30 degree slope. Plate Fillet > 30 degree slope.

GROOVE WELD TEST RESULTS

Visual Passed **Radiographic Results** NA

Guided Bend Test

Type and Figure No.	Results	Type and Figure No.	Results
(V) 5-18-10-5 Face - 4.12	Accept	(OH) 5-18-10-7 Root - 4.12	Accept
(V) 5-18-10-6 Root - 4.12	Accept	(OH) 5-18-10-8 Face – 4.12	Accept

Witnessed by: Reported as Barry Mitchell, Metrolina Steel
Test Conducted by: SteelFab , Inc. Bruce L Lanier
Inspector: B L Lanier SCWI #04090028 Date: 5-18- 2010

We certify that the statements in this record are correct and that the test weld(s) were prepared, welded and tested in accordance with the requirements of Section 4, ANSI/AWS D1.1-2008.

Organization: Metrolina Steel
By:
Date:

Qualification Tests: SteelFab, Inc
By: Bruce L Lanier
Date: 5-18-2010

Page 1 of 1

Figure A 94 Truss Pier Welder Certification (Continued)

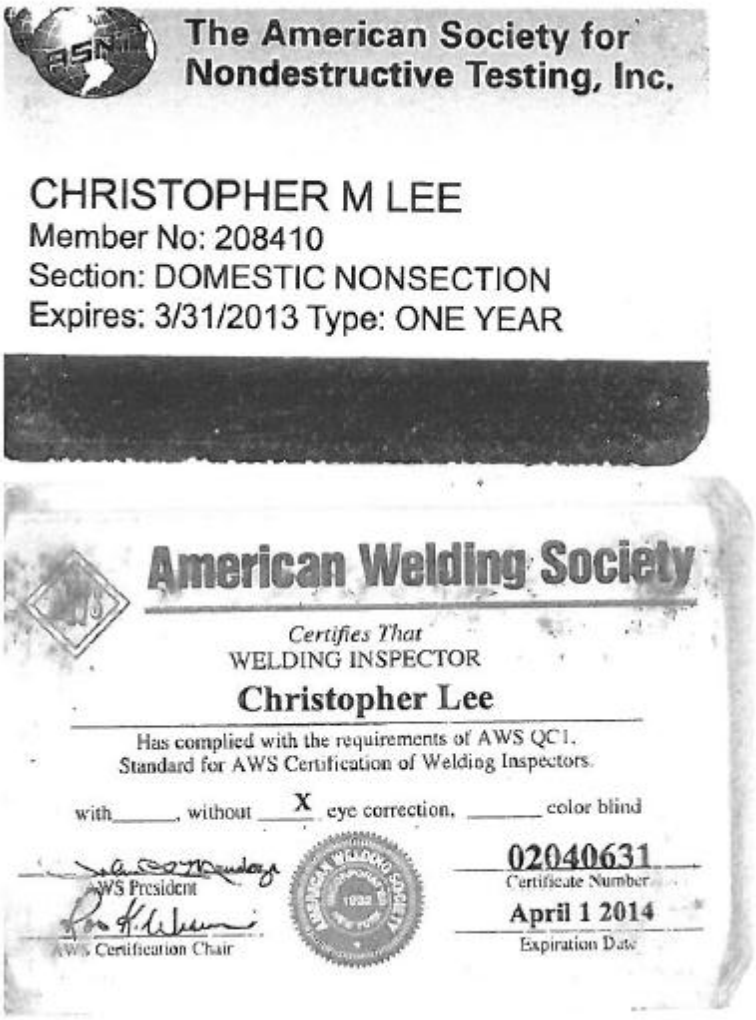

The American Society for Nondestructive Testing, Inc.

CHRISTOPHER M LEE
Member No: 208410
Section: DOMESTIC NONSECTION
Expires: 3/31/2013 Type: ONE YEAR

[redacted]

American Welding Society

Certifies That
WELDING INSPECTOR
Christopher Lee

Has complied with the requirements of AWS QC1,
Standard for AWS Certification of Welding Inspectors.

with_____, without ___X___ eye correction, _____ color blind

AWS President

AWS Certification Chair

02040631
Certificate Number

April 1 2014
Expiration Date

Figure A 95 Truss Pier Weld Inspector Certification

North Carolina Department of Transportation
Division of Highways
Materials and Tests Unit (Steel Section)
770A Park Centre Drive
Kernersville, NC 27284
Office Phone: 336-993-2300
Office Fax: 336-993-8740

Field Inspection Report

05/15-05/16/2012

ontract / Project Number:	N/A	**Resident / Project Engineer:**	Steven Fulmer
County:	Wake	**Contractor:**	Metrolina Steel
Division:	N/A	**M & T Inspector:**	Chris M. Lee
Project Location:	North Carolina State University Structural Laboratory		

Reason for Inspection:

- ☐ Material Inspection
- ☒ Welding Inspection
- ☐ Field Audit
- ☐ Other (explain):

Inspection Start Time: 0830
Inspection End Time: 1800

Personnel Present During Inspection (if any)	Company	Title
Steven Fulmer	NCSU	Graduate Student

Inspection Details:

05/15/2012-Mr. Steven Fulmer from NCSU requested fillet weld inspection and testing of a pier structure that will be destructively tested for Alaska Department of Transportation. Performed visual inspection on the ½" fillet weld joining the pipe pile to cap beams, welding was satisfactory.

05/16/2012-Continued visual inspection and testing of fillet welds for Mr. Steven Fulmer of NCSU. Performed visual inspection of ½" fillet weld joining pipe pile to cap beam. Minor grinding required removing sharp edges. Additional welding required assuring a smooth transition across the face of multiple pass welding application. Welding was in progress on interior bracing. Fillet welding joining pipe piles to cap beam had minor repairs, but was satisfactory. The interior bracing had excessive undercut in several locations. Left side diaphragm had a bead that appeared to be welded with "down-hill" progression. This weld needed removal. Welding on the interior bracing exceeded specified weld sizes at several locations. The weld sizes varied between approximately 5/16" fillets up to 5/8" fillet weld. Interior bracing with excessive undercut had additional weld passes which increased fillet weld sizes. Visual inspection of interior bracing after weld repairs was satisfactory. Several locations needed grinding to remove "Arc Striking". Magnetic Particle Testing was performed to assure weld soundness. Please see the MT report for results. This concludes the inspection and testing.

Figure A 96. Truss Pier Visual Weld Inspection Report

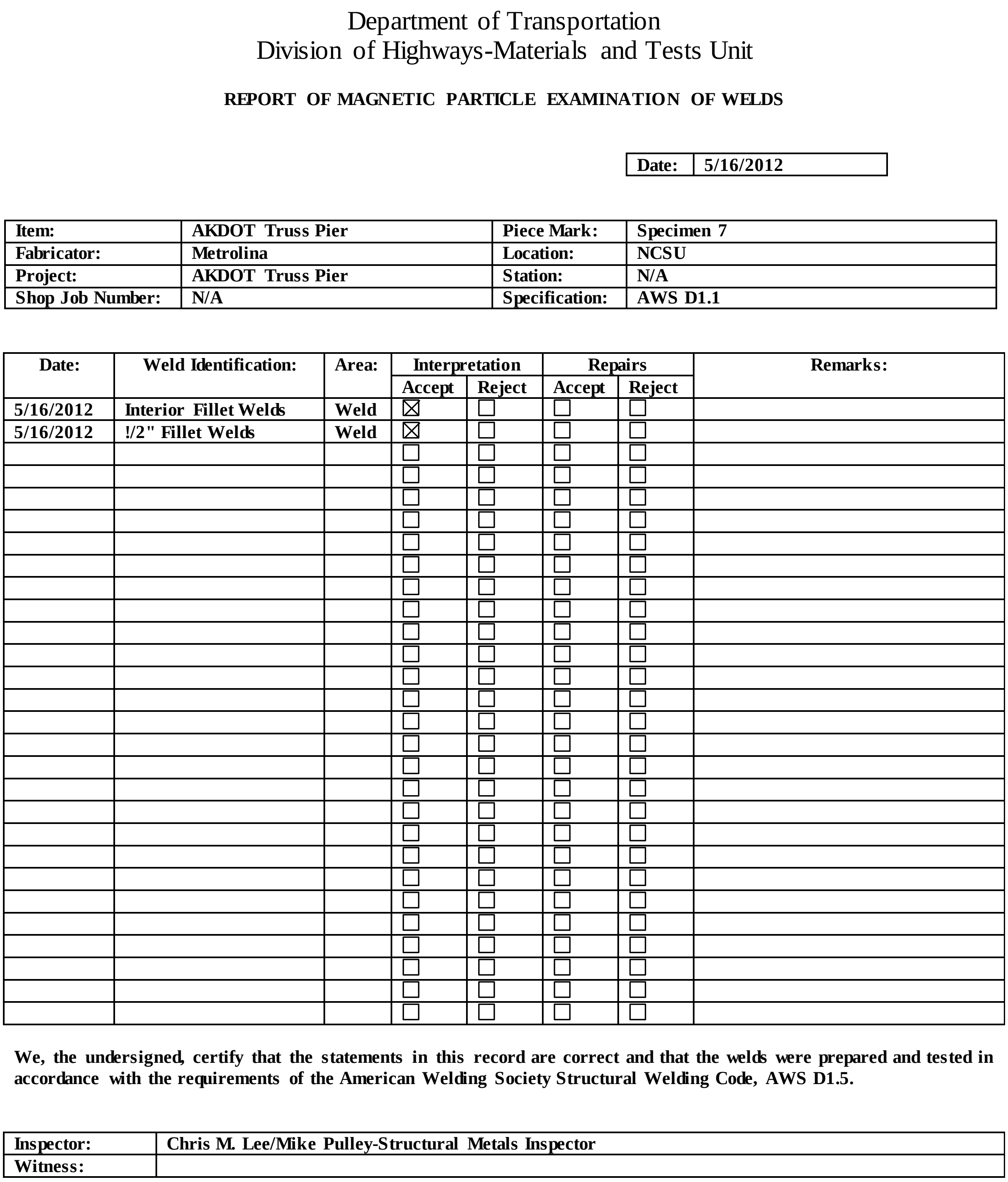

Department of Transportation
Division of Highways-Materials and Tests Unit

REPORT OF MAGNETIC PARTICLE EXAMINATION OF WELDS

Date:	**5/16/2012**

Item:	**AKDOT Truss Pier**	**Piece Mark:**	**Specimen 7**
Fabricator:	**Metrolina**	**Location:**	**NCSU**
Project:	**AKDOT Truss Pier**	**Station:**	**N/A**
Shop Job Number:	**N/A**	**Specification:**	**AWS D1.1**

Date:	**Weld Identification:**	**Area:**	**Interpretation**		**Repairs**		**Remarks:**
			Accept	**Reject**	**Accept**	**Reject**	
5/16/2012	**Interior Fillet Welds**	**Weld**	☒	☐	☐	☐	
5/16/2012	**!/2" Fillet Welds**	**Weld**	☒	☐	☐	☐	
			☐	☐	☐	☐	
			☐	☐	☐	☐	
			☐	☐	☐	☐	
			☐	☐	☐	☐	
			☐	☐	☐	☐	
			☐	☐	☐	☐	
			☐	☐	☐	☐	
			☐	☐	☐	☐	
			☐	☐	☐	☐	
			☐	☐	☐	☐	
			☐	☐	☐	☐	
			☐	☐	☐	☐	
			☐	☐	☐	☐	
			☐	☐	☐	☐	
			☐	☐	☐	☐	
			☐	☐	☐	☐	
			☐	☐	☐	☐	
			☐	☐	☐	☐	
			☐	☐	☐	☐	
			☐	☐	☐	☐	
			☐	☐	☐	☐	
			☐	☐	☐	☐	
			☐	☐	☐	☐	
			☐	☐	☐	☐	
			☐	☐	☐	☐	
			☐	☐	☐	☐	

We, the undersigned, certify that the statements in this record are correct and that the welds were prepared and tested in accordance with the requirements of the American Welding Society Structural Welding Code, AWS D1.5.

Inspector:	**Chris M. Lee/Mike Pulley-Structural Metals Inspector**
Witness:	

Figure A 97 Truss Pier MT Inspection Report

APPENDIX 4: Phase 2 Steel Pier Detailed Design Drawings

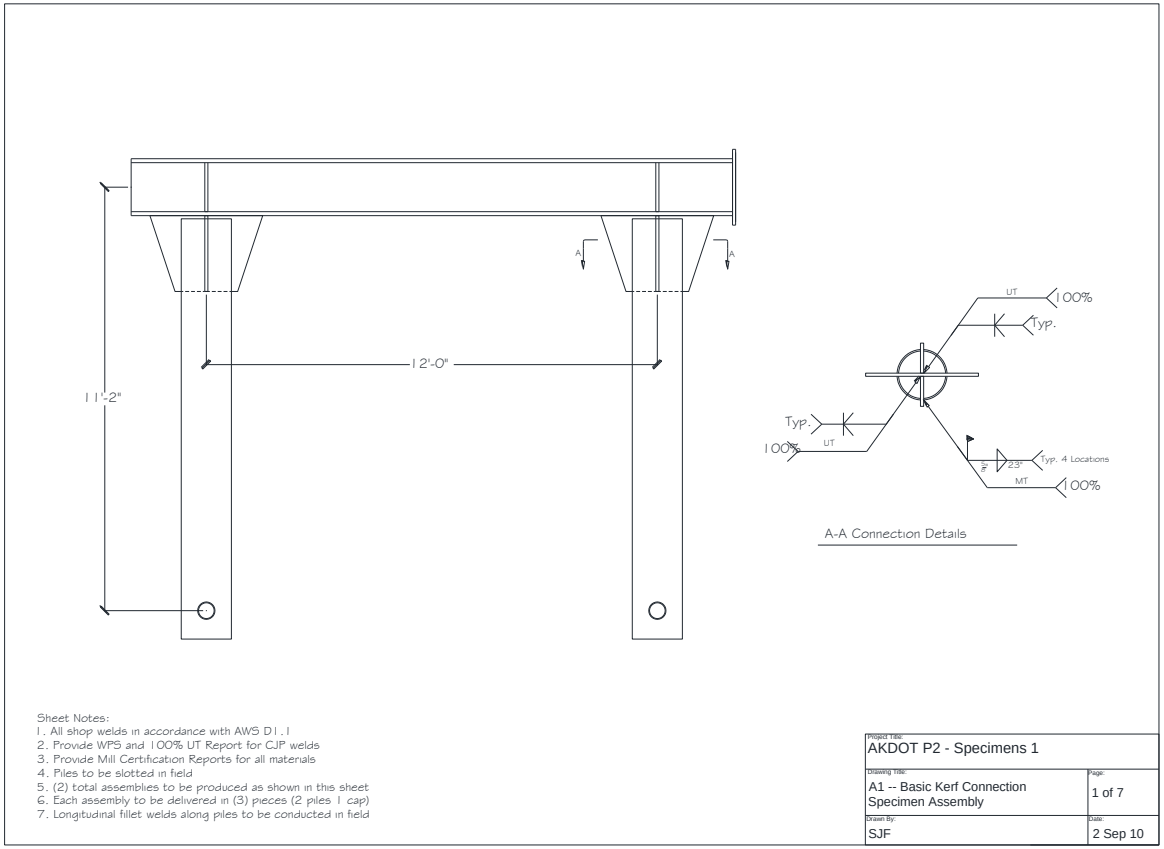

Figure A 98 Phase 2 Test 1 Kerf Connection Detailed Drawing

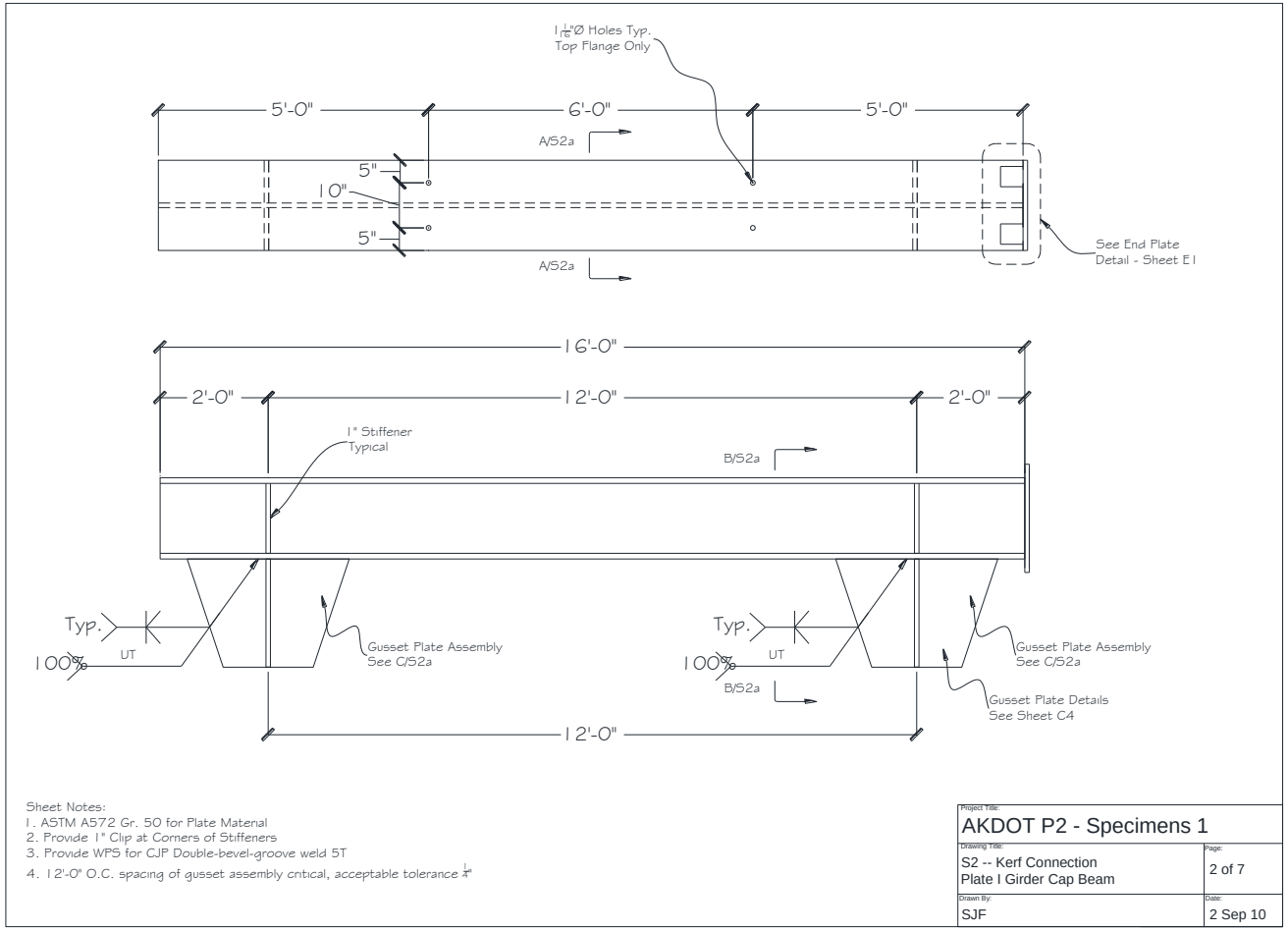

Figure A 99 Phase 2 Test 1 Kerf Connection Detailed Drawing

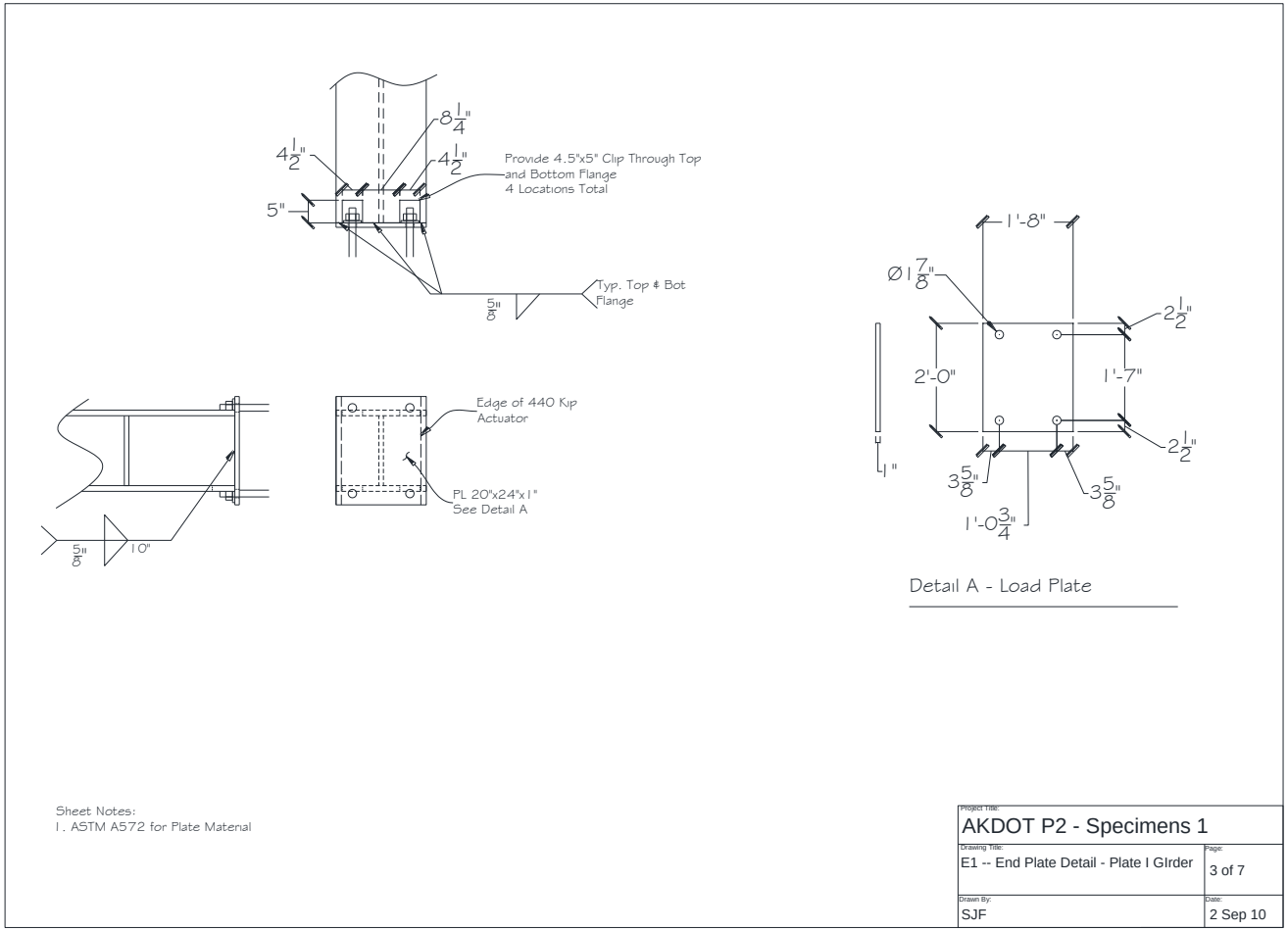

Figure A 100 Phase 2 Test 1 Kerf Connection Detailed Drawing

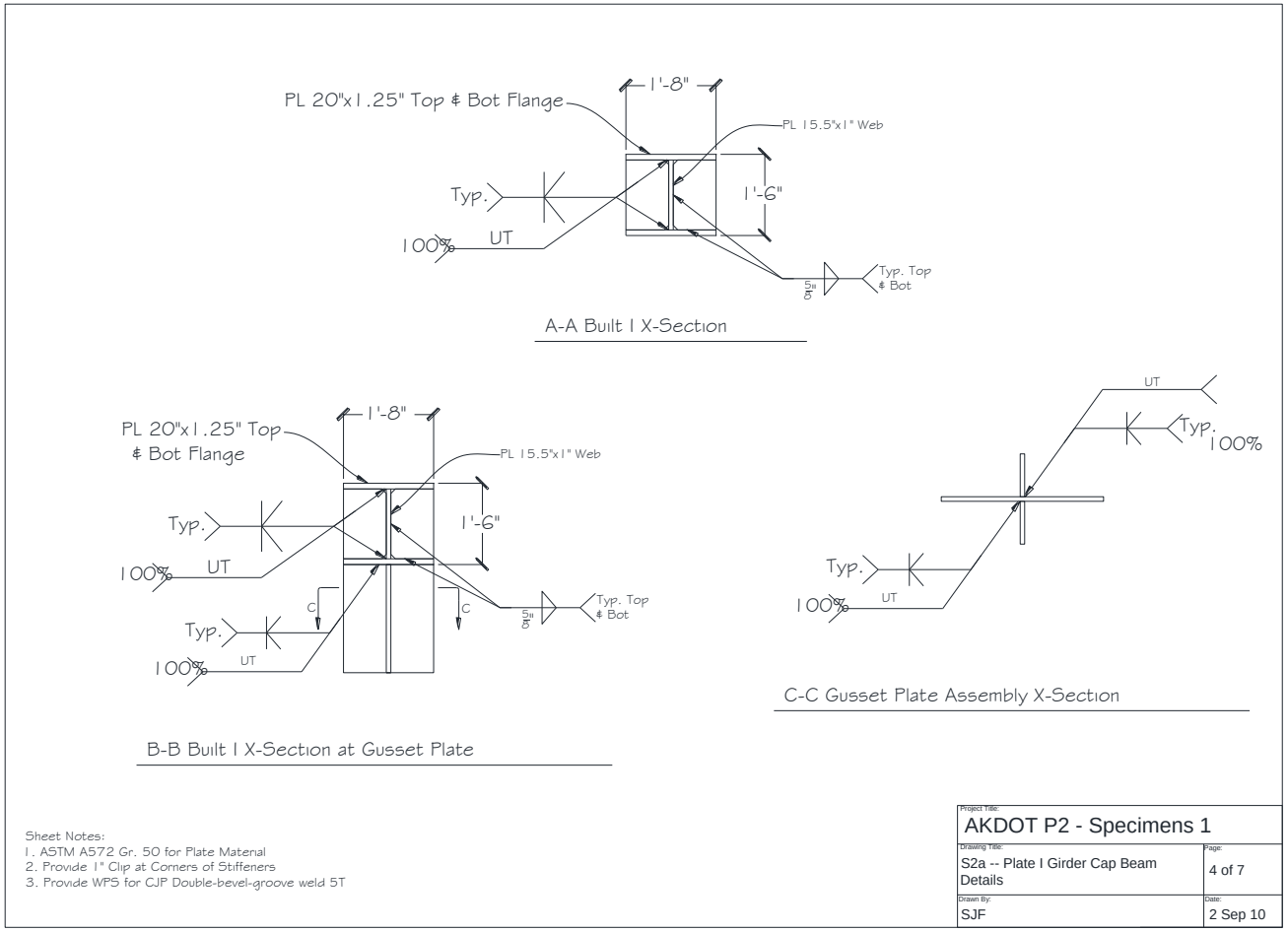

Figure A 101 Phase 2 Test 1 Kerf Connection Detailed Drawing

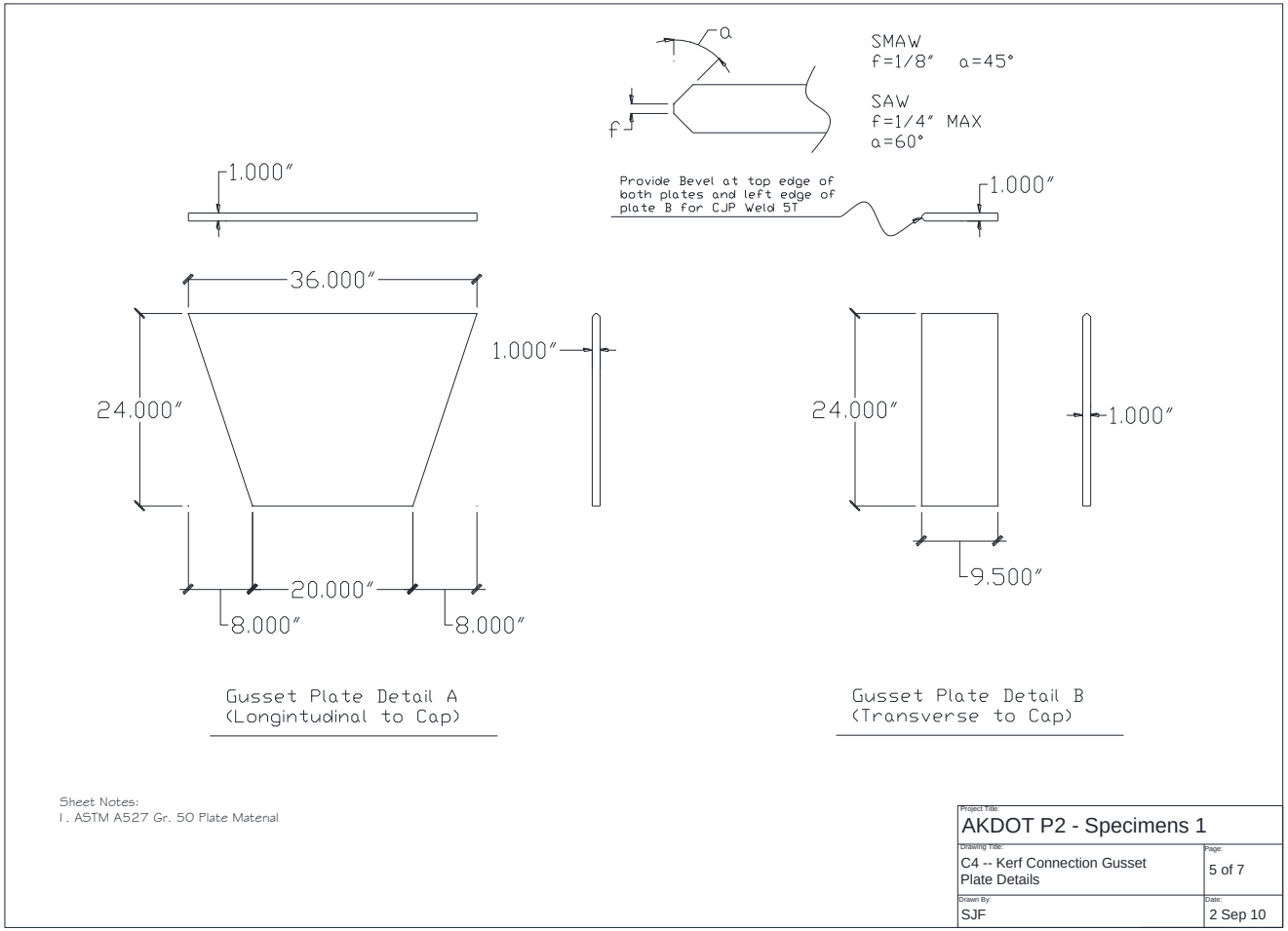

Figure A 102 Phase 2 Test 1 Kerf Connection Detailed Drawing

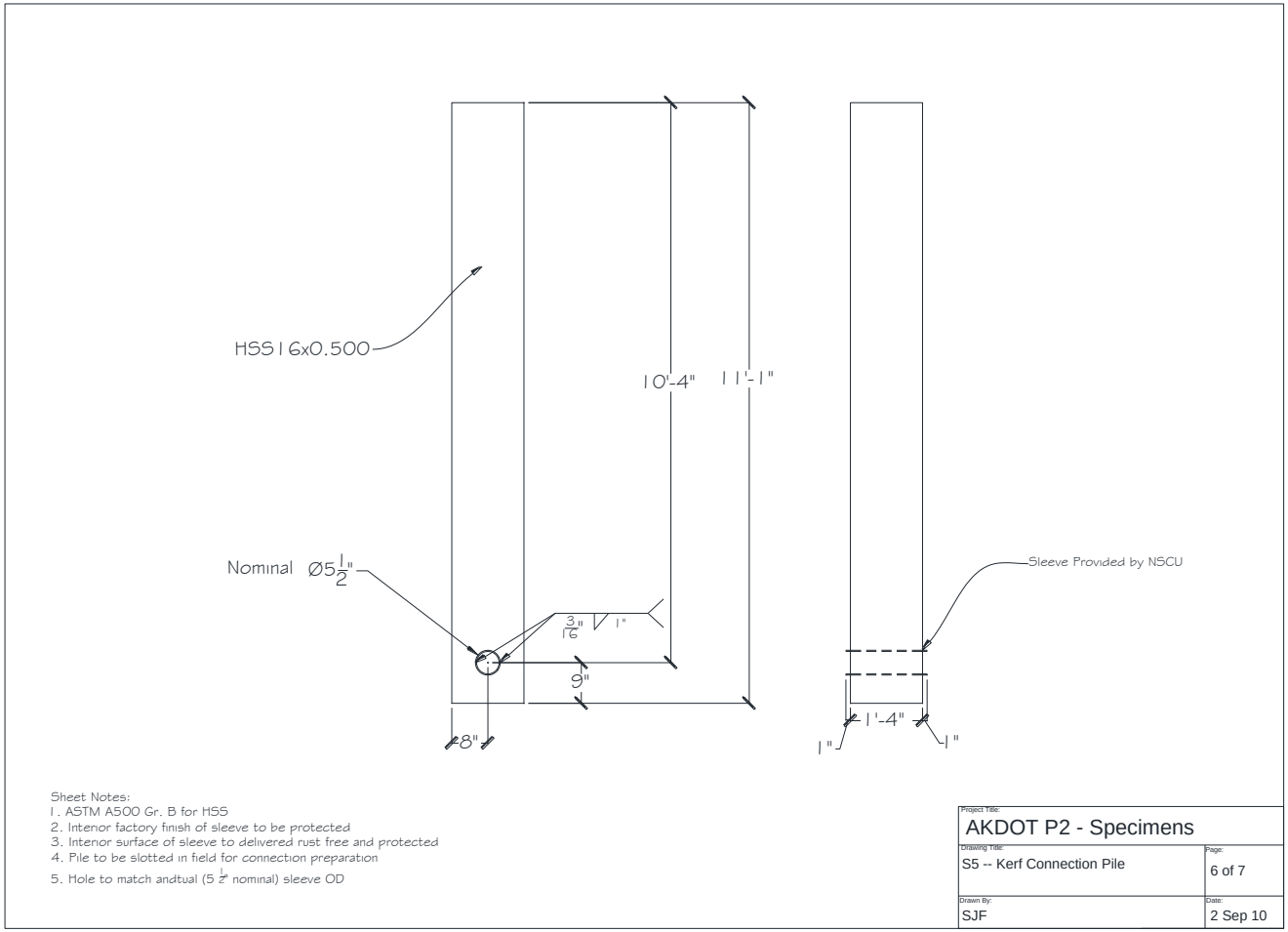

Figure A 103 Phase 2 Test 1 Kerf Connection Detailed Drawing

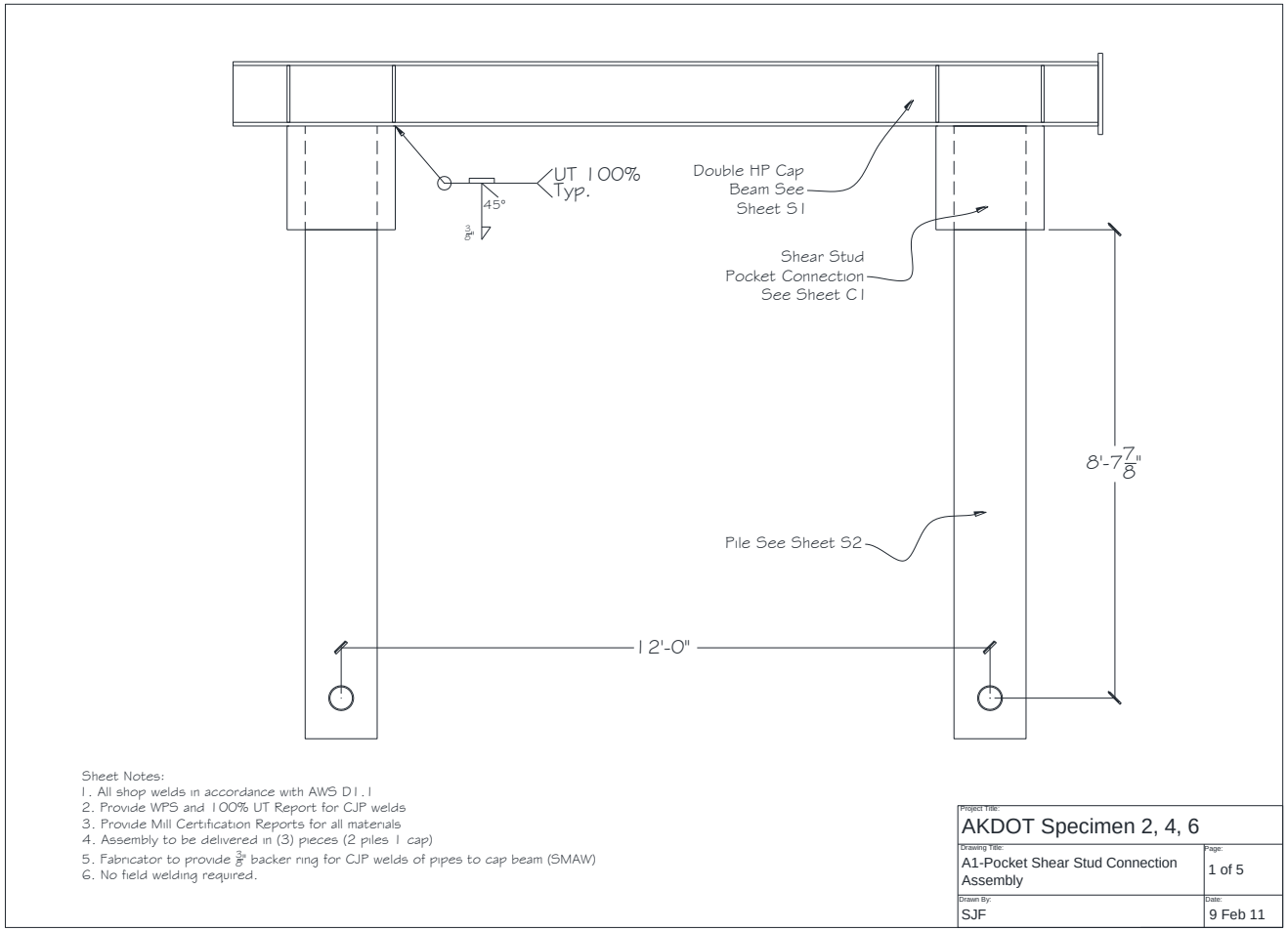

Figure A 104 Phase 2 Test 2, 4, and 6 G.S.C. Detailed Drawing

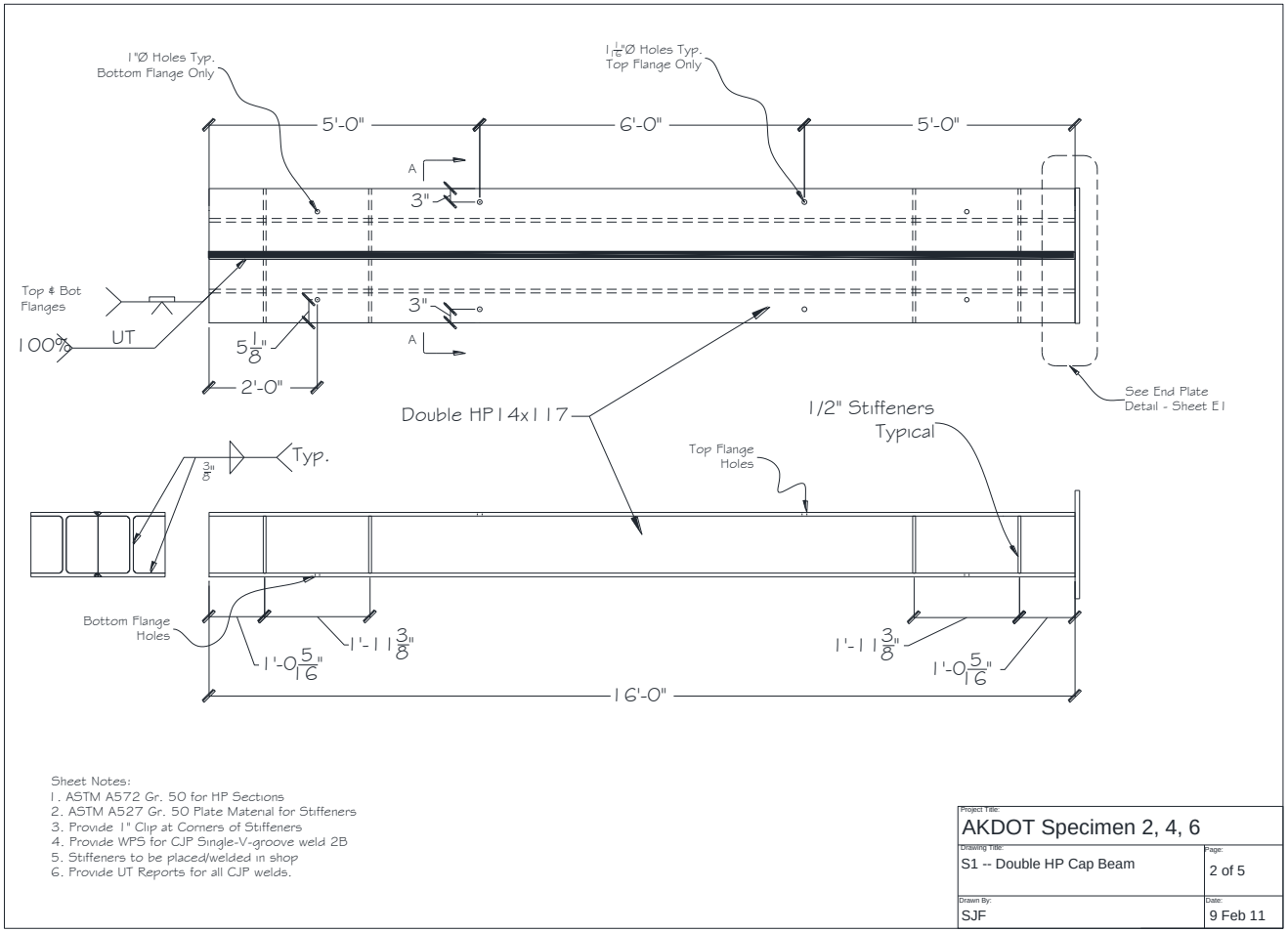

Figure A 105 Phase 2 Test 2, 4, and 6 G.S.C. Detailed Drawing

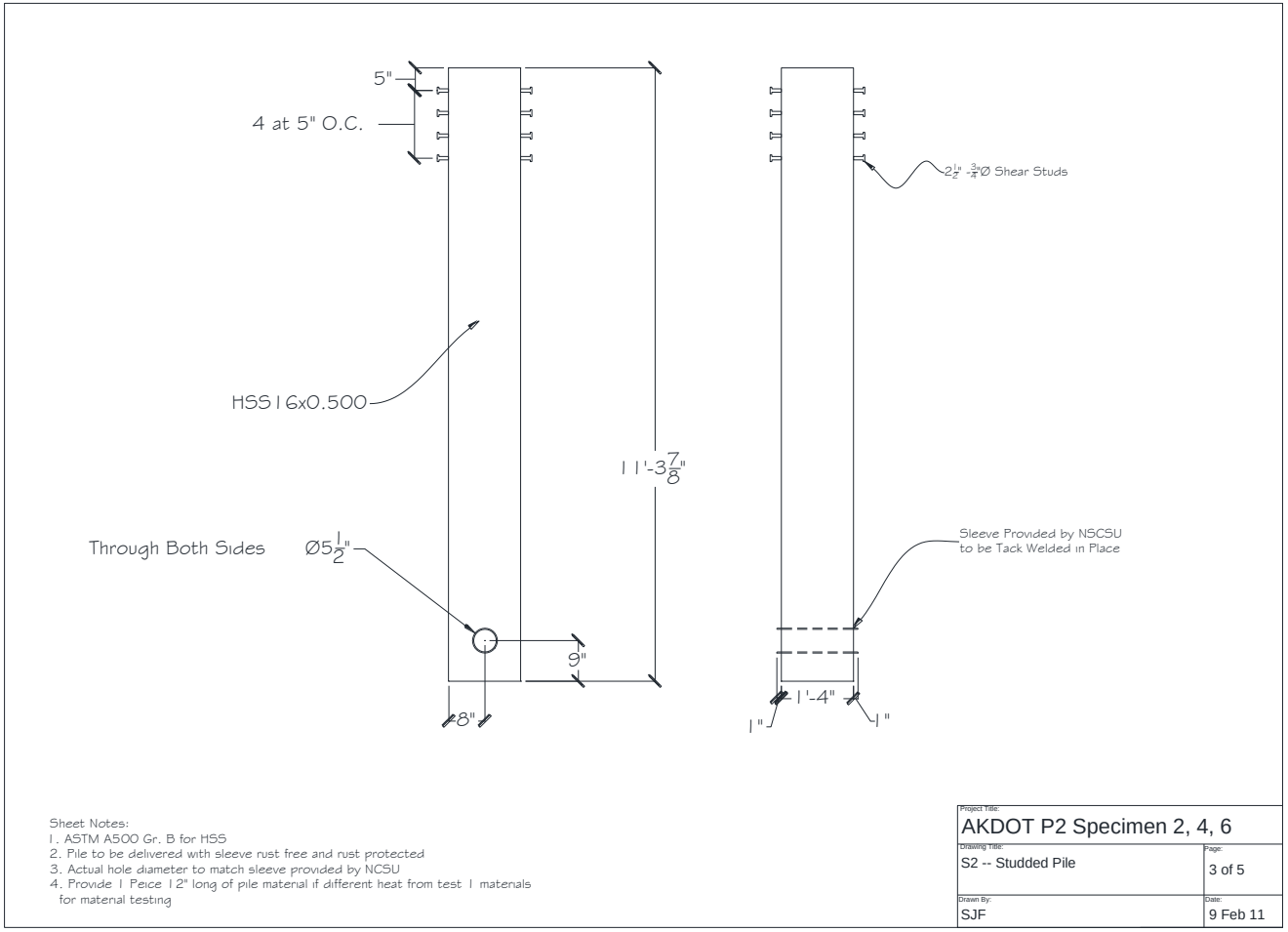

Figure A 106 Phase 2 Test 2, 4, and 6 G.S.C. Detailed Drawing

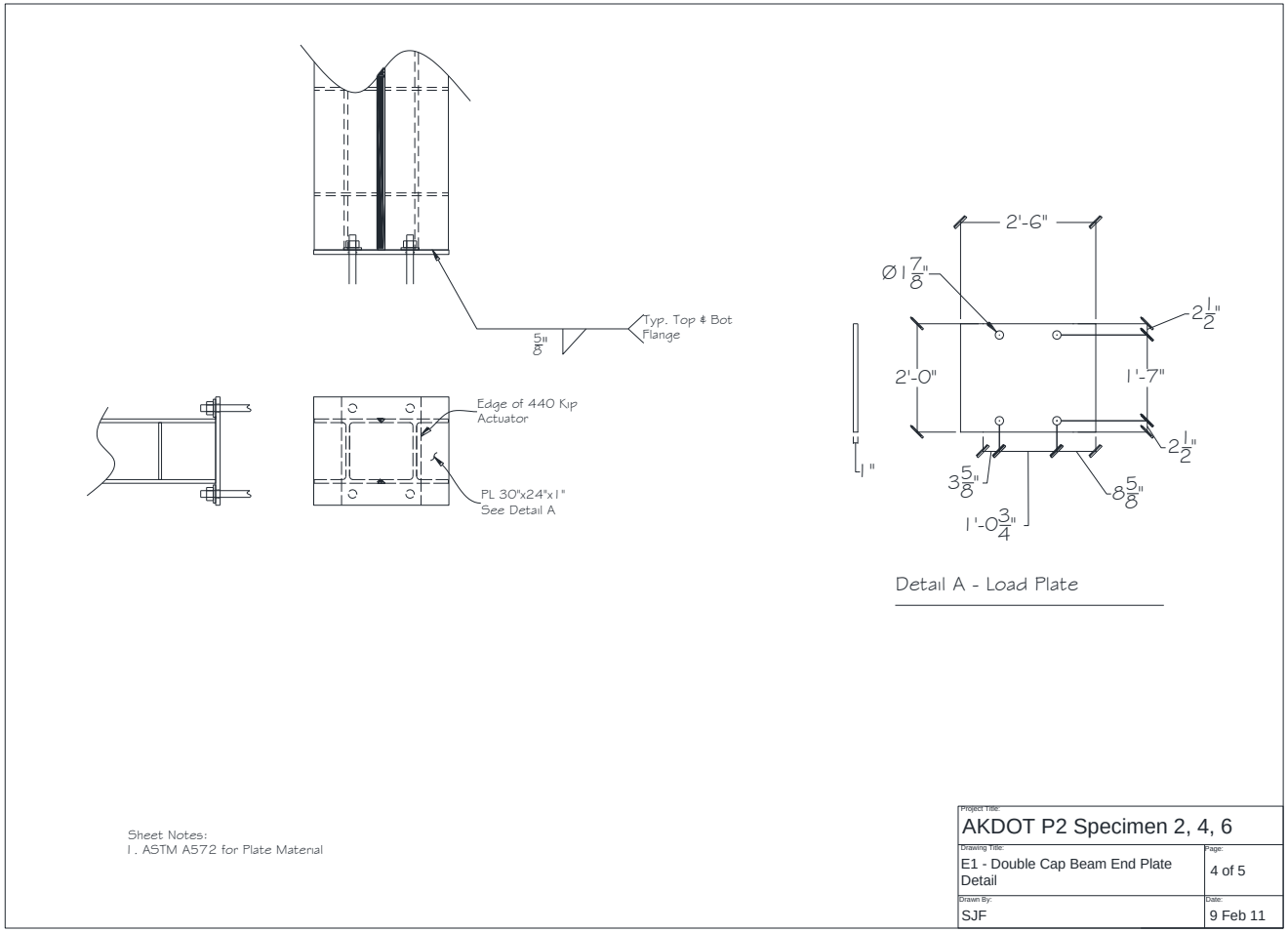

Figure A 107 Phase 2 Test 2, 4, and 6 G.S.C. Detailed Drawing

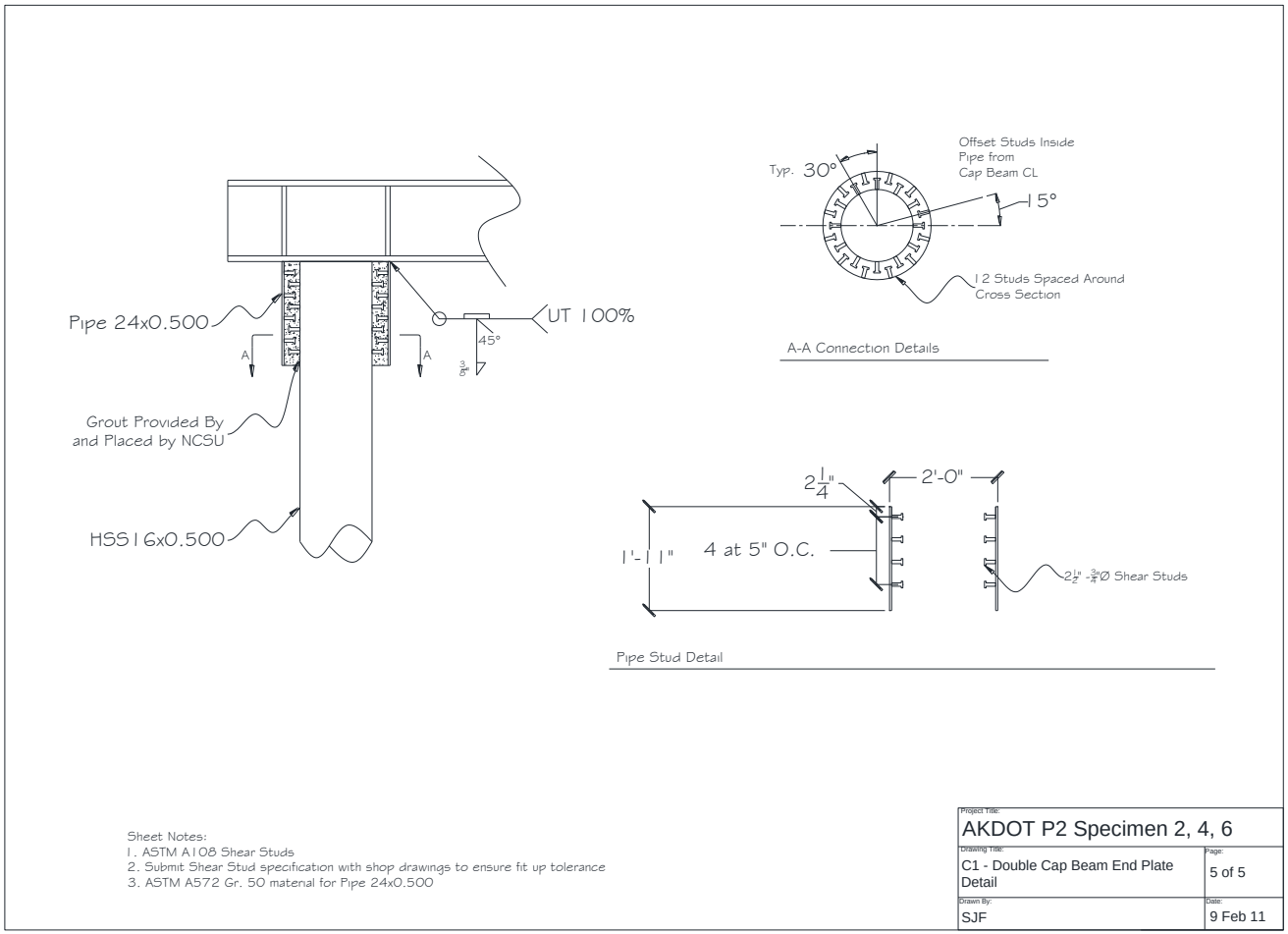

Figure A 108 Phase 2 Test 2, 4, and 6 G.S.C. Detailed Drawing

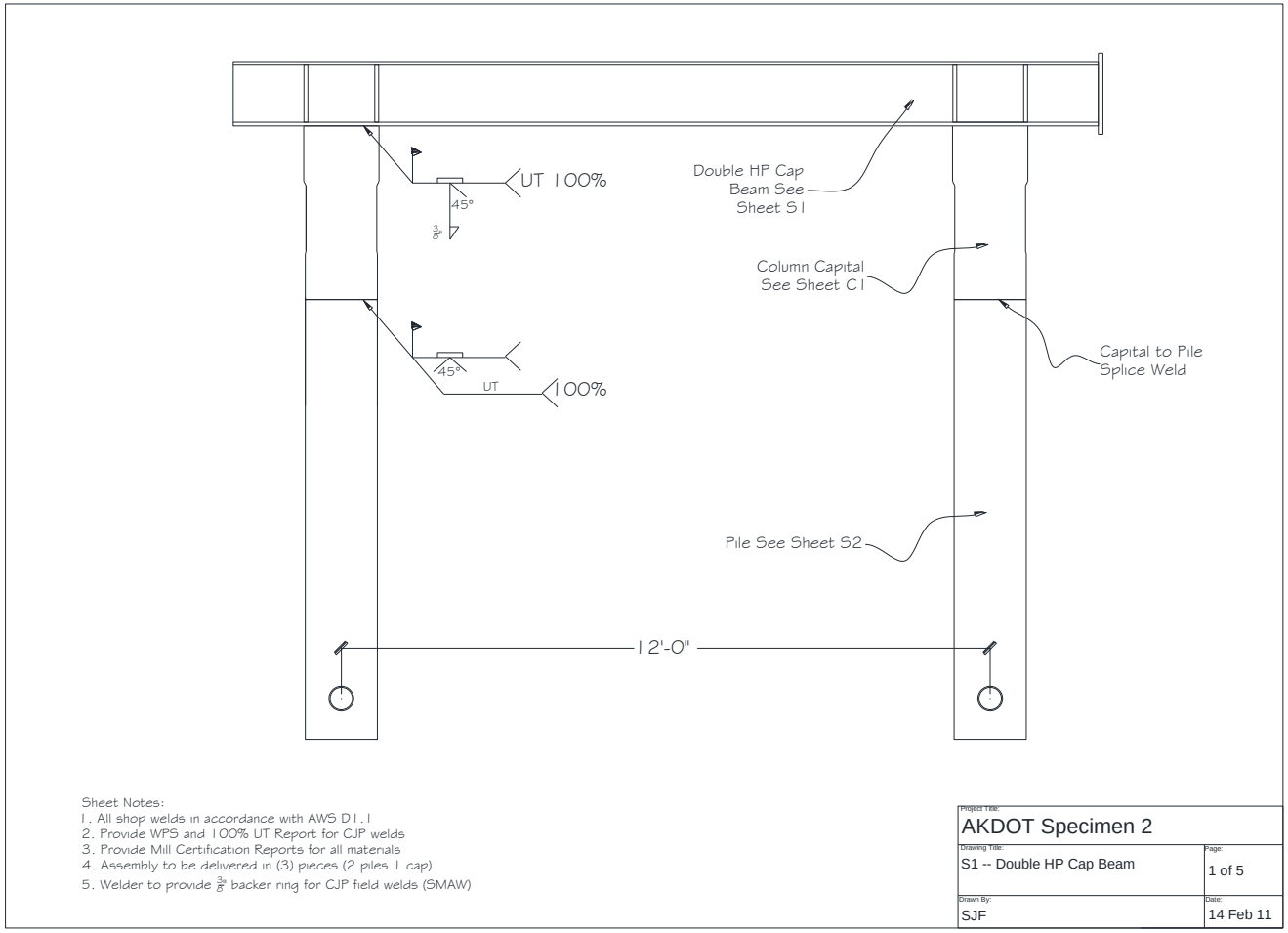

Figure A 109 Phase 2 Test 3 Modified Column Capital Detailed Drawing

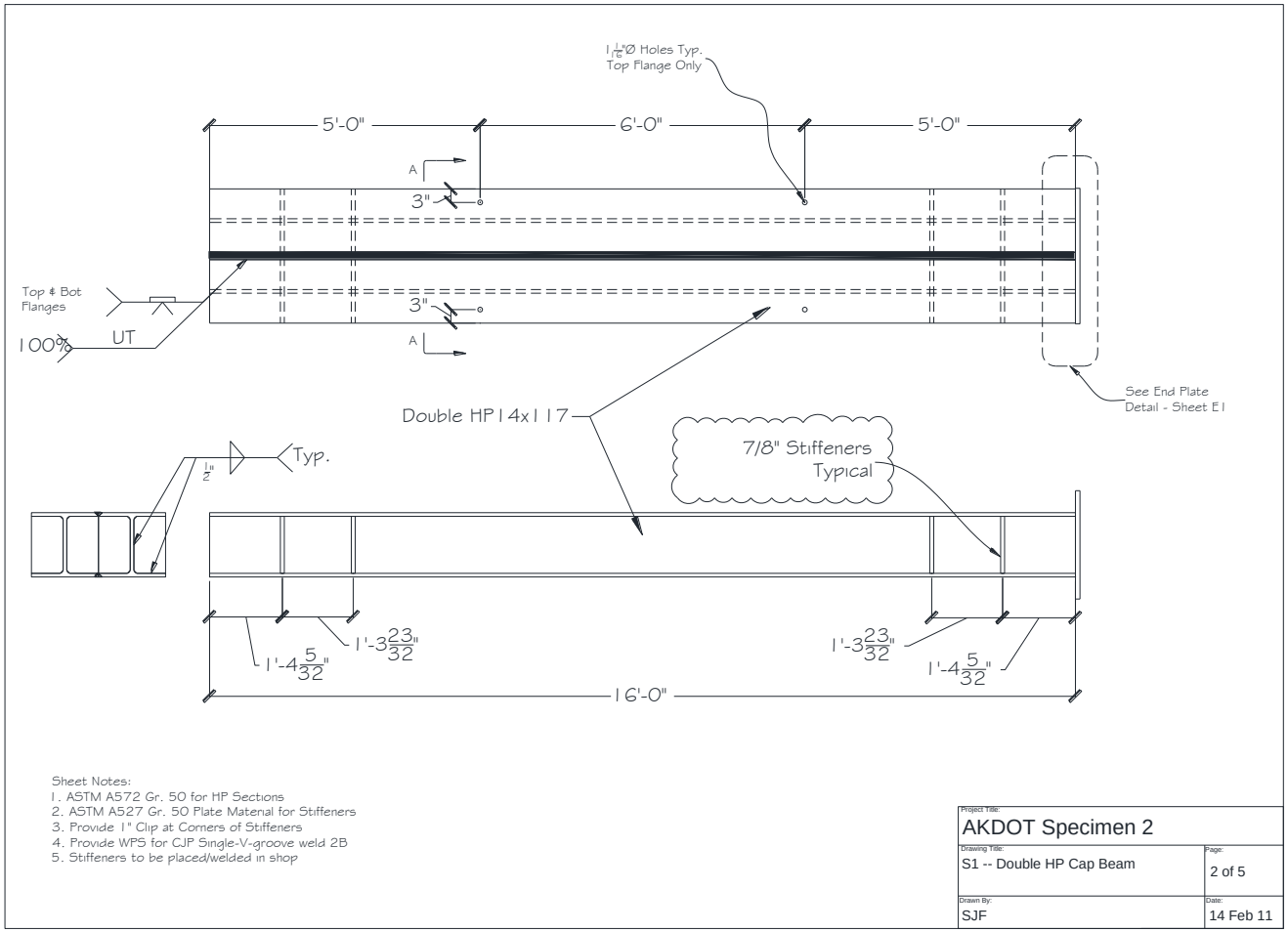

Figure A 110 Phase 2 Test 3 Modified Column Capital Detailed Drawing

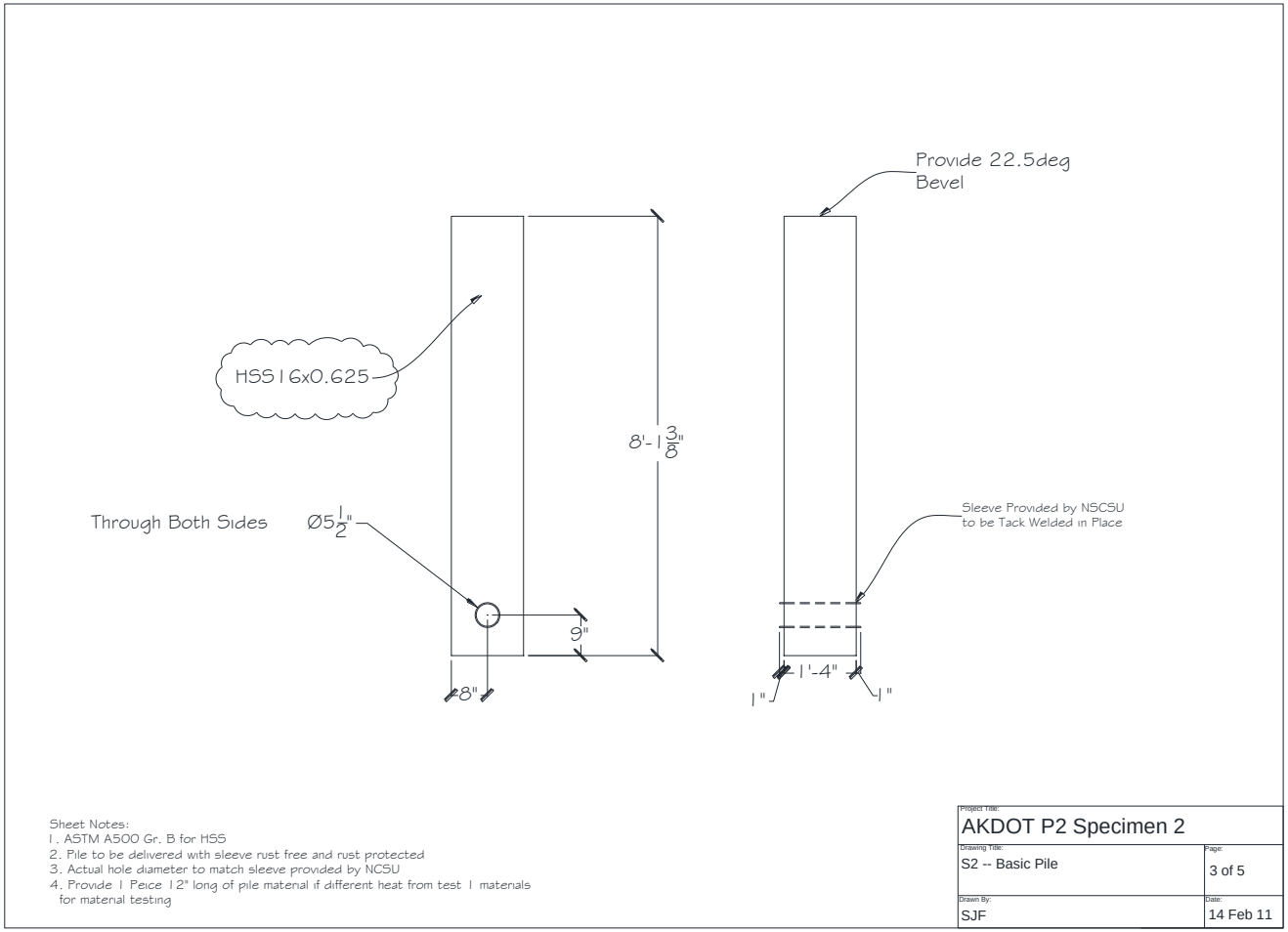

Figure A 111 Phase 2 Test 3 Modified Column Capital Detailed Drawing

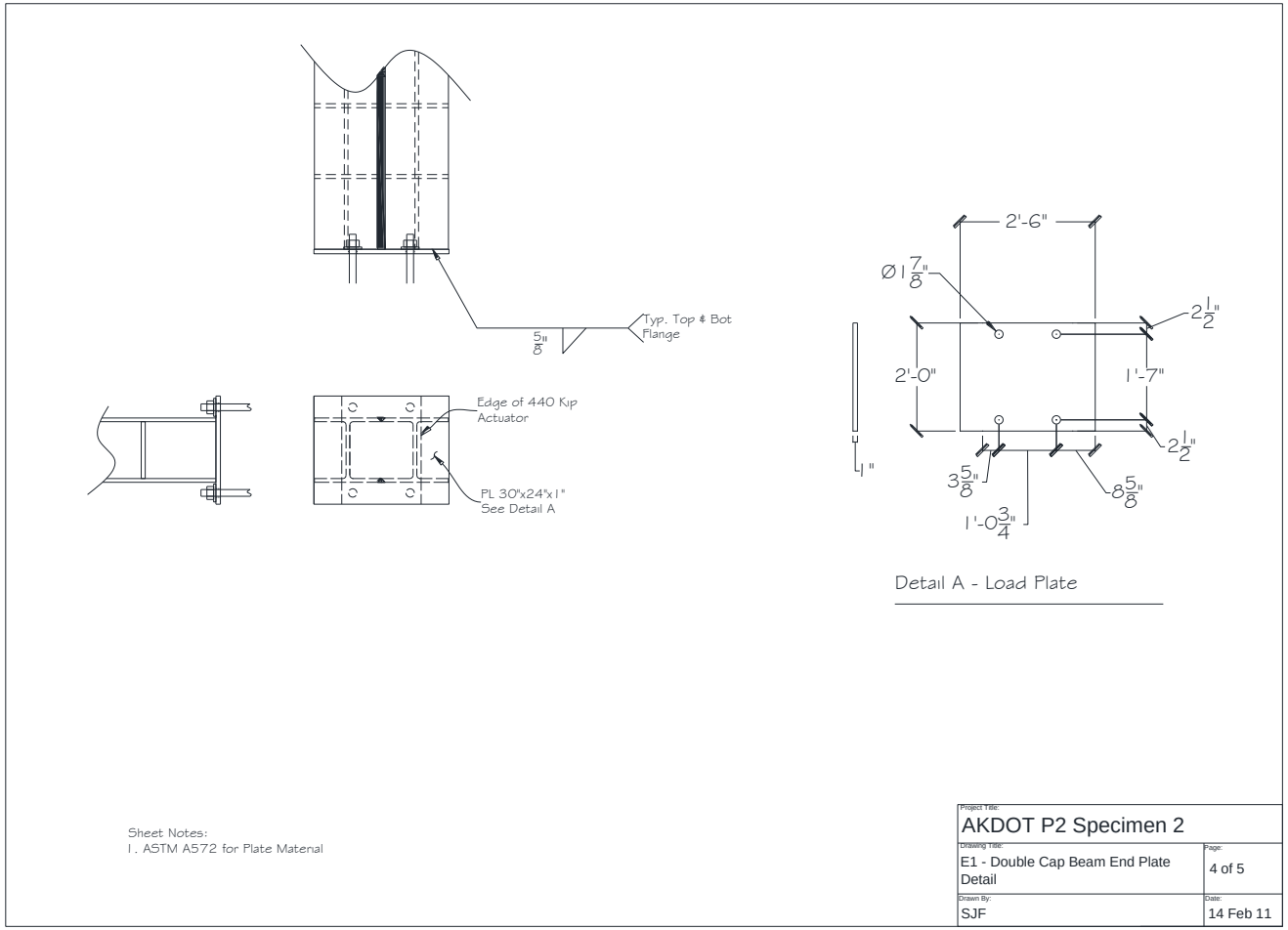

Figure A 112 Phase 2 Test 3 Modified Column Capital Detailed Drawing

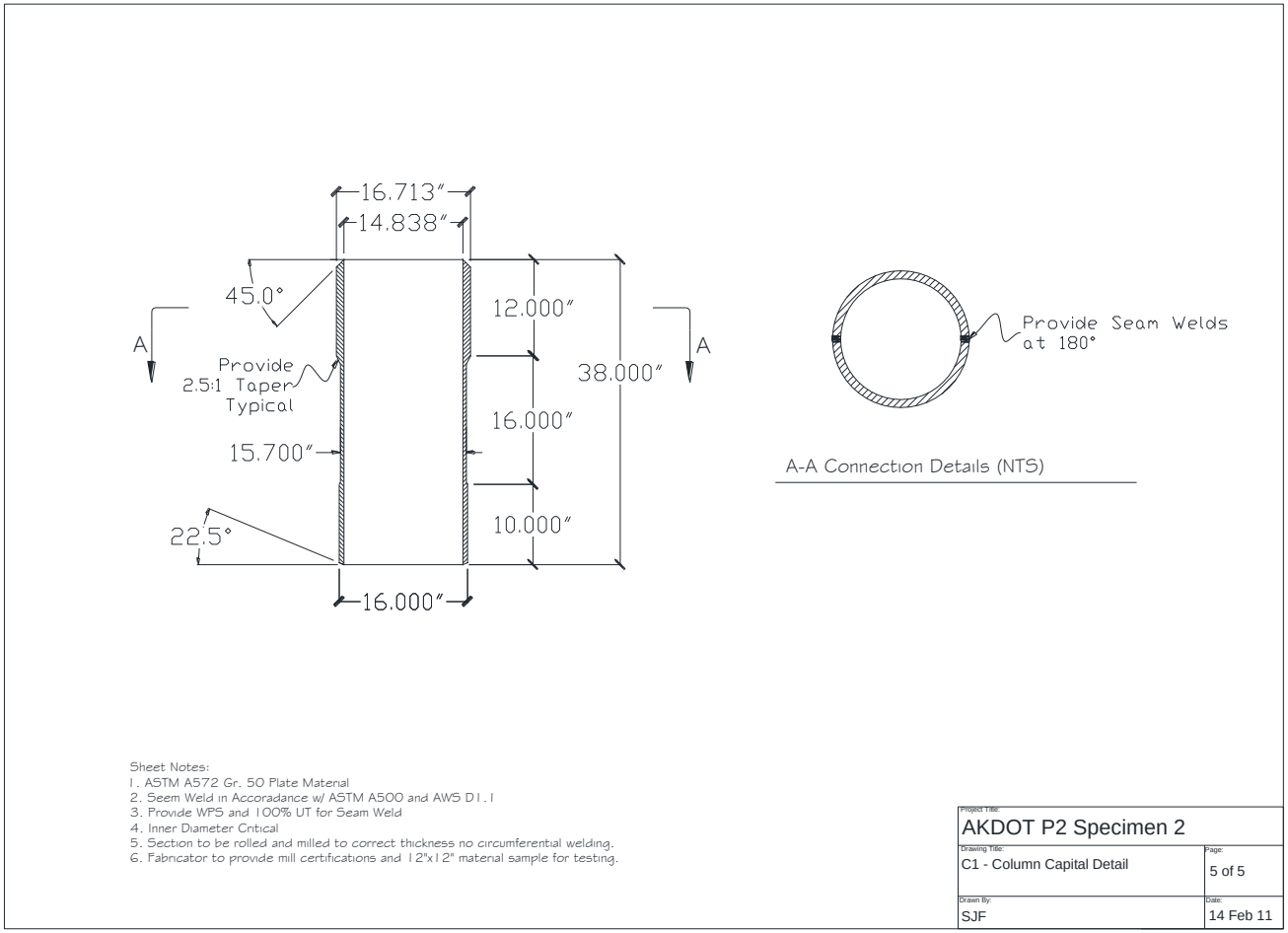

Figure A 113 Phase 2 Test 3 Modified Column Capital Detailed Drawing

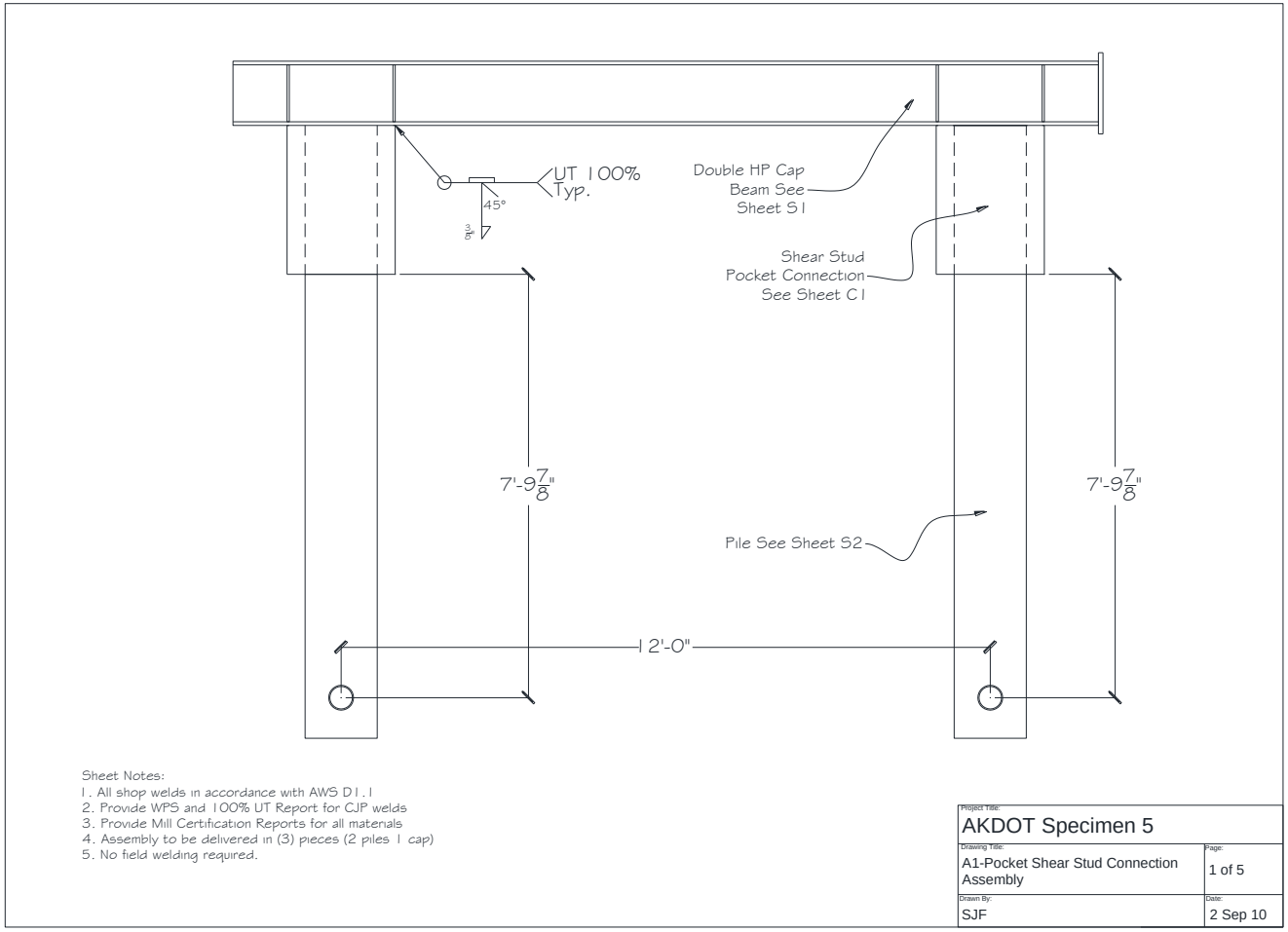

Figure A 114 Phase 2 Test 4 Modified B.R. – G.S.C. Detailed Drawing

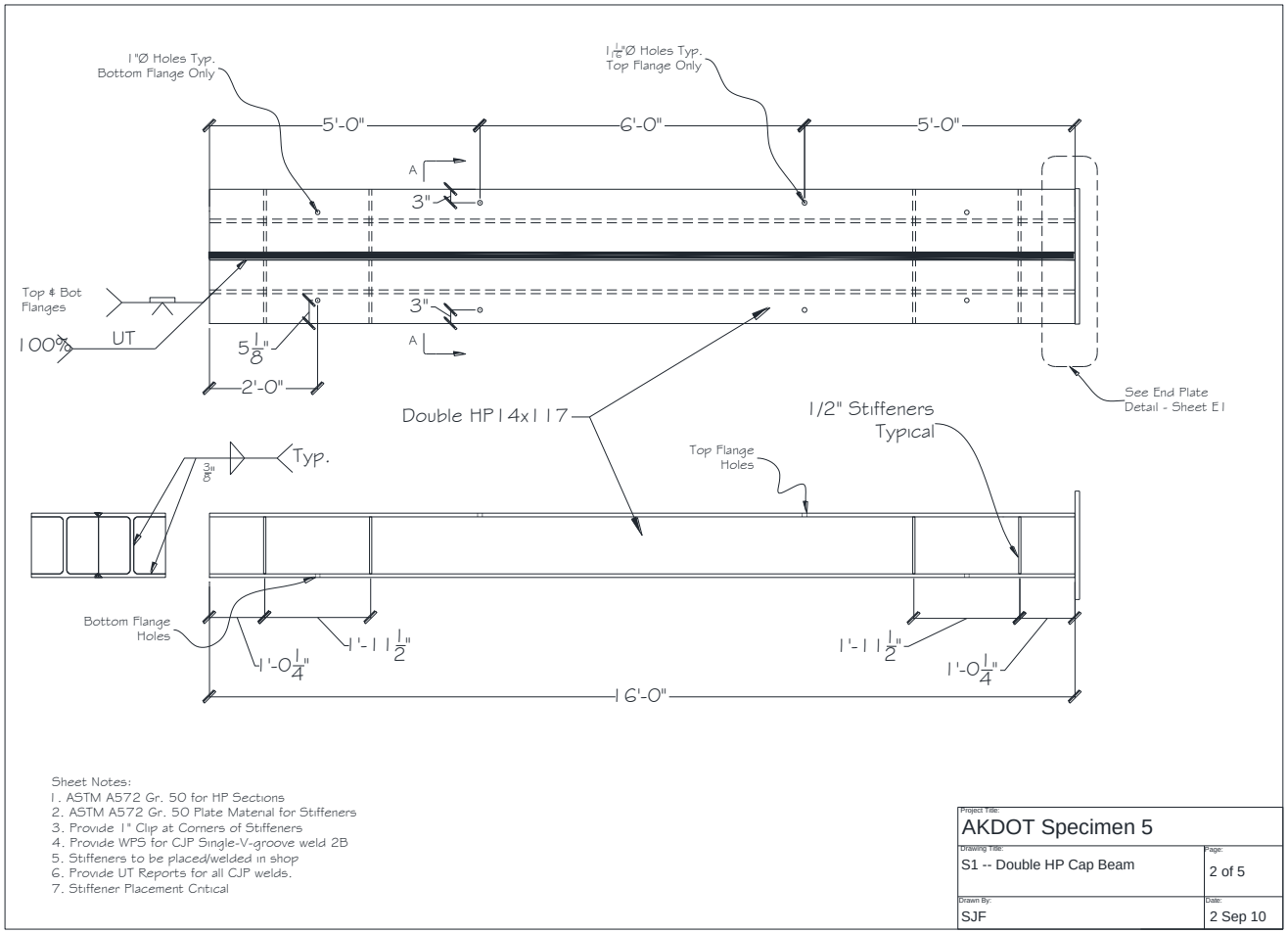

Figure A 115 Phase 2 Test 4 Modified B.R. – G.S.C. Detailed Drawing

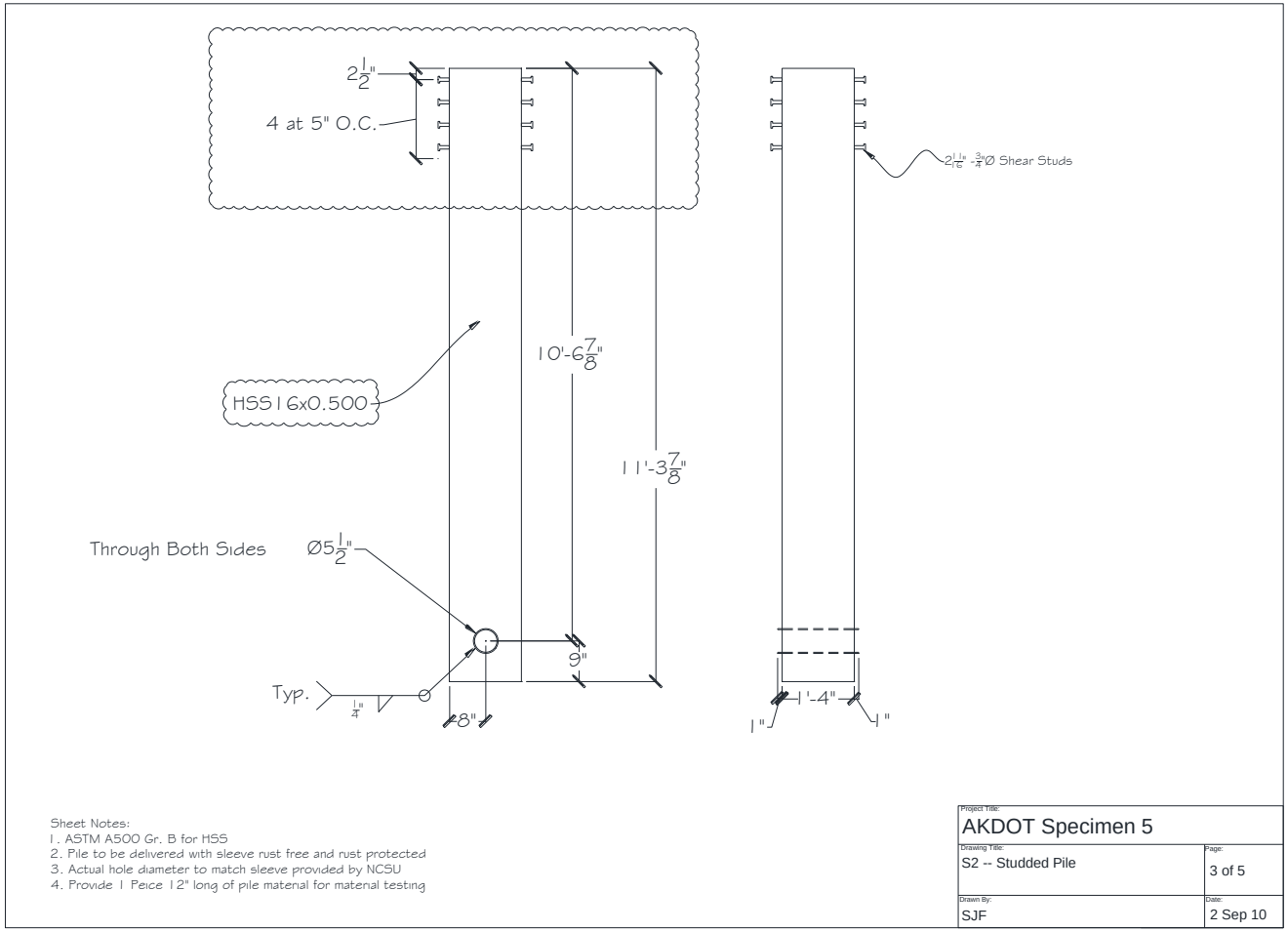

Figure A 116 Phase 2 Test 4 Modified B.R. – G.S.C. Detailed Drawing

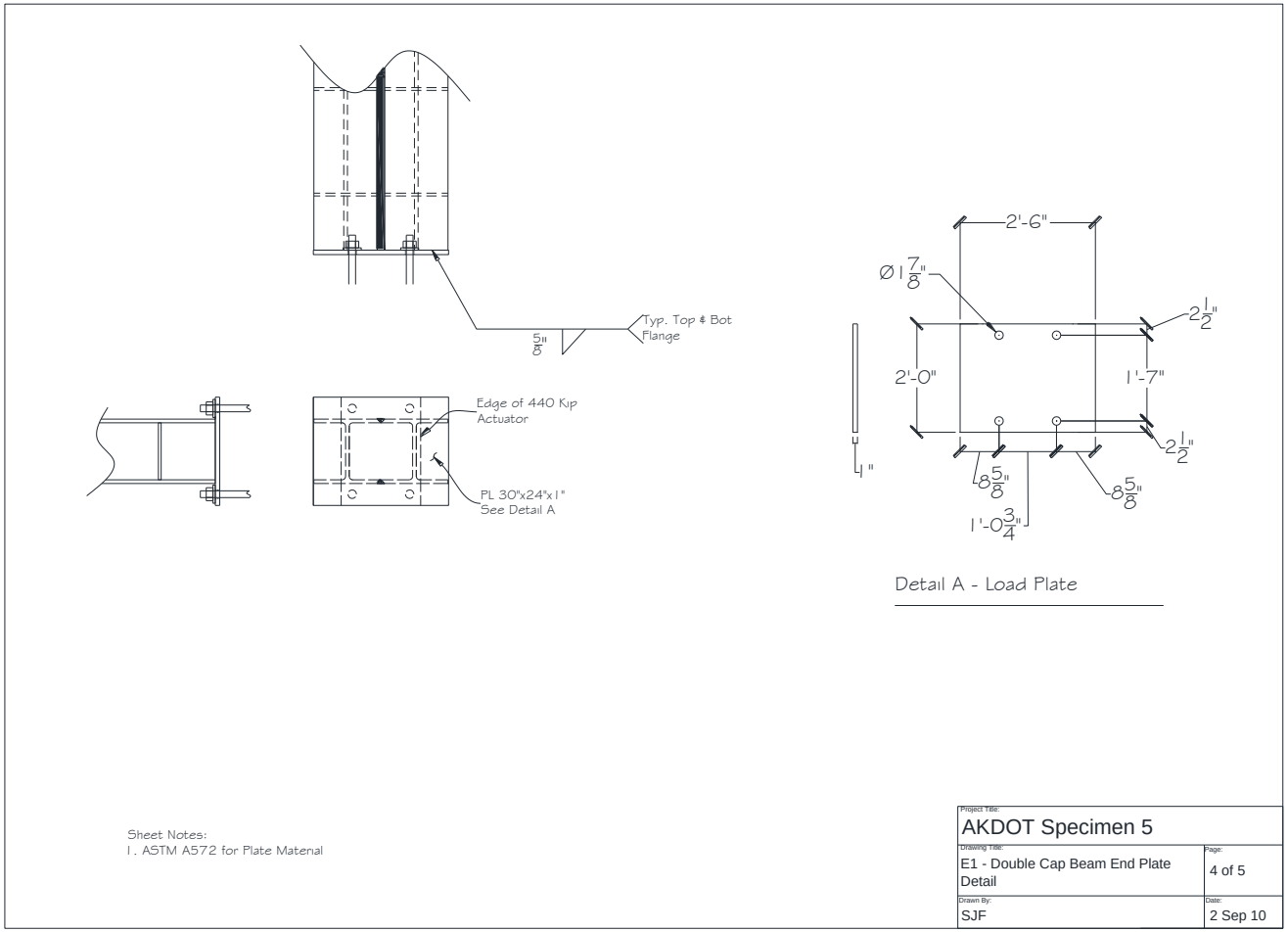

Figure A 117 Phase 2 Test 4 Modified B.R. – G.S.C. Detailed Drawing

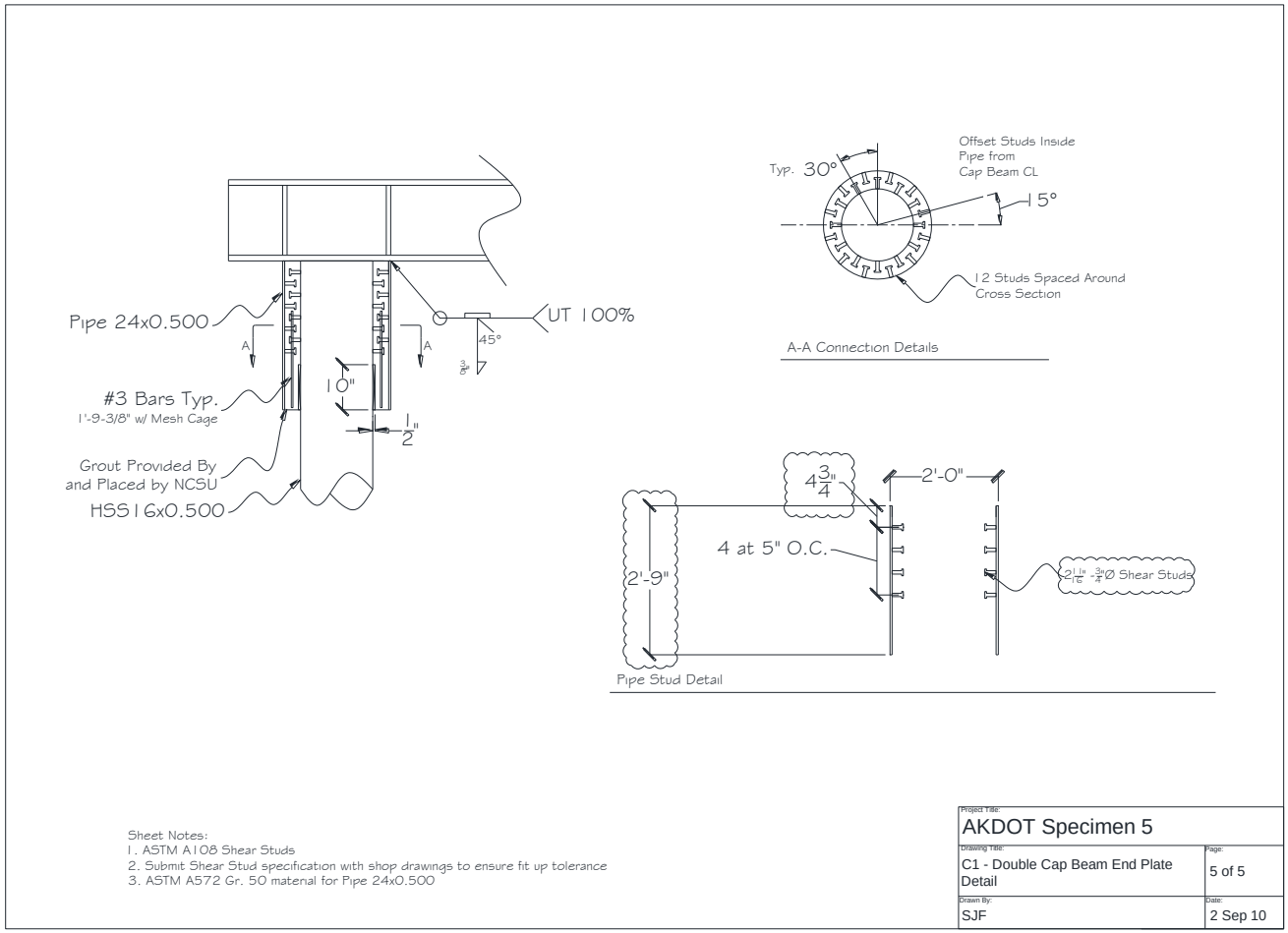

Figure A 118 Phase 2 Test 4 Modified B.R. – G.S.C. Detailed Drawing

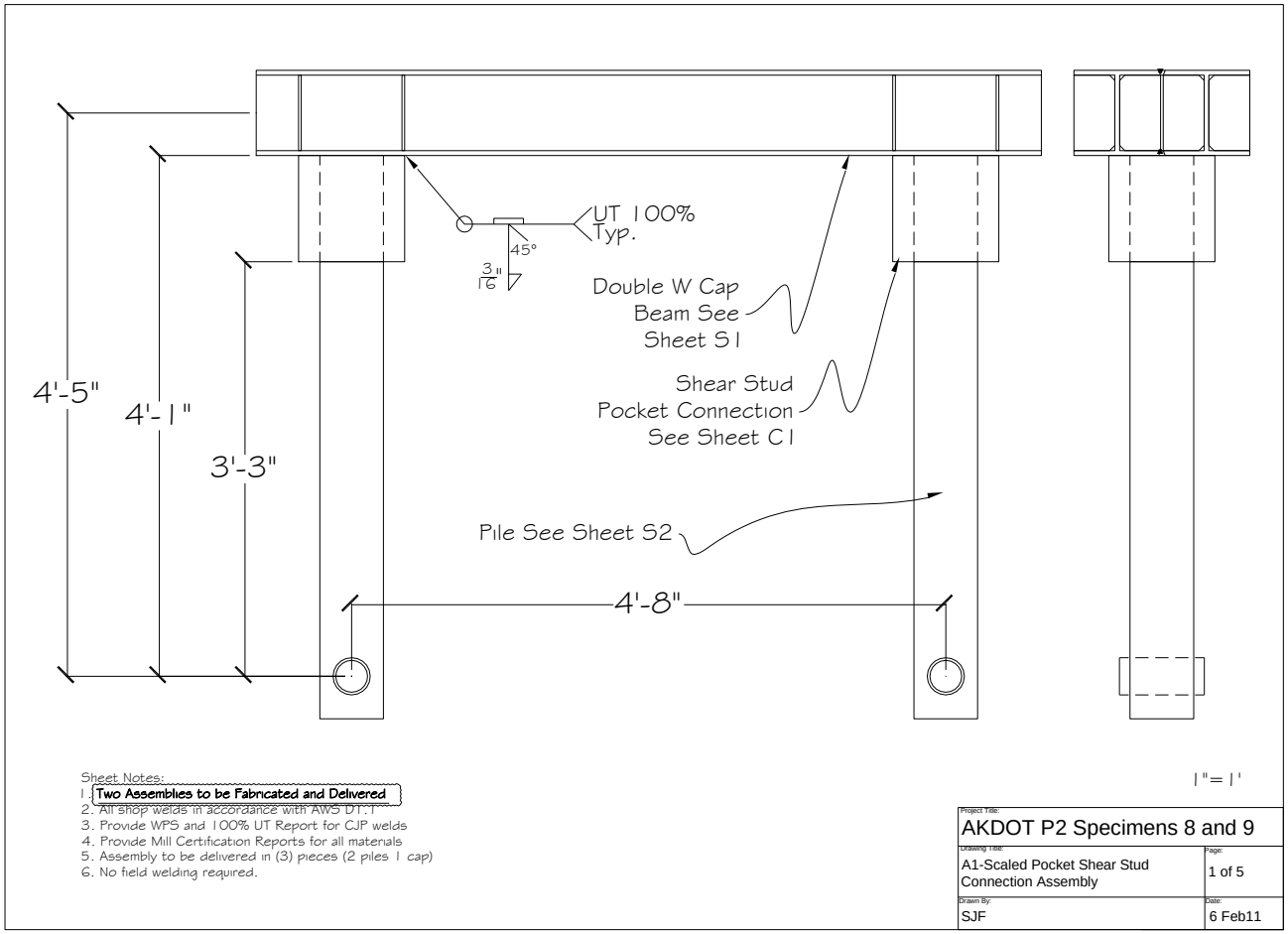

Figure A 119 Phase 2 Test 8, 9 Scaled Shake Table – G.S.C. Detailed Drawing

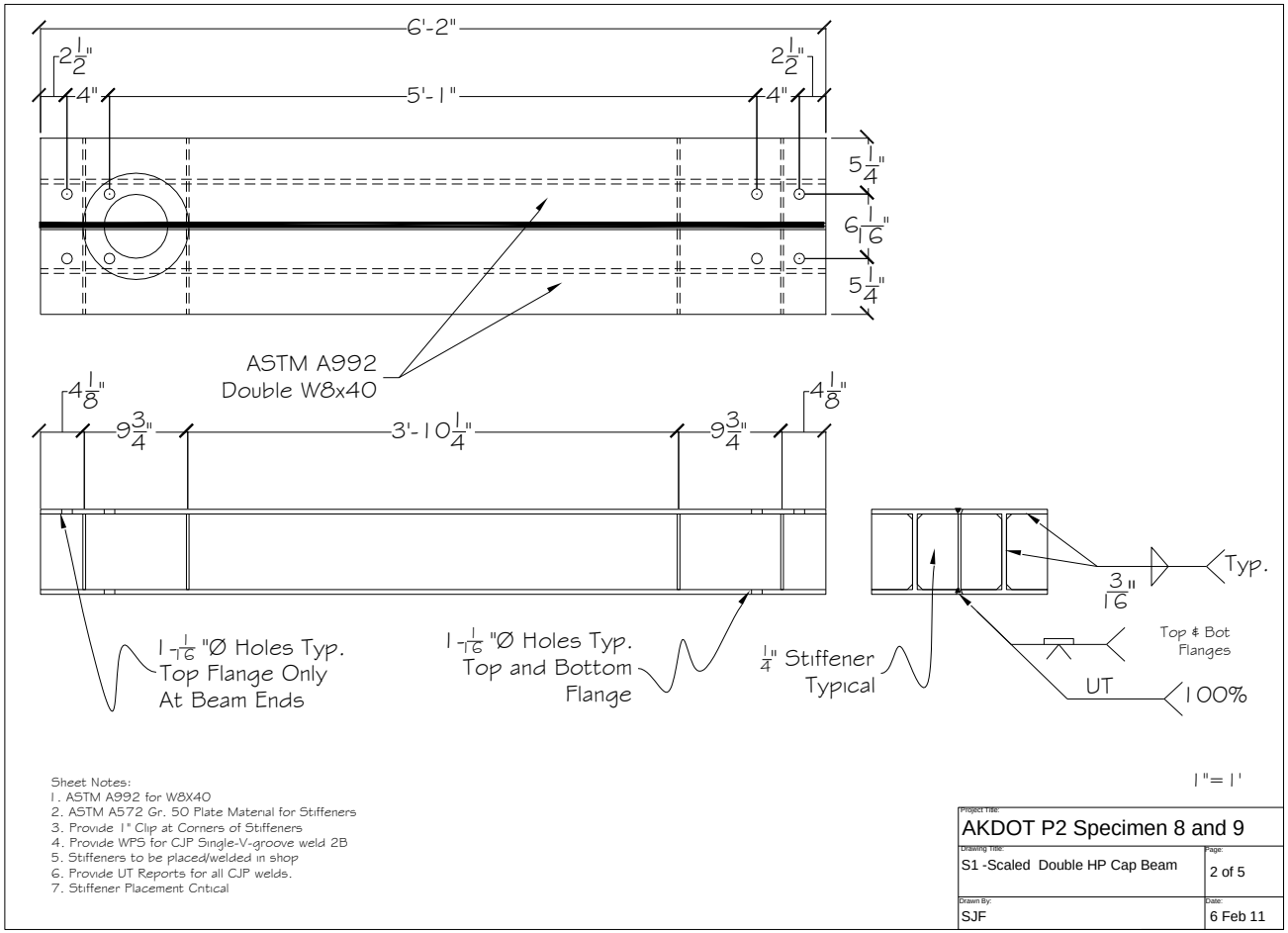

Figure A 120 Phase 2 Test 8, 9 Scaled Shake Table – G.S.C. Detailed Drawing

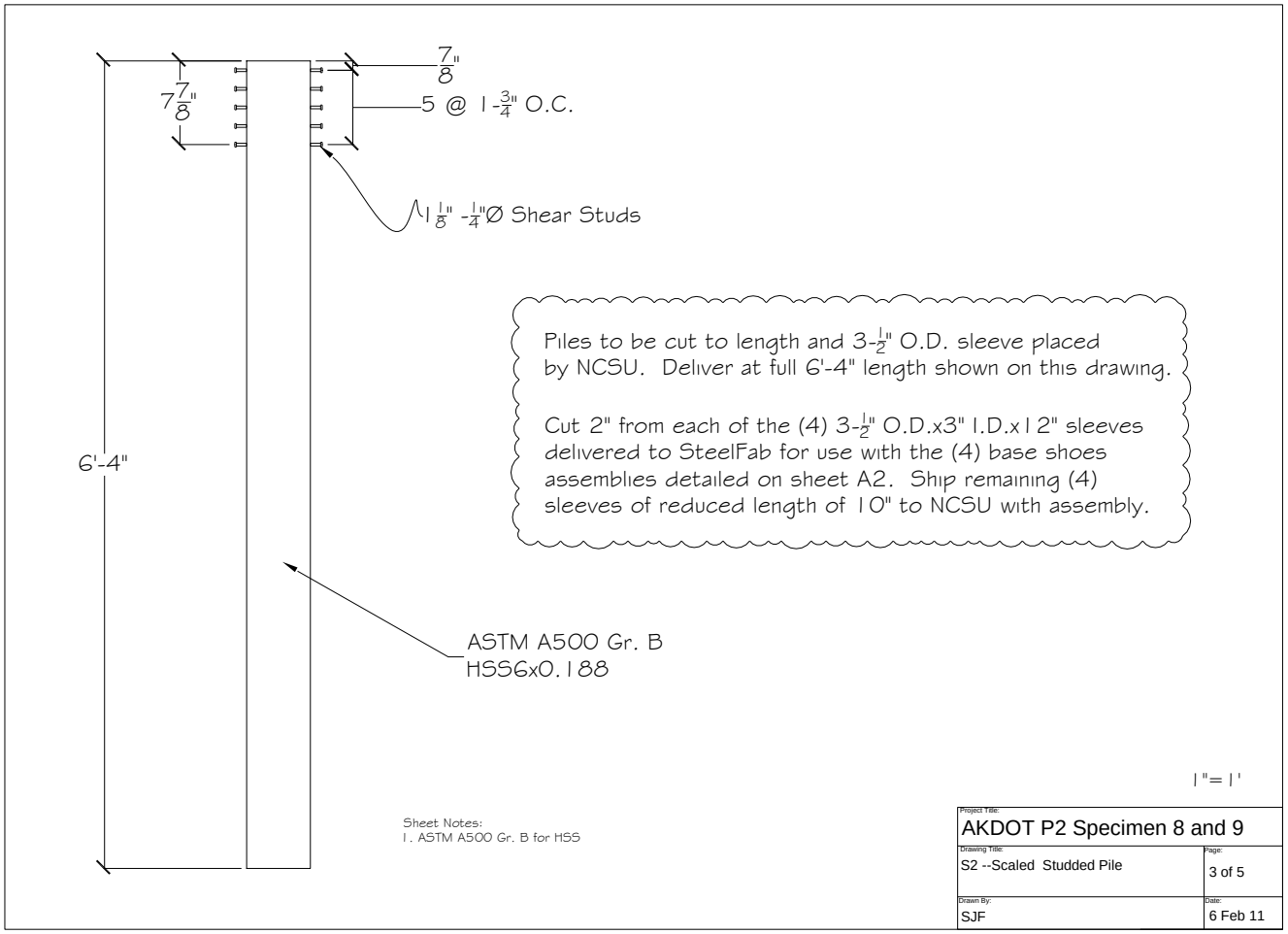

Figure A 121 Phase 2 Test 8, 9 Scaled Shake Table – G.S.C. Detailed Drawing

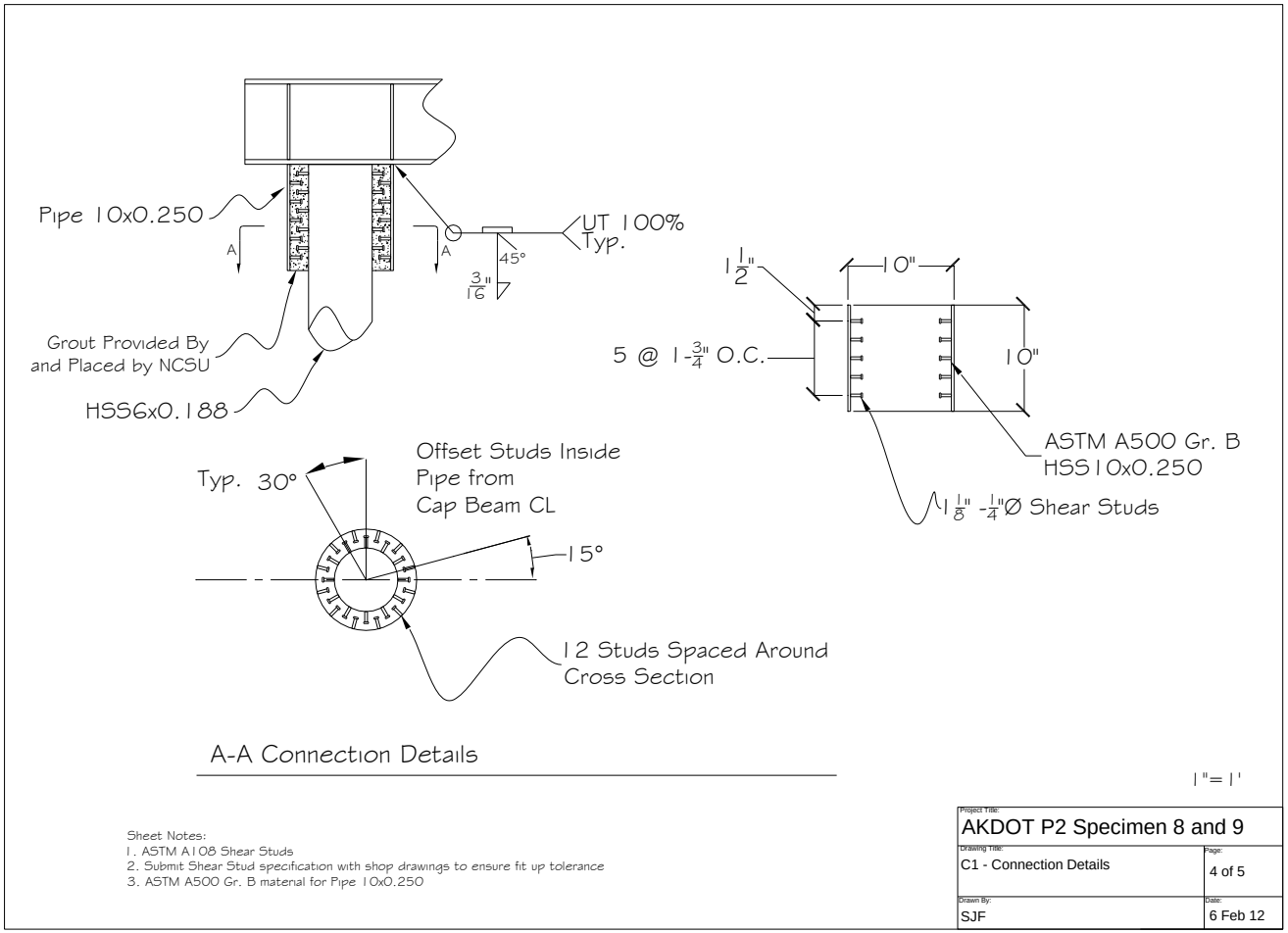

Figure A 122 Phase 2 Test 8, 9 Scaled Shake Table – G.S.C. Detailed Drawing

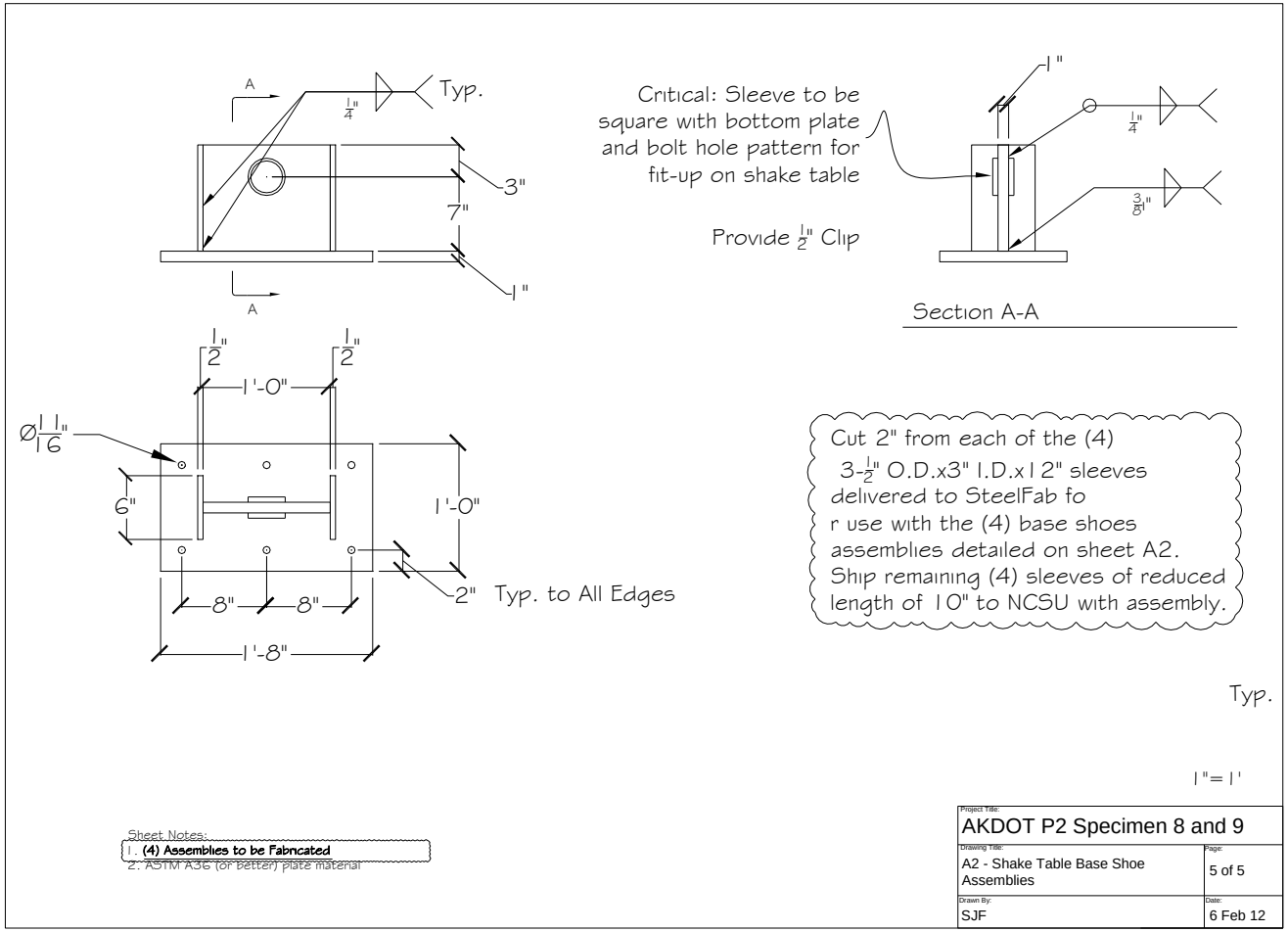

Figure A 123 Phase 2 Test 8, 9 Scaled Shake Table – Pinned Base Details

APPENDIX 5: Shake Table ARS and DRS Input / Output Comparisons

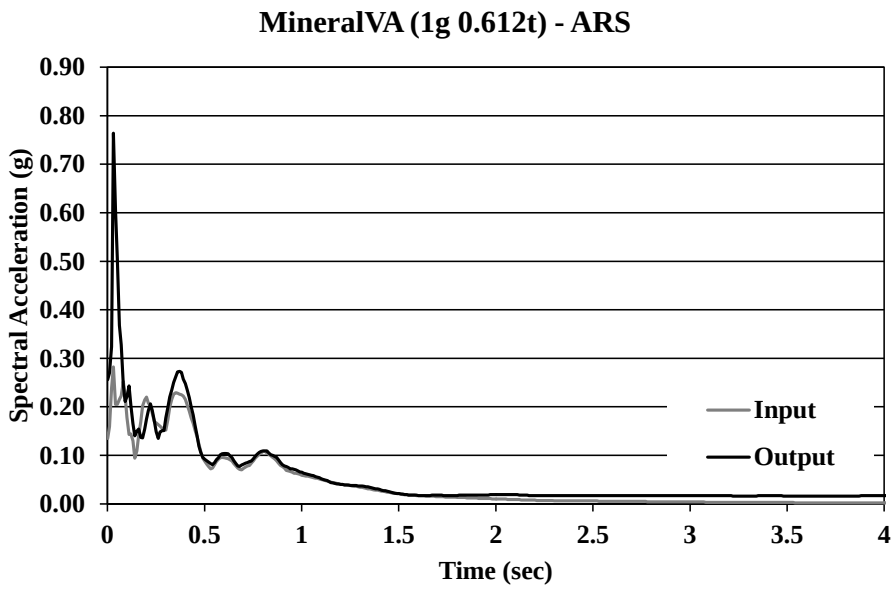

Figure A 124 Shake Table Test 1 – Mineral VA ARS Input / Output Comparison

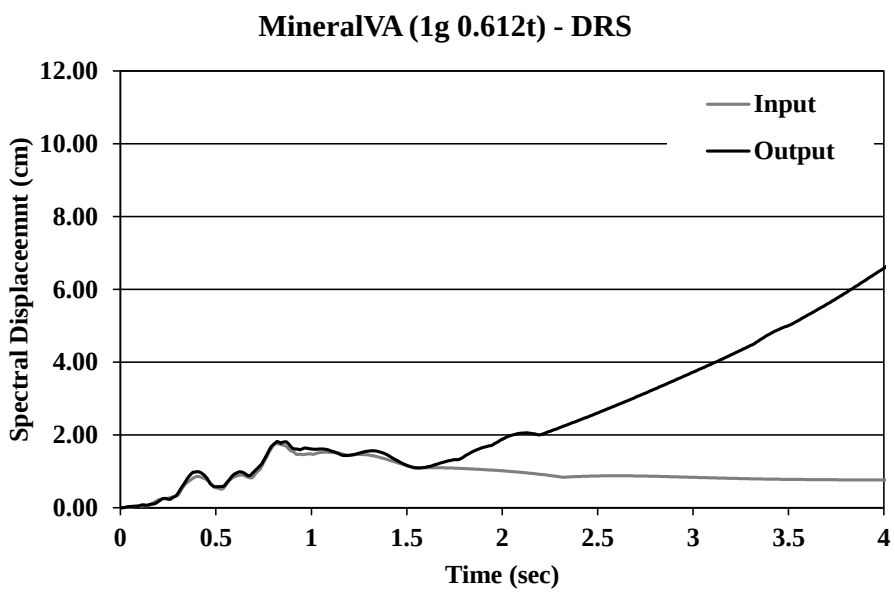

Figure A 125 Shake Table Test 1 – Mineral VA ARS Input / Output Comparison

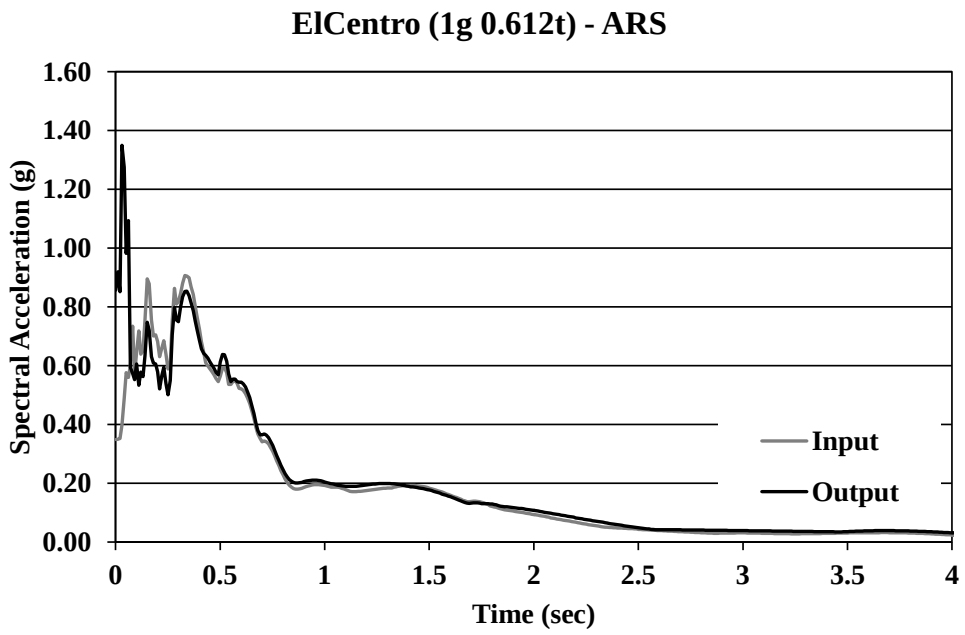

Figure A 126 Shake Table Test 1 – El Centro ARS Input / Output Comparison

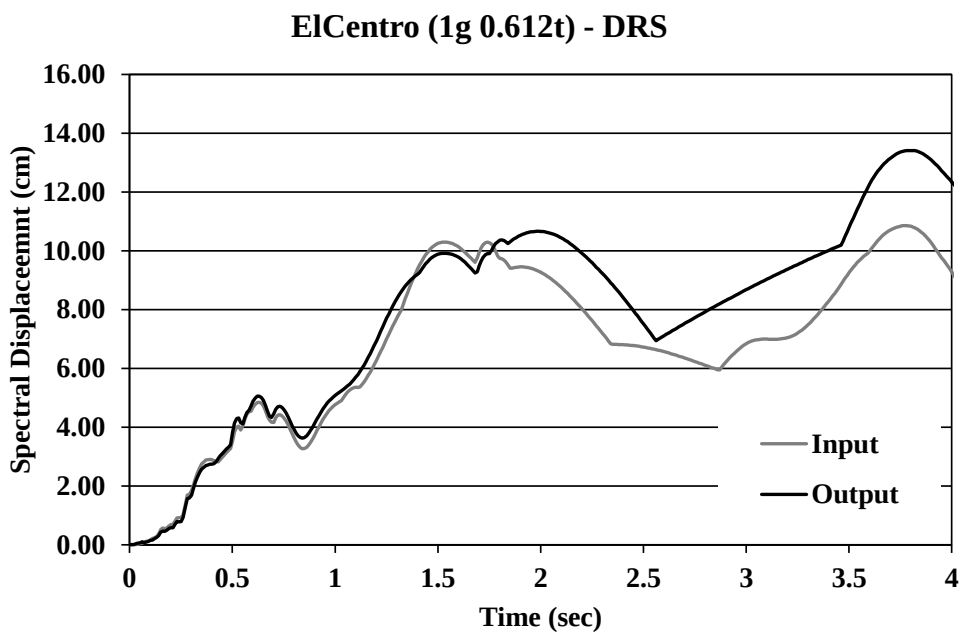

Figure A 127 Shake Table Test 1 – El Centro DRS Input / Output Comparison

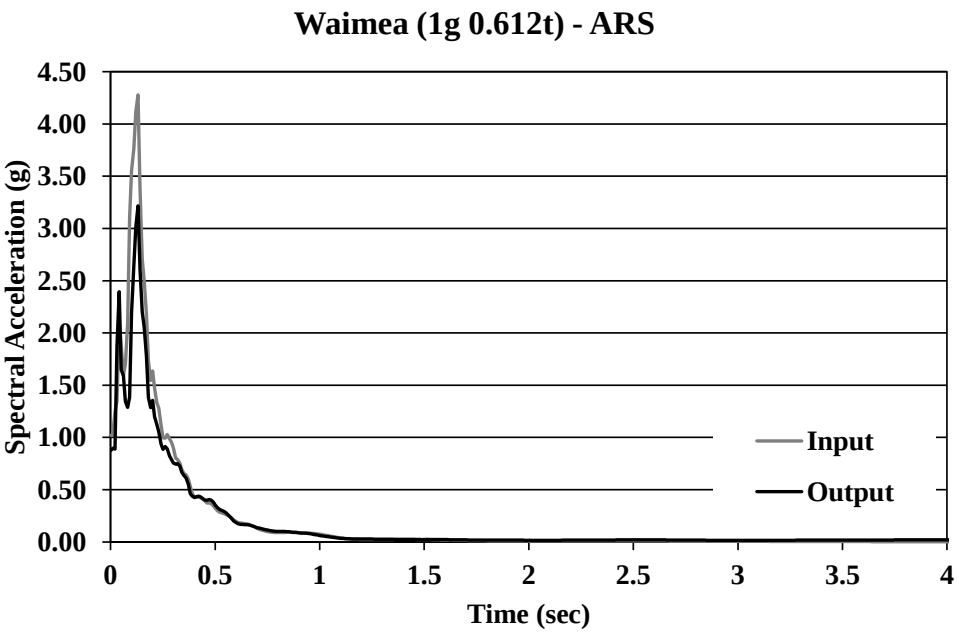

Figure A 128 Shake Table Test 1 – Waimea ARS Input / Output Comparison

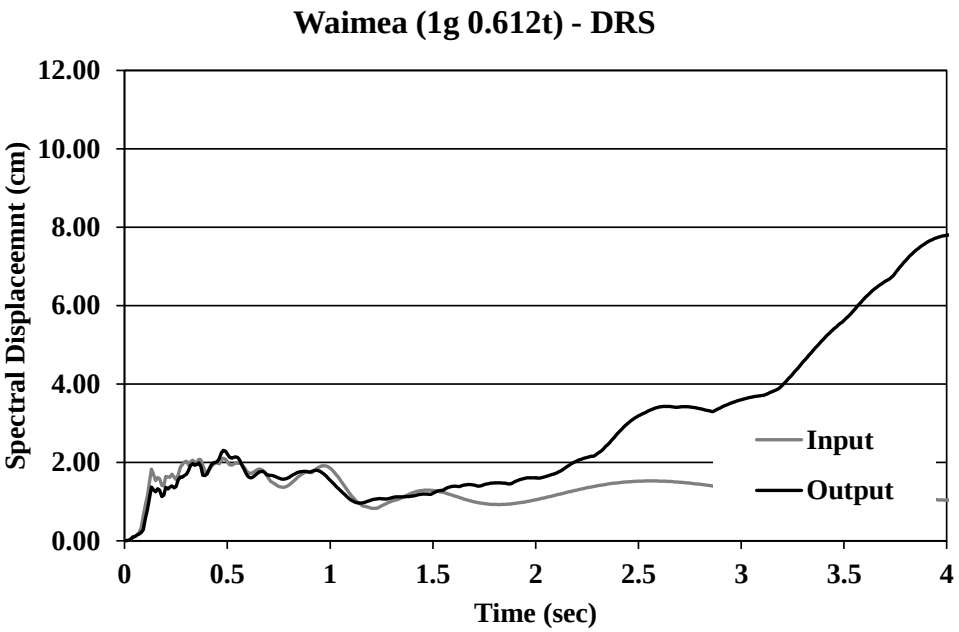

Figure A 129 Shake Table Test 1 – Waimea DRS Input / Output Comparison

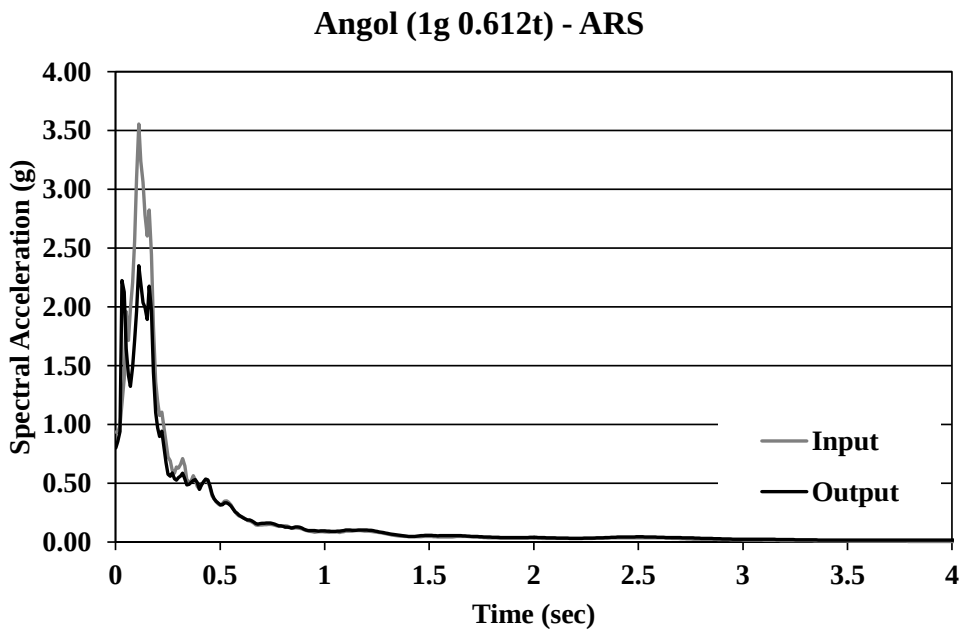

Figure A 130 Shake Table Test 1 – Angol ARS Input / Output Comparison

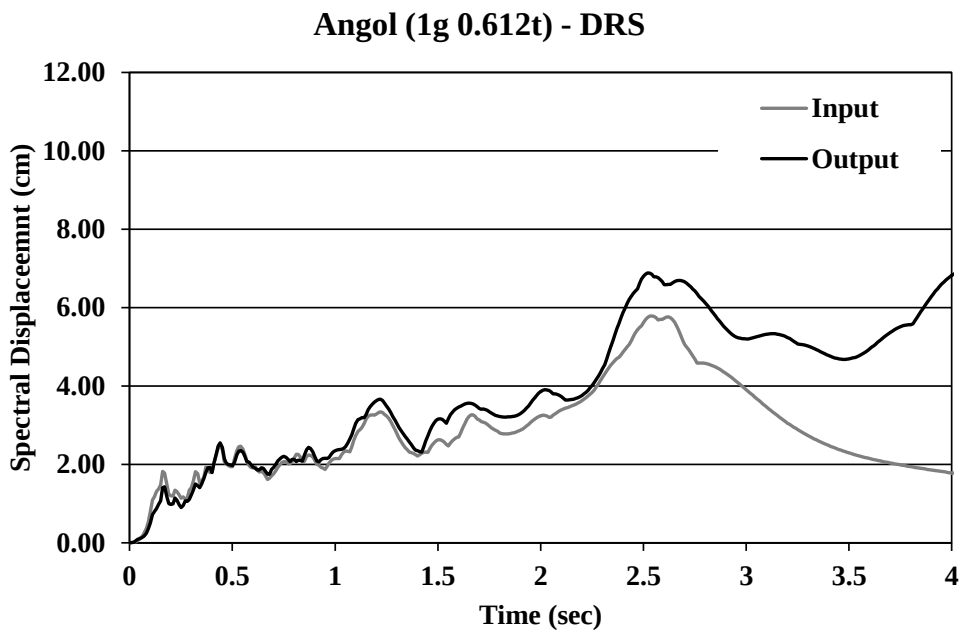

Figure A 131 Shake Table Test 1 – Angol DRS Input / Output Comparison

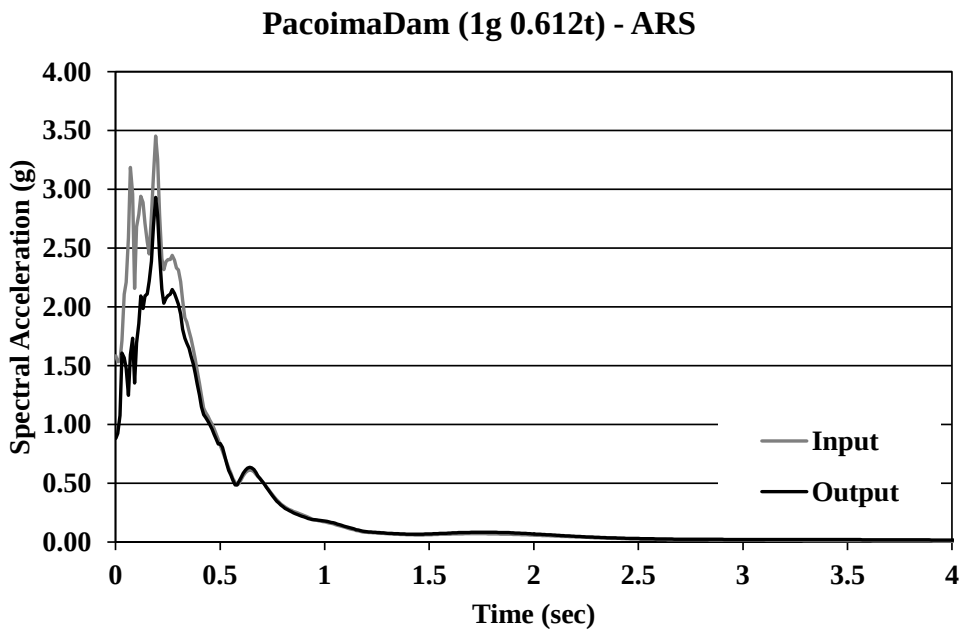

Figure A 132 Shake Table Test 1 – Pacoima Dam ARS Input / Output Comparison

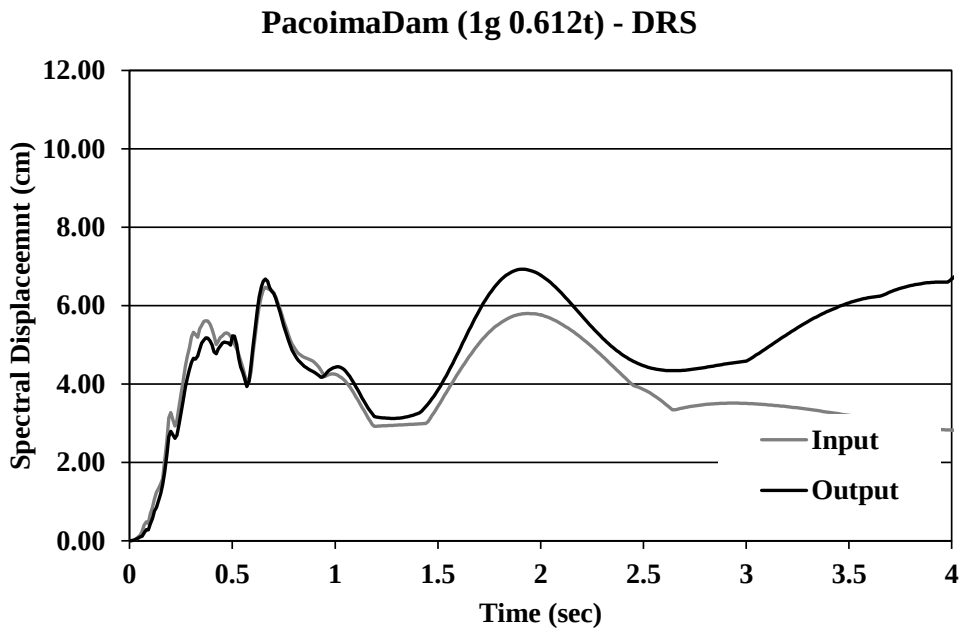

Figure A 133 Shake Table Test 1 – Pacoima Dam DRS Input / Output Comparison

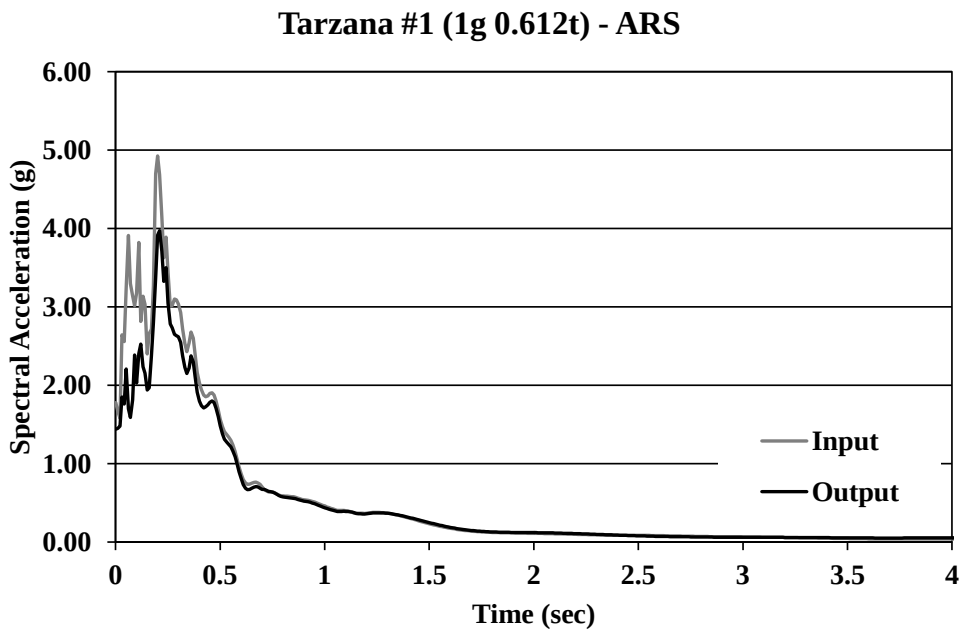

Figure A 134 Shake Table Test 1 – Tarzana #1 ARS Input / Output Comparison

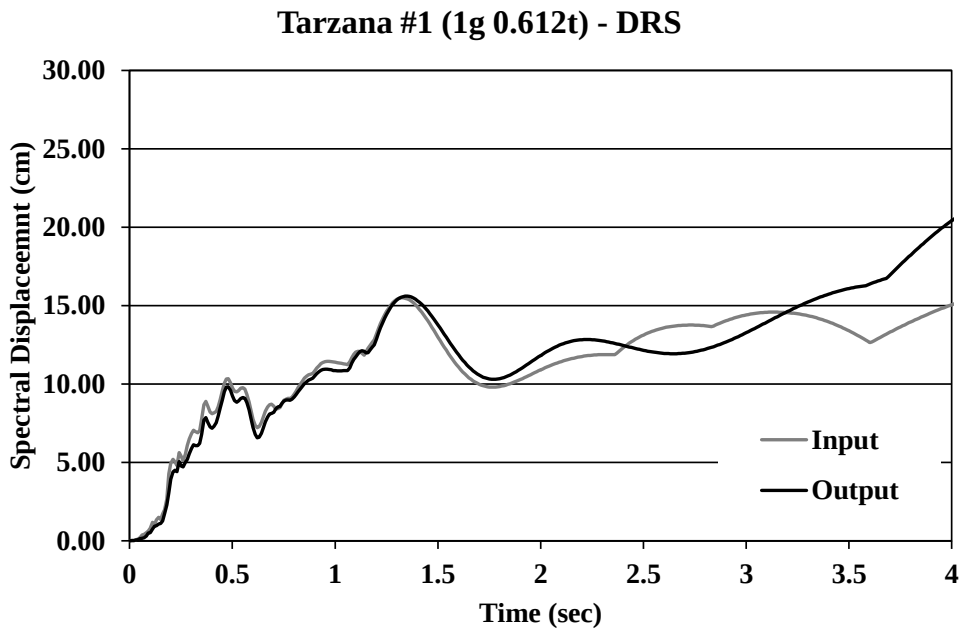

Figure A 135 Shake Table Test 1 – Tarzana #1 DRS Input / Output Comparison

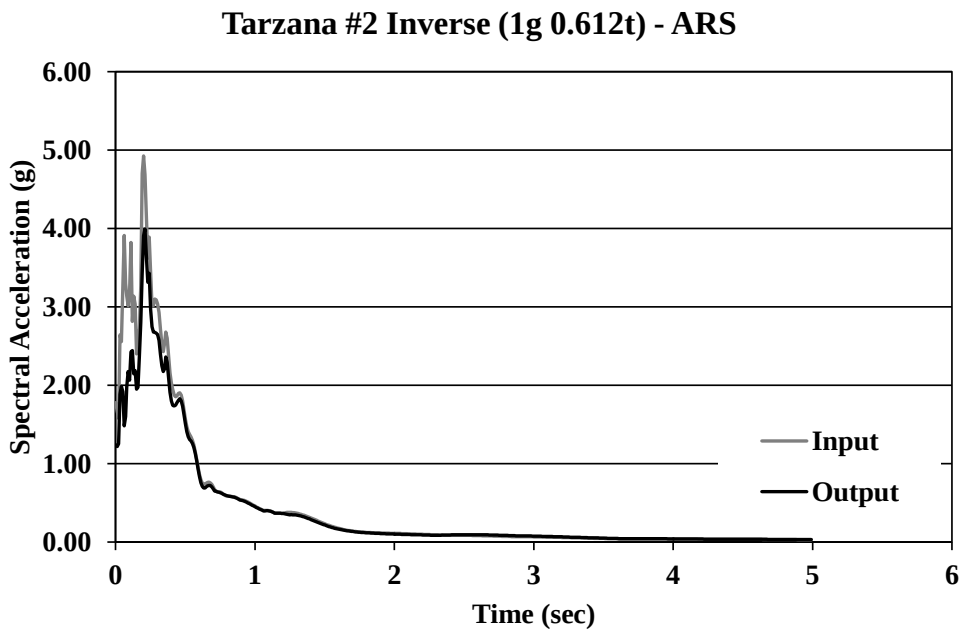

Figure A 136 Shake Table Test 1 – Tarzana #2 Inv. ARS Input / Output Comparison

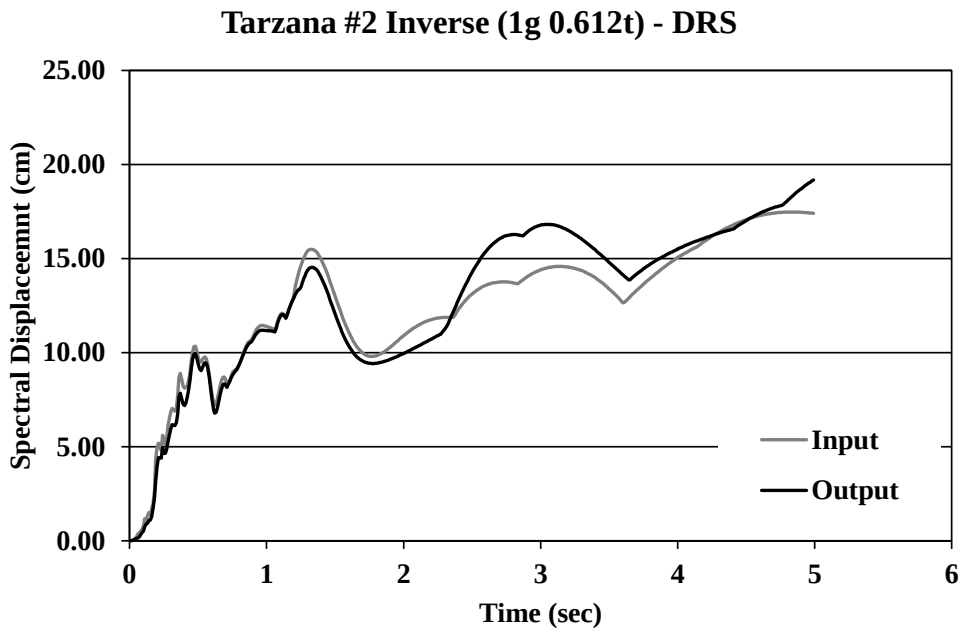

Figure A 137 Shake Table Test 1 – Tarzana #2 Inv. DRS Input / Output Comparison

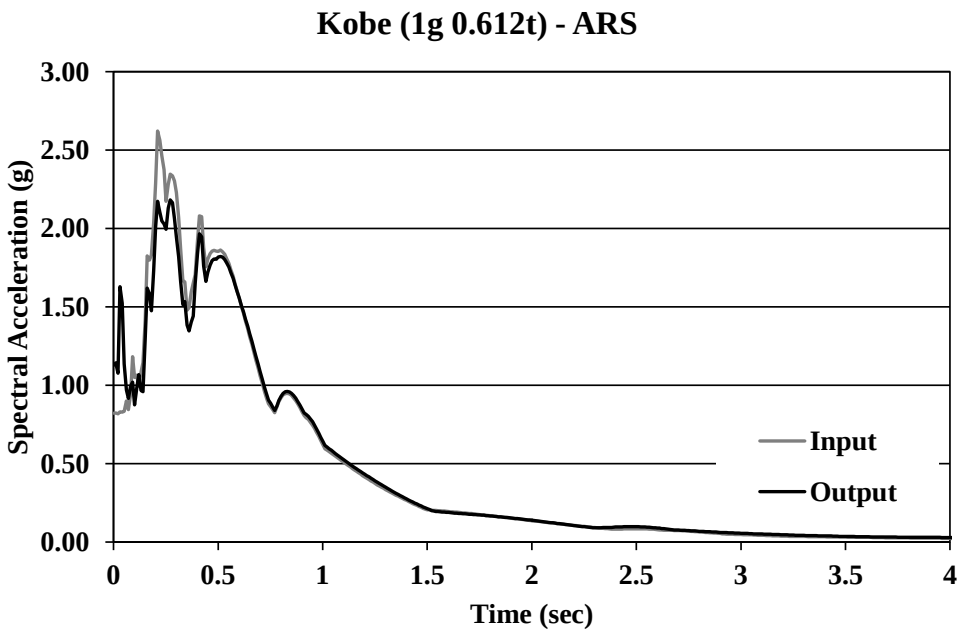

Figure A 138 Shake Table Test 1 – Kobe ARS Input / Output Comparison

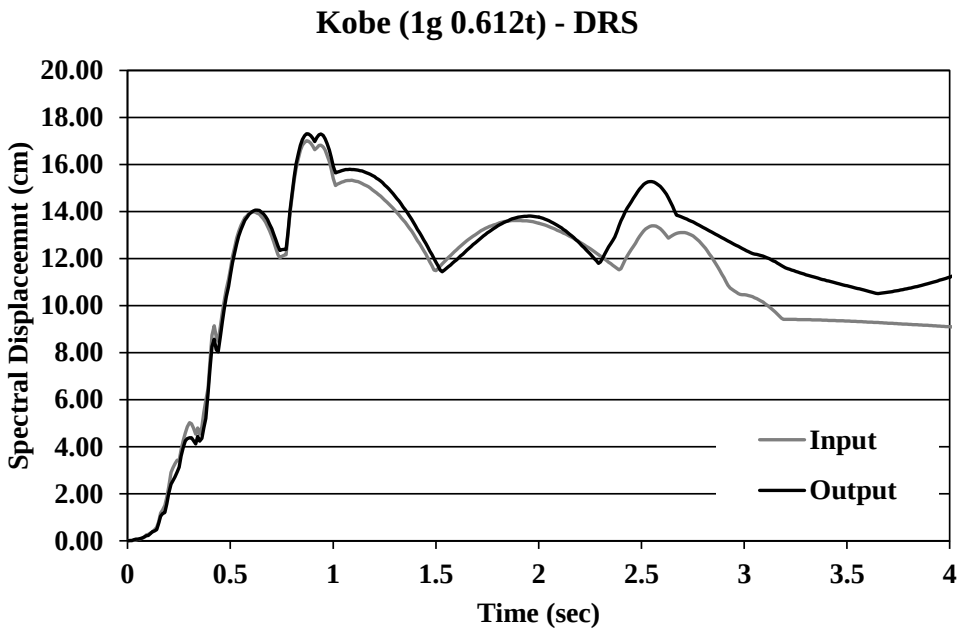

Figure A 139 Shake Table Test 1 – Kobe DRS Input / Output Comparison

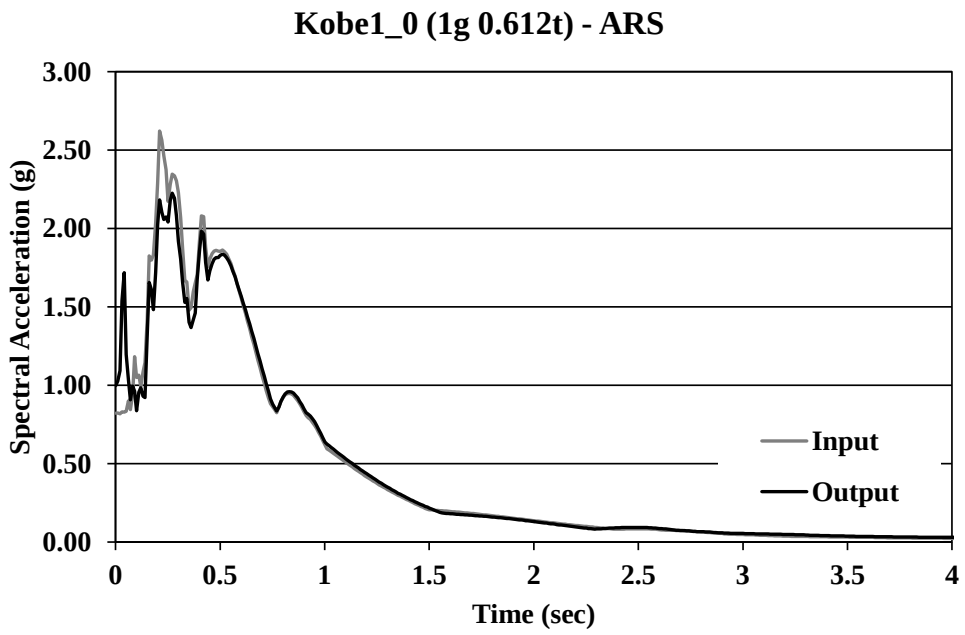

Figure A 140 Shake Table Test 2 – Kobe #1 ARS Input / Output Comparison

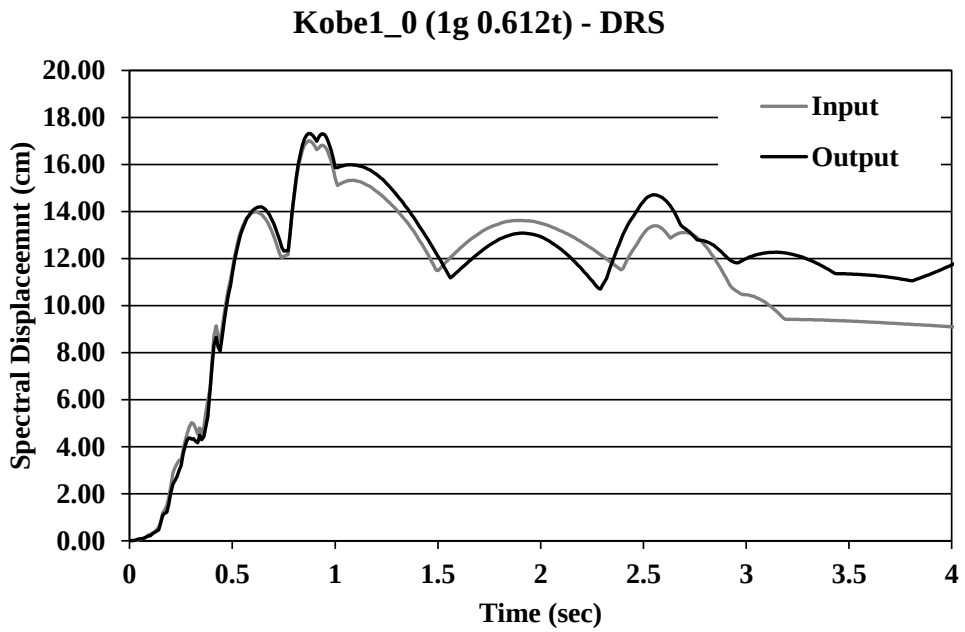

Figure A 141 Shake Table Test 2 – Kobe #1 DRS Input / Output Comparison

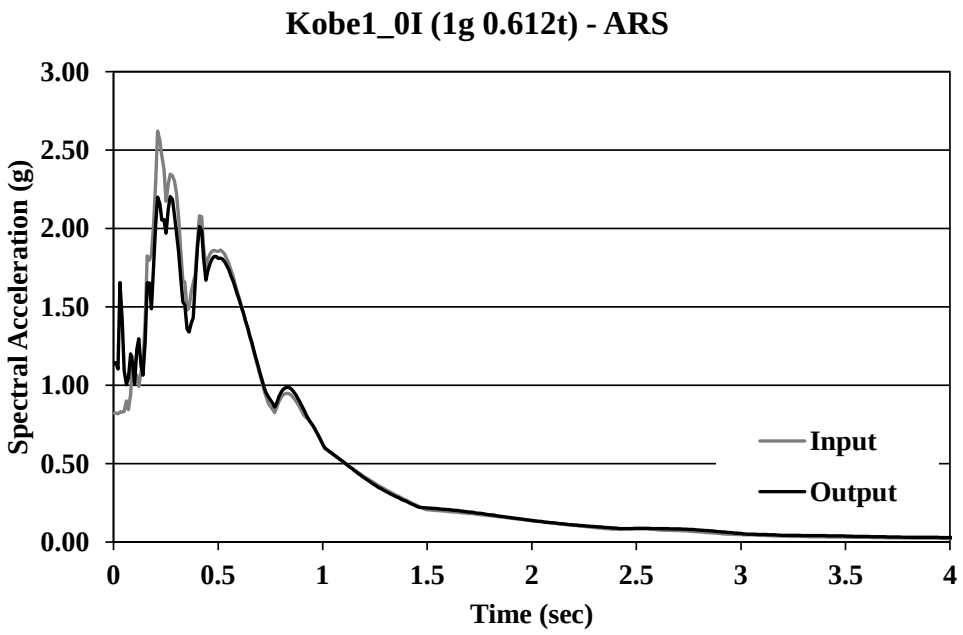

Figure A 142 Shake Table Test 2 – Kobe #2 Inv. ARS Input / Output Comparison

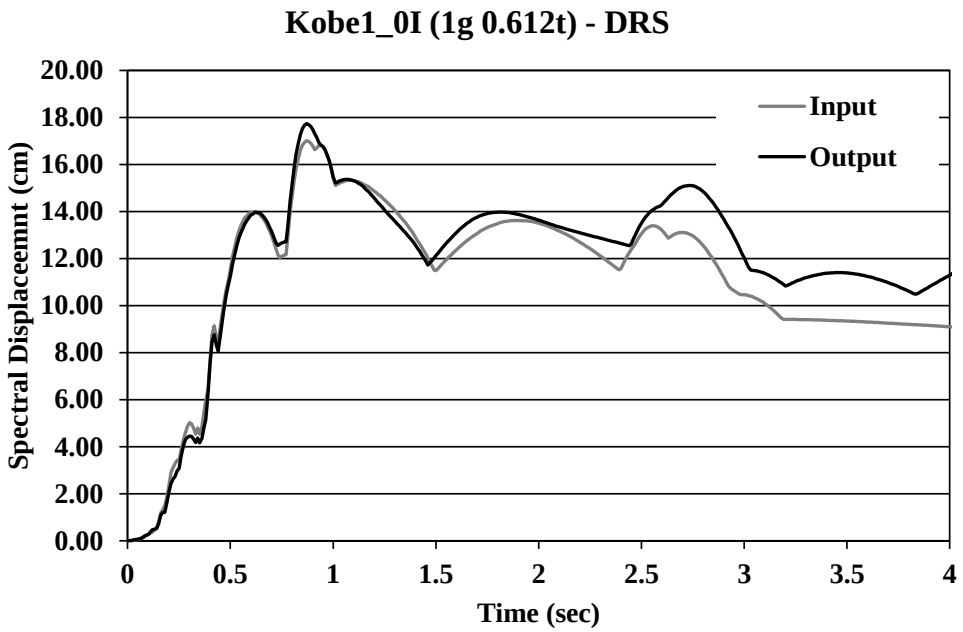

Figure A 143 Shake Table Test 2 – Kobe #2 Inv. DRS Input / Output Comparison